

Unclassified

ESC-TR-97-053

Project Report
ASAP-5
Volume 1

Proceedings of the Adaptive Sensor Array Processing (ASAP) Workshop 12-14 March 1997

G.M. O'Donovan
Editor

25 August 1997

Lincoln Laboratory

MASSACHUSETTS INSTITUTE OF TECHNOLOGY

LEXINGTON, MASSACHUSETTS



Prepared for the Defense Advanced Research Projects Agency and the U.S. Air Force under Contract F19628-95-C-0002.

Approved for public release; distribution is unlimited.

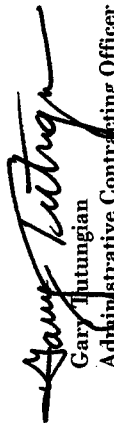
Unclassified

This report is based on studies performed at Lincoln Laboratory, a center for research operated by Massachusetts Institute of Technology. The work was sponsored in part by the Defense Advanced Research Projects Agency and in part by the U.S. Air Force under Contract F19628-95-C-0002.

This report may be reproduced to satisfy needs of U.S. Government agencies.

The ESC Public Affairs Office has reviewed this report, and it is releasable to the National Technical Information Service, where it will be available to the general public, including foreign nationals.

This technical report has been reviewed and is approved for publication.
FOR THE COMMANDER


Gary Tutungian
Administrative Contracting Officer
Contracted Support Management

Non-Lincoln Recipients

PLEASE DO NOT RETURN

Permission is given to destroy this document
when it is no longer needed.

Unclassified

MASSACHUSETTS INSTITUTE OF TECHNOLOGY
LINCOLN LABORATORY

**PROCEEDINGS OF THE ADAPTIVE SENSOR ARRAY
PROCESSING (ASAP) WORKSHOP
12-14 MARCH 1997**

*G.M. O'DONOVAN
EDITOR
Division 10*

PROJECT REPORT ASAP-5, VOLUME 1

25 AUGUST 1997

Approved for public release; distribution is unlimited.

19971001 030

DTIC QUALITY INSPECTED 3

LEXINGTON

MASSACHUSETTS

Unclassified

1997 ASAP Workshop Theme

This year marks the fifth annual ASAP workshop and is also the first ASAP workshop sponsored jointly by the DARPA Sensor Technology Office and Tactical Technology Office. This joint sponsorship is a result of the special attention to sonar given at this year's workshop. We wish to focus on the synergism between the sonar and radar ASAP communities and to encourage future efforts in this direction.

Although sonar was included in the first and third ASAP workshops, ASAP has traditionally concentrated on radar—core topics include airborne radar testbed systems, space-time adaptive processing, multipath jamming mitigation, theoretical limits in detection and estimation, and processor architectures. Parallel issues are likewise found in sonar, and both communities have developed adaptive techniques to reduce sensor vulnerability to undesired interference. The similarities between these two fields arise from the common technique of receiving energy on a sensor array, but different missions and propagation environments lead to different signal processing challenges. For airborne early warning (AEW) radar, real-time demands and free-space speed-of-light propagation generally lead to narrowband processing at high data processing throughput. For shallow-water anti-submarine warfare (ASW), the inhomogeneous, dispersive, and attenuation properties of underwater acoustic environments typically require broadband processing at low frequencies, oftentimes with unknown environmental characteristics.

The goal of ASAP '97 is to bring the sonar and radar ASAP communities together in a classified forum where the latest approaches to adaptive sensor array problems can be presented and discussed. Because this workshop will for many serve as an introduction to the other community, we have encouraged session chairs to provide broad overviews of the main ideas and a gentle introduction to the specific vocabulary of each subject. It is fitting to feature sonar and radar together in a workshop dedicated to national defense applications of ASAP. We hope that this interaction fosters an exchange of ideas within the geographically and professionally diverse adaptive processing community, highlights state-of-the-art developments, and focuses community efforts on outstanding problems. Finally, we hope that exposure to each community's new ideas broadens our horizons, above and below the water.

We welcome your participation in the fifth annual ASAP workshop.



Theo Koolij
DARPA/TTO
Maritime Systems
Program Manager

Dan Gammon
DARPA/STO
Advanced Signal Processing
Program Manager

Steering Committee

Kenneth D. Senne, Workshop Chairman / MIT Lincoln Laboratory
Lloyd J. Griffiths / University of Colorado
Arthur B. Baggeroer / MIT, Dept. of Ocean Engineering
Norman L. Owsley / Naval Undersea Warfare Center

ADAPTIVE SENSOR ARRAY PROCESSING WORKSHOP 12-14 MARCH 1997

SPEAKER PRESENTATIONS

VOLUME 1

SPEAKER	TITLE	PAGES
Norman Owsley Naval Undersea Warfare Center	Keynote Address Radar, Sonar and Whatever Happened to Finn Bryn?	1-28
Arthur Baggeroer MIT Ocean Engineering	SESSION I : Sonar and Underwater Acoustics Sessions	29-35
William Carey Massachusetts Inst. of Technology	The Determination of Signal Coherence Length Based on Signal Coherence and Gain Measurements in Deep and Shallow Water	37-65
Ira Ekhaus Synap Corporation	POSTER SESSION I Reduced Wavenumber Synthetic Aperture	69-85
Daniel Marshall MIT Lincoln Laboratory	Monostatic Clutter Spreading in Joint Terrain Scattered Jamming (TSJ) / Clutter Mitigation Architectures	87-109
Steven Smith and James Ward MIT Lincoln Laboratory	Fast Space-Time Clutter Covariance Matrix Computation	111-132
Brian Freburger and Donald Tufts Univ. of Rhode Island	On the Applicability of Principal Components Inverse (PCI) to Rapidly Adaptive Suppression of Terrain Scattered Interference (TSI)	133-151
William Ballance Hughes Aircraft Co.	SESSION II: Space-Time Adaptive Processing (STAP)	153-165

Peter Zulch USAF Rome Lab Joseph Guerci SAIC	The CREST Challenge - Overview and Analysis	167-191
William Melvin, Pinyuen Chen, and Michael Wicks USAF Rome Laboratory	Sample Selection for Improved Adaptive Airborne Radar	193-216
Timothy Barton and Steven Smith MIT Lincoln Laboratory	Structured Covariance Estimation for Space-Time Adaptive Processing	217-241
Michael Zatman MIT Lincoln Laboratory	The Effect of Bandwidth on Space-Time Adaptive Processing	243-276
James Day Lockheed Martin	SESSION III: Systems Applications of STAP	277-285
Robert Cooper Lockheed Martin	STAP Implementation Trades for a UHF Airborne Early Warning (AEW) Radar System	287-307
K. Akbulut, B. Suresh Babu, Richard Davis, and J Kramer The MITRE Corporation	Clutter Mitigation in an Airborne Radar Based Upon Phase-Weight Perturbation	309-332
S.U. Pillai, Y.L. Kim and Joseph Guerci, Polytechnic Univ.	An Efficient Implicit Interference Subspace Removal Techniques for STAP	333-346
Ronald Fante MITRE	SESSION IV: Terrain Scattered Interference	347-354
Lee Moyer and Douglas Page Technology Service Corp. James Arnits and David Fenner Northrop Grumman Corp. Ralph Kohler, Mike Little and David Mokay Rome Laboratory	Multi-Channel Airborne Bistatic Radar Data Collection	355-386
Daniel Rabideau MIT Lincoln Laboratory	Signal Modulation in Pulse-By-Pulse Adaptive Nulling Systems	387-415

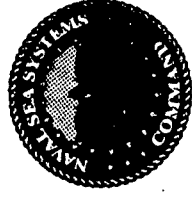
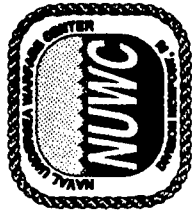
Stephen Kogon MIT Lincoln Laboratory E. Jeff Holder Georgia Tech Research Inst. Douglas Williams Georgia Inst. of Tech.	On the Use of Terrain Scattered Interference for Mainbeam Jammer Suppression	417-437
Scott Coutts MIT Lincoln Laboratory	3-D Emitter Localization Using Out-of-Plane Multipath	439-466
	SESSION V: Detection and Estimation	
Gary Hatke MIT Lincoln Laboratory	GAMMA: A Fast Adaptive Parameter Estimation Algorithm for Multidimensional Arrays	469-491
Christ Richmond MIT Lincoln Laboratory	Statistical Analysis of Clutter Editing Adaptive Detection Algorithm	493-523
Steven Smith MIT Lincoln Laboratory	Adaptive Detection Performance in Non-Ideal Conditions	525-546
	POSTER SESSION II: EMBEDDED COMPUTING	
Masahiro Arakawa and Robert Ford MIT Lincoln Laboratory	Seeker Algorithm and Architecture Study	549-559
Russell Brown, Richard Linderman, and Mark Linderman Rome Laboratory John Samson and David Grimm Honeywell Corporation Arnold Bramson, Bruce Havlicsek and Robert Warta Northrop Grumman Corporation	Processing Considerations and Performance Results for a Real-Time STAP Flight Demonstration	561-573
William Kostis, Gary Adams Robert Durie, and Adam Bojanczyk Cornell Univ.	Automated Application Synthesis for High-Performance Sensor Array Processing	575-587

Viktor Prasanna Univ. of Southern California	Data Remapping Techniques for High-Performance Embedded Signal Processing Applications	589-608
William Song MIT Lincoln Laboratory	Digital Radar Receiver	609-633
	SESSION VI: Sonar and Underwater Acoustics II	
J. Proakis and M. Stojanovic Northeastern Univ.	Reduced Complexity Receivers for Time-Dispersive Digital Communication Channels	637-655
	SESSION VII: Advanced Applications	
Donald Tufts and J.W. Cooley Univ. of Rhode Island Edward Real Sanders, Lockheed Martin	Fast Approximate Subspace Tracking	659-683
Alex Haimovich and A. Shah New Jersey Inst. of Tech.	STAP in Wireless Communications: Performance Analysis	685-714

Radar & Sonar: Together at Last

Norman L. Owsley
Naval Undersea Warfare Center
NUWC Div. Newport
Newport, RI 02840
tel: (401) 841-7505

Abstract The thirty-five year legacy of Finn Bryn, the first Viking to write $R^{-1}d$ for sonar, is surveyed. Particular emphasis is placed on submarine sensors and processing for both passive (beloved by submariners) and active (detested by submariners) sonar. Points of commonality and possible divergence between the radar and active sonar space-time adaptive processing (STAP) problems are examined. Comparisons and examples abound.



Radar, Sonar and Whatever Happened to Finn Bryn ?

Presented at:

1997 STAP Workshop

Lincoln Laboratories

March 1997

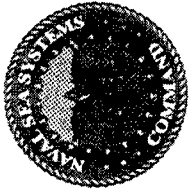
N.L.Owsley

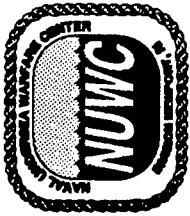
NUWC Submarine Sonar Department



SONAR and RADAR

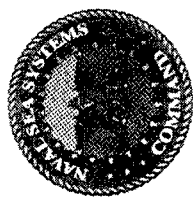
Together at Last





Outline

- Sonar since 1962
- Sensors
- STAP in Sonar?
- A Comparative Example of Active Sonar and Radar: Lessons to be Learned?
- The Trend: Multistatic Active Sonar
- Human Interest: Where is Finn Today?

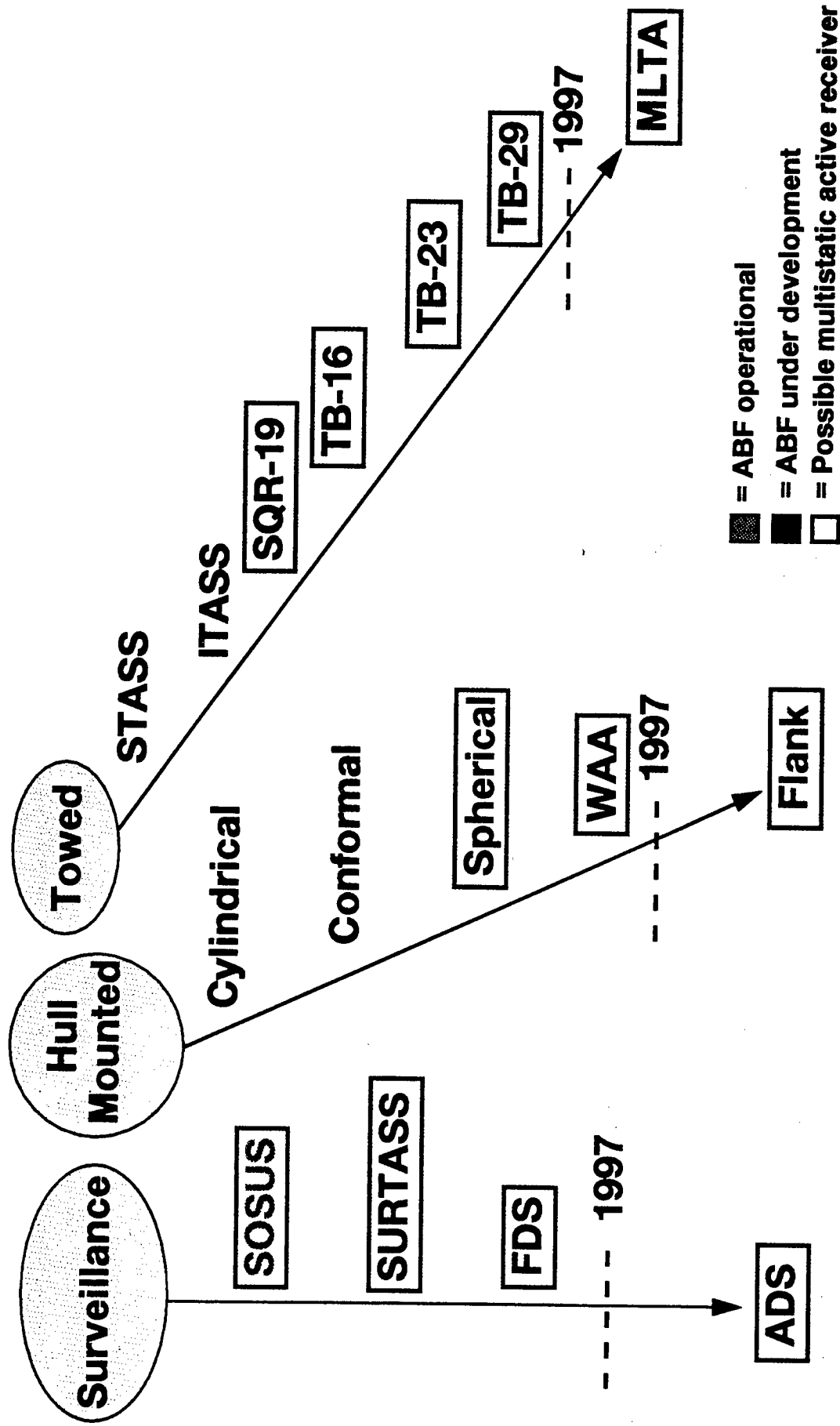


A high-contrast, black and white photograph of a person's legs and feet standing on a sandy beach. The person is wearing dark shorts and sandals. A small American flag is visible in the background on the left side.





Sensor Arrays: 1960s to 2000s





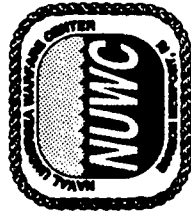
Sonar Array Gain (AG)

Noise Spatial Cross-Spectral Density Matrix (CSDM):

$$\mathbf{Q} = \alpha_0 \mathbf{I}_N + \alpha_1 \mathbf{Q}_1 + \alpha_2 \mathbf{Q}_2$$

$$\text{AG} = \frac{\text{SG}}{\alpha_0 \mathbf{N} \mathbf{G}_0 + \alpha_1 \mathbf{N} \mathbf{G}_1 + \alpha_2 \mathbf{N} \mathbf{G}_2}$$
$$\alpha_0 + \alpha_1 + \alpha_2 = 1$$

- Type 0: Uncorrelated self-noise (turbulent flow induced)
- Type 1: Extended (surface waves, biologics, bathymetric features)
- Type 2: Discrete (surface traffic, decoys, jammers, discrete facits)



Element Space(ES) vs. Beam Space(BS) Beamformer Array Gain

(SINGLE DISCRETE INTERFERENCE: N = NUMBER OF SENSORS $IN_0 R = r$, $SLL = L$)

CBF:

$$AG = \frac{N}{1 + rL}$$

ESMVDR:

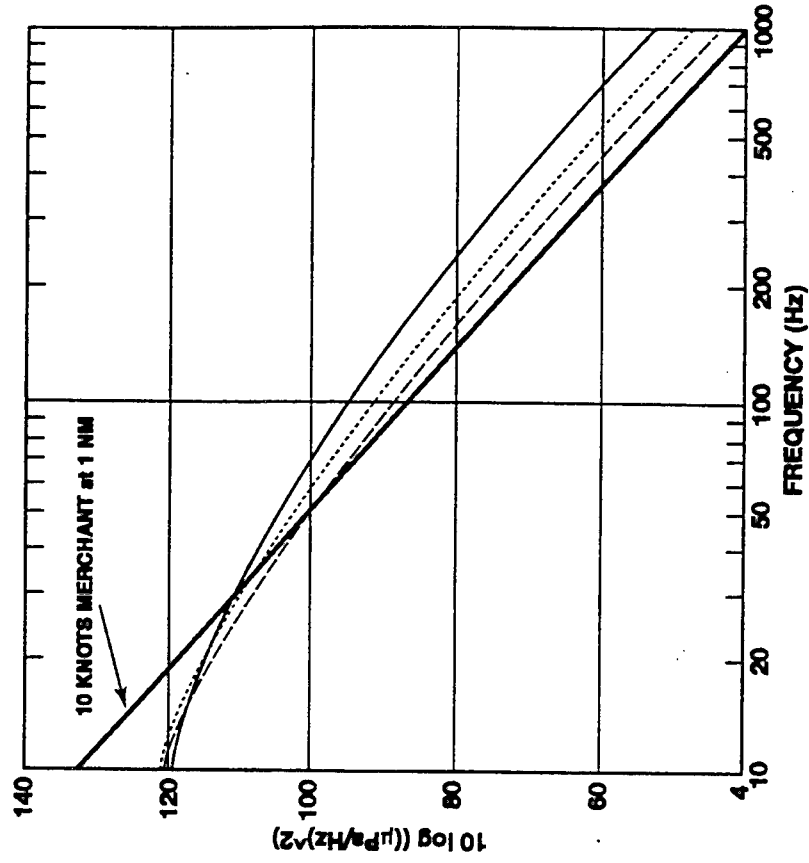
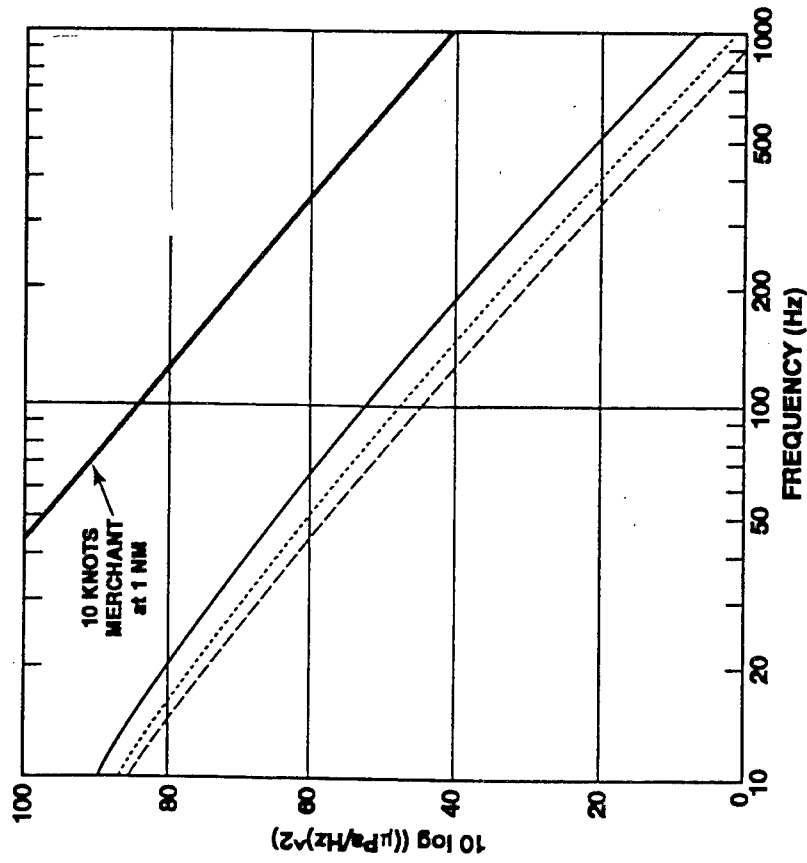
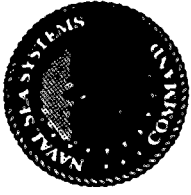
$$AG = N(1 - \frac{rL}{1 + r})$$

BSMVDR: (M = NUMBER OF ORTHOGONAL BEAMS)

$$AG = N(1 - \frac{rL}{1 + rML})$$



Passive Sonar Noise Levels



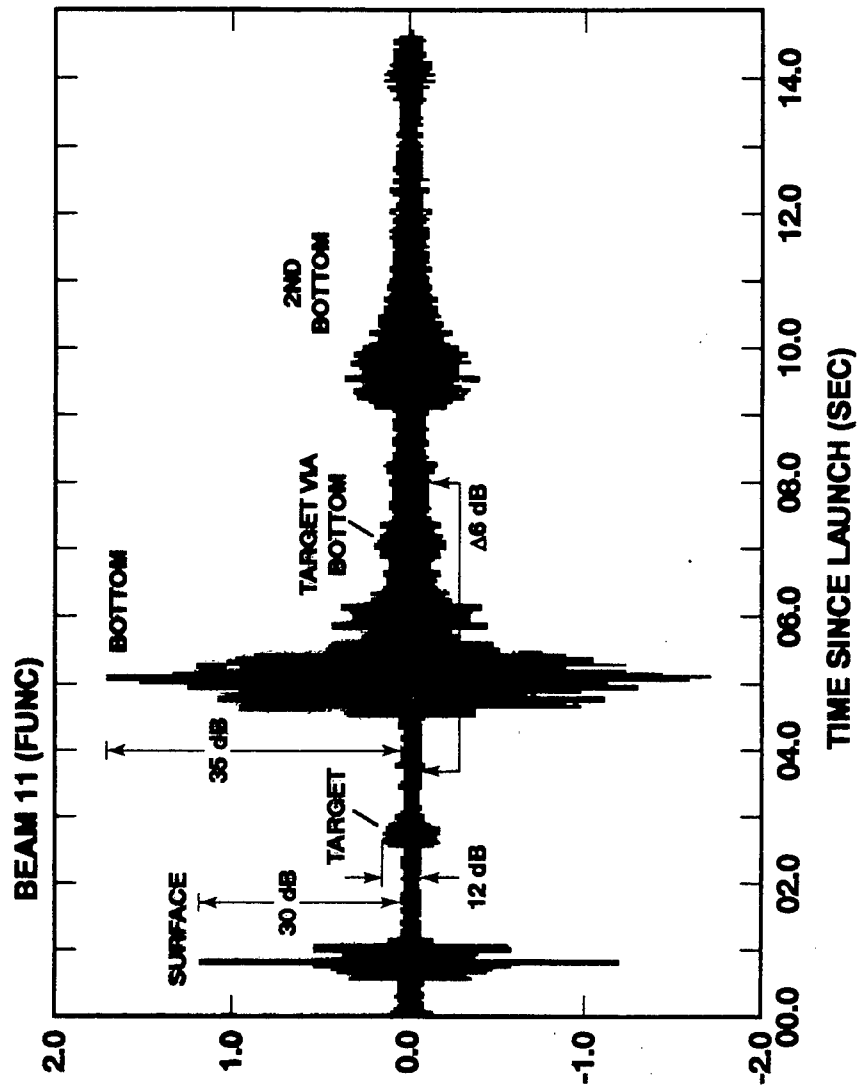


Active Sonar Noise Levels

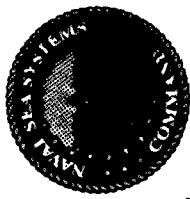
Towed Array re: Target Beam

64 element ULA with 0.5 m spacing

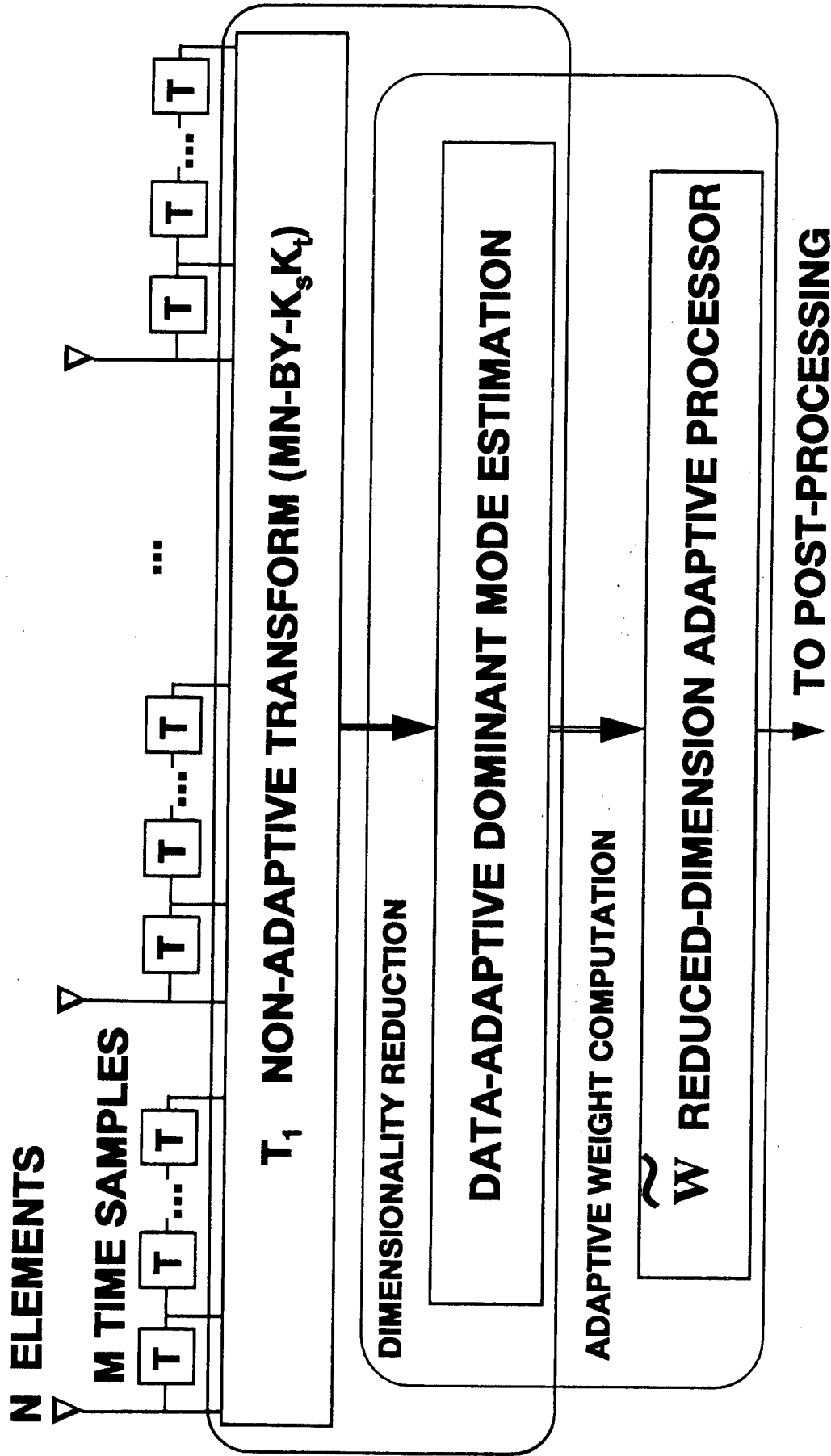
0.5 sec. LFM (1000 to 1260)



Matched Output for Entire Ping Cycle with No AGC

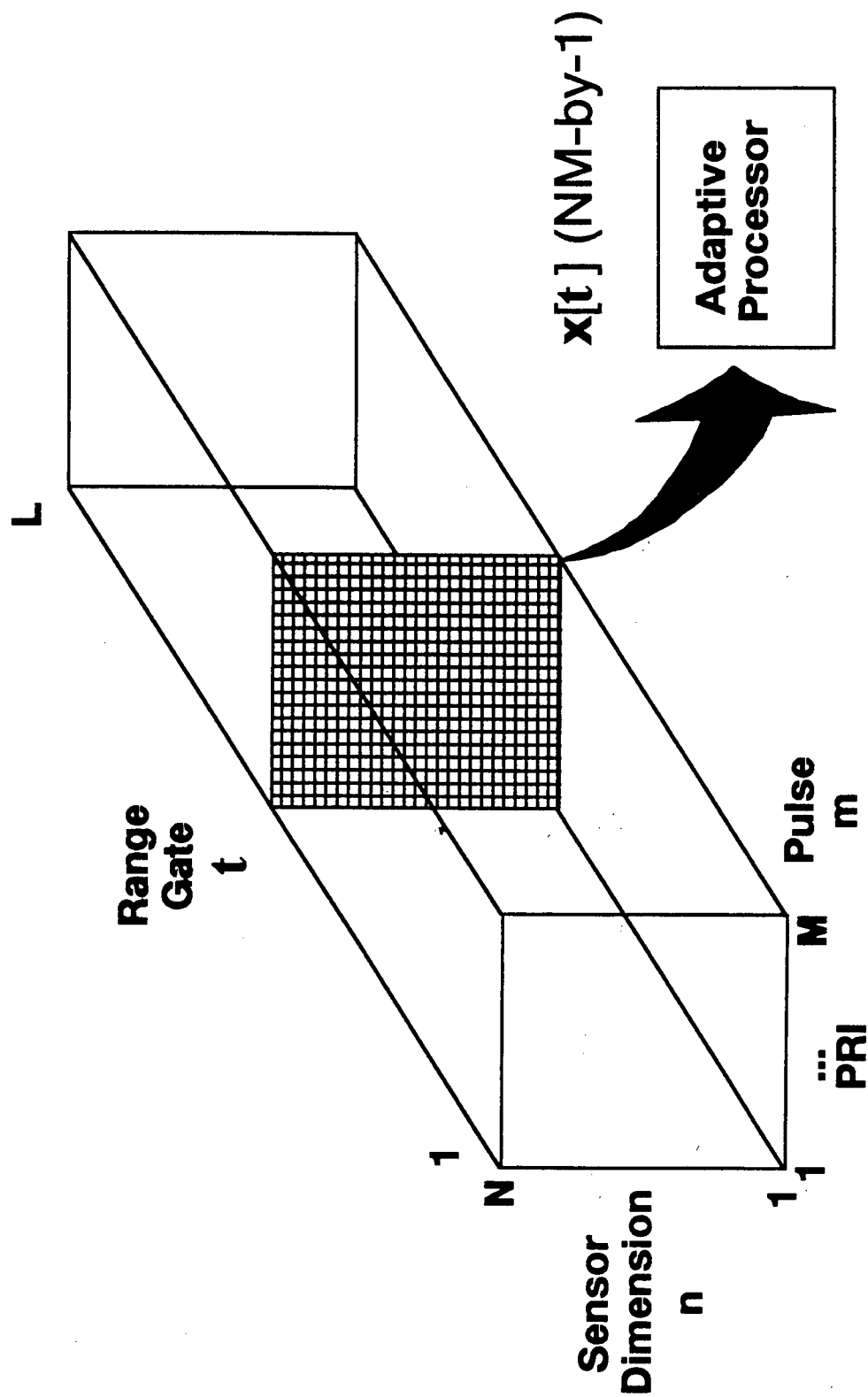


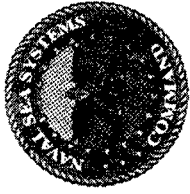
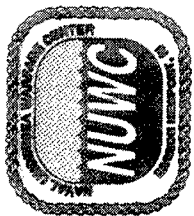
REDUCED-DIMENSION SPACE-TIME ADAPTIVE PROCESSOR





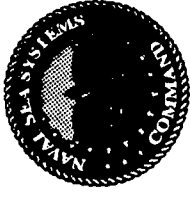
The Radar Coherent Processing Interval (CPI) Data Cube





$$C = 3 \times 10^8 \text{ m/sec}$$

$$C = 1.5 \times 10^3 \text{ m/sec}$$

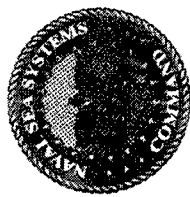
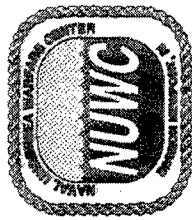


Question :

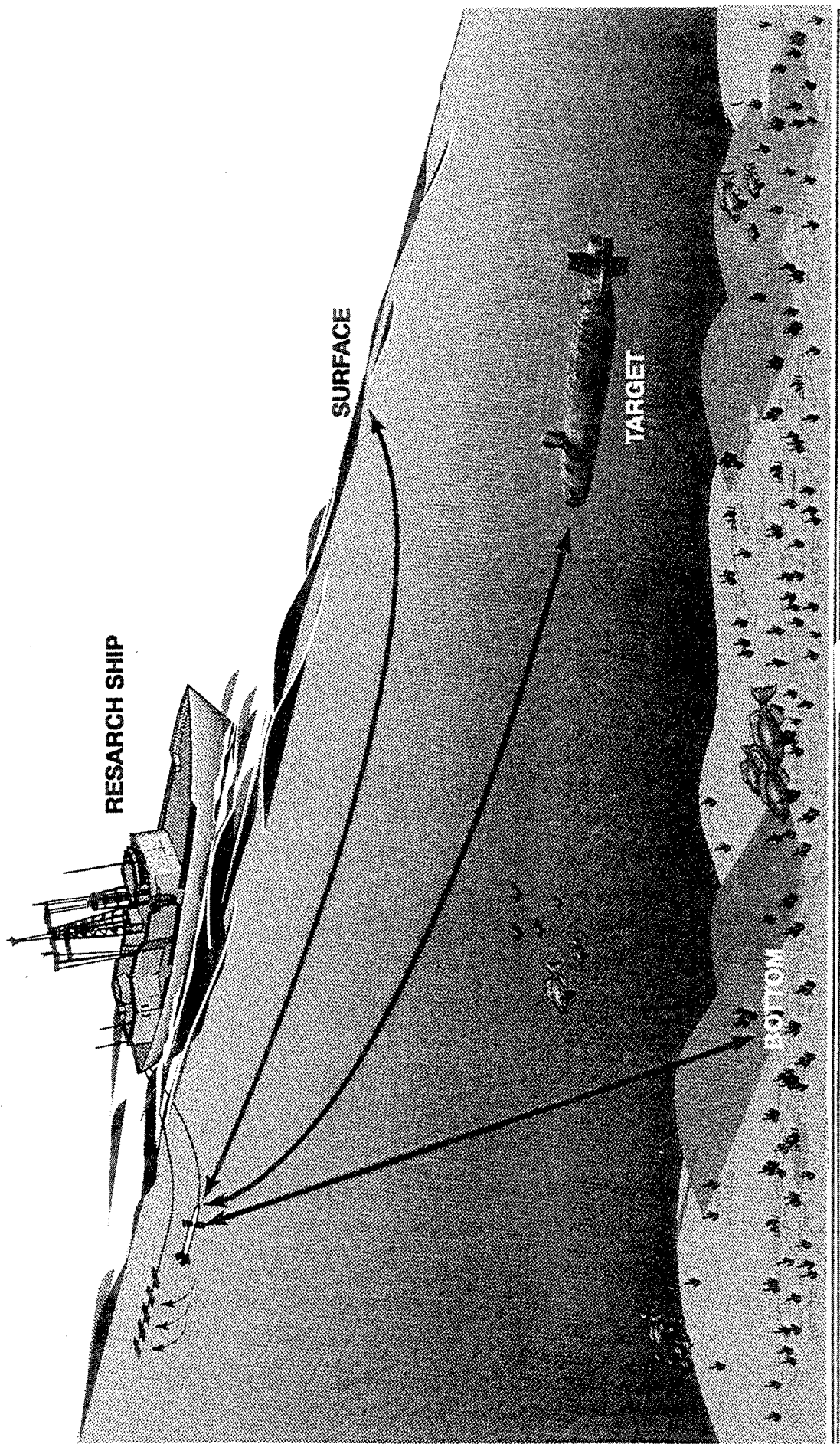
Can a sequence of M active sonar pulses be coherently processed as in the radar coherent processing interval (CPI) ?

	Radar	Sonar
c (m/sec)		1.5×10^3
PRI (sec)	3×10^8 (1/300)	60
Unambiguous Range (km)	500	45
Target Speed (knots)	600	6
Distance Moved in PRI (m)	1	185

Comment: Aspect angle rate would be critical.



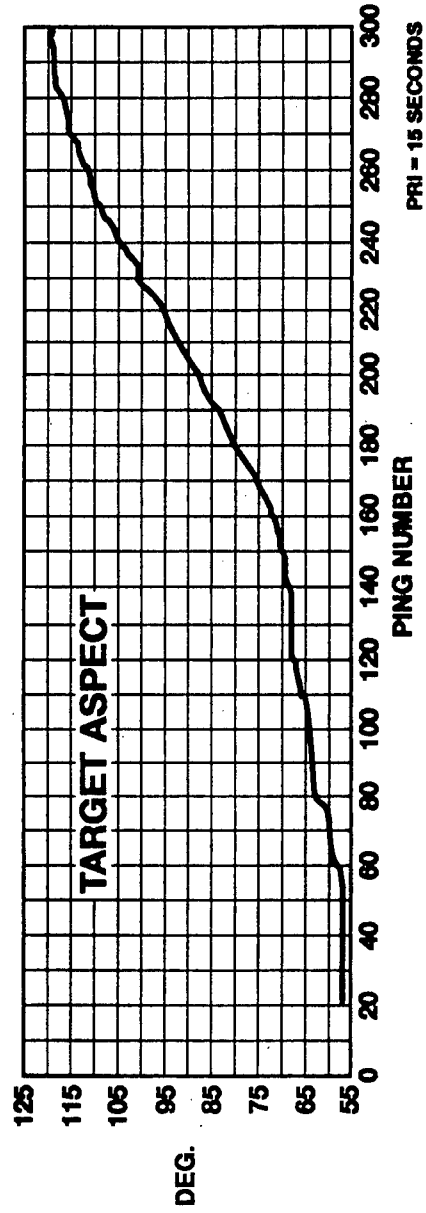
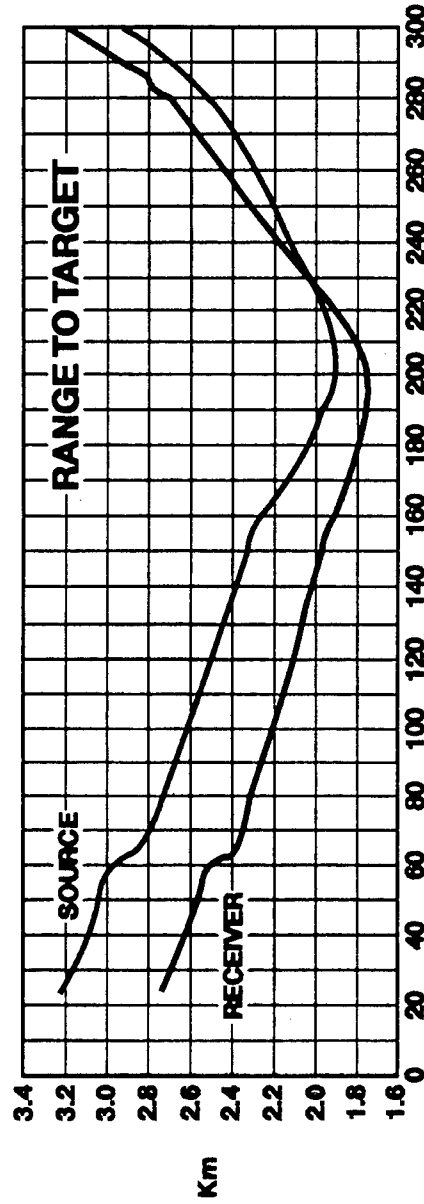
Adjacent Ping Correlation: Test Geometry (Stahl 1992)

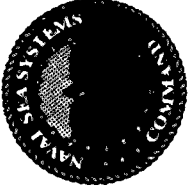




Adjacent Ping Correlation: Geometric Reconstruction

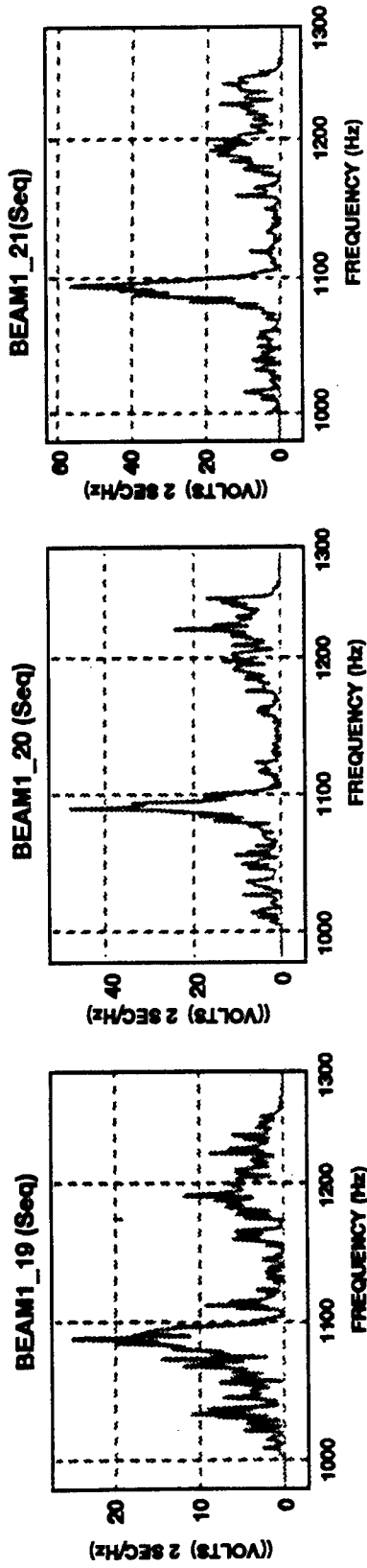
Maximum Bearing Rate = 1.6 deg/min



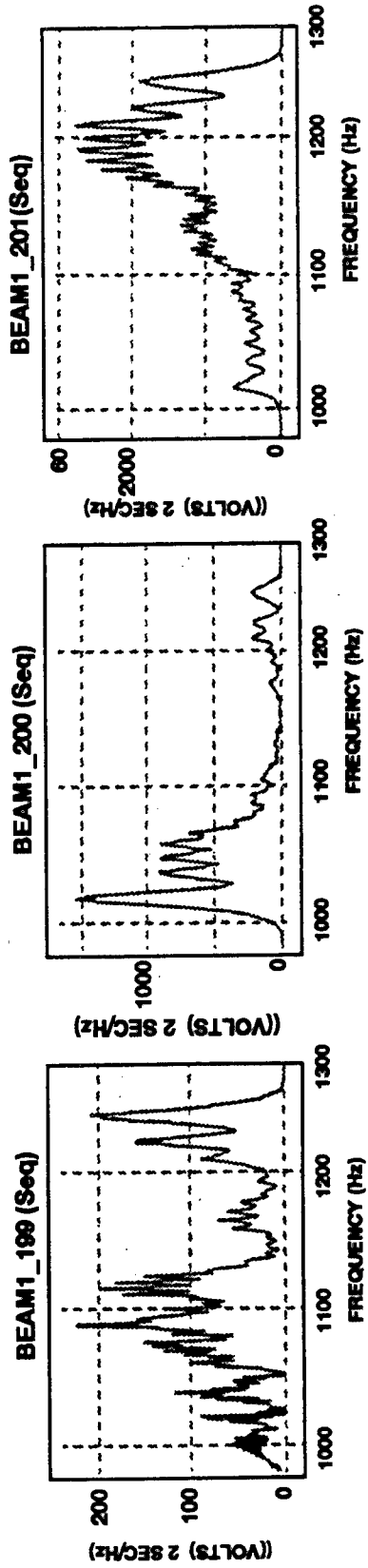


Adjacent Ping Correlation: Multiplying Spectra (PRI = 15 sec.)

Constant Aspect Angle

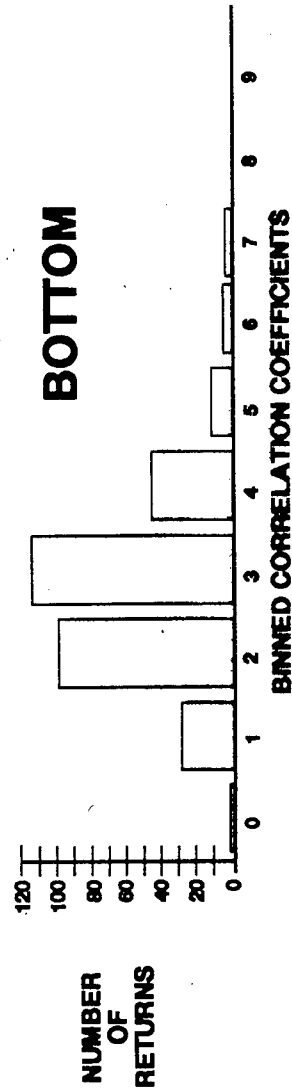
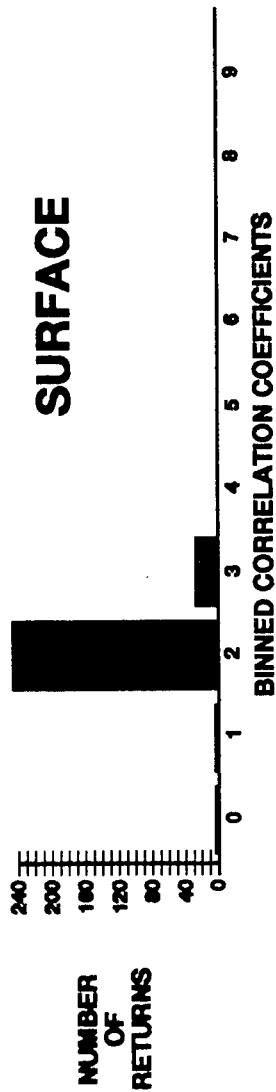
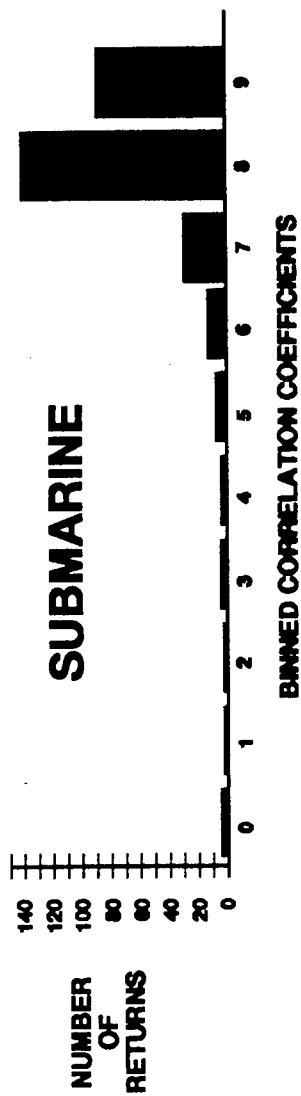


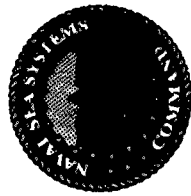
Variable Aspect Angle (aspect angle rate = 1.6 deg/min)





Adjacent Ping Correlation: Binned Correlation Coefficients (C_1)



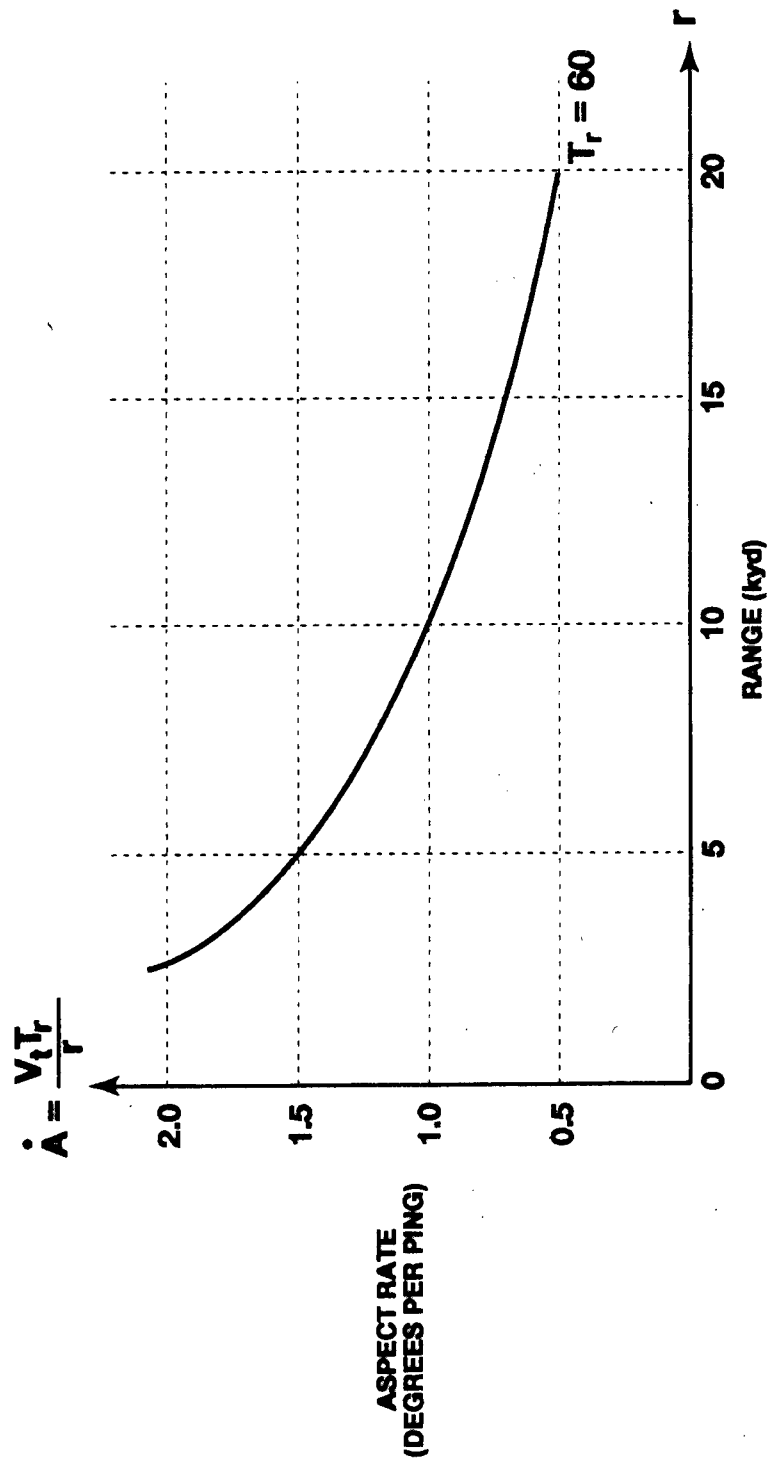


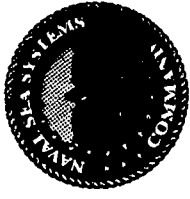
Aspect Angle Rate (A) vs. Range (r)

V_t = tangential SOA (knots)

T_r = PRI = pulse repetition interval (seconds)

r = range (kiloyards)





ADAPTIVE WEIGHT COMPUTATION

- **NON-ADAPTIVE TRANSFORMATIONS (DOF REDUCTION):**

$$\tilde{\mathbf{x}} = \mathbf{T}_1 \mathbf{x}, \tilde{\mathbf{d}}_0 = \mathbf{T}_1 \mathbf{d}_0, \tilde{\mathbf{C}} = \mathbf{T}_1 \mathbf{C}$$

- **MINIMUM VARIANCE:** $\sigma_y^2 = \mathbf{E}\{|\mathbf{w}^H \tilde{\mathbf{x}}|^2\}$
- **RESPONSE CONSTRAINT:** $\varepsilon^2 = |(\mathbf{w} - \tilde{\mathbf{d}}_0)^H \tilde{\mathbf{C}}|^2$
- **PROCESSOR DESIGN CRITERIA:**
minimize $(\sigma_y^2 + \lambda \varepsilon^2)$ w.r.t \mathbf{w}



ADAPTIVE WEIGHT SOLUTION

$$\mathbf{w} = [\mathbf{R}_{\mathbf{xx}}^{-1} + \lambda \mathbf{C} \mathbf{C}^H]^{-1} \mathbf{C} \mathbf{C}^H \mathbf{d}_0$$



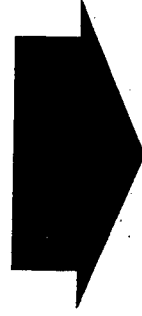
Something Old (1972): Adaptive Data Orthogonalization

For the rank one update:

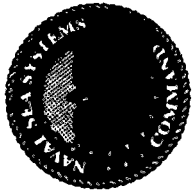
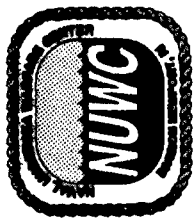
$$\mathbf{R}[t] = (1-\mu)\mathbf{R}[t-1] + \mu\mathbf{x}[t]\mathbf{x}[t]^H$$

Find

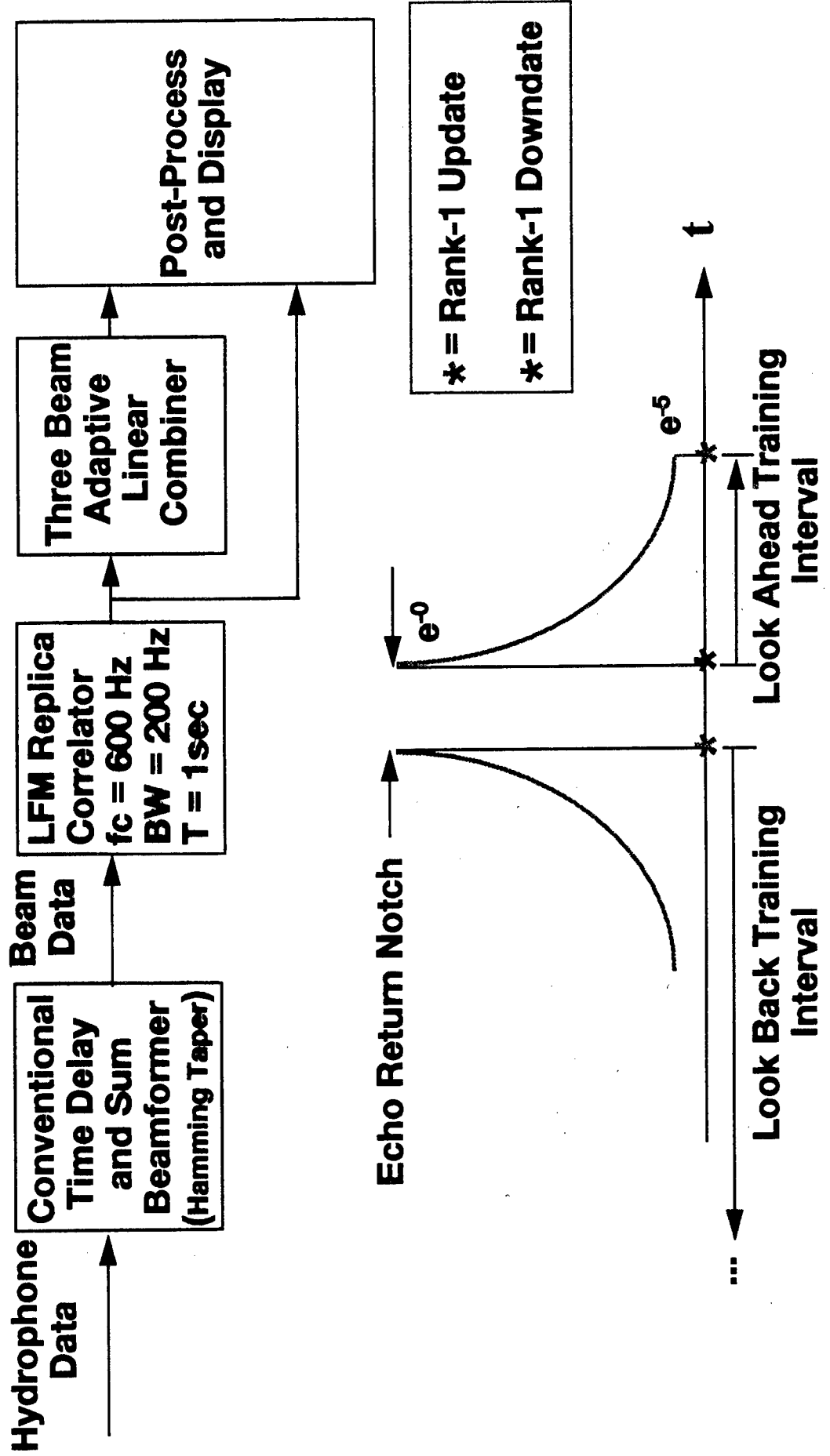
$$\max_{\mathbf{W}} \text{Trace}\{\mathbf{W}^H\mathbf{R}[t]\mathbf{W}\} \quad \text{subject to } \mathbf{W}^H\mathbf{W} = \mathbf{I}_D$$



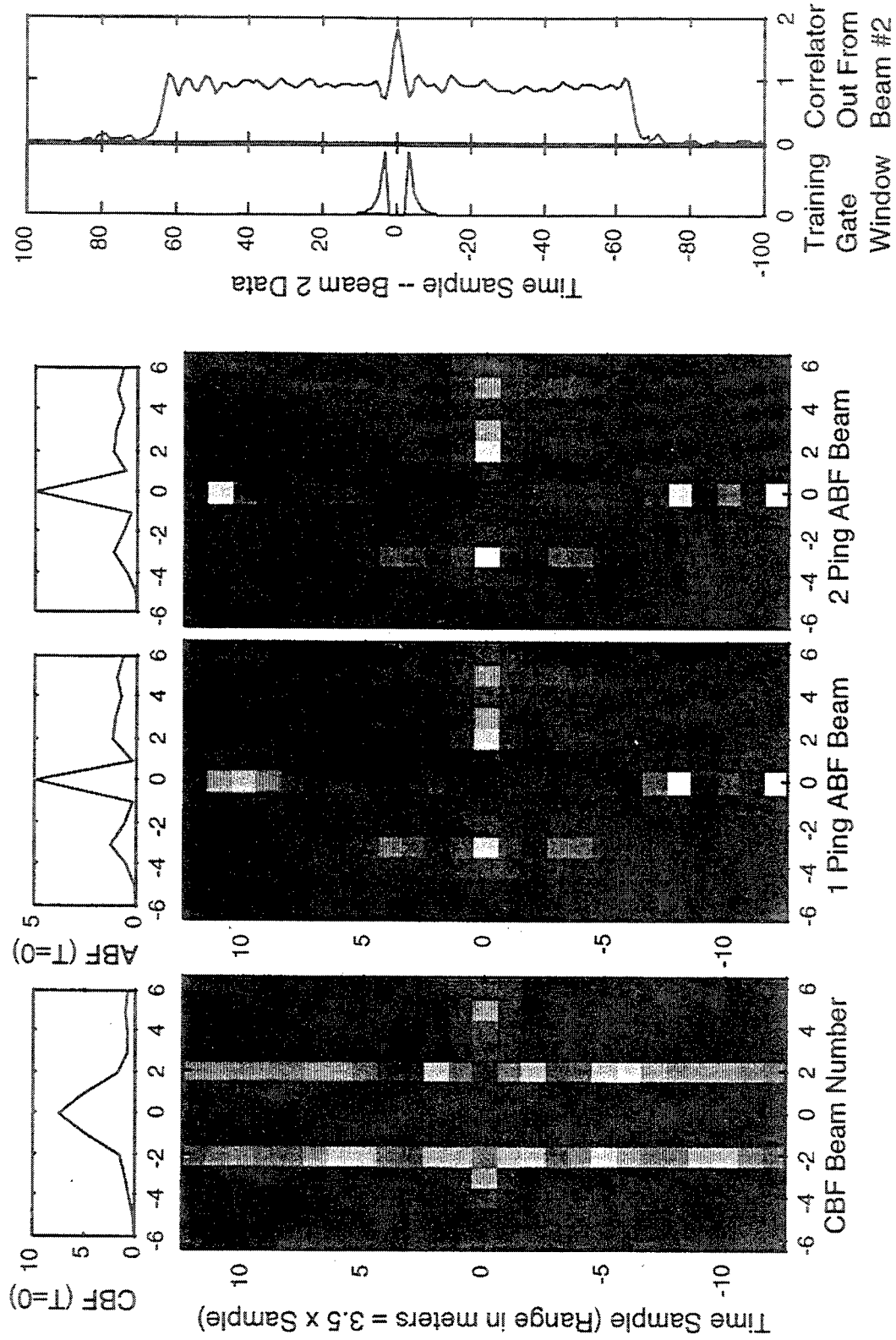
Coherent (multipath) target tracker, MUSIC, ESPRIT, subspace minimum variance distortionless response (MVDR) ABF (dominant mode rejection), subspace soft constrained MVDR ABF.

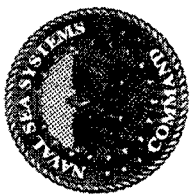
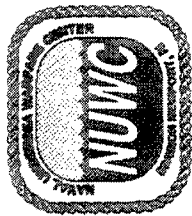


Beam-Space ABF with Exponential Sliding Notched Training

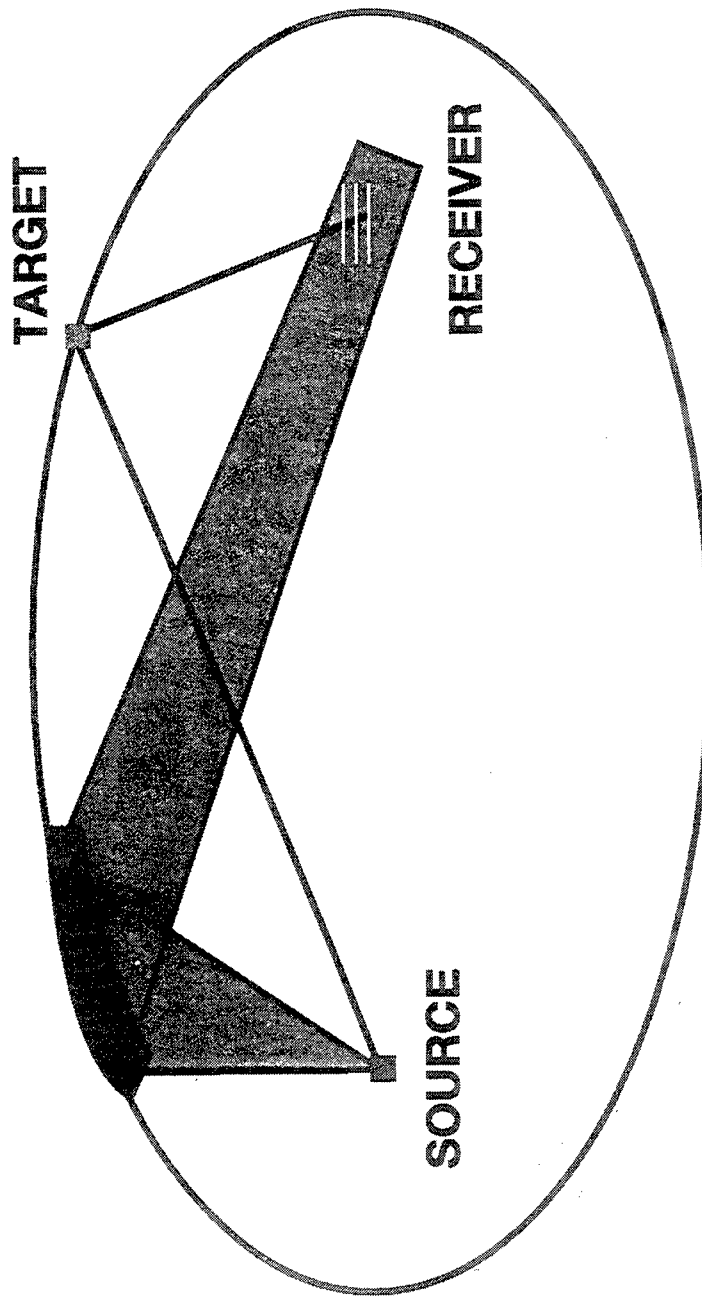


Interference = 4, Targets = [1 1 1], Noise = 1/16





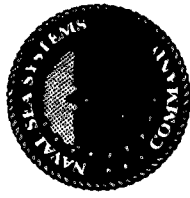
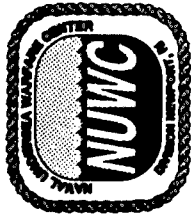
Multistatic Active Sonar CLUTTER





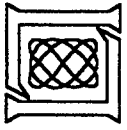
Summary

- **Cross-fertilization in the pursuit of computationally efficient adaptive algorithms has produced similar trends in radar and sonar.**
- **Because of the dramatically quieter threat, active sonar is regaining major importance.**
- **Multistatic active sonar is the major new thrust in active sonar and it does not completely compromise the stealth of the submarine as a receiver.**
- **Radar CPI STAP techniques may be very useful for active Doppler sensitive waveforms and low aspect angle rate targets.**



Some References

- [1] Bryn, F., "Optimum Signal Processing of Three-Dimensional Operating on Gaussian Signals and Noise," Journ. of the Acoust. Soc. of Amer., Vol. 34., No. 3, March 1962, pp. 289-297.
- [2] Ward, J., "Space-Time Adaptive Processing for Airborne Radar," MIT Lincoln Laboratory Technical Report 1015, December 1994.
- [3] Owsley, N., "Signal Subspace Based Minimum Variance Spatial Array Processing," Proceedings of the Twenty-Third Asilomar Conference on Signals, Systems and Computers, 1985, pp. 94-97.
- [4] Owsley, N and Abraham, D., "Beamforming with Dominant Mode Rejection," IEEE Oceans Conference Proceedings, 1990, pp. 470-475.
- [5] Owsley, N. "Enhanced Minimum Variance Beamforming (EMVDR)," in Underwater Acoustic Data Processing, Editor Y. Chan, NATO Advanced Study Institute Series, Kluwer, 1989, pp. 285-293.
- [6] Owsley, N and Abraham, D., "Preprocessing for High Resolution Beamforming," Proceedings of the Twenty-Third Asilomar Conference on Signals, Systems and Computers, October 1989.
- [6] Byerly, K. and Roberts, R., "Output Power Based Partial Adaptive Array Design," Asilomar, 1989.
- [7] Goldstein, J., Reed, I. and Tague, J., "Reduced Complexity, Robust CFAR Detectors for Large Arrays," Asilomar, 1996.

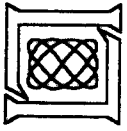


1997 Adaptive Sensor Array Processing Workshop
Sonar and Underwater Acoustics Sessions

Sessions Chairman

Arthur B. Baggeroer

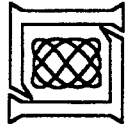
Departments of Ocean and Electrical Engineering
Massachusetts Institute of Technology
Cambridge, MA 02139



SONAR and Adaptive Array Processing

Passive versus Active Sonar

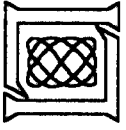
- Historical emphasis on passive
 - Surveillance - SOSUS (bottom mounted), SURTASS (towed array)
 - Submarine ASW - towed, forward spheres and conformal arrays
 - Surface ASW - towed arrays
 - Air ASW - sonobuoy fields
 - Bearing/time and frequency/azimuth processing
- Recent development of active
 - Response to threat quieting and diesel/electrics
 - Reverberation limited environments



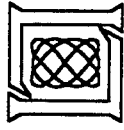
Acoustic propagation and signal gain

- Important environmental phenomena
 - Vertically inhomogeneous medium
 - multipath, multimodal and dispersive
 - long range, deep water and shallow water
 - Bandlimited α (dB/km) = .001 @ 100 Hz, 1 @ 10 kHz
 - reverberant - surface and bottom boundaries
 - random - dynamical sound speed perturbations, boundaries
 - range dependent

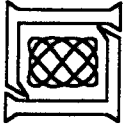
•



- **Receivers**
 - positional uncertainty
 - local multipath
 - precise calibration
 - high v/c

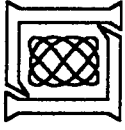


- Replicas for high signal gain beamformers
 - Operational systems
 - narrowband, plane wave models
 - horizontal arrays, limited vertical apertures
 - Multipath/multimode effects for large apertures
 - Coherence vs. propagation effects
 - Replica generation for large vertical apertures
 - Large search space dimensionality
 - Coherent, wideband processing
 - High ν/c limits on coherent pulse processing



Acoustic noise field and array gain

- **Passive environments**
 - Surface sea state - wind and rain
 - Shipping - local and distant (directional)
 - Seismic profiling (directional and high)
 - Biologics
- **Active environments**
 - Doppler spreading by sea surface
 - Range spreading by bottom bathymetric features



- **Self noise**
 - Self noise sources
 - Flow noise on sensor surfaces at high speeds
- **Noise gain limitations**
 - Covariance estimation with large arrays
 - Limited number of DOF's with active systems
 - Limits on narrowband representations

The Determination of Signal Coherence Length Based on Signal Coherence and Gain Measurements in Deep and Shallow Water

William M. Carey

Massachusetts Institute of Technology
77 Massachusetts Avenue, Room 5-211
Cambridge, MA 02139
tel: (617) 253-7639
email: wcarey@mit.edu

Abstract Experimental measurements of signal coherence and array signal gain are reviewed for deep and shallow water sound channels. The signal gain is related to the horizontal coherence length through relationships from the statistical theory of antennas. Signal gain measurements in the transverse direction are proffered as a practical measure of coherence length for both broad-band and narrow-band signals. Using this technique, measurements at frequencies near 400 Hz are presented that show for the deep water cases lengths on the order of 100 wavelengths can be achieved while under downward refraction conditions in shallow water waveguides with sand silt bottoms lengths on the order of 30 wavelengths are realized. The measurement of broad-band and narrow-band coherence functions are discussed with emphasis on the role of partly-coherent noise backgrounds, multipath interference effects, and averaging constraints. These results are interpreted with coherence models consistent with sound scattering from the volume and boundaries of the waveguide.

**The determination of signal coherence length
based on signal coherence and gain
measurements in deep and shallow water**

WILLIAM M. CAREY (MIT / DARPA)

Adaptive Sensor Array Processing Workshop

March 1997

The Sonar Equation:

- $SE = (SL - TL + ASG) - (NL + ANG) - DT$

Where the primary measures are ASG and ANG.

The ASG depends on signal coherence and ANG depends on the character of the noise field

- For a specific system of N elements

$$SE = (SL - TL) - (ASGT - ASGM) -$$

$$(NL + ANG - ASGT) - DT$$

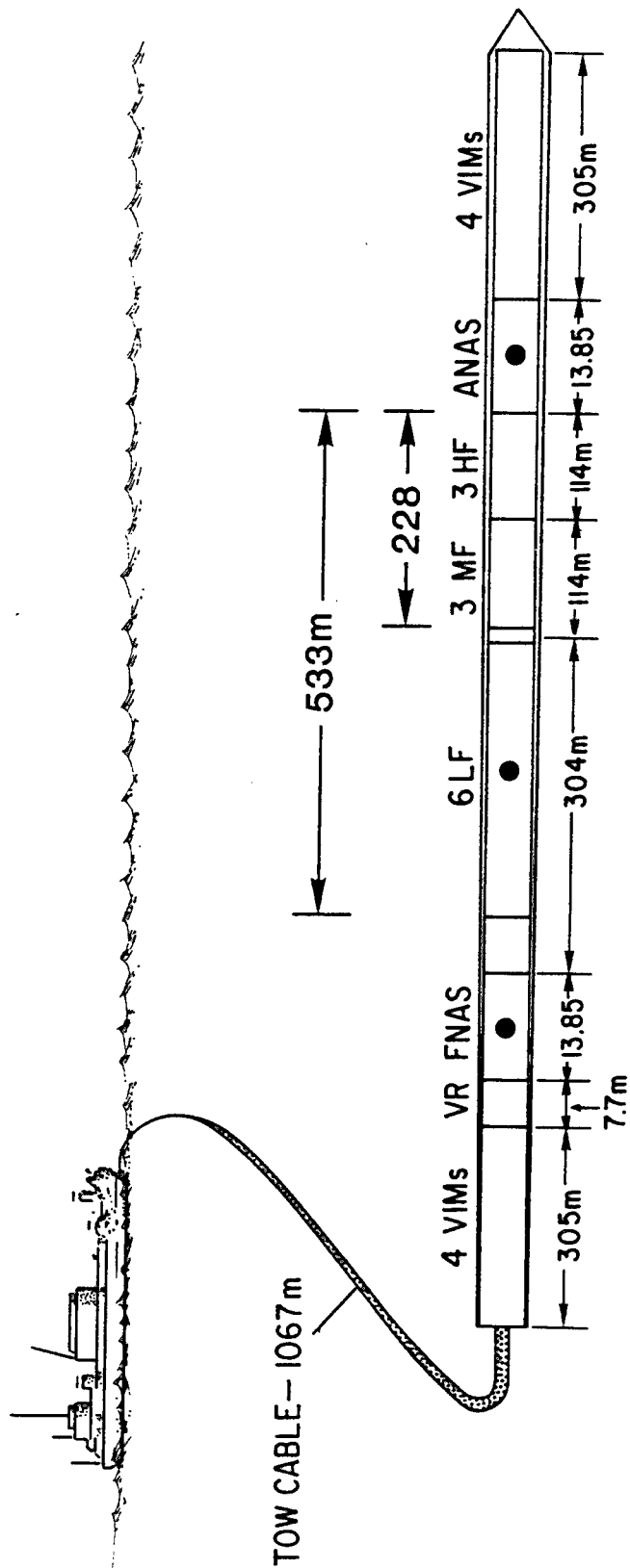
$$= RSL - ASGD - BNL - DT$$

Each term, (RSL, ASGD, BNL), are measurable quantities.

Summary of Array Investigations

For frequencies between 50 Hz and 1kHz:

- * ASGD (array signal gain degradation) is due to
 - # Multipath, shape and motion,
 - # Scattering.
- * BNLs (beam noise levels) are due to
 - # Tow Ship-directed and reflected,
 - # Dynamic distant shipping, resolved.
 - # Background noise - incoherent
- * AG may be greater than $10 \log(2L/\lambda)$.
- * Horiz. Coherence Lengths- 100λ DW and 30λ SW



LEGEND

VIM: VIBRATION SOLUTION MODULE
 VR: VOLTAGE REGULATOR
 FNAS: FORE NON-ACOUSTIC SENSORS
 ANAS: AFT NON-ACOUSTIC SENSORS
 LFM: LOW FREQUENCY MODULE
 MFM: MID FREQUENCY MODULE
 HFM: HIGH FREQUENCY MODULE

NOTE: ARRAY DIAMETER IS 8.9 CM.
 VIM DIAMETER IS 7.6

NESTED SUB ARRAY APERTURES

SUB-ARRAY	HF	MF	LF
NUMBER OF GROUPS	54	54	42
LENGTH OF ARRAY	114M	228M	533M
HALF WAVELENGTH FREQUENCY WITH C = 1467.6 m/sec	348 Hz	174 Hz	58Hz
GROUP SPACING	2.11M	4.22M	12.65M

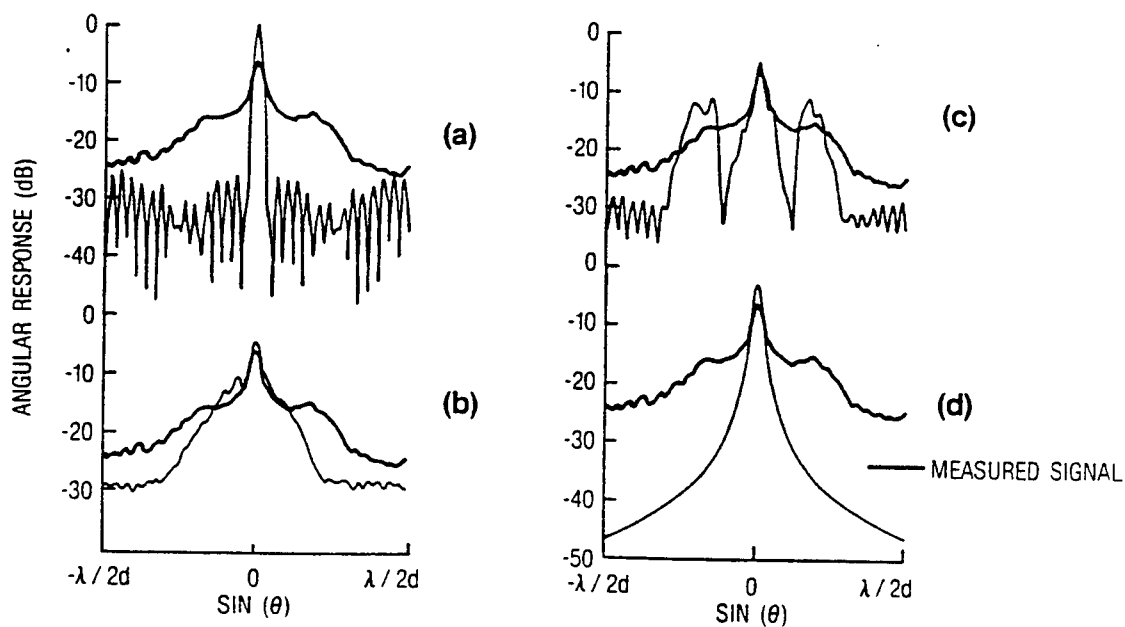


Figure The average-measured beam response (dB) versus $\sin\theta$ compared to computed beam response for (a) the case of an ideal array, (b) the case of a deformed array, (c) multipath interference, and (d) azimuthal scattering.

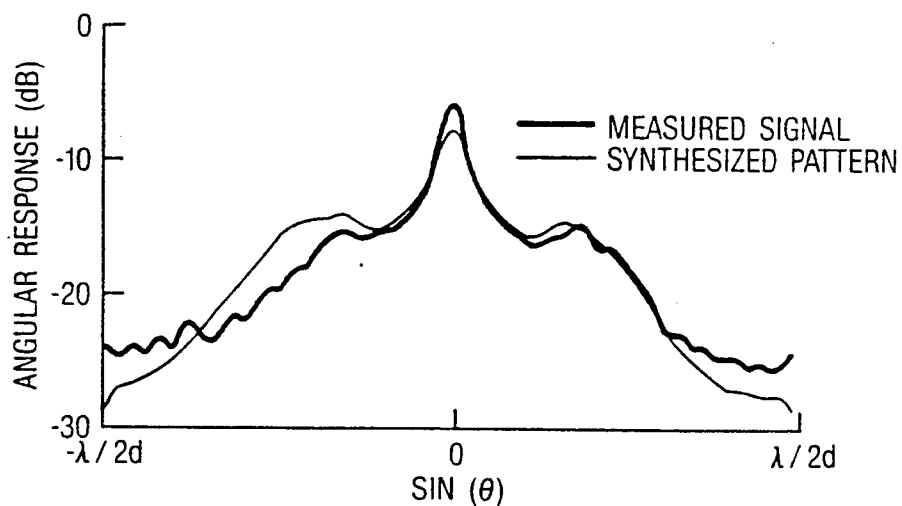
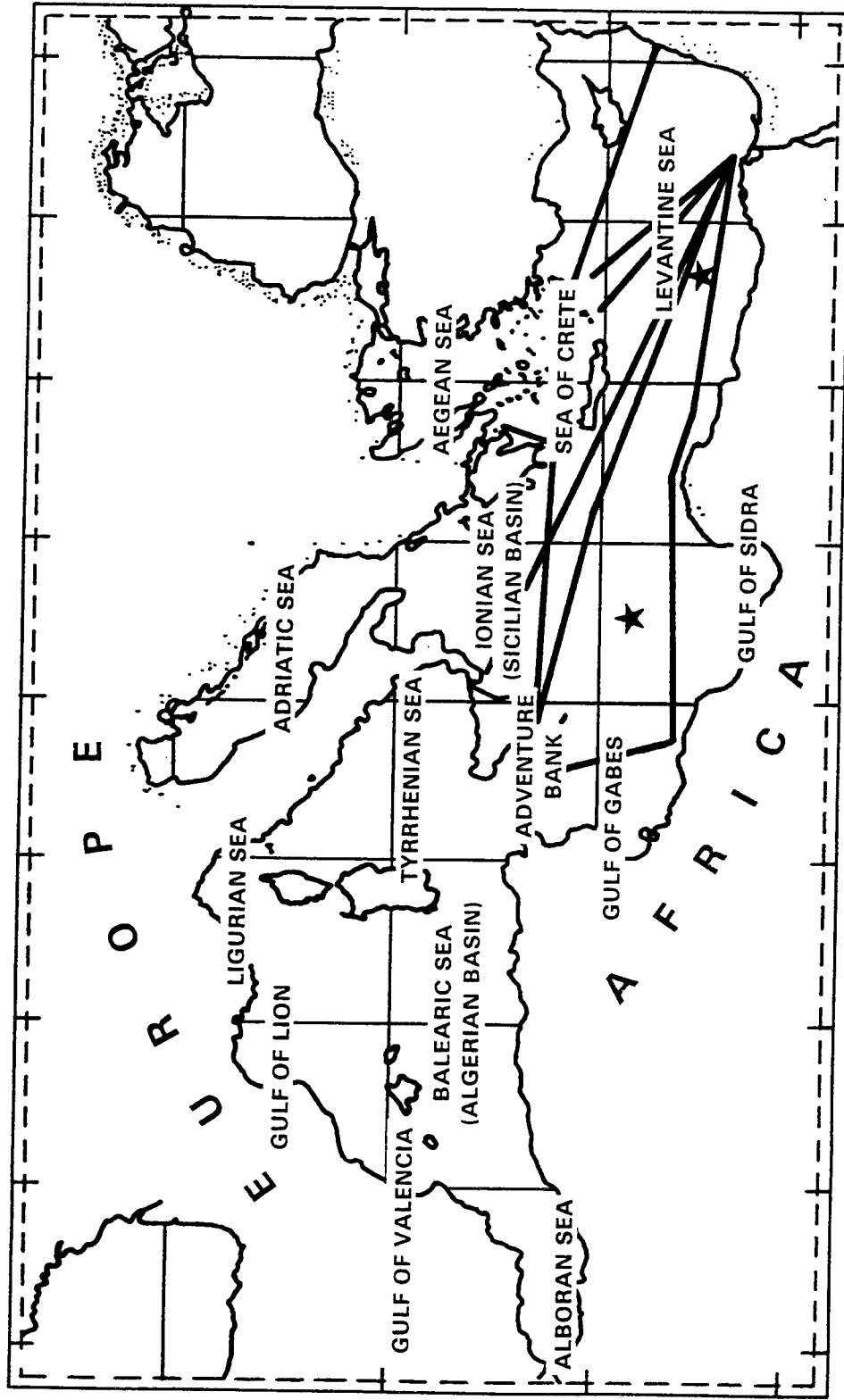
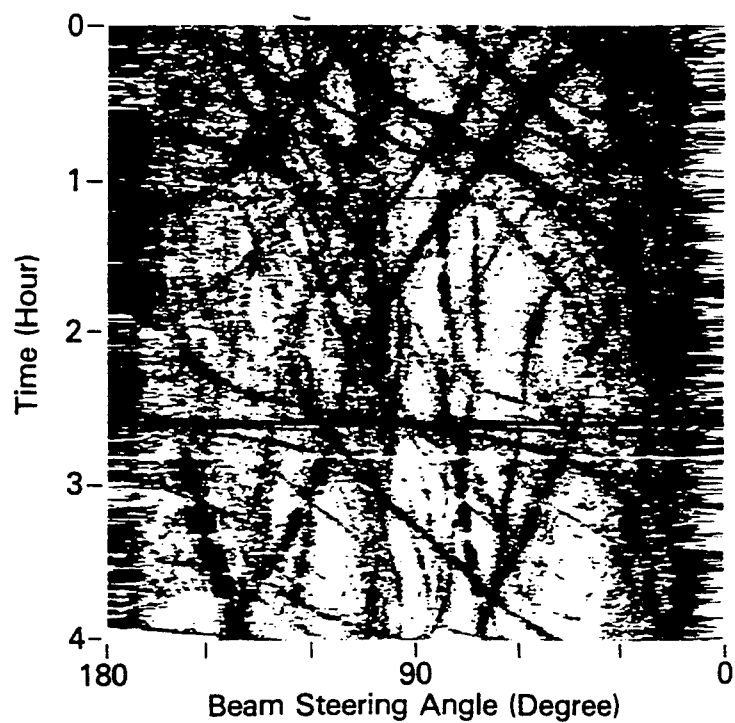


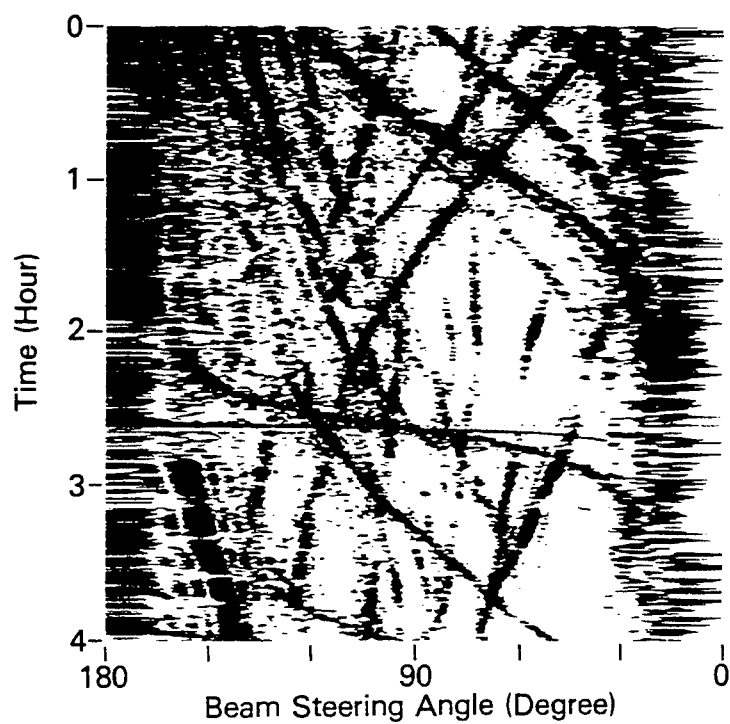
Figure Comparison of measured and calculated beam angular response versus $\sin\theta$ between $\pm\lambda/2d$

DEPLOYMENT SITES OF HIGH RESOLUTION ARRAYS





a. 110 Wavelengths, 105 Hydrophones



b. 24 Wavelengths, 54 Hydrophones

(UNCLASSIFIED)

(U) Figure 4. Beam Noise from Two Different Array Apertures

The Statistical Approach:

$$f_{lp}(k \sin \theta) = \int_{-l/2}^{l/2} P(y) \exp(ik \sin \theta) dy$$

Let $\psi = \pi l \sin \theta / \lambda$ and $x = 2y / l$

$$f(\psi) = \int_{-1}^1 P(x) \exp(i\psi x) dx \quad \text{where } P(x) = P_o \exp(i\phi(x))$$

$$\text{and } \langle \phi(x) \rangle = 0 ; \langle \phi(x)^2 \rangle = \sigma^2 = \alpha$$

$$R_\phi = \langle \phi_1 \phi_2^* \rangle / \sigma_1 \sigma_2 = \exp(-(x_1 - x_2)^2 / C)$$

$$C = 2\alpha / l$$

$$\langle f(\psi) \rangle = P_o \exp(-\sigma^2 / 2) \sin \psi / \psi$$

$$\begin{aligned} \langle |f(\psi)|^2 \rangle &= \iint P_o^2 \langle \exp(i(\phi_1 - \phi_2)) \rangle \exp(i\psi(x_1 - x_2)) dx_1 dx_2 \\ &= \iint P_o^2 \exp(\alpha R_\phi - \alpha + i\psi(x_1 - x_2)) dx_1 dx_2 \end{aligned}$$

Approach continued

$$\langle |f(\psi)|^2 \rangle = \iint P_o^2 \exp(\alpha R_\phi - \alpha + i\psi(x_1 - x_2)) dx_1 dx_2$$

When $R_\phi = \exp(-(x_1 - x_2)^2 / C^2) \equiv 1 - |x_1 - x_2|^2 / C^2$

$$\langle |f(\psi)|^2 \rangle = \iint P_o^2 \exp(-|x_1 - x_2|^2 / C^2 / \alpha) \exp(i\psi(x_1 - x_2)) dx_1 dx_2$$

recognize $P_o^2 \exp(-|x_1 - x_2|^2 / C^2 / \alpha) = P_o^2 \exp(-|x_1 - x_2|^2 / L_h^2)$
as the quadratic (Gaussian) coherence function.

THE EXPECTATION VALUE OF THE MAGNITUDE SQUARED RESPONSE FUNCTION:

$$\langle f_{lp}(k \sin \theta) \cdot f_{ij}^*(k \sin \theta) \rangle = \int_{-L/2}^{+L/2} P_p \cdot P_j^* \exp\left(-\left[(x_p - x_j) / L_h\right]^2\right) \cdot \exp(ik \sin \theta (x_p - x_j)) dx_p dx_j$$

This expression may be written in matrix notation:

$$P(k \sin \theta, \omega) = \langle f_{lp}(k \sin \theta) \cdot f_{ij}^*(k \sin \theta) \rangle \\ = C^T \cdot R_{CPS} \cdot C$$

$$\text{WHERE } R_{CPS} = \left\| P_p \cdot P_j^* \exp\left(-\left[(x_p - x_j) / L_h\right]^2\right) \right\| \cdot$$

Volume scattering relations

The Beran-McCoy-Adams Formulation:

Transverse Coherence Function is

$$\begin{aligned}\Gamma(\Delta y) &= R_p(R, f, \Delta y, z) / I(z) = \exp\left(-(\Delta y / L_{hc})^{3/2}\right) \\ &= \exp\left(-E_f f^{5/2} R(\Delta y)^{3/2}\right) = \exp\left(-E_k k^{5/2} R(\Delta y)^{3/2}\right)\end{aligned}$$

where $E_f = 1.136 \cdot 10^{-6} E_k = 1.136 \cdot 10^{-6} (\varepsilon \cdot 10^{-10})$
and $L_{hc}^{-1} = f^{5/2} (E_f R)^{2/3}$.

The Flatte-Dashen Formulation:

$$\Gamma(\Delta y) = R_p(R, f, \Delta y, z) / I(z) = \exp\left(-D_{1,2} / 2\right) = \exp\left(-(\Phi \Delta y / L_{hc} \sqrt{2})^2\right)$$

Generally we write: $\Gamma(\Delta y) = \exp\left(-(\Delta y / L_{hc})^n\right)$.

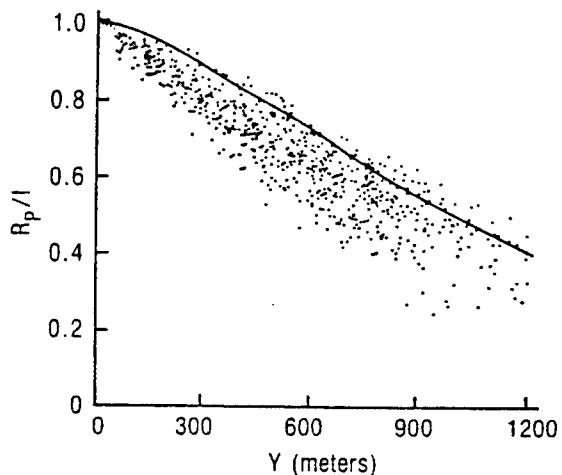


Figure Acoustic correlation versus transverse receiver separation: experiment three; range, 137 km; frequency, 400 Hz; curve represents theory.

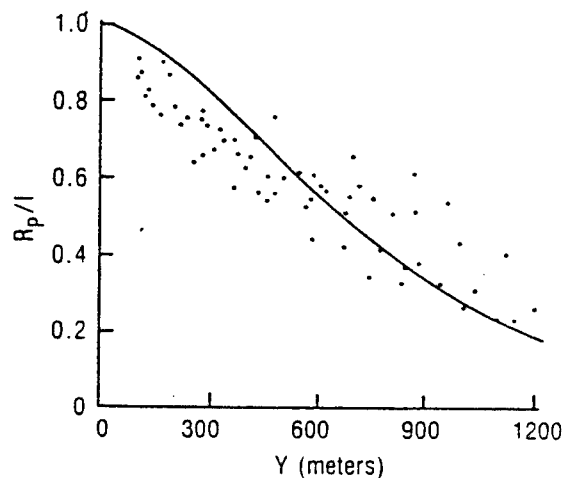


Figure Acoustic correlation versus transverse receiver separation: experiment one; 259 km; frequency, 400 Hz; curve represents theory.

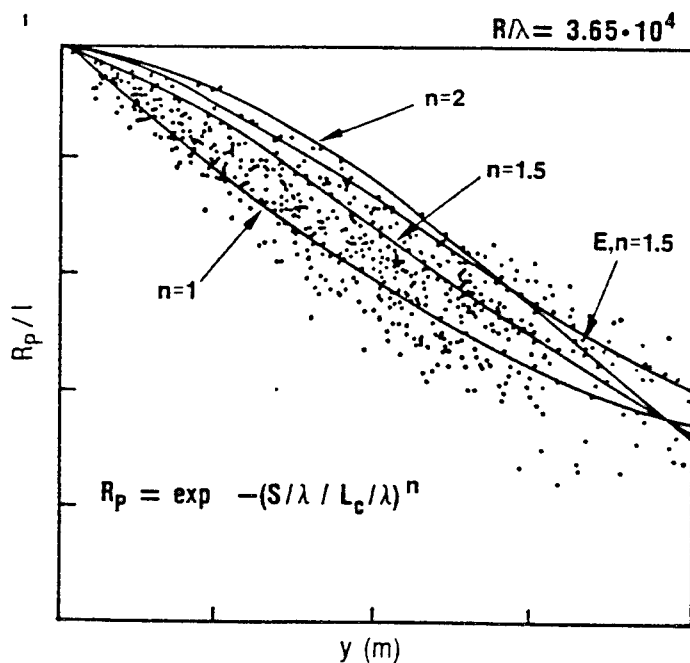
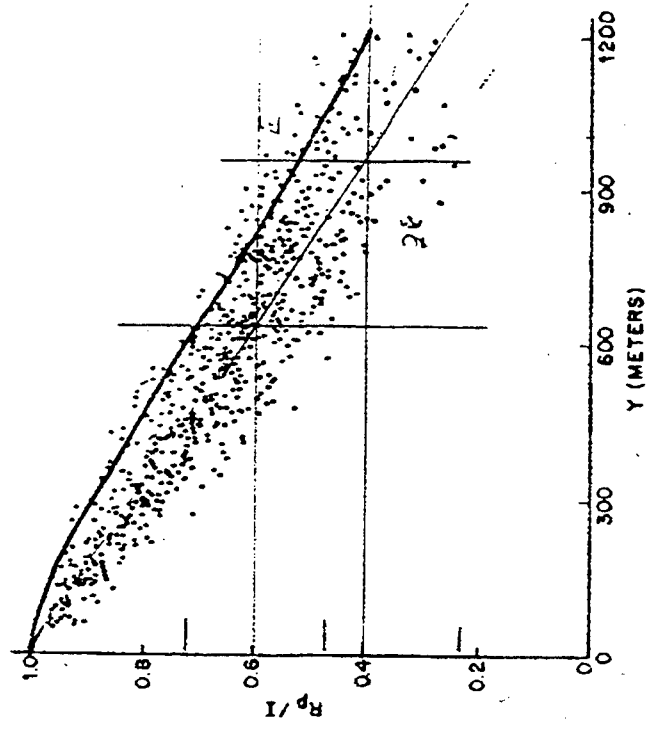
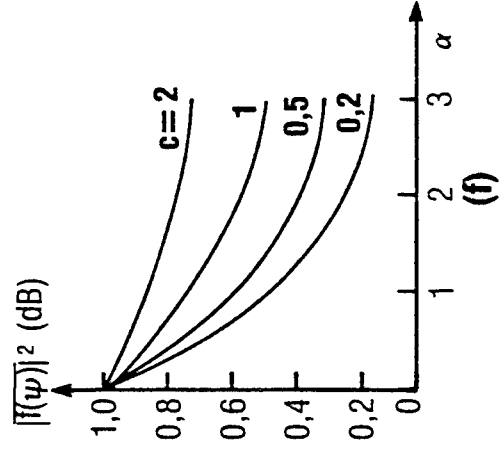
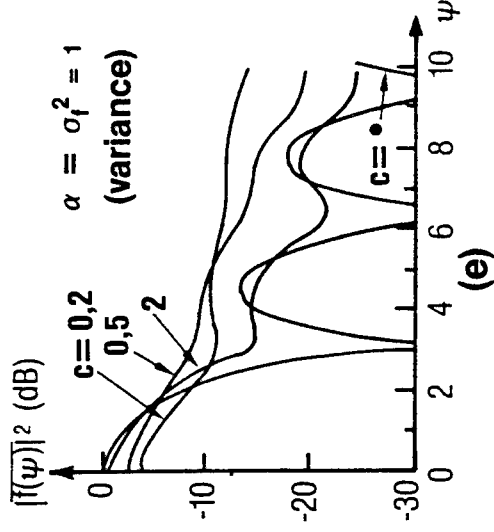
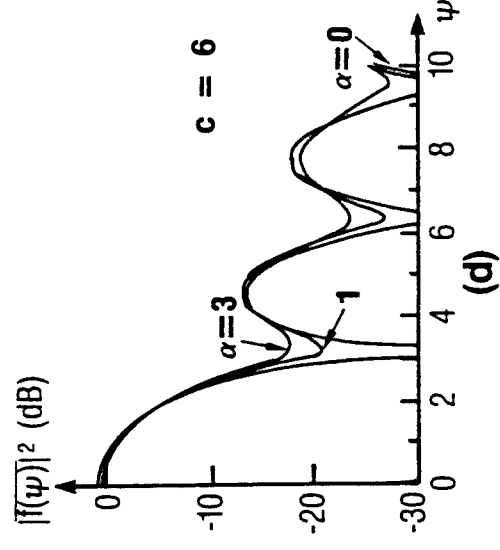
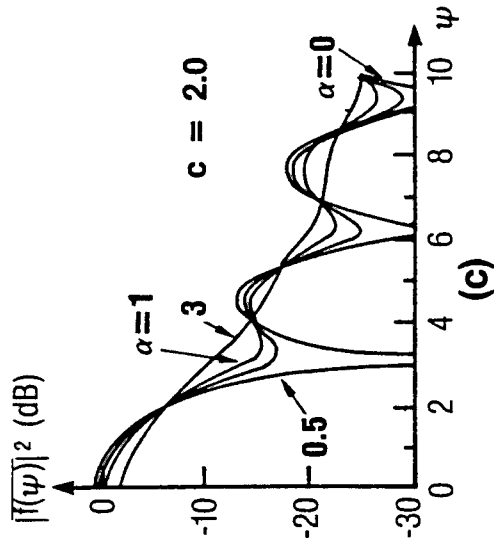
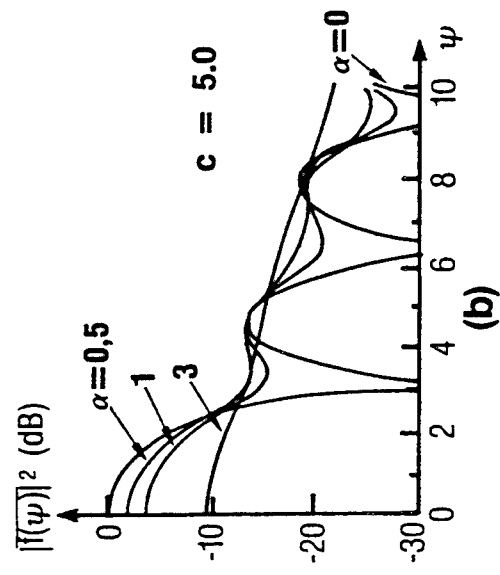
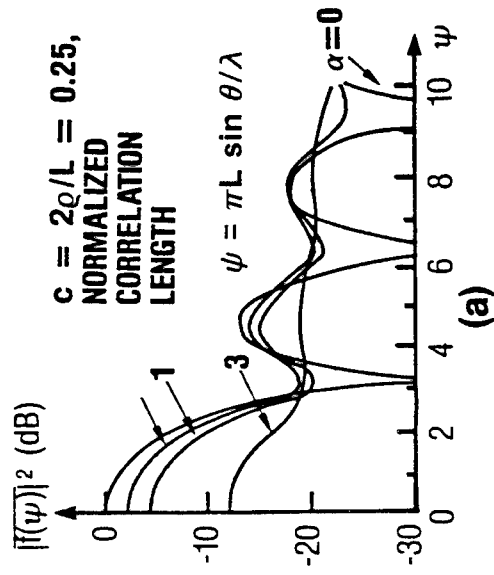


Figure A comparison of $\exp(-(y/L_c)^n)$ with acoustic correlation versus transverse separation at 400 Hz.

Coherence length estimates at 400 Hz.



R(km)	L_h	L_h / λ	$E_{fm} \times 10^{+17}$
137	1143	306	5.9
139	1677	450	3.4
259	1067	286	3.5
268	1067	286	--
507	381	102	8.2
963	350	94	4.96



MATCH THE ENVIRONMENTAL ANGLE SPREAD TO THE BEAMWIDTH OF THE HALF POWER POINTS!

$$S(k \sin \theta) = \int_{-\infty}^{\infty} \exp(-(y / L_h)^n) \exp(ik \sin \theta) dy$$

where $\exp(-(y / L_h)^n)$ is the coherence function.

	$n = 1$	$n = 1.5$	$n = 2$	$\Delta \theta_{hp}$
$BW(\text{radian})$	0.318 λ / L	0.457	0.530	$0.886 \lambda / L$
$BW(\text{degrees})$	18.2°	26.2°	30.36°	$50.76^\circ \lambda / L$
L_a / L_h	2.72	1.89	1.64	

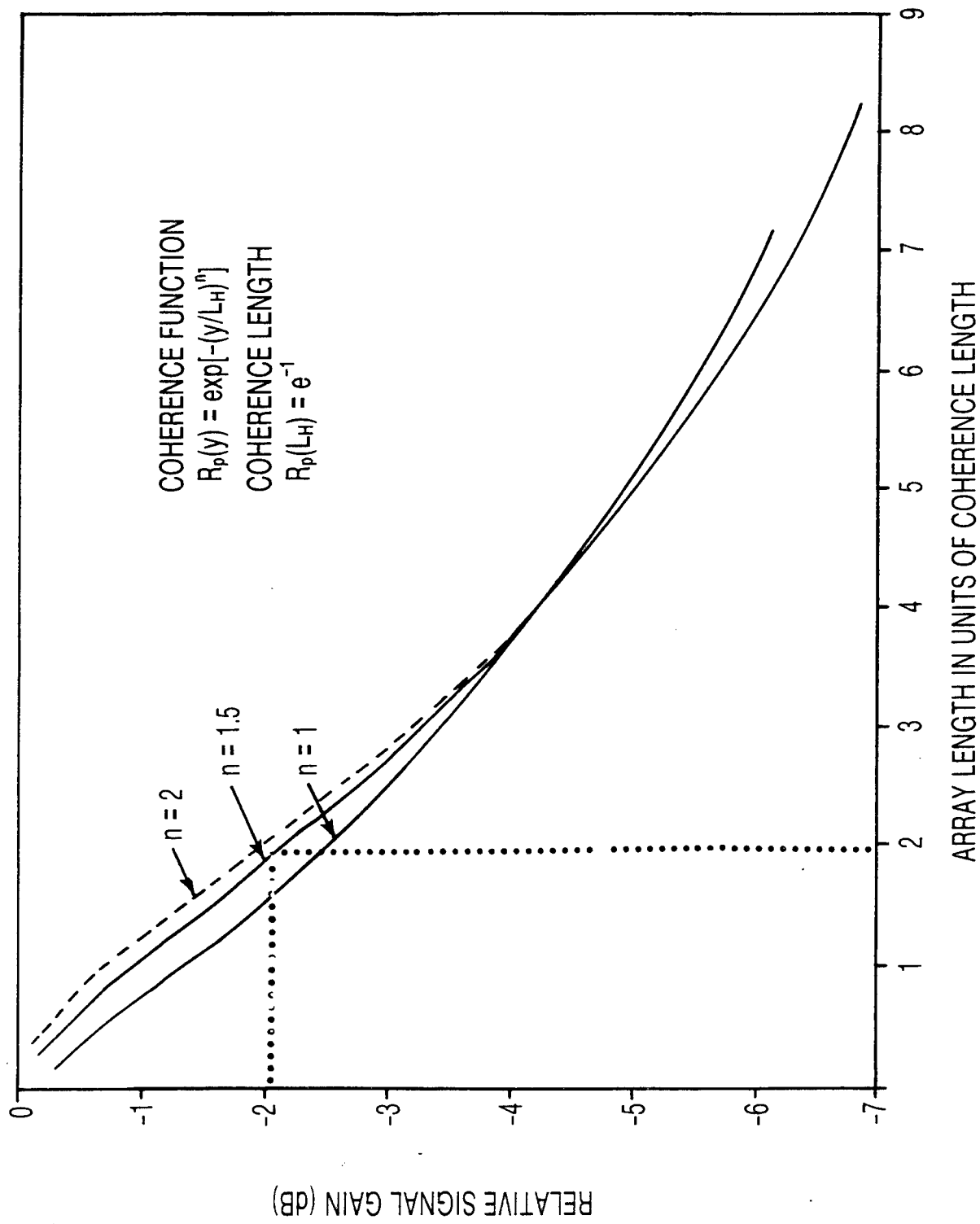
The relative signal gain is:

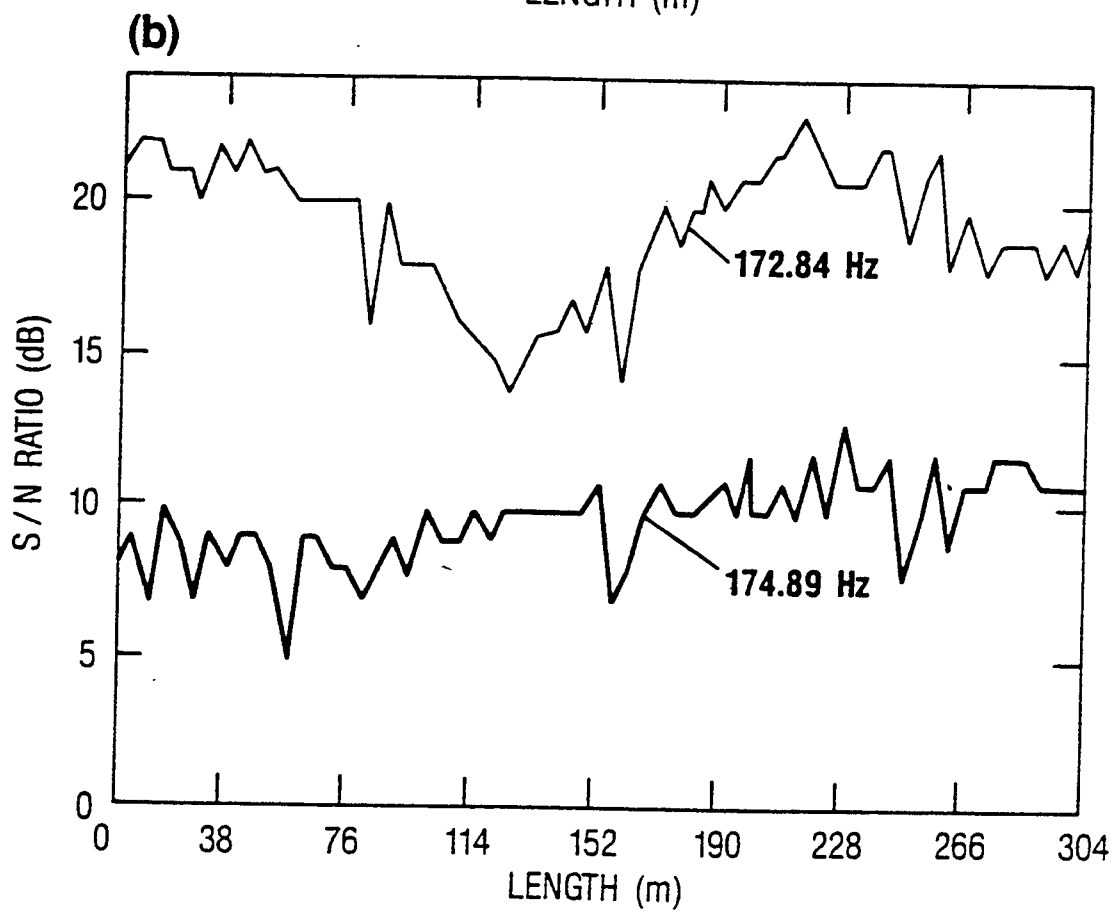
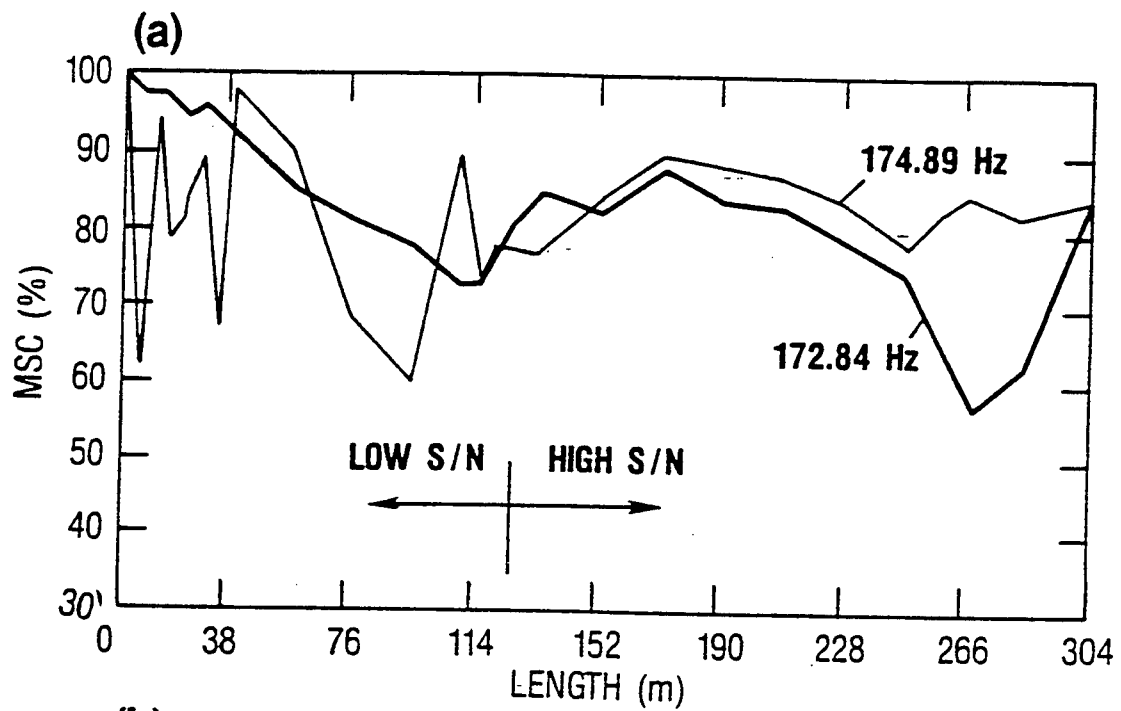
$$RSG = (L_a / L_h)^2 \cdot \int_{-L_a/L_h}^{+L_a/L_h} (L_a / L_h - |x|) \exp(x^n) dx$$

Thus the gain of the array is related to the coherence length — provided we have a criterion and a coherence functional form!

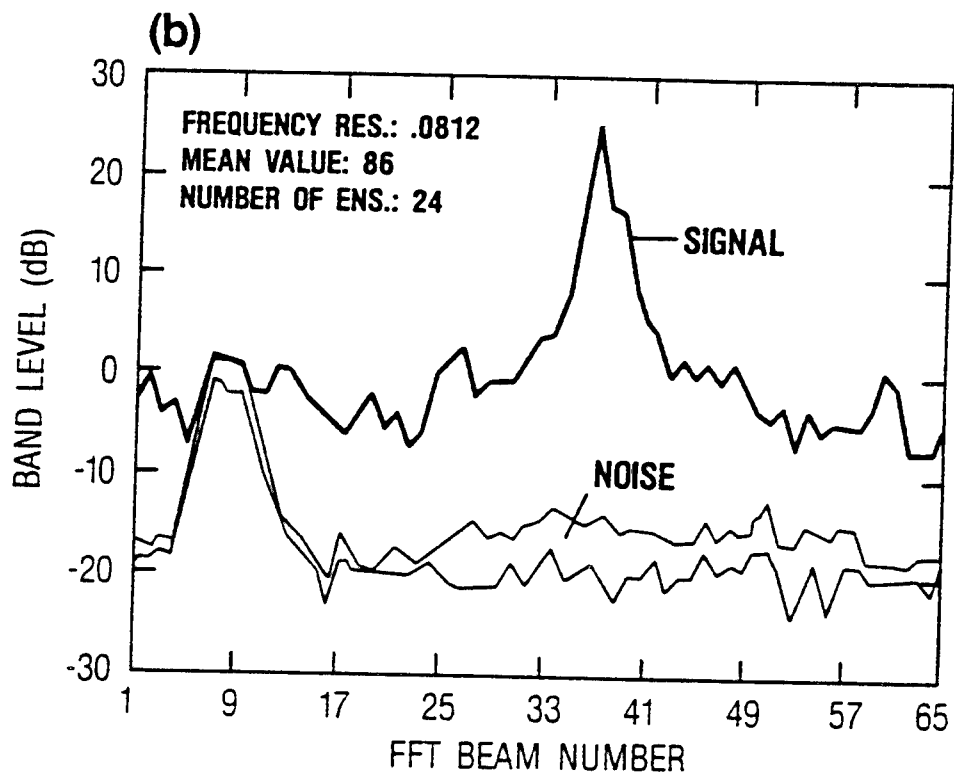
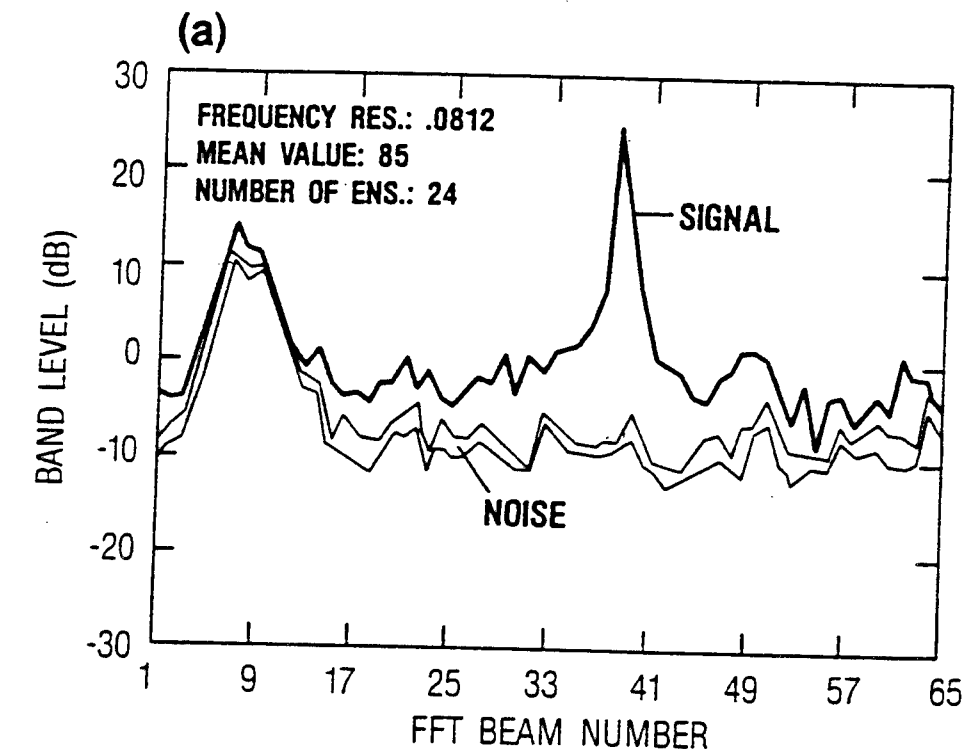
THE RELATIVE SIGNAL GAIN

$$rsg \approx (L_h / L_a - |y|) \int_{-L_h/L_a}^{L_h/L_a} (L_h / L_a - |y|''') dy \quad RSG = 10 \log(rsg)$$





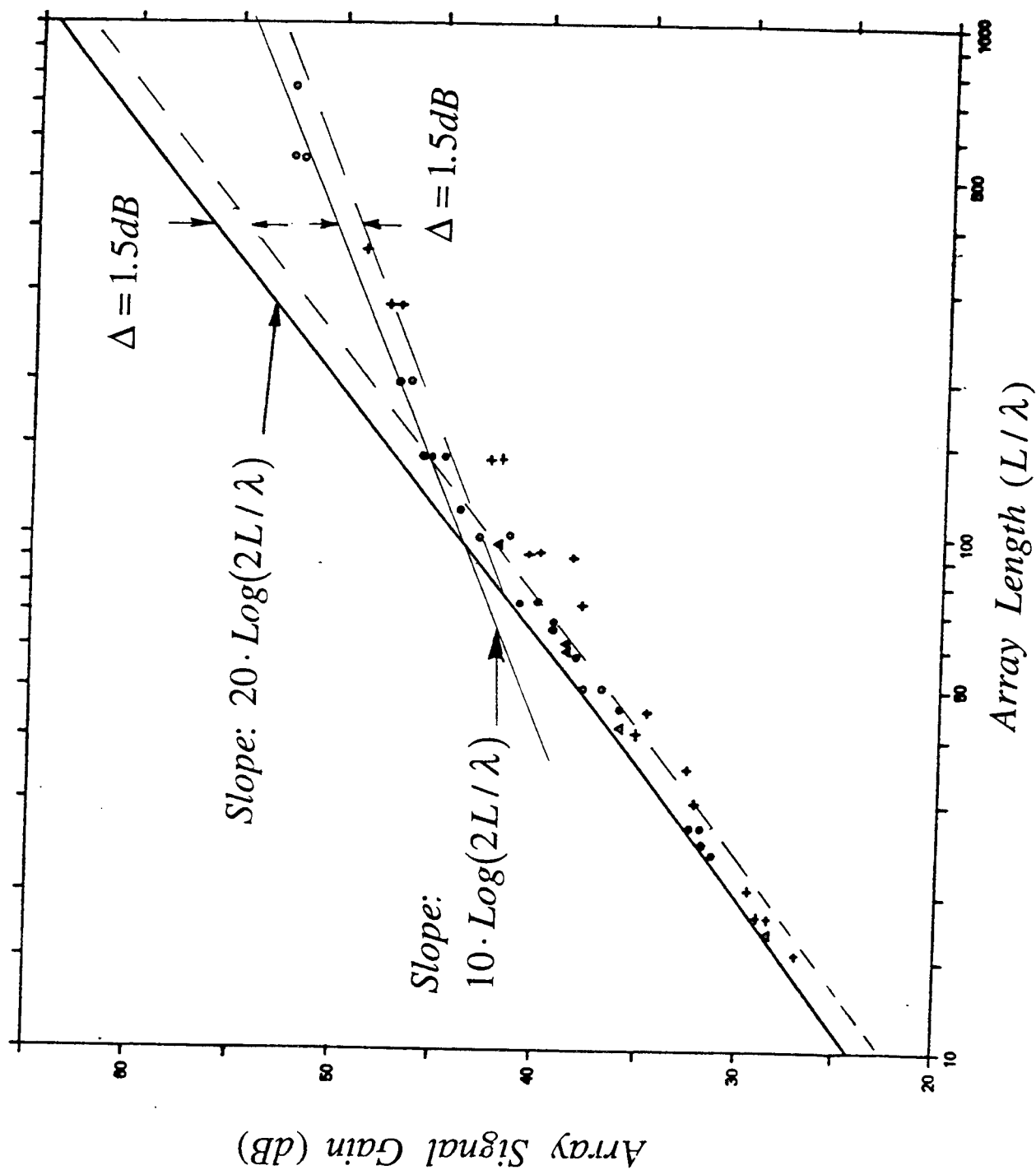
Steered Beam Response Measurement



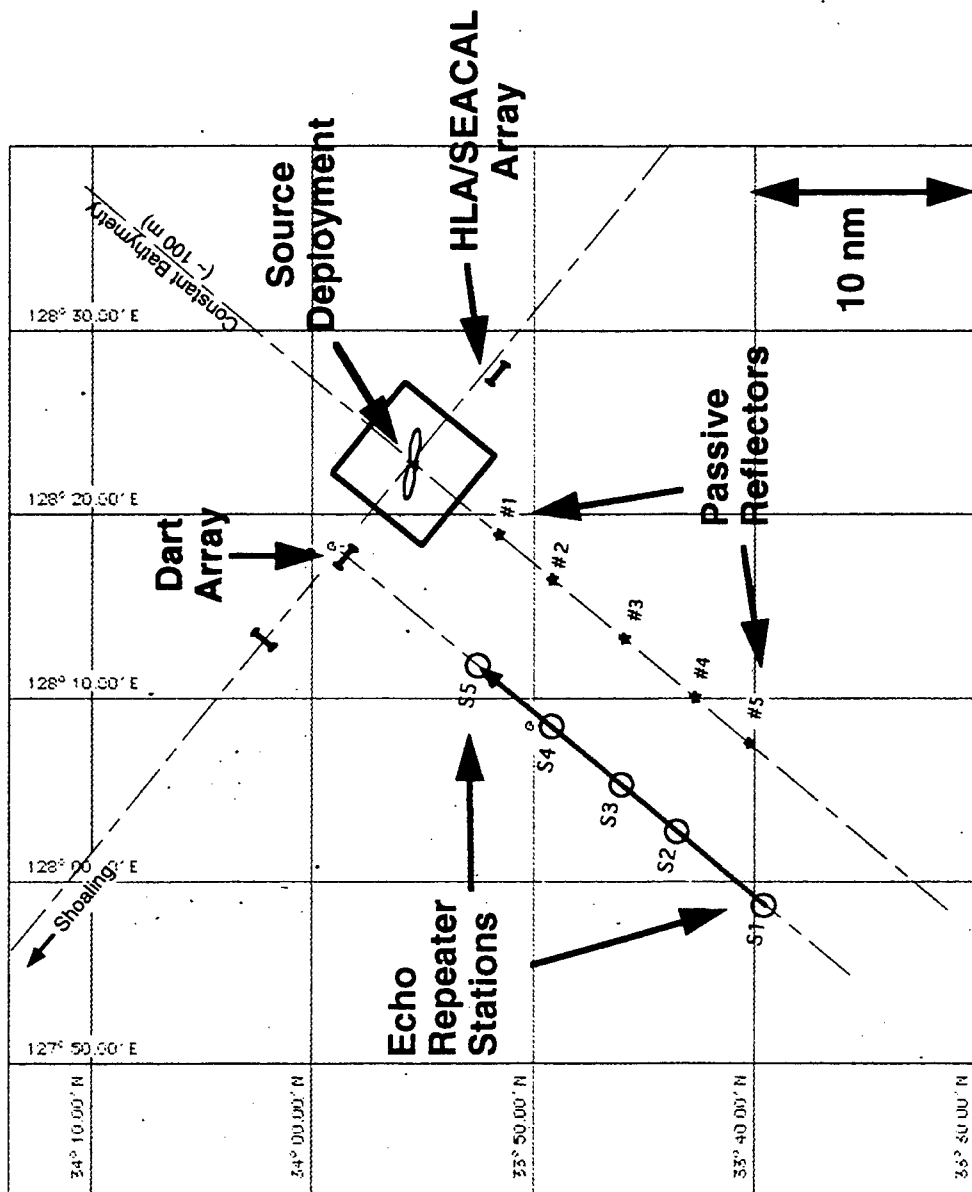
Measurements with Arrays

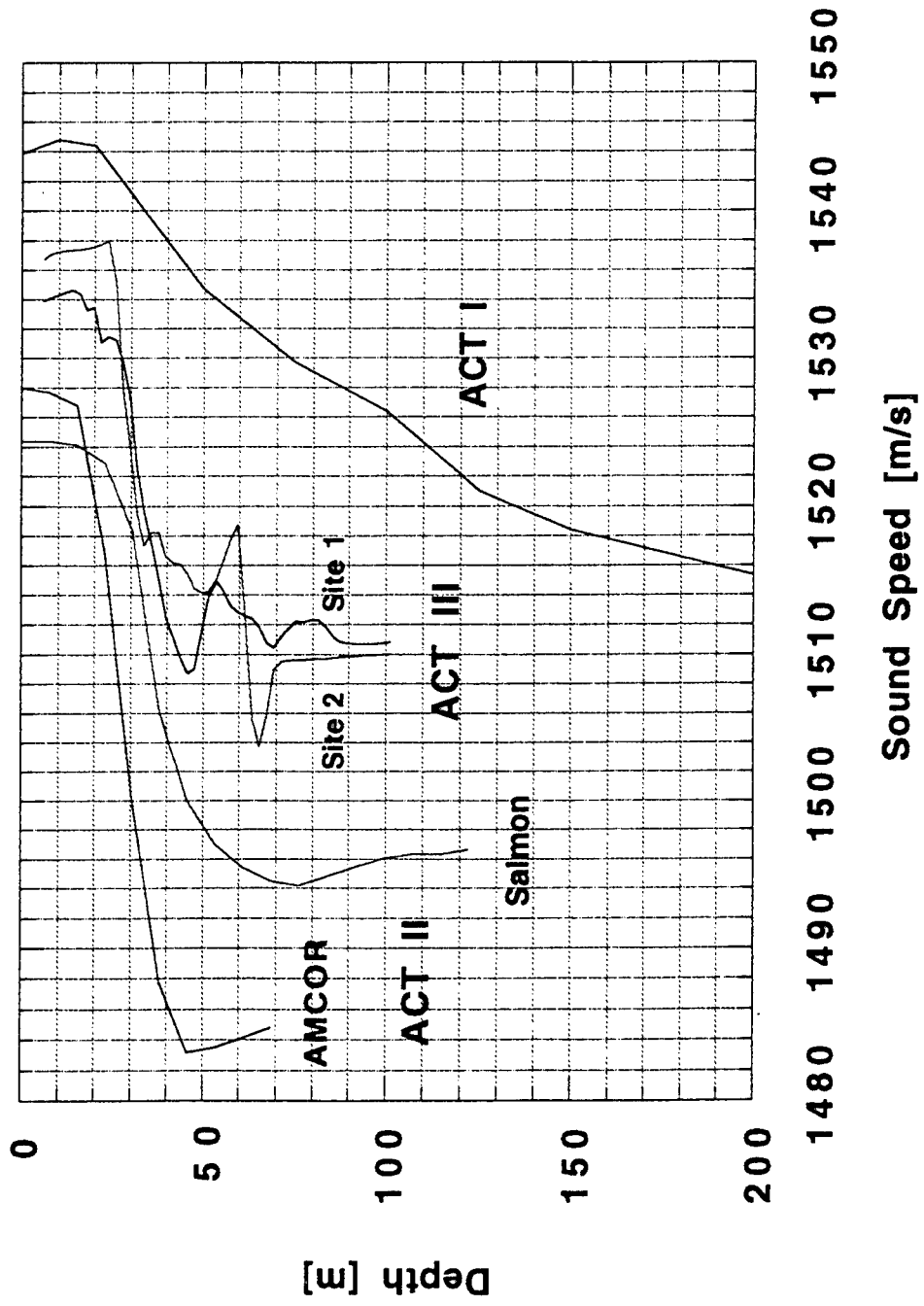
Array Estimates of L_h / λ

Basin	frequency, f	range, r	L_a / λ	ASGD	L_h / λ
Ionian	337	≤ 300 km	143	1.5	95
N.W. Atl.	337	582 km	143	1.12	127
N.W. Atl	337	≤ 600 km	143	2.0-2.4	72-60
Levantine	323	≤ 800 km	112	1.2	96



Straits of Korea **Run A- SE-1 (Approximate geometry)**





ACT III Site 1A

111 Hz, ch (6-32), Aperture length= 140.35 m (10.3 wavelengths), broadside

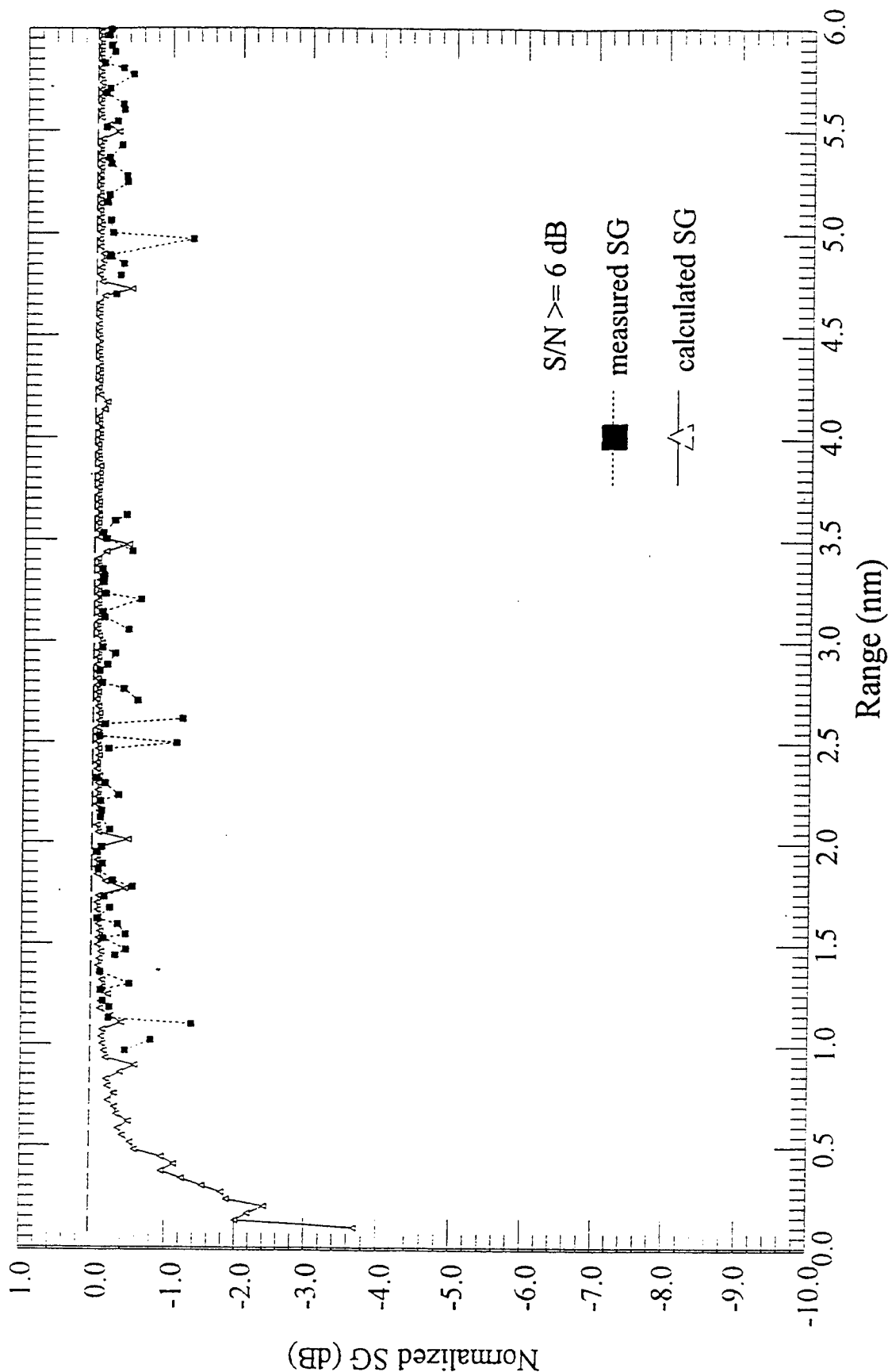


FIGURE 3-2. ACT III SITE 1A BROADSIDE LEG CALCULATED AND MEASURED SIGNAL GAIN VS. RANGE 111 Hz., DART I, CH 6-32, APERTURE LENGTH = 140.35 m (10.3 WAVELENGTHS)

ACT III Site 1A

Calculated and Measured Signal Gain vs. Range
 354 Hz, ch (6-32), Aperture length= 140.35 m (32.9 wavelengths), broadside

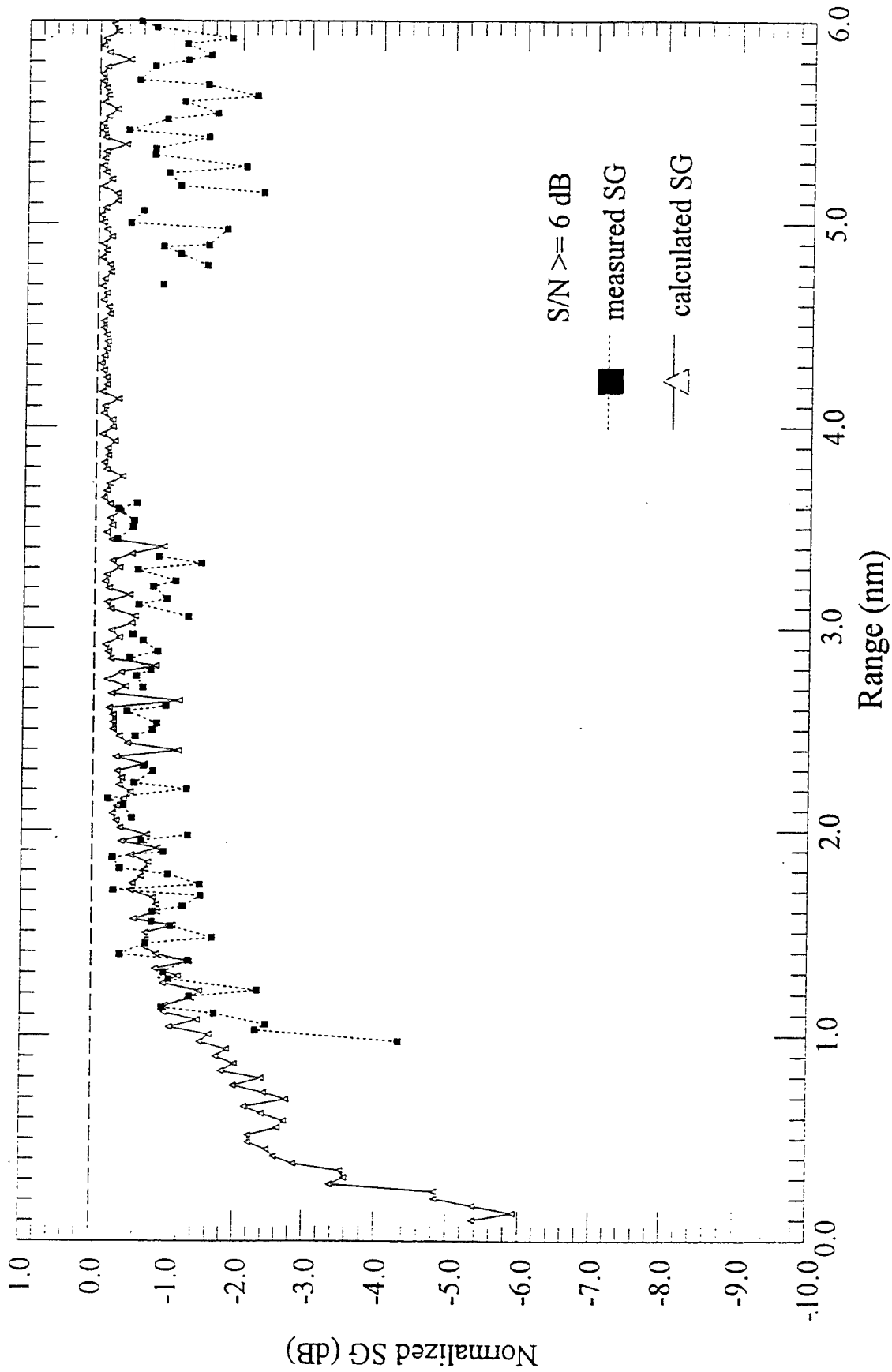


FIGURE 3-3. ACT III SITE 1A BROADSIDE LEG CALCULATED AND MEASURED SIGNAL GAIN VS. RANGE 354 Hz., DART I,
 CH 6-32, APERTURE LENGTH = 140.35 M (32.9 WAVELENGTHS)

ACT III Site 1A

Calculated and Measured Signal Gain vs. Range

604 Hz, ch (6-32), Aperture length= 140.35 m (56.1 wavelengths), broadband

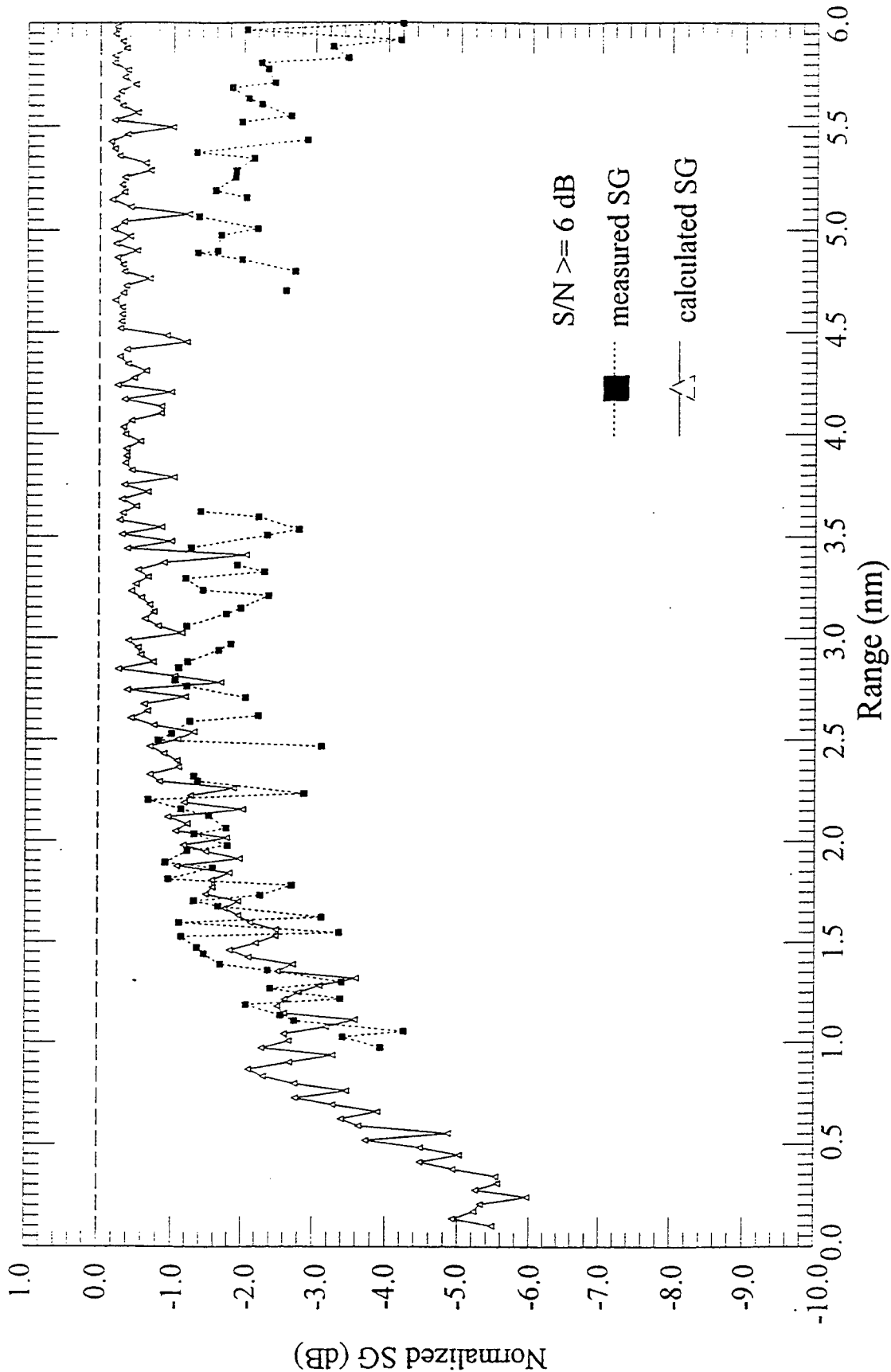


FIGURE 3-4. ACT III SITE 1A BROADSIDE LEG CALCULATED AND MEASURED SIGNAL GAIN VS. RANGE 604 HZ., DART I, CH 6-32, APERTURE LENGTH = 140.35 m (56.1 WAVELENGTHS)

Table 5, Shallow water coherence length results.

Ref.	[14]	[15]	[16]	[17]	[17]	[17]	[17]
Location	N. Sea	N.W. Atl.	GOMWFE	GOMFS	NWA/IS	SOK	[17]
SVP	ISV	DR	DR	DR	DR	DR	SOK
WD	65m	.1-1 km	.1-1km	200m	100m	100m	DR
Bottom	S	S-SC	S-SC	S-SC	S-SC	S-SC	100m
f ₁ (Hz)	400	135	173-175	200-400	200-400	354	S-SC
f ₂	800			400-800	400-600	600	300
f ₃	1.6 kHz				600-800		500
Range	7.4 km	100 km	25 km	9.3 km	4-22 km	7-11 km	700
(L_c / λ) ₁	18	31	21	30	23	35	5-45 km
(L_c / λ) ₂	10			32	25	35	29
(L_c / λ) ₃	6				21		31
Source	Exp.	CW	CW	Exp.	Exp.	CW	31
SD	21m	18m	100m	100m	52m	46m	Exp.
RD	15m	750m	400m	200m	100m	100m	52m
COV	8%	4%	6%	4%	4%	4%	100m
L _h -COV	40%	300%	67%			41%	5%
							230%

SVP=Sound Velocity Profile; ISV= Isovelocity; Downward Refracting; WD= Water Depth;
S= Sand; S-SC= Silty- Clay; SD=Source Depth; RD= Receiver Depth. COV=coef
ficient of variation in measured results.

Summary and Conclusions

Coherence lengths can be estimated by the mutual coherence function or array signal gain.

Array signal gain is primarily degraded by motional effects; but when these are controlled coherence lengths can be estimated.

Deep water coherence lengths in the absence of surface interactions are on the order of 100 wavelengths near 400 Hz..

Shallow water coherence lengths under downward refraction are on the order of 30 wavelengths near 400 Hz.

Measurements in shallow water can be made under known conditions to isolate dominate mechanisms.

POSTER SESSION I

Reduced Wavenumber Synthetic Aperture

Ira Ekhaus

Synap Corporation
100 Wildwood Avenue
Arlington, VA 02174
email: ekhaus@synapcorp.com

Abstract Underwater acoustic imaging applications such as mine countermeasures and side scan sea floor surveys would benefit from an operational synthetic aperture sonar system. While the potential of high resolution Synthetic Aperture (SA) Sonar designs to provide unprecedented detection and discrimination performance is clear, the real world issues of residual platform motion and temporal/spatial variations in sound speed (SSP) have prevented operational deployment of existing designs. High azimuthal resolution requires a synthesized aperture of lengths approaching ten thousand wavelengths. This imposes tight constraints on residual motion error and environmental scenarios where present designs could potentially operate. These problems have provided much incentive for research in autofocusing and motion compensation techniques as they apply to the sonar environment. Synap Corporation has developed the Reduced Wavenumber Synthetic Aperture (REWSA) algorithm/design based on an interferometric preprocessing stage operating on multiple element baseband receptions, and a unique inversion stage. The system specification is shown to develop a reduced wavenumber characteristic that is inherently robust to the effects of the sonar environment. The REWSA algorithm is shown to be a quadratic generalization of wavenumber decomposition SA techniques. Where traditional SA techniques can be cast as a 2-D Fourier inversion, REWSA can be interpreted as a 3-D Fourier inversion where two dimensions of the data set form a two spatial (and frequency) correlation function that are inverted to obtain a final image estimate of the reflectivity of the target field. Simulation of time records for a variety of target scenarios reinforce a discussion of spatial sampling and aperture requirements.

**REDUCED WAVENUMBER SYNTHETIC APERTURE
(REWSA)**

**Ira Ekhaus
Synap Corporation
Arlington, MA
ekhaus@synapcorp.com**

March 12, 1997

SPONSORED BY NOAA UNDER 50-DKNA-5-00206

ACOUSTIC REMOTE SENSING GOALS

HIGH COVERAGE RATE (NM^2 / HOUR)

HIGH RESOLUTION (ALONG TRACK, ACROSS TRACK)

ROBUST, SIMPLE OPERATION

CANDIDATE TECHNOLOGY: SYNTHETIC APERTURE SONAR (SAS)

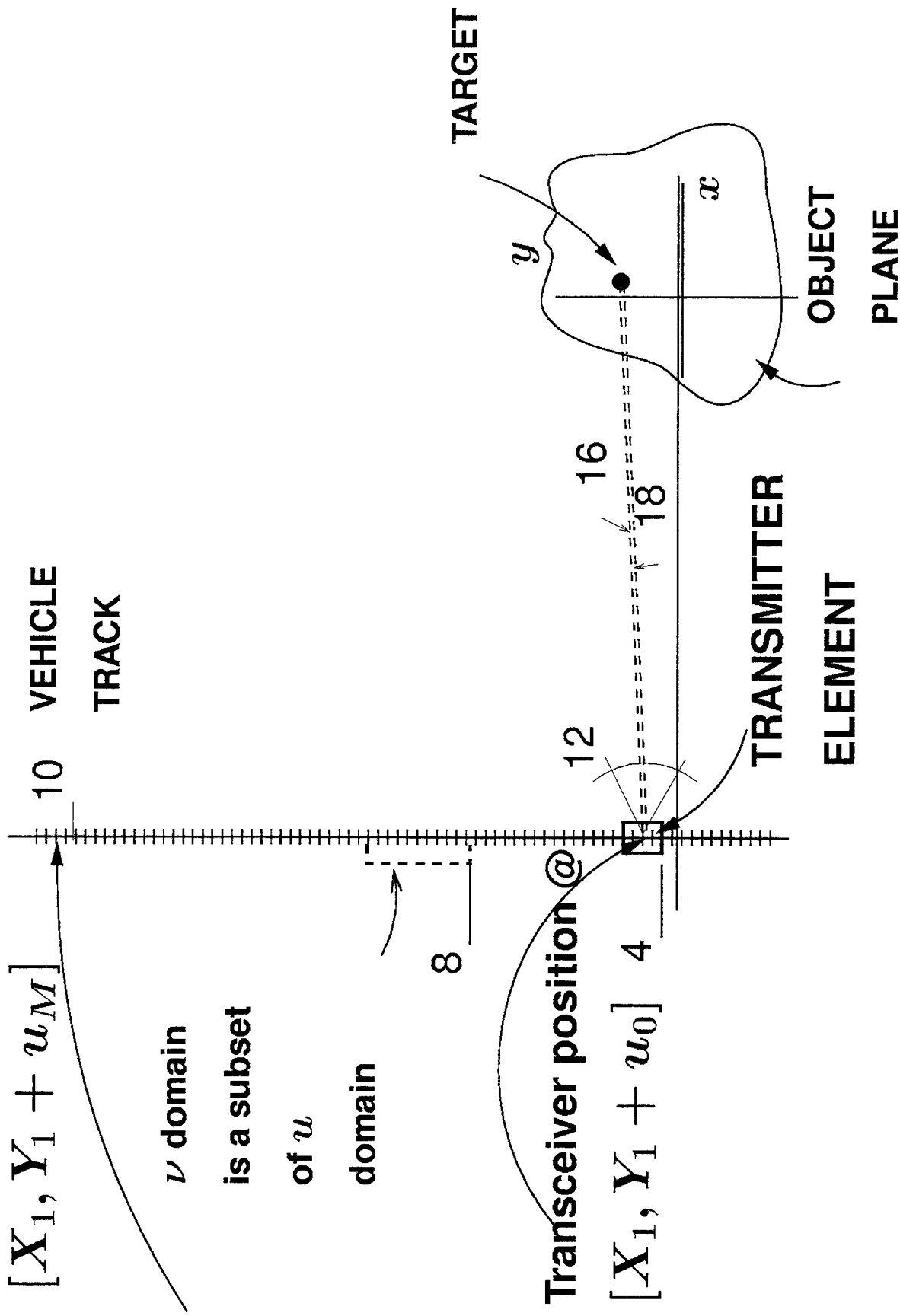
- ✓ VERY HIGH RESOLUTION
- ✓ VERY HIGH COVERAGE RATE (USING MULTISTATIC RECEPTION)
- X EXTREME SENSITIVITY TO VEHICLE MOTION.
- X EXTREME SENSITIVITY TO ENVIRONMENTAL PHASE NOISE .
- ? ENVIRONMENTALLY ROBUST OPERATIONAL SYSTEMS

Diagram illustrating the geometry of a fan beam sonar system. The diagram shows a vehicle moving in a direction, emitting a fan beam of sound. The resulting resolution cells on the sea floor are shown, along with the unprocessed data and the footprint of the system.

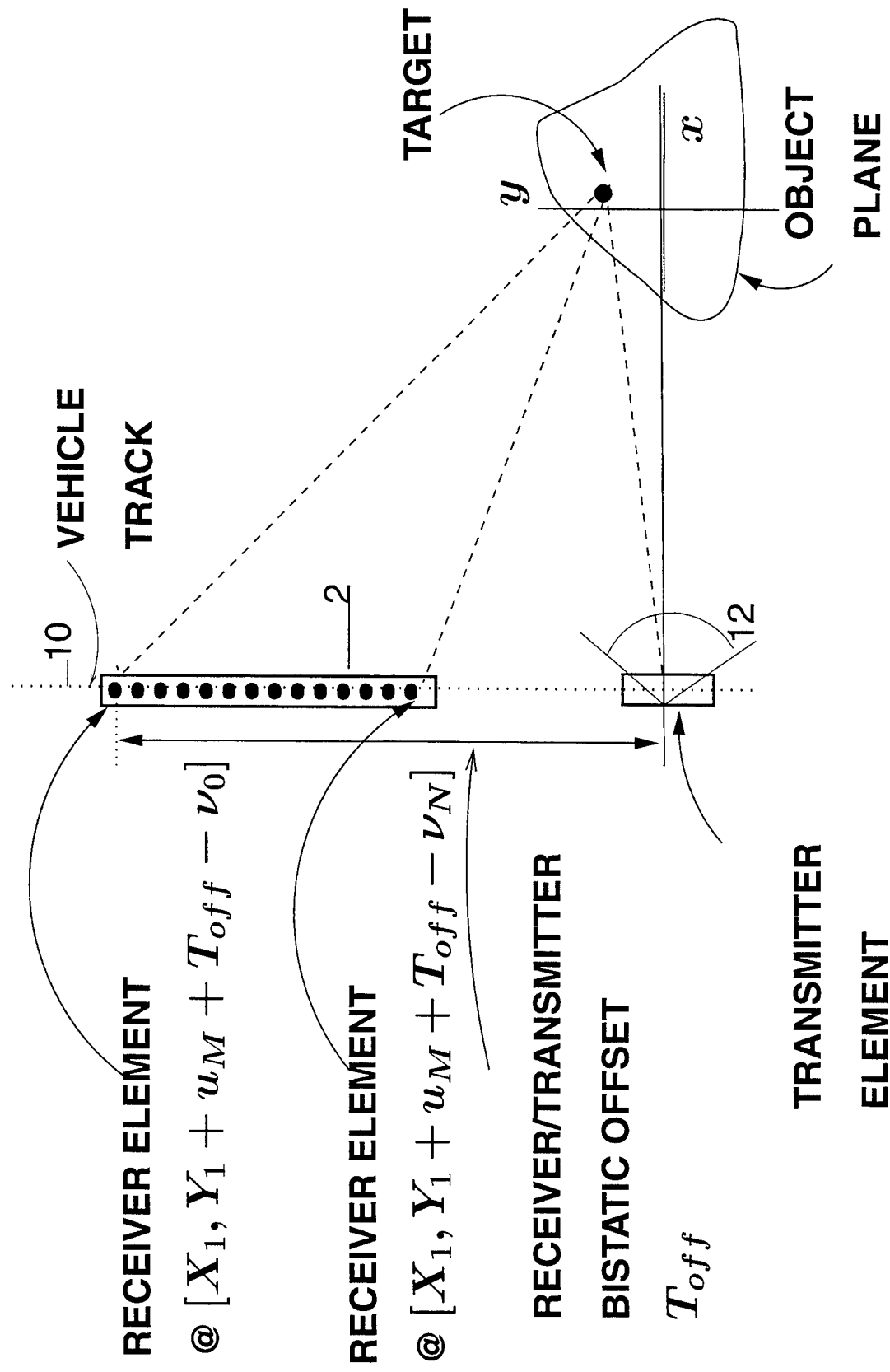
Labels and components:

- VEHICLE DIRECTION
- DIRECTION OF SOUND
- PROPAGATION
- FAN BEAM
- $B = \frac{\lambda}{L}$
- B_{hor}
- B_{ver}
- OCEAN SURFACE
- SEA FLOOR
- BOTTOM LAYING OBJECT
- UNPROCESSED
- SEAFLOOR RESOLUTION
- SCATTERERS CELL
- (FOOTPRINT)

Monostatic SAR (SAS) MEASUREMENT SCENARIO



MULTISTATIC MEASUREMENT



SYNTHETIC APERTURE PROCESSING SEQUENCE

$$s(t, u) \equiv \int \int \underbrace{\alpha(x, y)}_{\text{TARGET REFLECTIVITY}} p \left[t - \underbrace{\frac{2 | X_1 - x, Y_1 + u - y |}{C}}_{\text{TRANSMIT SIGNAL}} \right] dx dy \quad (1)$$

$$s(\omega, u) = P(w) \int_{-2k}^{2k} E[-j(k_x X_1 + k_u Y_1)] \Psi(k_x, k_u) E[jk_u u] dk_u \quad (2)$$

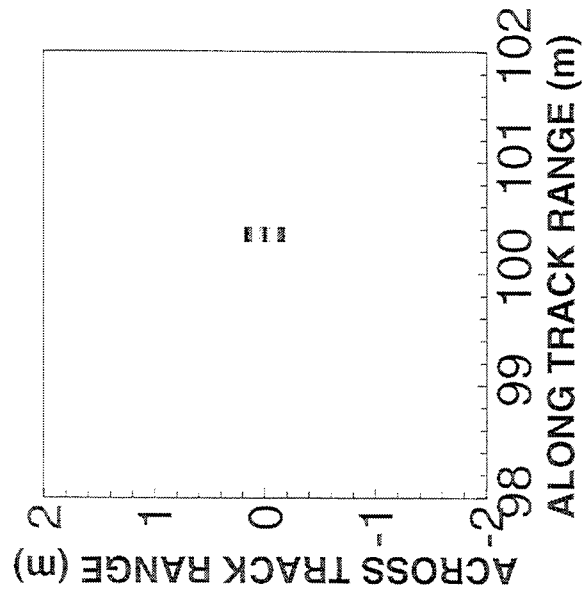
$$\text{where } k_x = \sqrt{4k^2 - k_u^2}, \quad k_y = k_u, \quad \alpha(x, y) \leftrightarrow_{FT} \Psi(k_x, k_y) \quad (3)$$

$$S(\omega, k_u) = P(w) E[jk_x X_1 + jk_u Y_1] \Psi(k_x(w, k_u), k_u) \quad (4)$$

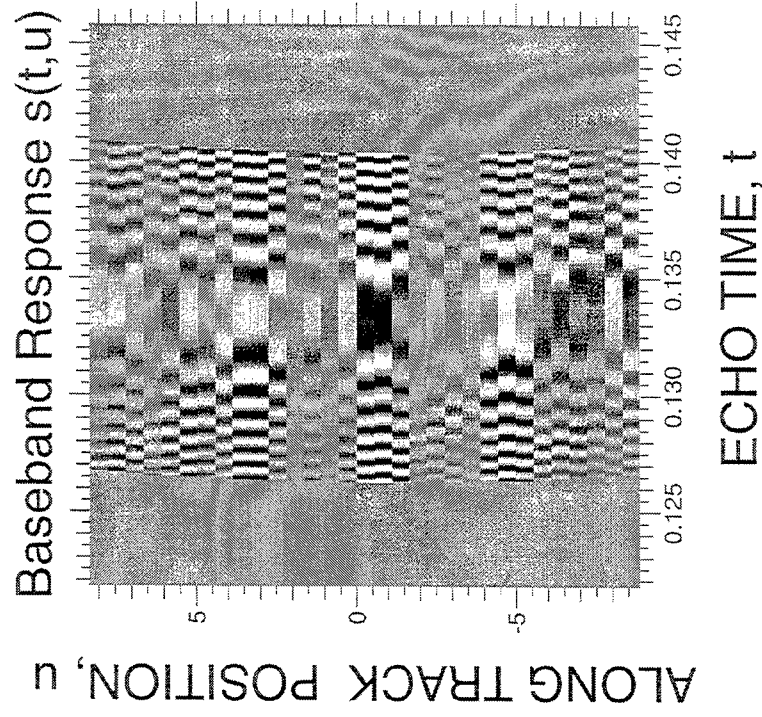
$$\hat{\Psi}(k_x(\omega, k_u), k_y) \leftarrow \text{interpolate } P^{-1}(\omega) \underbrace{E[-jk_x X_1 - jk_u Y_1]}_{\substack{\text{PHASE CORRECTION} \\ \text{REQUIRES GREAT PRECISION}}} S(\omega, k_u) \quad (5)$$

$$\hat{\alpha}(x, y) = FT^{-1}(\hat{\Psi}(k_x, k_y)) \quad (6)$$

TYPICAL SAS RETURN

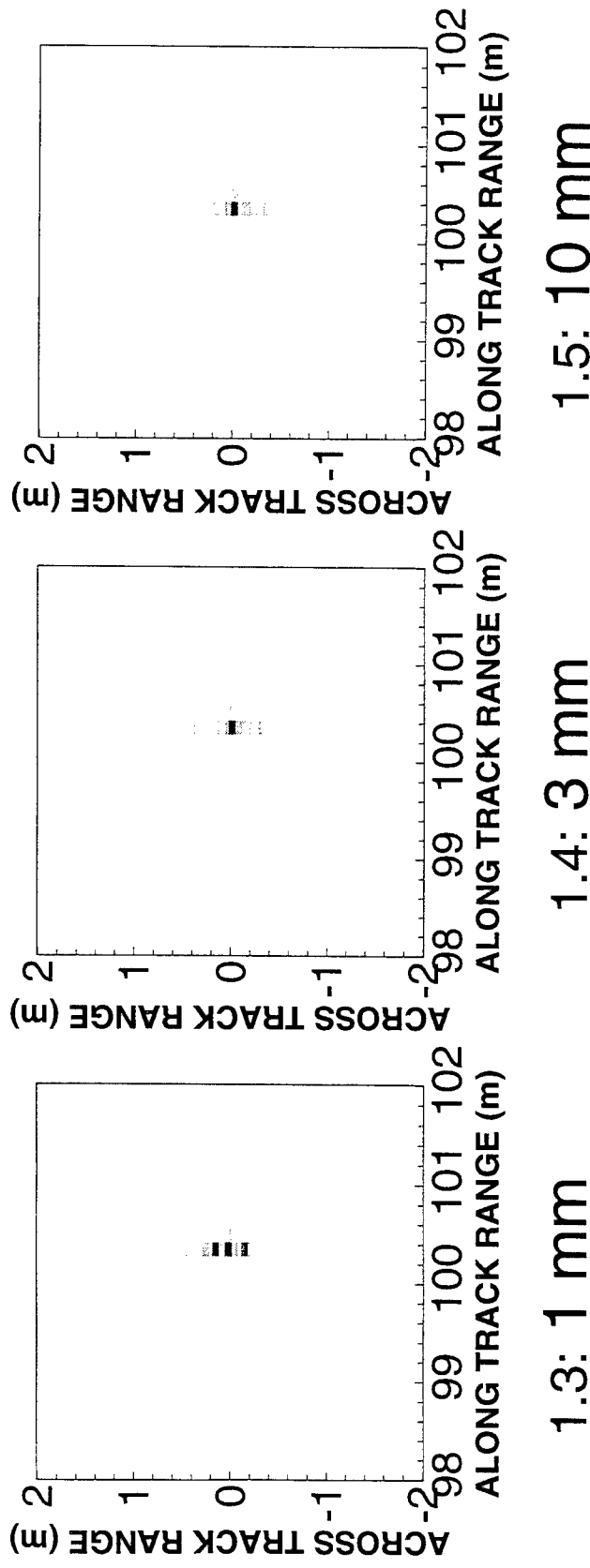


1.1: 3 PT TARGET
FIELD



1.2: BASEBAND RESPONSE
 $s(t, u)$ vs TIME t and TRACK
 u

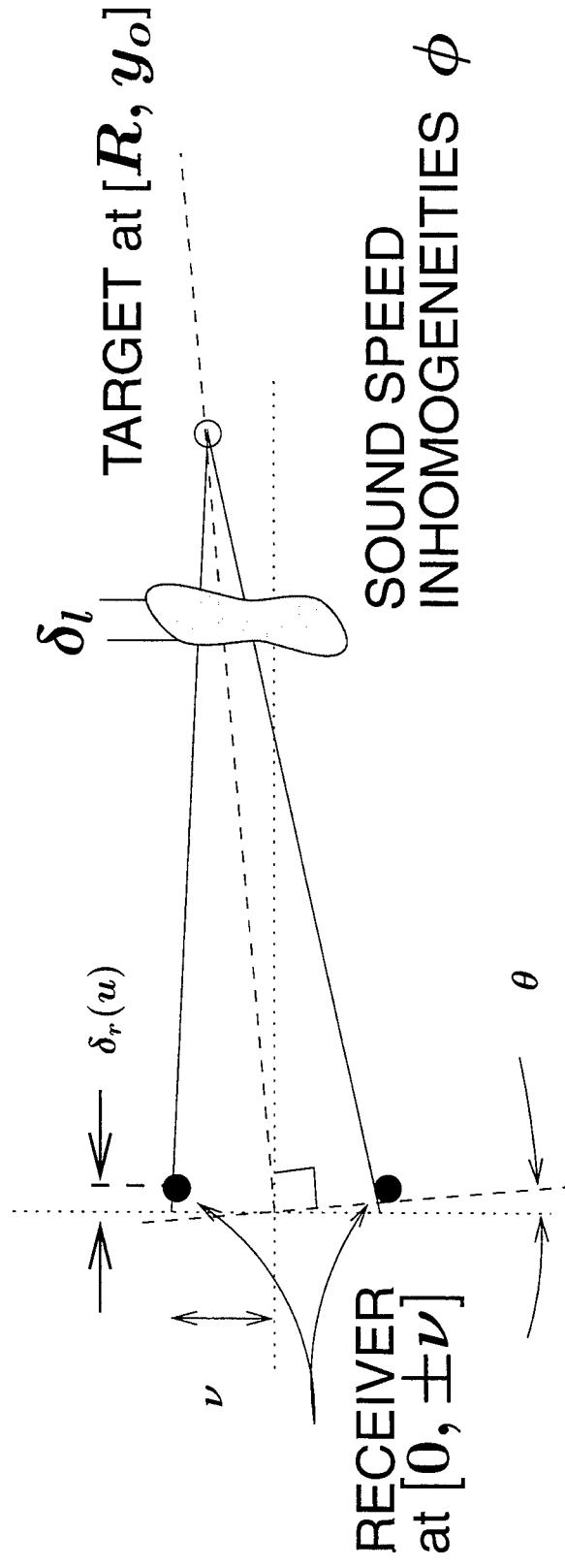
IMAGE DEGRADATION UNDER SAS DUE TO RESIDUAL ACROSS TRACK MOTION (RMS)



EXISTING TECHNIQUES (MOTION COMPENSATION and AUTOFOCUSING) MUST REDUCE RESIDUAL ERROR TO A FRACTION OF A WAVELENGTH.

THE ALTERNATIVE IS TO REDUCE THE EFFECTIVE WAVELENGTH SEEN BY THE SYSTEM.

INTERFEROMETRY "REDUCES" the EFFECTIVE WAVENUMBER K_x



THE PAIRWISE INTERFEROMETRIC PRODUCT :

$$\Gamma(t, \nu) = s(t; +\nu) s^*(t; -\nu) \sim \underbrace{[p(t - 2K\delta_r - \delta_l\phi)]^2}_{\text{envelope}} E[-j2K\nu \sin(\theta)]$$

MOTION δ_r AND ENVIRONMENTAL PHASE NOISE $\delta_l\phi$ PRIMARILY AFFECT ENVELOPE; HIGH WAVENUMBER SENSITIVITY $E[j2K\delta_r]$ HAS BEEN STRIPPED OFF.

REWSA OVERVIEW

TAKE THE CORRELATION OF THE ORIGINAL SAS SIGNAL $s(t, u)$, ON LAG VARIABLES τ, ν , (ν IS EITHER A SUBSET OF MONOSTATIC u OR DISTINCT MULTISTATIC RECEPTIONS.)

$$\Gamma(t, \tau, u, \nu) = \underbrace{s(t + \tau, u + \nu) s^*(t - \tau, u - \nu)}_{\text{INTERFEROMETRIC PRODUCT}}$$

THROUGH A 4D FT, TO YIELD A SPECTRAL, WAVENUMBER DATABASE

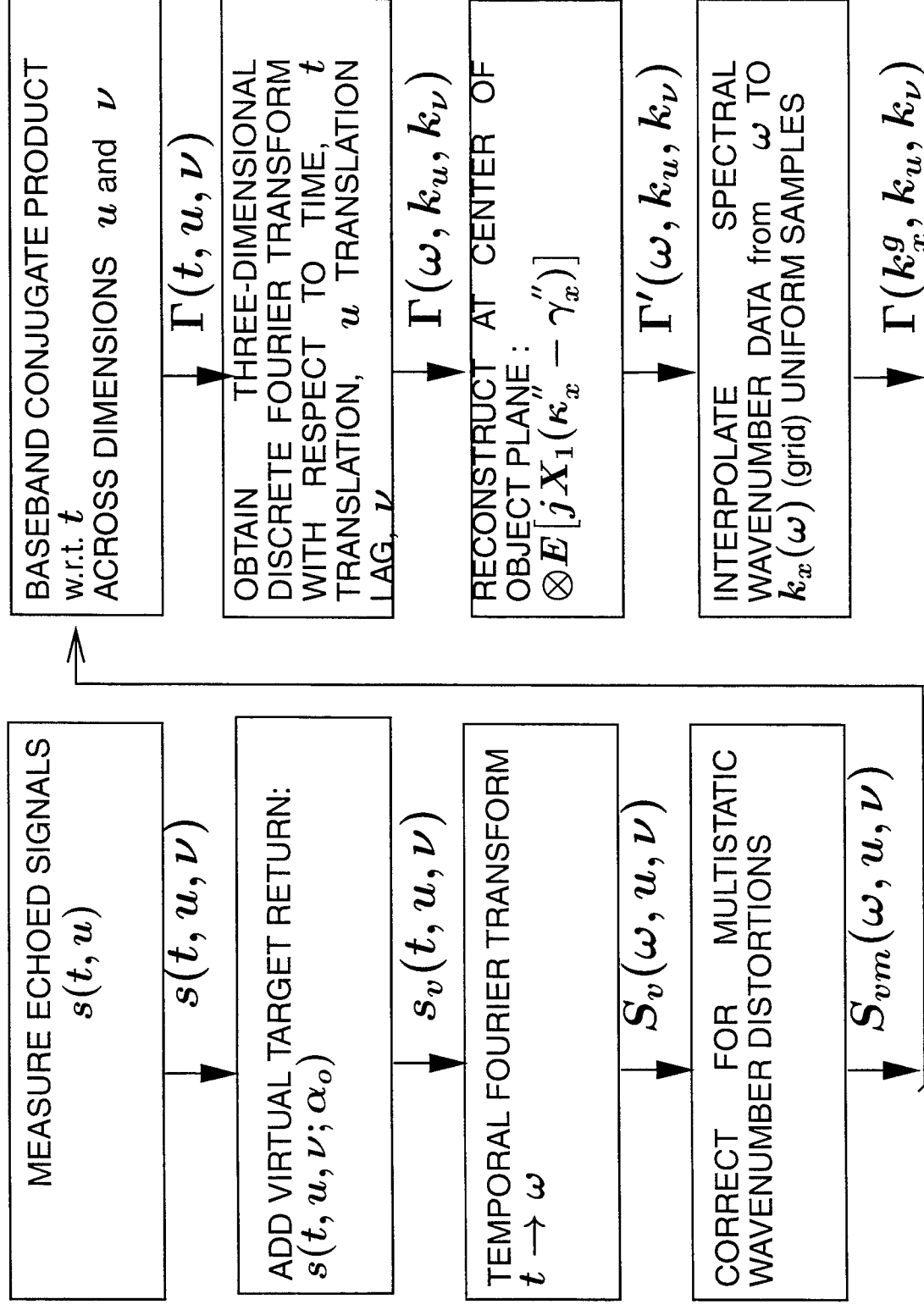
$$\Gamma(w_o, \Theta, k_u, k_\nu) = \underbrace{E[jY_1(k_u)] E[jX_1(\kappa_x'' - \gamma_x'')]}_{\text{PHASE FUNCTION}} \underbrace{\Psi(\kappa_x'', \frac{k_\nu + k_u}{2}) \Psi^*(\gamma_x'', \frac{k_u - k_\nu}{2})}_{\text{TWO WAVENUMBER CORRELATION FUNCTION}} \quad (7)$$

WITH EQUIVALENT ACROSS TRACK WAVENUMBER K_x^e ,

$$\frac{\kappa_x'' - \gamma_x''}{2} \sim \frac{K_\nu K_u}{4 K_C} + \frac{(K_u^2 + K_\nu^2) K_o + 2 K_\nu K_u K_\Theta}{8 K_C^2} + \dots \quad (8)$$

THAT IS MUCH SMALLER THAN PROPAGATION WAVENUMBER K_C . THEN, ANALOGOUS TO STEP 5 OF SAS SEQUENCE, CORRECT FOR PHASE AND INVERT TO OBTAIN IMAGE.

REWSA ALGORITHM FLOWCHART (I)



REWSA ALGORITHM FLOWCHART (II)

↓ $\Gamma(k_x^g, k_u, k_\nu)$

TWO-WAVENUMBER CORRELATION → TWO-VARIABLE
CORRELATION:

$$\Gamma^g(k_x, k_u, k_\nu) - > \alpha'(k_x, u, \nu)$$

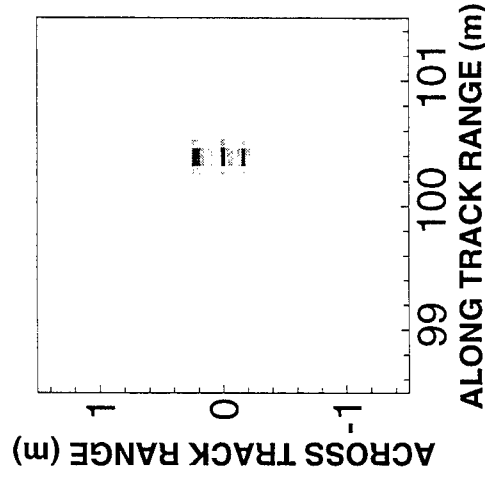
TWO-VARIABLE CORRELATION → SINGLE VARIABLE:
EVALUATE AT $u = \nu/2$, DIVIDE THROUGH BY $\alpha^*(k_x, 0)$:
 $\alpha'(k_x, \nu/2, \nu) \rightarrow \alpha(k_x, u)$

INVERSE FOURIER TRANSFORM $k_x \rightarrow x$:
 $\alpha(k_x, u) \rightarrow \alpha_o(x, y) \oplus \alpha(x, y)$

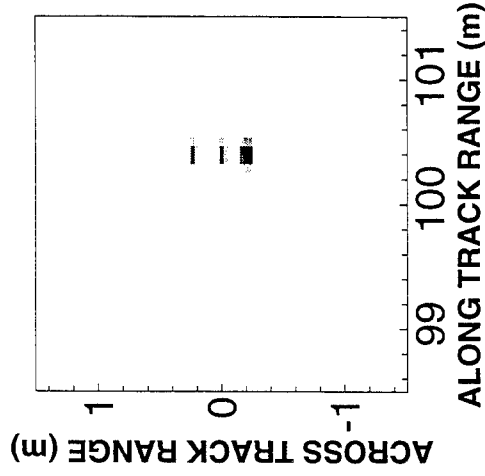
SUBTRACT VIRTUAL TARGET, TAKE MAGNITUDE
→ $|\hat{\alpha}(x, y)|$

FINAL IMAGE

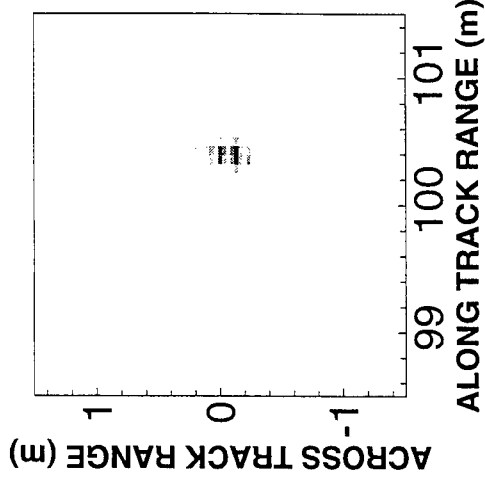
IMAGE DEGRADATION UNDER REWSA DUE TO RESIDUAL ACROSS TRACK MOTION (RMS)



1.6: 3 mm



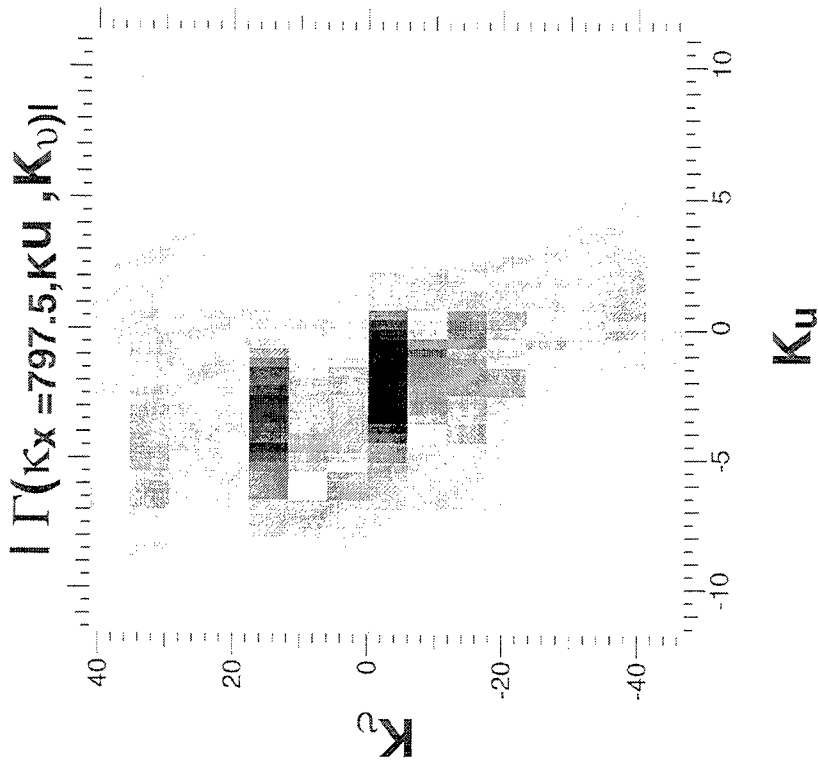
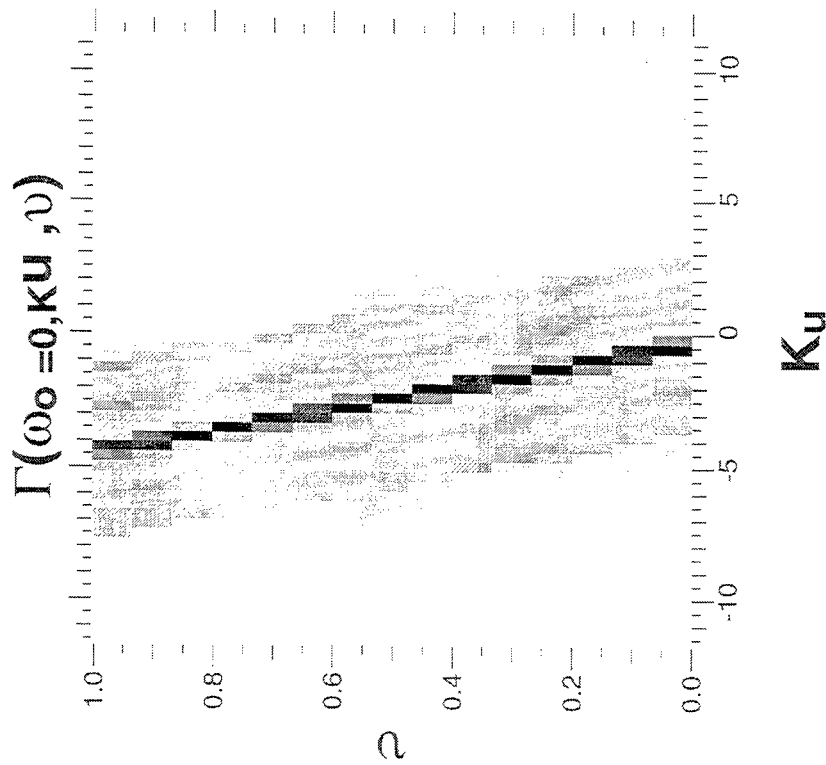
1.7: 10 mm



1.8: 30 mm

THE EFFECTIVE WAVENUMBER IS REDUCED TO THE EQUIVALENT OF THE BANDWIDTH ; APPROXIMATELY 10 TIMES MORE ROBUST THAN UNCOMPENSATED SAS.

INTERMEDIATE DATA IN REWSA



1.9: K_u/K_ν SLOPE RELATES TO TOWSPEED

1.10: K_u/K_ν IS THE WAVENUMBER CORRELATION DOMAIN

HIGH SPATIAL FREQUENCY DATA NOW RESIDES IN K_ν , MODULATION W.R.T. K_ν , DUE TO MULTIPLE TARGETS.

Summary:

PROBLEM:

- MCM REQUIRES HIGHEST POSSIBLE (ACOUSTIC) RESOLUTION/COVERAGE RATE.
- SYNTHETIC APERTURE (SA) TECHNIQUES HAVE POTENTIAL.
- SYNTHETIC APERTURE (SA) TECHNIQUES ARE ENVIRONMENTALLY FRAIL .
- REWSA = ENVIRONMENTALLY ROBUST SYNTHETIC APERTURE

NEAR TERM:

- OPEN WATER EXPERIMENTS

LONG TERM:

- MUCH HIGHER DATA QUALITY AND COVERAGE RATES
- POTENTIAL FOR A.T.D.T.R. AND OTHER RADAR POST-PROCESSING TECHNIQUES

Monostatic Clutter Spreading in Joint Terrain Scattered Jamming (TSJ) / Clutter Mitigation Architectures

Daniel F. Marshall

MIT Lincoln Laboratory
244 Wood Street
Lexington, MA 02173-9108
tel: (617) 981-0807
email: dmars@ll.mit.edu

Abstract Research is ongoing into architectures for mitigating monostatic clutter interference and terrain-scattered jamming (TSJ) when both occur simultaneously. A difficulty which may arise in such architectures is that the process of mitigating the TSJ can spread the clutter energy off of its characteristic low-dimensional locus in the signal space. The consequences of this phenomenon are that target detection is impeded in those areas of the signal space to which clutter is spread, and that additional adaptive degrees of freedom are required to null the clutter. The latter occurrence has the potential to overwhelm the adaptive clutter nulling process, resulting in incomplete nulling of all of the clutter which is present. Different forms of clutter spreading have been predicted based on a number of hypothetical mechanisms. In this paper, a technique is developed for identifying such instances of clutter spreading in real data. Then, an example of clutter spreading in Mountaintop data after joint mitigation processing is given. This example is examined to identify the mechanisms responsible for it. The performance loss due to clutter spreading is compared for several joint mitigation architectures.

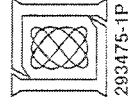
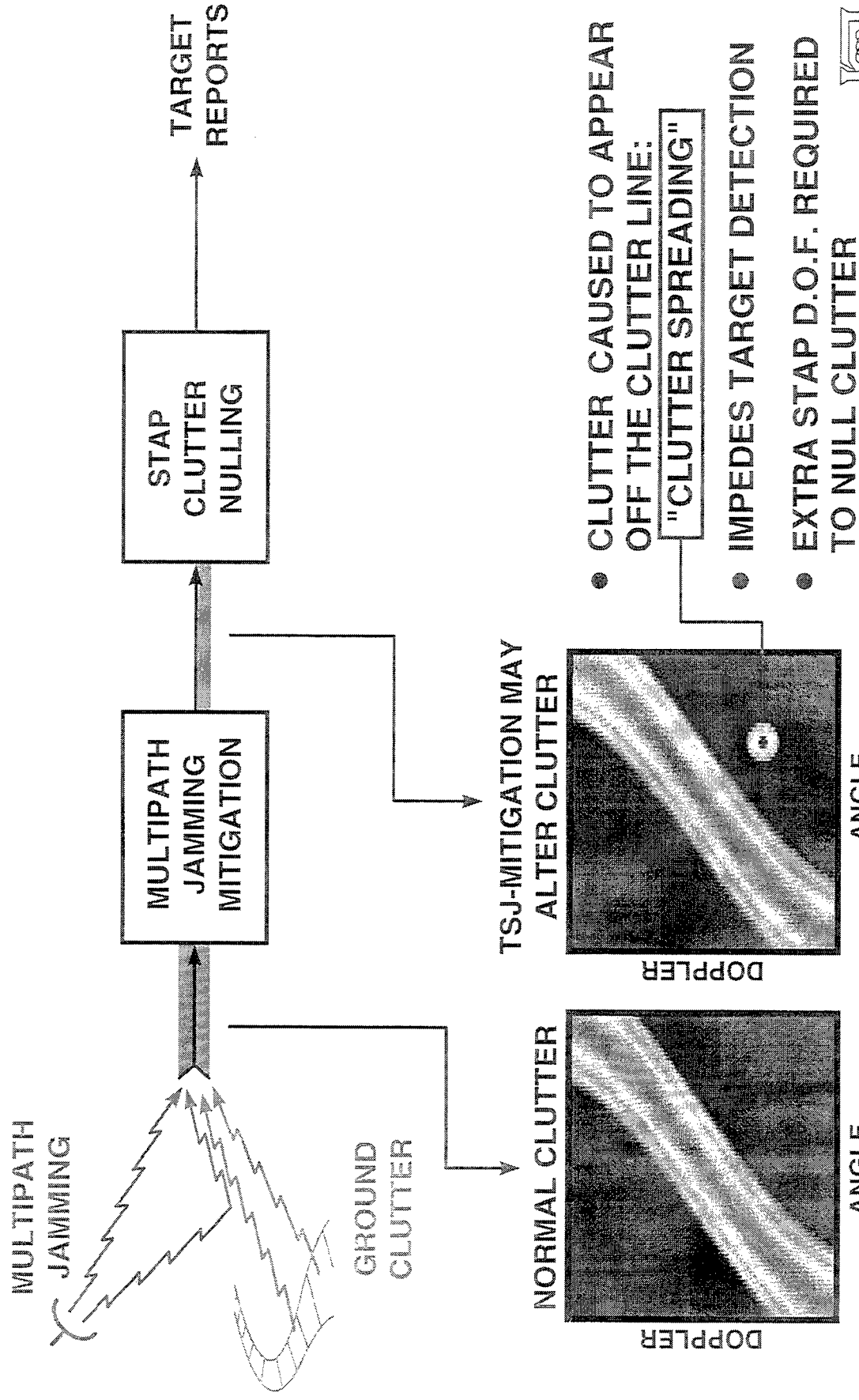
MONOSTATIC CLUTTER SPREADING IN JOINT TSJ/CLUTTER MITIGATION ARCHITECTURES

Daniel F. Marshall
MIT Lincoln Laboratory

OUTLINE: THE PROBLEM
A CASE STUDY
RESULTS
CONCLUSIONS

PROBLEM DESCRIPTION

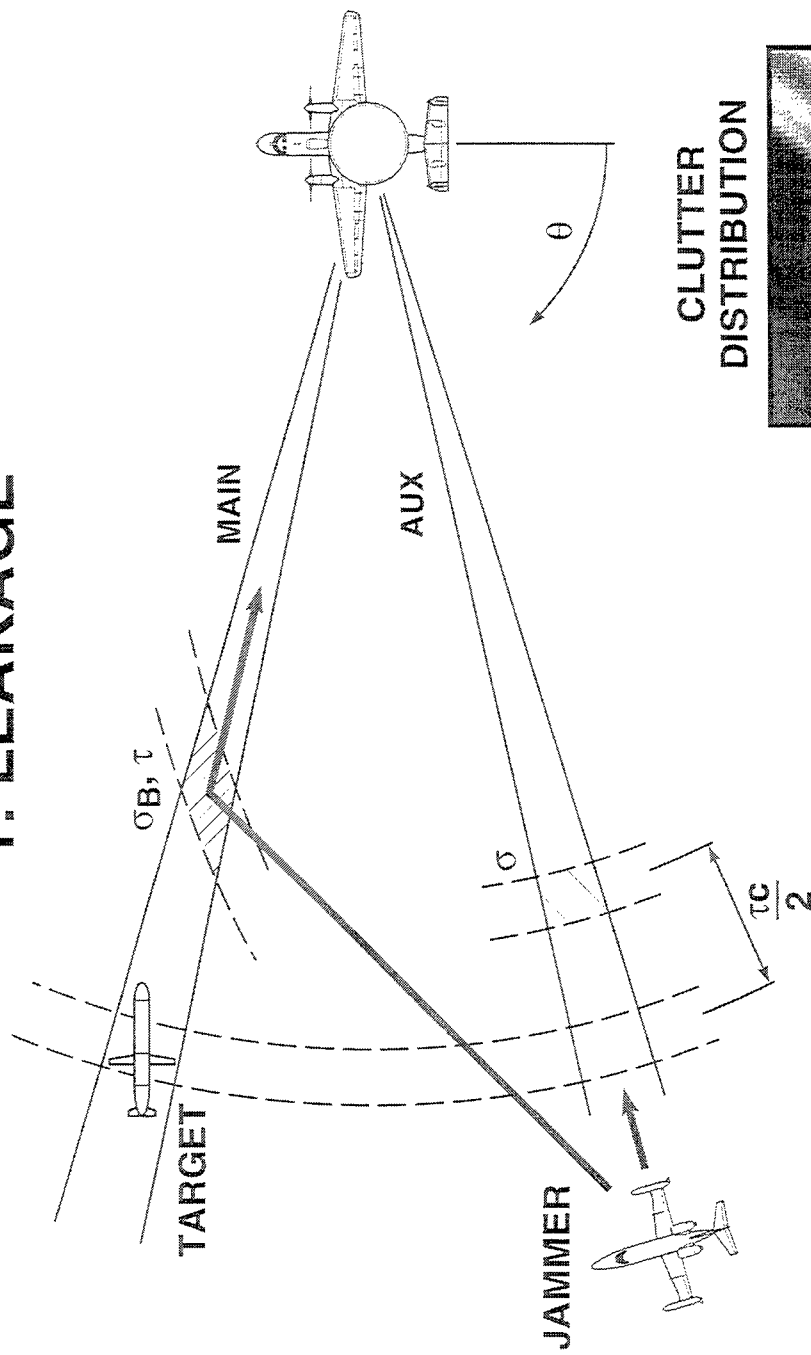
JOINT INTERFERENCE MITIGATION ARCHITECTURE



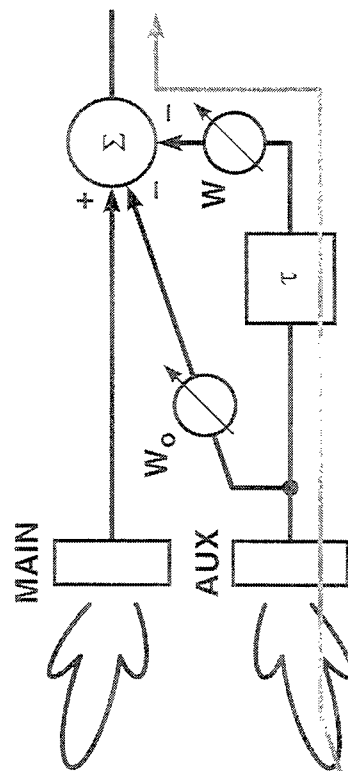
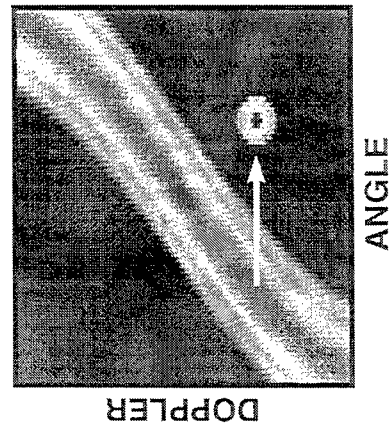
293475-1P

POSSIBLE MECHANISMS FOR CLUTTER SPREADING

1: LEAKAGE



CLUTTER DISTRIBUTION

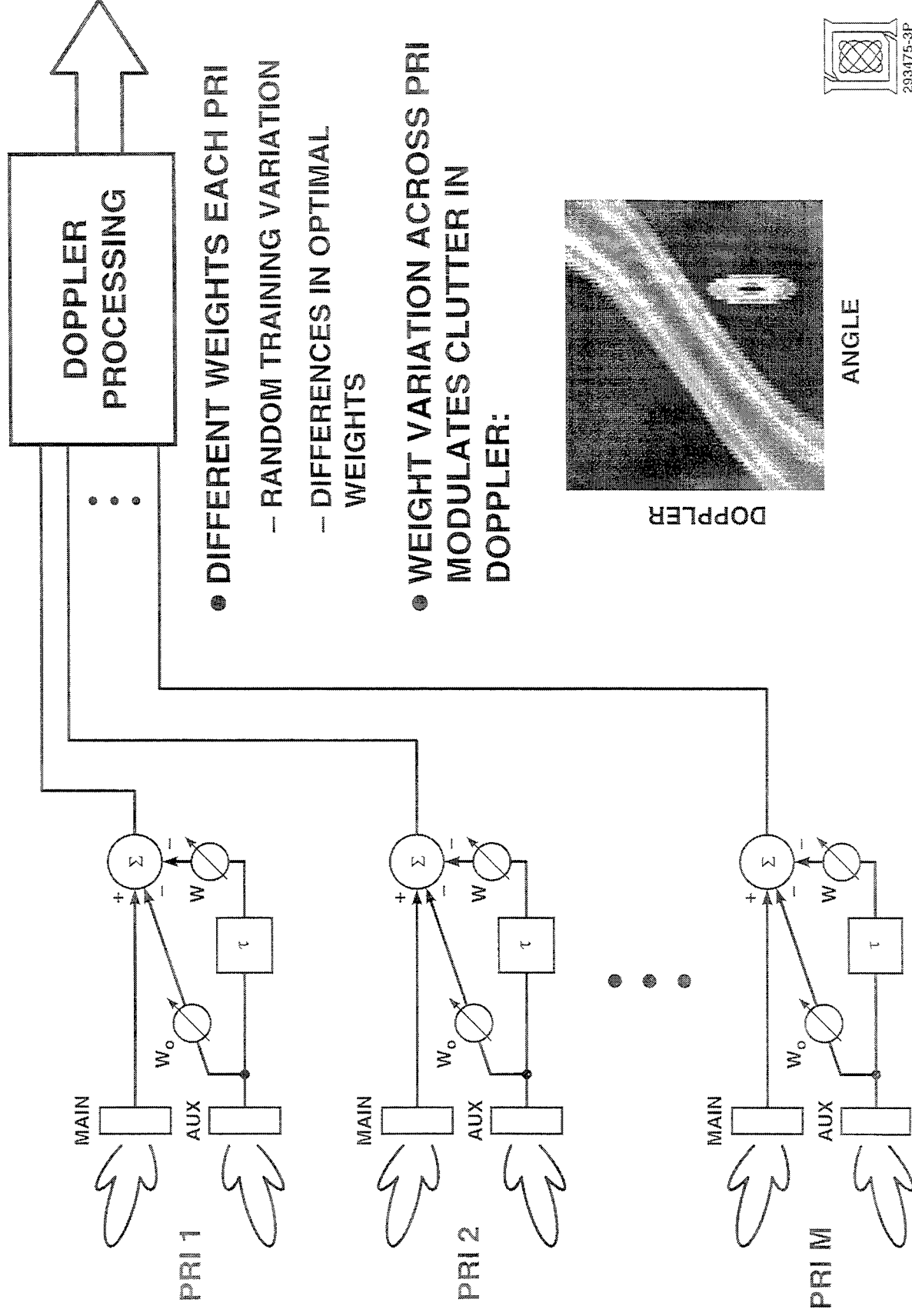


TSI MITIGATION

- **REFERENCE:** Robert A. Gabel, “Monostatic Clutter Spreading from TSI Mitigation,” 4th DARPA Advanced Signal Processing Hot Clutter Technical Interchange Meeting, Rome, NY, 7–8 August 1996.

POSSIBLE MECHANISMS FOR CLUTTER SPREADING

2: MODULATION

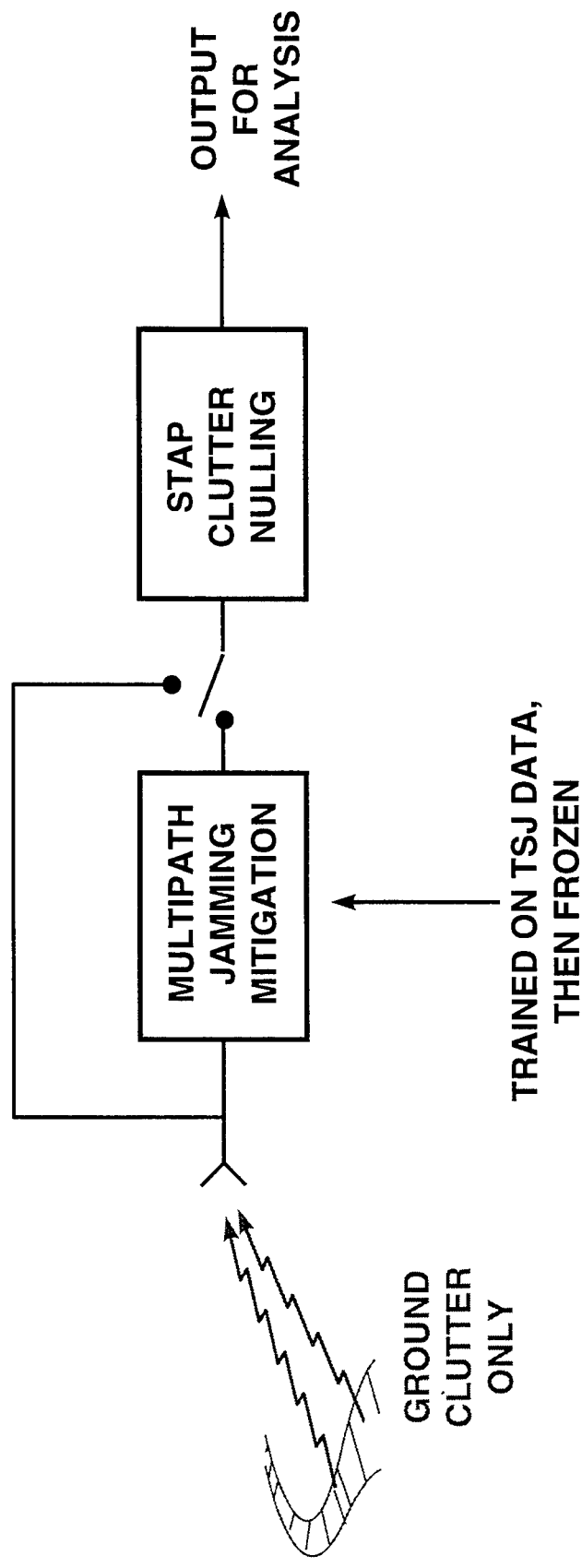


- **REFERENCE: Daniel J. Rabideau, “Signal Modulation in Pulse-by-Pulse Adaptive Nulling Systems,”**

ASAP’97, THURSDAY 13 MARCH, 9:30 a.m.

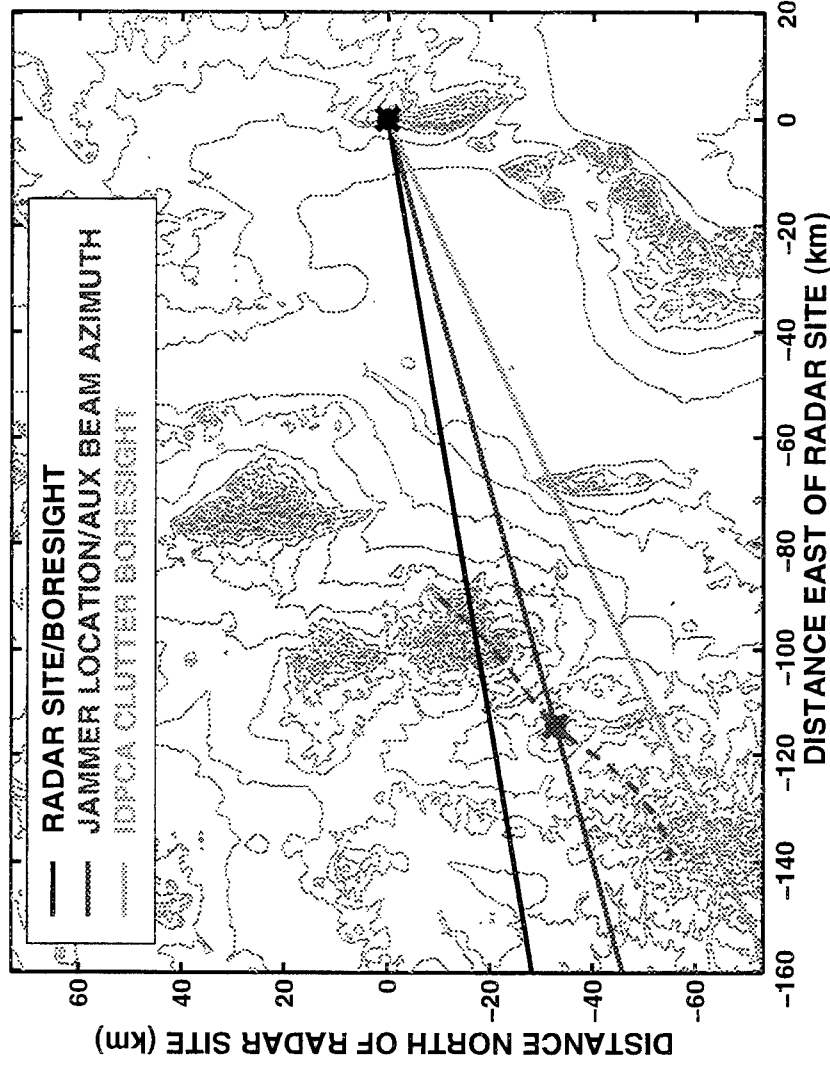
CASE STUDY: AN EPISODE OF CLUTTER SMEARING OBSERVED IN REAL DATA FROM THE MOUNTAINTOP DATABASE

METHOD:



JAMMER AND BORESIGHT GEOMETRY

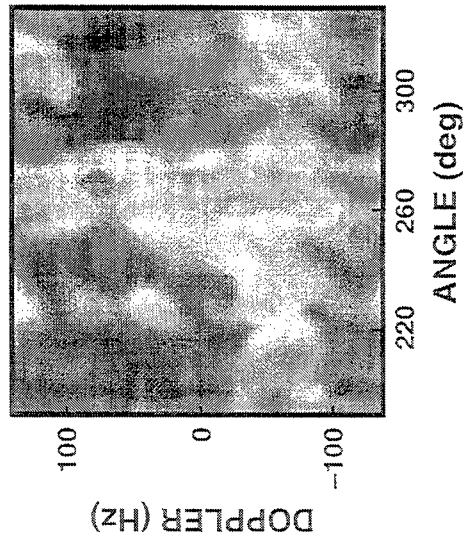
RSTER RADAR AT NORTH OSCURA PEAK
WHITE SANDS MISSILE RANGE, 6 APRIL 1994



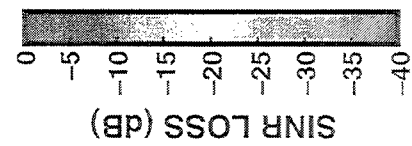
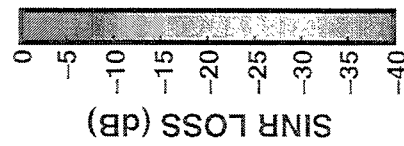
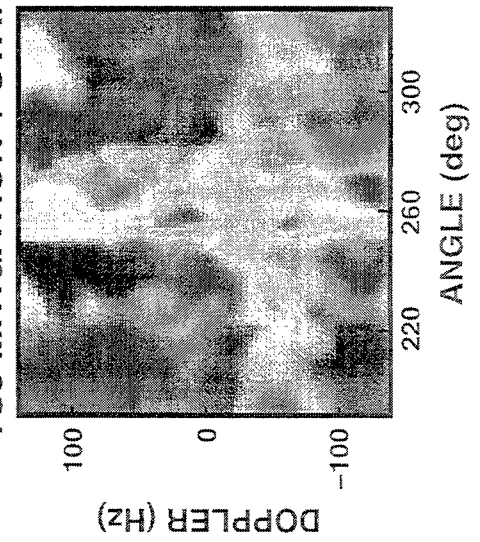
- DATA FILE HOT6065: TSJ AND IDPCA CLUTTER
 - TSJ-ONLY DATA BEYOND CLUTTER HORIZON
- DATA FILE HOT6007: IDPCA CLUTTER ONLY

RESULT:

**SINR LOSS
STAP ONLY**

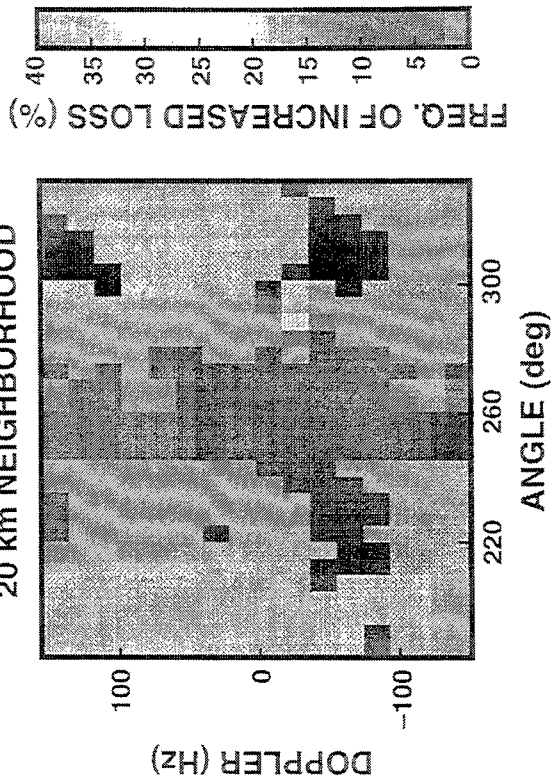


TSJ MITIGATION + STAP

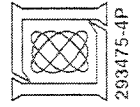


**STATISTICAL ANALYSIS
OF DIFFERENCE**

20 km NEIGHBORHOOD



**CLUTTER SPREADING IS
WEAK BUT PERSISTENT:
STATISTICALLY
SIGNIFICANT**

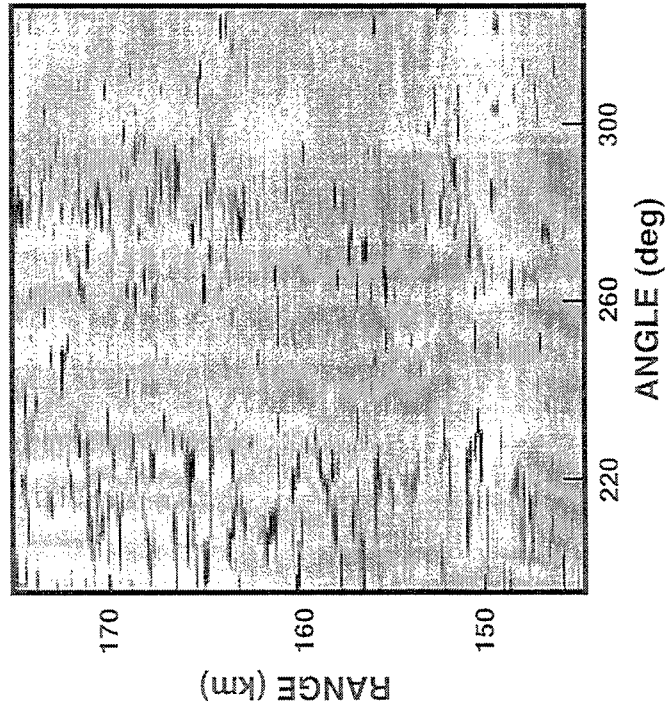


- WEAK SPREADING HERE
- STRONG SPREADING EXPECTED IN OTHER SCENARIOS
- THIS OBSERVATION PROVIDES REAL-WORLD EXPERIENCE OF CLUTTER SPREADING
 - NO SIMULATION
 - OPPORTUNITY FOR STUDY OF CLUTTER SPREADING PHENOMENOLOGY

RESULTS

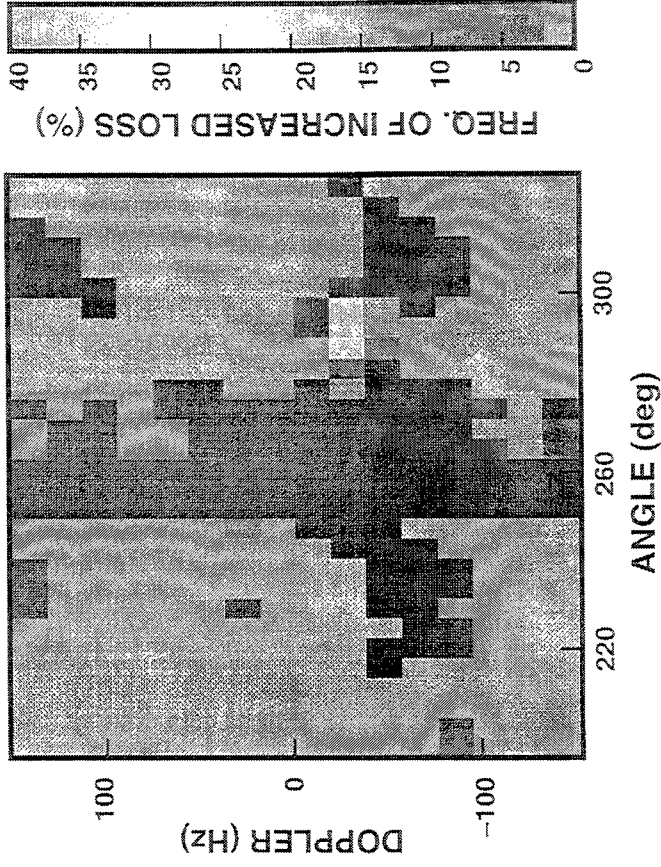
- ELEMENT SPACE TSJ MITIGATION
- SEPARATELY TRAINED WEIGHTS EACH PRI
- ELEMENT SPACE POST-DOPPLER STAP

TSJ AND CLUTTER
PERFORMANCE

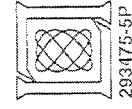


RESIDUAL INTERFERENCE
ABOVE NOISE

CLUTTER SPREADING
PERFORMANCE



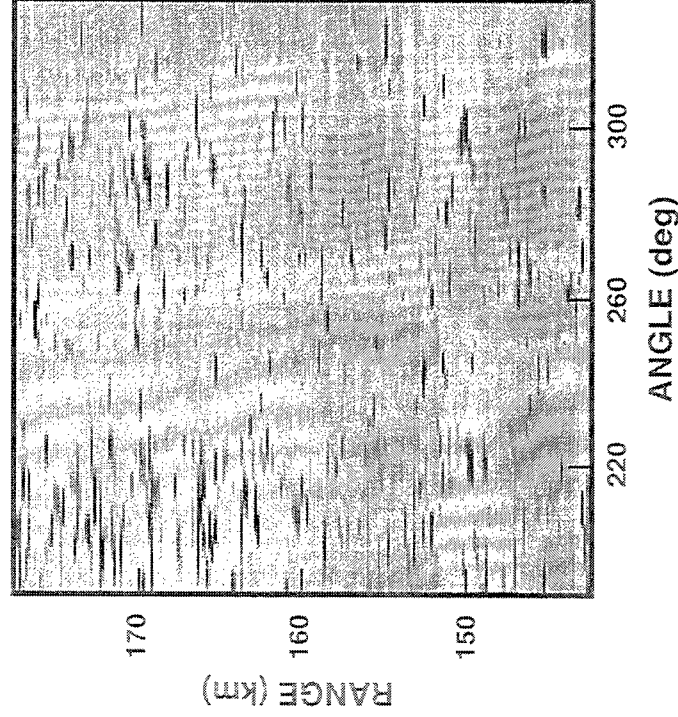
FREQUENCY OF INCREASED
LOSS DUE TO TSJ-MITIGATION



RESULTS

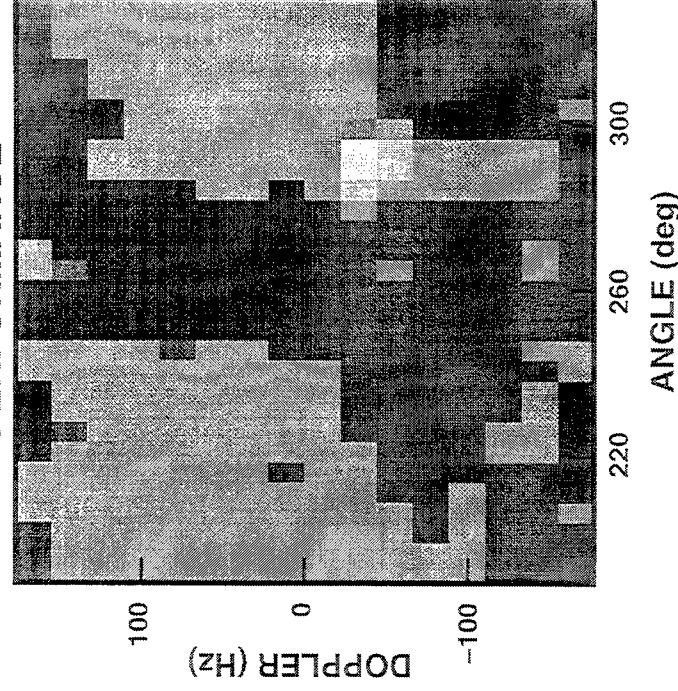
- ELEMENT SPACE TSJ MITIGATION
- SEPARATELY TRAINED WEIGHTS EACH PRI
- ELEMENT SPACE PRE-DOPPLER STAP

TSJ AND CLUTTER
PERFORMANCE

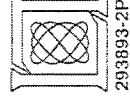
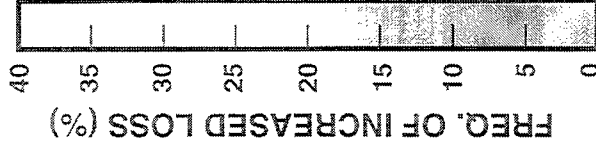


RESIDUAL INTERFERENCE
ABOVE NOISE

CLUTTER SPREADING
PERFORMANCE



FREQUENCY OF INCREASED
LOSS DUE TO TSJ-MITIGATION

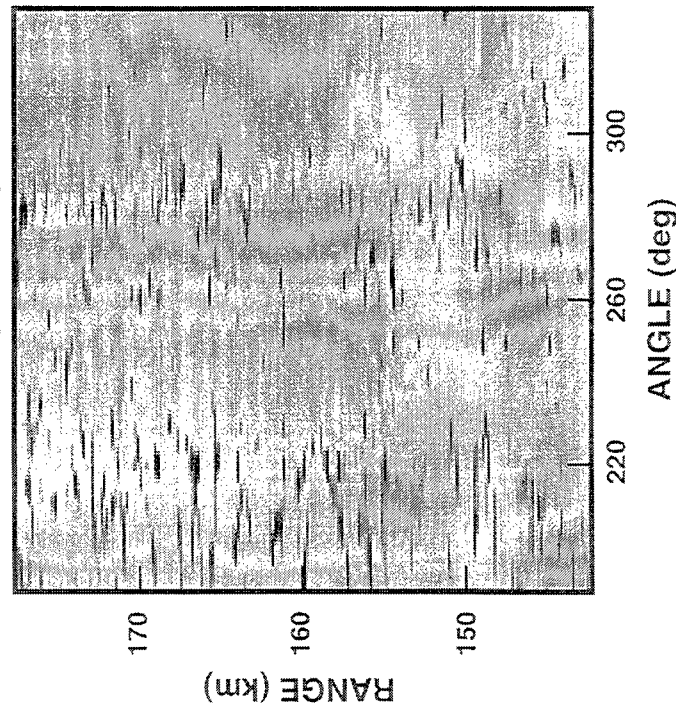


293893-2P

RESULTS

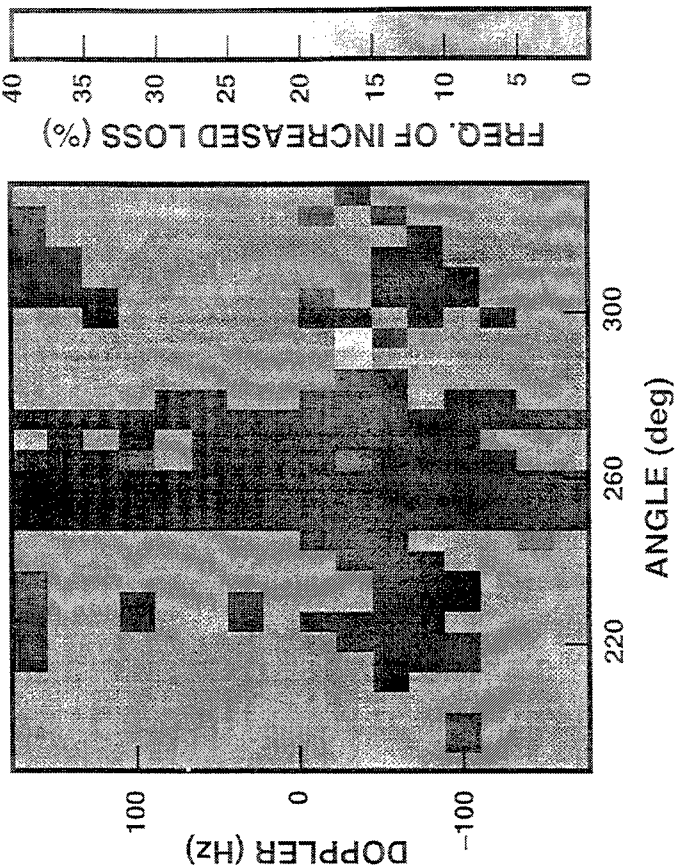
- BEAM SPACE TSJ MITIGATION
- SEPARATELY TRAINED WEIGHTS EACH PRI
- BEAM SPACE POST-DOPPLER STAP

TSJ AND CLUTTER
PERFORMANCE

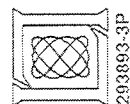


RESIDUAL INTERFERENCE
ABOVE NOISE

CLUTTER SPREADING
PERFORMANCE



FREQUENCY OF INCREASED
LOSS DUE TO TSJ-MITIGATION

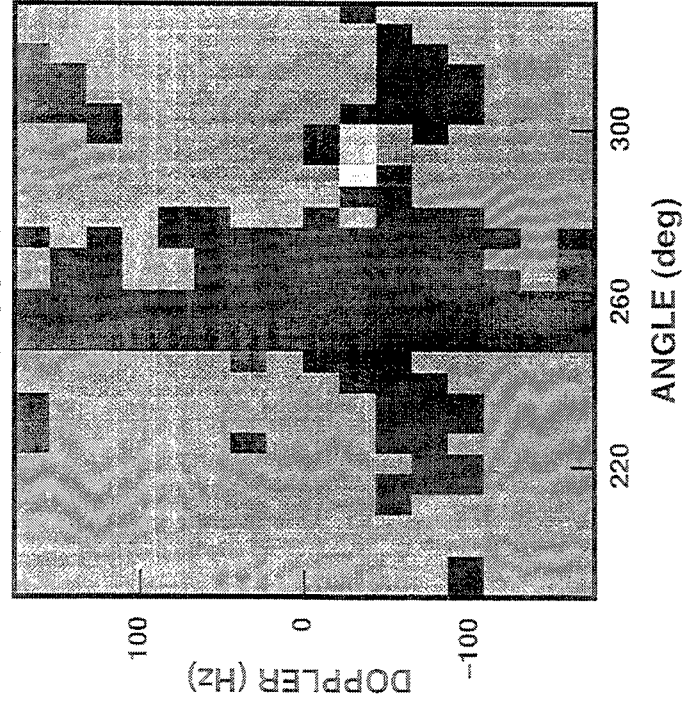


293893-3P

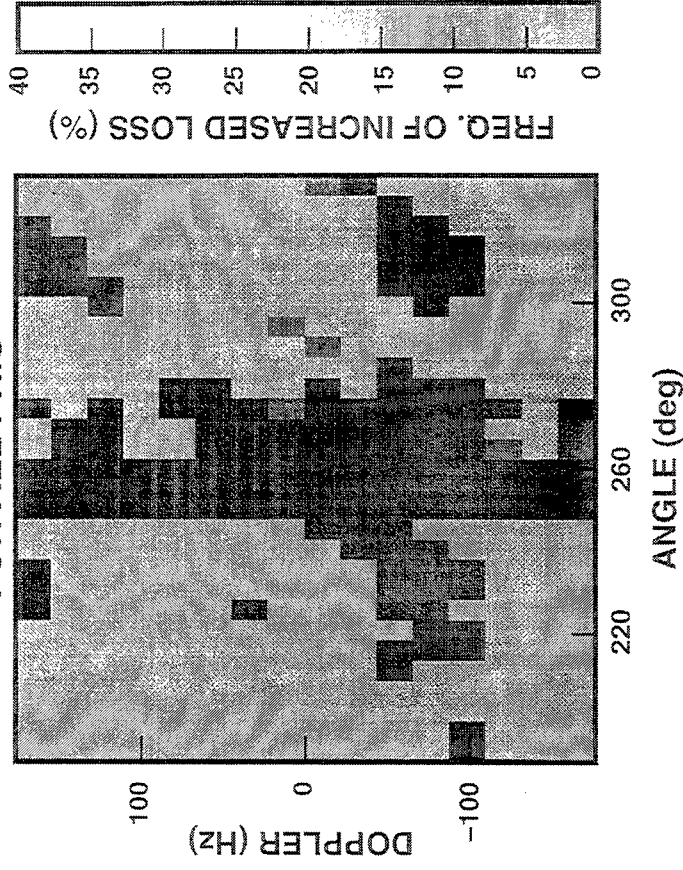
ANALYSIS

WHAT CAUSES THE OBSERVED CLUTTER SPREADING?

OBSERVED
RESULT



PRI #1 WEIGHTS USED
FOR ALL PRIS

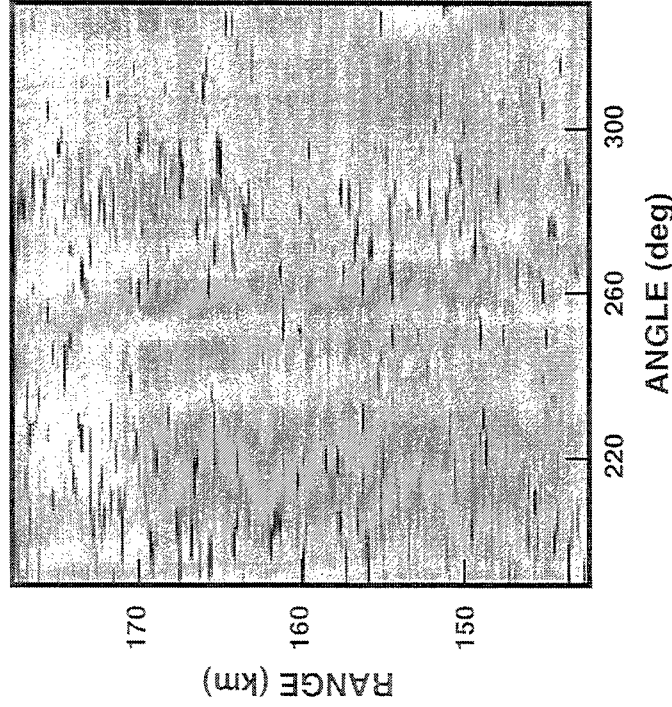


- CLUTTER SPREADING VANISHES

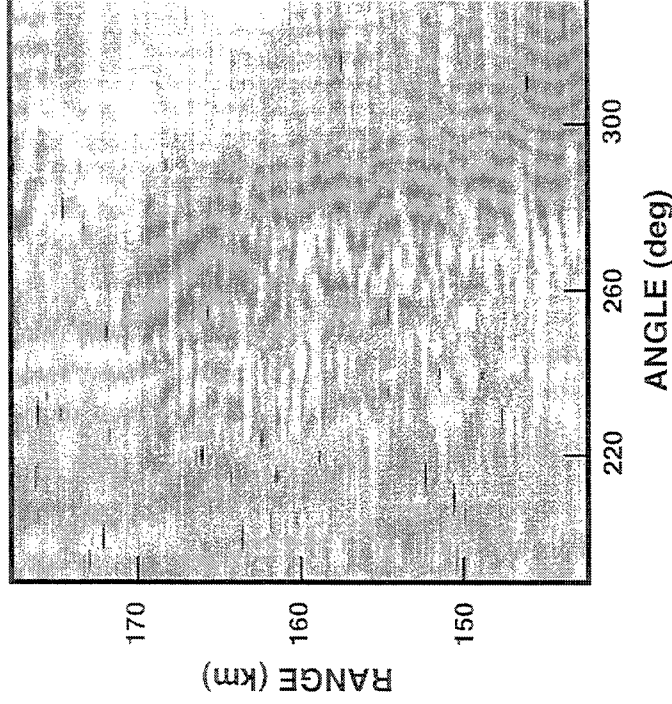
⇒ THIS SPREADING IS CAUSED BY MODULATION

BUT TSJ PERFORMANCE IS DEGRADED:

BASELINE
POWER OUT



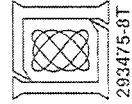
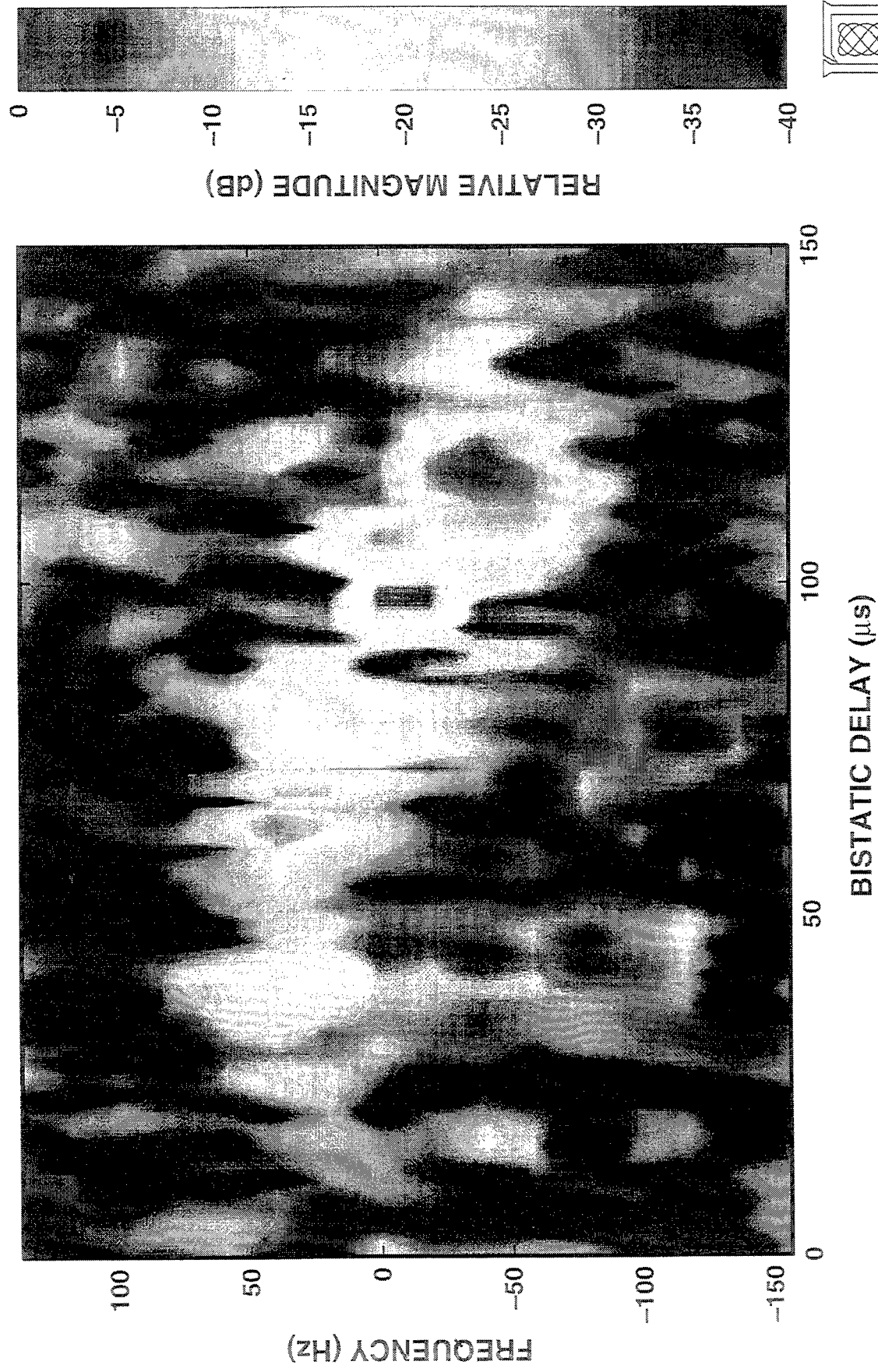
PRI #1 WEIGHTS USED
FOR ALL PRIS



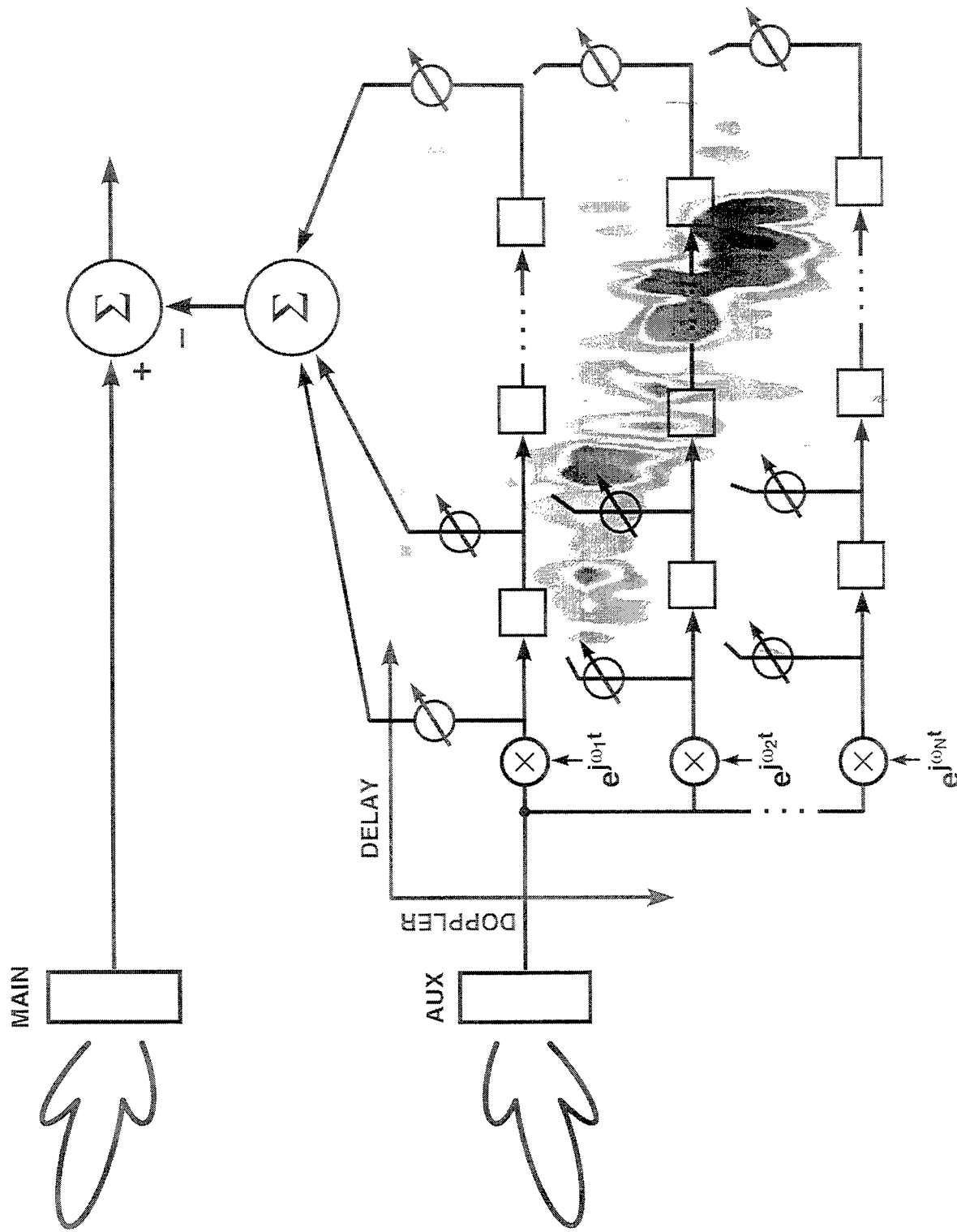
- SUGGESTS THAT CLUTTER SPREADING CAN BE MITIGATED BY MINIMIZING WEIGHT VARIATION ACROSS THE CPI
- BUT MUST MAINTAIN TSJ MITIGATION PERFORMANCE



TSJ MAGNITUDE vs DELAY AND DOPPLER



DOPPLER COMPENSATED ARCHITECTURE FOR TSJ MITIGATION

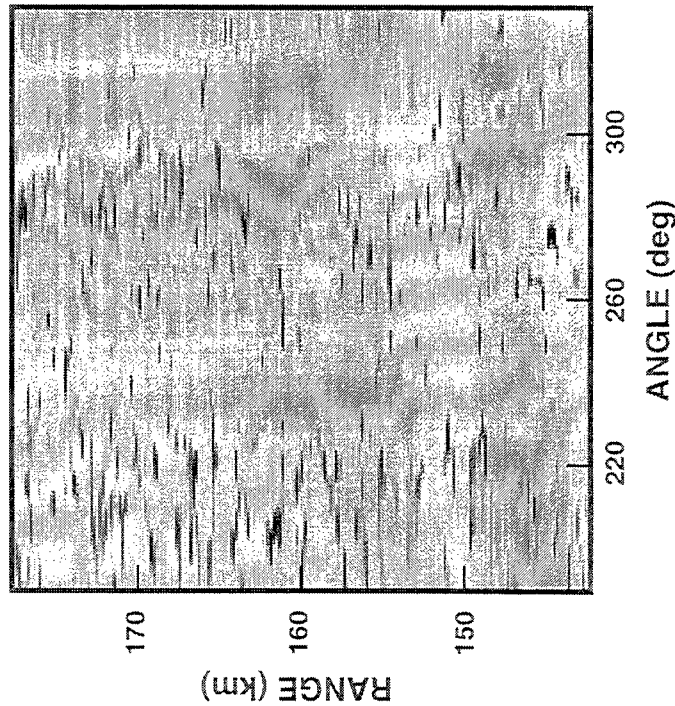


- DOPPLER-DELAY TREND DETERMINES WHICH WEIGHTS ARE NEEDED TO MITIGATE THE TSJ: WEIGHT THINNING
 - DOPPLER-DELAY TREND CAN BE ESTIMATED FROM DATA
- THESE WEIGHTS CAN BE TRAINED AND HELD CONSTANT OVER ENTIRE CPI
 - WITHOUT LOSS OF TSJ MITIGATION PERFORMANCE
 - BECAUSE LINEAR-PHASE TIME VARIATION IS APPLIED SEPARATELY
 - REMOVES RANDOM TRAINING VARIATION ACROSS PRI—
MINIMIZES MODULATION-INDUCED CLUTTER SPREADING

RESULTS

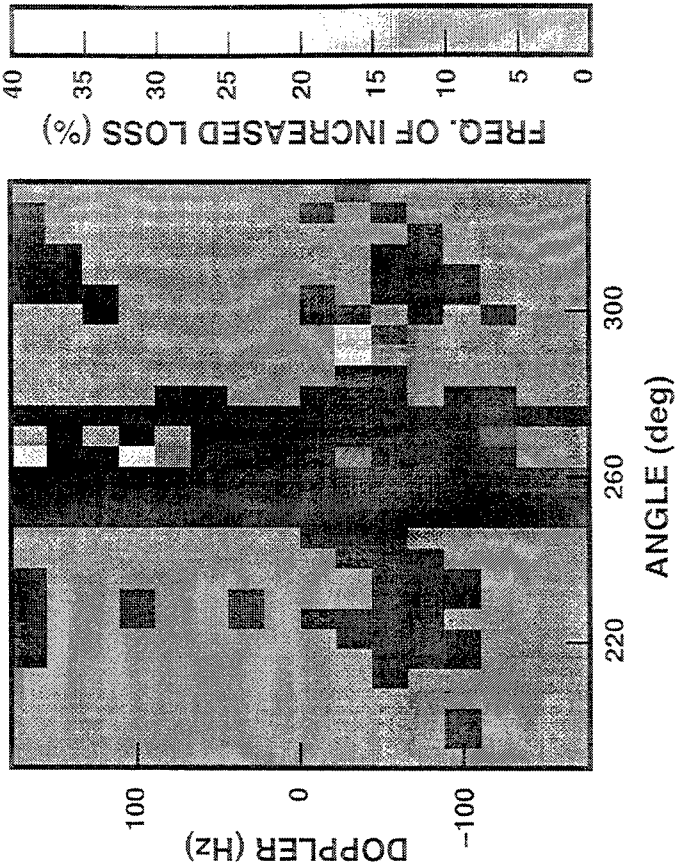
- BEAM SPACE TSJ MITIGATION
- WEIGHTS TRAINED OVER ENTIRE CPI, SAME WEIGHTS USED FOR ALL PRIS
- BEAM SPACE POST-DOPPLER STAP

TSJ AND CLUTTER PERFORMANCE

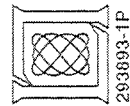


RESIDUAL INTERFERENCE ABOVE NOISE

CLUTTER SPREADING PERFORMANCE



FREQUENCY OF INCREASED LOSS DUE TO TSJ-MITIGATION



293893-1P

- **TSJ MITIGATION PERFORMANCE IS MAINTAINED**
- **BUT CLUTTER SPREADING PERFORMANCE IS NOT IMPROVED**
- **THUS DOPPLER PHASE VARIATION CAUSES CLUTTER SPREADING**

CONCLUSIONS

- **CLUTTER SPREADING OBSERVED IN REAL-WORLD SCENARIO**
 - **VALIDATES PREDICTIONS OF CLUTTER SPREADING**
- **MODULATION WAS MAJOR CAUSE OF PERFORMANCE DEGRADATION**
 - **STRONG LEAKAGE-INDUCED SPREADING NOT OBSERVED WHEN MODULATION WAS REMOVED; MAY OCCUR IN OTHER SCENARIOS**
- **SIMILAR PERFORMANCE FOR SEVERAL DIFFERENT ALGORITHMS**
 - **NO ALGORITHM PROVIDED SIGNIFICANT PERFORMANCE ADVANTAGE**
 - **ONLY CASCADE-TYPE JOINT MITIGATION ALGORITHMS STUDIED HERE**
 - **OTHER ALGORITHMS OR APPROACHES MAY MITIGATE CLUTTER SPREADING**

Fast Space-Time Clutter Covariance Matrix Computation

Steven T. Smith and James Ward

MIT Lincoln Laboratory
244 Wood Street
Lexington, MA 02173-9108
tel: (617) 981-3106
email: stsmith@ll.mit.edu

Abstract Initial analysis of adaptive radar system performance is oftentimes performed using ideal covariance matrix and time-series analysis. If the radar must operate in the presence of clutter interference, then STAP algorithms are appropriate and the space-time clutter covariance matrix must be computed. Because this matrix's size is determined by the product of the aperture and CPI length, huge matrices result for even moderately sized radars. Nevertheless, space-time clutter covariance matrices containing hundreds of thousands of elements may be computed in a few seconds by exploiting Toeplitz structure and a trick involving the Fourier-Bessel expansion of the ground's reflected energy, i.e., a discretization in frequency. This method is typically several orders of magnitude faster than a direct approach of discretization in azimuth. The only assumption necessary is independent patch-to-patch clutter interference, i.e., no terrain scattered interference. Aside from this restriction, arbitrary illumination and reflectance patterns are treated. Furthermore, the following cases are easily incorporated into this framework at limited or no computational cost: clutter with zero pitch, clutter with nonzero pitch, internal clutter motion on the ground (Billingsly's model is used as one example), and nonzero signal bandwidth. The consideration of such details can add integrity to a performance study. As an additional benefit, a block Toeplitz data structure is easily obtained, resulting in potentially large savings in storage cost, and matrix-vector and matrix inversion operations. This talk presents these results, which are greatly expanded and enhanced from previously published work, and uses them to explore some implications for STAP performance of pitch, ICM, and bandwidth.

FAST SPACE-TIME CLUTTER COVARIANCE MATRIX COMPUTATION

STEVEN T. SMITH

JAMES WARD

LINCOLN LABORATORY

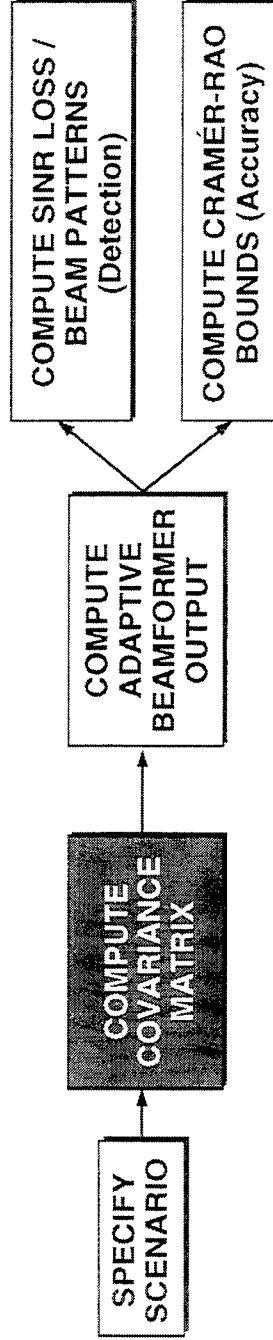
MASSACHUSETTS INSTITUTE OF TECHNOLOGY

1997 ASAP WORKSHOP



MAIN IDEA

- ANALYSIS TOOL FOR ADAPTIVE RADAR PERFORMANCE



ASSUMPTIONS / FEATURES

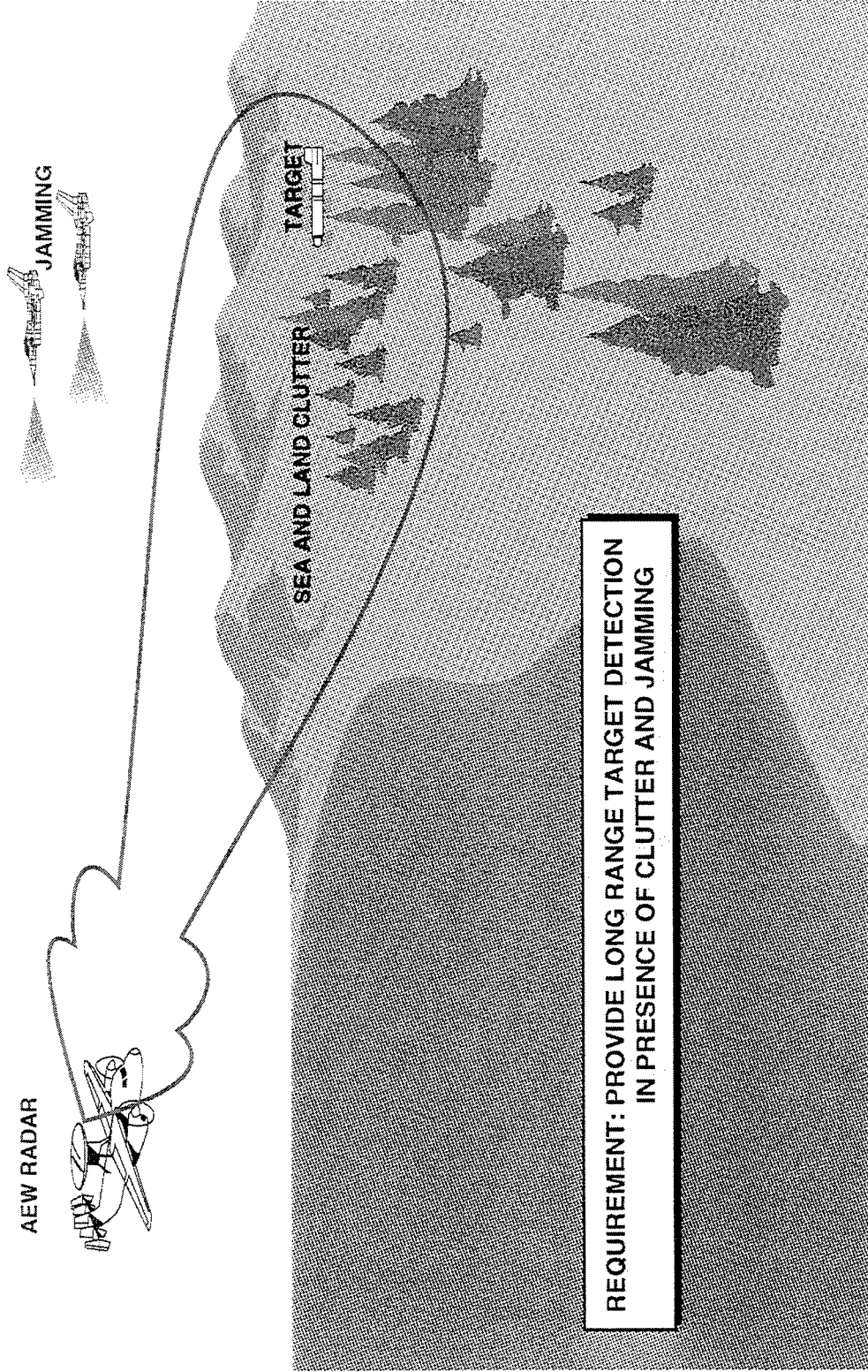
- INDEPENDENT PATCH-TO-PATCH CLUTTER
- NO PULSE OR ELEMENT MISMATCHES
- ARBITRARY TRANSMIT PATTERN AND GROUND REFLECTIVITY
- INCLUDES INTERNAL CLUTTER MOTION AND BANDWIDTH EFFECTS

OUTLINE

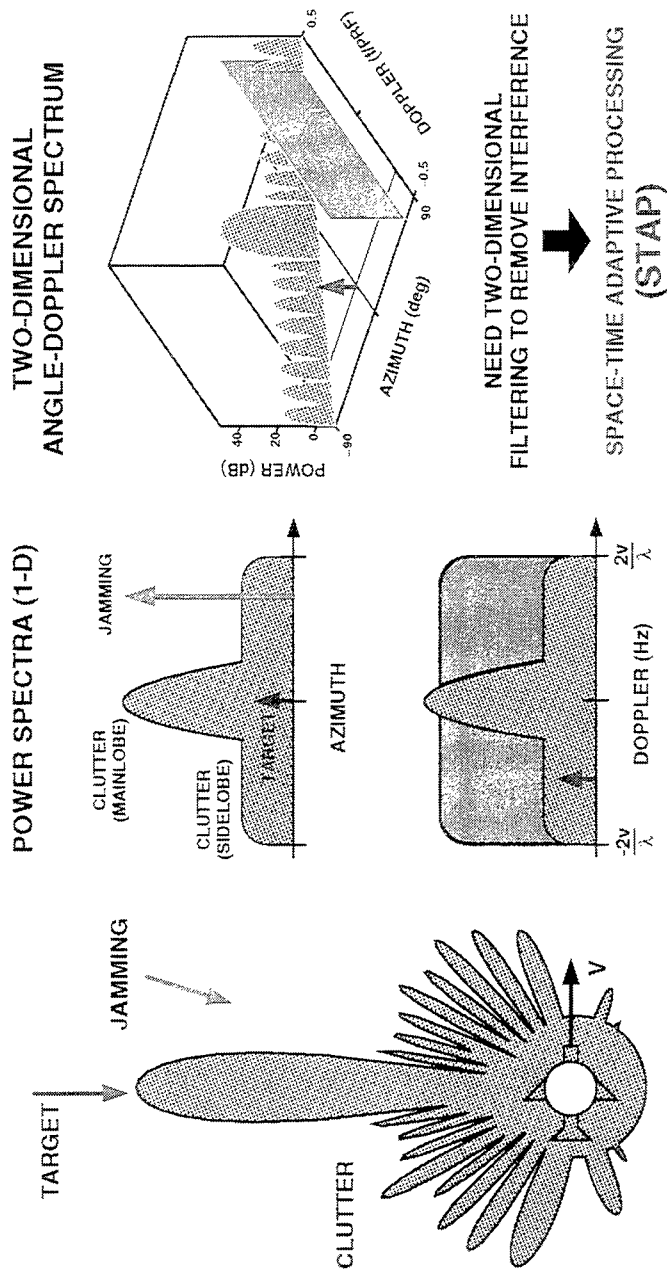
- INTRODUCTION
- STAP COVARIANCE ALGORITHM
- EXAMPLES
- CONCLUSIONS



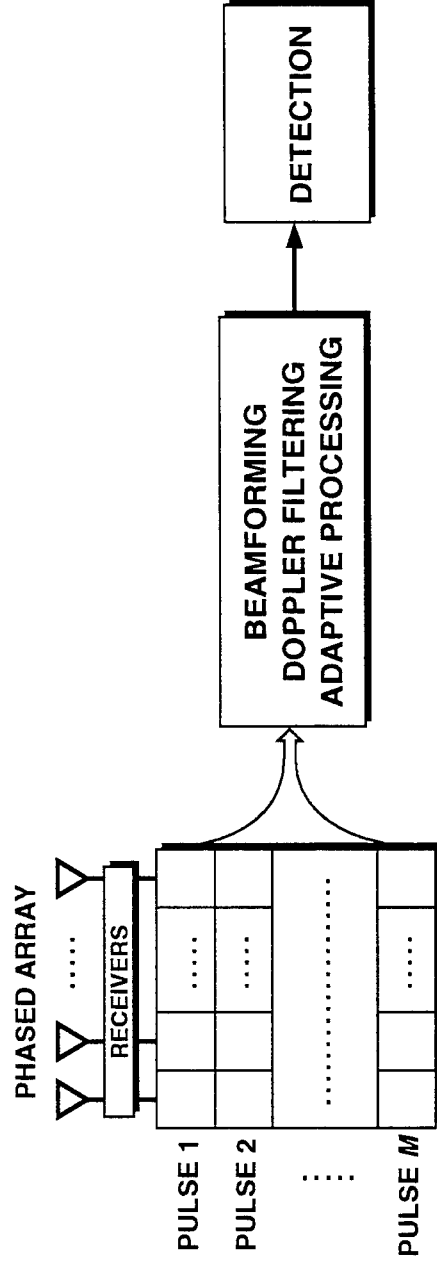
AIRBORNE EARLY WARNING (AEW) RADAR ENVIRONMENT



AEW RADAR SIGNAL SCENARIO



STAP BLOCK DIAGRAM

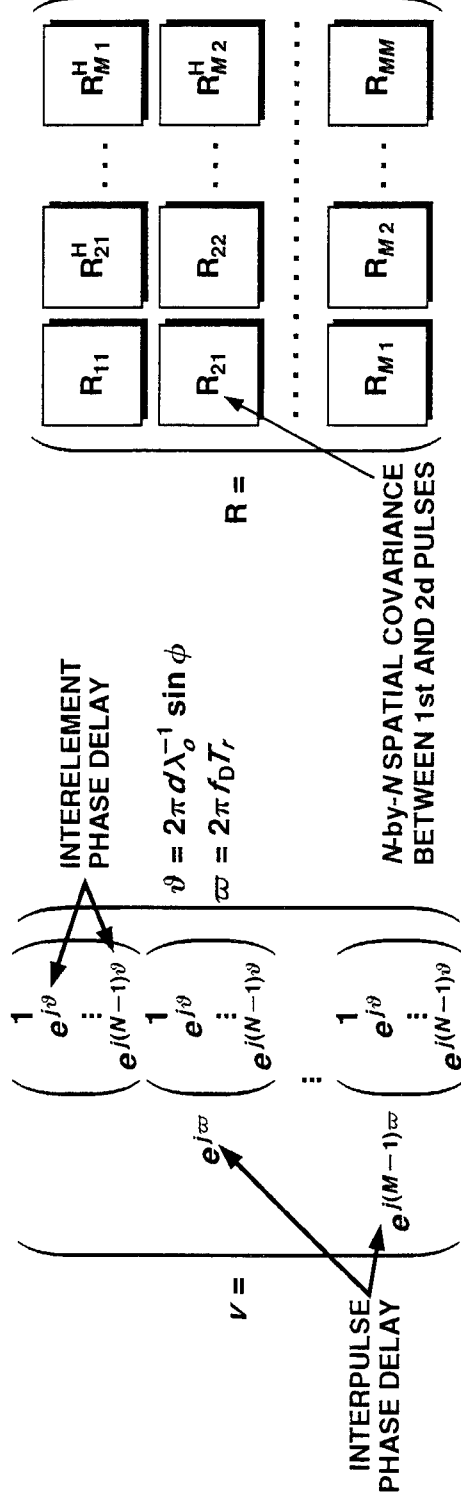


STAP AND SPACE-TIME COVARIANCE MATRICES

- FULLY ADAPTIVE WEIGHTS GIVEN BY

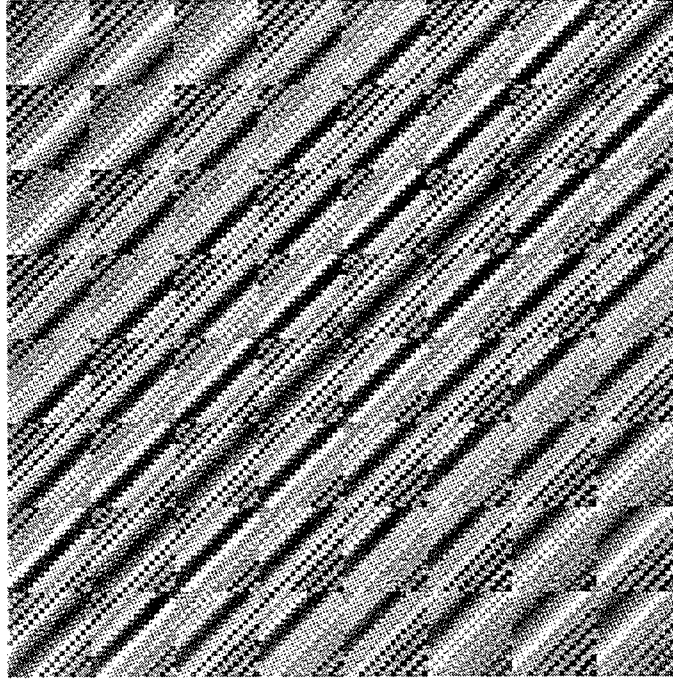
$$W = R^{-1}V$$

- $R = E[xx^H]$ = COVARIANCE MATRIX OF INTERFERENCE+NOISE
- V STEERED TO DESIRED ANGLE AND DOPPLER



- STAP REQUIRES ESTIMATE OF R

SPACE-TIME CLUTTER COVARIANCE MATRIX



$R_c =$

16 ELEMENTS
8 PULSES

ASAP '97 COVER:

```
N = 16;
M = 8;
cnr = 30;
beta = 2;
phin = 45;
cc = [0 2*20];

Rc = stccov(cnr,M,N,beta,phin,cc);

colormap('default'); colormap(jet); clf
imagesc(10*log10(abs(Rc)))
axis equal; axis off;
```



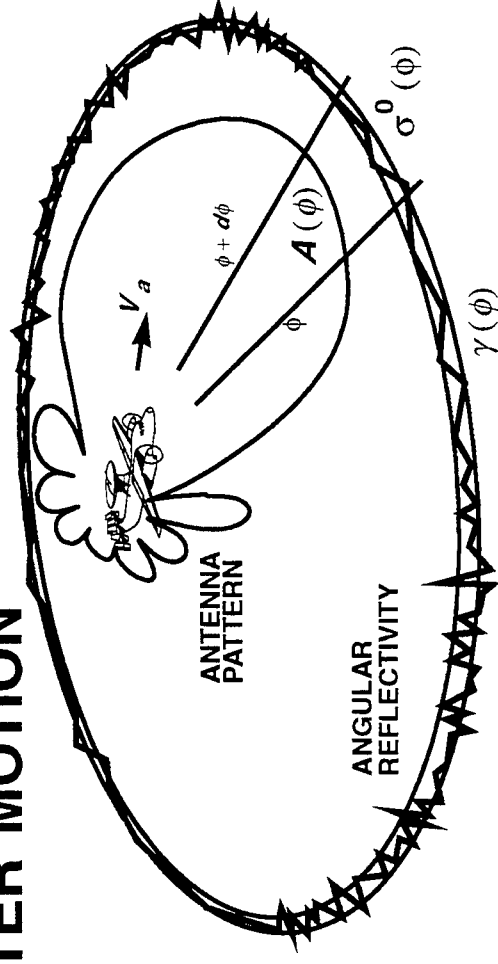
OUTLINE

- INTRODUCTION
- STAP COVARIANCE ALGORITHM
- EXAMPLES
- CONCLUSIONS



BASIC ASSUMPTIONS

- NO INTERNAL CLUTTER MOTION
- NARROWBAND



$$x_{mp} = \oint A(\phi) e^{j2\pi(m\varpi(\phi) + p\vartheta(\phi))} d\gamma(\phi) \quad \left(\begin{matrix} m\text{th Pulse} \\ p\text{th Element} \end{matrix} \right)$$

$\vartheta(\phi)$ = SPATIAL FREQUENCY

$\varpi(\phi)$ = DOPPLER FREQUENCY

$\gamma(\phi)$ = STOCHASTIC MODEL

} CLUTTER (Infinitesimal Patch)



SPACE-TIME CLUTTER COVARIANCE MATRIX

UNCORRELATED PATCH-TO-PATCH CLUTTER

$$(R_c)_{mn;pq} = E[x_{mp}x_{nq}^*] = \oint |A(\phi)|^2 \sigma^0(\phi) e^{j(z \sin \phi + w \cos \phi)} d\phi$$

- $(R_c)_{mn;pq}$ IS COVARIANCE BETWEEN mn -th PULSE AND pq -th ELEMENT PAIRS

$$z = 2\pi\xi((p - q) \cos \theta_d \sin \phi_d + (m - n)\beta \cos \theta_v \sin \phi_v)$$

$$w = 2\pi\xi((p - q) \cos \theta_d \cos \phi_d + (m - n)\beta \cos \theta_v \cos \phi_v)$$

$$\xi = d/\lambda_o \quad (\text{Interelement Spacing in Wavelengths})$$

$$\beta = 2v_a T_r / d \quad (\text{Slope of Clutter Ridge})$$

- R_c IS A TOEPLITZ-BLOCK-TOEPLITZ MATRIX

$$R_c = \begin{bmatrix} R_0 & R_1^H & R_2^H \\ R_1 & R_0 & R_1^H \\ R_2 & R_1 & R_0 \end{bmatrix}$$



COVARIANCE MATRIX COMPUTATION

- THE ELEMENTS OF R_c MAY BE EXPRESSED USING A FOURIER-BESSEL SERIES

$$(R_c)_{ik,jl} = C_0 J_0(a) + 2 \sum_{n=1}^{\infty} J_{2n}(a) C_{2n} \cos(2n\psi + \varphi_{2n}) + 2j \sum_{n=0}^{\infty} J_{2n+1}(a) C_{2n+1} \sin((2n+1)\psi + \varphi_{2n+1})$$

$$- a = (z^2 + w^2)^{1/2}, \quad \psi = \arg(z, w)$$

$J_\nu(a)$ IS A BESSEL FUNCTION OF THE FIRST KIND

C_n, φ_n ARE FOURIER COEFFICIENTS OF $|A(\phi)|^2 \sigma^0(\phi)$

MAIN CONTRIBUTIONS

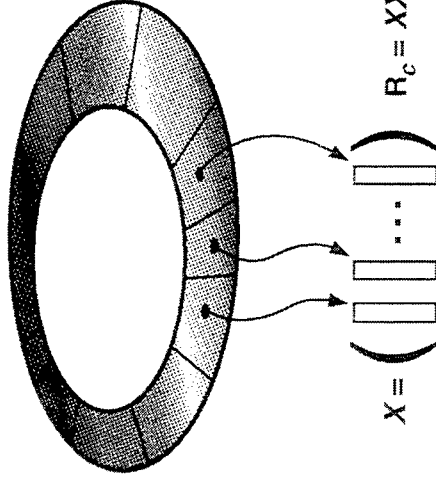
- FOURIER-BESSEL SERIES
- EXPLOIT TOEPLITZ STRUCTURE



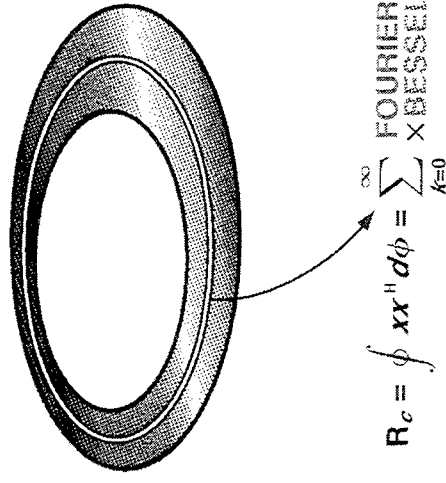
COVARIANCE MATRIX COMPUTATION

AZIMUTHAL VS. FOURIER DISCRETIZATION

RIEMANN SUM



FOURIER-BESSEL

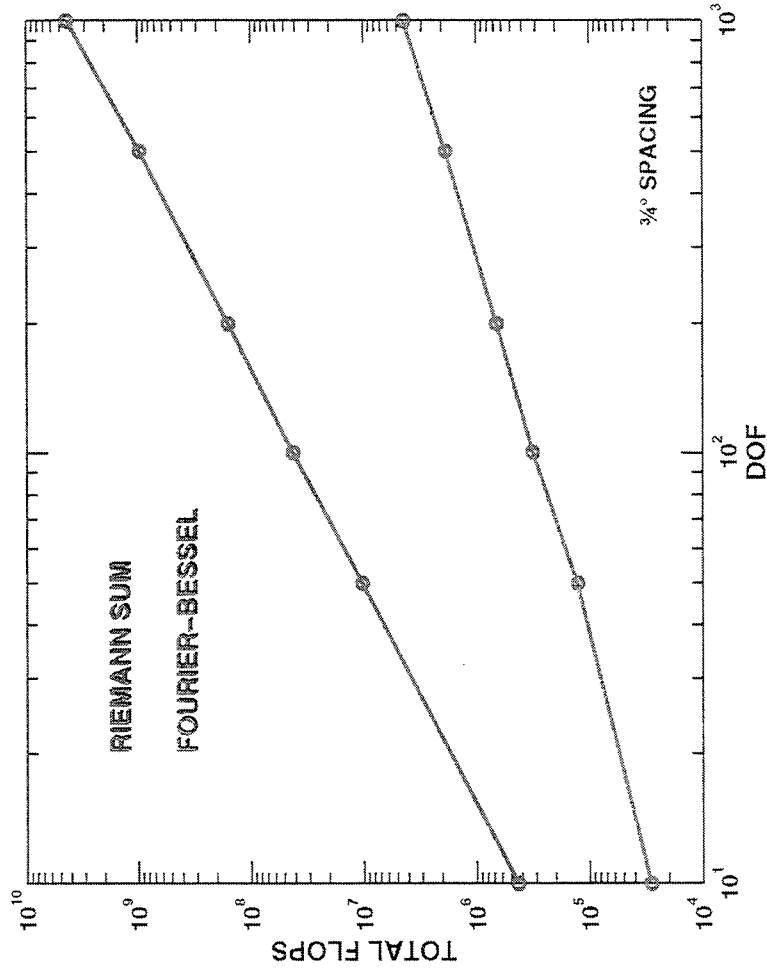


FOURIER-BESSEL BENEFITS

- FASTER
 - 100-1000x FOR $MN = 100-1000$, $3/4^\circ$ SPACING
- MORE ACCURATE
 - NO INADVERTANT CLUTTER DISCRETES

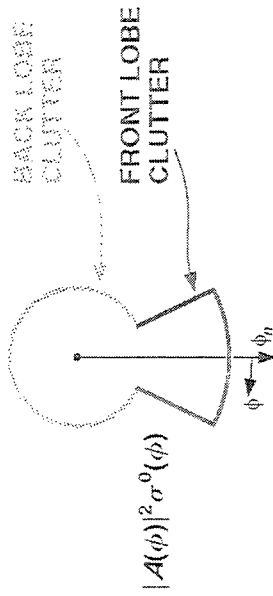
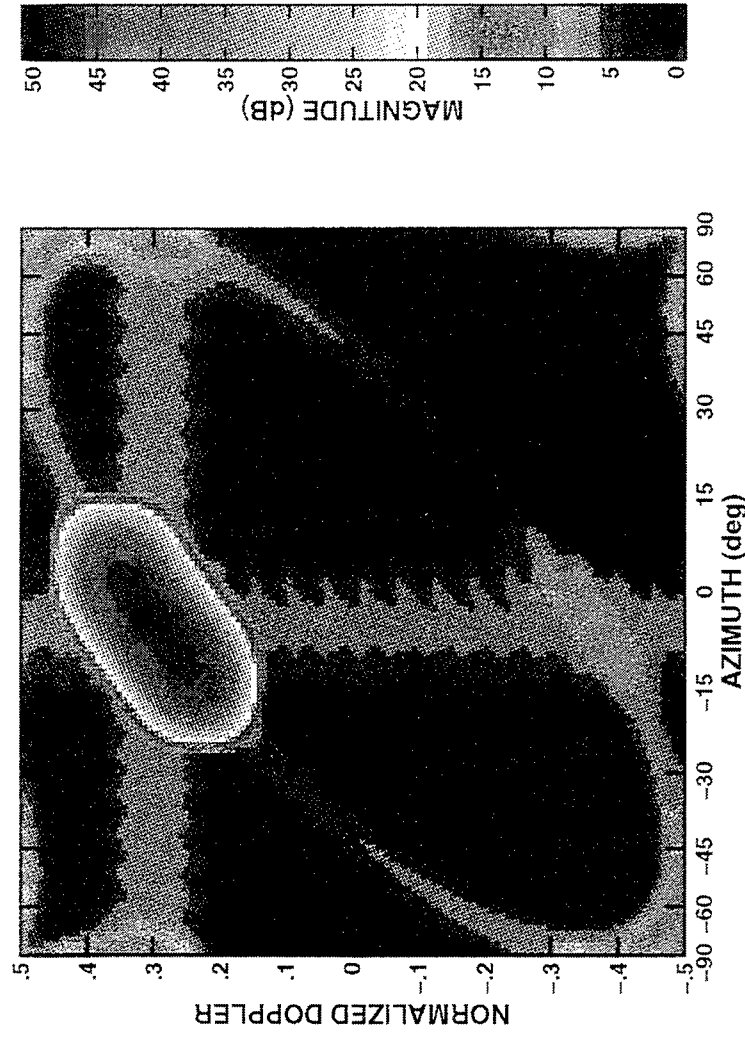
COST COMPARISON

RIEMANN SUM VS. FOURIER-BESSEL SERIES



CLUTTER POWER SPECTRAL DENSITY

EXAMPLE: KEYHOLE CLUTTER

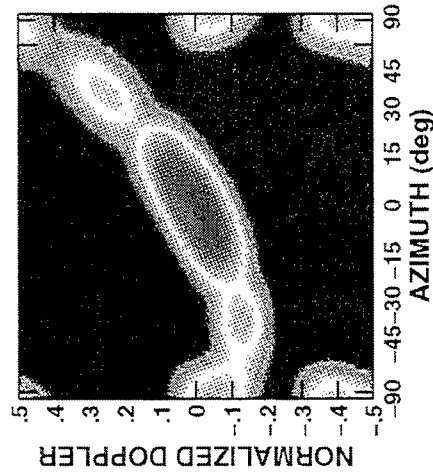


- 30 dB CNR BETWEEN -15° AND 5°
- 0 dB CNR ELSEWHERE
- 40 dB CHEBYSHEV SPATIAL AND DOPPLER TAPERS

PREDICTED VS. MEASURED CLUTTER RIDGE

MOUNTAINTOP DATA

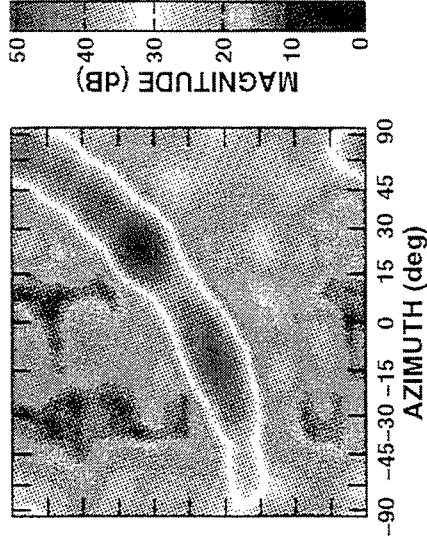
PREDICTED



SIMILARITIES

- CLUTTER RIDGE LOCATION
- ARRAY PARAMETERS
- TACCAR COMPENSATED

MEASURED



DIFFERENCES

- POWER ALONG CLUTTER RIDGE
- IDEAL VS. REAL DATA
- MOUNTAINS AND VALLEYS

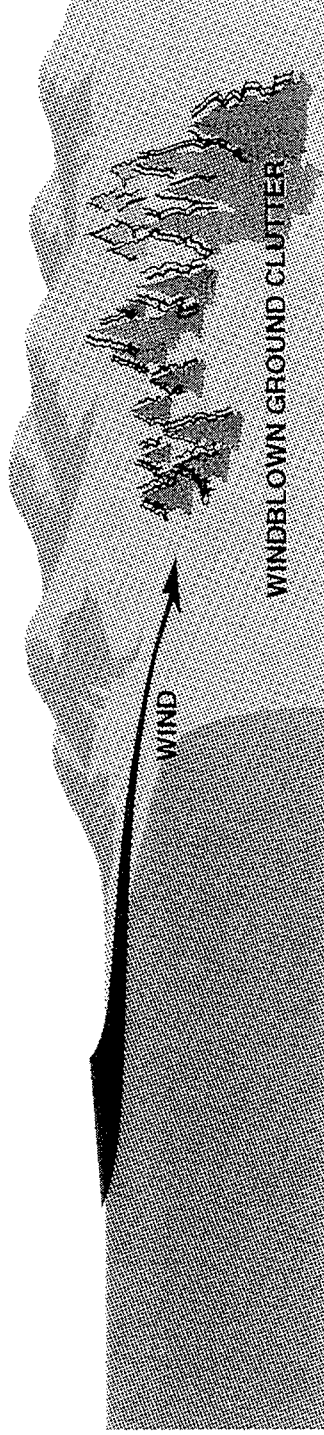


OUTLINE

- INTRODUCTION
- STAP COVARIANCE ALGORITHM
- EXAMPLES
 - BASELINE SCENARIO
 - ADDITIONAL EFFECTS
 - INTERNAL CLUTTER MOTION
 - BANDWIDTH EFFECTS
 - REDUCED DIMENSION STAP
- CONCLUSIONS



INTERNAL CLUTTER MOTION



• COVARIANCE MATRIX WITH ICM:

$$R_c = R_{ICM} \odot R_{NO \text{ ICM}}$$

- WHERE $R_{ICM} = \text{FOURIER}^{-1}(\text{ICM PSD}(\omega))$
- BILLINGSLEY'S ICM MODEL:

$$(R_{ICM})_{mn} = \frac{r}{r+1} + \frac{1/(r+1)}{1 + \left(\frac{\omega(m-n)}{\beta} \right)^2}, \quad \omega = \frac{2\pi}{\lambda \cdot \text{PRF}} \quad \beta = \text{PARAMETER}$$

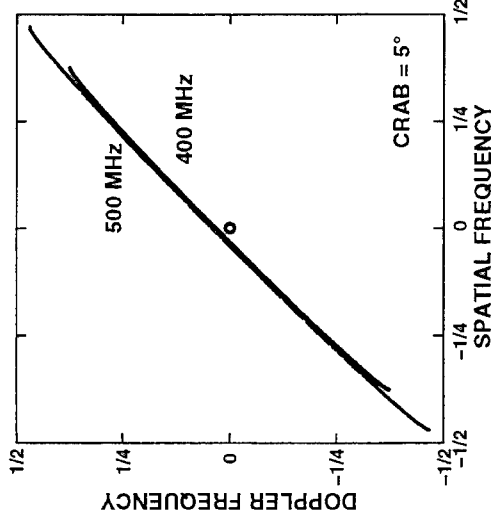
$$10 \log_{10} r = -15.5 \log_{10} v_w \text{ (dBmph)} - 12.1 \log_{10} f \text{ (dBMHz)} + 63.2$$



BANDWIDTH EFFECTS

- WIDEBAND:

$$R_c = \int_{BW} \psi(f) R_c(f) df$$



- $\psi(f)$ = WAVEFORM POWER SPECTRAL DENSITY
- LINEAR DILATION OF ZERO BANDWIDTH CLUTTER BY FRACTIONAL BANDWIDTH ABOUT DC (o)

- IMPLEMENT USING SLIGHTLY MODIFIED CODE



REDUCED DIMENSION STAP

- MANY REDUCED DIMENSION STAP ALGORITHMS HAVE SIMILAR TOEPLITZ STRUCTURE
 - PRI-STAGGERED POST-DOPPLER
 - BEAMSPACE POST-DOPPLER

- USE IDENTICAL FORMULATION:

$$\tilde{\mathbf{R}}_c = \oint \tilde{\mathbf{P}}(\phi) \tilde{\mathbf{v}}(\phi) \tilde{\mathbf{v}}^H(\phi) d\phi$$

$\tilde{\mathbf{P}}(\phi)$ = FILTERED PSD

$\tilde{\mathbf{v}}(\phi)$ = FILTERED STEERING VECTOR



SUMMARY

- **ANALYSIS TOOL FOR ADAPTIVE RADAR PERFORMANCE**
- **CLOSED FORM EXPRESSION DERIVED FOR CLUTTER COVARIANCE MATRIX**
 - COVERS BROAD RANGE OF SCENARIOS
- **FAST ALGORITHM DEVELOPED FOR COVARIANCE MATRIX COMPUTATION**
 - ABOUT 2 SECONDS FOR BASIC CASE, DOF = 300, ON HP WORKSTATION



On the Applicability of Principal Component Inverse (PCI) to Rapidly Adaptive Suppression of Terrain Scattered Interference (TSI)

Brian E. Freburger and Donald W. Tufts

University of Rhode Island

Kingston, RI 02881

email: brain@ele.uri.edu

Abstract Reduced-rank weight calculations are investigated to provide the faster adaptation required for effective suppression of Terrain Scattered Interference (TSI). Both element space Principal Component Inverse (PCI) and reduced-rank least squares for the generalized sidelobe canceller (GSLC) in beamspace are compared with each other and with their Sample Matrix Inverse (SMI) counterparts. More specifically, the case where training data is limited due to the non-stationarity of the jammer signal is considered. It is demonstrated using the Mountaintop data that in non-stationary environments such as an airborne jammer, using the reduced rank methods with training on the same data interval on which the weight vector will be applied yields better residual signal to jammer ratio than training on a nearby data interval. In fact the performance in this case is better than training on the entire pulse repetition interval using a full-rank or reduced-rank method. In addition the reduced-rank methods outperform the full-rank versions in the case where training data is limited by the availability or stationarity of the noise. Both reduced-rank methods investigated have similar performance, however, the element space PCI does not require recalculation of the weight vector for different matching vectors giving it a computational advantage.

On the Applicability of Principal Component Inverse (PCI) to Rapidly Adaptive Suppression of Terrain Scattered Interference (TSI)

B. E. Freburger and D.W. Tufts
Department of Electrical and Computer Engineering
University of Rhode Island
Kingston, RI 02881

Reduced-rank weight calculations are investigated to provide the faster adaptation required for effective suppression of Terrain Scattered Interference (TSI). Both element based Principal Component Inverse (PCI) and reduced-rank least squares for the generalized sidelobe canceller (RR-GSLC) in beamspace are compared with each other and with their Sample Matrix Inverse counterparts. More specifically, the case where training data is limited due to the non-stationarity of the received jamming is considered. We consider the case in which the reduced rank methods, PCI and reduced-rank generalized sidelobe canceling, are trained on the same data interval within which the associated weight vector will be applied. Using the Mountaintop data, we find that this procedure yields a significantly better residual signal-to-interference ratio than training on a nearby interval. In fact the performance in this case is comparable to or better than training on the entire pulse repetition interval using a full rank or reduced rank method. In addition the reduced rank methods outperform the full rank versions in the case where training data is limited by the availability or stationarity of the noise.

Both reduced rank methods investigated have similar performance, however the element based PCI does not require recalculation of the weight vector for different matching vectors giving it a computational advantage. A fast algorithm has been developed for the reduced rank method ("Fast Approximate Subspace Tracking (FAST)", D. W. Tufts, E. C. Real, J. W. Cooley).

This work was supported by the Statistical Signal Processing Program of the Office of Naval Research, Dr. Douglas Lake, Program Director.



OVERVIEW

- ADVANTAGES OF PCI APPROACH
- SPACE-TIME ADAPTIVE PCI
- RANK SELECTION PROCEDURE
- FOUR APPROACHES TO BE COMPARED
- EXPERIMENTS WITH MOUNTAINTOP DATA
- SLIDING WINDOW UPDATE METHOD
- CONCLUSIONS

ADVANTAGES OF PCI APPROACH

- FASTER ADAPTATION NEEDED FOR NON-STATIONARY DATA
- ABILITY TO TRAIN AND DETECT ON SAME INTERVAL
- SIMULTANEOUS CANCELLATION OF JAMMER IN ALL LOOK DIRECTIONS
- BECOMES CONVENTIONAL BEAM-DOPPLER STAP IN THE ABSENCE OF STRONG INTERFERENCE
- UTILIZE FAST LOW RANK ALGORITHMS FOR LOWER COMPUTATION

“Fast Approximate Subspace Tracking (FAST),” Tufts D.W., Real E.C. Cooley J.W,
ICASSP97, ASAP97

SPACE-TIME ADAPTIVE PCI

(HARRISON & TUFTS ASAP94, KIRSTEINS & TUFTS IEEE AES 1994)
DETECTION OF A RANDOM PHASE SIGNAL

$H_0 : X = V$ V IS A SPACE-TIME ZERO MEAN GAUSSIAN COLUMN VECTOR

$H_1 : X = e^{j\phi} S + V$ S IS A KNOWN SPACE-TIME SIGNAL VECTOR

$R = E(VV^H) = Q + \sigma^2 I$ COVARIANCE OF THE NOISE

WHERE Q IS LOW RANK AND ϕ IS UNIFORM $[0, 2\pi]$.

LIKELIHOOD RATIO TEST STATISTIC $LRT = \frac{1}{2} |S^H R^{-1} X| = \frac{1}{2} |S^H (I - WP) X|$

$WP = \sum_{k=1}^n \frac{\lambda_k}{\lambda_k + \sigma^2} Q_k Q_k^H$ A WEIGHTED PROJECTION MATRIX

Q_k IS THE k^{th} SINGULAR VECTOR OF Q .

SPACE-TIME ADAPTIVE PCI

SMI: ESTIMATE R AND USE $GLRT = \left| S^H \hat{R}^{-1} X \right|$ (REED, MALLET & BRENNAN 1974)

PCI: ESTIMATE WP AND USE $GLRT = \left| S^H (I - \hat{WP}) X \right|$ (HARRISON & TUFTS, ASAP94)
(KIRSTEINS & TUFTS ICASSP85)

IF Q IS THE COVARIANCE OF r STRONG JAMMER COMPONENTS THEN

$$\lambda_k \gg \sigma^2 \text{ for } 1 \leq k \leq r \text{ and } \lambda_k \approx 0 \text{ for } k > r$$

AND SO, THE WEIGHTED PROJECTION IS APPROXIMATELY A PROJECTION

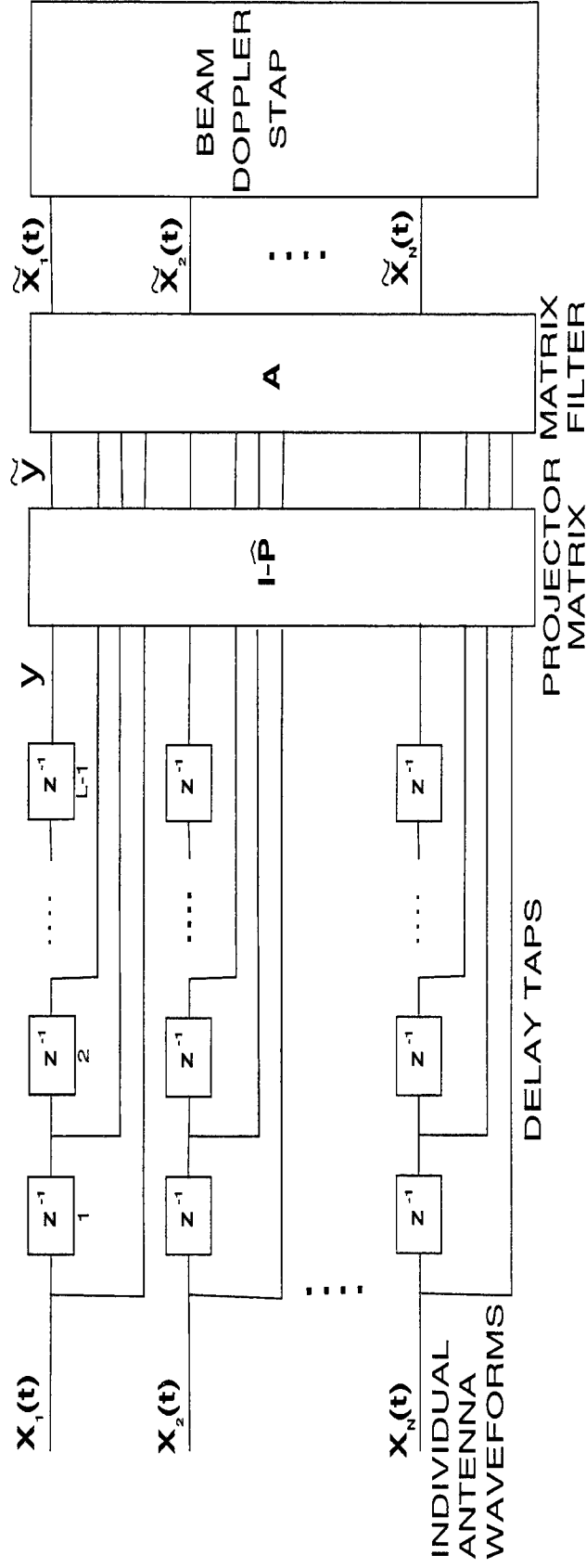
$$WP \approx P = \sum_{k=1}^r Q_k Q_k^H$$

THE TEST WITH ESTIMATED REDUCED RANK COVARIANCE IS THEN GIVEN BY

$$GLRT = \left| S^H \left(I - \sum_{k=1}^r \hat{Q}_k \hat{Q}_k^H \right) X \right|$$

VECTORIZED SPACE-TIME ADAPTIVE PCI (VST/PCI)

VECTORIZED SPACE-TIME PCI (VST/PCI)



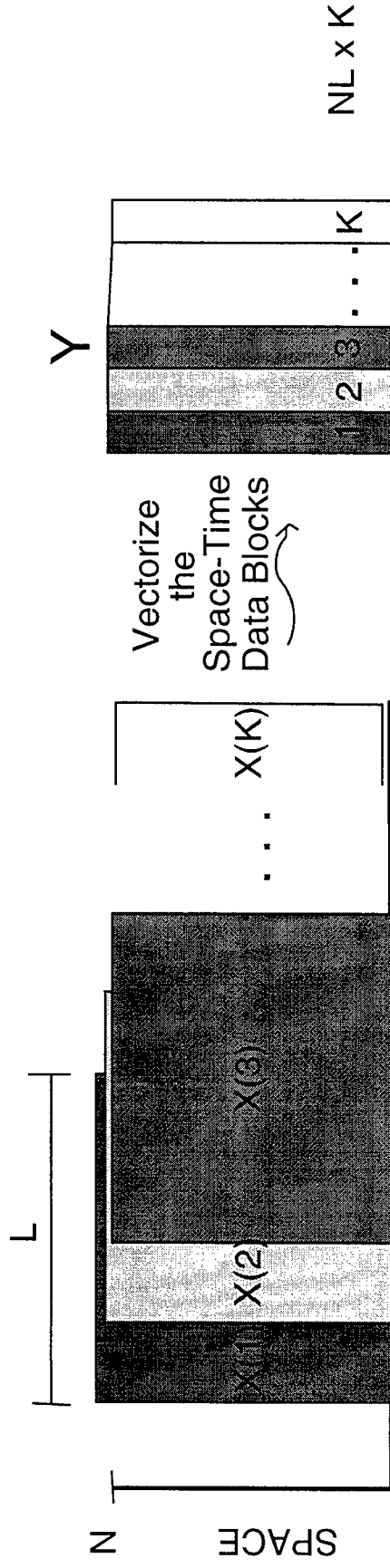
MATRIX A OPERATES ON THE SUBSPACE DATA TO PRODUCE A "CLEANED" VERSION OF THE INDIVIDUAL ANTENNA WAVEFORMS.

IN CONTRAST TO BEAMSPACE CANCELLER, ONLY ONE CLEANING OPERATION REQUIRED FOR ALL ANGLES OF ARRIVAL.

CONVENTIONAL STAP PROCESSING THEN FOLLOWS.

ESTIMATE of PROJECTION MATRIX

A MATRIX Y IS FORMED USING VECTORIZED SPACE-TIME DATA BLOCKS



TIME SAMPLES WITHIN PRI

TRAINING DATA MATRIX

$$Y = [\text{vec}(X(1)) \text{ vec}(X(2)) \text{ vec}(X(3)) \dots \text{vec}(X(K))]$$

THE PROJECTION IS THEN CALCULATED AS

$$\hat{P} = U_r U_r^H$$

WHERE U_r CONTAINS THE r SINGULAR VECTORS CORRESPONDING TO THE r LARGEST SINGULAR VALUES OF $Y = U \Sigma V^H$.

RANK SELECTION

BASIC PRINCIPLES:

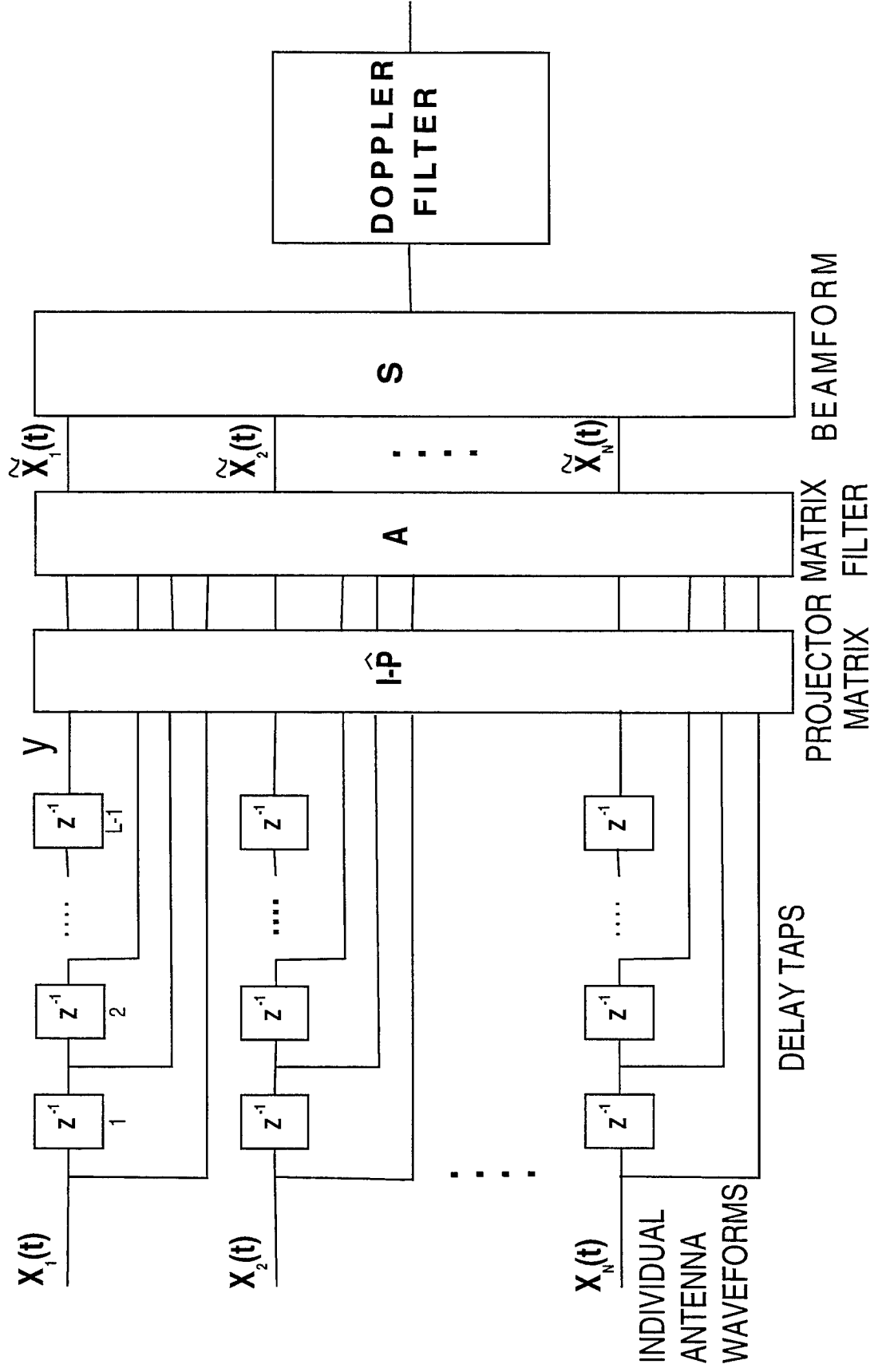
1.) UNDER CONDITIONS OF NO STRONG JAMMING, ANTENNA WAVEFORMS SHOULD PASS THROUGH PCI PROCESSING UNCHANGED

2.) THRESHOLD SHOULD ALLOW MAX EXPECTED SIGNAL AT CURRENT RANGE AND LOW LEVEL CLUTTER TO PASS THROUGH PCI PROCESSING UNCHANGED

- FIND SMALLEST S , S_{\min} FOR WHICH $\sum_{k=0}^S \sigma_{N-k}^2 > T$ WHERE σ_k IS THE k^{th} SINGULAR VALUE OF THE SPACE-TIME DATA MATRIX Y . CHOOSE $\text{RANK} = N - S_{\min}$ WHERE N IS THE ROW DIMENSION OF Y AND T IS THE THRESHOLD VALUE.
- WHEN $S_{\min} = N$ THEN THE $\text{RANK} = 0$ AND NO INTERFERENCE SUPPRESSION IS APPLIED (THAT IS PCI IS TURNED OFF)

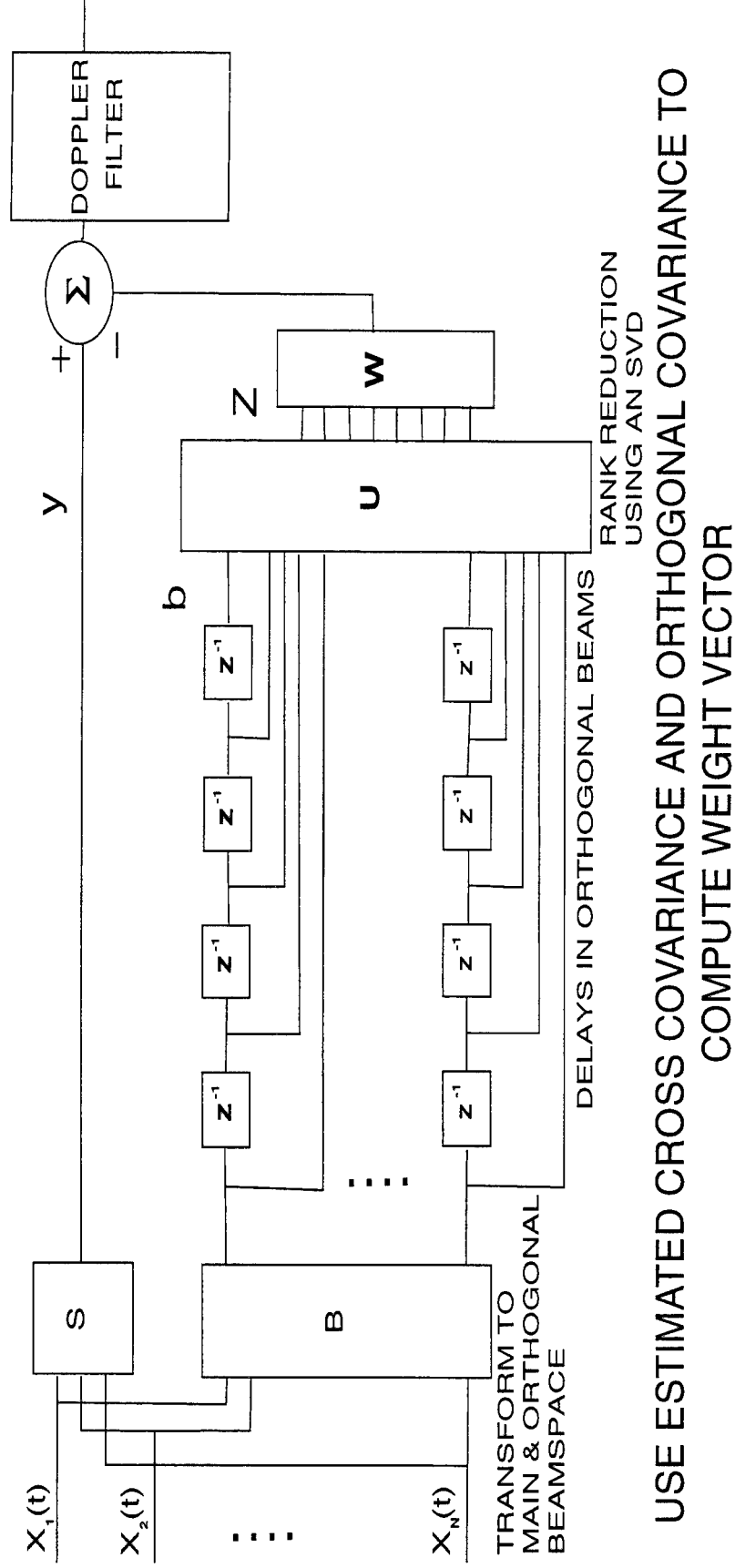
VECTORIZED SPACE TIME PCI (VST/PCI)

VECTORIZED SPACE-TIME PCI (VST/PCI) (PLOT A BELOW)



BEAMSPACE CANCELLER STRUCTURE

(FULL RANK VERSION - KOGON S.M., WILLIAMS D.B. & HOLDER E.J. 1996)



$$\hat{W} = \hat{R}_z^{-1} \hat{r}_{yz}$$

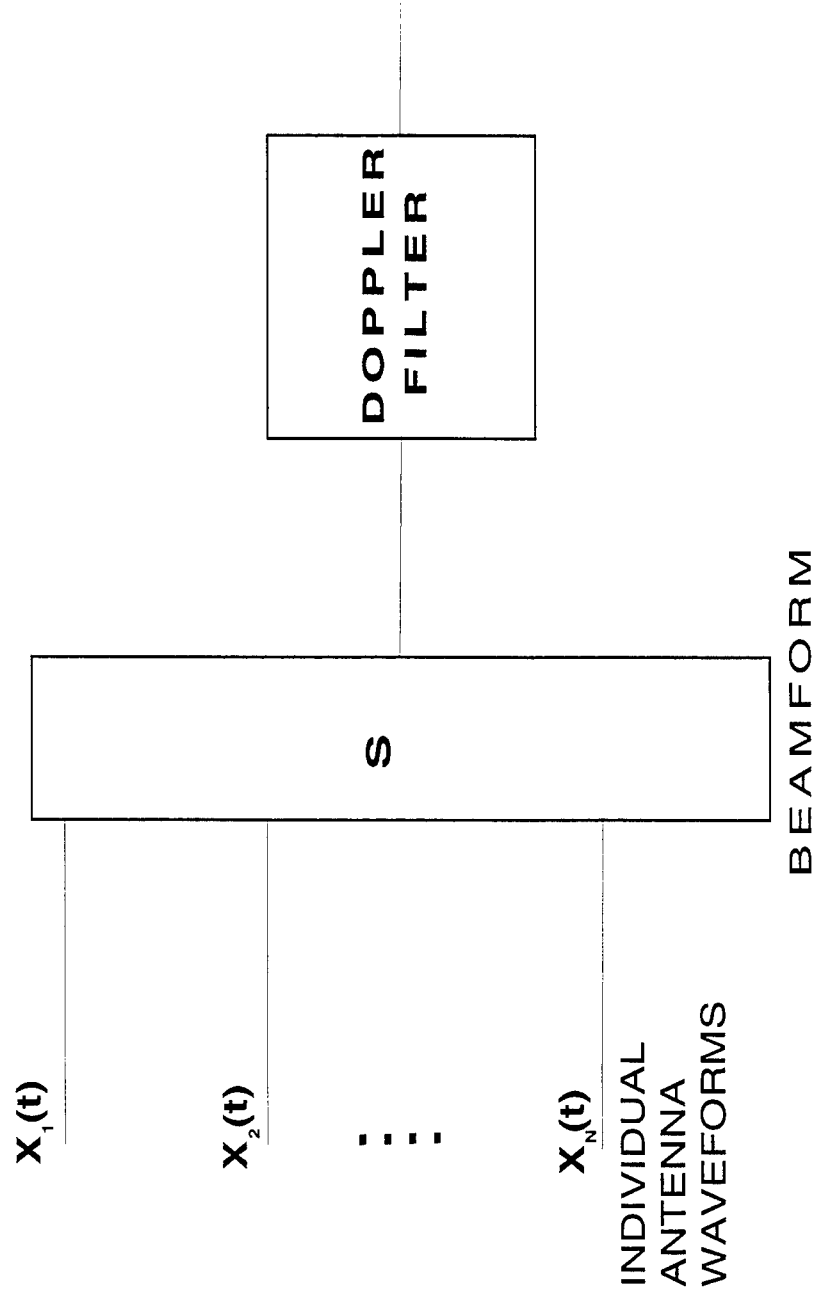
FULL RANK BEAMSPACE CANCELLER, $U = I$ (PLOT C BELOW)

REDUCED RANK BEAMSPACE CANCELLER, U REDUCES THE DIMENSION OF THE

SPACE USING r SINGULAR VECTORS OF \hat{R}_b . (PLOT B BELOW)

CONVENTIONAL PROCESSING

CONVENTIONAL PROCESSING (PLOT D BELOW)



THIS BASELINE APPROACH IS INCLUDED FOR COMPARISON.



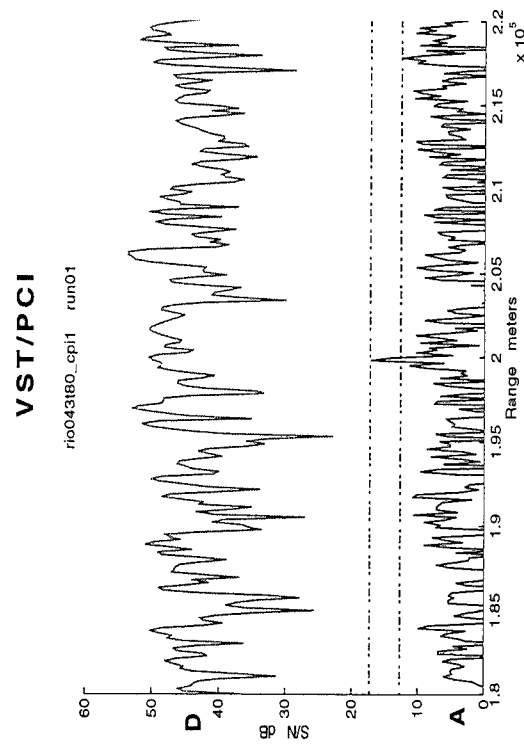
TARGET WITHIN TRAINING INTERVAL

IMPROVED RESIDUAL SNR ON LOCAL INTERVAL TRAINING

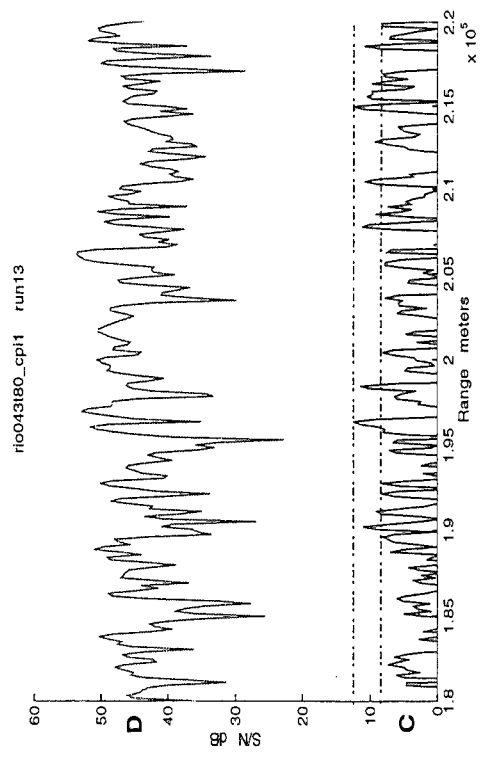
AIRBORNE JAMMER - RIO043
 4 PULSES 40 TAPS
 INJECTED TARGET 24 dB SNR at 200 Km,
 150Hz, BROADSIDE
 TRAINING 150 - 250 Km

Table 1: S to Peak N in Suppression Interval

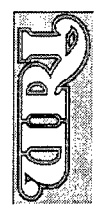
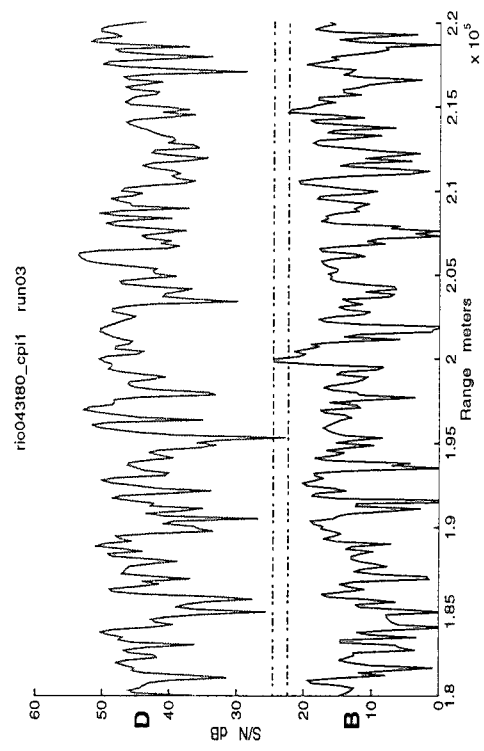
	VST/PCI (A)	RR-BC (B)	FR-BC (C)
S to Pk N	~ +5 dB	~ +2.5 dB	~ -5 dB



FULL RANK BEAMSPEACE CANCELLER



REDUCED RANK BEAMSPEACE CANCELLER



TARGET NEARBY TRAINING INTERVAL

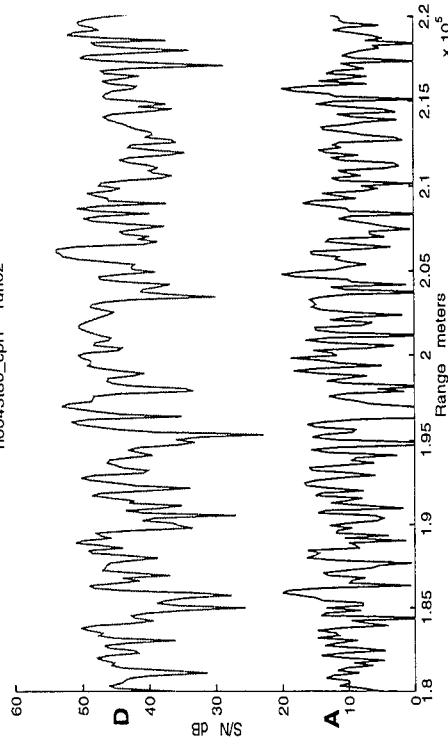
DEGRADED PERFORMANCE COMPARED TO LOCAL TRAINING

AIRBORNE JAMMER - RIO043
 4 PULSES 40 TAPS
 INJECTED TARGET 24 dB SNR at 200 Km,
 150Hz, BROADSIDE
 TRAINING 250 - 350 Km

RESIDUAL JAMMER OBSCURES TARGET
 FOR ALL THREE METHODS
 DATA IS NON-STATIONARY

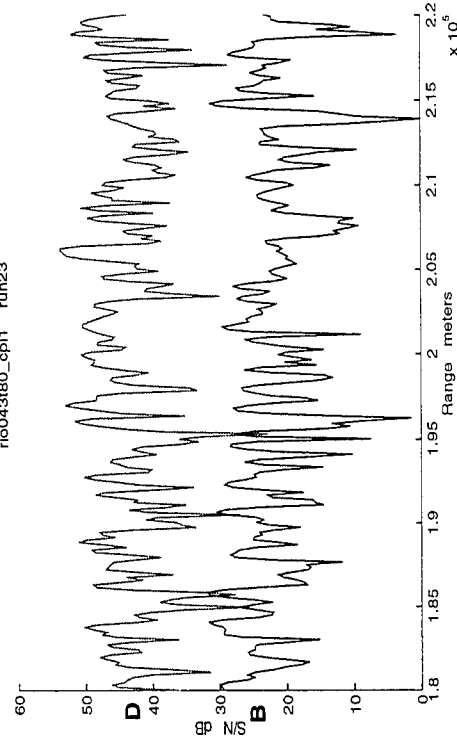
VST/PCI

rio043180_cpi1 run02



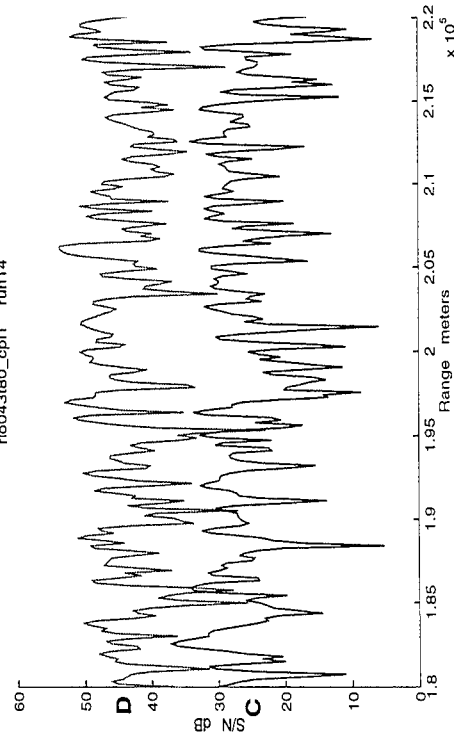
REDUCED RANK BEAMSPE CANCELLER

rio043180_cpi1 run23



FULL RANK BEAMSPE CANCELLER

rio043180_cpi1 run14



FULL PRI TRAINING

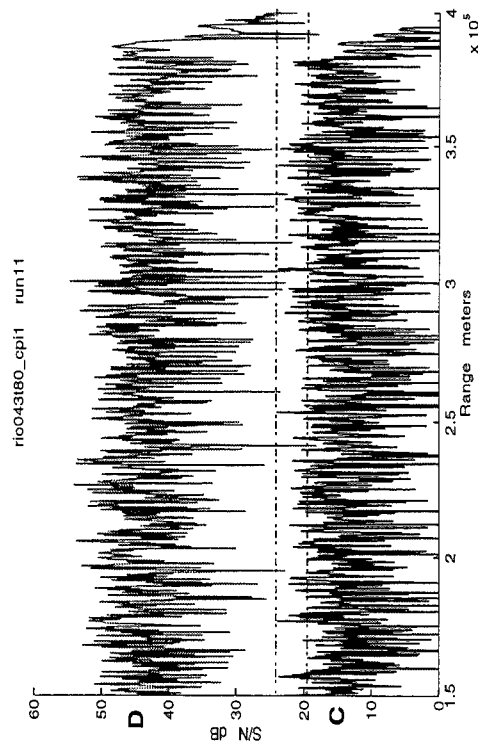
IMPROVED RESIDUAL SNR WITH FULL PRI TRAINING

AIRBORNE JAMMER - RIO043
 4 PULSES 40 TAPS
 INJECTED TARGET 24 dB SNR at 200 Km,
 150Hz, BROADSIDE
 TRAINING - FULL PRI

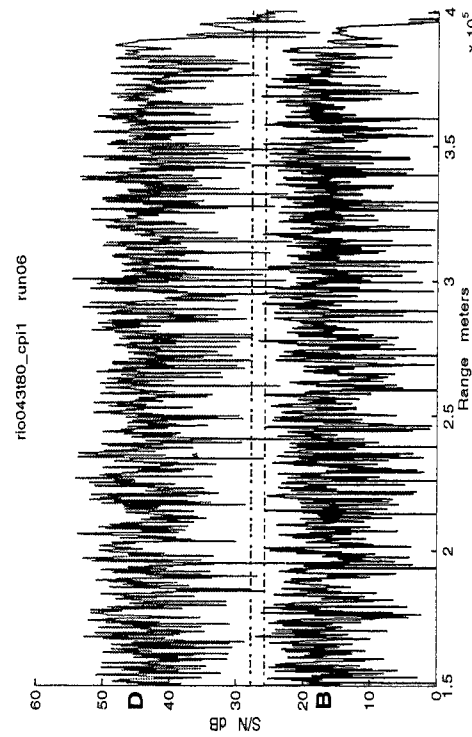
Table 1: S to Peak N in Suppression Interval

	VST/PCI (A)	RR-BC (B)	FR-BC (C)
S to Pk N	~ +5 dB	~ -2 dB	~ -5 dB

FULL RANK BEAMSPEACE CANCELLER

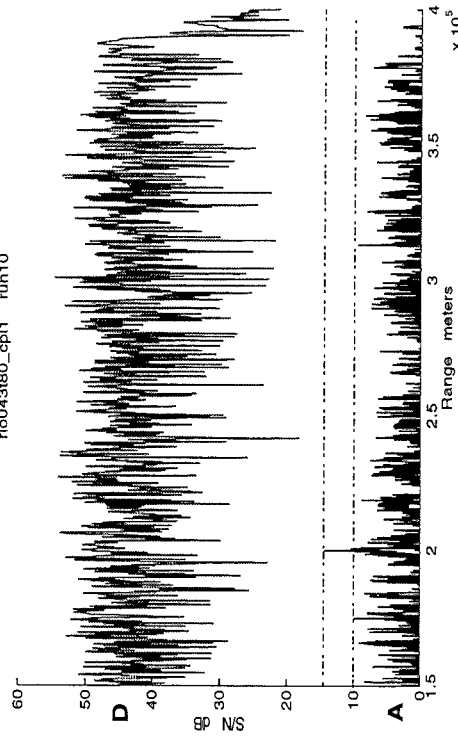


REDUCED RANK BEAMSPEACE CANCELLER

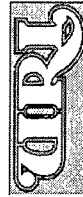


VST/PCI

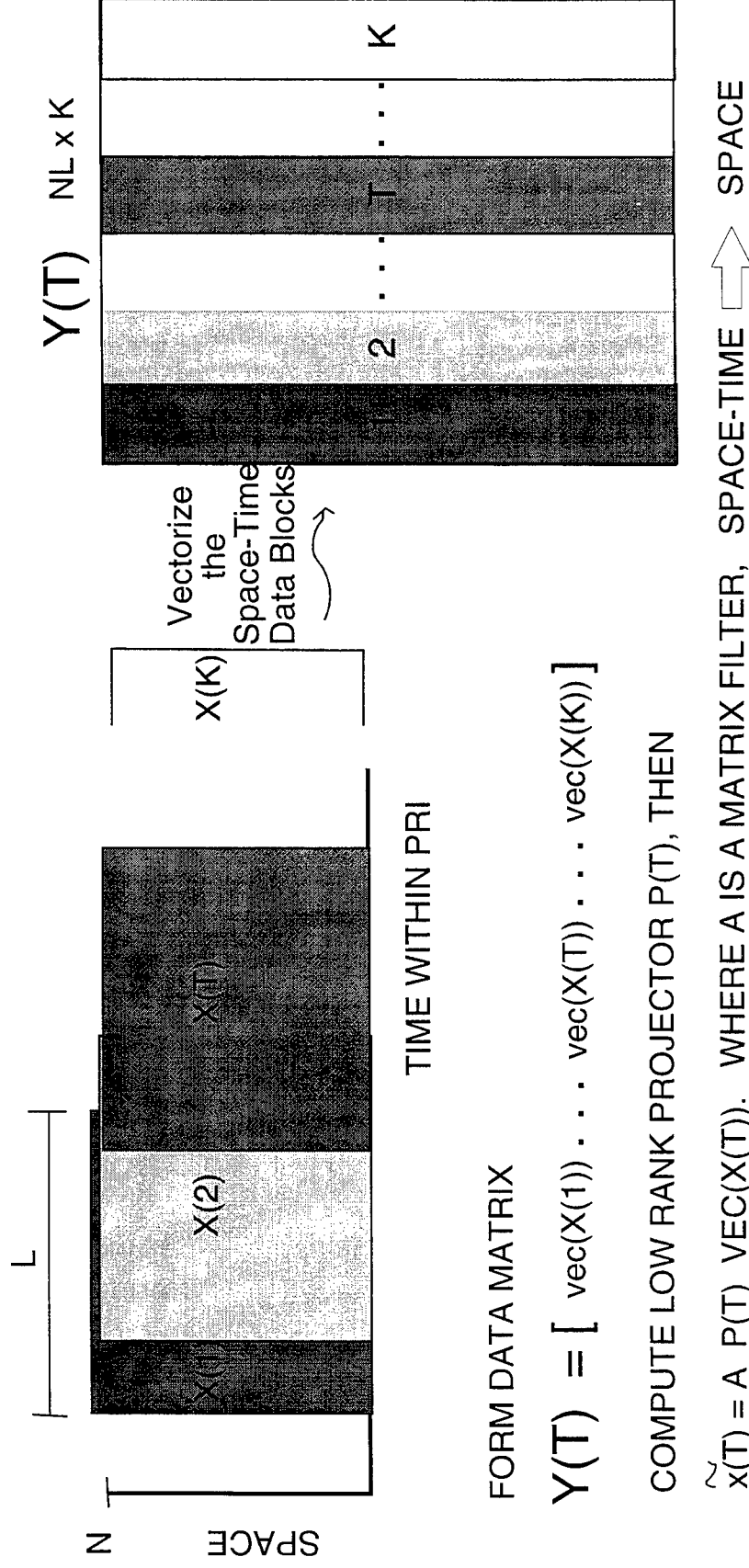
rio043180_cpl1 run10



rio043180_cpl1 run06



SLIDING WINDOW UPDATE METHOD



FORM DATA MATRIX

$$Y(T) = [\text{vec}(X(1)) \dots \text{vec}(X(T)) \dots \text{vec}(X(K))]$$

COMPUTE LOW RANK PROJECTOR $P(T)$, THEN

$\tilde{x}(T) = A P(T) \text{VEC}(X(T))$. WHERE A IS A MATRIX FILTER, SPACE-TIME \rightarrow SPACE

$\tilde{x}(T)$ IS THE "CLEANED" SNAPSHOT AT TIME T .

SLIDE WINDOWS FOR NEW MATRIX

$$Y(T+1) = [\text{vec}(X(2)) \dots \text{vec}(X(T+1)) \dots \text{vec}(X(K+1))]$$

USE SVD UPDATE ALGORITHM TO COMPUTE $P(T+1)$, THEN $\tilde{x}(T+1)$.

SLIDING WINDOW METHOD

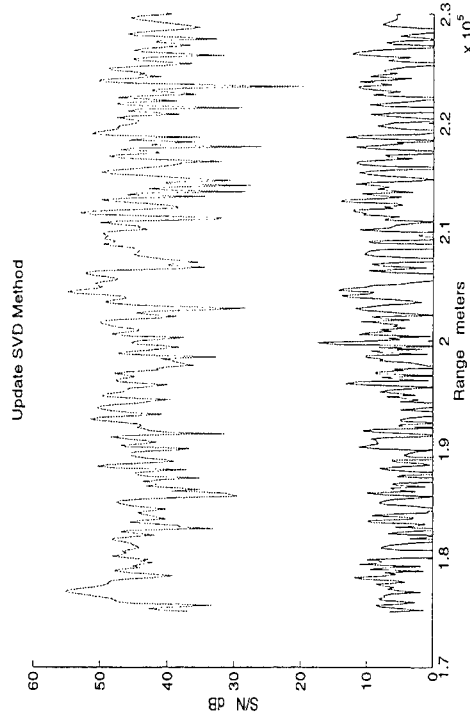
SLIDING WINDOW METHOD REDUCES RESIDUAL AT 225 Km

AIRBORNE JAMMER - RIO043
1 PULSE 40 TAPS
INJECTED TARGET 28dB SNR at 200 Km,
150Hz, BROADSIDE

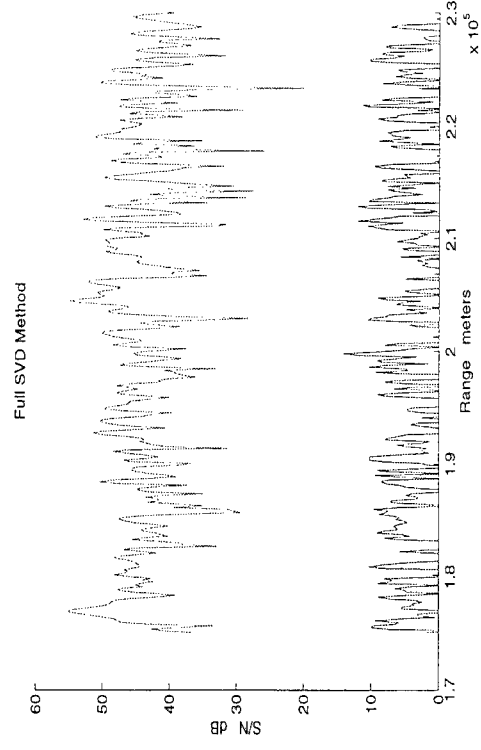
Table 1: COMPUTATION MATLAB FLOPS

	VST/PCI	SVD UPDATE	SVD FULL
MATLAB FLOPS	8.3E09	3.9E11	3.3E12

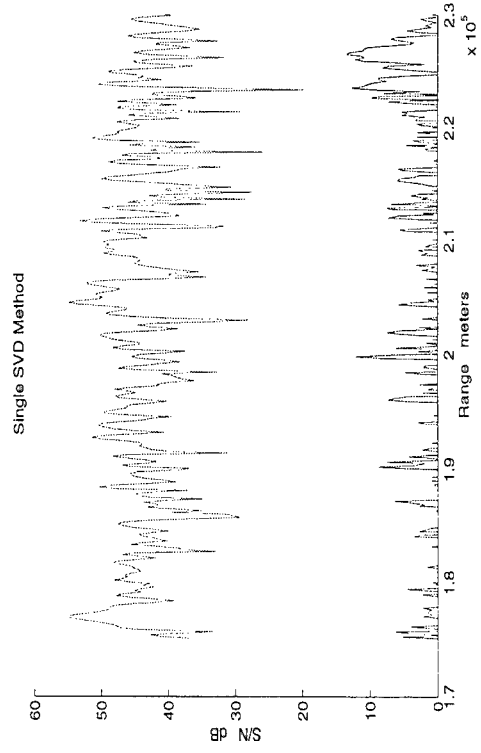
SLIDING WINDOW PCI w/SVD UPDATE



SLIDING WINDOW PCI w/FULL SVD



VST/PCI



CONCLUSIONS

- VST/PCI PROVIDED HIGHER RESIDUAL SIGNAL TO JAMMER RATIO FOR LOCAL AND FULL PRI TRAINING THAN THE FULL OR REDUCED RANK BEAMSPACE CANCELLER
- THE REDUCED RANK METHODS (VST/PCI AND RR-BEAMSPACE) PERFORMED BETTER WITH LOCAL TRAINING THAN FULL RANK BEAMSPACE
- IMPROVED PERFORMANCE IS OBTAINED WITH LOCAL TRAINING DATA FOR THE NON-STATIONARY AIRBORNE JAMMER CASE
- SLIDING WINDOW METHOD MAY BE NECESSARY IN HIGHLY NON-STATIONARY ENVIRONMENTS

**SESSION II:
SPACE-TIME ADAPTIVE PROCESSING
(STAP)**

DR. WILLIAM P. BALLANCE
SESSION CHAIR

12 MARCH 1997

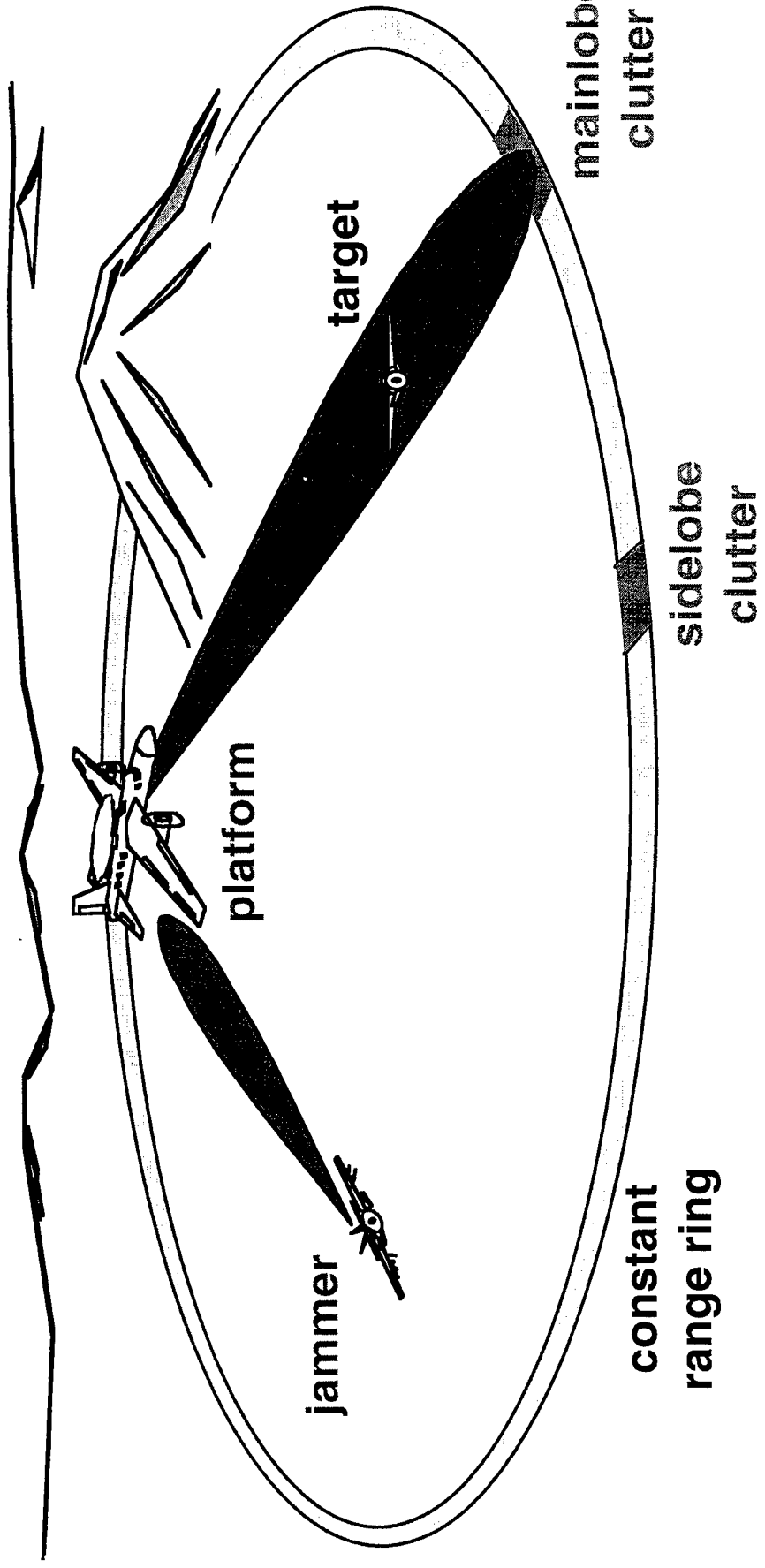
OUTLINE



- **PROBLEM DESCRIPTION**
- **CHALLENGES / RESEARCH AREAS**
- **OVERVIEW OF PAPERS IN SESSION**

AIRBORNE RADAR SCENARIO

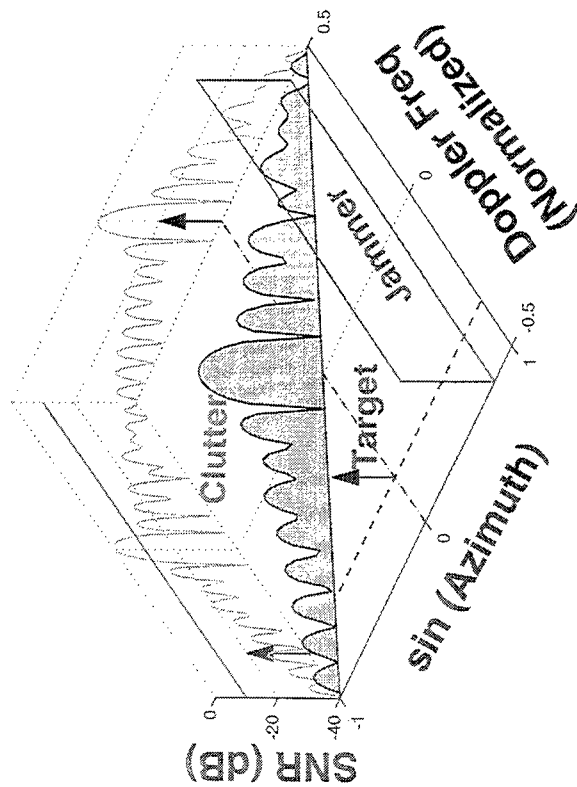
HUGHES
AIRCRAFT



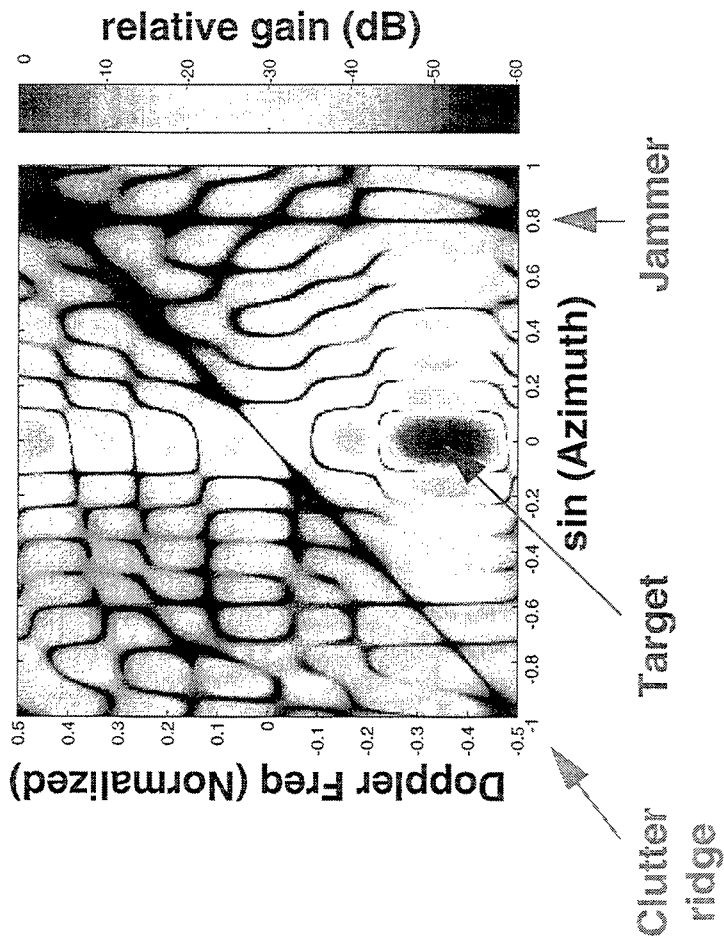
SPATIAL-DOPPLER SPECTRUM OF CLUTTER AND JAMMING

HUGHES
AIRCRAFT

SPECTRUM



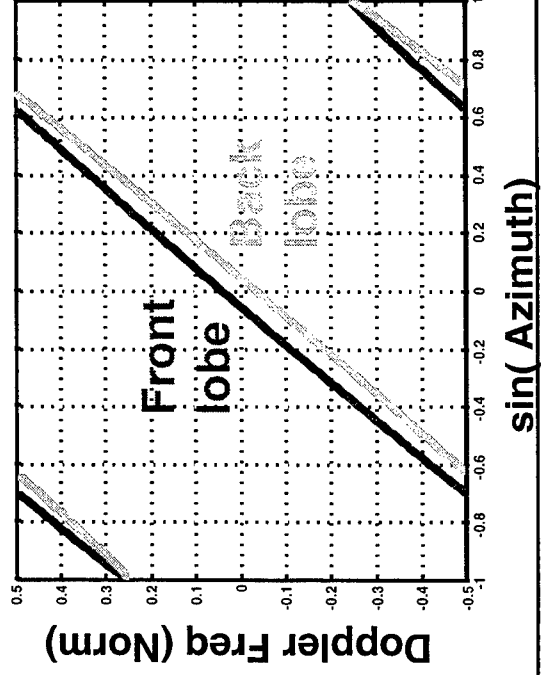
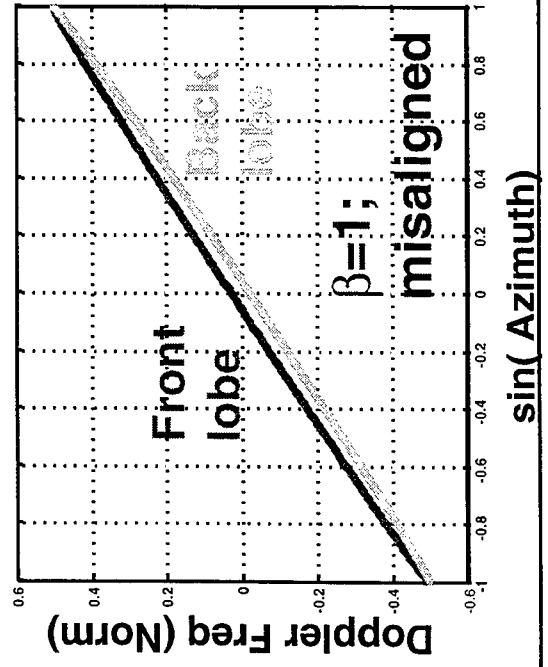
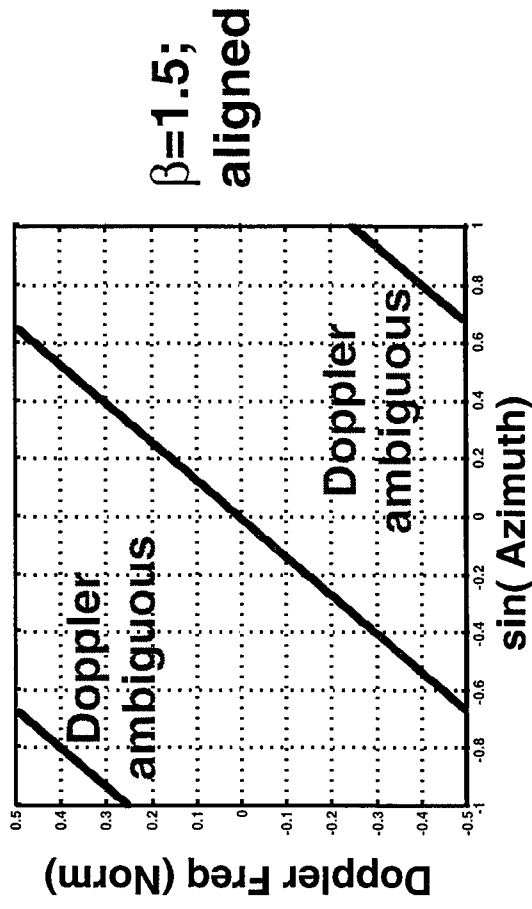
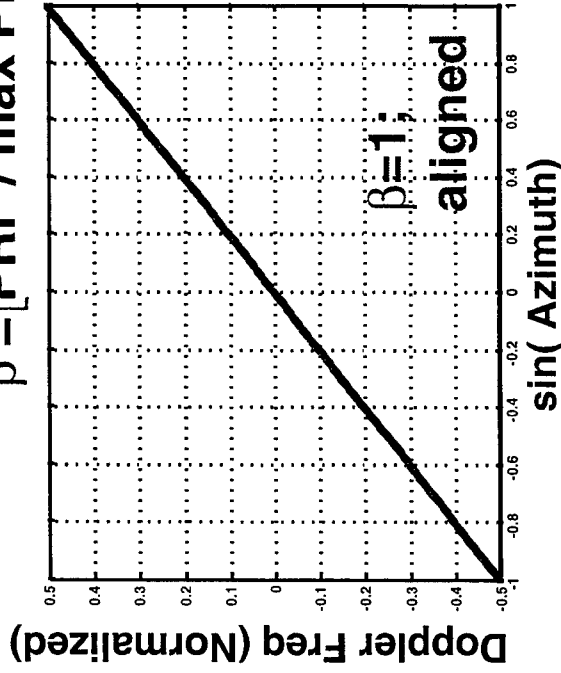
ADAPTED SPACE-TIME PATTERN



CLUTTER RIDGE: IMPACT OF PRF AND OF ARRAY MISALIGNMENT

HUGHES
AIRCRAFT

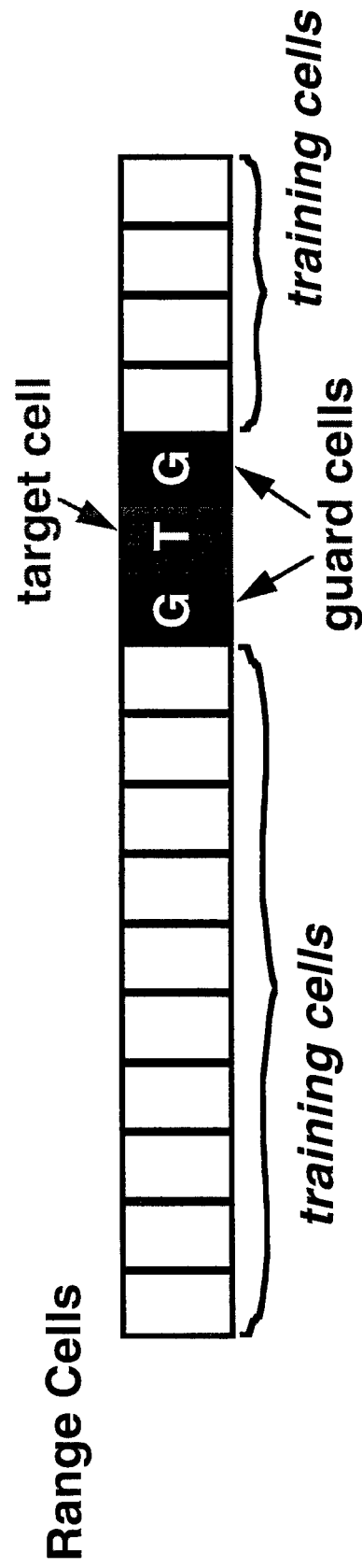
$\beta = [\text{PRF} / \text{max PRF with no clutter Doppler ambiguity}]^{-1}$



WEIGHT ESTIMATION / TRAINING

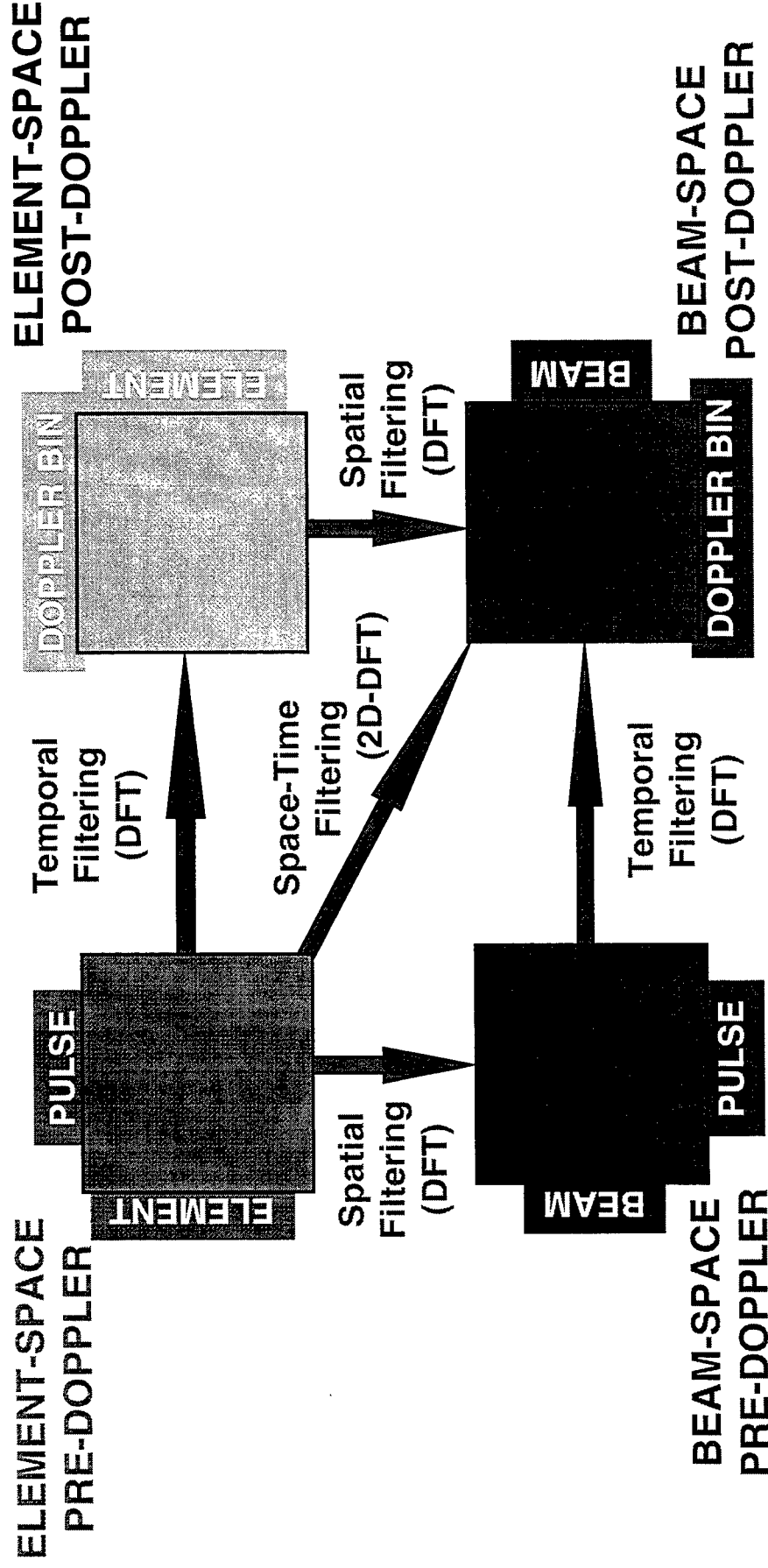


Terrain Can Vary as a Function of Range
Within the Beam



A TAXONOMY OF STAP ARCHITECTURES*

HUGHES
AIRCRAFT



Architectures Classified By:

- Type of preprocessor
- Domain in which adaptive weighting occurs

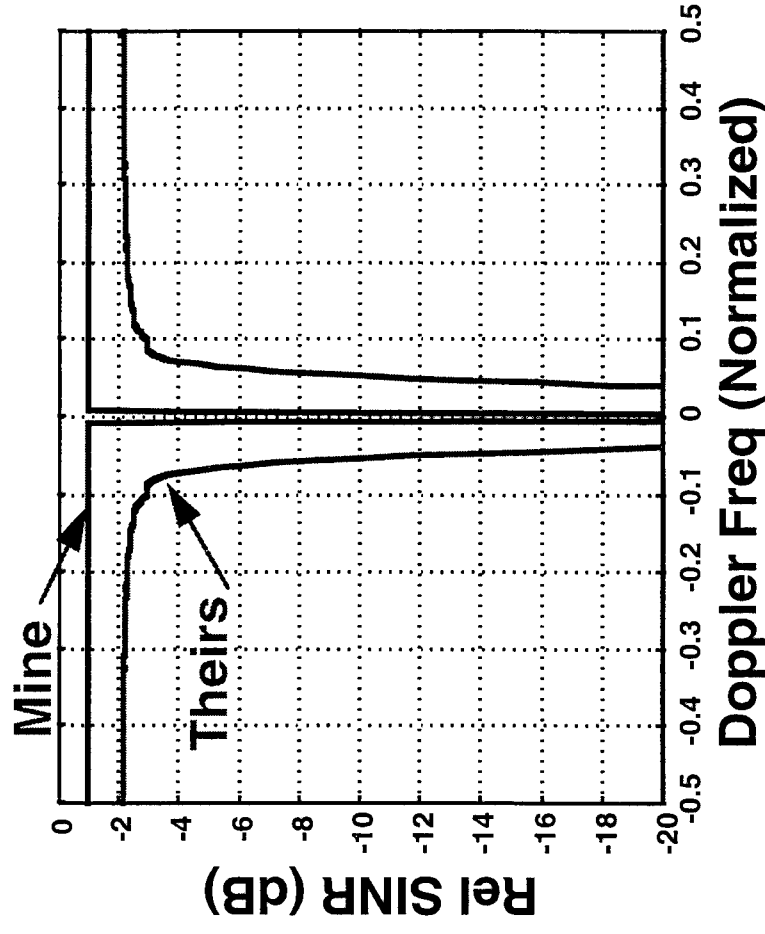
*courtesy of
Jim Ward, MIT/LL

SINR PERFORMANCE

HUGHES
AIRCRAFT

- SINR: Signal to Interference plus Noise Ratio
 - interference is clutter + jamming
- SINR is relative to the SINR that would be achieved in a benign (noise only) environment, with no spatial or Doppler taper losses

- *The plot is for a single azimuth/elevation receive beam.*
- *The dip in performance is due to mainlobe clutter.*



CHALLENGES / RESEARCH AREAS



- **FIRST AND FOREMOST: TO DEVELOP REALIZABLE ALGORITHMS THAT PERFORM WELL ON REAL DATA**
- **REDUCED DOF REQUIREMENT SO FEWER SAMPLES NEEDED FOR WEIGHT ESTIMATION**
- **COMPUTATIONAL BURDEN**
- **WEIGHT ESTIMATION/TRAINING FOR NON-HOMOGENEOUS CLUTTER**
- **POST-STAP PROCESSING/CFAR**
- **LOWER MINIMUM DETECTABLE VELOCITY (MDV)**
- **CLUTTER AND JAMMER NULLING WITH WIDER BANDWIDTHS**
- **JOINT SUPPRESSION OF COLD CLUTTER AND HOT CLUTTER (TERRAIN SCATTERED INTERFERENCE, JAMMER MULTIPATH)**

SESSION PAPER: 1



- The CREST Challenge, Overview and Analysis

Peter A. Zulch and Joseph R. Guerici

- Definition of Terms
 - CREST: Common Research Environment for STAP Technology at the Maui High Performance Computing Center (MHPCC)
 - RLSTAP: Rome Laboratory STAP Tool, with a Khoros-based GUI
- The Challenge
 - Given four simulated STAP data sets created using RLSTAP, resolve all target information.
 - The sets contain multiple targets, clutter and jamming. The last three sets contain site specific non-homogeneous clutter, including shadowing.
- The Winning Solution
 - Details, including STAP rank selection, weight estimation/training, post-STAP processing and computational burden

SESSION PAPER: 2



- Sample Selection for Improved Adaptive Airborne Radar

William L. Melvin, Pinyuen Chen and Michael C. Wicks

- The Problem
 - Spatially non-homogeneous clutter returns can result in poor quality estimates for the clutter in the test cell of interest, resulting in degraded adaptive weights and nulling performance
- Proposed Solution
 - Detect non-homogeneous regions and modify training accordingly
- Tested with Collected MCARM Data
 - MCARM: Rome Laboratory Multichannel Airborne Radar Measurements Program
 - L-band radar on a BAC-111 aircraft, 2 kW of TX power, 22 digitized elements, 1 MHz instantaneous bandwidth with IF sampling and channel equalization, 2 kHz PRF, CPI contains 200 PRIs

SESSION PAPER: 3



- Structured Covariance Estimation for Space-Time Adaptive Proc.

Timothy A. Barton and Steven T. Smith

- The Problem
 - Limited sample support degrades adaptive nulling performance
- Proposed Solution
 - Exploit structure of covariance matrix to lessen number of samples required, e.g., block Toeplitz structure
 - Several covariance estimators considered. Used with fully optimal STAP as well as reduced dimension sub-optimum STAP.
 - New EM (expectation-maximization) algorithm based ML estimator
- Examined Using Simulated and Collected Mountaintop Data
 - Mountaintop radar: UHF-band ground-based radar on mountain top. 18-element IDPCA TX array providing 16 pulse motion emulation with 625 Hz PRF (variable). RX using 14 digitized-element RSTER array, approx. 1 MHz instantaneous bandwidth with IF sampling and channel equalization

SESSION PAPER: 4



• The Effect of Bandwidth on Space-Time Adaptive Processing

Michael Zatman

- The Problem
 - To date most STAP analysis has relied on narrowband clutter and jamming models
 - Bandwidth leads to dispersion in two dimensions, both across the array in the spatial domain and across the CPI in the Doppler domain. Phase $2\pi f t$
 - When the array is not aligned with the platform's velocity vector, dispersion is shown to result in MDV (minimum detectable velocity) degradation. The degradation is shown to be greater for Post-Doppler STAP algorithms than for Pre-Doppler algorithms.
- Proposed Solution
 - Time delay steering in both the spatial and Doppler dimension
- Examined Using Simulated Data

The CREST Challenge—Overview and Analysis

Peter A. Zulch and Joseph R. Guerçi¹

USAF Rome Laboratory
Advanced Technology Group
Rome, NY 13441-4514
email: zulchp@rl.af.mil

¹Science Applications International Corporation
Air Defense Technology Group
4001 No. Fairfax Drive, Suite 400
Arlington, VA 22203

Abstract In support of the DARPA Advanced Signal Processing Program a challenge had been issued to the radar and signal processing community. Several simulated data sets that emulate a flying phased array surveillance radar were created as a challenge to the STAP community to resolve all target information. There were four data sets created for the challenge using the Rome Laboratory Space Time Adaptive Processing Tool (RLSTAP). The first three data sets contained returns from a single coherent processing interval (cpi) over different clutter types and target/jammer scenarios. The fourth data set contained ten cpi's worth of data and simulated a typical airborne radar scenario where the radar would revisit a point on the ground ten different times with a 30 sec revisit time. The first portion of this presentation will describe the CREST challenge data sets and how to access them via the World Wide Web for future STAP investigations. The second part of the talk will be a discussion of the approach employed by the winning strategy. Issues highlighted will include robust and computationally efficient strategies for STAP rank selection, weight calculation, as well as post-STAP and CFAR processing.



The CREST Challenge, Overview and Analysis

Peter A. Zulch

USAF Rome Laboratory (RL/OCSA)

Rome, NY

zulchp@rl.af.mil

Joseph R. Guerci

SAIC-Air Defense Technology

Arlington, VA

1997 ASAP Workshop

March 12-14, 1997



CREST Challenge Overview



- **Description:**
 - contest - April 96 to December 96
 - provide simulated airborne phased array data sets with challenging scenarios
 - 4 data sets
- **Objective:**
 - challenge RADAR community to resolve target information
 - awareness of CREST
 - » recorded radar data
 - » MHPCC
 - » RLSTAP/ADT

<http://wwwcrest.mhpcc.edu>
(under “Events”)



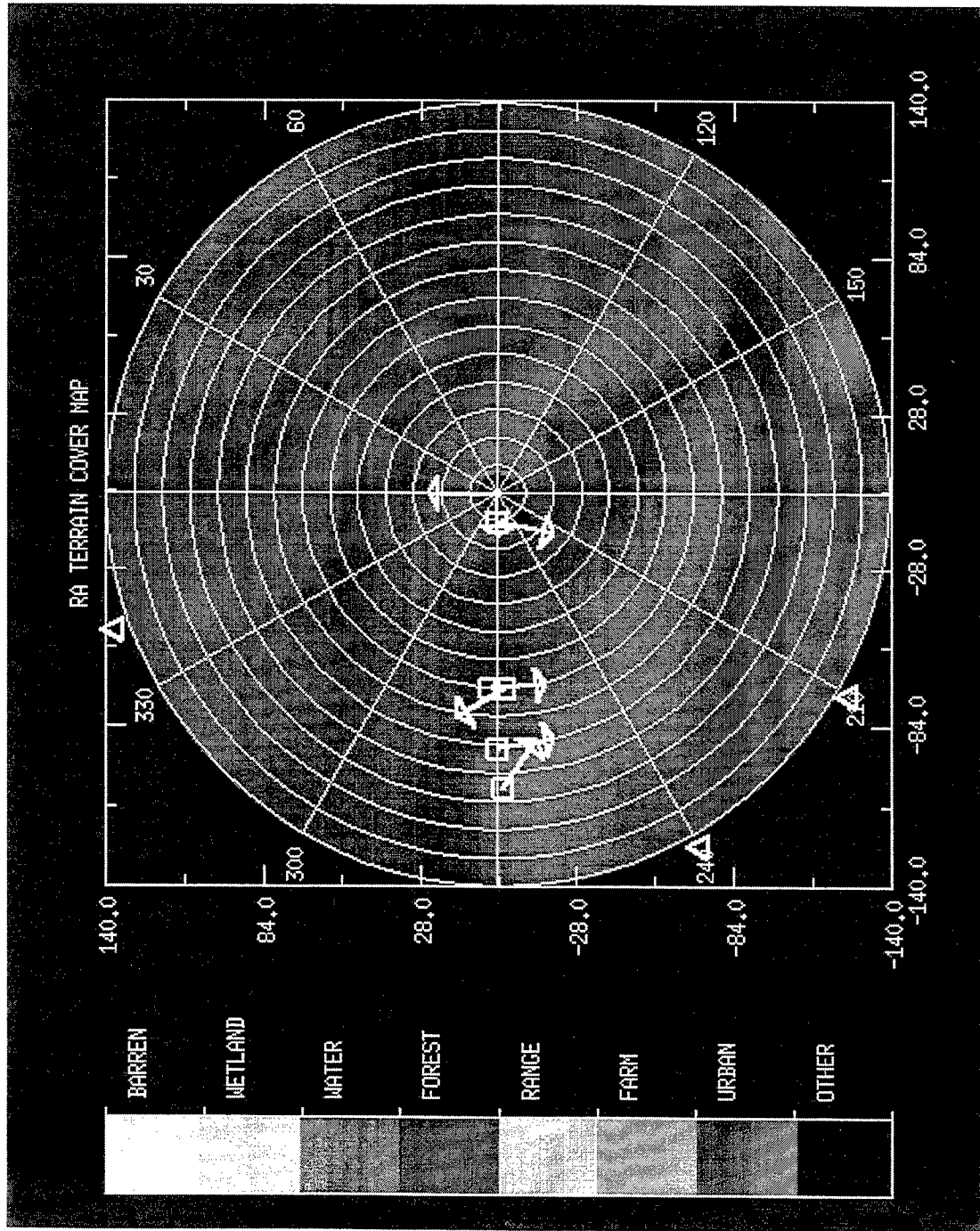
RADAR Parameters



Transmit Frequency	450 MHz
Pulse Width	50 μsec.
Waveform	LFM
Bandwidth	0.5 MHz
PRF	1000 Hz
Channels	20
Pulses	18
Element Spacing	$.5\lambda$
TX Az. Beamwidth	5^0 (rect. weighted)
TX El. Beamwidth	13^0 (32.5 Dolph Cheb. weighted)



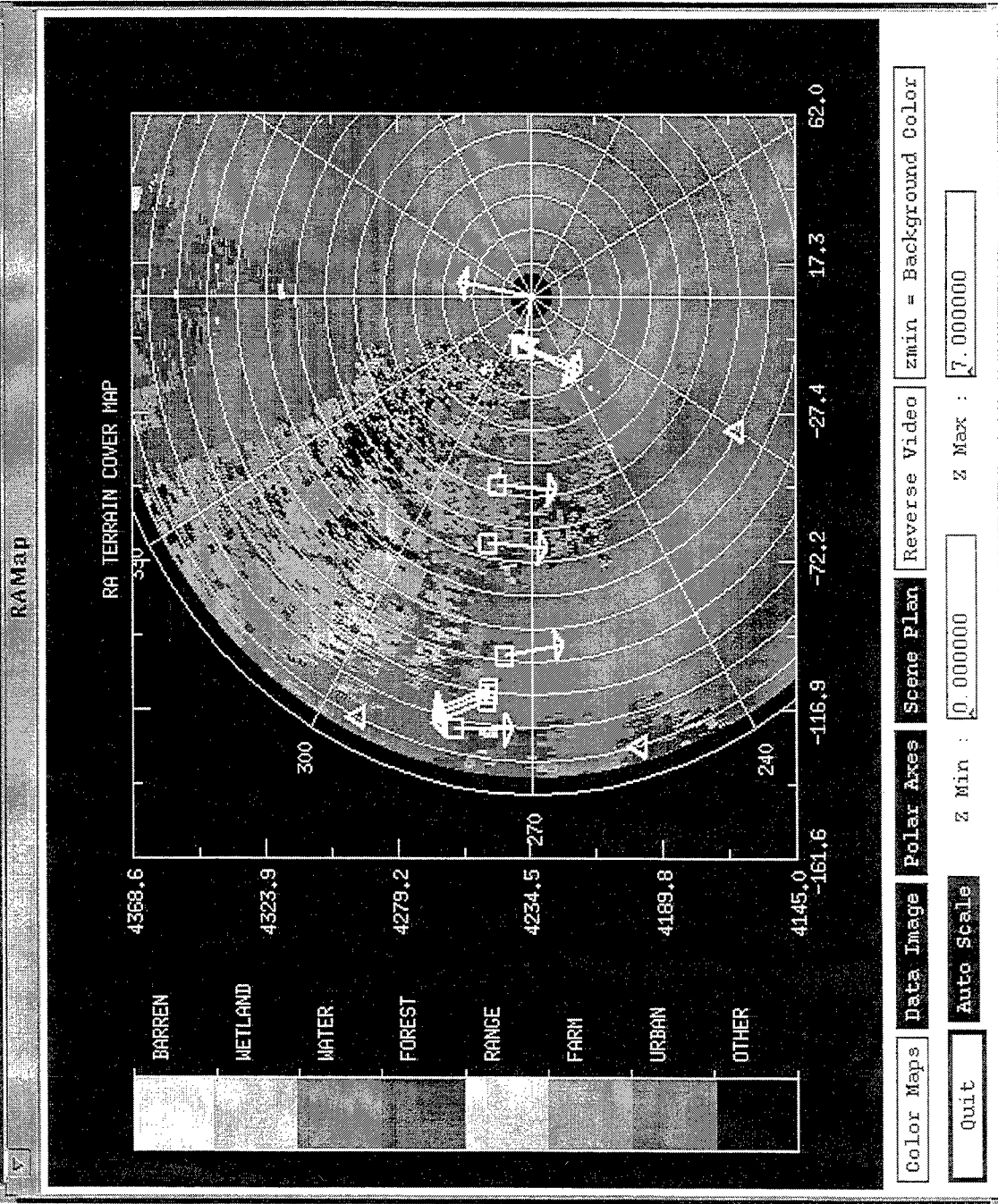
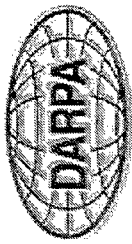
Data Set 1 - CREST1



- warm-up
- homogeneous clutter
- platform-20000', heading North, boresight pointed West,
- 5 targets
- 3 jammers
- 888 range bins



Data Set 2 - CREST2

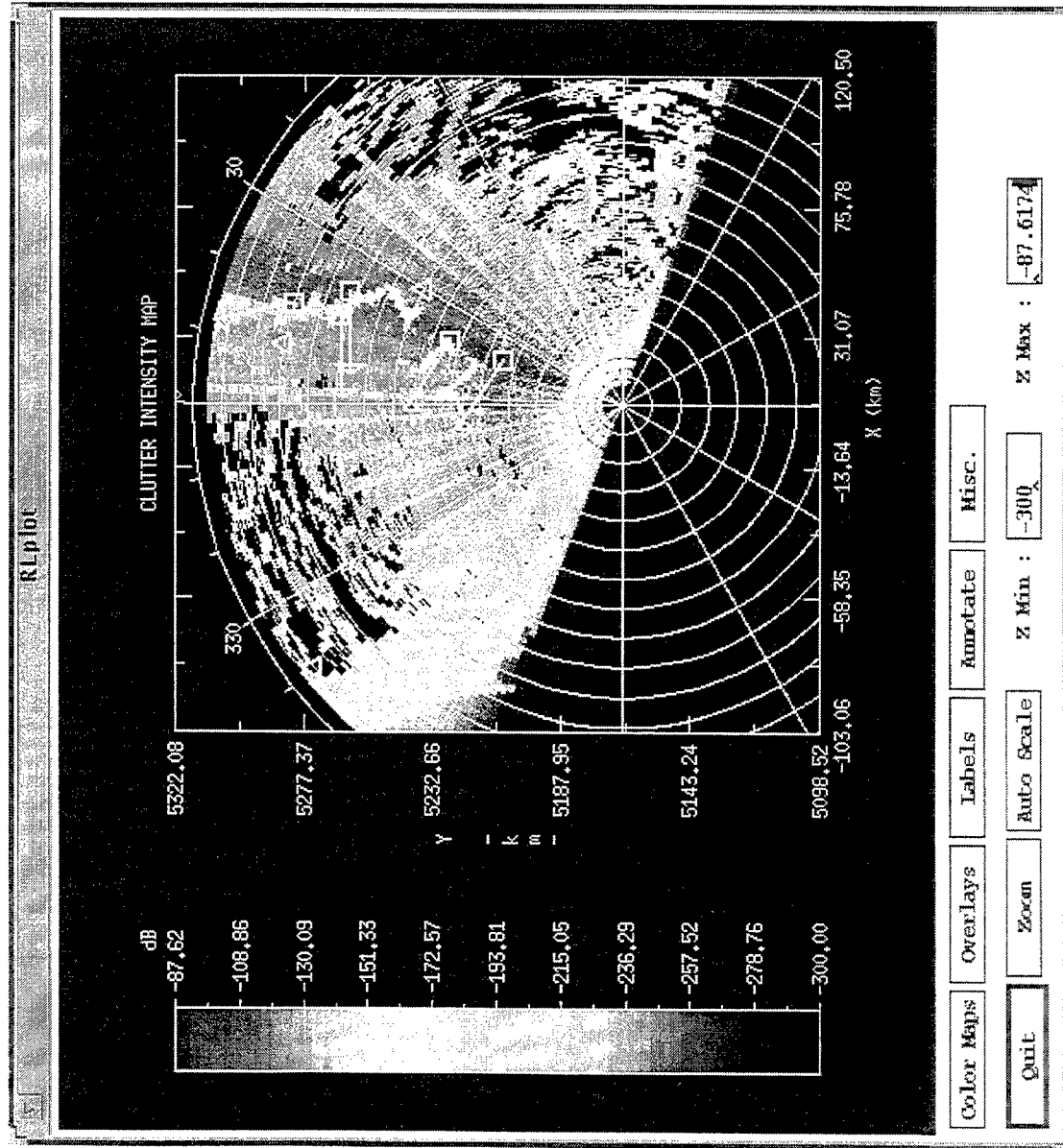


- site specific clutter - Delmar, MD
- platform-20000', heading 10°, boresight -80°
- 9 targets
- 3 jammers
- 920 range bins

ASAP97cc



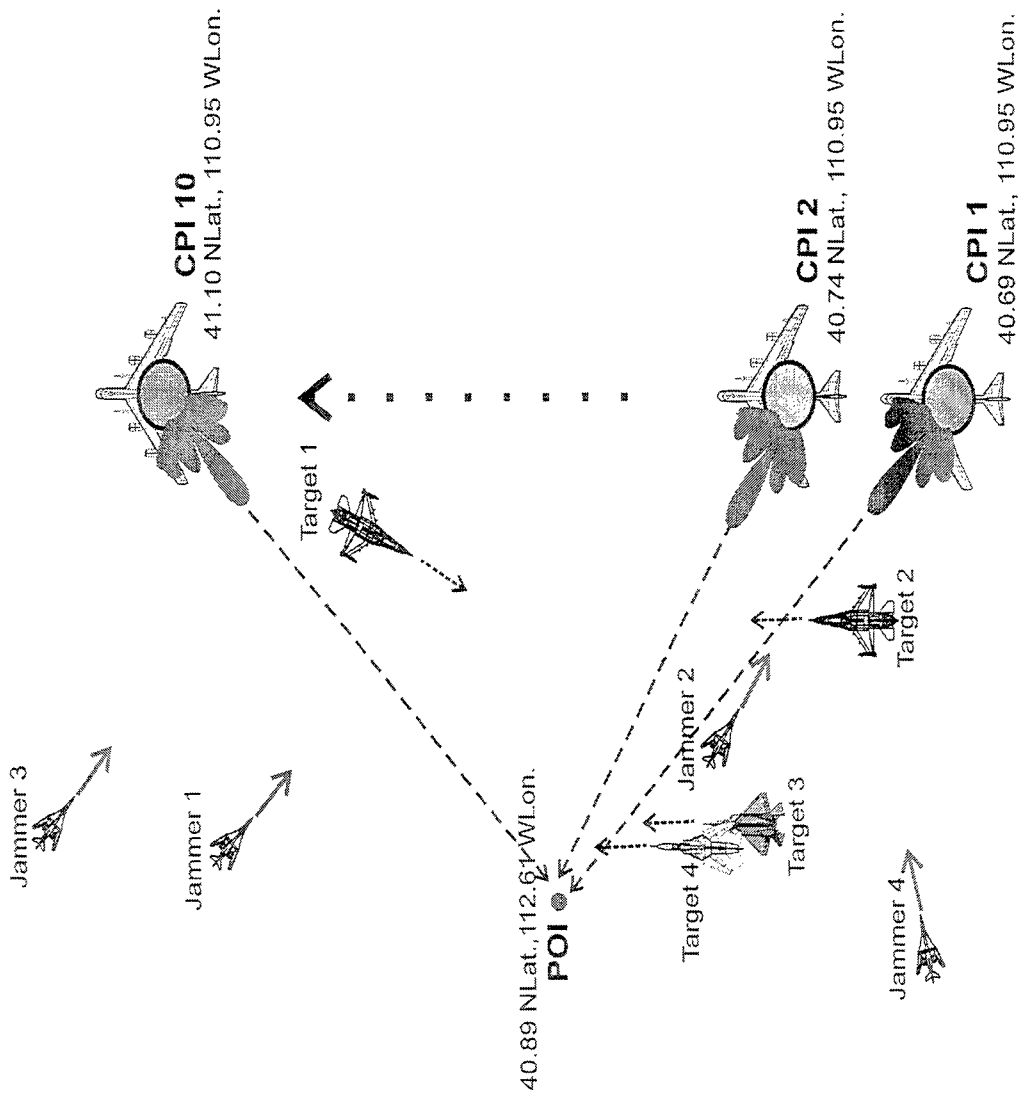
Data Set 3 - CREST3



- site specific clutter
 - Olympia, WA
- platform-20000', heading -40°, boresight 20°
- 5 targets
- 4 jammers
- 920 range bins



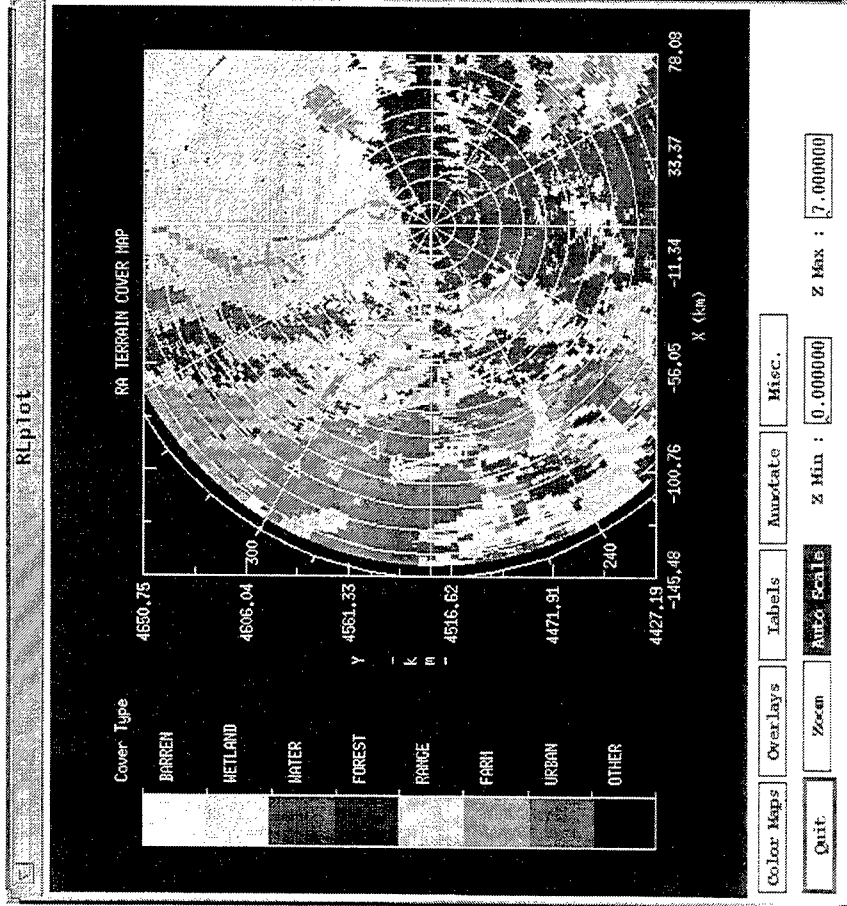
Data Set 4 - CREST4*



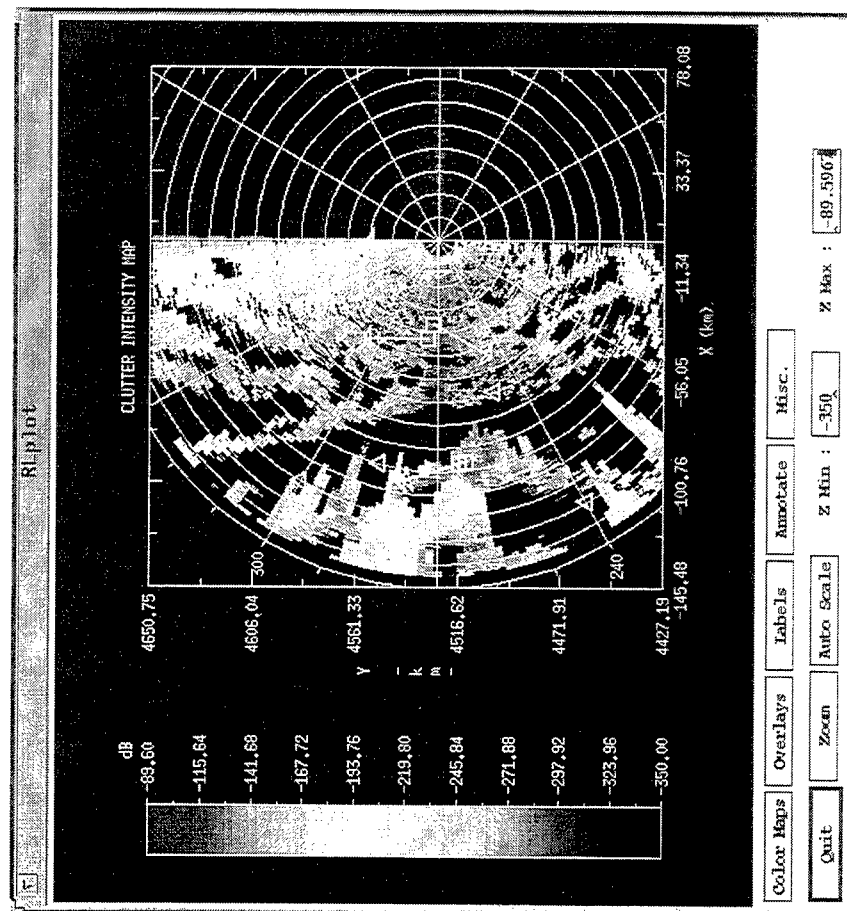
- site specific clutter - Salt Lake City UT
- platform-20000', heading North, boresight towards POI
- 10 CPIs (*10 data sets)
- 30 second revisit time
- 4 targets
- 4 jammers
- 920 range bins



Data Set 4 - CREST4



Terrain Cover



Clutter Intensity



CREST Challenge Winner

Dr. Joseph R. Guerci

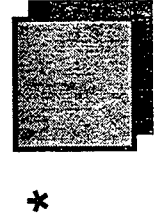
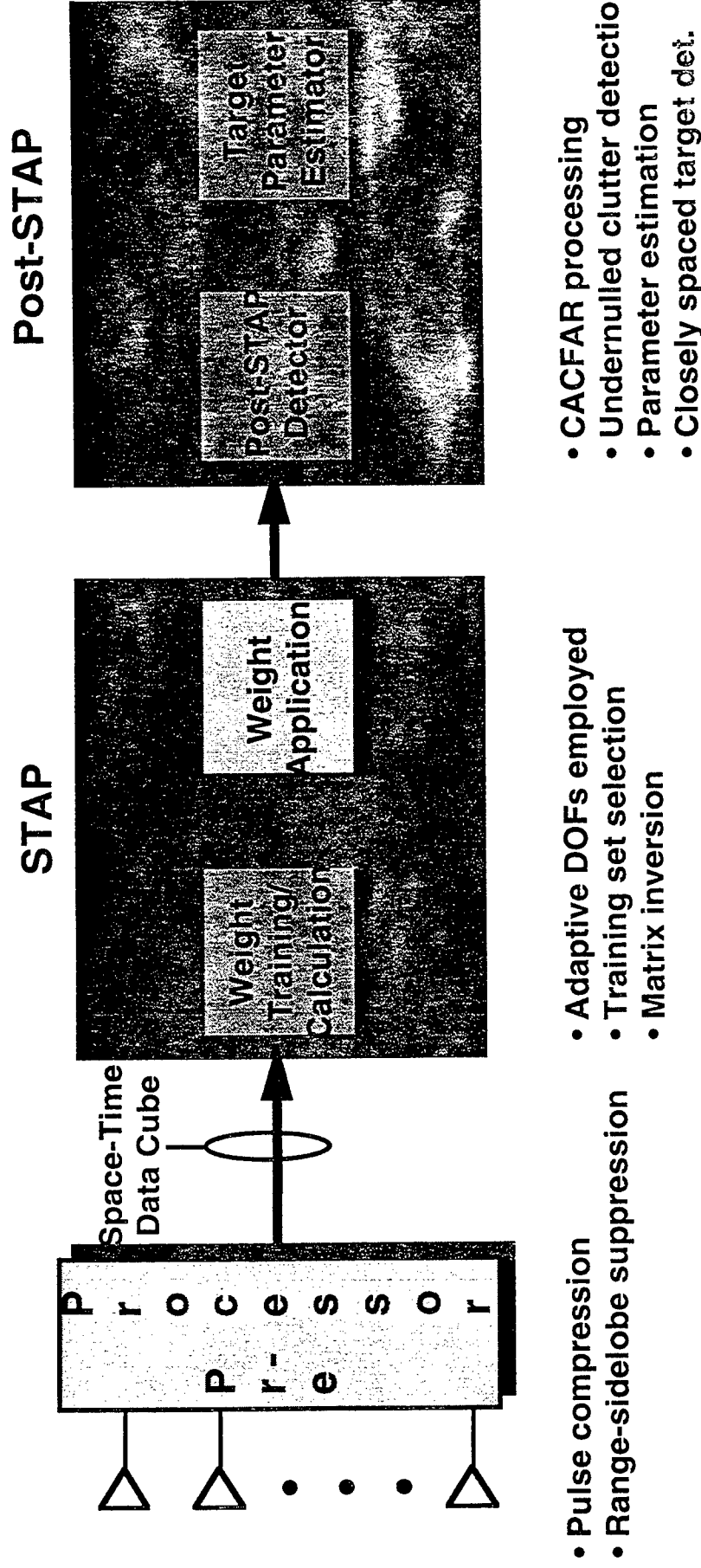
SAIC

**Air Defense Technology Division
Arlington, VA**

Outline

- **Signal processing chain**
- **STAP algorithm selection**
- **Post-STAP detector design**
- **Application to the CREST data sets**
- **Summary and discussion**

Basic Signal Processing Chain



Critical design element (performance/computation)

STAP/Post STAP "Sources"

• E. J. Baranoski, "Improved Pre-Doppler STAP Algorithm for Adaptive Clutter Nulling in Airborne Radars" ¹	Basic STAP Algorithm Selection
• J. K. Day, "Space Time Adaptive Processing from an Airborne Early Warning Perspective" ¹	—
• J. R. Guerci, S. U. Pillai, Y. L. Kim, "Efficient Space-Time Adaptive Processing for Airborne MTI-Mode Radar" ²	—
• G. K. Borsari, A. O. Steinhardt, "Cost-Efficient Training Strategies for Space-Time Adaptive Processing Algorithms" ¹	Training Strategies
• D. E. Kreithen, A. O. Steinhardt, "Target Detection in Post-STAP Undernull Clutter" ¹	Undernull Clutter
• B. D. Carlson, "Covariance Matrix Estimation Errors and Diagonal Loading in Adaptive Arrays" ³	Robust Sample Matrix Inversion

1. Proceedings of the Twenty-Ninth Asilomar Conference on Signals, Systems, & Computers, Pacific Grove, CA., October 30 - November 1, 1995.

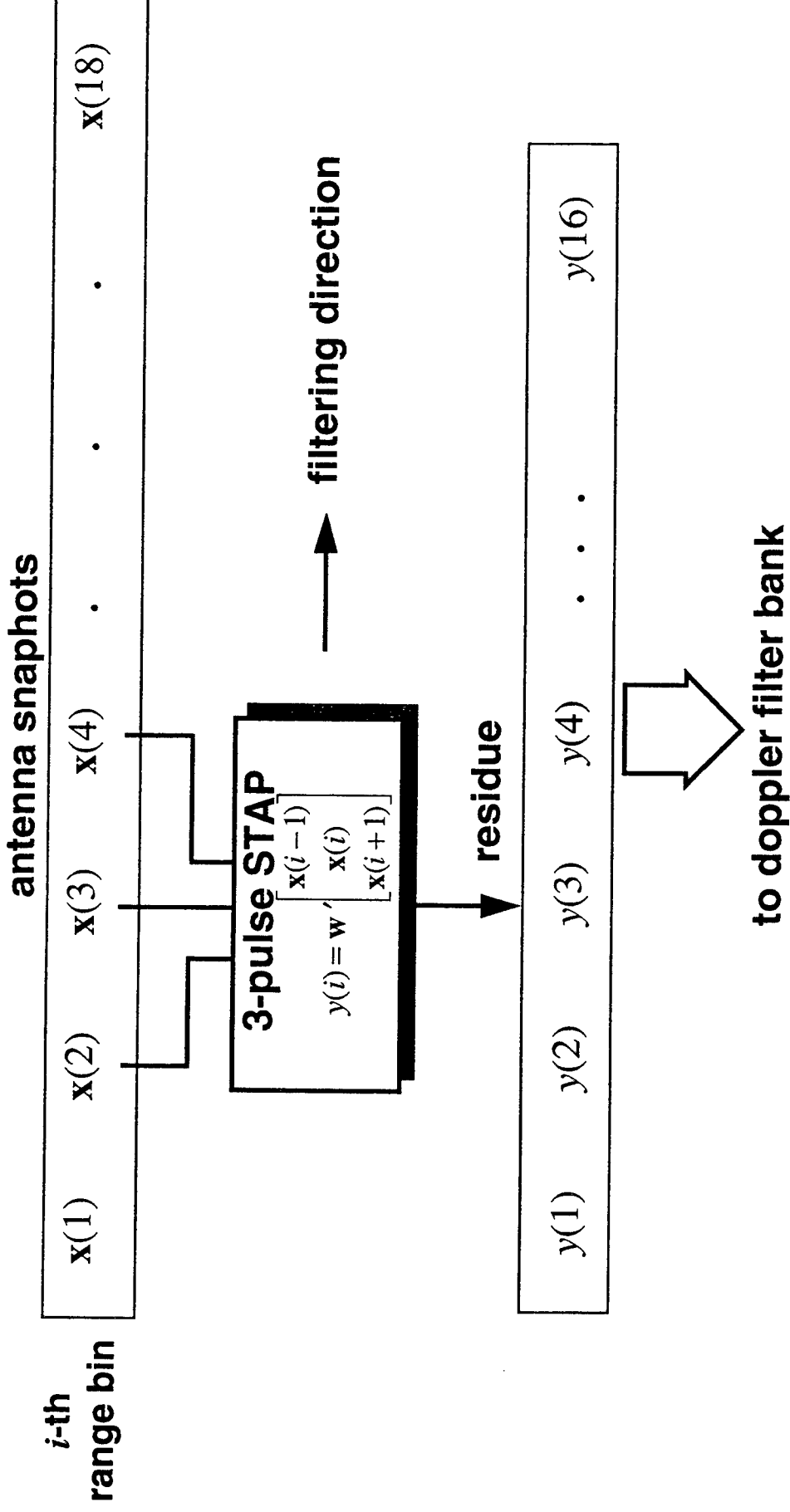
2. Proceedings of the 1996 IEEE ICASSP, Atlanta, GA, May 7-10, 1996.

3. IEEE Transactions on Aerospace & Electronic Systems, July 1988.

STAP Algorithm Selection

- **Contest criteria placed a premium on computational burden**
- **Post-Doppler is approximately 2 ~ 4 times more complex (GFlops/sec)**
- **Recent research and analysis bolsters the efficacy of Pre-Doppler approaches:**
 - **Baranoski's "Adaptive Taper"**
 - Performance essentially equivalent to Post-Doppler
 - **Analyses conducted with Mountain Top data suggests choice of sub-CPI DOFs and weight training are most critical**
- **Selection: Sub-CPI Pre-Doppler**
 - **DOFs chosen off-line (based on known platform speed, PRF, etc.)**

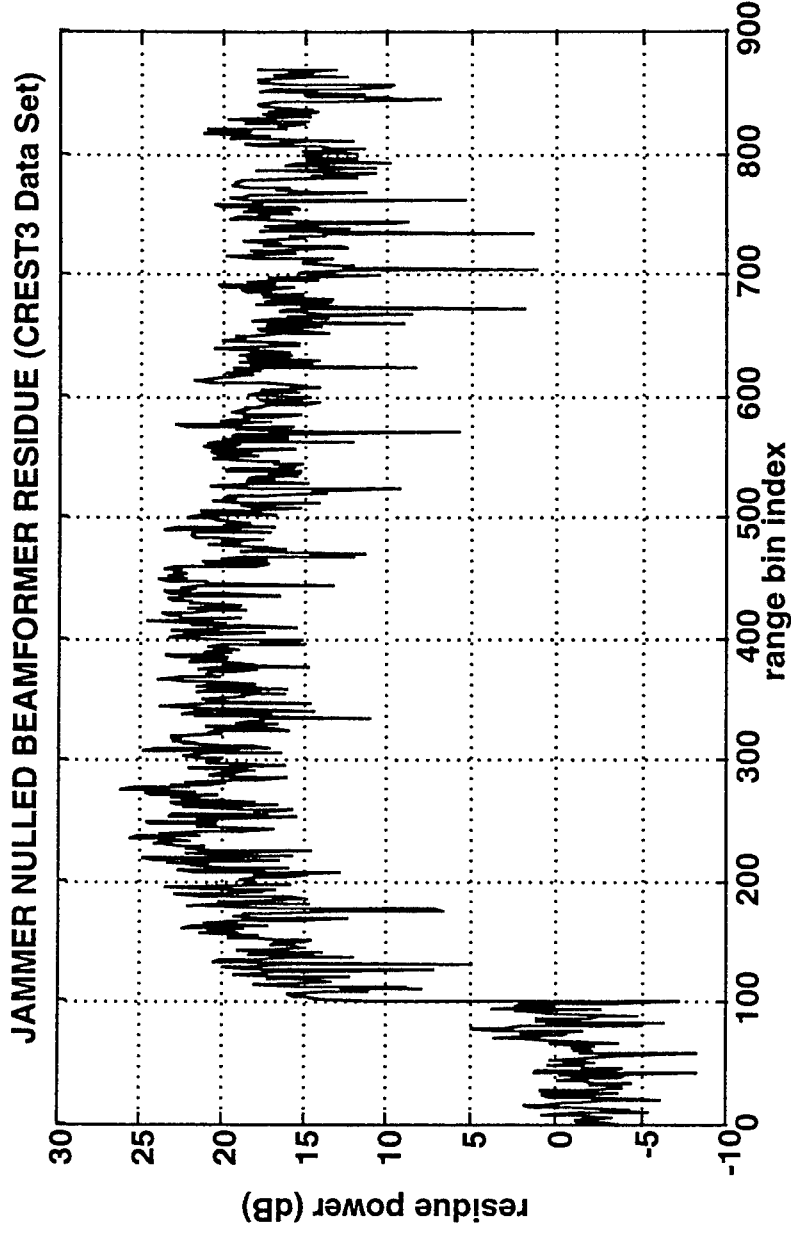
Pre-Doppler Sub-CPI STAP



where: $\mathbf{w} = \hat{R}^{-1}(\mathbf{t} \otimes \mathbf{v})$, for non-adaptive taper: $\mathbf{t} = [1 \ -2 \ 1]'$

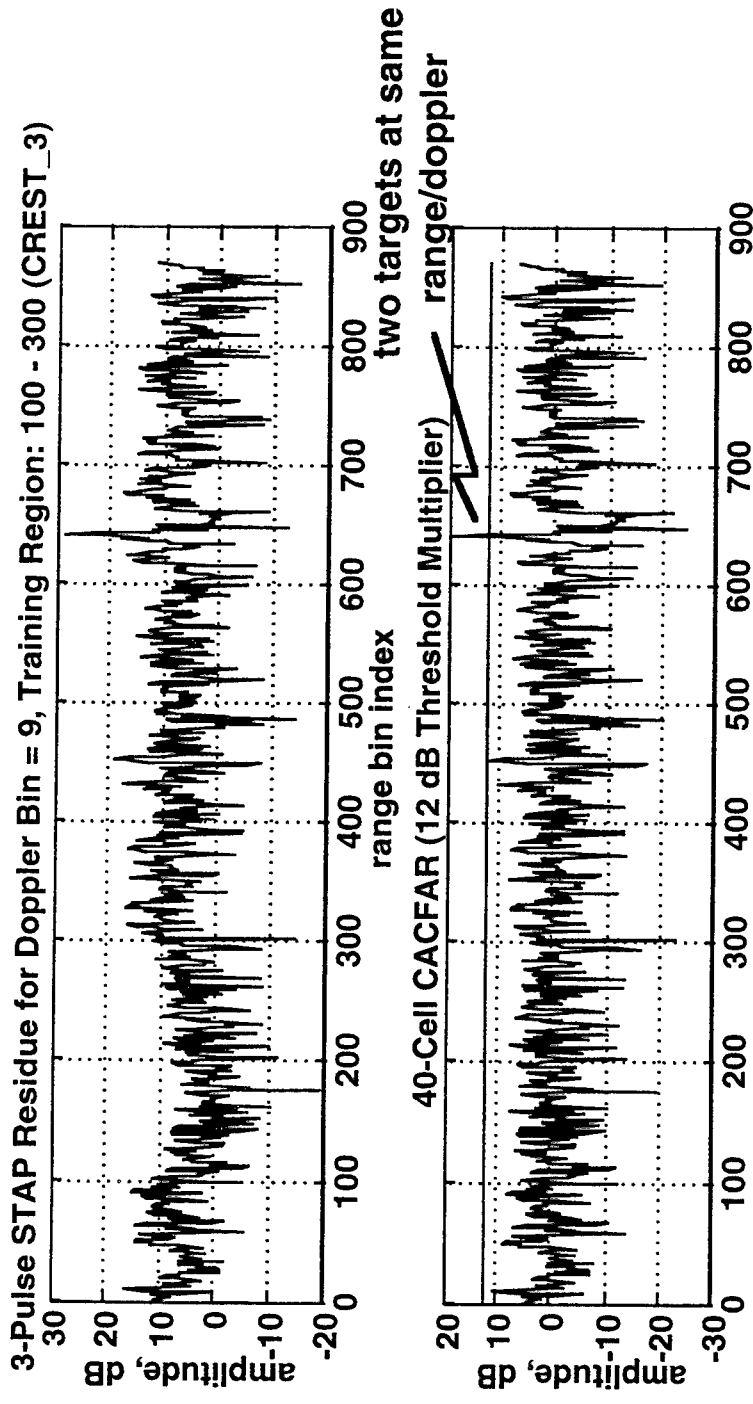
Weight Training Procedure

- “Freeze” Training
 - Very low complexity
 - “Overnulling” problem (Loss of gain-on-target)
 - Requires CACFAR to compensate for power discrepancies



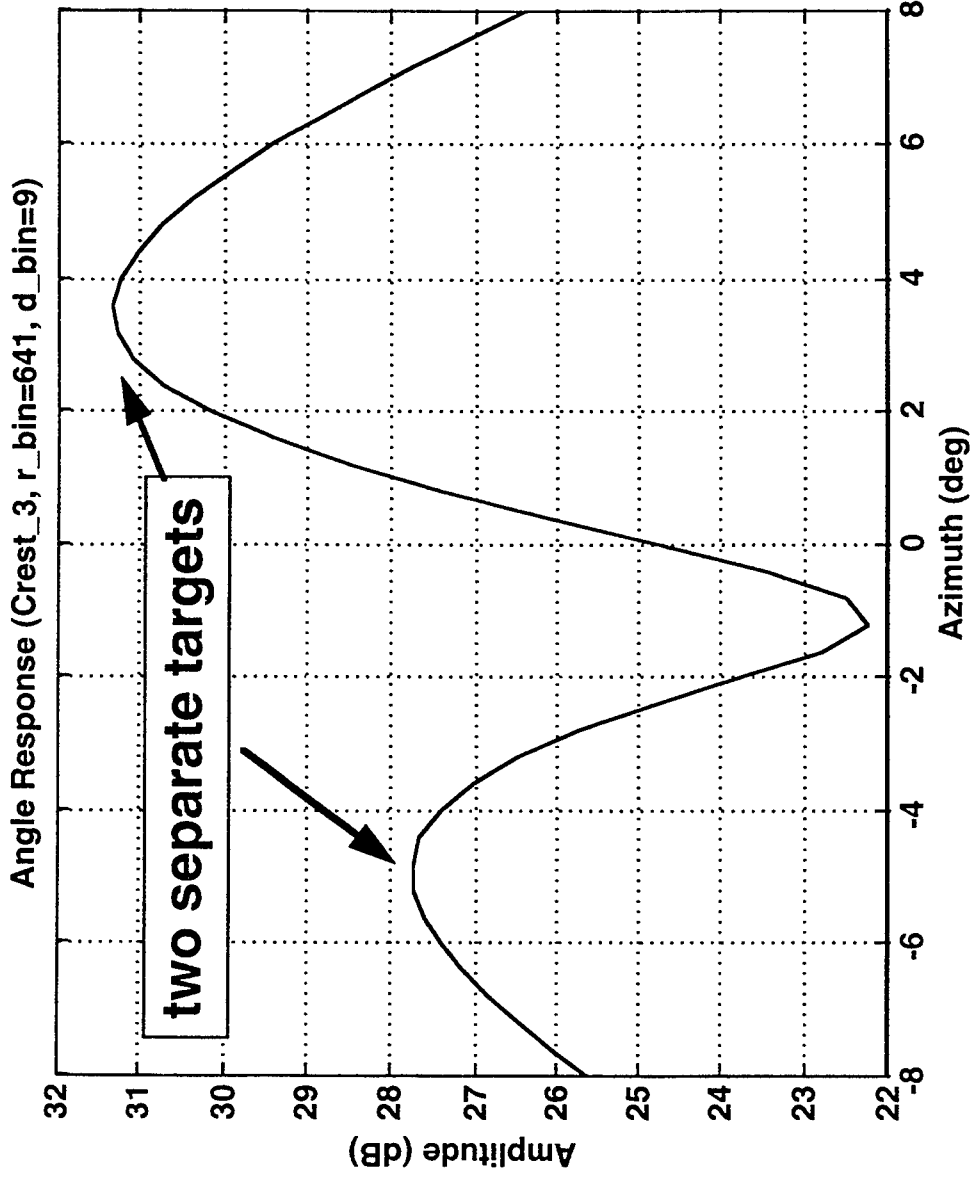
Post-STAP CACFAR Detection

- **Multi-pass CACFAR** (40-cell, ~ 12 dB threshold multiplier)
 - Second pass required for closely spaced targets and “undernullled” clutter
- **Low dimensionality of Post-STAP residue allows for very complex CACFAR processing without incurring a large computational penalty**



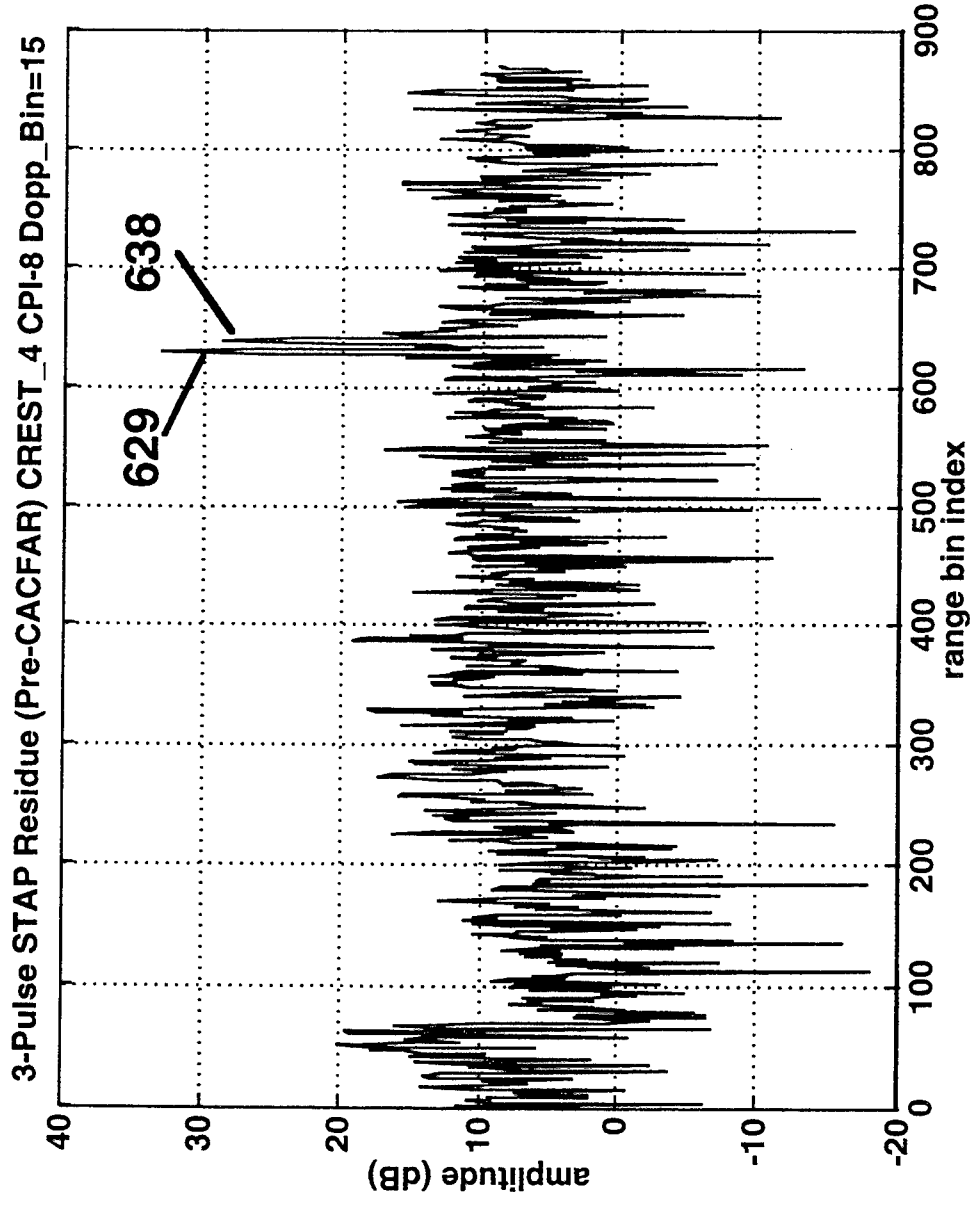
Post-STAP CACFAR Detection

- Closely spaced targets (same range and doppler)
 - Requires angle response method



Post-STAP CACFAR Detection

- Closely spaced targets (target contaminated reference cells)
 - Many remedies available (chose “outlier” removal approach)



Post-STAP Undernulled Clutter Problem

- Problem is particularly acute with:
 - Freeze training methods
 - Heterogeneous terrain
- Raises P_{fa}
- Requires a method for “predicting” where undernulling is likely to occur
- For Pre-Doppler STAP, a multipass CACFAR incorporating the “Point Beams at Clutter (PBC)”[†] technique seems promising

[†] D. E. Kriethen and A. O. Steinhardt, “Target Detection in Post-STAP Undernulled Clutter”, *Proceedings of ASILOMAR-29*, pp. 1203-1207, 1995.

Undernulled Clutter Detection (for Pre-Dopp STAP)

- “Predict” degree of nulling expected for each initial CACFAR detect

– “Leakage Factor”:
$$L_f \triangleq \frac{|w_i' v_i|^2}{|w_i' w_i| |v_i' v_i|}$$

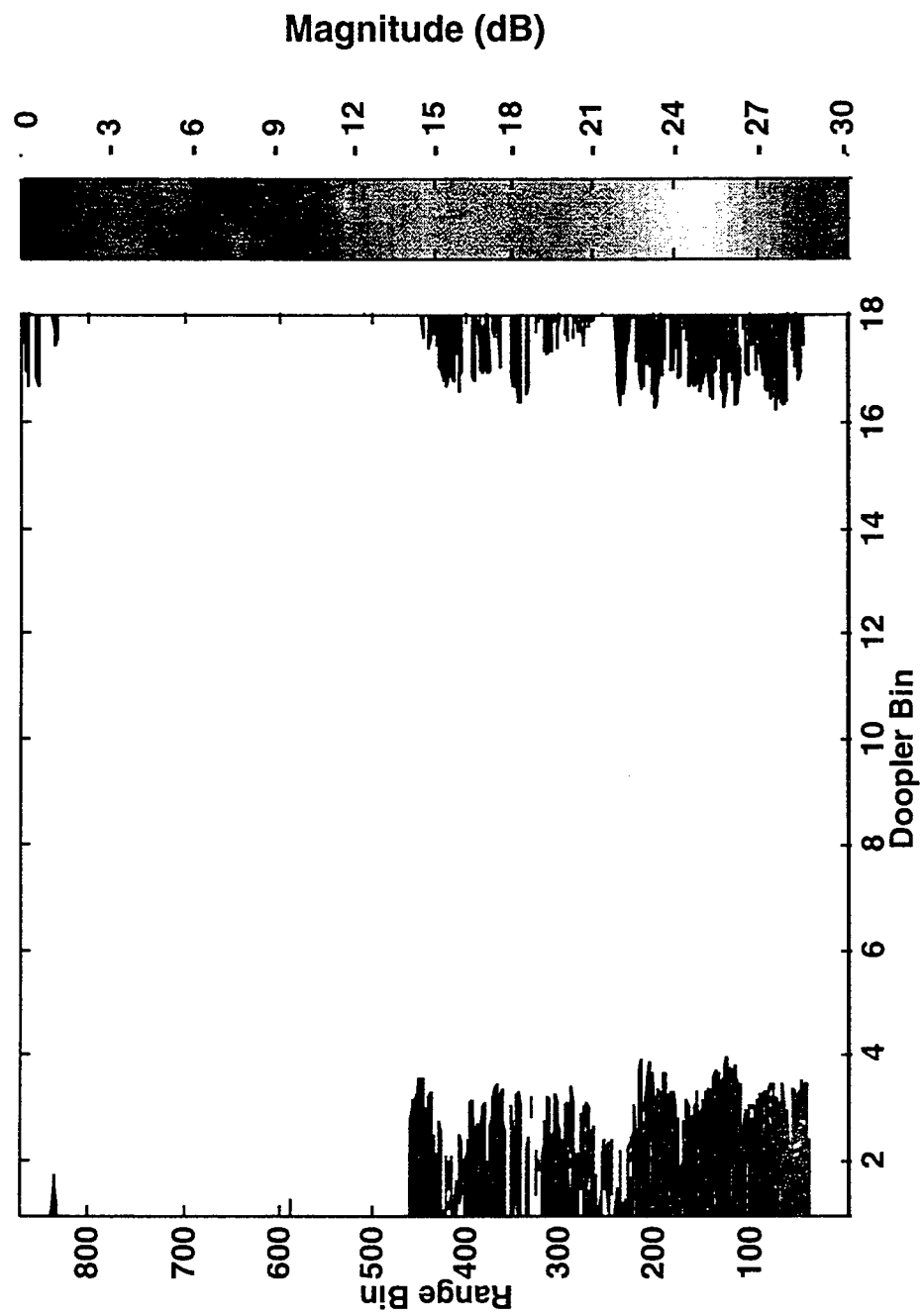
– “PBC” Map:
$$PBC_i \triangleq \frac{|v_i' x|^2}{|v_i' v_i|}$$

where: w_i = ST weight vector for the i -th detect
 v_i = ST steering vector for interfering clutter
 x = ST data vector for range bin of interest

- Adjust threshold based on predicted nulling
- Note: If jamming present, replace v_i with spatially pre-whitened ST clutter steering vector

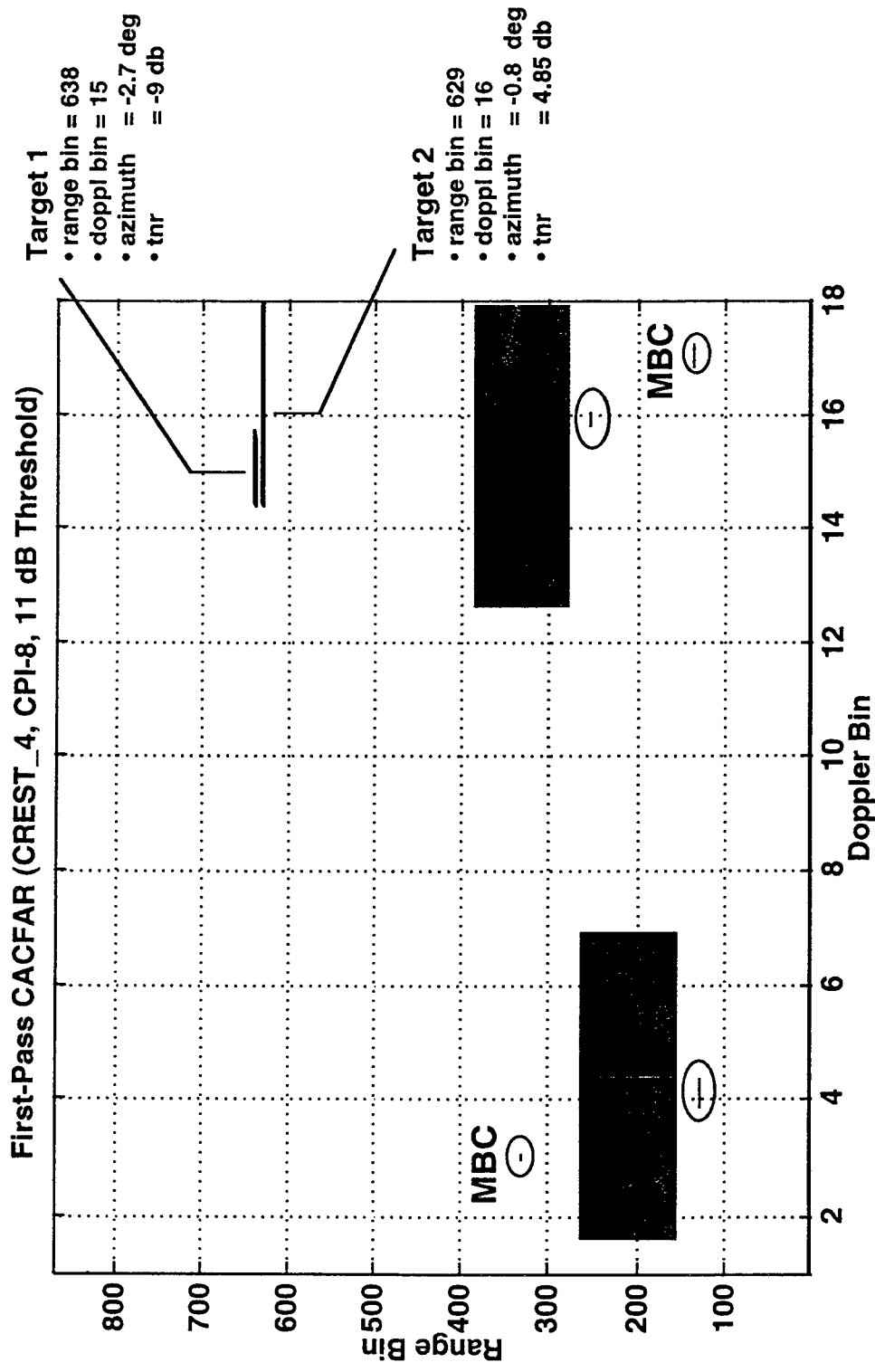
Undernulled Clutter Example

Estimated Clutter Distribution for CREST_4 CPI-8 (CNR ~ 54 dB)



Undernulled Clutter Example

- Post-STAP CACFAR with lowered threshold



Summary

- **Pre-Doppler Sub-CPI STAP with CACFAR**
 - Good trade-off between performance & complexity
 - Can be significantly enhanced with modest cost:
 - “Adaptive Taper” for improved MDV (Baranoski)
 - PBC for undernulled clutter & lower detection threshold (Kriethen & Steinhardt)
- **However... Post-Doppler can:**
 - Inherently address “sidelobe” targets
 - Naturally integrate with PBC approach
 - Easier/better target parameter estimation

“The last thing one discovers in composing a work, is what to put first”.

Blaise Pascal

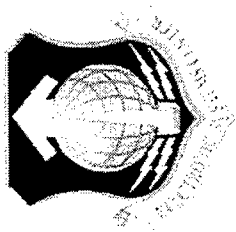
Sample Selection For Improved Adaptive Airborne Radar

William L. Melvin, Pinyuen Chen*, and Michael C. Wicks

USAF Rome Laboratory
26 Electronics Parkway
Rome, NY 13441-4514
tel: (315) 330-1896
fax: 315-330-2139
email: melvinw@rl.af.mil

Abstract This presentation shall discuss the challenges of fielding an adaptive airborne radar in the presence of nonhomogeneous interference. We discuss the impact of corrupted, nonhomogeneous sample data on the formulation of the adaptive filter weights. We then propose several solutions to improve the performance of the adaptive processor. Measured airborne radar data from the Multichannel Airborne Radar Measurements (MCARM) Program shall be used in the analysis. This presentation will include discussion of the following topics: an overview of the challenge nonhomogeneous interference poses for adaptive systems; detection of nonhomogeneous interference based on several test statistics; comparison of methods; performance of adaptive training strategies using measured airborne data; and analysis of MCARM data.

*Visiting Scientist under the Intergovernmental Personnel Act (IPA)



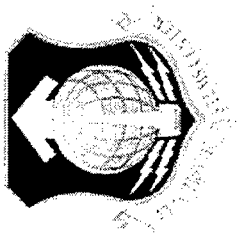
Sample Selection for Improved Adaptive Airborne Radar

William L. Melvin, Michael C. Wicks and Pinyuen Chen
United States Air Force Rome Laboratory

26 Electronic Pky

Rome, NY 13441-4514

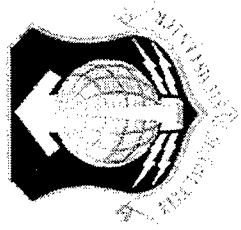
Ph. 315-330-1896 Fax 315-330-2528



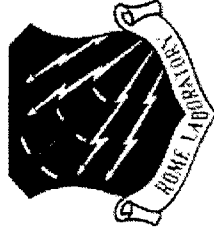
Outline



- Overview and problem statement
 - Impact of nonhomogeneous interference on space-time adaptive processing (STAP) for airborne radar
 - Corruption of adaptive filter response
 - Detection threshold misplacement
- Nonhomogeneity detectors
 - Test homogeneity of secondary data based on selected measure
 - Generalized inner product, sample matrix inversion test statistic, inner product
- Examples using measured airborne radar data from the Multichannel Airborne Radar Measurements (MCARM) Program
- Relationship to ongoing work



Preliminaries



$$y_k = W_k^H X_k ; \quad W_k^H = s^H \bar{\bar{R}}_k^{-1}$$

(Adaptive filter output and adaptive weights [1])

$$\bar{\bar{R}}_k = \frac{1}{P} \sum_i X_i X_i^H$$

(Minimum mean square error (MMSE)
estimate of interference covariance matrix)

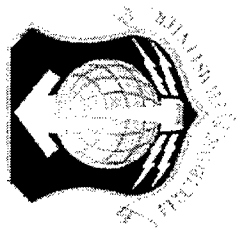
$X_i = NM \times 1$ space-time or reduced-dimension signal vector for i^{th} range cell

s = target steering vector

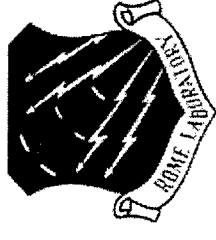
When X_i are independent and identically distributed (iid), then $\bar{\bar{R}}_k \rightarrow R_k$ as $P \uparrow$,

where $R_k = E[X_{k/H_0} X_{k/H_0}^H]$ (ie., converges in distribution)

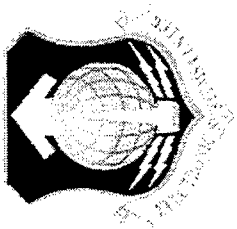
Question: How do we select secondary data from a limited population of potentially non-iid realizations to best estimate R_k ?



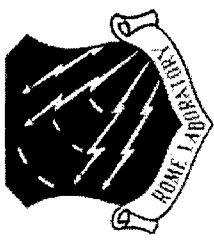
Brief Perspective



- For Gaussian-distributed interference, selecting 2 NM iid secondary data yields an average loss ratio between adaptive and optimal systems of less than 3 dB (NM = degrees of freedom) [2]
- In addition to mitigating computational burden, Joint-Domain Localized processing by Wang and Cai attempts to minimize sample support in nonhomogeneous environments [3]
- Marshall discusses training strategies applied to Mountaintop data [4]
 - Range Segmentation, Sliding-Window, Freeze Training, Power-Weighted Freeze Training
- Melvin, Wicks and Brown demonstrate impact of training data selection on STAP performance using MCARM data [5]
 - Use of generalized inner product to rank and exclude outliers for improved covariance matrix estimation
- Rabideau and Steinhardt demonstrate improved clutter nulling using Mountaintop data by training on strongest in power [6]



Nonhomogeneous Interference



- Definition: Two signal vectors, X_i and X_j , are approximately homogeneous under the Gaussian assumption provided

$$R_i R_j^{-1} \approx I_{NM}$$

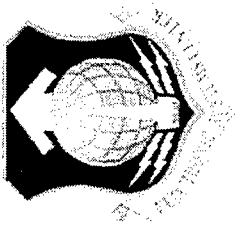
$$R_i = E[X_i X_i^H] \quad R_j = E[X_j X_j^H] \quad I_{NM} = NM \times NM \text{ Identity Matrix}$$

- Definition: Homogeneous secondary data represent the majority, taking the form

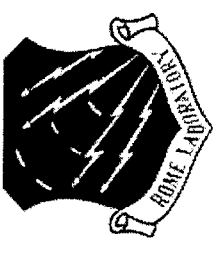
$$X_i = X_{i/H_0} = C_i + N_i + I_i$$

A minority of the secondary data may appear nonhomogeneous, taking the form

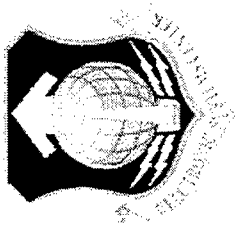
$$X_i = C_i + N_i + I_i + O_i$$



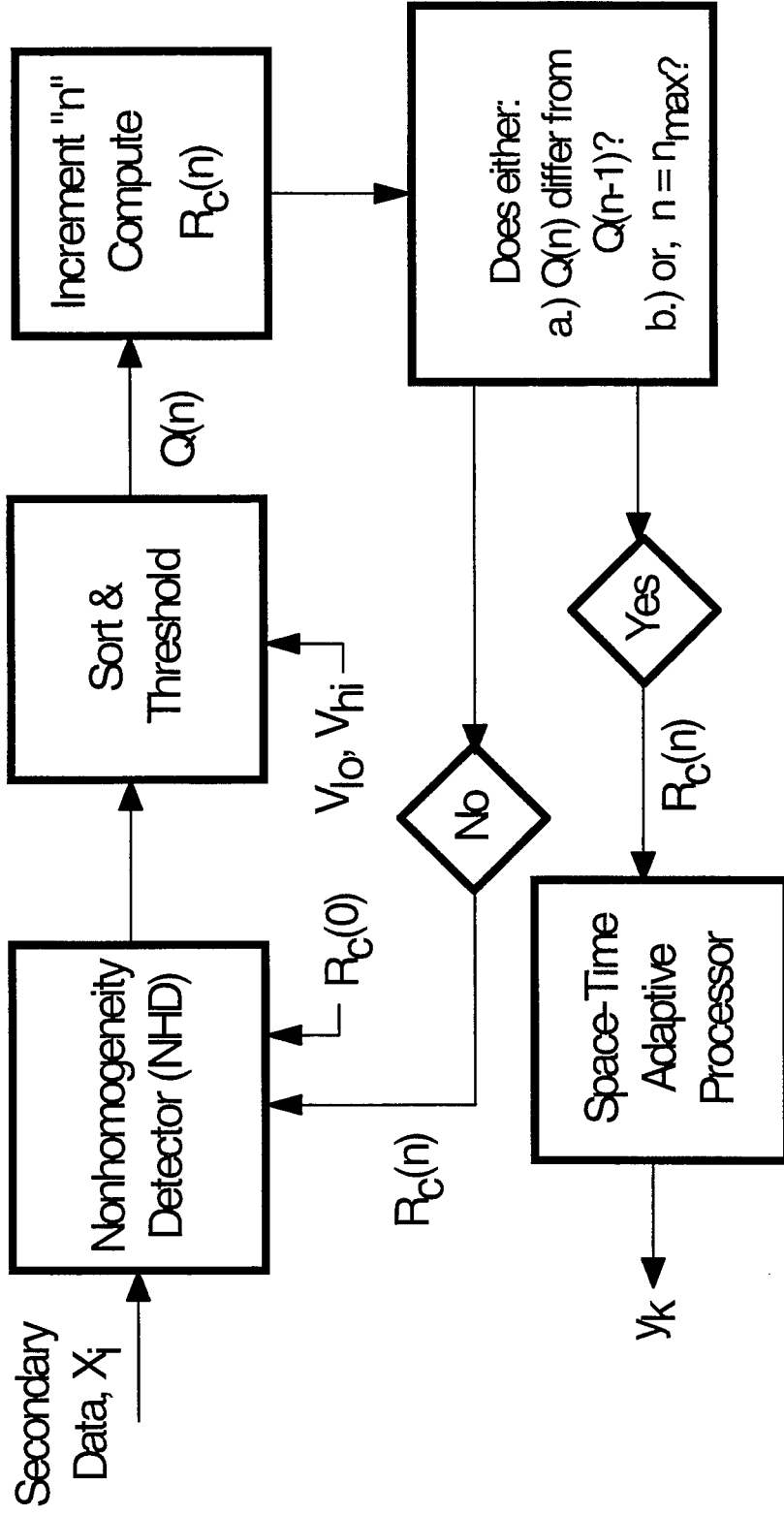
Nonhomogeneous Environments

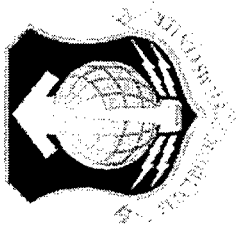


- A variety of factors create a nonhomogeneous environment, including:
 - Spatial variation in clutter, system errors exacerbating spatial clutter variation, shadowing, moving scatterers, interfering targets, deceptive jamming, etc.
- We wish to reject homogeneous interference by training on homogeneous secondary data, thereby improving performance in the majority of the instances
- Nonhomogeneous interference should pass through the filter
 - Targets fall in this category
 - Post-STAP processing should make the final determination of target presence or false alarm



Sample Selection for Airborne Radar





Nonhomogeneity Detectors (NHDs)



- Inner Product

$$d_i = X_i^H X_i = \sum_{i=1}^{NM} x_i^* x_i$$

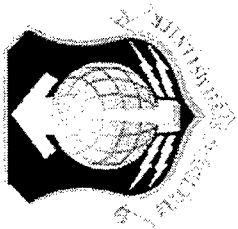
- Generalized Inner Product

$$g_i = X_i^H R_C^{-1} X_i$$

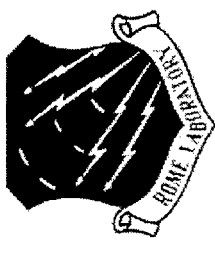
- Sample Matrix Inversion (SMI) Test Statistic

$$\eta_i = \left| s^H R_i^{-1} X_i \right|^2$$

- R_C is the test covariance matrix (sample covariance matrix derived from the data)
- Similar form for either space-time or reduced-dimension signal vector, X_i



Inner Product



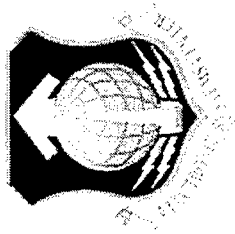
$$d_i = X_i^H X_i = \sum_{i=1}^{NM} x_i^* x_i$$

- Observe that two signal vectors may be characterized by dissimilar covariance matrices while exhibiting similar inner products

$$E[d_i] = \text{trace}(R_i) \quad (\text{expected value of inner product})$$

where

$$R_i = E[X_i X_i^H]$$



Generalized Inner Product

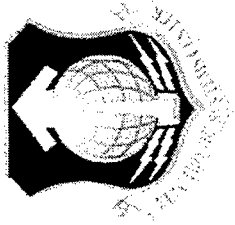
$$g_i = X_i^H R_C^{-1} X_i = (X_i^H R_C^{-1/2})(R_C^{-1/2} X_i) = \overline{X_i}^H \overline{X_i}$$

- g_i is equivalent to the sum of the squares of the signal vector, X_i , “whitened” or “partially whitened” by the filter, $R_C^{-1/2}$
- $R_C^{-1/2}$ is Hermitian because R_C is positive definite

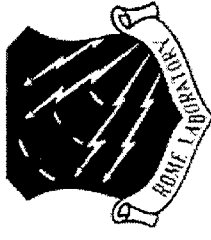
$$\overline{R_i} = E[\overline{X_i} \overline{X_i}^H] = R_C^{-1/2} E[X_i X_i^H] R_C^{-1/2} = R_C^{-1/2} R_i R_C^{-1/2}$$

$$\text{If } R_i \approx R_C \text{ then } \overline{R_i} \approx I_{NM} \text{ and } E[g_i] \approx NM$$

- We consider signal vectors with similar values of g_i as homogeneous with covariance matrices similar to R_C



SMI Test Statistic



- Let $\bar{\bar{R}}_i = R_C$ and define $W = R_C^{-1}$ s. Then,

$$\eta_i = |y_i|^2 = y_i y_i^* = W^H X_i X_i^H W$$

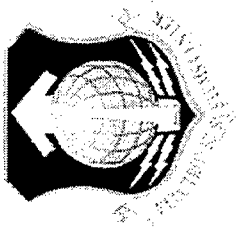
- In the homogeneous case,

$$E[\eta_i] \approx W^H R_C W \quad R_C \approx E[(C_i + N_i + I_i)(C_i + N_i + I_i)^H]$$

- In the nonhomogeneous case,

$$E[\eta_i] \approx W^H R_C W + W^H (R_{OC} + R_{CO} + R_O) W$$

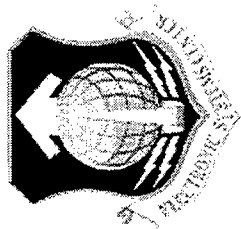
$$R_O = E[O_i O_i^H] \quad R_{OC} = E[O_i (C_i + N_i + I_i)^H] \quad R_{CO} = R_{OC}^H$$



Computational Considerations



- The Matrix Inversion Lemma [7] should be used to improve computational efficiency
- After computing the interference covariance matrix inverse using standard techniques (eg., QR decomposition), the matrix inversion lemma can be used to either add homogeneous samples or remove nonhomogeneous samples in a straightforward manner from the already computed matrix inverse
 - Significantly reduces computational burden over recomputing matrix inverse

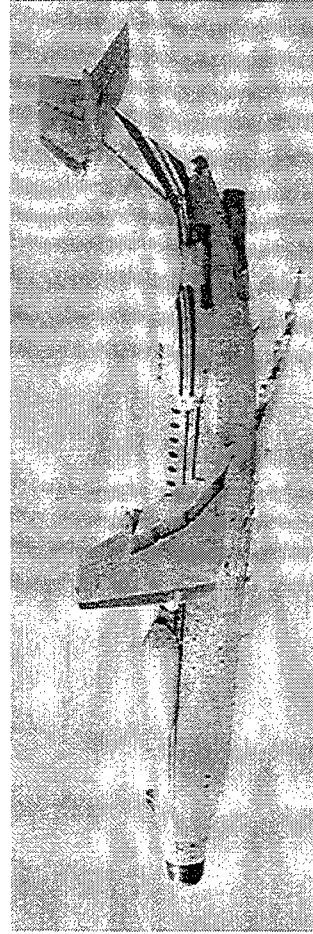


Measured Data Results

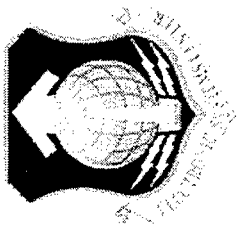
Some Relevant MCARM Data Information



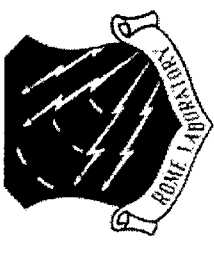
- Transmit Frequency: 1240 MHz
- Peak Transmit Power: 20 kW
- IF Center Frequency: 1.25 MHz
- IF Sampling Rate: 5 MHz
- Receiver Bandwidth: 0.8 MHz
- Coherent Processing Interval: 128 Pulses
- Sidemounted Array
- Subarray Configuration: Planar, 11 over 11 array
- Pulse Repetition Frequency: 2 kHz
- Data Collected in DELMARVA Peninsula Area - Flt. 5, Acq. 575
- Transmit Direction from Array Normal: 0 degrees (Broadside)
- Crab Angle: -7 degrees
- Injected Signal: Doppler 10, Range 290 (16.4 miles), SCNR of -56 dB w.r.t. mainbeam clutter and -25 dB w.r.t. sidelobe clutter
- For more MCARM information, see: <http://sunrise.oc.rl.af.mil/>



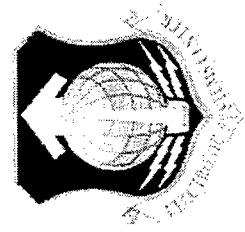
BAC 1-11



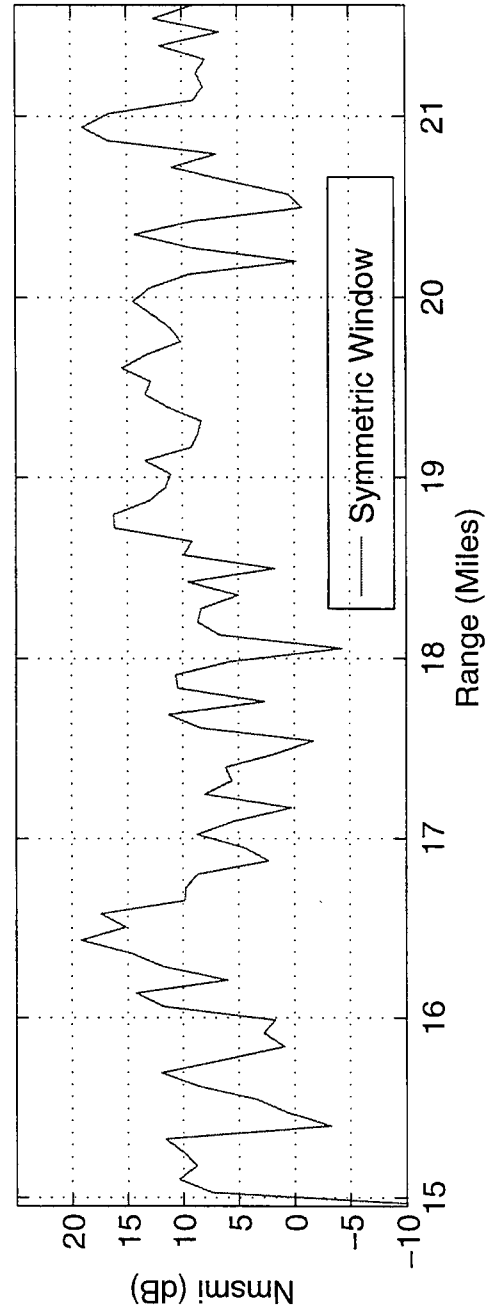
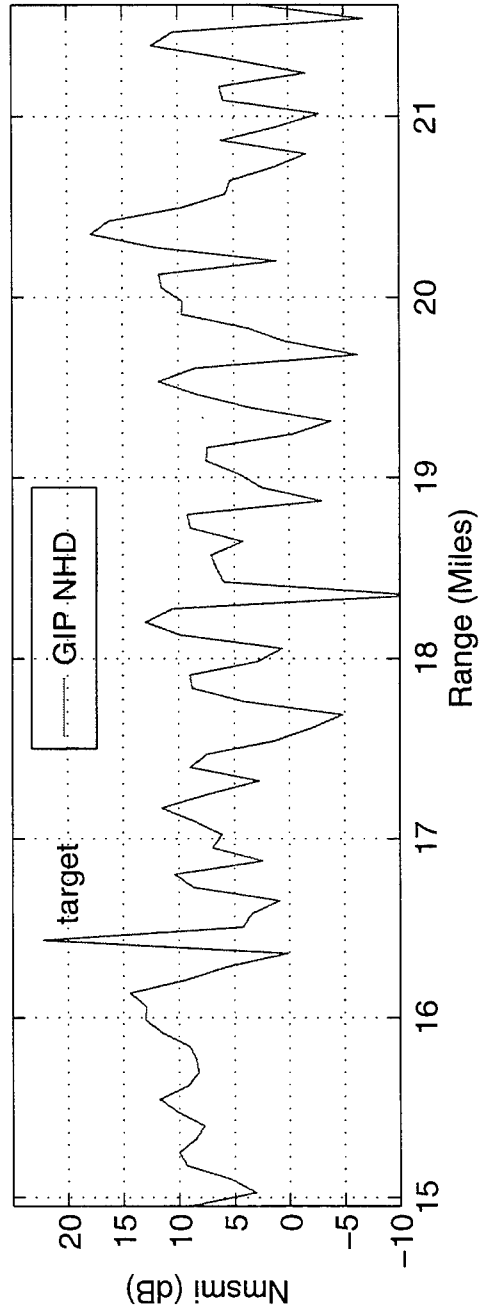
Data Analysis Example

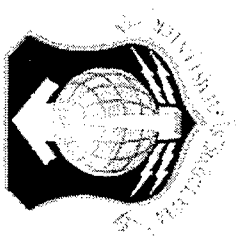


- Example of the importance of sample selection/demonstration of the preceding nonhomogeneity detectors - Apply the Factored Time-Space architecture to MCARM data with varying methods of sample selection - Single-pass NHD
 - Symmetric Window (SW) chooses 44 samples, 22 on each side of the cell under test (CUT) - Compute a new weight vector for each range cell as the window slides
 - Generalized Inner Product (GIP) chooses a single secondary data set of 44 samples appearing most homogeneous in terms of the GIP - Compute essentially a single weight vector over range from these 44 samples - Thresholds for Doppler 10 are $V_{lo}=0.7$, $V_{hi}=1.1$
 - SMI Test Statistic (SMI) applied in same way as GIP to select 44 samples for a homogeneous secondary data set - Threshold for Doppler 10 are $V_{lo}=0.1$, $V_{hi}=0.5$
 - Inner Product (IP) and strongest IP applied as SMI and GIP - The IP case chooses 44 samples most homogeneous in terms of their IP, whereas strongest IP chooses a nonhomogeneous set of 44 samples appearing strongest in power after [6]
- We plot the modified SMI test statistic (N_{msmi}), with its embedded CFAR characteristic to facilitate the comparison

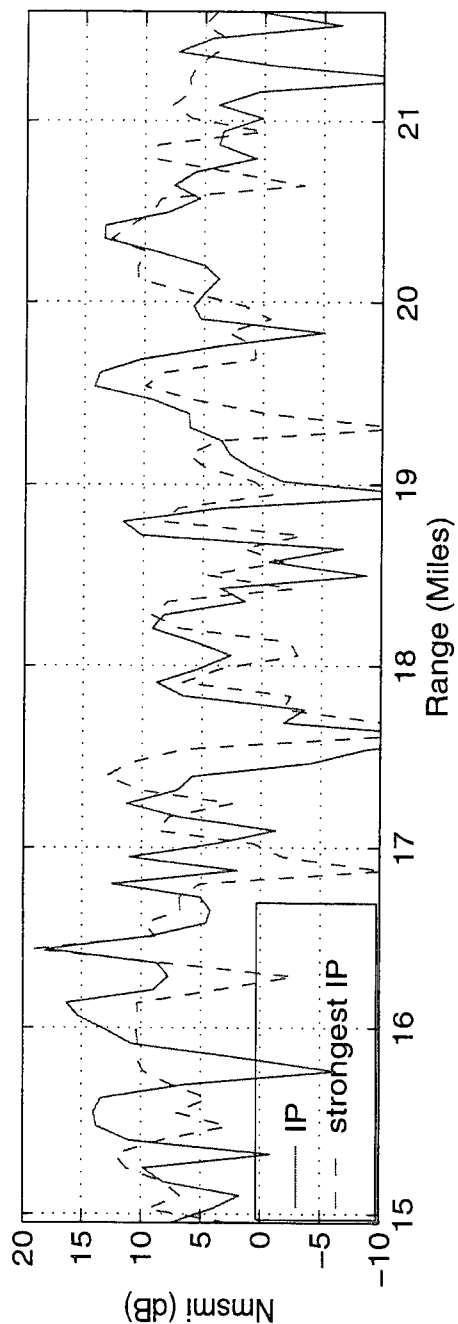
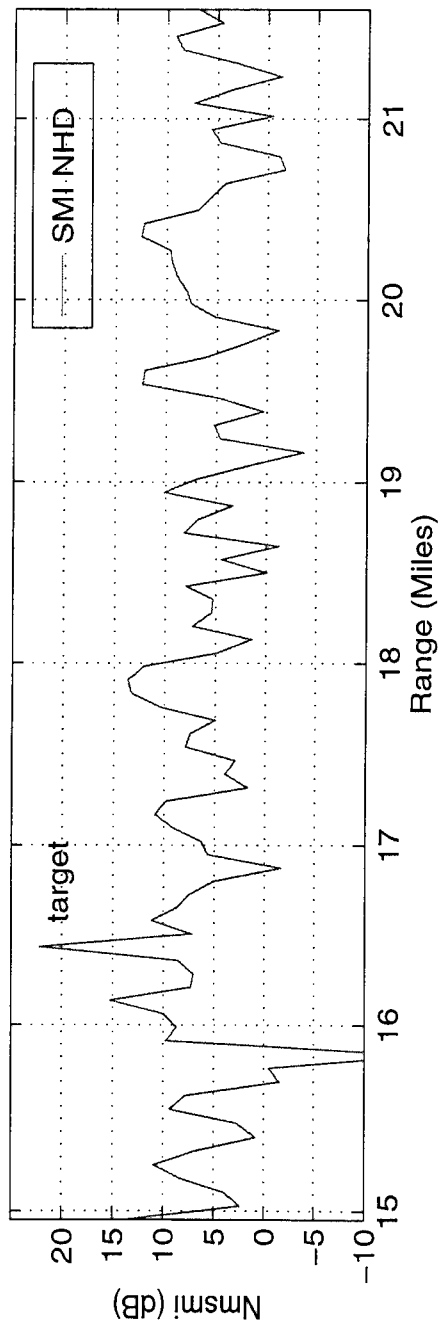


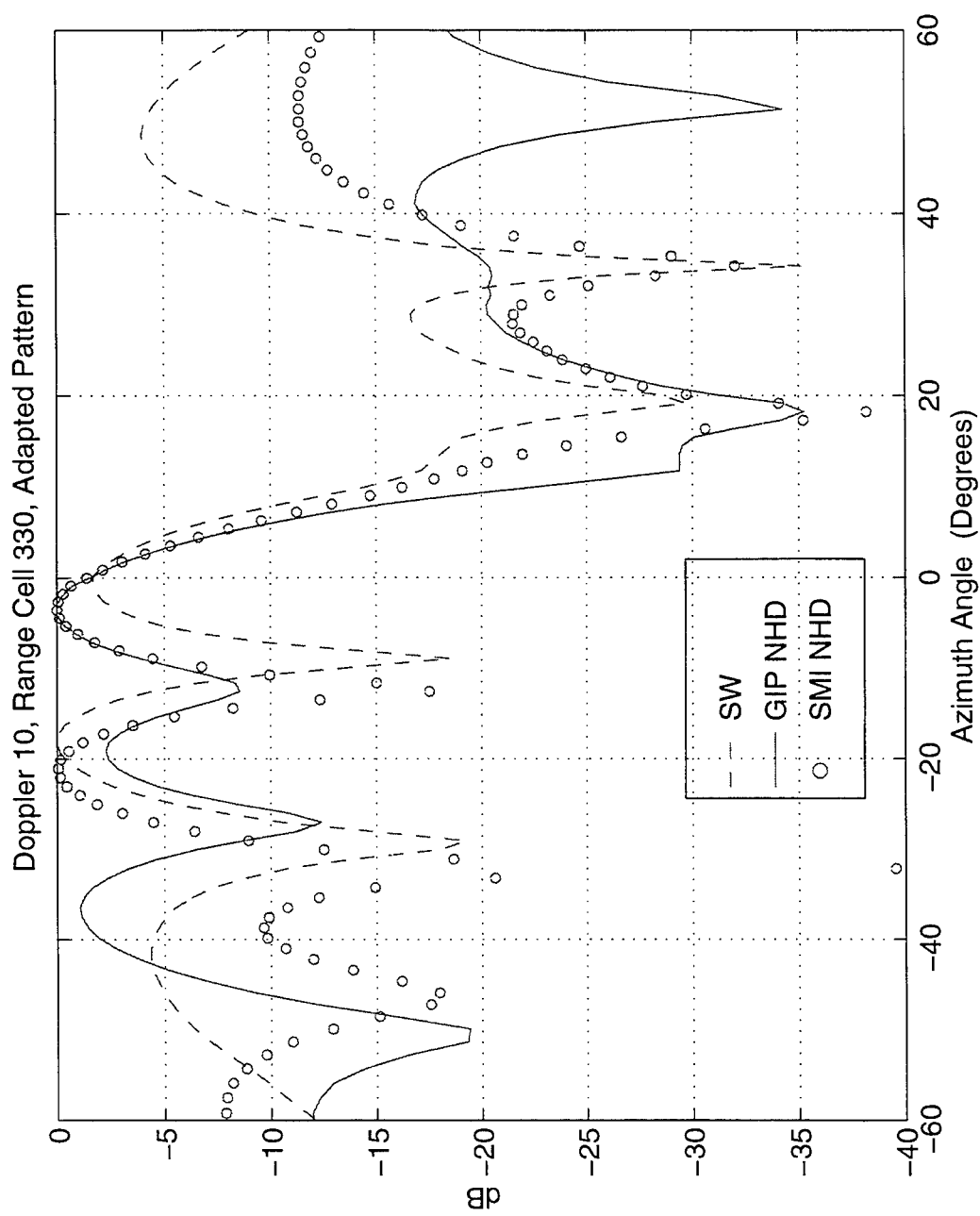
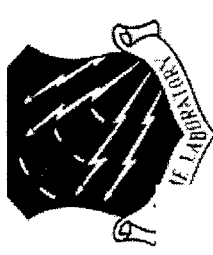
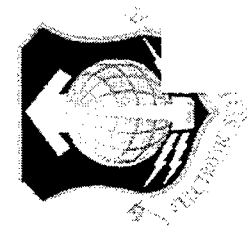
Doppler 10, MSMI test statistic vs. range

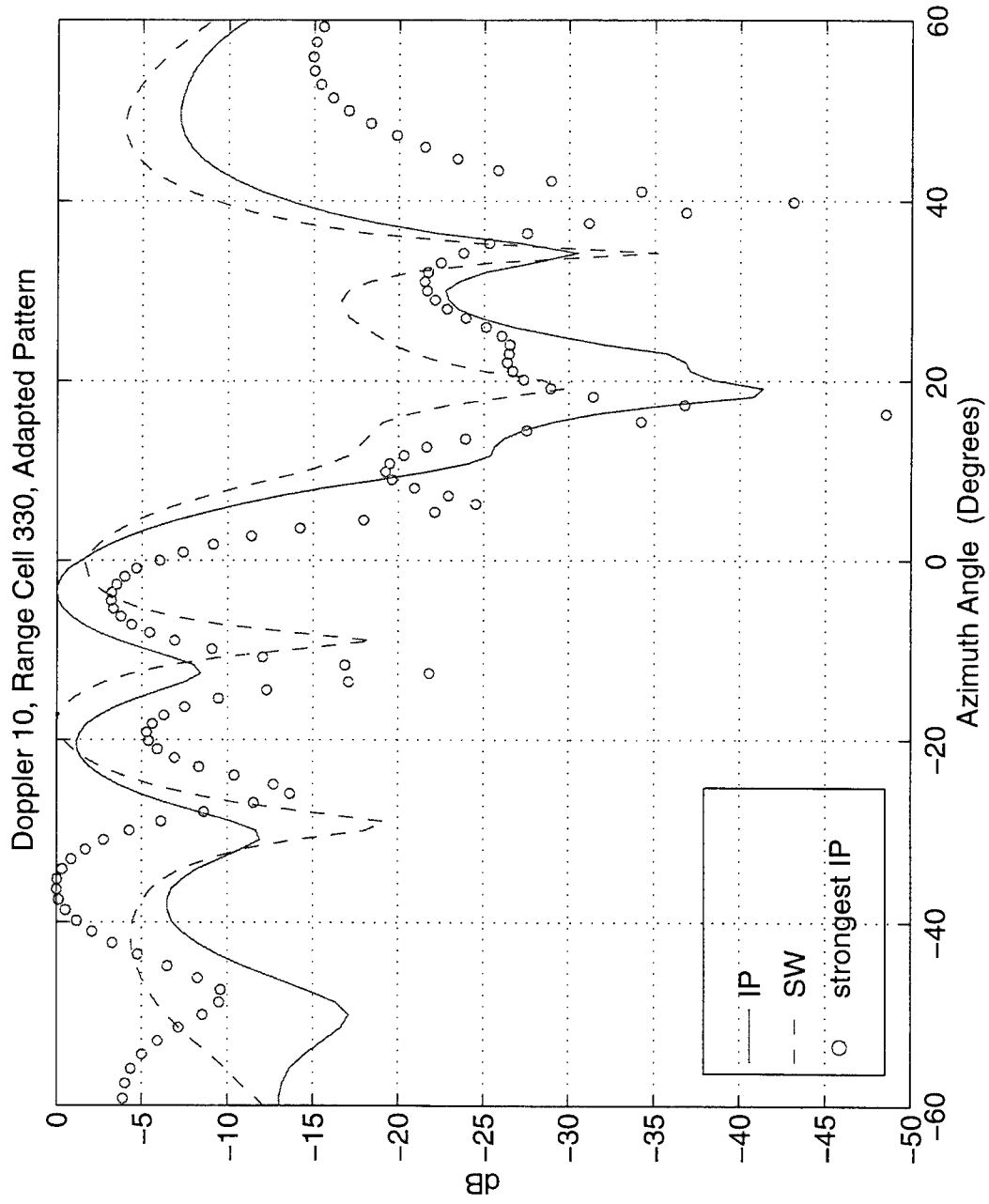
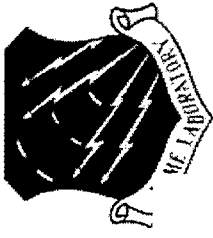
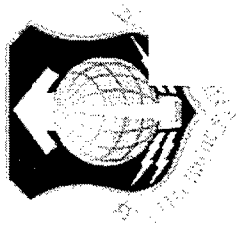


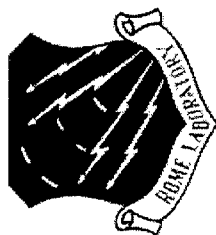
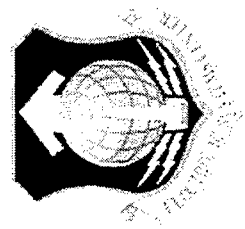


Doppler 10, MSMI test statistic vs. range

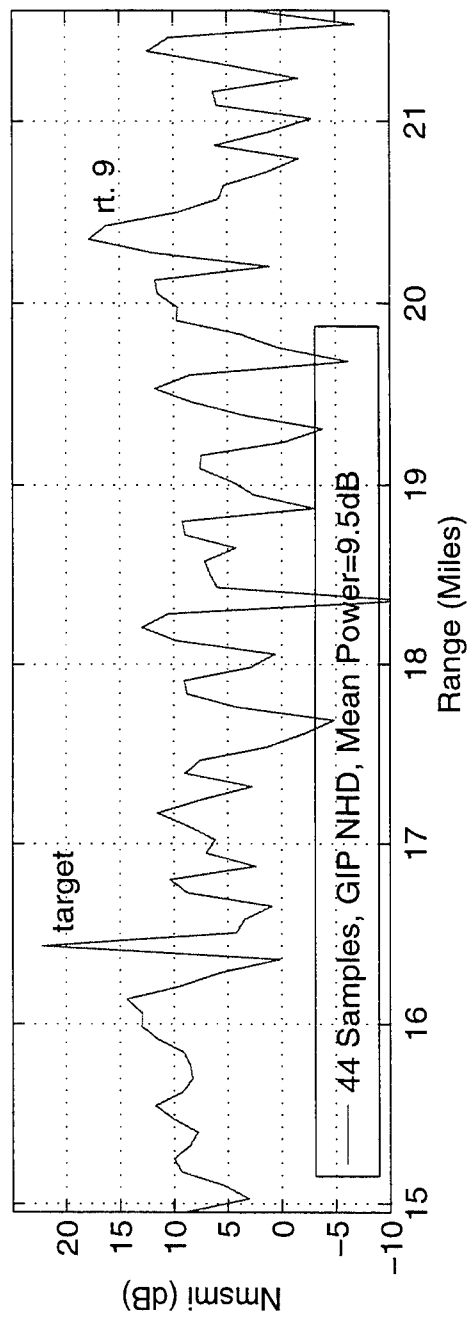
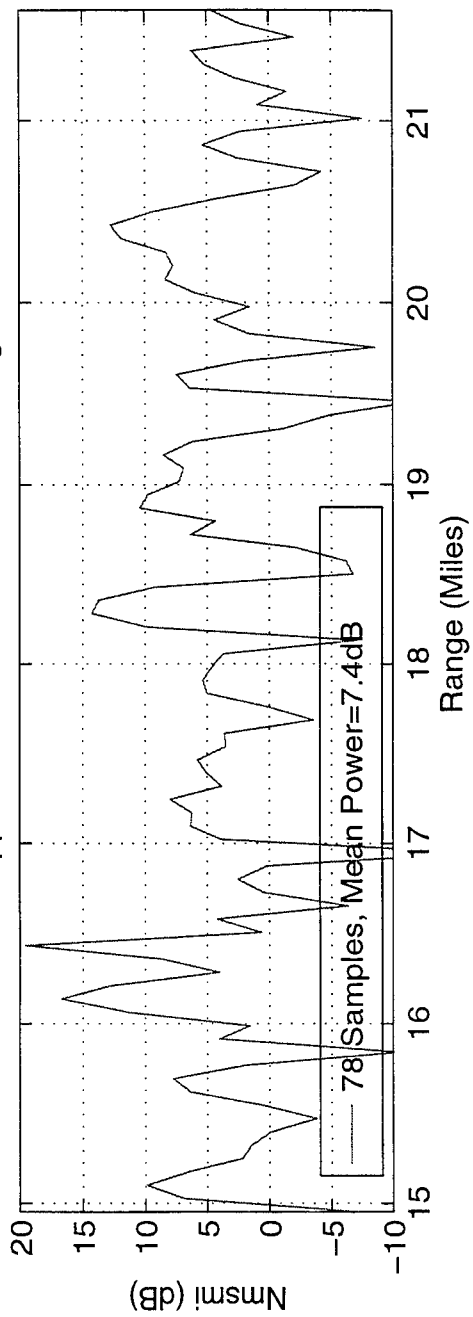


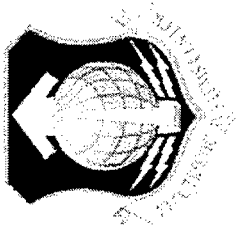






Doppler 10, MSML test statistic vs. range

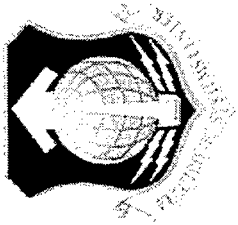




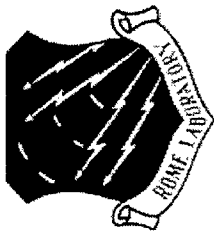
Relationship to Ongoing Work



- Knowledge-based applications to radar signal processing
 - Use of *a priori* knowledge, such as mapping and communication data, flight profile information, etc., combined with traditional data-derived information
- Bistatic space-time adaptive processing (Bi-STAP)
 - Use of STAP needed to mitigate severe bistatic clutter
 - However, sample selection is quite difficult, varying dramatically with geometry and thereby requiring improved sample selection techniques



Conclusions

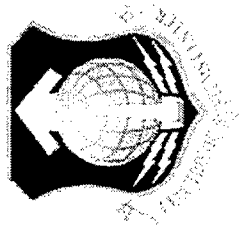


In this presentation, we:

- Provided a definition of “Nonhomogeneous”
- Discussed three nonhomogeneity detectors based on the generalized inner product, sample matrix inversion test statistic and inner product
- Analyzed measured data from the MCHARM program, demonstrating that improved sample selection methods yield improved STAP performance

Future research will focus on:

- Analyzing more measured monostatic data
- Developing better nonhomogeneity detectors
- Applying our methods to the bistatic problem



References

- [1] L.E. Brennan and I.S. Reed, "Theory of adaptive radar," *IEEE Trans. AES*, Vol. 9, No. 2, pp. 237-252, March 1973.
- [2] I.S. Reed, J.D. Mallett and L.E. Brennan, "Rapid convergence in adaptive arrays," *IEEE Trans. AES*, Vol. 10, No. 6, pp. 853-863, November 1974.
- [3] H. Wang and L. Cai, "On adaptive spatial-temporal processing for airborne surveillance radar systems," *IEEE Trans. AES*, Vol. 30, No. 3, pp. 660-670, July 1994.
- [4] D. Marshall, "Evaluation of STAP training strategies with Mountaintop data," MIT Lincoln Laboratory, TR MTP-5, 1996.
- [5] W.L. Melvin, M.C. Wicks, and R.D. Brown, "Assessment of multichannel airborne radar measurements for analysis and design of space-time processing architectures and algorithms," *Proc. 1996 IEEE Natl. Radar Conf.*, Ann Arbor, MI, pp. 130-135, May 13-16, 1996.
- [6] D.J. Rabideau and A.O. Steinhardt, "Improving the performance of adaptive arrays in nonstationary environments through data-adaptive training," *Proc. 30th Asilomar Conf. on Signal, Systems and Computers*, Pacific Grove, CA, 3-6 November, in press.
- [7] S. Haykin, *Adaptive Filter Theory*, 3rd Ed., Upper Saddle River, NJ: Prentice-Hall, 1996.

Structured Covariance Estimation for Space-Time Adaptive Processing

Timothy A. Barton and Steven T. Smith

MIT Lincoln Laboratory
244 Wood Street
Lexington, MA 02173-9108
tel: (617) 981-3278
email: barton@ll.mit.edu

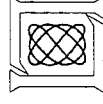
Abstract Adaptive nulling algorithms require a good estimate of the interference covariance matrix. In situations with limited sample support, such an estimate is not available unless there is covariance structure to be exploited. In applications such as space-time adaptive processing (STAP), where one may be attempting to null clutter in range and doppler, the underlying covariance matrix may be structured (e.g., block Toeplitz), and it is possible to exploit this structure to arrive at improved covariance estimates. Several structured covariance matrix estimators have been proposed for this purpose, including estimators that project the sample covariance matrix into the structured covariance matrix constraint set, as well as maximum likelihood (ML) estimators. The efficacy of several of these are analyzed in this talk in the context of a fully optimum STAP algorithm as well as several reduced-dimension sub-optimum STAP algorithms. The SINR losses resulting from these different algorithms are compared. In particular, an example illustrating the superior performance resulting from a new maximum likelihood algorithm (based on the expectation-maximization (EM) algorithm) is demonstrated using simulation and experimental data from the Mountaintop data set. It is shown specifically that for a low sample support, positive definite, sample covariance matrix, the SINR losses achieved away from main lobe clutter can be much greater for the projection covariance matrix estimators than that achieved using the EM algorithm-based ML estimator. In addition, the doppler coverage near main lobe clutter may also be significantly reduced when using the considered non-ML covariance matrix estimators.

STRUCTURED COVARIANCE ESTIMATION FOR SPACE-TIME ADAPTIVE PROCESSING

**TIMOTHY A. BARTON
STEVEN T. SMITH**

MIT LINCOLN LABORATORY

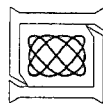
**ASAP WORKSHOP
MARCH 12, 1997**



3/10/97
TAB-ASAP97

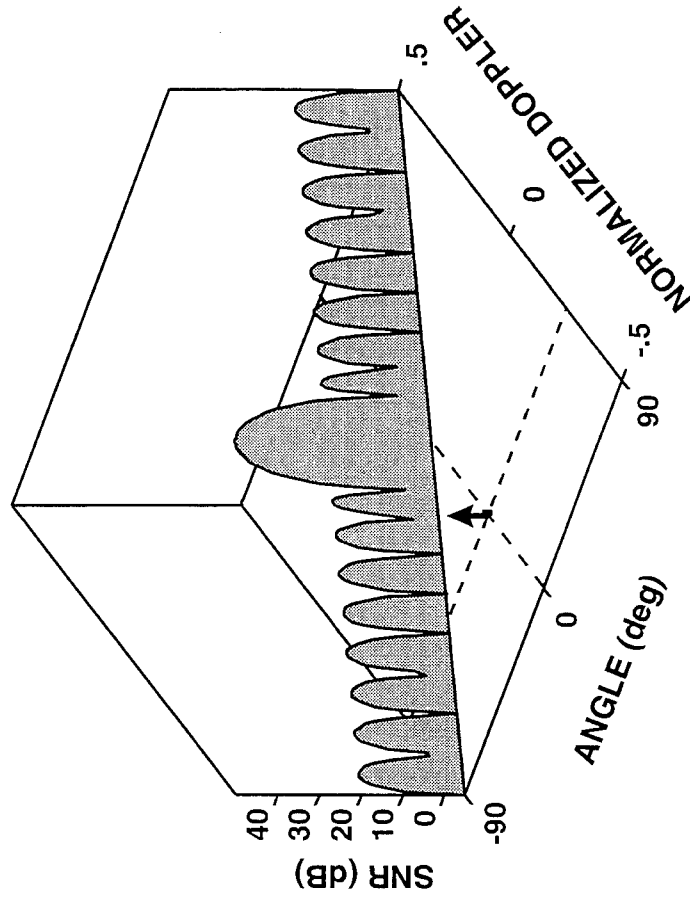
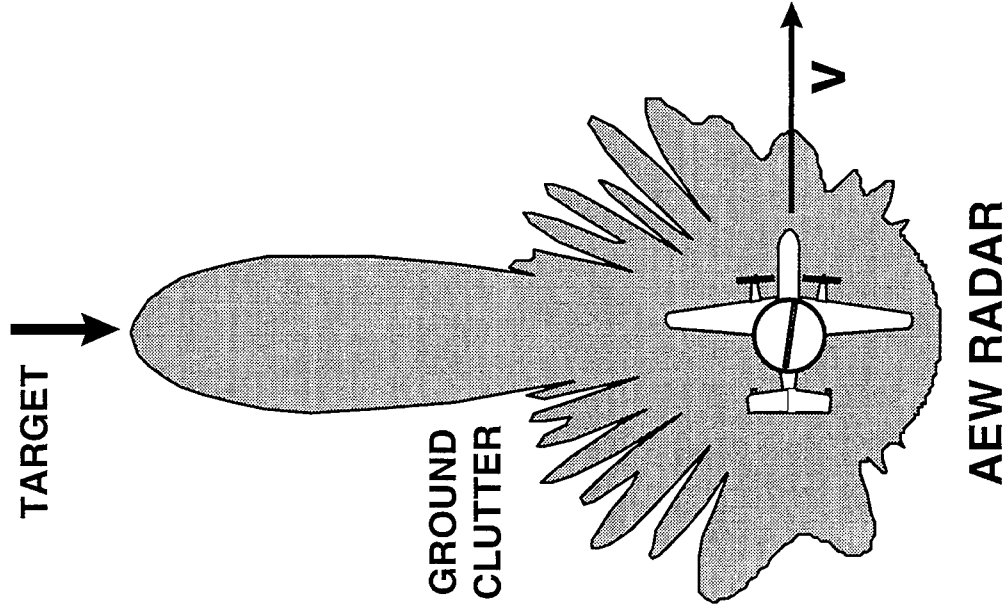
OUTLINE

- INTRODUCTION
- STRUCTURED COVARIANCE ESTIMATION TECHNIQUES
- ANALYSIS
- SUMMARY AND CONCLUSIONS



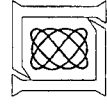
3/10/97
TAB-ASAP97

SPACE-TIME ADAPTIVE PROCESSING (STAP)



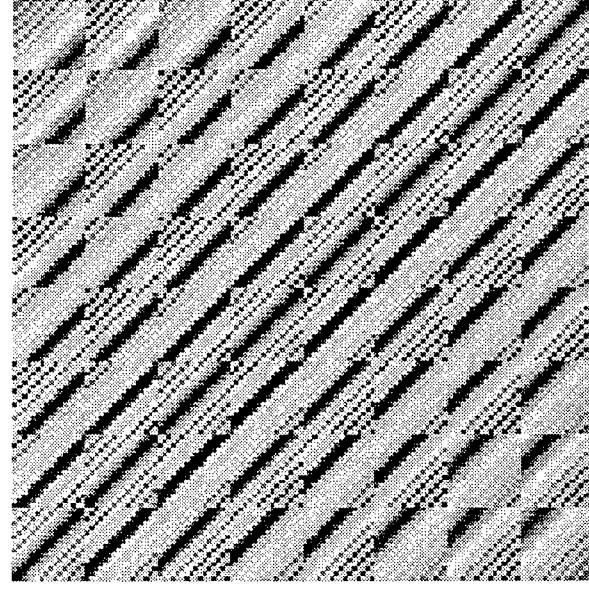
TWO-DIMENSIONAL FILTERING REQUIRED
TO CANCEL GROUND CLUTTER

SPACE-TIME ADAPTIVE PROCESSING
(STAP)

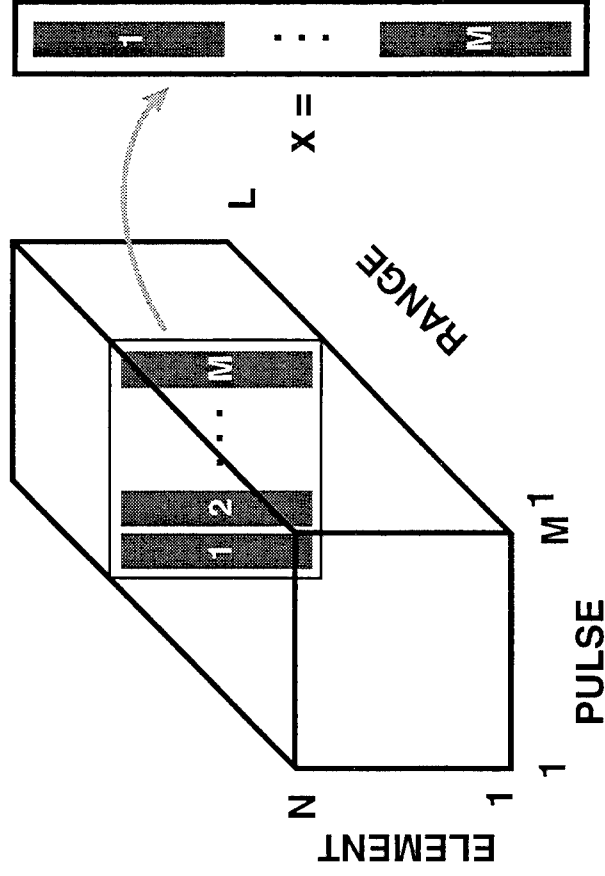


COVARIANCE MATRIX STRUCTURE FOR STAP

TOEPLITZ BLOCK TOEPLITZ
CLUTTER COVARIANCE MATRIX
 $MN \times MN$

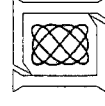


PULSE DOPPLER
DATA CUBE



• BLOCK ROW: M BLOCKS EACH
OF SIZE $N \times N$

- UNIFORM LINEAR ARRAY
- FIXED PRI



WHY PERFORM STRUCTURED COVARIANCE MATRIX ESTIMATION FOR STAP?

$$w = \hat{R}^{-1}v \quad \hat{R} = f\left(\frac{1}{K} \sum_{k=1}^K x_k x_k^H\right) = f(S)$$

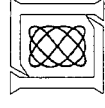
- IMPROVED ADAPTIVE PROCESSING PERFORMANCE FOR A GIVEN SAMPLE SUPPORT K
- REASONABLE OR IMPROVED ADAPTIVE PROCESSING PERFORMANCE IN A LIMITED SAMPLE SUPPORT SCENARIO

$$K < 2N_{\text{DOF}}$$

- LARGE N_{DOF}
- NONSTATIONARITY

- FOR $N = 8$ ELEMENTS AND $M = 8$ PULSES:

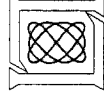
- FREE PARAMETERS IN S: $(MN)^2 = 4096$
- FREE PARAMETERS IN A BLOCK TOEPLITZ COVARIANCE MATRIX: $(2M-1)N^2 = 960$




OBJECTIVES

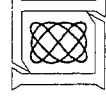
IN AN ADAPTIVE NULLING FRAMEWORK WITH LIMITED SAMPLE SUPPORT:

- WHAT ARE “REASONABLE” METHODS OF STRUCTURED COVARIANCE ESTIMATION?
- WHAT ARE THE ADAPTIVE PROCESSING PERFORMANCE CONSEQUENCES OF THESE STRUCTURED COVARIANCE MATRIX ESTIMATORS?



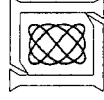
OUTLINE

- INTRODUCTION
-  STRUCTURED COVARIANCE ESTIMATION TECHNIQUES
 - PROJECTION
 - MAXIMUM LIKELIHOOD (ML)
- ANALYSIS
- SUMMARY AND CONCLUSIONS



BLOCK TOEPLITZ COVARIANCE ESTIMATION TECHNIQUES

BLOCK TOEPLITZ COVARIANCE MATRIX ESTIMATOR	CHARACTERISTICS (LOW SAMPLE SUPPORT)
<div> <div>PROJECTED</div> <div>WEIGHTED PROJECTED</div> </div>	<div> <div>LOW COMPUTATIONAL COMPLEXITY</div> <div>POOR STAP PERFORMANCE</div> </div>
<div> <div>MAXIMUM LIKELIHOOD (EXPECTATION-MAXIMIZATION ALGORITHM)</div> </div>	<div> <div>IMPROVED STAP PERFORMANCE</div> <div>HIGH COMPUTATIONAL COMPLEXITY</div> </div>



THE PROJECTED BLOCK TOEPLITZ COVARIANCE MATRIX ESTIMATOR

$$S = \frac{1}{K} \sum_{k=1}^K x_k x_k^H$$

- DIAGONAL BLOCKS OF \hat{R}_P ARE COMPUTED BY AVERAGING DOWN BLOCK-DIAGONALS OF S

\hat{R}_{11}	\hat{R}_{12}	\hat{R}_{13}
\hat{R}_{12}^H	\hat{R}_{11}	\hat{R}_{12}
\hat{R}_{13}^H	\hat{R}_{12}^H	\hat{R}_{11}

$$\hat{R}_P =$$

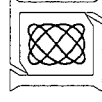
$$\hat{R}_{11} = (S_{11} + S_{22} + S_{33}) / 3$$

$$\hat{R}_{12} = (S_{12} + S_{23}) / 2$$

$$\hat{R}_{13} = (S_{13}) / 1$$

- EVEN IF S IS P.D., \hat{R}_P IS NOT GUARANTEED TO BE P.D.

- COMPUTATION: $O[\text{SAMPLE SUPPORT} \times N_{\text{DOF}}^3]$



THE WEIGHTED PROJECTED BLOCK TOEPLITZ COVARIANCE MATRIX ESTIMATOR

- DIAGONAL BLOCKS OF \hat{R}_{WP} ARE COMPUTED BY CALCULATING WEIGHTED AVERAGE DOWN BLOCK-DIAGONALS OF S

\hat{R}_{11}	\hat{R}_{12}	\hat{R}_{13}
\hat{R}_{12}^H	\hat{R}_{11}	\hat{R}_{12}
\hat{R}_{13}^H	\hat{R}_{12}^H	\hat{R}_{11}

$$\hat{R}_{WP} =$$

$$\hat{R}_{11} = S_{11} + S_{22} + S_{33}$$

$$\hat{R}_{12} = S_{12} + S_{23}$$

$$\hat{R}_{13} = S_{13}$$

IF S IS P.D., \hat{R}_{WP} IS GUARANTEED TO BE P.D.

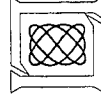
- COMPUTATION: $O[\text{SAMPLE SUPPORT} \times N_{\text{DOF}}^3]$

ML STRUCTURED COVARIANCE MATRIX ESTIMATION

$$p(\mathbf{S}; \mathbf{R}) = \frac{1}{\pi^{(MN)K} |\mathbf{R}|^K} \exp(-K \operatorname{tr}(\mathbf{R}^{-1} \mathbf{S})) \quad L_{\text{ID}}(\mathbf{S}; \mathbf{R}) = -K \log |\mathbf{R}| - K \operatorname{tr}(\mathbf{R}^{-1} \mathbf{S})$$

$\hat{\mathbf{R}} = \max(\text{LOG-LIKELIHOOD}) \text{ OVER CONSTRAINT SET}$

- FOR MOST STRUCTURED COVARIANCE CONSTRAINT SETS
NO CLOSED FORM SOLUTION IS KNOWN
- ITERATIVE TECHNIQUES
 - BURG, LUENBERGER, AND WENGER
 - SNYDER, MILLER, AND FUHRMANN



THE EXPECTATION-MAXIMIZATION (EM) ALGORITHM

- ASSUMPTIONS

$$L_{ID}(\Theta) = \log [p(\text{incomplete data} \mid \Theta)]$$

$$L_{CD}(\Theta) = \log [p(\text{complete data} \mid \Theta)]$$

- ITERATION SEQUENCE

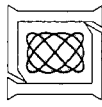
- E-STEP

$$Q(\Theta \mid \hat{\Theta}_p) = E \{ L_{CD}(\Theta \mid \text{incomplete data}, \hat{\Theta}_p) \}$$

- M-STEP

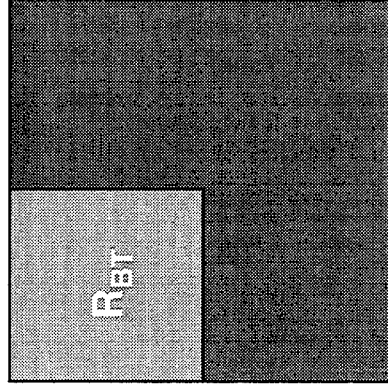
$$\hat{\Theta}_{p+1} = \max_{\Theta \in \Theta} [Q(\Theta \mid \hat{\Theta}_p)]$$

THE SEQUENCE OF INCOMPLETE DATA LOG-LIKELIHOOD
 $L_{ID}(\hat{\Theta}_p)$ IS NON-DECREASING



ML BLOCK TOEPLITZ COVARIANCE MATRIX ESTIMATION

THE EM ALGORITHM ASSUMPTIONS

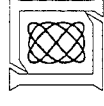


$$R_{BC} = [W_Q \otimes I_N] \Sigma [W_Q \otimes I_N]^H$$

- $R_{BC} = QN \times QN$ BLOCK CIRCULANT COVARIANCE MATRIX ($Q > M$)
- $\Sigma = QN \times QN$ BLOCK DIAGONAL COVARIANCE MATRIX
- BLOCK SIZE N

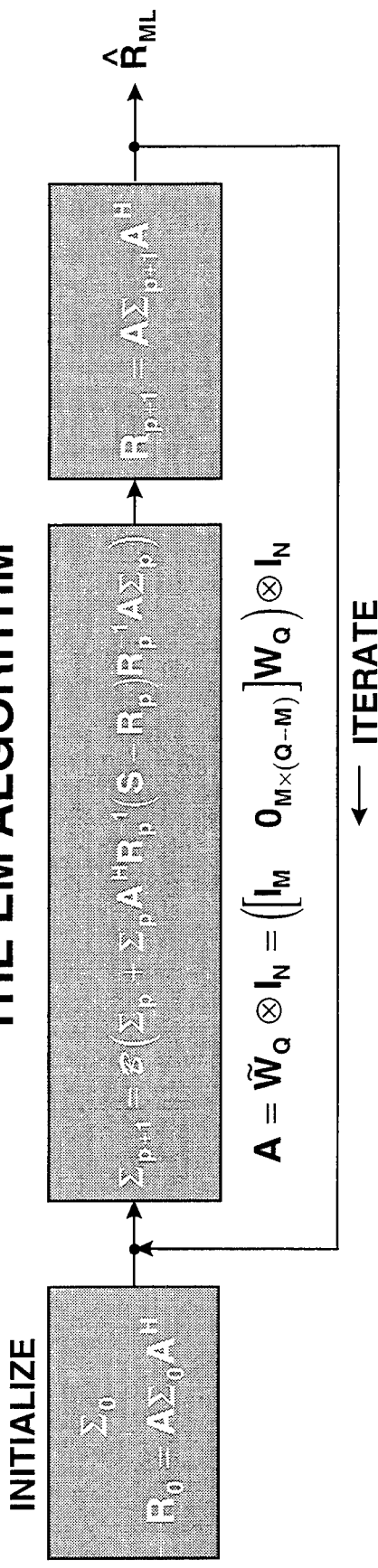
- $R_{BT} = MN \times MN$ BLOCK TOEPLITZ COVARIANCE MATRIX

$$R_{BT} = A \Sigma A^H \quad A = \tilde{W}_Q \otimes I_N \quad \tilde{W}_Q = \begin{bmatrix} I_M & 0_{M \times (Q-M)} \end{bmatrix} W_Q$$



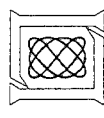
ML BLOCK TOEPLITZ COVARIANCE MATRIX ESTIMATION

THE EM ALGORITHM



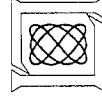
IF S AND Σ_0 ARE P.D., \hat{R}_{ML} IS GUARANTEED TO BE P.D.

- NON-DECREASING $L_{ID}(S;R)$
- MAXIMIZES $L_{ID}(S;R)$ (Locally)
- COMPUTATION:
 $O[(\text{ITERATIONS} + \text{SAMPLE SUPPORT}) \times N_{\text{DOF}}^3]$



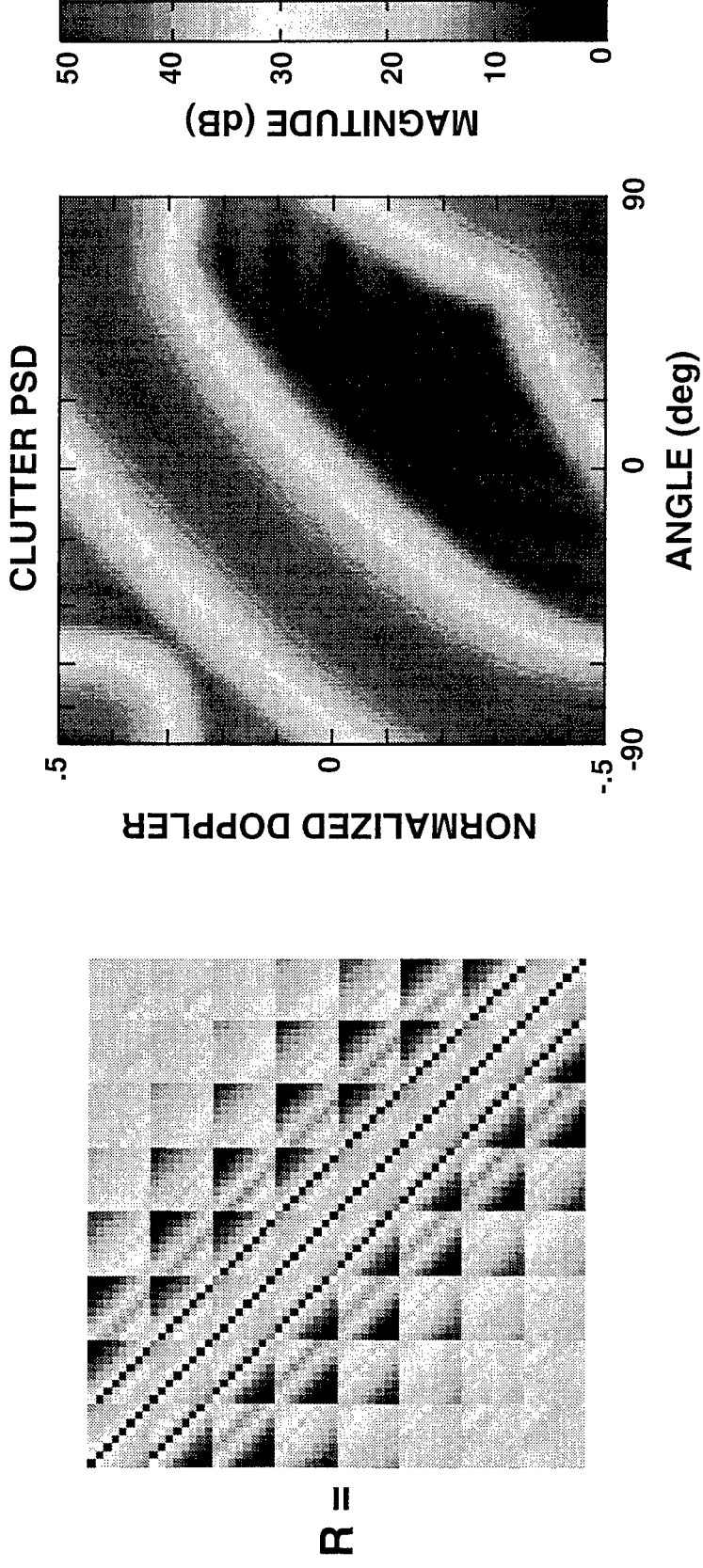
OUTLINE

- INTRODUCTION
- STRUCTURED COVARIANCE ESTIMATION TECHNIQUES
- ANALYSIS
 - SIMULATION
 - MOUNTAINTOP DATA
- SUMMARY AND CONCLUSIONS

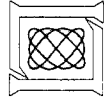


STAP SIMULATION SCENARIO

- 8 ELEMENTS / 8 PULSES $\rightarrow N_{\text{DOF}} = 64$
- 40 dB CNR



ASSUME BLOCK TOEPLITZ COVARIANCE MATRIX STRUCTURE



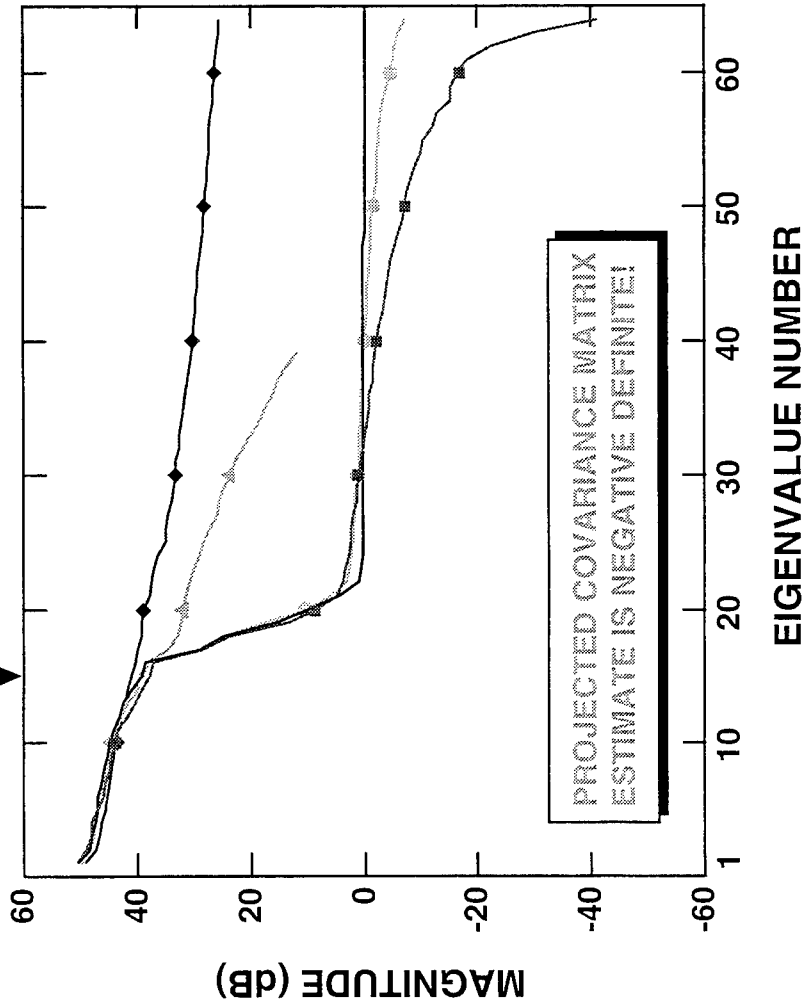
BLOCK TOEPLITZ COVARIANCE MATRIX ESTIMATE EIGENVALUES

- 8 ELEMENTS / 8 PULSES
- $N_{\text{DOF}} = 64$
- SAMPLE SUPPORT = 64

LOW SAMPLE SUPPORT

BRENNAN'S RULE

$$r_c \approx \left\lfloor N + (M - 1)\beta \right\rfloor = 15$$



MAGNITUDE (dB)

EIGENVALUE NUMBER

COVARIANCE ESTIMATORS

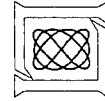
IDEAL

SAMPLE

PROJECTED

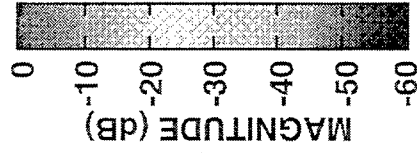
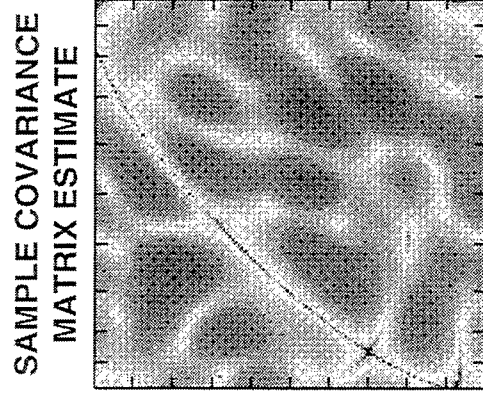
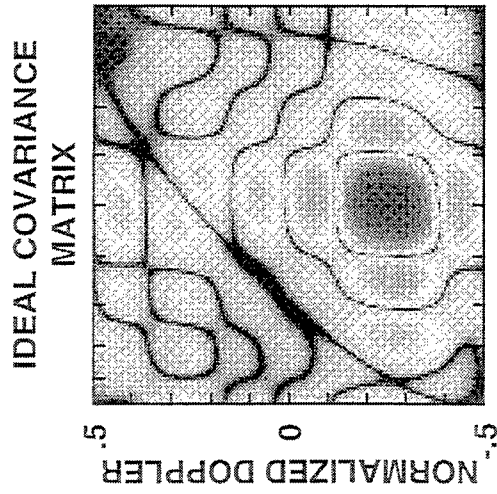
WEIGHTED PROJECTED

ML



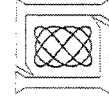
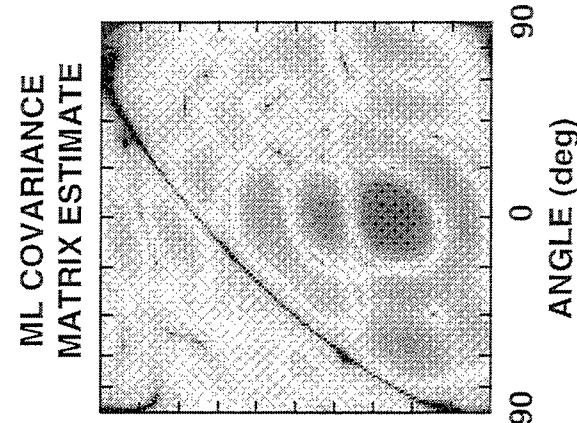
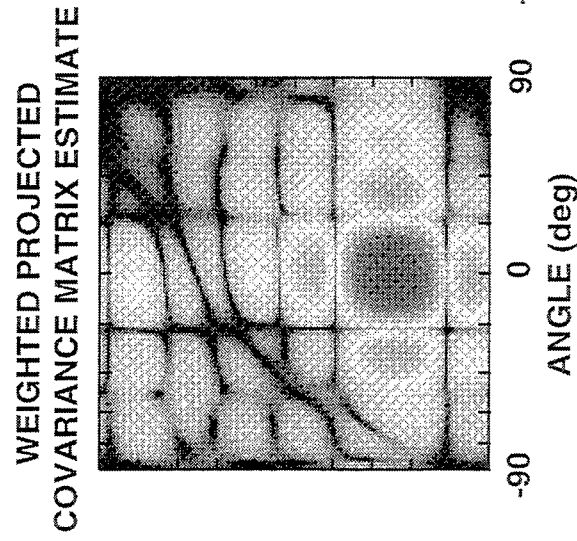
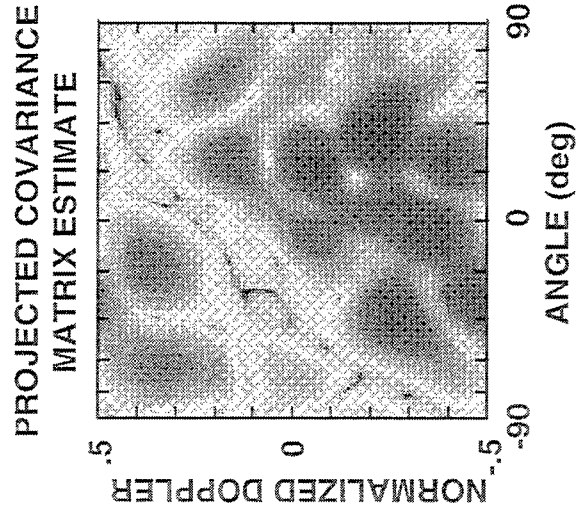
3/10/97
TAB-ASAP97

ADAPTIVE ANTENNA PATTERNS FOR FULLY ADAPTIVE STAP



- 8 ELEMENTS / 8 PULSES
- $N_{\text{DOF}} = 64$
- SAMPLE SUPPORT = 64

LOW SAMPLE SUPPORT



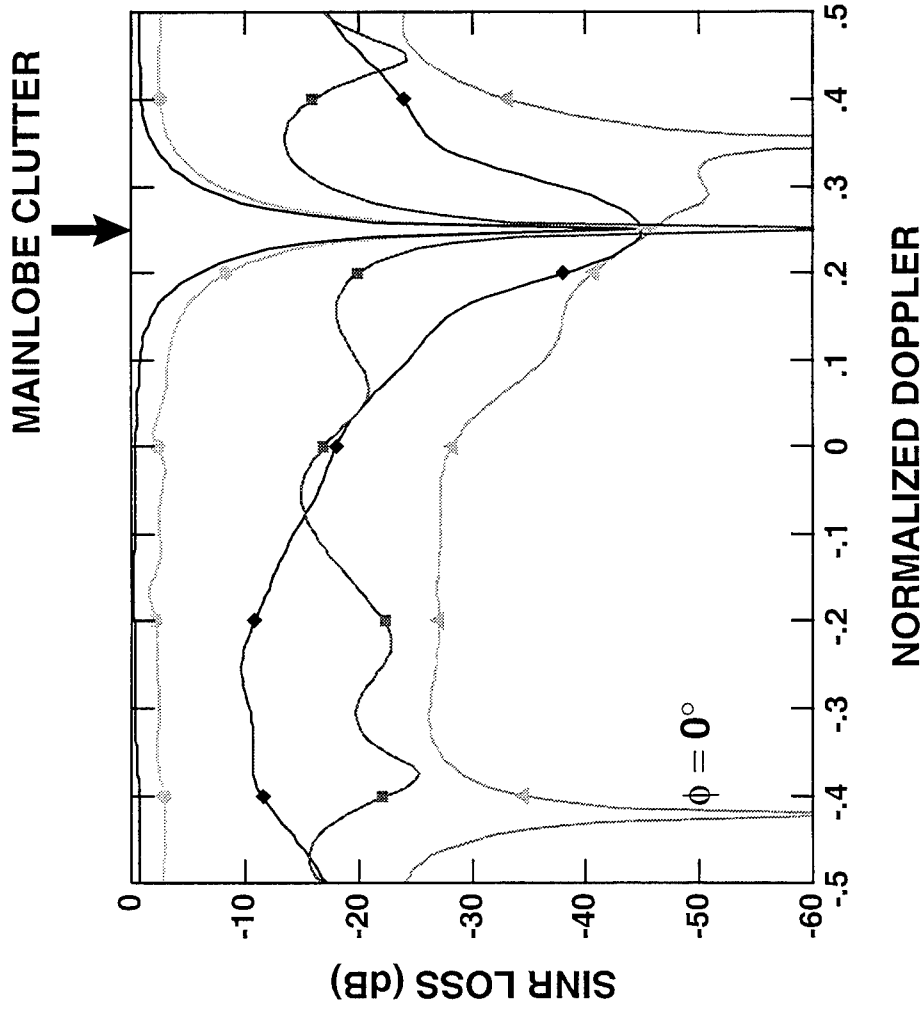
3/10/97
TAB-ASAP97

SINR LOSS FOR FULLY ADAPTIVE STAP

ELEMENT SPACE PRE-DOPPLER

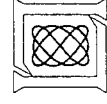
- 8 ELEMENTS / 8 PULSES
- $N_{\text{DOF}} = 64$
- SAMPLE SUPPORT = 64

LOW SAMPLE SUPPORT



COVARIANCE ESTIMATORS

- IDEAL
- SAMPLE
- ▲— PROJECTED
- ◆— WEIGHTED PROJECTED
- ML



3/10/97
TAB-ASAP97

COMPUTATIONAL CONSIDERATIONS

FOR $N_{\text{DOF}} = 64$:

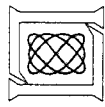
- THE ML (EM ALGORITHM) BLOCK TOEPLITZ COVARIANCE MATRIX ESTIMATOR REQUIRES:

$$O[(\text{ITERATIONS} + 1) \times N_{\text{DOF}}^3] \approx 40 \text{ MFLOPS}$$

- IF THE SAMPLE SUPPORT EXISTS:
EQUIVALENT STAP PERFORMANCE USING THE SAMPLE COVARIANCE MATRIX ESTIMATOR REQUIRES $3 \times N_{\text{DOF}}$ SAMPLE SUPPORT:

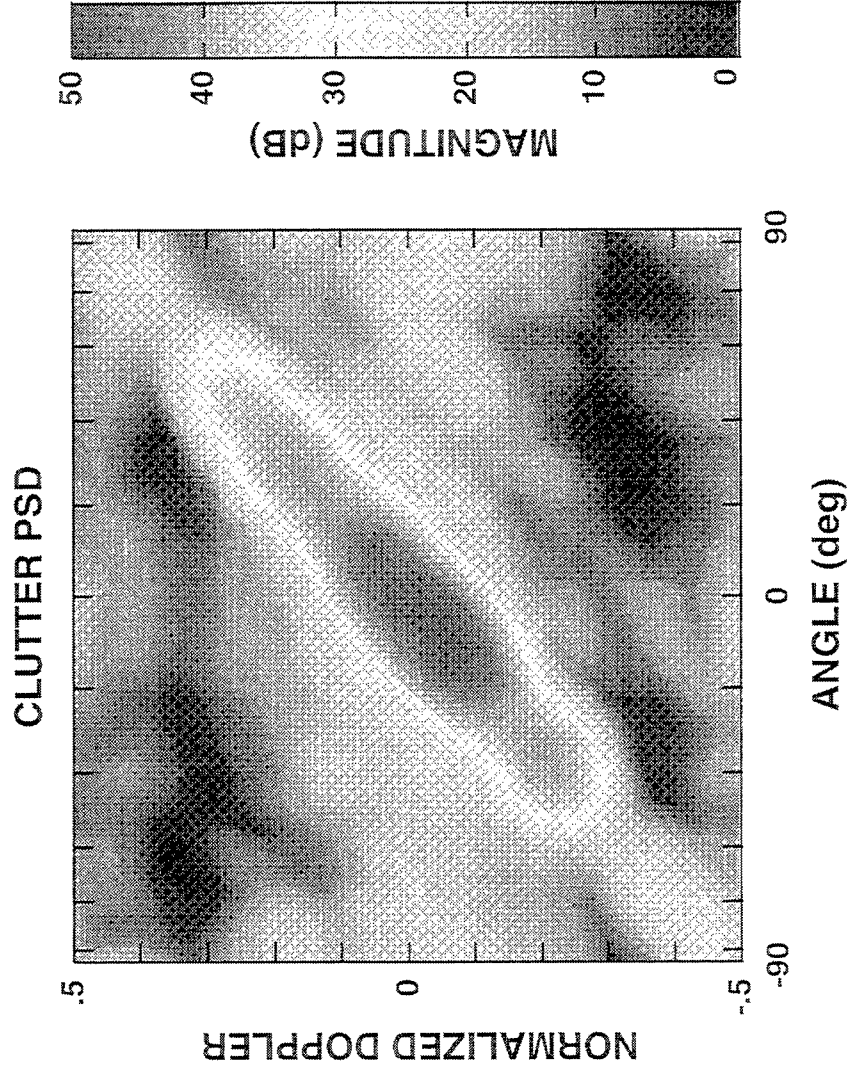
$$O[3 \times N_{\text{DOF}}^3] \approx 0.8 \text{ MFLOPS}$$

- FOR EQUIVALENT STAP PERFORMANCE, THE ML ESTIMATOR REQUIRES ≈ 50 TIMES THE COMPUTATION REQUIRED BY THE SAMPLE COVARIANCE ESTIMATOR AND 1/3 THE SAMPLE SUPPORT



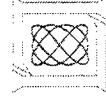
MOUNTAINTOP DATA EXAMPLE

CLUTTER ENVIRONMENT



- 14 ELEMENTS / 16 PULSES

- $N_{\text{DOF}} = 224$



3/10/97
TAB-ASAP97

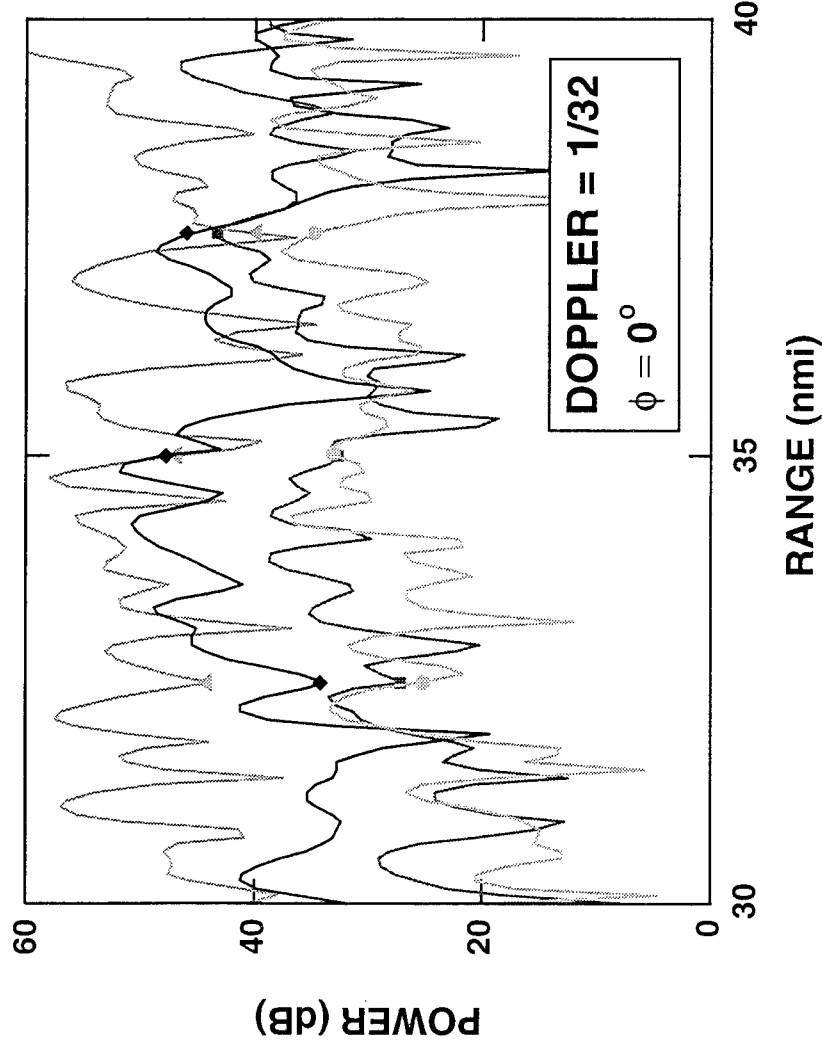
MOUNTAINTOP DATA EXAMPLE

DISPLACED PHASE CENTER PRE-DOPPLER STAP

- 14 ELEMENTS / 16 PULSES
 - 3 SUBAPERTURES
 - $N_{\text{DOF}} = 48$
 - SAMPLE SUPPORT = 61
- TRAIN: 25 - 30 nmi

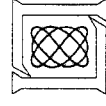
LOW SAMPLE SUPPORT

RESIDUAL CLUTTER-PLUS-NOISE
OUTPUT POWER



COVARIANCE ESTIMATORS

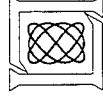
- SAMPLE
- ▲--- PROJECTED
- ◆— WEIGHTED PROJECTED
- ML



3/10/97
TAB-ASAP97

SUMMARY

- CHARACTERIZED LOW SAMPLE SUPPORT STAP PERFORMANCE FOR BLOCK TOEPLITZ COVARIANCE ESTIMATION TECHNIQUES
- THE PROJECTED ESTIMATORS PROVIDE:
 - COMPUTATION: $O[\text{SAMPLE SUPPORT} \times N_{\text{DOF}}^3]$
 - 10-30 dB SINR LOSS AWAY FROM MAINLOBE CLUTTER
 - DECREASED DOPPLER COVERAGE NEAR MAINLOBE CLUTTER
- THE ML (EM Algorithm) ESTIMATOR PROVIDES:
 - 2-4 dB SINR LOSS AWAY FROM MAINLOBE CLUTTER
 - NEAR IDEAL DOPPLER COVERAGE NEAR MAINLOBE CLUTTER
 - COMPUTATION: $O[(\text{ITERATIONS} + \text{SAMPLE SUPPORT}) \times N_{\text{DOF}}^3]$
- FOR THE MOUNTAINTOP DATA EXAMPLE, THE ML ESTIMATOR PROVIDES > 13 dB IMPROVED RESIDUAL CLUTTER-PLUS-NOISE PERFORMANCE



The Effect of Bandwidth on Space-Time Adaptive Processing (STAP)

Michael A. Zatman

MIT Lincoln Laboratory
244 Wood Street
Lexington, MA 02173-9108
tel: (617) 981-2543
email: zatman@ll.mit.edu

Abstract In the airborne radar environment, STAP is used to suppress ground clutter returns. Most of the analysis on space-time adaptive processing to date has used the narrowband signal model. In this paper new results on the effect of bandwidth on STAP are presented. Bandwidth leads to dispersion in two dimensions, both across the array in the angle domain and across the coherent processing interval in the Doppler domain. When the array is not aligned with the platform's velocity vector the dispersion leads to a broadening of the clutter ridge and a degradation in the radar's minimum detectable velocity performance. However, in the absence of misalignment between the array and the platform's velocity vector the effects of bandwidth are negligible. For reasons of computational complexity and sample support, reduced dimension algorithms are required for the practical implementation of STAP. Previous analysis using the narrowband signal model shows that postDoppler STAP algorithms perform better than their pre-Doppler counterparts. However, we show that the coherent gain on clutter due to the Doppler filtering applied to the data prior to adaptive processing makes post-Doppler STAP algorithms more susceptible to the effects of bandwidth. Time delay steering (TDS) has been proposed as a method of mitigating the effects of dispersion. While conventional (spatial) TDS improves angular coverage in the presence of jamming, it does not compensate for the Doppler component of dispersion when suppressing clutter. In STAP minimizing both the spatial and Doppler dispersion on the mainlobe clutter with TDS in both domains provides the most improvement.

THE EFFECT OF BANDWIDTH ON SPACE-TIME ADAPTIVE PROCESSING

MICHAEL ZATMAN, MIT LINCOLN LABORATORY

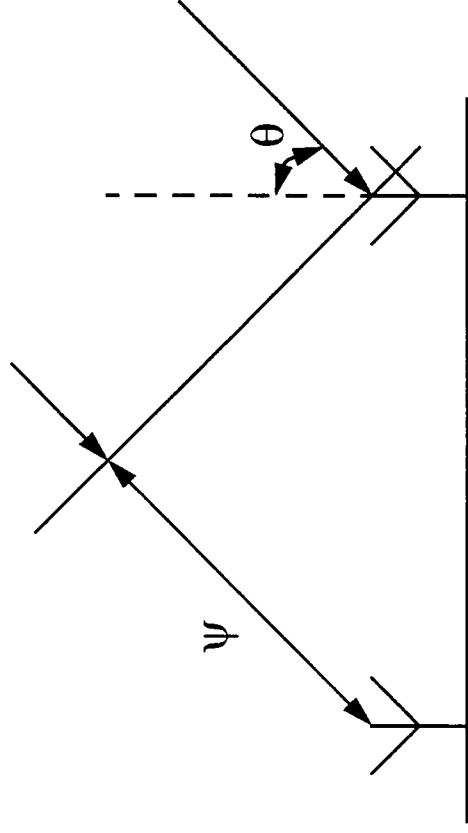
ASAP WORKSHOP, MARCH 12TH 1997



OUTLINE

- INTRODUCTION
- THE EFFECT OF BANDWIDTH ON ADAPTIVE BEAMFORMING
- THE EFFECT OF BANDWIDTH ON STAP
- TIME DELAY STEERING
- CONCLUSIONS

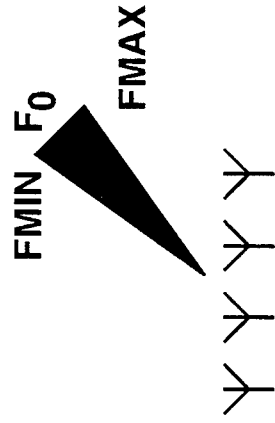
WHAT IS DISPERSION ?



$$\psi = 2\pi d \lambda^{-1} \sin(\theta)$$

- PHASE DEPENDS ON BOTH WAVELENGTH AND ANGLE

FMIN F₀ FMAX



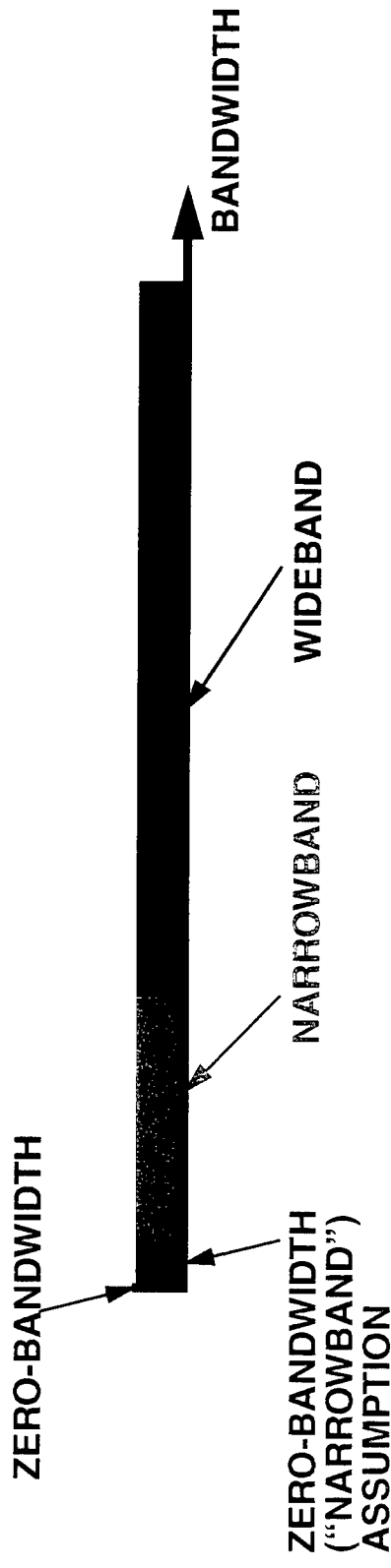
ZERO BANDWIDTH SOURCE APPEARS AS A SINGLE ANGLE OF ARRIVAL ~ 1 DOF

NON-ZERO BANDWIDTH SOURCE SPANS AN ANGULAR SECTOR ~ >1 DOF

INTERFERENCE RANK ~ NUMBER OF DOF NEEDED TO SUPPRESS THE INTERFERENCE



MOTIVATION



- STAP IS WELL STUDIED FOR THE ZERO-BANDWIDTH ASSUMPTION
- WHERE DOES THE ZERO-BANDWIDTH ASSUMPTION FAIL ?
- HOW DOES STAP PERFORM IN THE NARROWBAND SCENARIO ?
- HOW CAN NARROWBAND STAP PERFORMANCE BE IMPROVED ?

OUTLINE

- **INTRODUCTION**
- **THE EFFECT OF BANDWIDTH ON ADAPTIVE BEAMFORMING**
- **THE EFFECT OF BANDWIDTH ON STAP**
- **TIME DELAY STEERING**
- **CONCLUSIONS**

THE NON-ZERO BANDWIDTH COVARIANCE MATRIX

$$R = R_1 + R_2 + \dots + R_M + \sigma^2 I$$

TOTAL = SUM OF INDIVIDUALS + NOISE

- FOR EACH COMPONENT WRITE AS

ZERO BANDWIDTH MODEL

$$\mathbf{R}_m = \mathbf{S}_m \mathbf{a}(\theta_m) \mathbf{a}(\theta_m)^H$$

$$r_{mkl} = s_m e^{j2\pi\tau_{kl}f_0} \mathbf{A}$$

**TIME DELAY BETWEEN
kth AND #th ELEMENTS**

$$\tau_{k|} = \frac{d_k - d_l}{c} \sin(\theta)$$

$$\tau_{k|l} = \frac{d_k - d_l}{c} \sin(\theta)$$

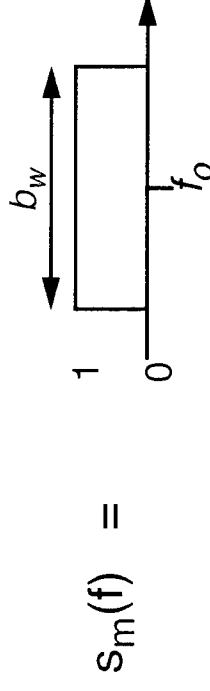
- **COMPACT FORM FOR COVARIANCE MATRIX**

$$-R^{m_{\text{WIDE}}} = R^{m_{\text{NABB}}} \bullet A$$

- $a_{kl} = \text{sinc}(b_w \tau_{kl})$

NON-ZERO BANDWIDTH MODEL

CORRELATION IS THE I.F.T. OF THE POWER SPECTRUM

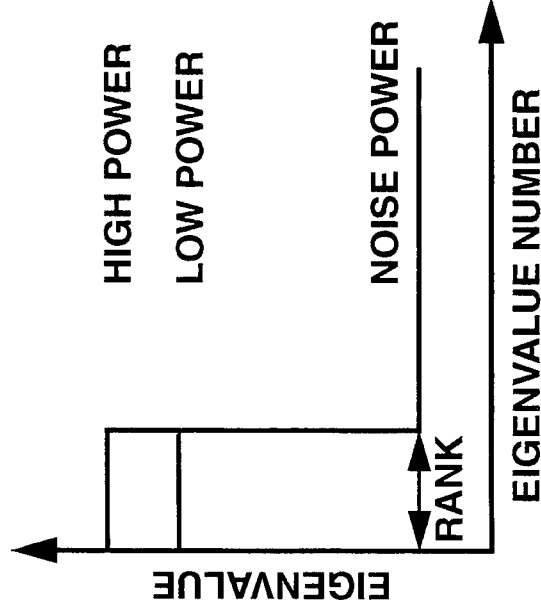


$$r_{m_{kl}} = \int_{f_0 - \frac{b_w}{2}}^{f_0 + \frac{b_w}{2}} s_m(f) e^{j2\pi\tau_{kl}f} df = \text{sinc}(b_w\tau_{kl}) s_m e^{j2\pi\tau_{kl}f_0}$$

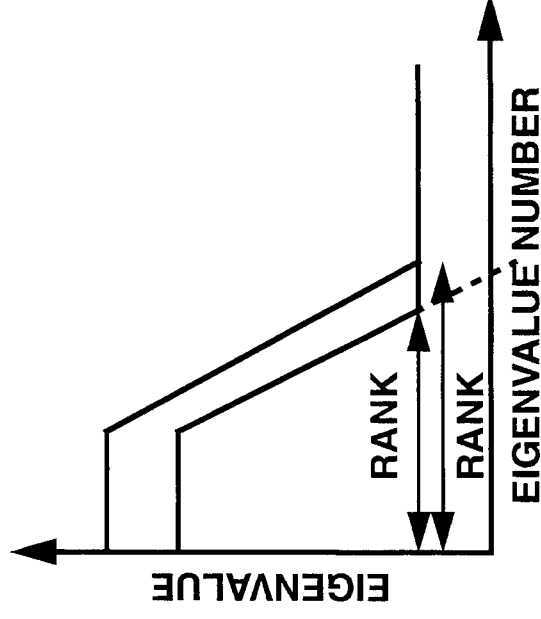


RANK AND INTERFERENCE POWER

ZERO BANDWIDTH MODEL

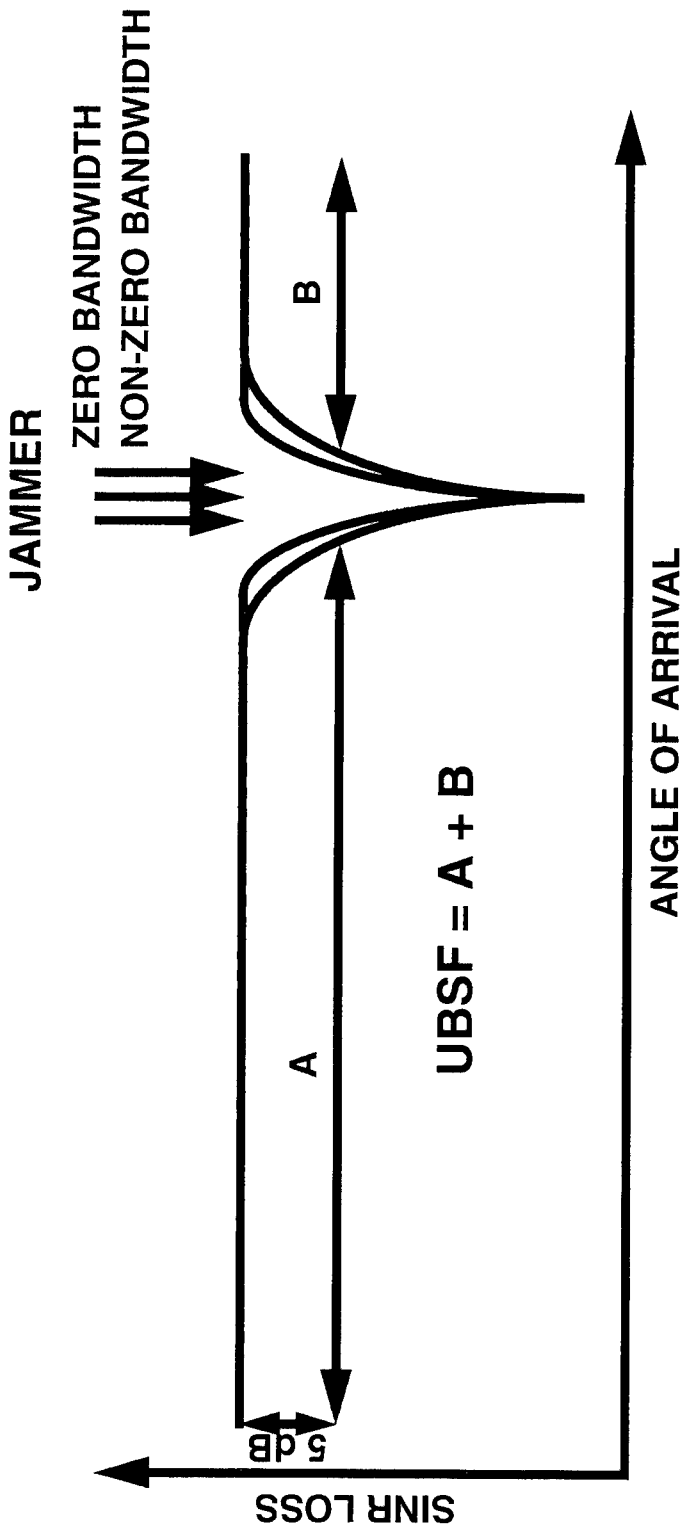


NON-ZERO BANDWIDTH MODEL



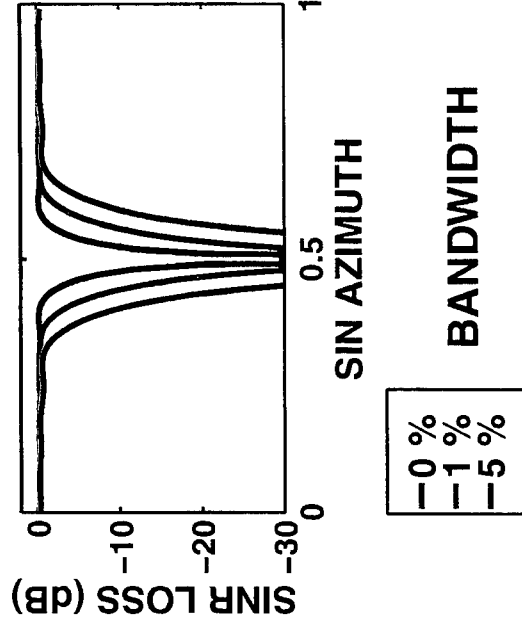
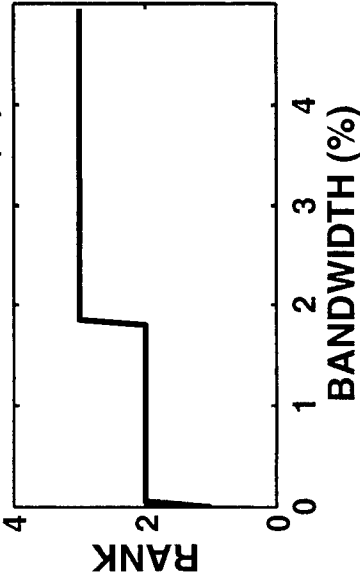
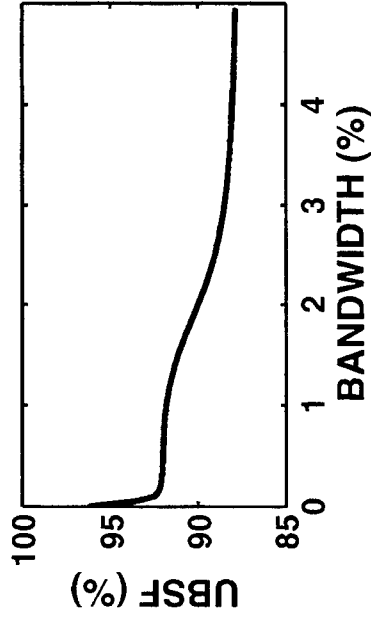
- FOR NON-ZERO BANDWIDTHS RANK INCREASES WITH INTERFERENCE POWER
- RANK DEPENDS ON POWER, BANDWIDTH, AOA AND APERTURE

PERFORMANCE LOSS



- INCREASING BANDWIDTH RESULTS IN INCREASED DOF AND REDUCED ANGULAR COVERAGE
- USEABLE BEAMSPACE FRACTION (UBSF) USED AS A METRIC
 - UBSF (MEASURED IN PERCENT) IS A MEASURE OF MINIMUM DETECTABLE VELOCITY

CHANGE IN UBSF WITH BANDWIDTH



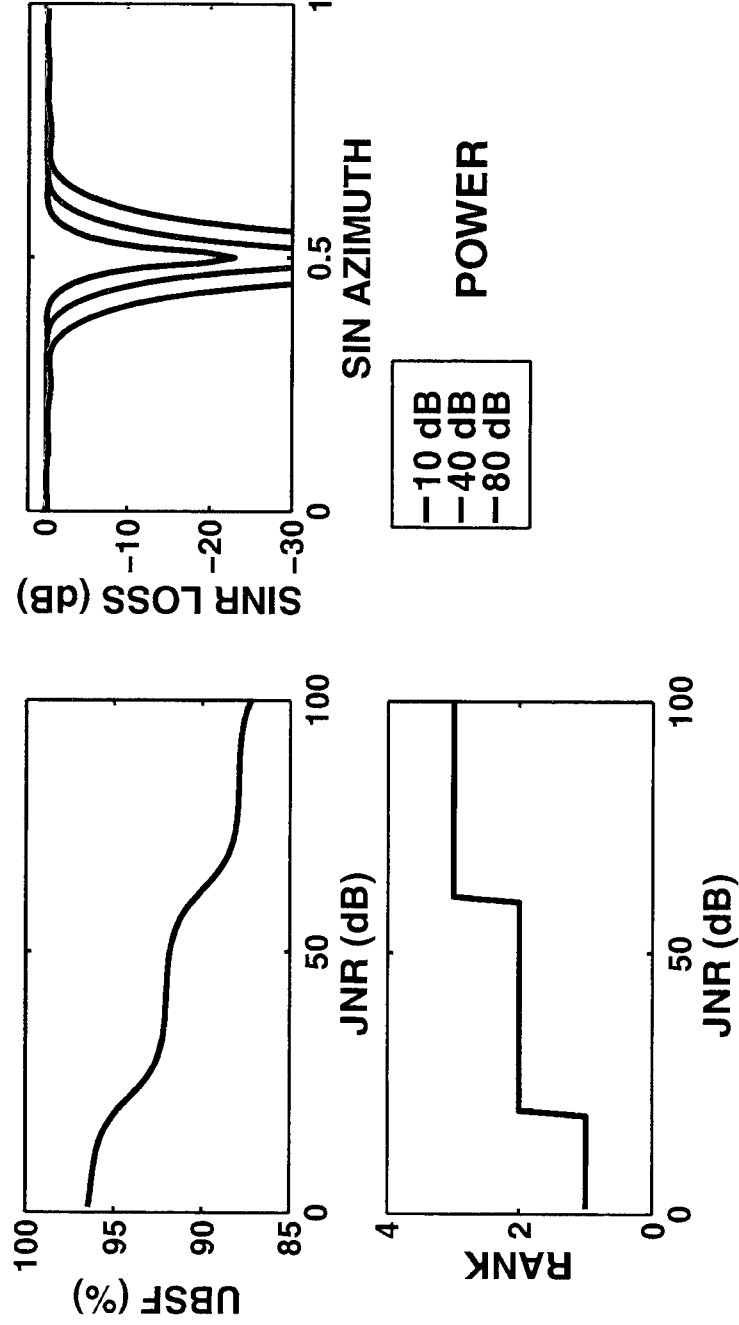
*18 ELEMENT ARRAY, JNR=50 dB, JAMMER AOA=30°

- USEABLE SPACE DECREASES WITH INTERFERENCE RANK
- RANK INCREASES WITH BANDWIDTH



ZAT 030397

CHANGE IN UBSF WITH POWER

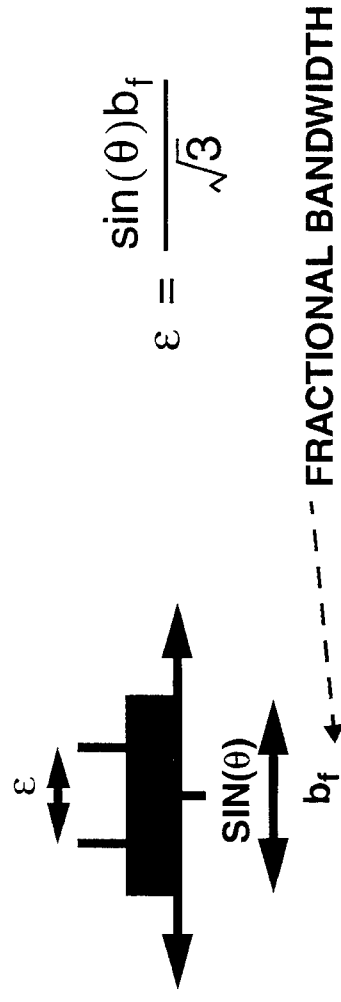


*18 ELEMENT ARRAY, JAMMER AOA=30°, BW=1%

- RANK INCREASES WITH JAMMER POWER
- USEABLE SPACE DECREASES WITH JAMMER POWER

HOW NARROW IS NARROWBAND ?

- NARROWBAND SIGNAL MODEL WRONG WHEN $\lambda_2 > \text{NOISE}$
- USE RANK 2 APPROXIMATION OF A NON-ZERO BANDWIDTH SIGNAL



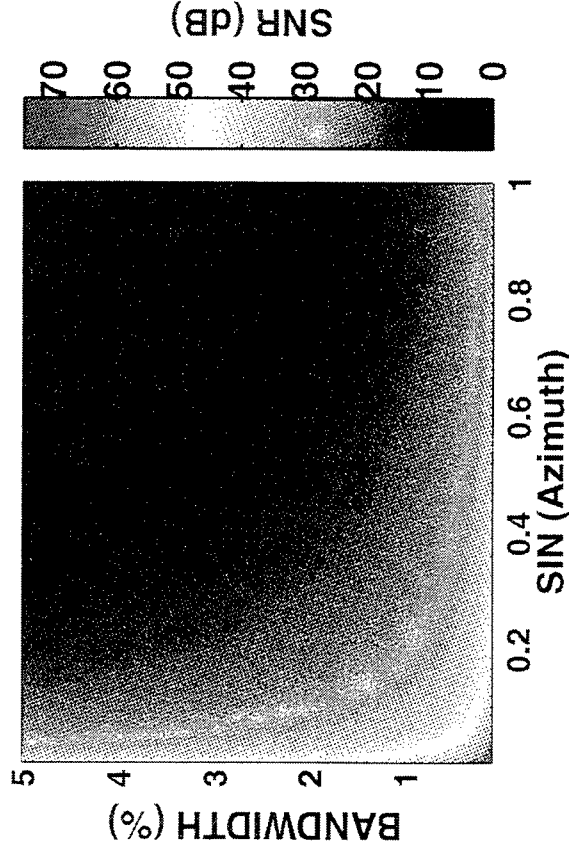
$$\epsilon = \frac{\sin(\theta)b_f}{\sqrt{3}}$$

ELEMENTS

$$\lambda_2 = \frac{N}{4}(\text{JNR}) \left(1 - \left[\frac{\sin\left(\frac{N\pi\epsilon}{2}\right)^2}{N \sin\left(\frac{N\pi\epsilon}{2}\right)} \right] \right)$$

DIRICHLET FUNCTION

18 ELEMENT ARRAY EXAMPLE



- THE 'NARROWBAND' ASSUMPTION IS ONLY CORRECT IF

- $\theta = 30^\circ$ AND $JNR = 50$ dB FOR BANDWIDTHS $< 0.027\%$
- $\theta = 30^\circ$ AND BANDWIDTH $= 0.222\%$ FOR $JNR < 32$ dB
- BANDWIDTH $= 0.222\%$ AND $JNR = 50$ dB FOR $\theta < 3.55^\circ$

- NARROWBAND SIGNAL MODEL INAPPROPRIATE FOR RADAR BANDWIDTHS OF INTEREST



ZAT 9 30 96

OUTLINE

- **INTRODUCTION**
- **THE EFFECT OF BANDWIDTH ON ADAPTIVE BEAMFORMING**
- **THE EFFECT OF BANDWIDTH ON STAP**
- **TIME DELAY STEERING**
- **CONCLUSIONS**

THE CLUTTER COVARIANCE MATRIX

$$R = R_1 + R_2 + \dots + R_M + \sigma^2 I$$

TOTAL = SUM OF COMPONENTS (PATCHES) + NOISE

- FOR EACH COMPONENT (PATCH) WRITE AS

ZERO BANDWIDTH MODEL

$$R_m = S_m \mathbf{a}(\theta_m, f_m) \mathbf{a}(\theta_m, f_m)^H$$

$$r_{m_{klmn}} = S_m e^{j2\pi(\tau_{kl} - \tau_{mn})\omega} f_o$$

TIME DELAY BETWEEN ELEMENTS

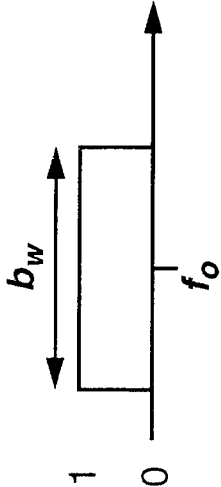
TIME DELAY BETWEEN PULSES

NORMALIZED DOPPLER $\omega = \frac{f}{f_o}$

• COMPACT FORM FOR COVARIANCE MATRIX

- $R_{m_{WIDE}} = R_{m_{NARR}} \bullet A$
- $a_{klmn} = \text{sinc}(b_w(\tau_{kl} - \tau_{mn}))$

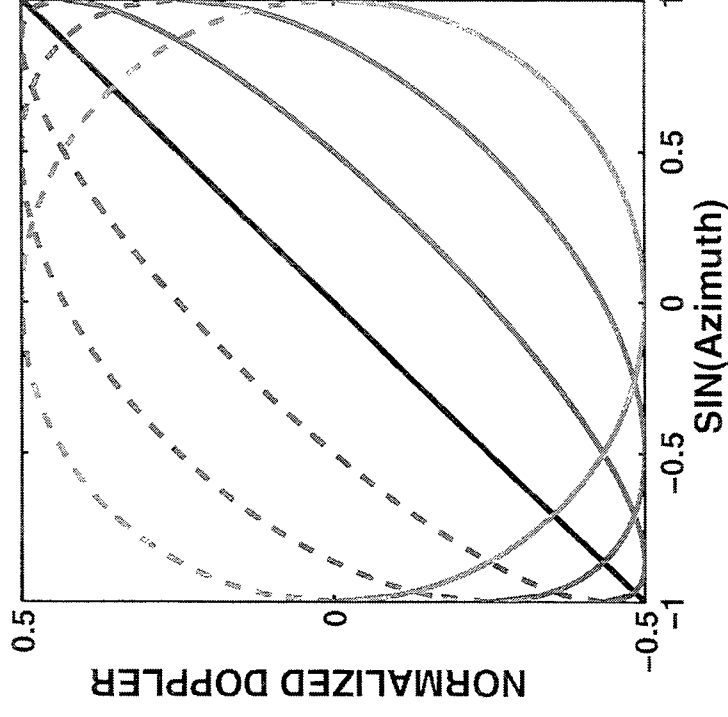
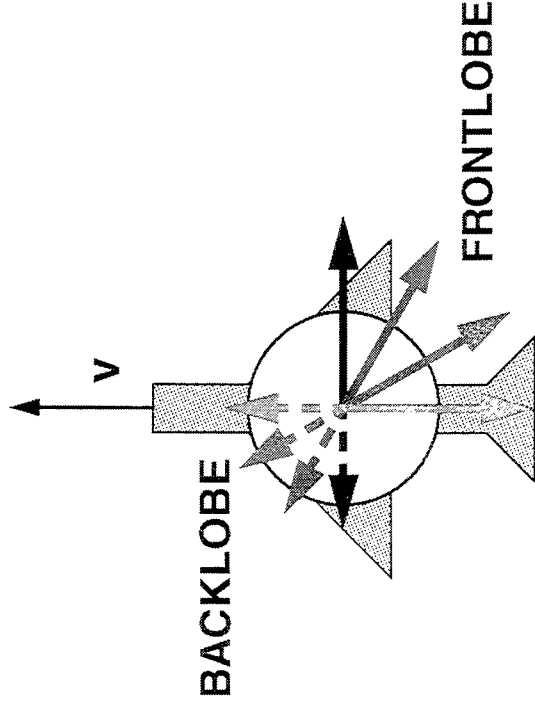
NON-ZERO BANDWIDTH MODEL



$$r_{m_{kl}} = \int_{f_o - \frac{b_w}{2}}^{f_o + \frac{b_w}{2}} S_m e^{j2\pi(\tau_{kl} - \tau_{mn})f} df$$

$$= \text{sinc}(b_w(\tau_{kl} - \tau_{mn})) S_m e^{j2\pi(\tau_{kl} - \tau_{mn})f_o}$$

LOCUS OF THE CLUTTER RIDGE



- CLUTTER LOCUS DEPENDS ON MISALIGNMENT BETWEEN
ARRAY AND PLATFORM VELOCITY VECTOR
 - MISALIGNMENT DUE TO ARRAY ROTATION OR AIRCRAFT CRAB

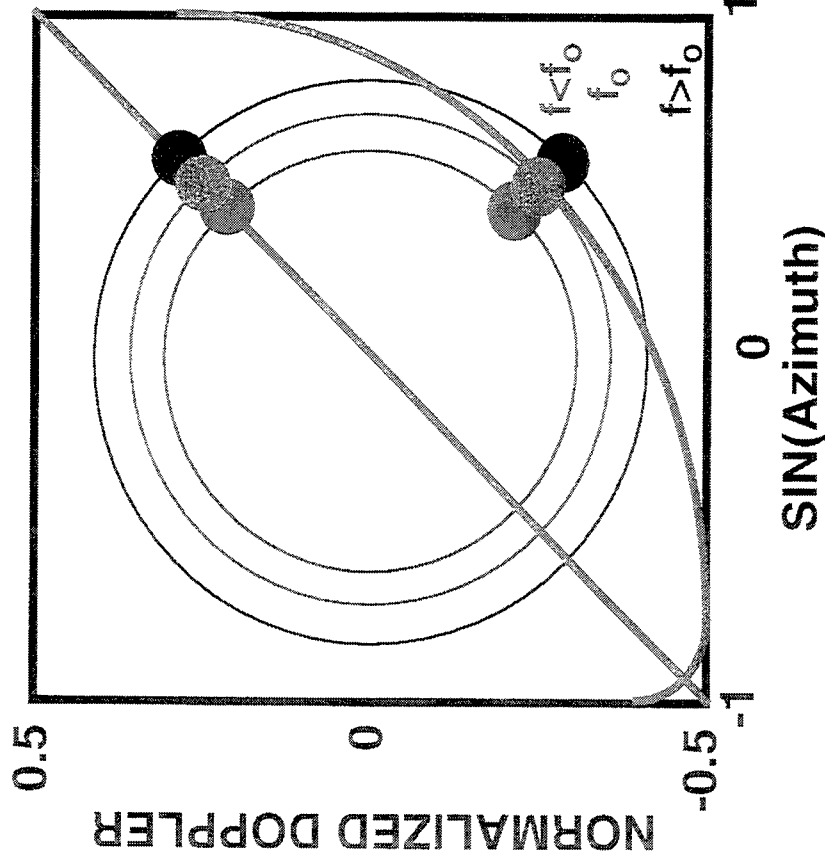
DISPERSION IN STAP

- INTER-ELEMENT AND INTER-PULSE PHASE ARE BOTH A FUNCTION OF INSTANTANEOUS FREQUENCY

- DISPERSION INCREASES RADially FROM BROADSIDE AND ZERO DOPPLER

$$\text{DOPPLER} \quad \phi = 4\pi v \lambda^{-1}$$

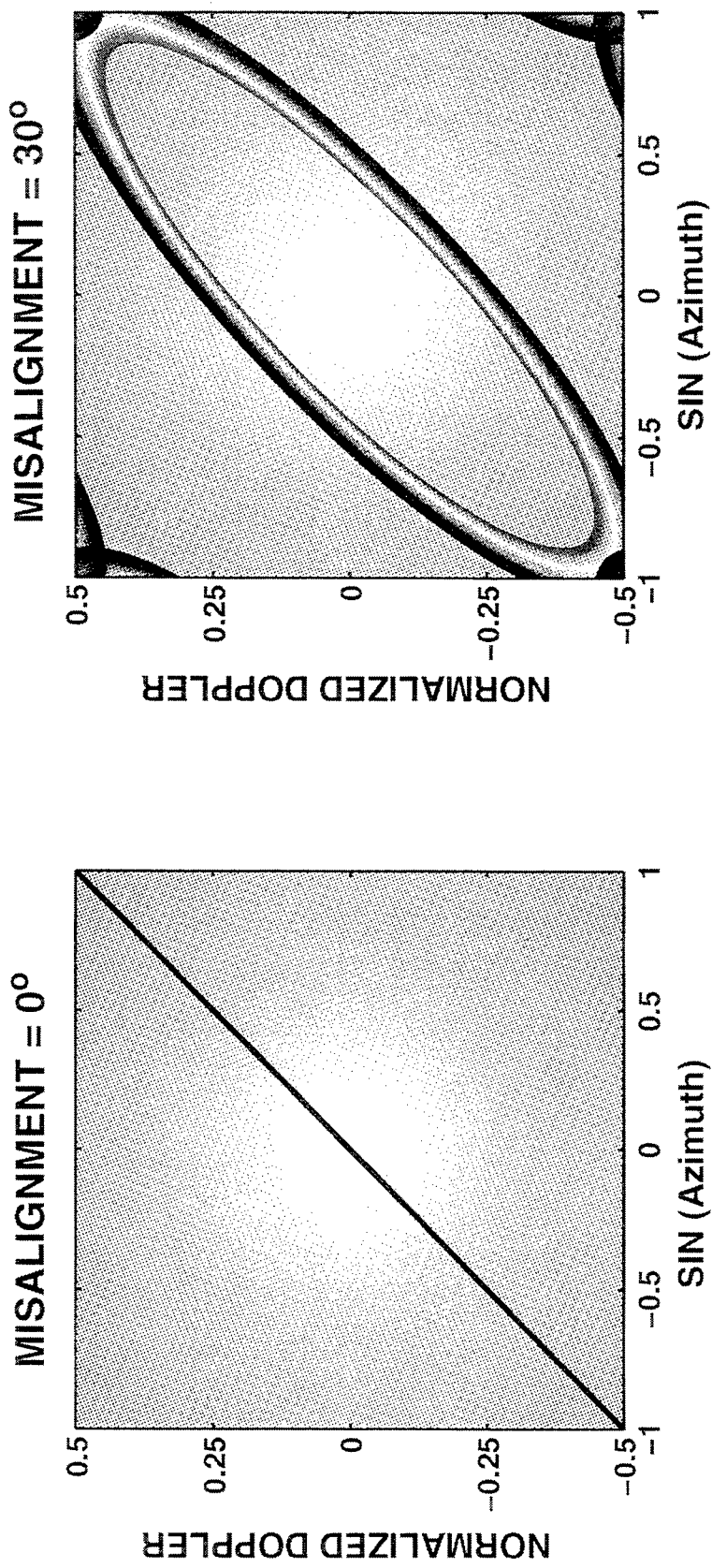
$$\text{SPATIAL} \quad \psi = 2\pi d \lambda^{-1} \sin(\theta)$$



- EFFECT ON CLUTTER RIDGES DEPENDS ON ARRAY MISALIGNMENT
 - NO MISALIGNMENT ~ DISPERSION IS ALONG THE ZERO BANDWIDTH CLUTTER LOCUS
 - MISALIGNMENT ~ DISPERSION CAUSES THE CLUTTER RIGES TO SPREAD

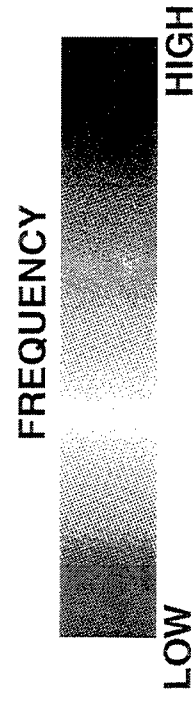
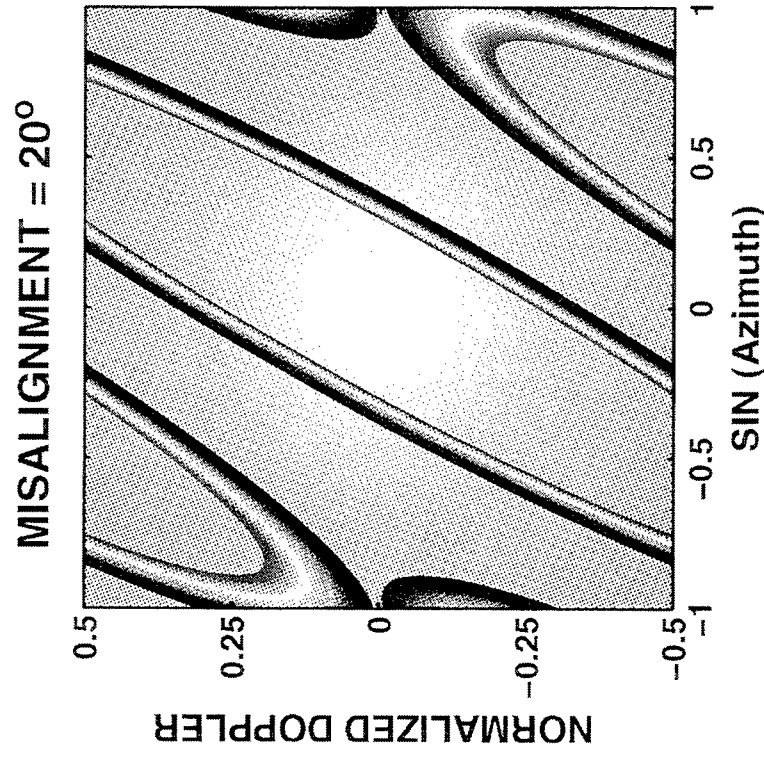
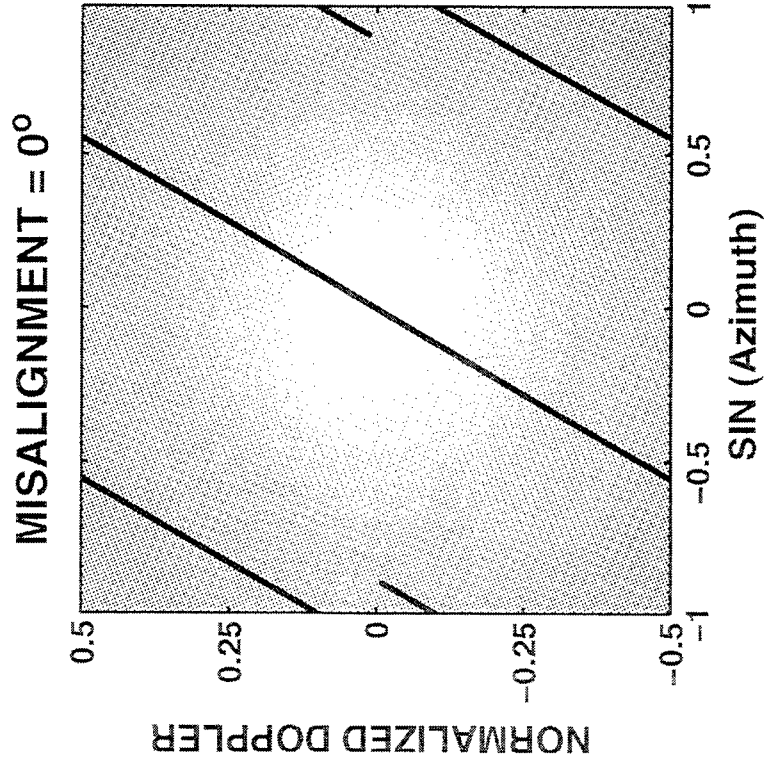
CLUTTER RIDGE LOCI

DOPPLER UNAMBIGUOUS ($\beta=1$)



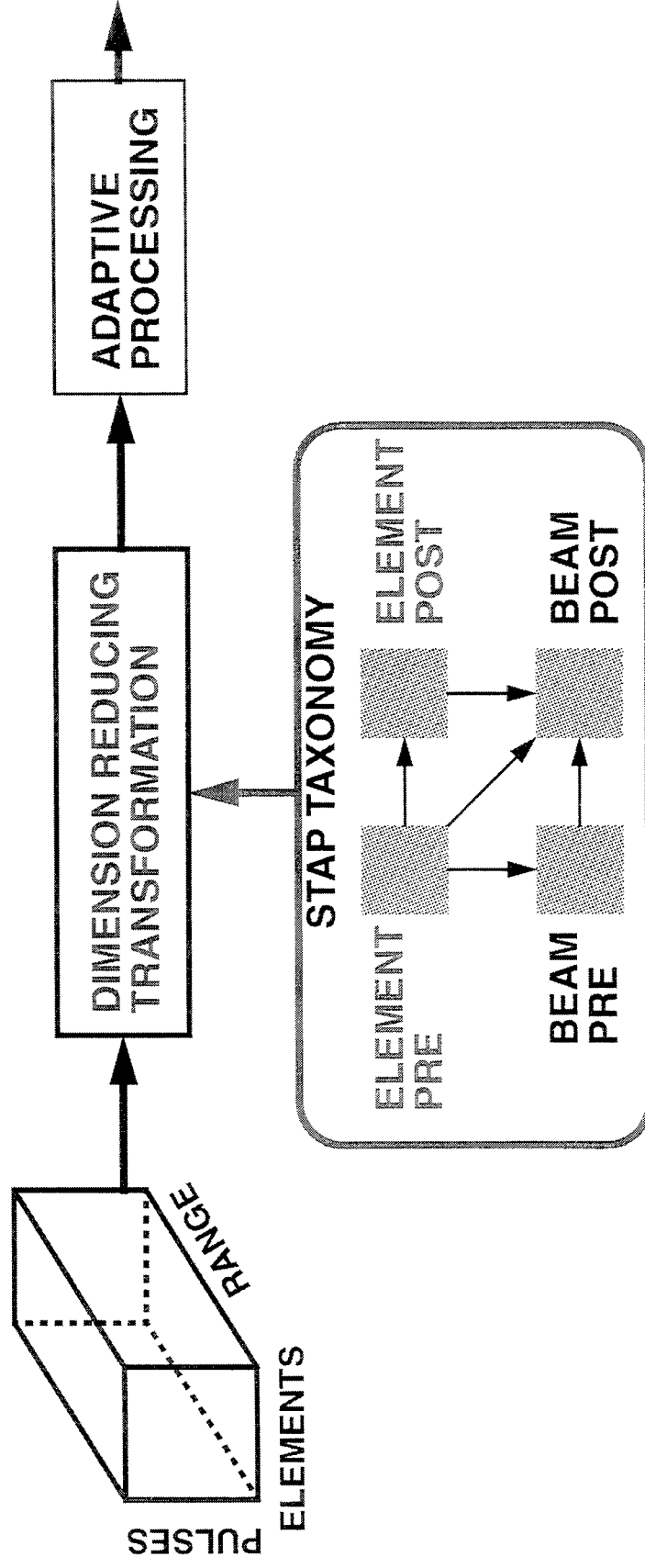
CLUTTER RIDGE LOCI

DOPPLER AMBIGUOUS ($\beta=1.8$)



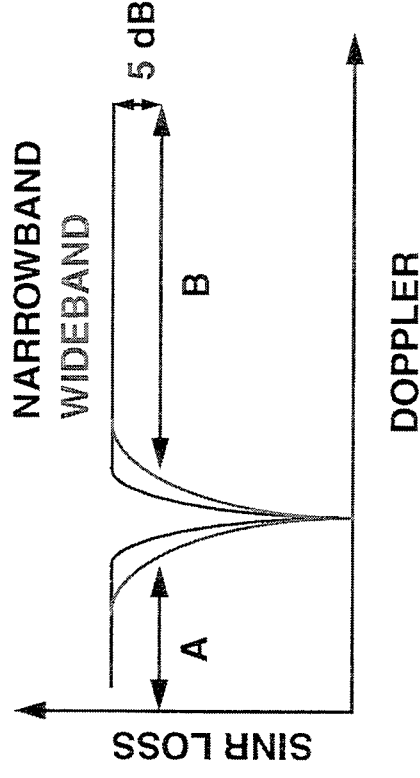
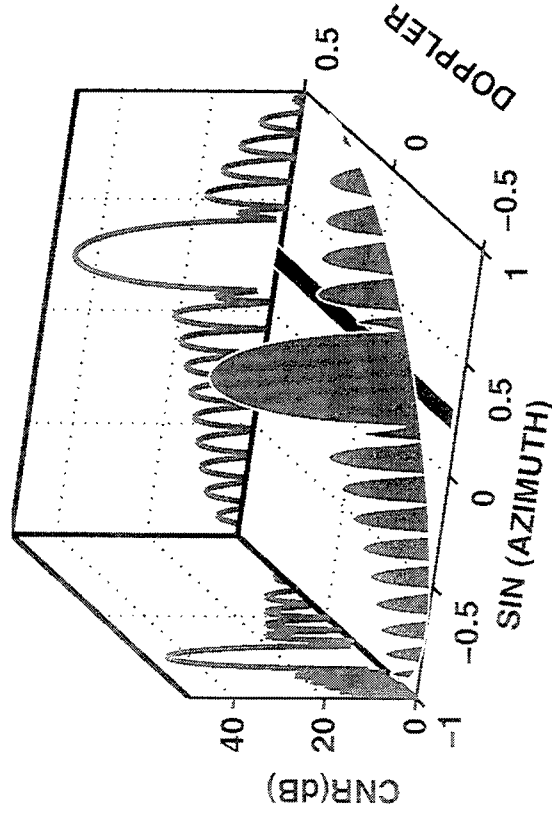
REDUCED DIMENSION STAP

STAP DATA FLOW



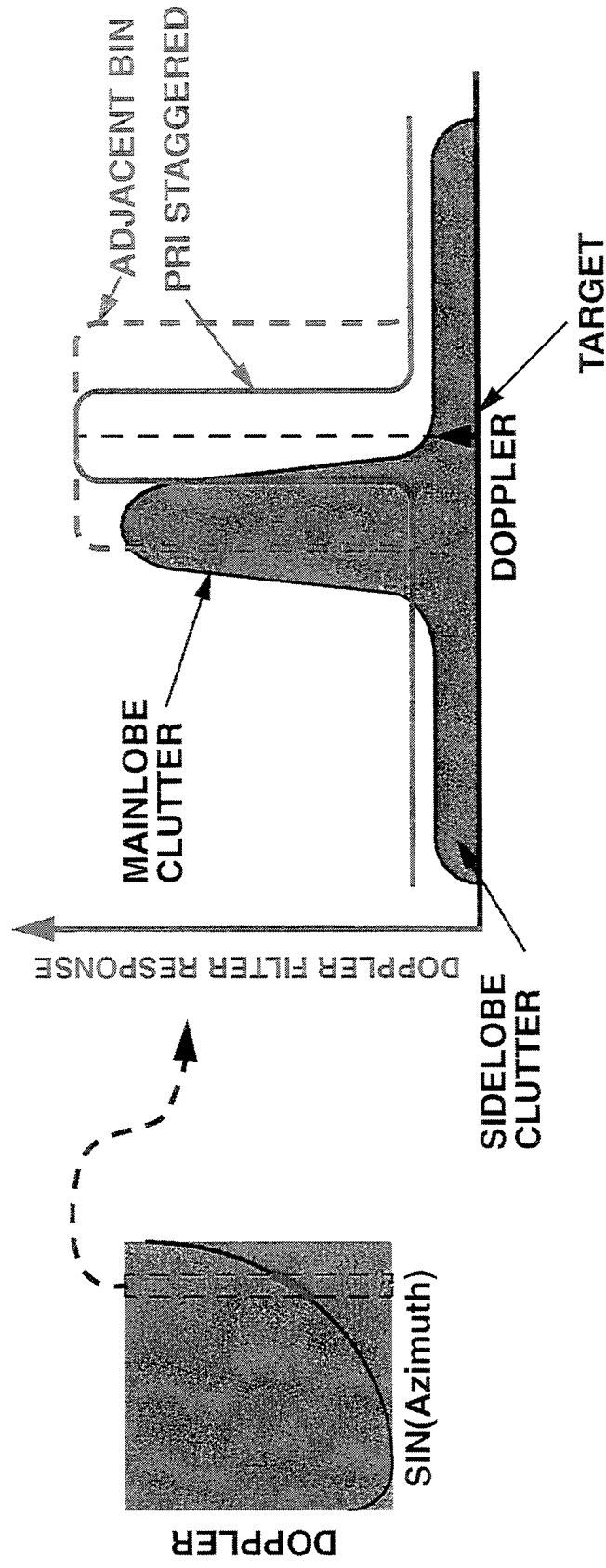
- DIMENSION REDUCING TRANSFORMATION MAY ALTER THE CLUTTER TO NOISE RATIO (CNR)
- BANDWIDTH DEGRADATION DEPENDS ON THE CNR

PERFORMANCE LOSS WITH CLUTTER



- USABLE DOPPLER SPACE FRACTION (UDSF) = $A + B$
 - AMOUNT OF DOPPLER SPACE WHERE SINR LOSS < 5 dB
RELATED TO THE MINIMUM DETECTABLE VELOCITY

POST DOPPLER STAP



- CLUTTER POWER INCREASED IN DOPPLER BINS NEAR MAIN LOBE CLUTTER

– BANDWIDTH EFFECTS DEPEND ON CLUTTER POWER

- ADJACENT BIN ALGORITHM HAS WIDER DOPPLER FILTERS

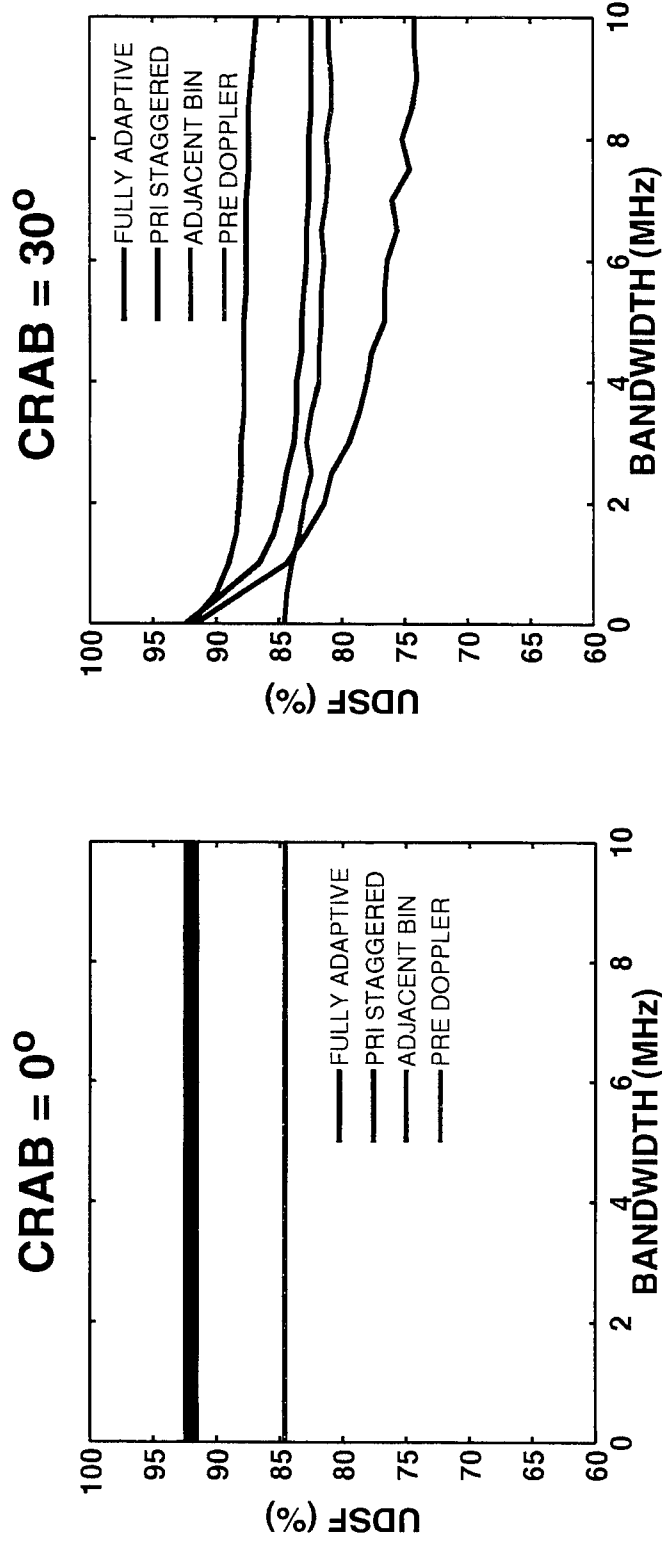
– ADJACENT BIN MORE SENSITIVE TO BANDWIDTH

SIMULATION PARAMETERS

- 18 ELEMENT ARRAY - 30 dB CHEBYCHEV TAPER
- 18 PULSES - 40dB CHEBYCHEV TAPER
- RADAR OPERATING FREQUENCY - 450 MHz
- $\beta=1$
- MAINBEAM STEERED -20° FROM BROADSIDE
- “COVARIANCE ANALYSIS”
- 54 D.O.F. REDUCED DIMENSION STAP (18 SPATIAL x 3 TEMPORAL)

SIMULATION RESULTS - CRAB

18 ELEMENT 18 PULSE STAP SIMULATION 35 dB CNR

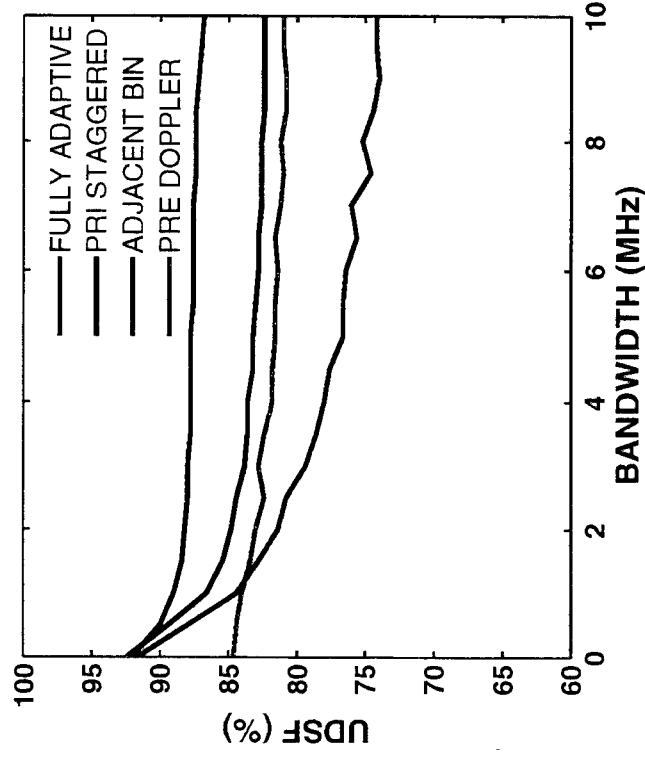


- BANDWIDTH EFFECTS STAP PERFORMANCE IN THE PRESENCE OF CRAB

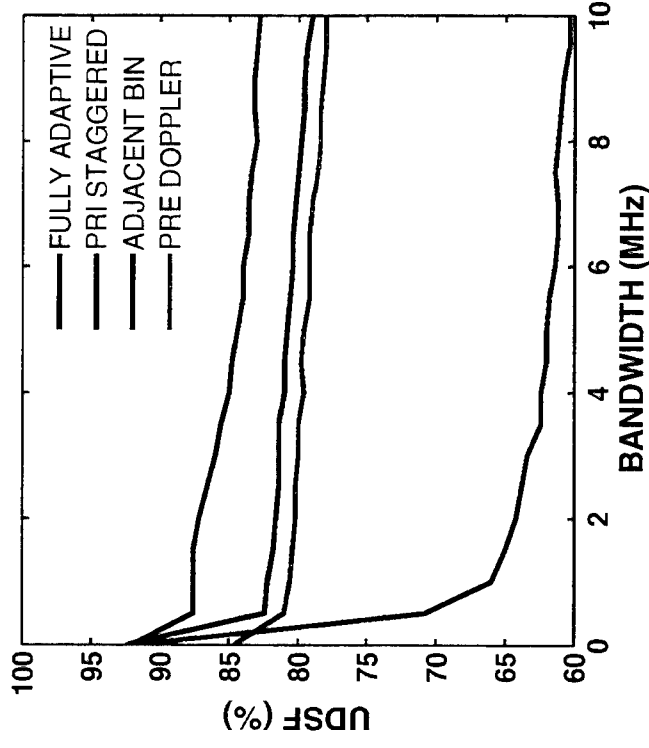
SIMULATION RESULTS - POWER

18 ELEMENT 18 PULSE STAP SIMULATION 30° CRAB

35 dB CNR



60 dB CNR



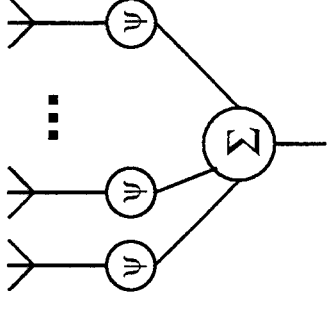
- POST DOPPLER ALGORITHMS DEGRADE QUICKER
- ADJACENT BIN 'WORSE' THAN PRI STAGGERED

OUTLINE

- **INTRODUCTION**
- **THE EFFECT OF BANDWIDTH ON ADAPTIVE BEAMFORMING**
- **THE EFFECT OF BANDWIDTH ON STAP**
- **TIME DELAY STEERING**
- **CONCLUSIONS**

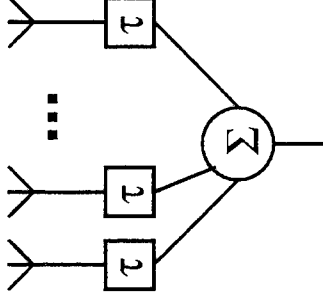
ARRAY STEERING ARCHITECTURES

- CONVENTIONAL PHASE DELAYS
 - SIMPLE PHASE SHIFTER IMPLEMENTATION
 - DOES NOT ACCOUNT FOR DISPERSION



- TIME DELAY STEERING

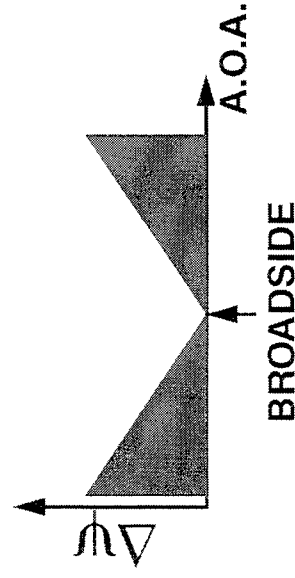
- ACCOUNTS FOR DISPERSION IN LOOK DIRECTION
- IMPLEMENTED USING FIR FILTER
- EQUALIZATION / PULSE COMPRESSION FILTERS USED
- LITTLE EXTRA COMPUTATION



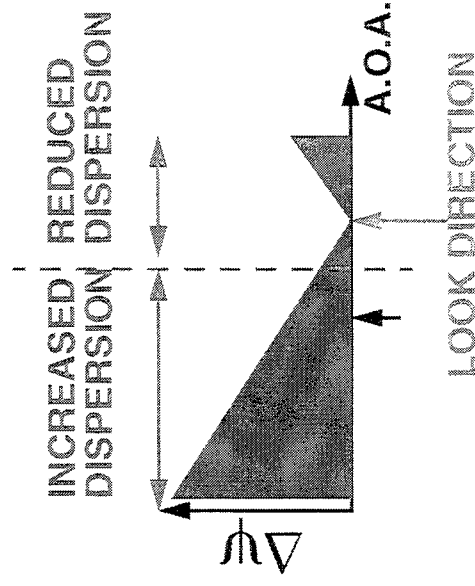
- OTHER METHODS REQUIRE MUCH MORE COMPUTATION
 - ADDING 'FAST TIME' TAPS
 - SUB-BAND ARCHITECTURES

EFFECT OF TIME DELAY STEERING ON DISPERSION

CONVENTIONAL STEERING



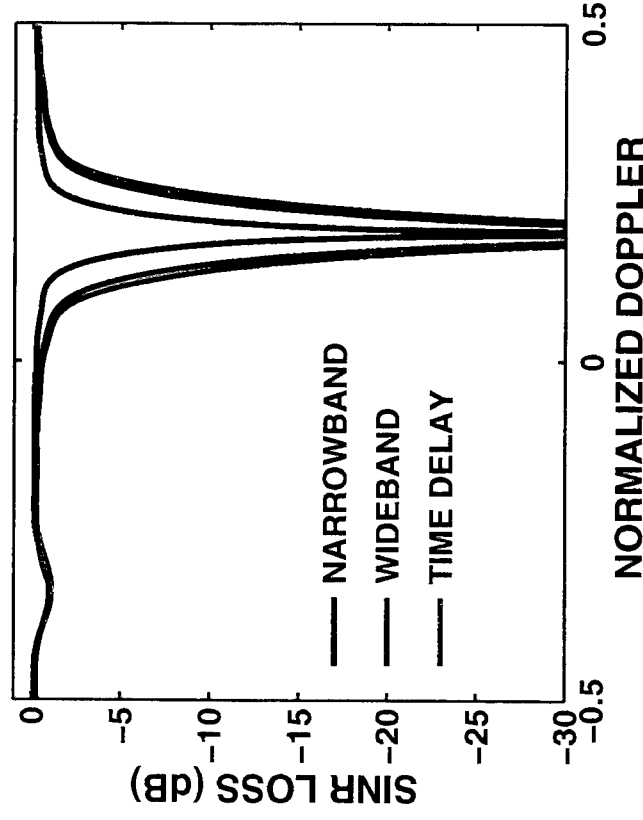
TIME DELAY STEERING



- TIME DELAY STEERING MITIGATES DISPERSION IN THE LOOK DIRECTION

- TIME DELAY STEERING INCREASES DISPERSION FOR MOST ANGLES OF ARRIVAL

STAP PERFORMANCE WITH TIME DELAY STEERING

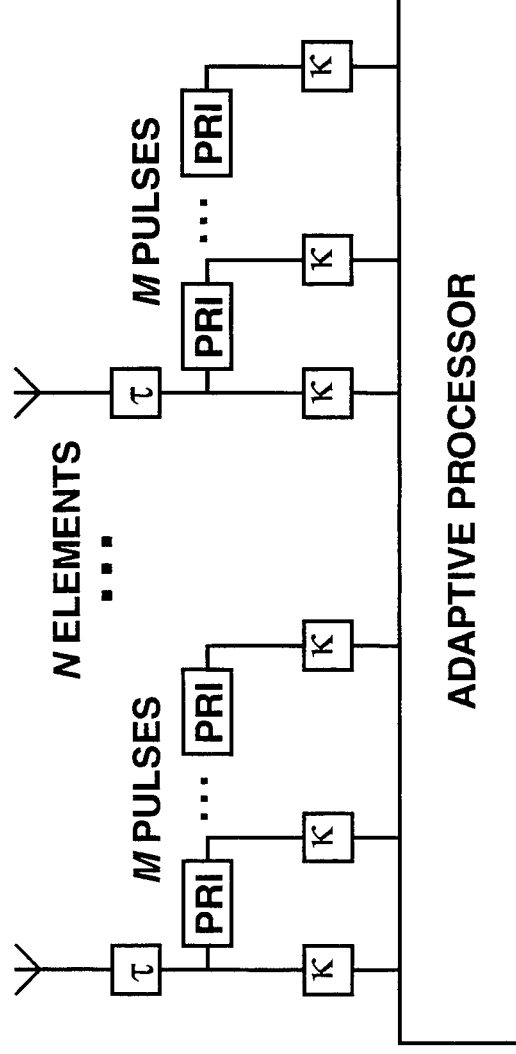


* $\beta=1.8$, CNR=45 dB, CRAB = 20°, LOOK DIR.= 30°, BW = 1 %

• TIME DELAY STEERING RESULTS IN WORSE MDV

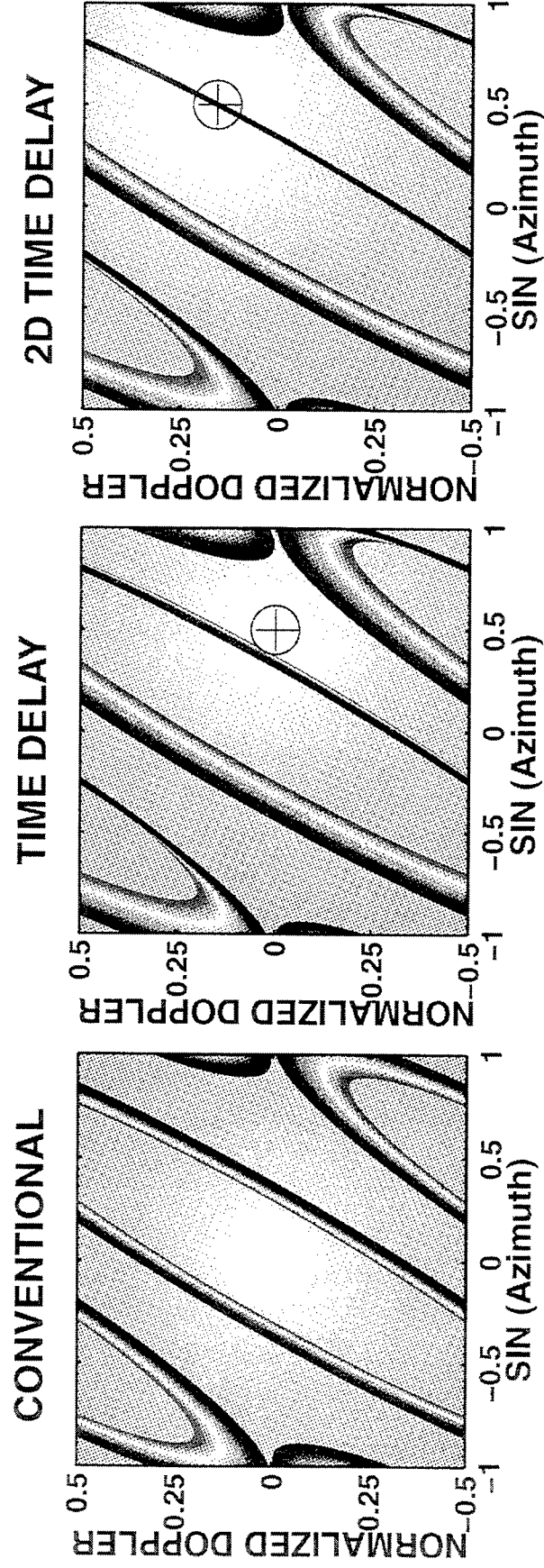
- DOES NOT ACCOUNT FOR DOPPLER DISPERSION
- INCREASES OVERALL CLUTTER RANK

2D TIME DELAY STEERING



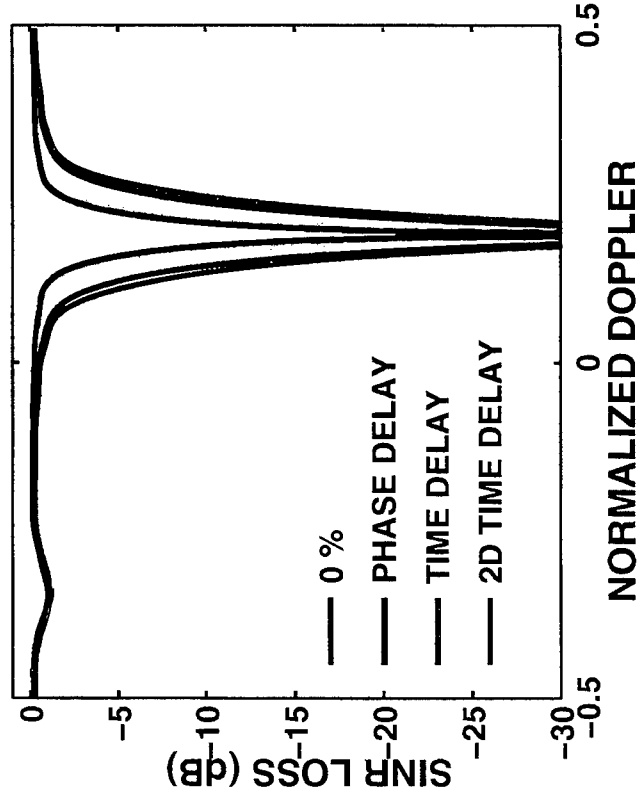
- COMPENSATION IN BOTH THE ANGLE AND DOPPLER DOMAINS
- CHOOSE τ AND κ TO ZERO DISPERSION ON LOOK DIRECTION CLUTTER
- SEVERAL IMPLEMENTATION SCHEMES
 - EQUALIZATION / PULSE COMPRESSION FIR FILTERS
 - STAGGER TRANSMITTED WAVEFORM
 - DPCA

CLUTTER RIDGE LOCI



- ONLY 2D TIME DELAY STEERING MINIMIZES DISPERSION ON THE MAINBEAM CLUTTER

STAP PERFORMANCE WITH 2D TIME DELAY STEERING



* $\beta=1.8$, CNR=45 dB, CRAB = 20°, LOOK DIR.= 30°, BW = 1 %

- MDV PERFORMANCE SIGNIFICANTLY IMPROVED WITH 2D TIME DELAY STEERING

CONCLUSIONS

- STAP SIGNAL MODEL EXTENDED TO INCLUDE BANDWIDTH
- REDUCTION IN COVERAGE DUE TO BANDWIDTH QUANTIFIED
 - ANGULAR COVERAGE
 - MINIMUM DETECTABLE VELOCITY
- POST DOPPLER STAP MORE SENSITIVE TO BANDWIDTH
 - ADJACENT BIN MORE SENSITIVE THAN PRI STAGGERED
- TWO DIMENSIONAL TIME DELAY STEERING IMPROVES STAP PERFORMANCE FOR MOST SCENARIOS

SESSION III: Systems Applications of STAP

(James K. Day, Lockheed Martin Corp.)

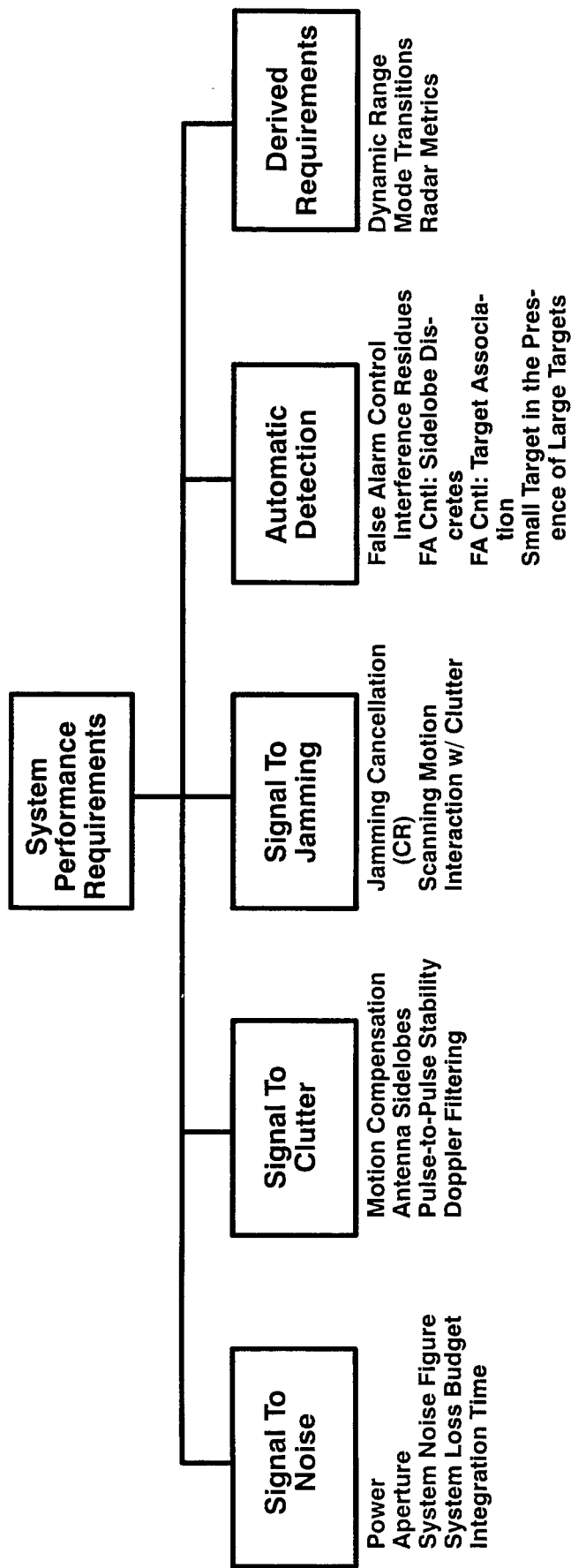
SYSTEM REQUIREMENTS FLOWDOWN TO STAP

- **TYPICAL RADAR REQUIREMENTS**
 - TARGET TRACING
 - Track Initiation, Track Life, Metric Accuracy
 - TARGET DETECTION
 - P_d , P_{fa} At Various Stages (CPI, Dwell, Multiple Looks...)
 - ENVIRONMENT:
 - Clutter (Land, sea, Littoral), Jamming (cold, hot, ...), EMI
- **TYPICAL STAP ANALYSIS RESULTS**
 - SELECTED STAP ARCHITECTURE
 - Pre-Doppler Element Space, Post-Doppler Beamspace ...
 - PERFORMANCE PREDICTIONS (OFTEN SINGLE CPI)
 - $SINR_{loss}$, $S/C_{enhancement}$, $S/J_{enhancement}$, $USDF(\%)$
 - Metric Accuracies
 - SELECTED IMPLEMENTATION/REQUIREMENTS
 - Digital Receivers, Beamforming
 - STAP/Detection Processor Approach

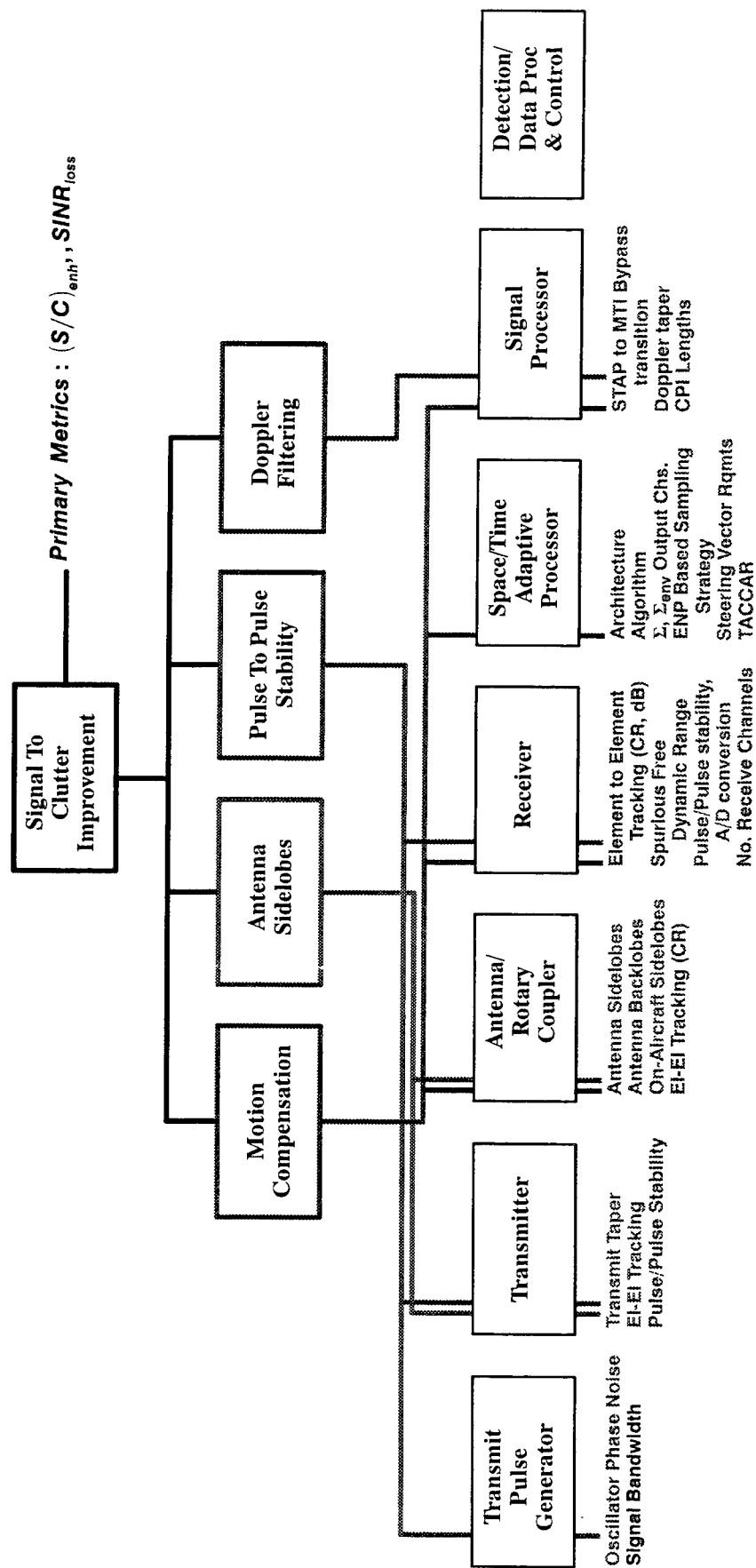
**FLOWDOWN OF REQUIREMENTS & ROLL-UP OF
RESULTS MUST BE CAREFULLY ADDRESSED**



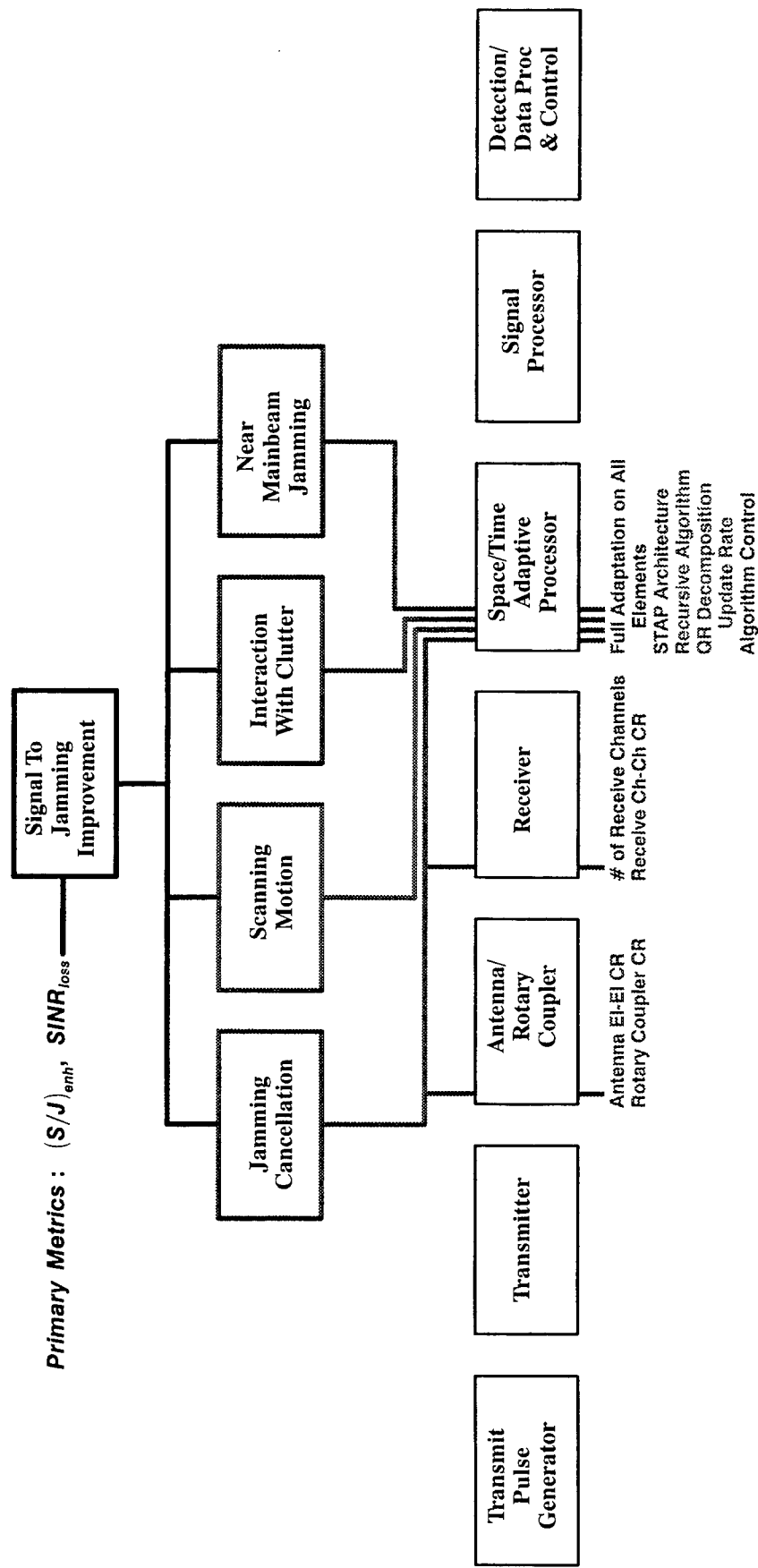
REQUIREMENTS FLOWDOWN -- FIRST LAYER



REQUIREMENTS FLOWDOWN: SIGNAL-TO-CLUTTER



REQUIREMENTS FLOWDOWN: SIGNAL-TO-JAMMING

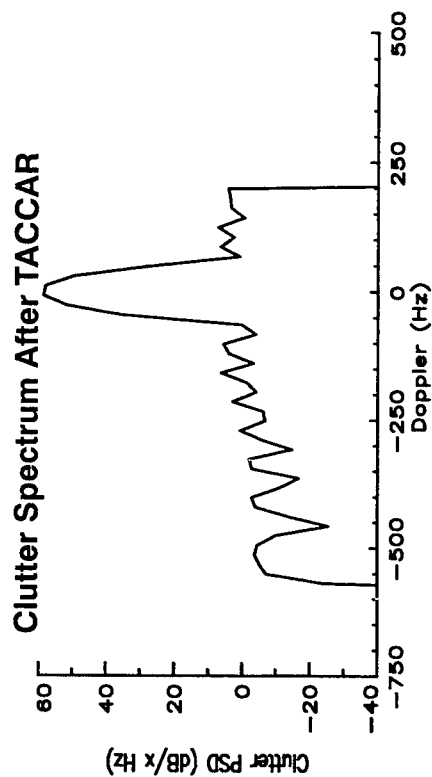


APPLICATION DEPENDENCE OF FUNCTIONAL FLOWDOWN

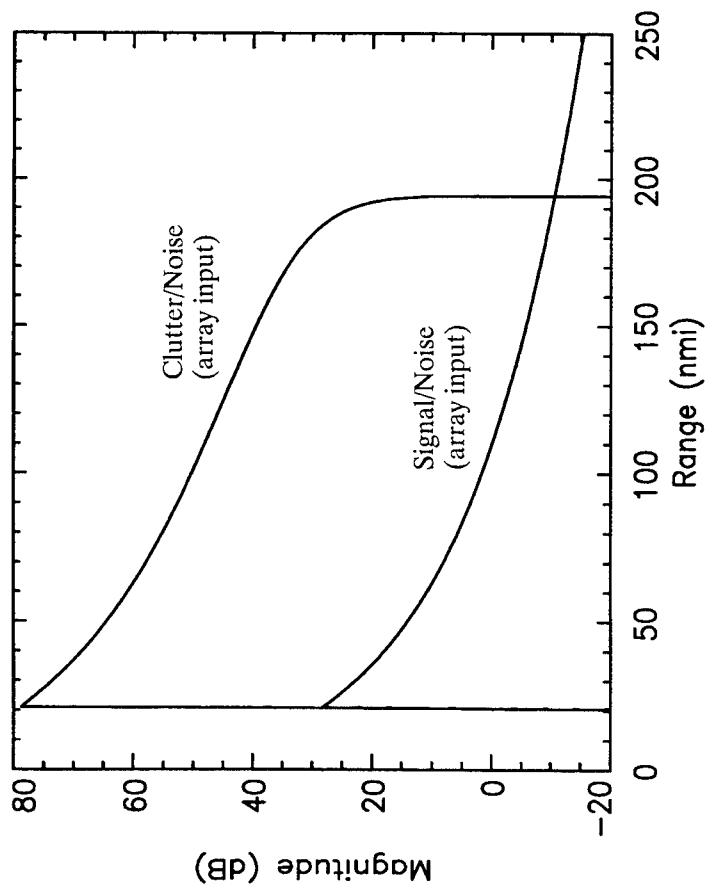
- **AEW RADAR SOLUTIONS AS AN EXAMPLE**
- **E-3A AWACS**
 - LARGE PLATFORM, LARGE ANTENNA
 - S-BAND, PRIMARILY MEDIUM/HIGH PRF
- **E-2C HAWKEYE**
 - SMALL PLATFORM, SMALLER ANTENNA
 - UHF, LOW PRF
- **VERY DIFFERENT REQUIREMENTS FLOWDOWN FOR STAP**
 - ANTENNA SIZE (IN λ) HAS DRAMATIC IMPACT ON ARCHITECTURE:
 - Element Space, Beamspace, Subarrays...
 - PRF SELECTION HAS DRAMATIC IMPACT ON CLUTTER PROCESSING
 - Low PRF: Doppler Foldover, Range Dependent Falloff
 - High PRF: Doppler Clutter Free Region, Range Foldover



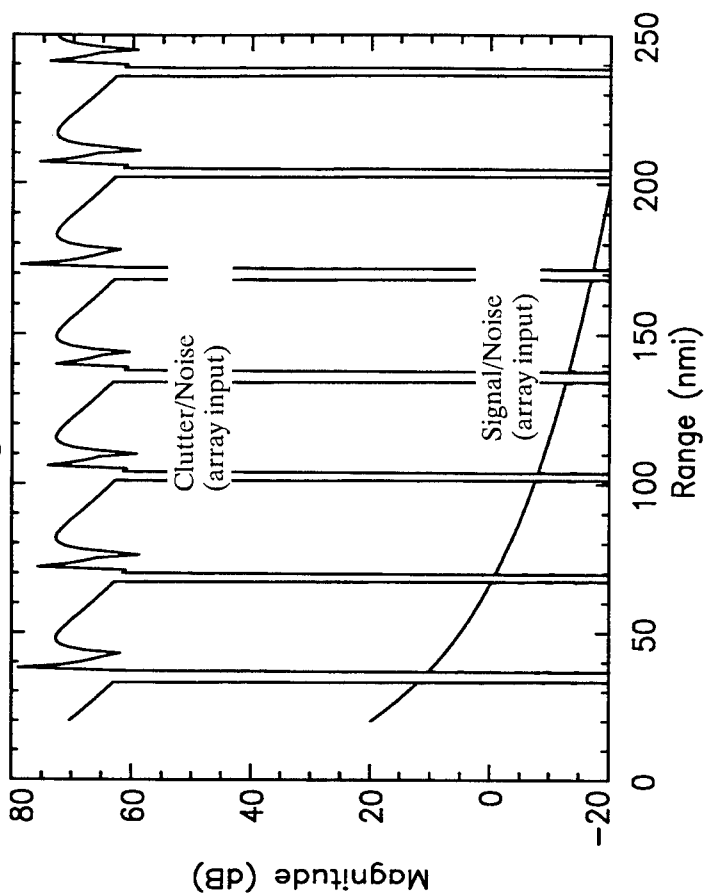
SIGNAL AND CLUTTER VERSUS RANGE



Low PRF



High PRF



CHALLENGE FOR STAP RADAR COMMUNITY

- **CAREFUL ATTENTION TO REQUIREMENTS FLOWDOWN**
 - FUNCTIONAL FLOWDOWN, NOT IMPLEMENTATION FLOWDOWN
 - ITERATIVE PROCESS
- **CAREFUL SELECTION OF STAP METRICS**
 - LIMITATIONS OF ANY SINGLE METRIC
 - DESIRE FOR SMALL NUMBER OF METRICS TO MINIMIZE COMPLEXITY OF PERFORMANCE COMPARISONS
- **REVISIT THE PERFORMANCE ROLL-UP PROCESS OFTEN**
 - SINGLE CPI RESULTS MOST PRACTICAL
 - MULTIPLE CPI, MULTIPLE LOOK DETECTION AND TRACKING RESULTS ARE THE REQUIRED RESULTS



SESSION PAPERS

- **Space Time Adaptive Processing Implementation Trades for a UHF Airborne Early Warning Radar**
R. M. Cooper, Lockheed Martin Corporation
- **Clutter Mitigation in An Airborne Radar Based Upon Phase—Weight Perturbation**
K. Akbulut, The MITRE Corporation
- **A Robust and Low Computational Burden Implicit Subspace Interference Removal Technique for STAP**
J. Guerci, Polytechnic University

STAP Implementation Trades for a UHF Airborne Early Warning (AEW) Radar System

Robert M. Cooper

Lockheed Martin

P.O. Box 4840

Syracuse, NY 13221-4840

tel: (315) 456-2495

email: cooper@syr.lmco.com

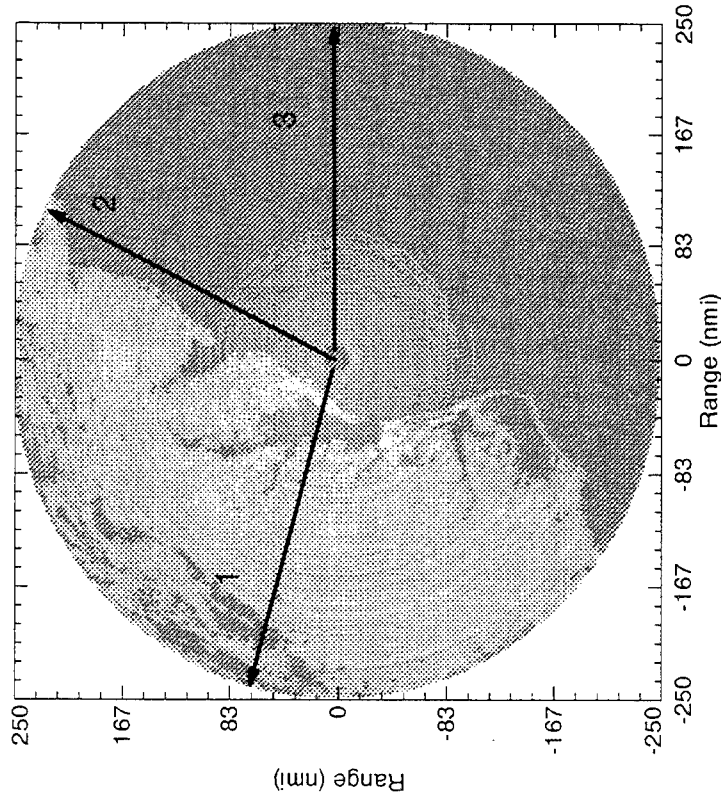
Abstract This presentation addresses the use of Space-Time Adaptive Processing (STAP) for clutter and jamming mitigation in a carrier based airborne early warning (AEW) radar system. A UHF, low PRF system has been chosen as the baseline, and the system is characterized by severe size, weight and power constraints, a relatively wide bandwidth and a rotating antenna, all of which effect the choice and implementation of a STAP algorithm. Broadband measured antenna data from the ADS-18S antenna, and realistic clutter models generated with the Rome Lab STAP Algorithm Development Tool (RLSTAP/ADT) are utilized to create simulated performance results. An overview of the fundamental characteristics of low PRF radars, alternative STAP clutter and jamming cancellation techniques, and a selection of candidate STAP architectures for detailed simulated performance comparisons are presented. Because of Doppler ambiguities inherent in a low PRF radar, platform motion compensation techniques over a sub-CPI become the preferred adaptive approach rather than spatial nulling for clutter cancellation. STAP performance with both narrow band and wideband models, and with both stationary and rotating antennas are used when comparing the interference mitigation capabilities of alternative STAP subsystem architectures. Finally, a summary of computational requirements for alternative STAP and signal processing implementations is presented. Tradeoffs with respect to the location of the pulse compressor before or after the STAP subsystem are presented in terms of computational requirements, STAP sample selection, and target cancellation concerns. The computational advantages of using a recursive QR decomposition algorithm such as the Recursive Modified Gram Schmidt (RMGS) algorithm rather than a block algorithm for a pre-Doppler STAP approach are explained. The implementation of this algorithm in a High Performance Scalable Computer implementation utilizing the Analog Devices SHARC processor and Myrinet™ LAN technology is summarized.

SPACE TIME ADAPTIVE PROCESSING IMPLEMENTATION TRADES FOR A UHF AIRBORNE EARLY WARNING RADAR

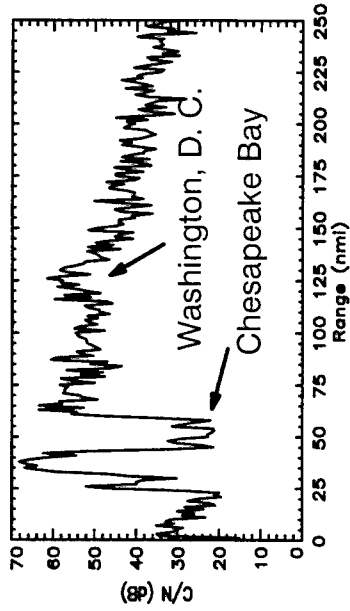
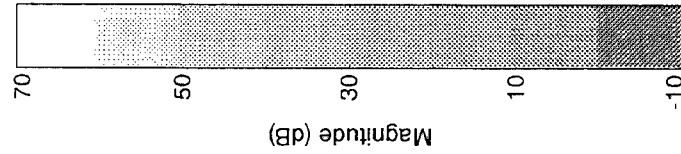
**ROBERT M. COOPER
LOCKHEED MARTIN
OCEAN, RADAR AND SENSOR SYSTEMS
SYRACUSE, NY 13221
cooperr@syr.lmco.com**

RLSTAP MODEL RESULTS

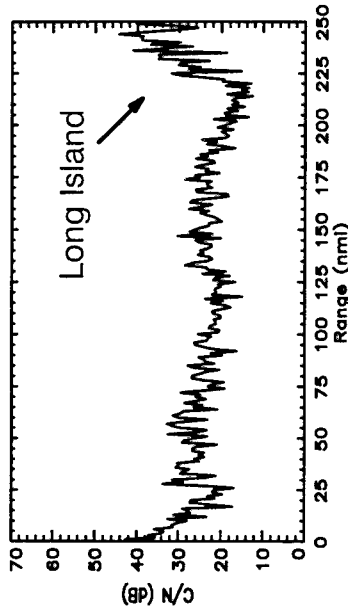
CLUTTER/NOISE VERSUS RANGE



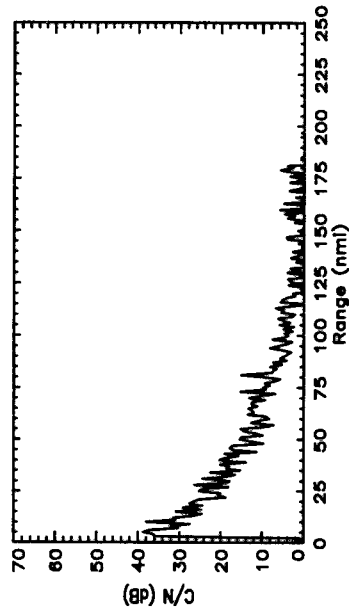
CLUTTER MAP MADE WITH
RLSTAP MAPPING CAPABILITY



C/N LOOKING INLAND (LINE 1)



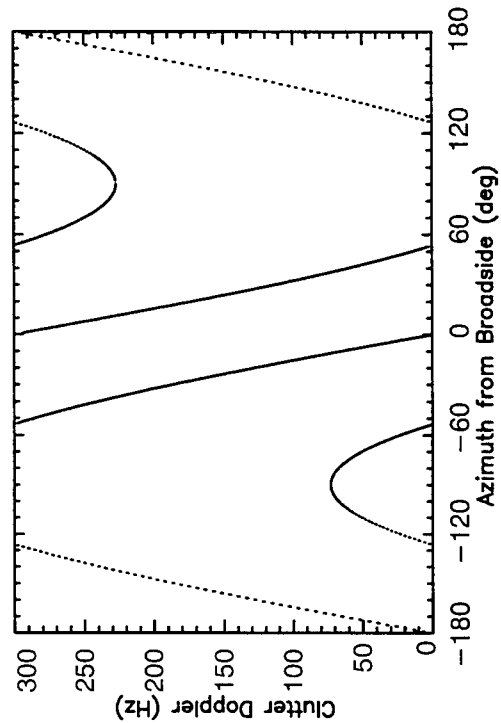
C/N LOOKING ALONG THE COAST (LINE 2)



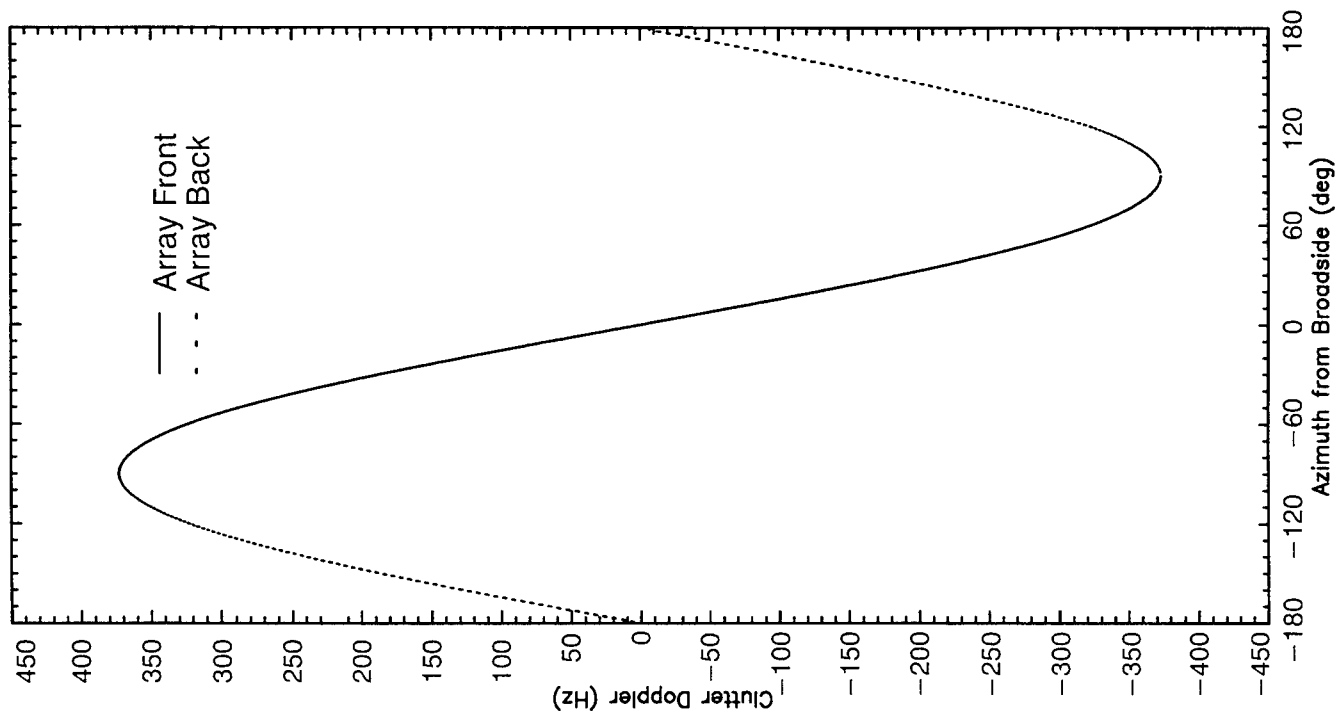
C/N LOOKING OUT TO SEA (LINE 3)

LOW PRF CLUTTER SPECTRUM FOLDOVER

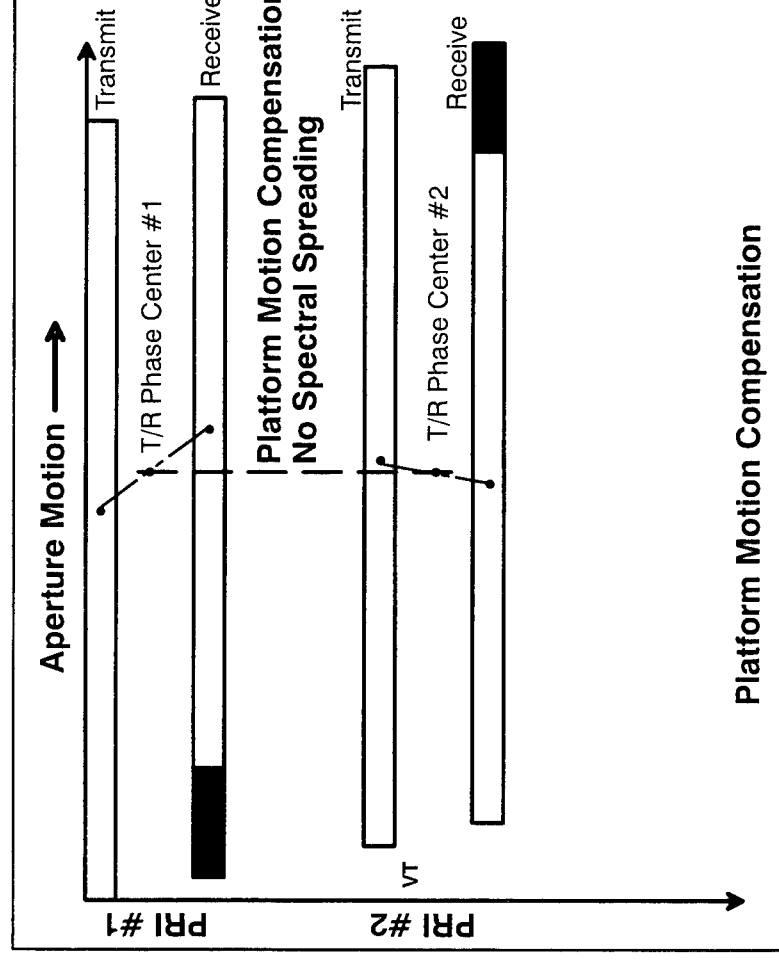
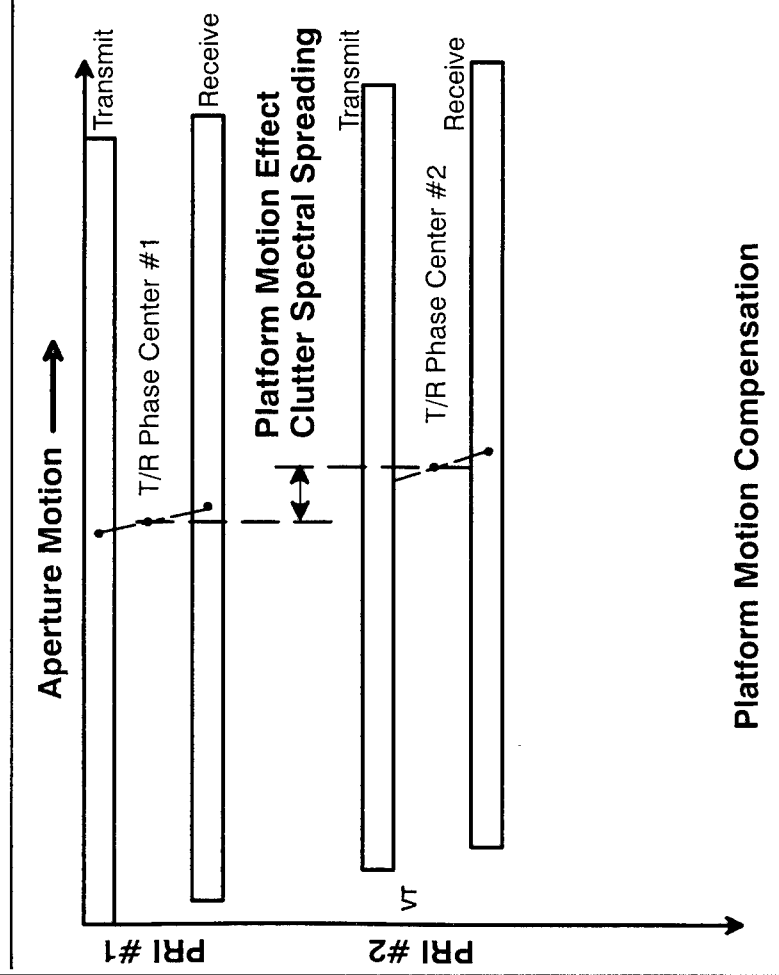
CLUTTER DOPPLER WITH THE
ANTENNA BROADSIDE 90°
FROM THE AIRCRAFT HEADING



- THE DOPPLER FREQUENCY OF CLUTTER HAS A SINUSOIDAL RELATIONSHIP WITH THE ANGLE FROM ARRAY BROADSIDE
- LOW PRF CLUTTER SPECTRUM FOLDS AT MULTIPLES OF THE PRF WHICH CREATES AMBIGUITIES

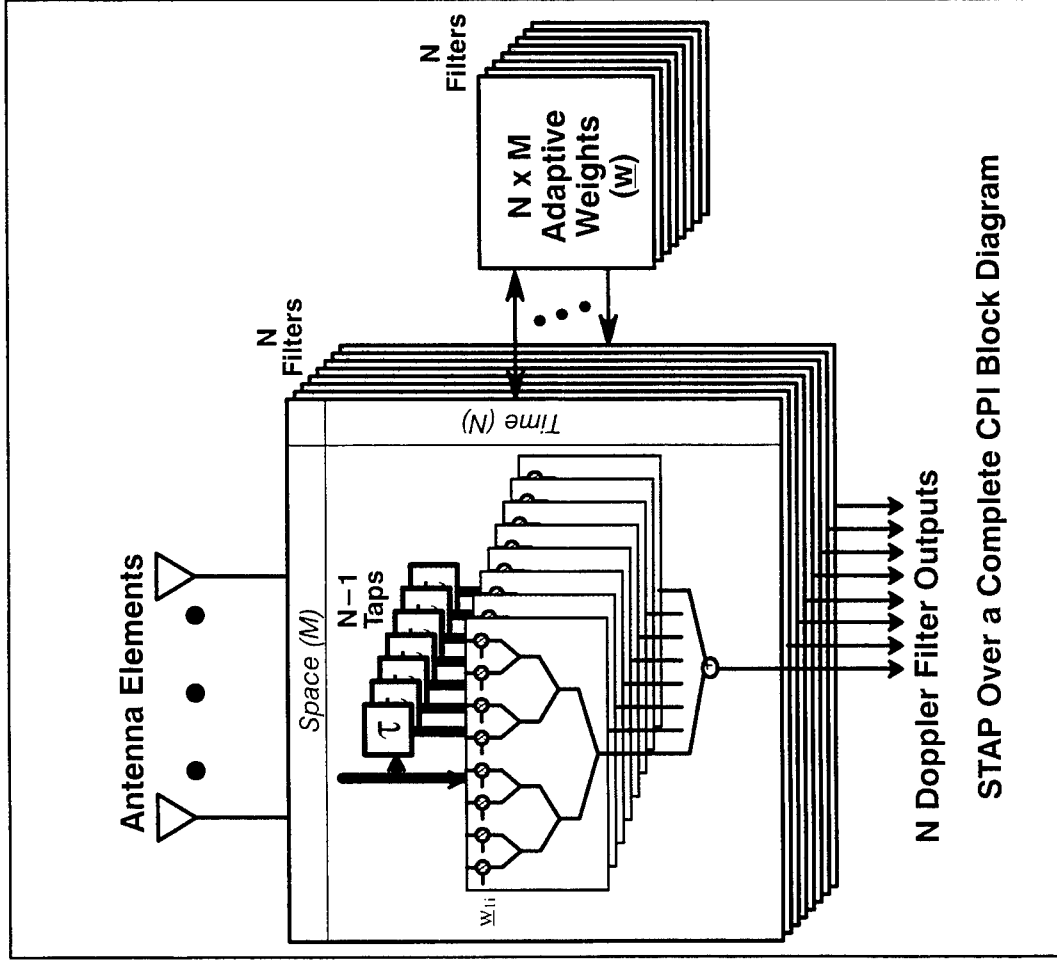


PLATFORM MOTION EFFECT AND COMPENSATION TECHNIQUE



STAP INTEGRATED OVER A COMPLETE CPI

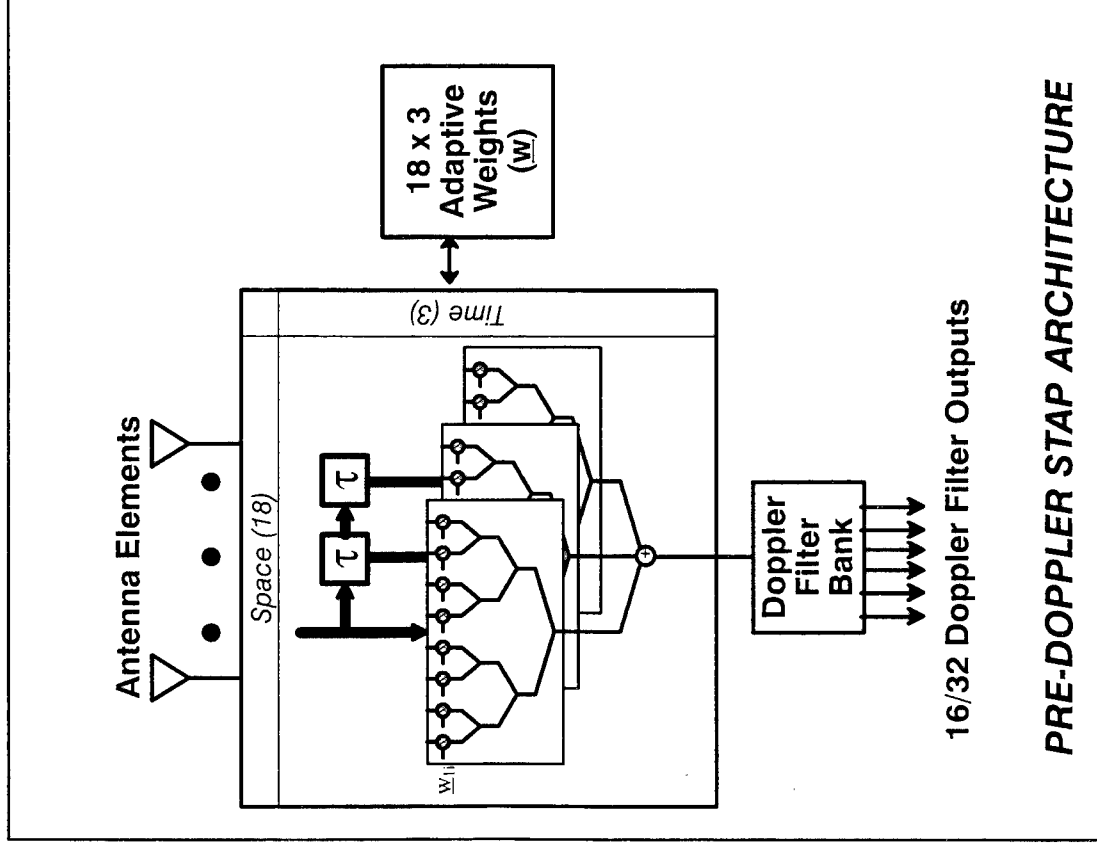
(Joint Optimum STAP)



- COMBINE STAP AND DOPPLER PROCESSING THROUGH CHOICE OF REFERENCE VECTOR AND DESIRED RESPONSE
- NOT CONSIDERED PRACTICAL DUE TO LARGE NUMBER OF ADAPTIVE WEIGHTS
- JAMMERS ARE CANCELLED SPATIALLY
- CLUTTER IS CANCELLED WITH MULTIPLE PRI PLATFORM MOTION COMPENSATION PROCESSING

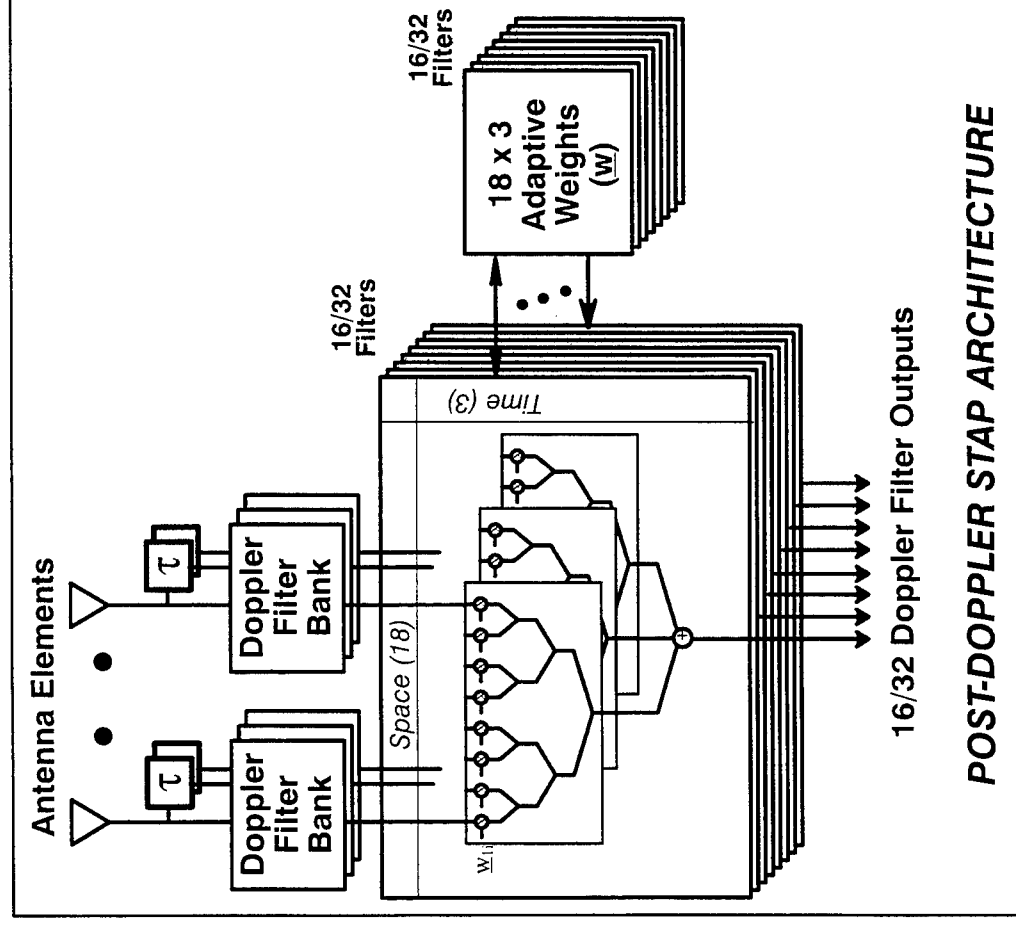
3 PULSE PRE-DOPPLER STAP PROCESSING

- REQUIRES DOPPLER PROCESSING FOR OUTPUT BEAMS ONLY
- DOPPLER PROCESSORS FOR SUM, DIFFERENCE AND OMNI CHANNELS
- JAMMERS ARE CANCELLED SPATIALLY
- CLUTTER IS CANCELLED WITH MULTIPLE PRI PLATFORM MOTION COMPENSATION PROCESSING



3 PULSE POST DOPPLER STAP PROCESSING

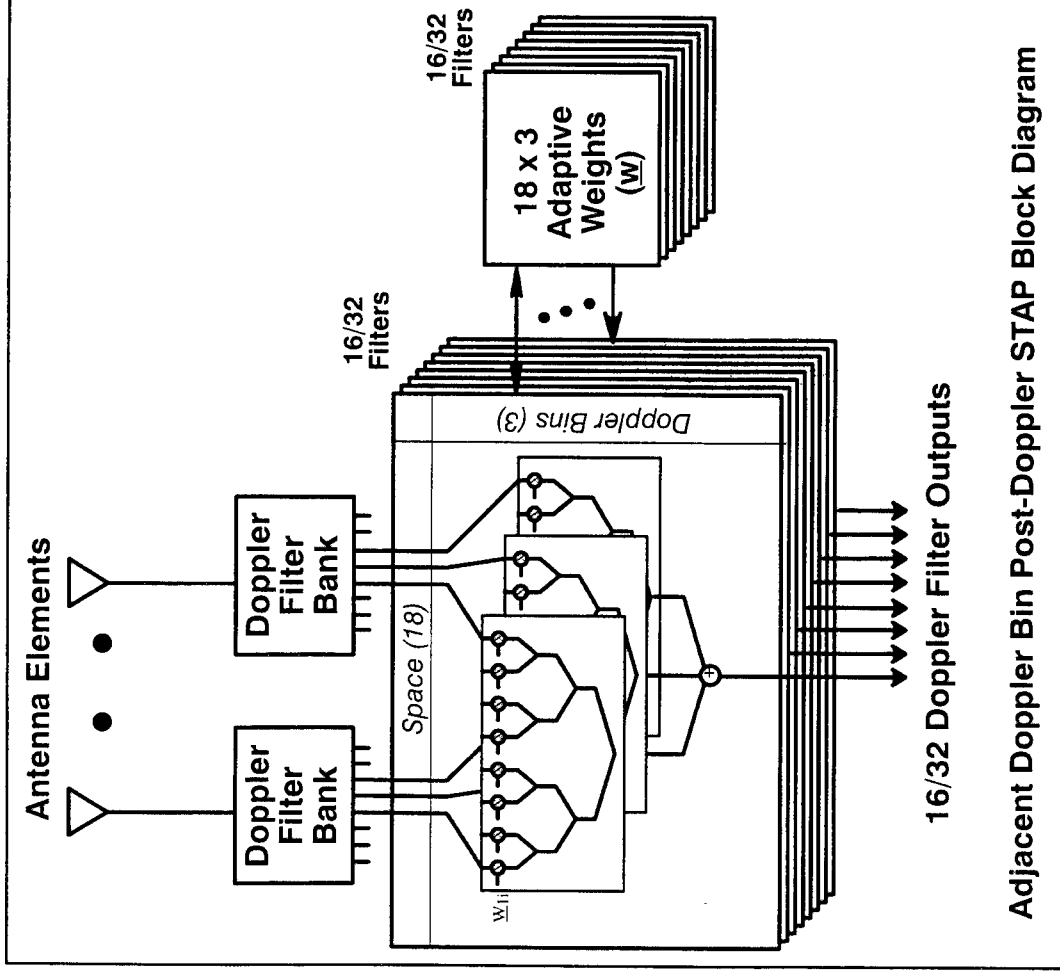
- REQUIRES DOPPLER PROCESSING FOR UNDELAYED, SINGLE DELAYED AND DOUBLE DELAYED OUTPUTS OF EACH ELEMENT CHANNEL
- TOTAL OF 54 DOPPLER PROCESSORS
- JAMMERS ARE CANCELLED SPATIALLY
- CLUTTER IS CANCELLED WITH MULTIPLE PRI PROCESSING SEPARATELY FOR EACH DOPPLER BIN



ADJACENT DOPPLER BIN STAP PROCESSING

(Post-Doppler STAP)

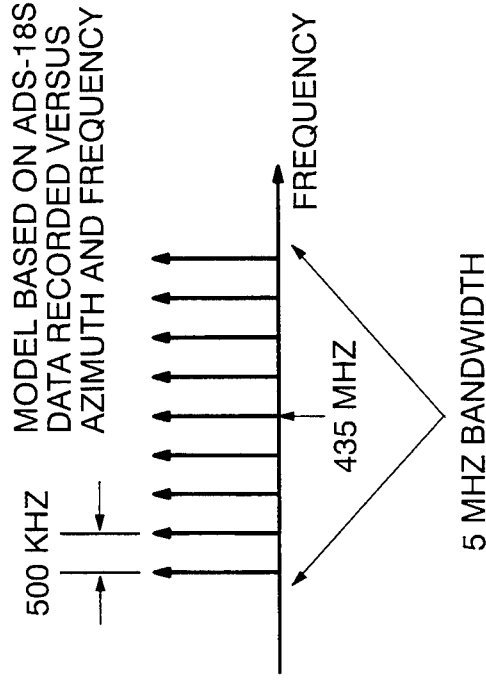
- REQUIRES DOPPLER PROCESSING ON EACH ELEMENT CHANNEL
- TOTAL OF 18 DOPPLER PROCESSORS
- JAMMERS ARE CANCELLED SPATIALLY
- CLUTTER IS CANCELLED WITH ADJACENT DOPPLER FILTER BINS



Adjacent Doppler Bin Post-Doppler STAP Block Diagram

CLUTTER AND JAMMING SIMULATED ENVIRONMENT

Parameter	Value
PRF	300 Hz
Bandwidth	5 MHz
Range of Data	30 to 250 nmi
Platform Altitude	30,000 ft
Platform Velocity	250 knots
Array Broadside wrt Heading	95°
Antenna Element Model	ADS-18S – 18 Yagi Element Array
Elect Scan wrt Array Broadside	0°
Array Mechanical Scanning	6 RPM – $\sigma_c = 1.5$ Hz, $\sigma_v = 0.525$ m/s
Clutter Internal Motion	
– Sea State 3 Clutter	$\sigma_c = 2.28$ Hz, $\sigma_v = 0.8$ m/s
– Wooded Clutter	$\sigma_c = .285$ Hz, $\sigma_v = 0.1$ m/s
– Urban Clutter	$\sigma_c = .114$ Hz, $\sigma_v = 0.04$ m/s



COVARIANCE MATRIX FORMATION:

$$\sum \#Scats \underline{v_c} \underline{v_c}' = \underline{C_c}$$

ADS-18S DATA WAS RECORDED BY RANDTRON SYSTEMS IN 1991,
AND HAS BEEN PROVIDED COURTESY OF NORTHRUP GRUMMAN

PERFORMANCE METRICS: SINR LOSS

$$\text{SINR}_{\text{loss}} = \frac{\left(\frac{S}{C+J+N}\right)_{\text{Adapted}}}{\left(\frac{S}{N}\right)_{\text{Quiescent}}}$$

- COMPUTED VERSUS DOPPLER
- AVERAGED OVER DATA SAMPLES FOR TIME SAMPLE SIMULATIONS

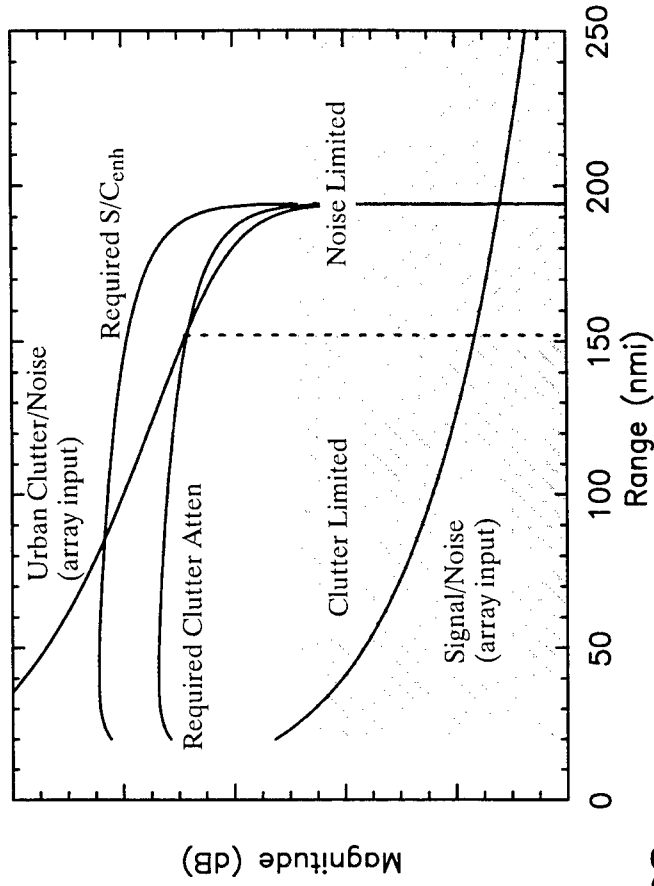
SINR LOSS COMBINES SIGNAL LOSS AND INTERFERENCE RESIDUE INTO A SINGLE METRIC

PERFORMANCE METRICS: S/C ENHANCEMENT

$$(S/C)_{\text{enh}} = \frac{\left(\frac{S}{C}\right)_{\text{Adapted}}}{\left(\frac{S}{C}\right)_{\text{Quiescent}}}$$

- S/C ENHANCEMENT REQUIRES
 - SPECIFIED TARGET MODEL
 - SPECIFIED CLUTTER MODEL
 - SPECIFIED RADAR PARAMETERS

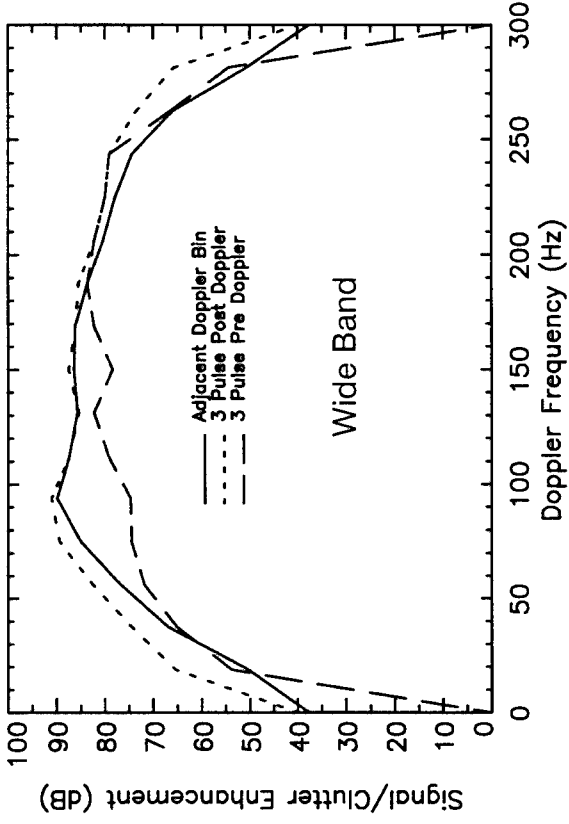
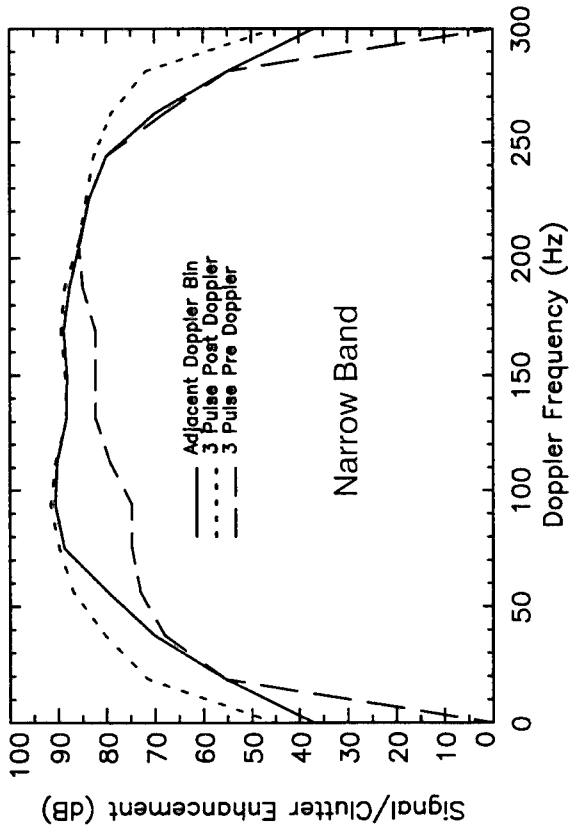
SIGNAL/CLUTTER ENHANCEMENT VS RANGE



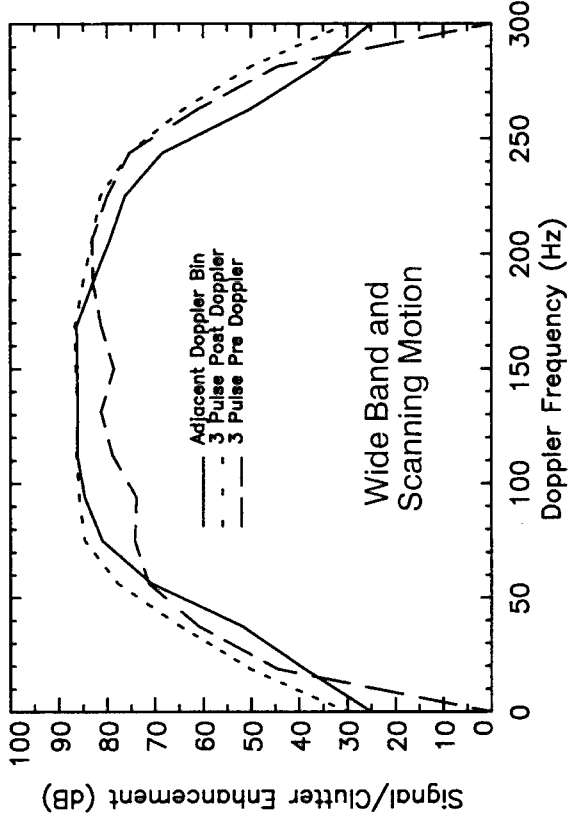
**S/C ENHANCEMENT TRANSLATES
DIRECTLY INTO SYSTEM REQUIREMENTS**

SIMULATION PERFORMANCE EXAMPLES

COVARIANCE MATRIX SIMULATIONS

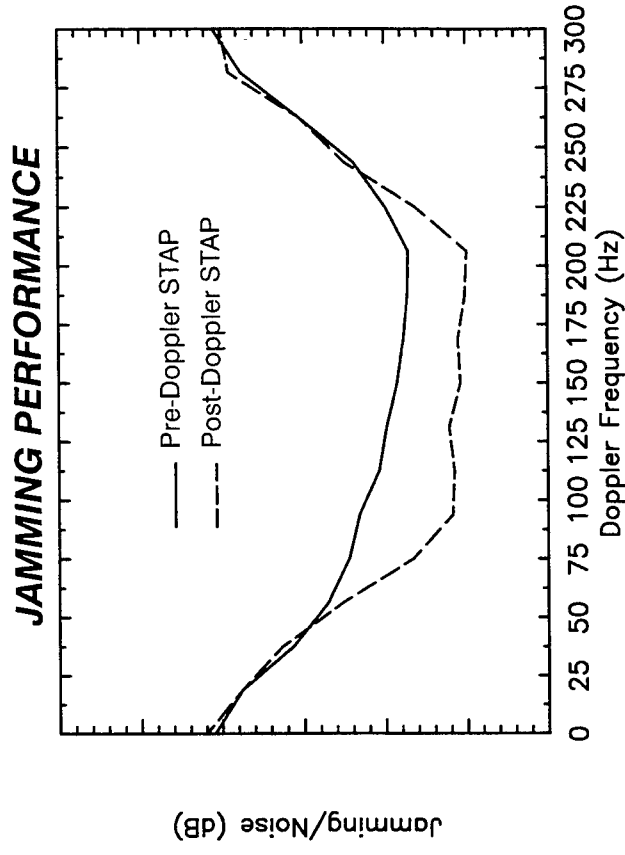
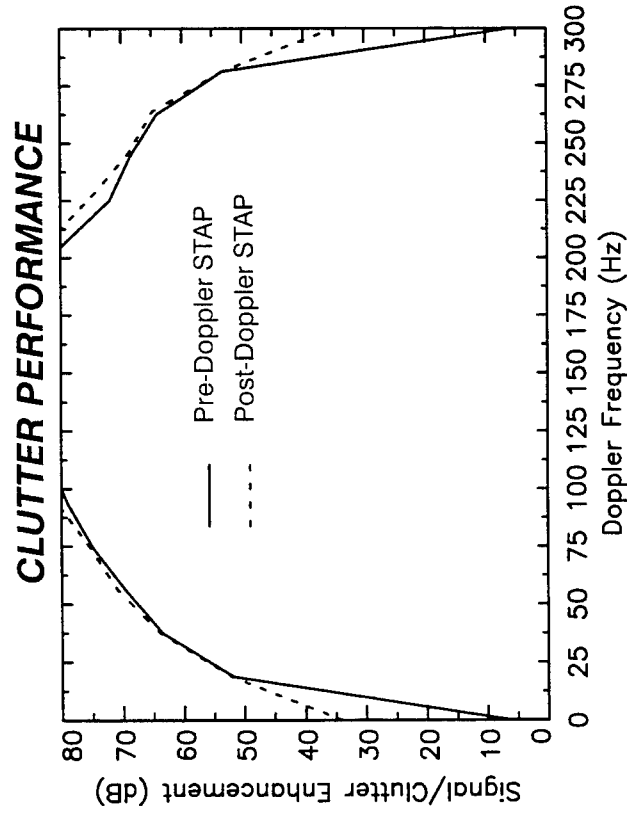


- NOTCH WIDTH IS THE MOST CRITICAL PERFORMANCE METRIC
- PERFORMANCE IN THE 60 TO 70 DB S/C ENHANCEMENT RANGE DEFINES THE NOTCH WIDTH
- PERFORMANCE WITH THE ADJACENT DOPPLER BIN APPROACH DEGRADES WITH BANDWIDTH AND SCANNING MOTION EFFECTS



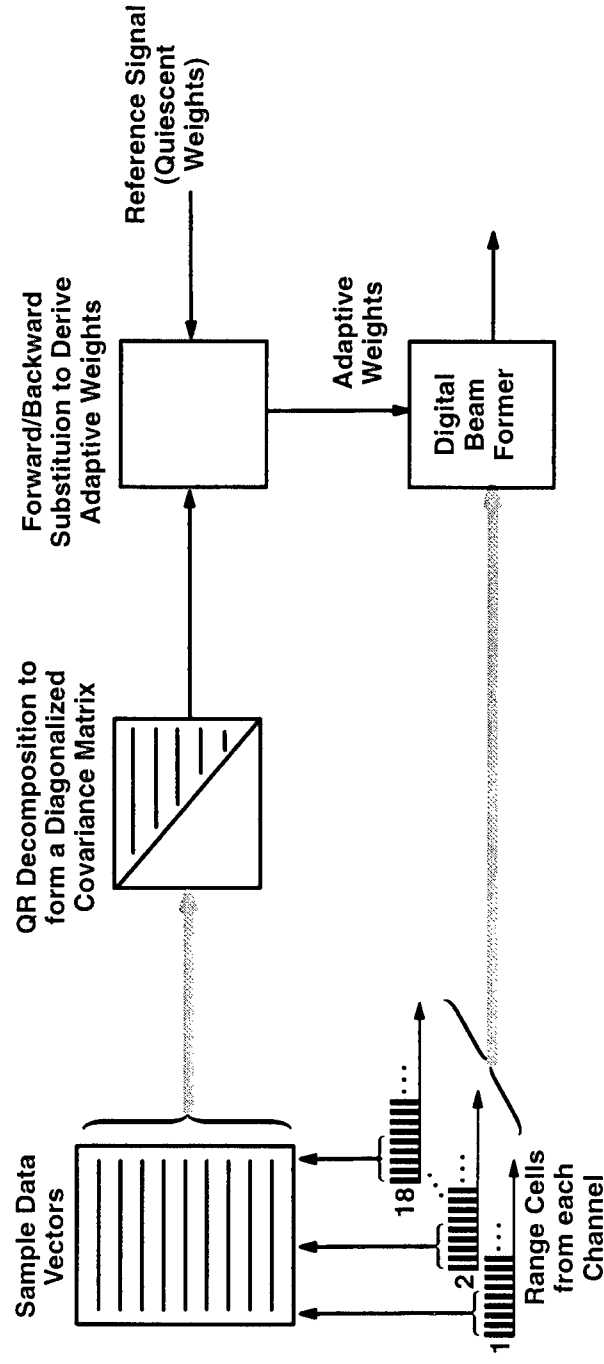
SIMULATION PERFORMANCE EXAMPLES

TIME SAMPLE SIMULATIONS



**JAMMING PERFORMANCE IS IMPROVED IN THE
CENTER DOPPLER FILTERS WITH POST-DOPPLER STAP**

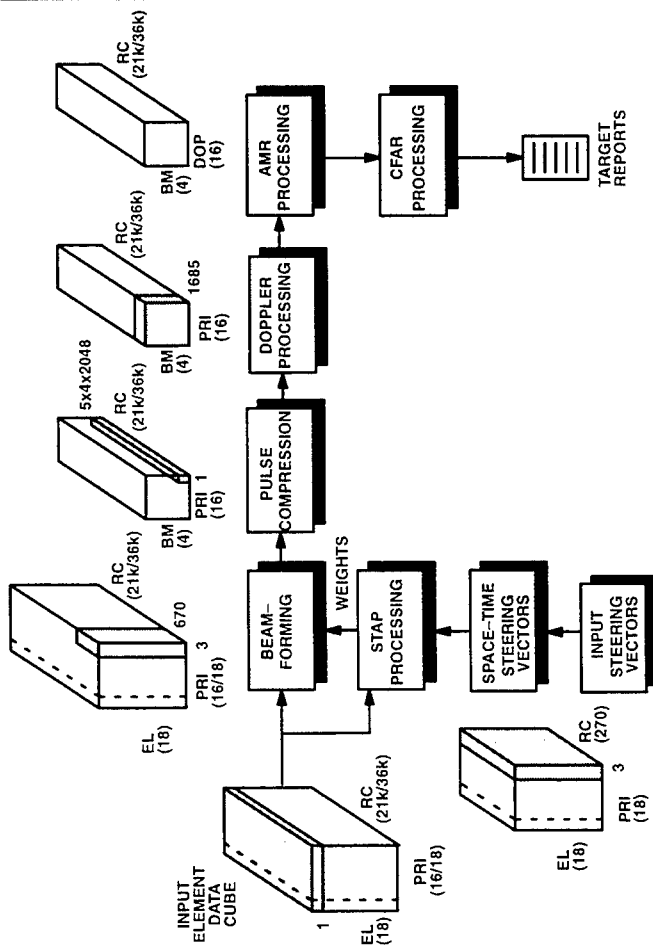
ADAPTIVE ALGORITHM BASIC STEPS



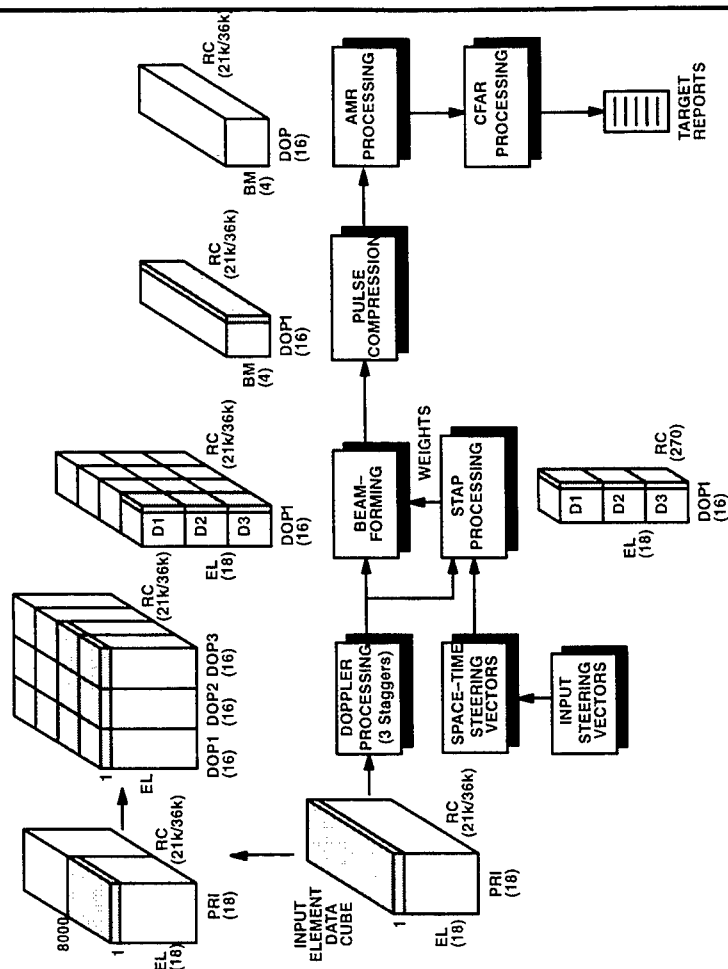
- BASIC EQUATION TO BE SOLVED: $W = A^{-1}b$
- USE QR DECOMPOSITION TO SOLVE FOR W WITHOUT PERFORMING AN EXPLICIT MATRIX INVERSE
- FOR PRE-DOPPLER STAP, A RECURSIVE ALGORITHM WILL EASE THE COMPUTATIONAL BURDEN
 - STAP SOLUTION FOR ONE PRI IS COMPUTED BASED ON THE SOLUTION FOR THE PREVIOUS PRI
 - REQUIRES HALF THE SAMPLE SUPPORT PER PRI

ADAPTIVE ALGORITHM FUNCTIONAL PARTITIONING

PRE-DOPPLER STAP ARCHITECTURE

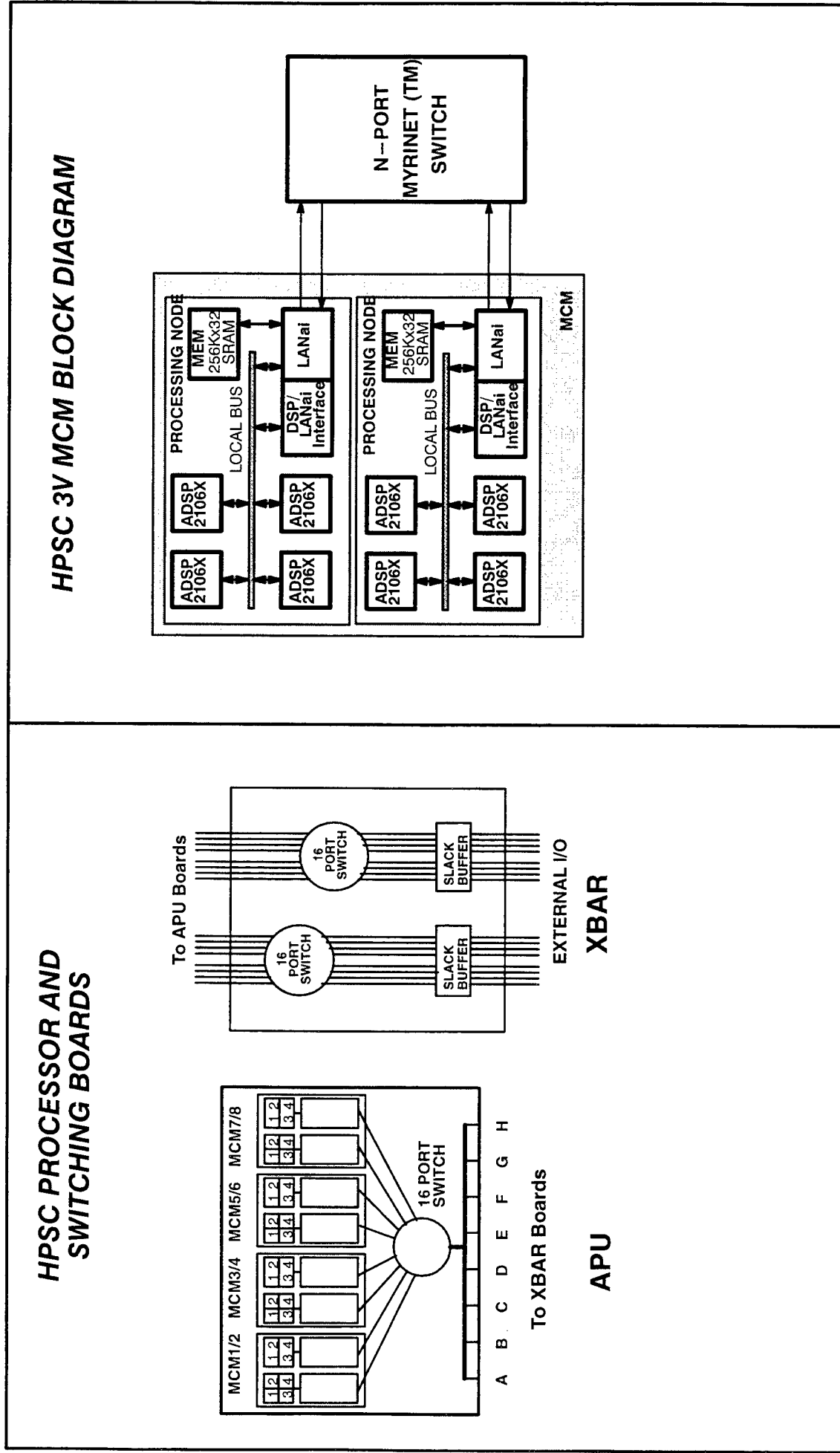


POST-DOPPLER STAP ARCHITECTURE



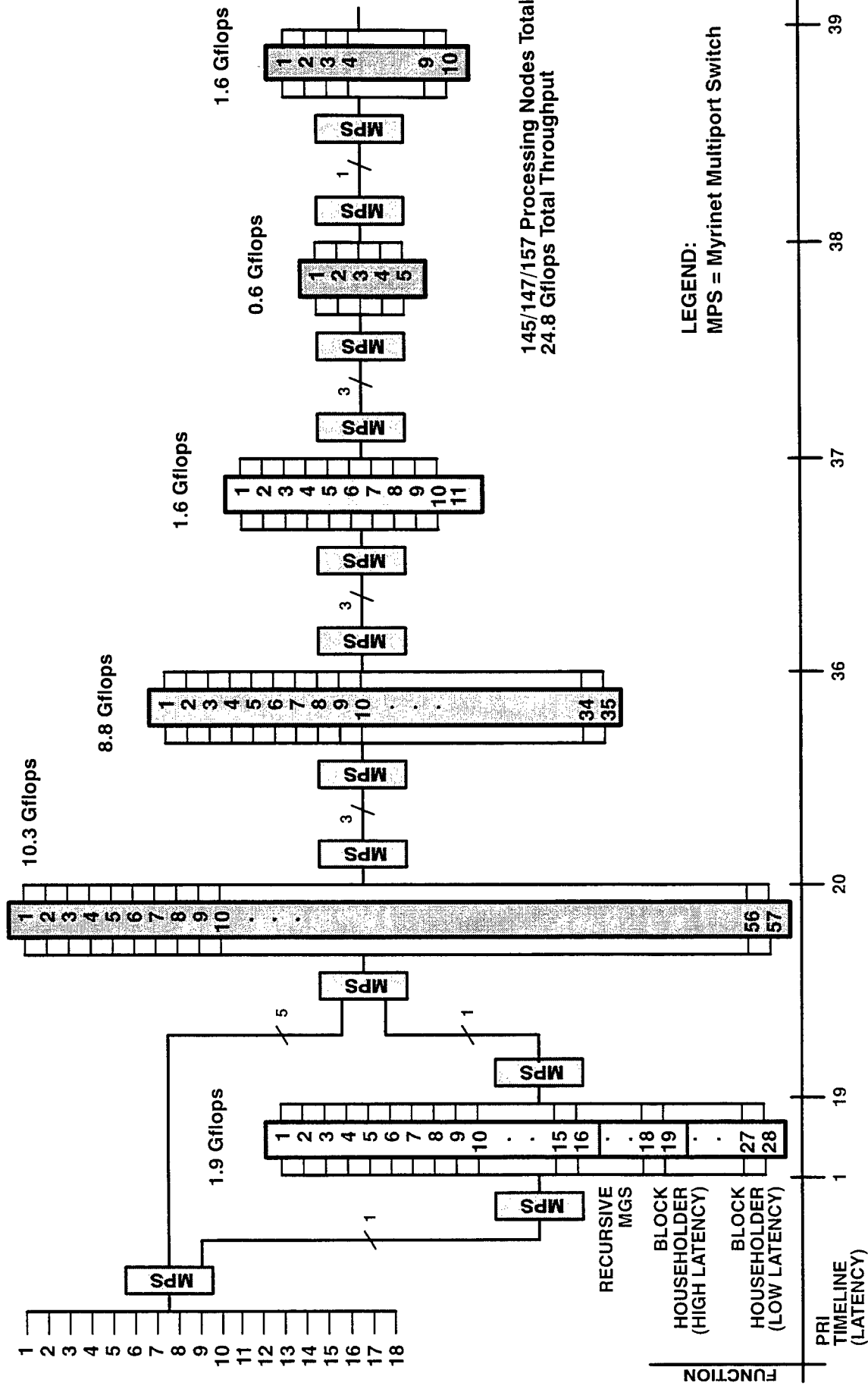
ADAPTIVE PROCESSOR BUILDING BLOCKS

HIGH PERFORMANCE SCALABLE COMPUTER

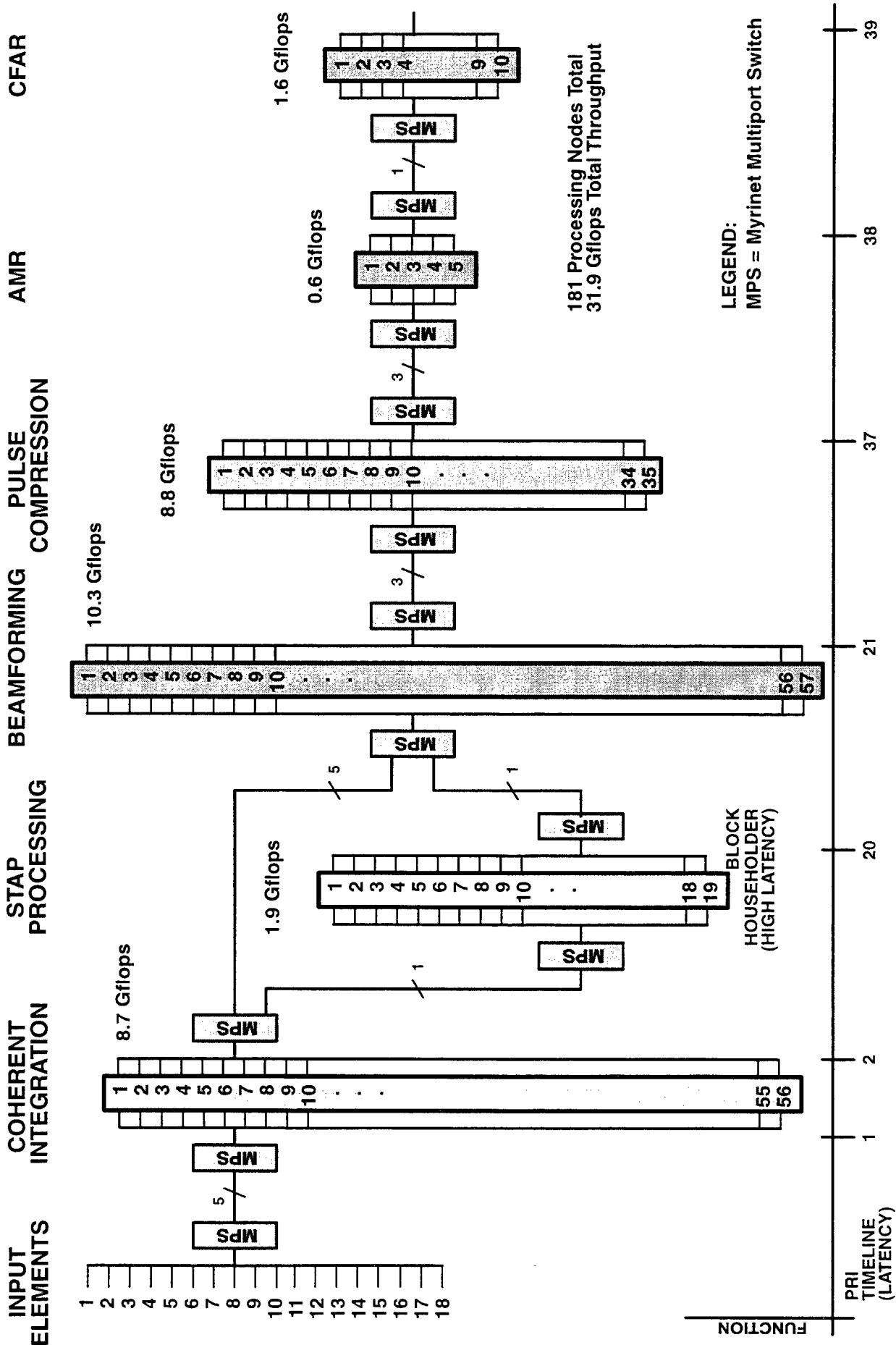


PRE-DOPPLER STAP PARTITIONING DIAGRAM

INPUT ELEMENTS STAP PROCESSING BEAMFORMING PULSE COMPRESSION COHERENT INTEGRATION AMR CFAR



POST-DOPPLER STAP PARTITIONING DIAGRAM



CONCLUSIONS

- THE ADJACENT DOPPLER BIN STAP PERFORMANCE SUFFERS WHEN BANDWIDTH AND SCANNING MOTION EFFECTS ARE CONSIDERED
- THE POST-DOPPLER STAP ARCHITECTURE PROVIDES THE GREATEST CLUTTER AND JAMMING MITIGATION CAPABILITY
- THE SIZE, WEIGHT AND POWER CONSTRAINTS OF A CARRIER BASED AEW PLATFORM MAY HAVE AN IMPACT ON THE ARCHITECTURE OF A NEAR FUTURE FIELDDED SYSTEM
- THE HIGH SPEED SCALABLE COMPUTER APPROACH RESULTS IN A FLEXIBLE PROCESSOR ARCHITECTURE DESIGN CAPABILITY

Clutter Mitigation in an Airborne Radar Based Upon Phase-Weight Perturbation

***K.R. Akbulut, B.N. Suresh Babu,
R.M. Davis, and J.D.R. Kramer***

The MITRE Corporation
202 Burlington Road
Bedford, MA 01730

Abstract In an airborne surveillance radar, the sensitivity for detecting low velocity targets is often limited by ground clutter that fills the low Doppler frequency filters. In order to reduce the clutter, it is necessary to reduce the antenna sidelobes where the clutter is most significant. In this paper, we describe a low cost sidelobe canceller that minimizes the clutter by using a phase perturbation algorithm. The antenna is modeled as a rotating planar array. The adaptive phases are applied to the row phase shifters. The same phase is applied on both transmit and receive and the phase settings remain fixed during a coherent processing interval. The environment seen by the canceller will be non-stationary due to the rotation of the antenna and motion of the aircraft. The canceller adaptively modifies the phase shifter settings to lower the elevation sidelobes, thereby, suppressing sidelobe clutter. Orthogonal binary sequences are used to provide the phase perturbations to those rows that are made adaptive. A gradient based algorithm updates the adaptive phases. An estimate of the gradient is obtained by cross-correlating the binary codes with the instantaneous output power. Only the output power needs to be measured. The phase-only perturbation algorithm eliminates the need for separate receivers on the adaptive channels and supports low cost retrofitting of adaptive nulling on phased arrays using conventional beam-steering circuits to apply the adaptive weights. This paper describes the perturbation algorithm and the simulation being developed to evaluate its ability to reduce sidelobe clutter.

Clutter Mitigation in an Airborne Radar Based Upon Phased-Weight Perturbations

K. R. Akbulut

B. N. Suresh Babu

R. M. Davis

J. D. R. Kramer

Adaptive Sensor Array Processing Workshop

12-14 March 1997

MITRE

Background and Application

- Target detection in airborne radars is limited by antenna sidelobe clutter
- Detection of low speed targets in high prf airborne radars is limited by high elevation sidelobes where near-in clutter competes with targets at long range
- High elevation sidelobes can be reduced in three ways
 - Closed loop multiport adaptive techniques
 - Open loop (predictive nulling techniques)
 - Closed loop single-port adaptive techniques(require making only a single power measurement)

Objective, Approach, Status

- Objective

- Lower principal plane near-in elevation sidelobes to reduce sidelobe clutter and improve detection of low speed targets
- Goal is 5-10 dB reduction in sidelobes over 30-degree sector
- Intent is to compensate for antenna errors, radome effects, and other platform to platform variations without modifying antenna

- Approach

- Use phase-only perturbation adaptive algorithm
- Perform adaptation in the spatial (elevation angle) domain
- Adaptive phases are settings on phase shifters at ends of rows in antenna
- Minimize clutter in defined range-Doppler cells as fly over region with uniform clutter (e.g., ocean)

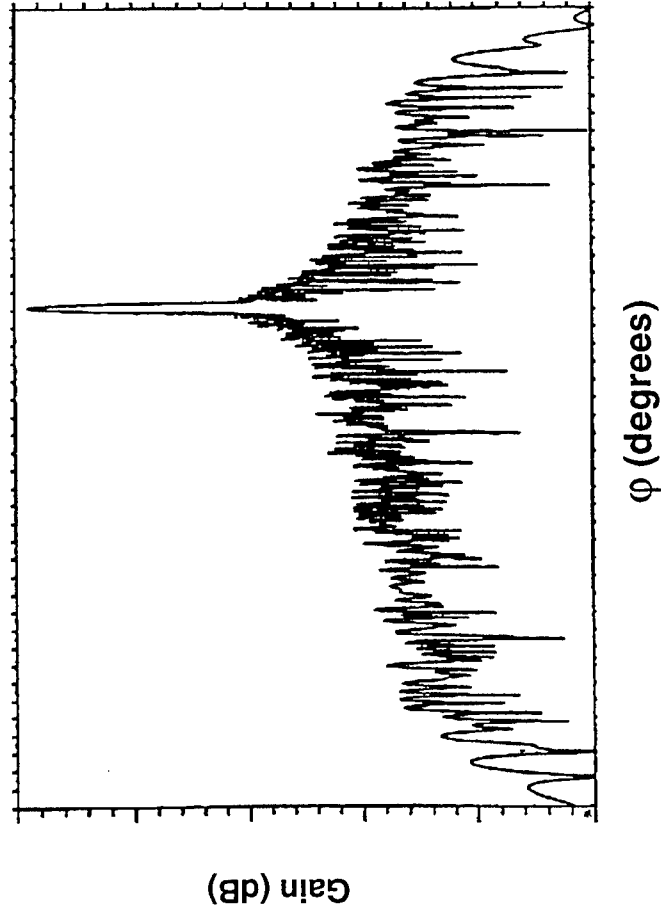
- Status

- Simulation being developed to evaluate algorithm and demonstrate potential capability of technique. Work in progress

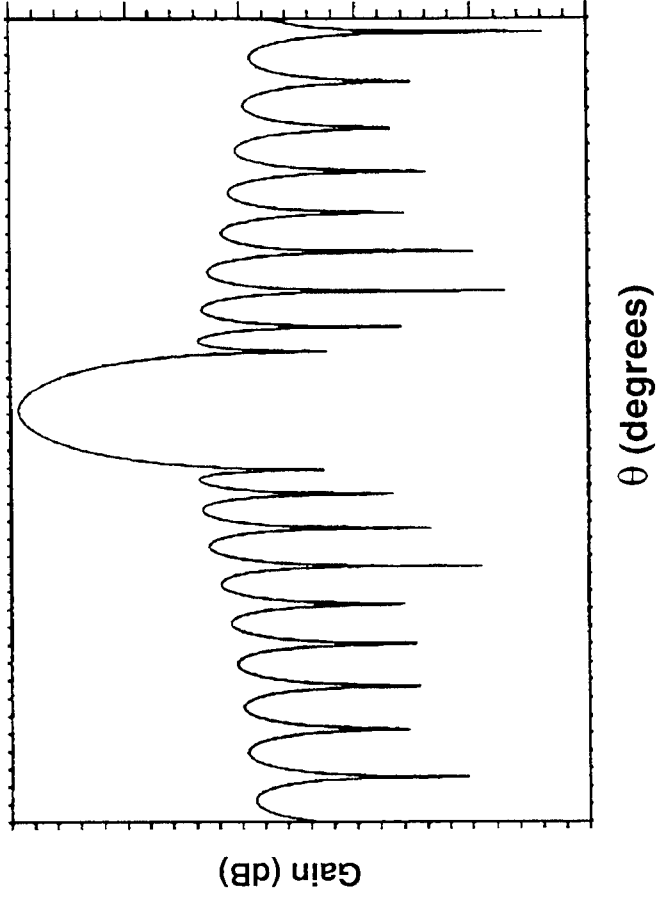
Statement of Problem

- Antenna is planar elliptical array of N serial-fed rows
- Phase shifters at end of each row can be independently controlled (voltages from each row are not available)
- Phase shifters cannot be changed during a coherent processing interval (CPI)
 - Adaptive phases must be applied on transmit as well as receive
- Antenna rotates one revolution every 10 sec
- Antenna assumed to have ultra-low azimuth and intercardinal plane sidelobes
- Only available measurements per CPI are powers in range-Doppler cells
 - Implies single port algorithm

Free Space Azimuth and Conical Elevation Antenna Patterns



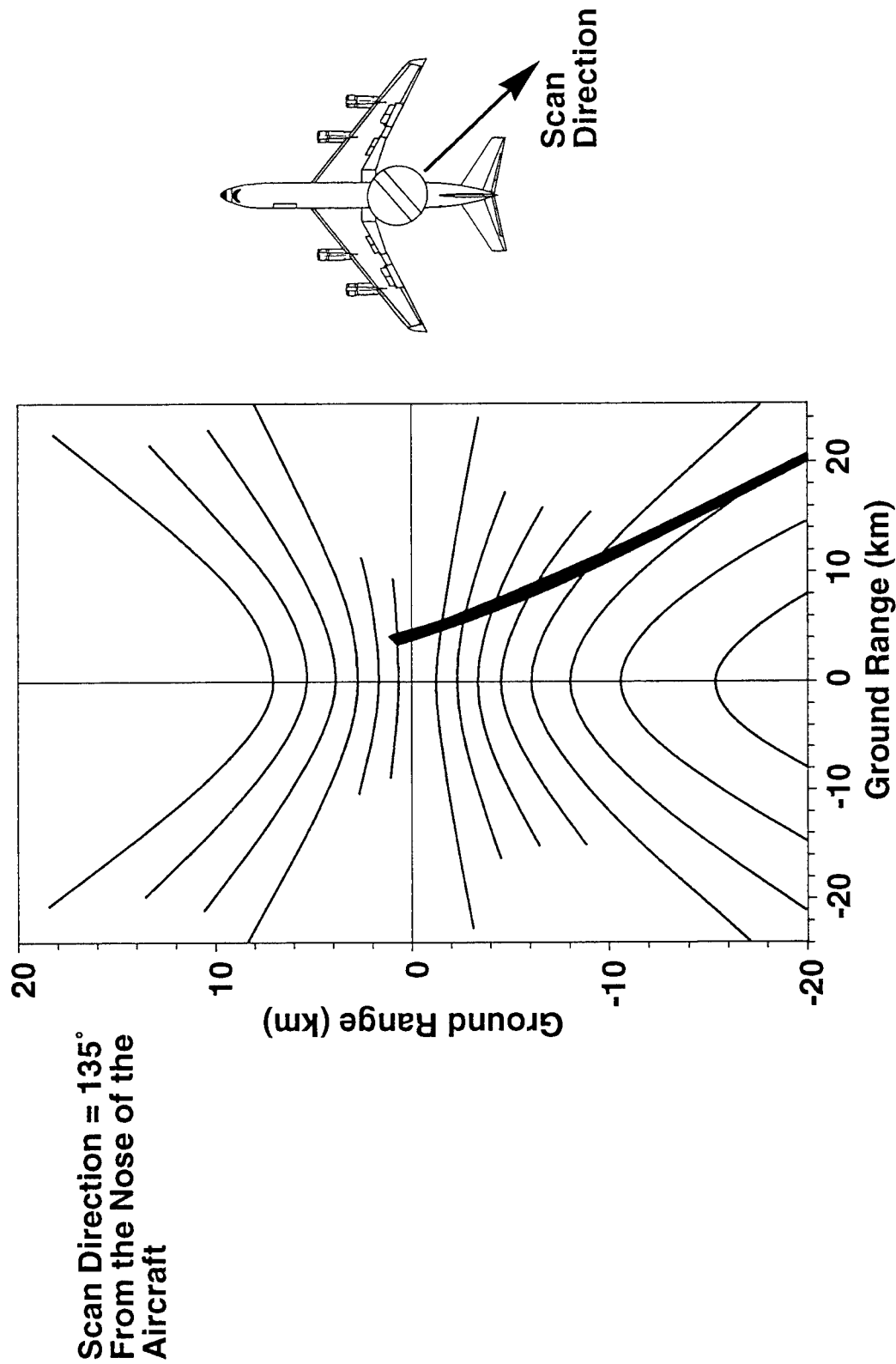
**Free Space Azimuth Beam
Antenna Pattern**



**Free Space Conical
Elevation Beam**

MITRE

Intersection of Conical Elevation Beam With Isodop Contours (Scan 135° From the Nose of the Aircraft)



MITRE

Clutter RCS Model

- Constant amplitude random phase

$$\sigma_{\text{patch}} = \frac{R_p \theta_{AZ} C \tau_c \Gamma \tan(\gamma_p)}{2} \exp(j\psi_p)$$

- Random amplitude, random phase

$$\sigma_{\text{patch}} = \frac{R_p \theta_{AZ} C \tau_c \Gamma \tan(\gamma_p)}{2} \left(\frac{X_p + jY_p}{\sqrt{2}} \right)$$

where:

R_p = Range to clutter

θ_{AZ} = Azimuth beamwidth

τ_c = Compressed pulse width

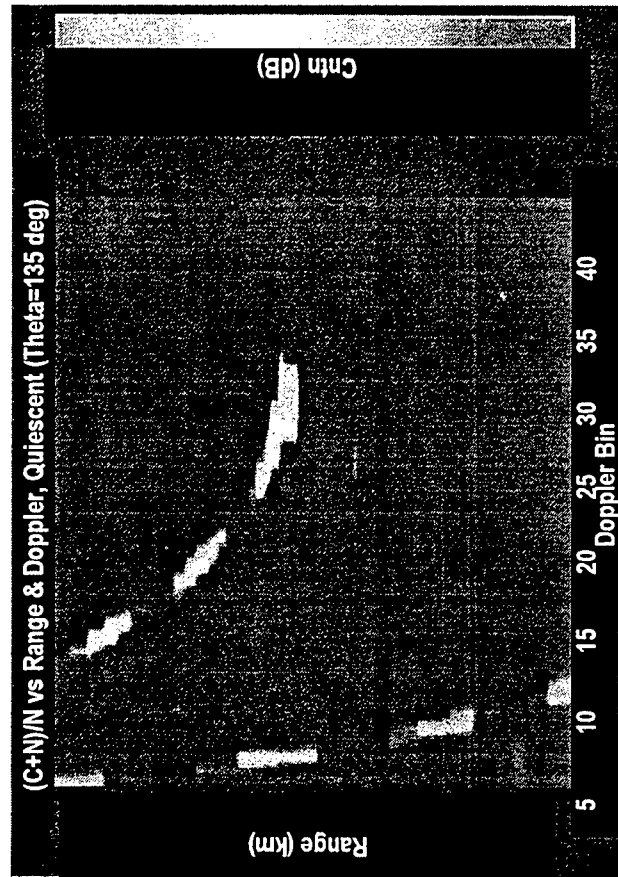
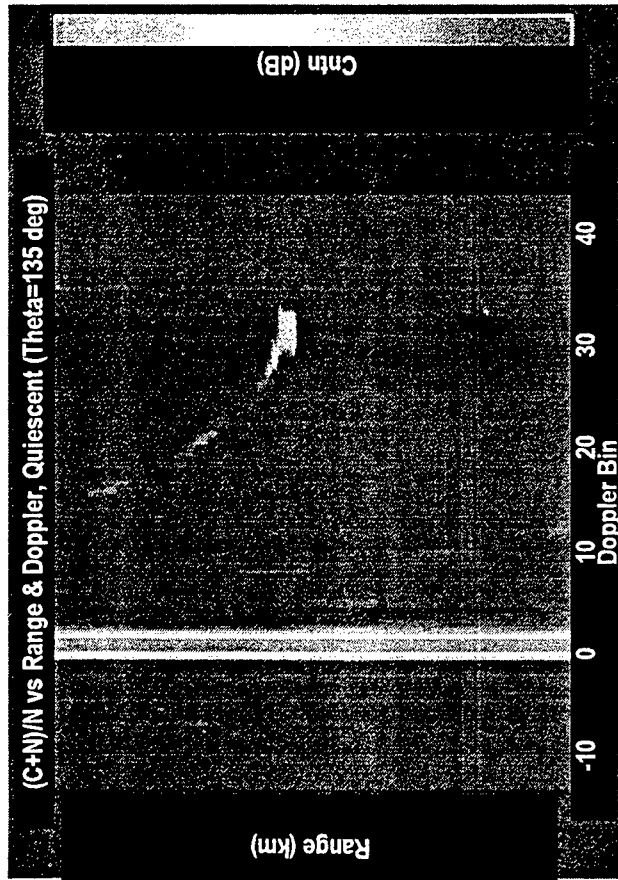
Γ = Reflection coefficient

γ_p = Grazing angle

ψ_p = Random variable uniformly distributed $0 - 2\pi$

X_p, Y_p = Zero mean unit variance Gaussian variates

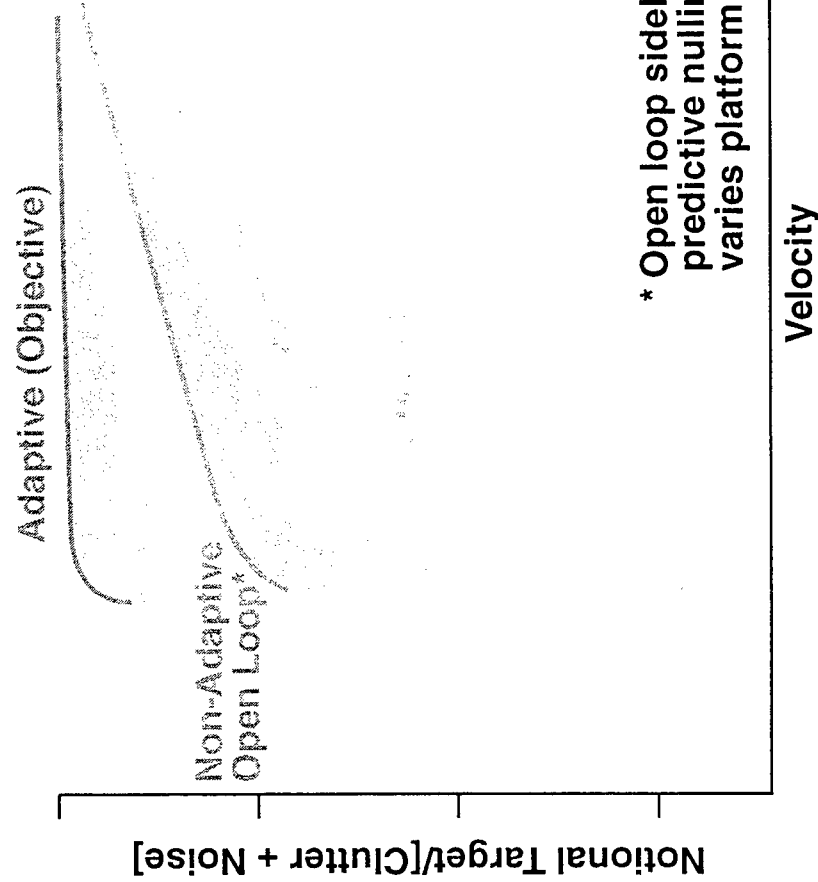
Clutter Plus Noise-to-Noise Ratio Contour vs Range and Doppler (Beam Position 135° From the Nose of the Aircraft)



Note: Sidelobe Clutter is Concentrated in
Relatively Small Number of Range-Doppler Cells

MITRE

Low-Velocity Target Surveillance Performance



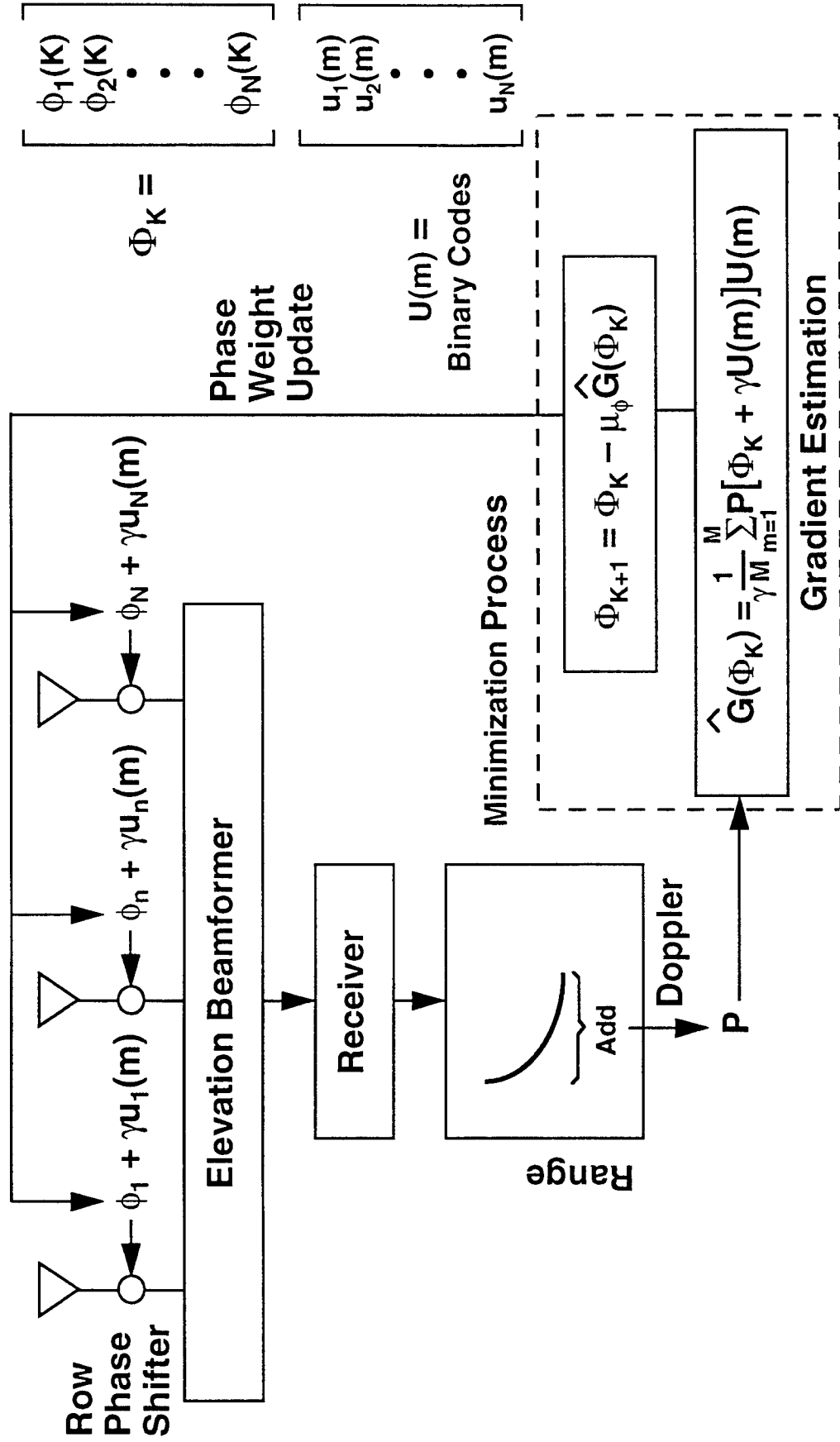
* Open loop sidelobe control called predictive nulling. Performance varies platform to platform.

MITRE

Overview of Simulation

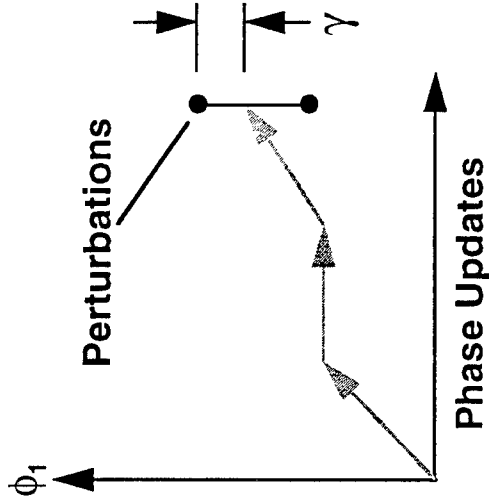
- Minimize power in Doppler filters using gradient based single-port adaptive algorithm
 - Perturb row shifters using binary sequences (codes)
 - Measure power variations in low velocity Doppler filters caused by perturbations
 - Calculate new gradients to be used in updating adaptive phases by cross-correlating binary sequences with measured output powers
 - Update phase shifter settings on row phase shifters using the calculated gradients
 - Repeat the procedure described above until the phases converge to their steady-state values
 - Make the amplitude of the perturbations proportional to the output power. The perturbations will then shut themselves off as the algorithm converges

Phase-Only Perturbation Algorithm With Doppler Processing: Block Diagram



P = Some Combination of Range-Doppler Cells in Which Power is to be Minimized

Phase Weight Perturbation Codes



The perturbation codes applied to the row phase shifters must have zero mean and must be mutually orthogonal.

Consider canceller with four adaptive phases. One possible code set is:

	<i>m</i> = sample time															
	1	2	3	4	5	6	7	8	9	10	11	12	13	14	15	16
$u_1(m)$	1	1	-1	-1	1	1	-1	-1	0	0	0	0	0	0	0	0
$u_2(m)$	1	1	1	1	-1	-1	-1	-1	0	0	0	0	0	0	0	0
$u_3(m)$	0	0	0	0	0	0	0	0	1	1	-1	-1	1	1	-1	-1
$u_4(m)$	0	0	0	0	0	0	0	0	1	1	1	1	-1	-1	-1	-1

M = 16

Time Multiplex Pair Code

Algorithm: Picking Weight Step Size (μ_ϕ) and Perturbation Amplitude (γ)

3/17/07

13

- μ_ϕ = weight step size = $\frac{1}{10\hat{g}_{\max}}$

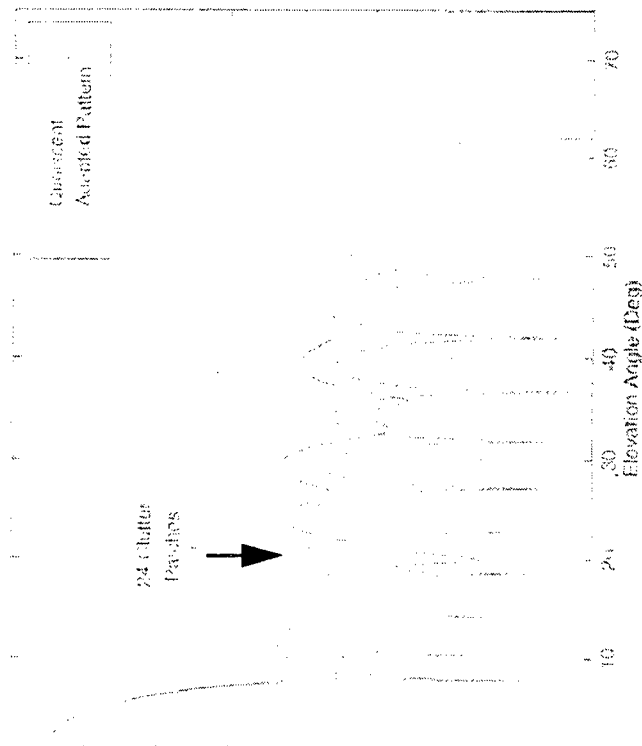
where \hat{g}_{\max} = maximum component of gradient during first weight update interval

- If any component $\hat{G}(\Phi_K)$ exceeds \hat{g}_{\max} on subsequent weight updates, do not update the corresponding weight
- Make perturbation amplitude (γ) time-varying and proportional to output power

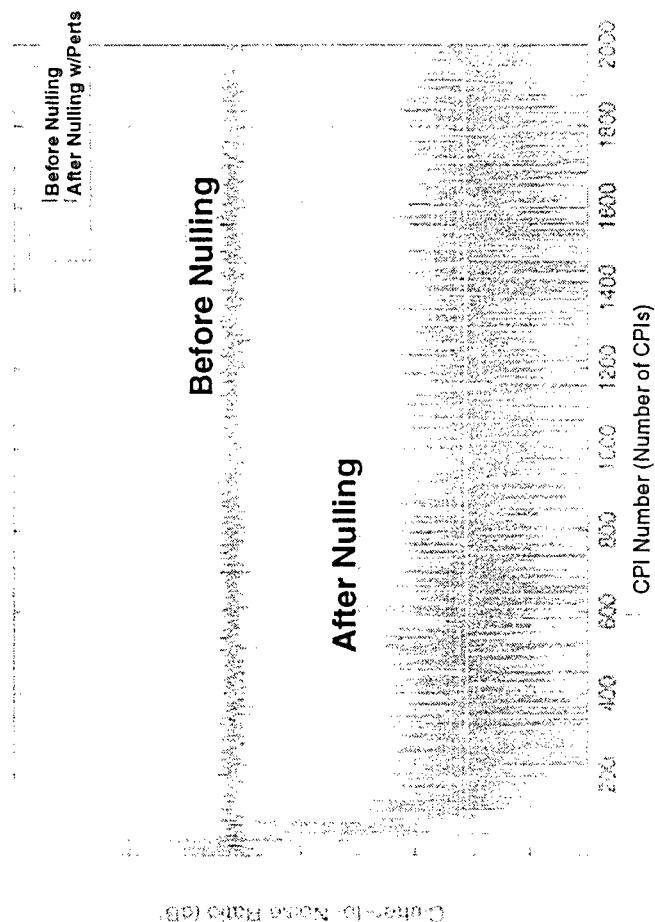
$$\gamma_{K+1} = \gamma_o \left[\frac{\sum_{m=1}^M |e_{KM+m}(\Phi_K + \gamma U_m)|^2}{\sum_{m=1}^M |e_m(\Phi_o + \gamma U_m)|^2} \right]^{1/2}$$

Performance of Phase Perturbation Algorithm On Non-Rotating Elliptical Planar Array; Power Minimized in Doppler Bin 3

One Way Antenna Patterns (Nulling in Doppler Bin 3)



Performance Without Rotation: Nulling in Doppler Bin 3

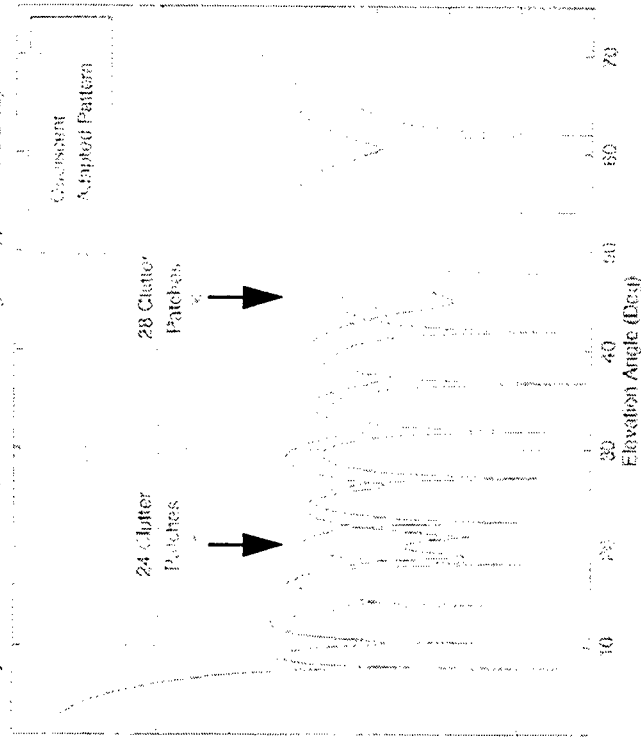


12 Adaptive Phases
Constant Amplitude Clutter Model

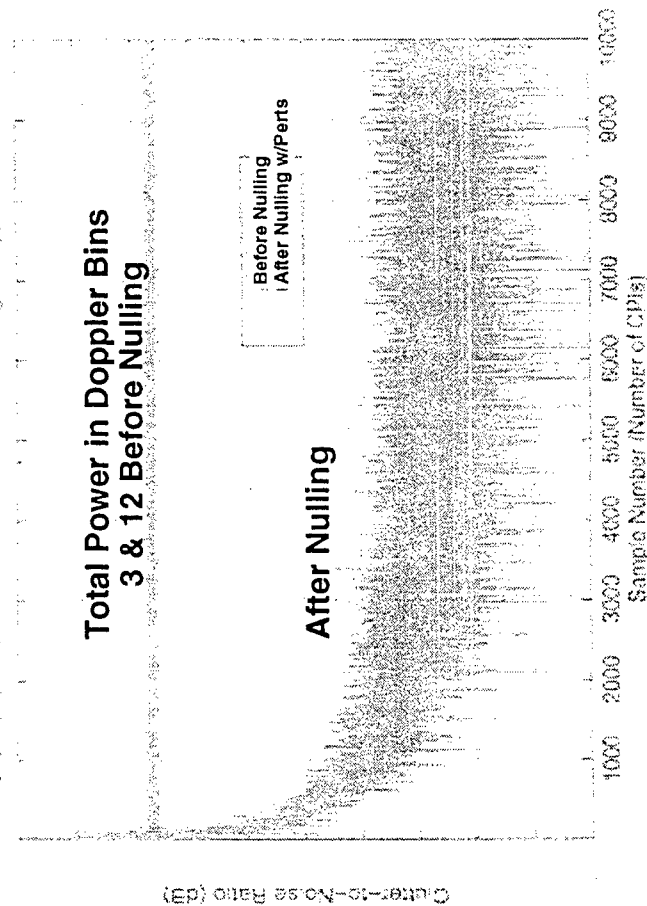
MITRE

Performance of Phase Perturbation Algorithm On Non-Rotating Elliptical Planar Array; Power Minimized in Doppler Bins 3 and 12

One Way Antenna Patterns (Simultaneous Nulling in Doppler Bins 3 & 12)



Performance Without Rotation: Simultaneous Nulling in Doppler Bins 3 & 12

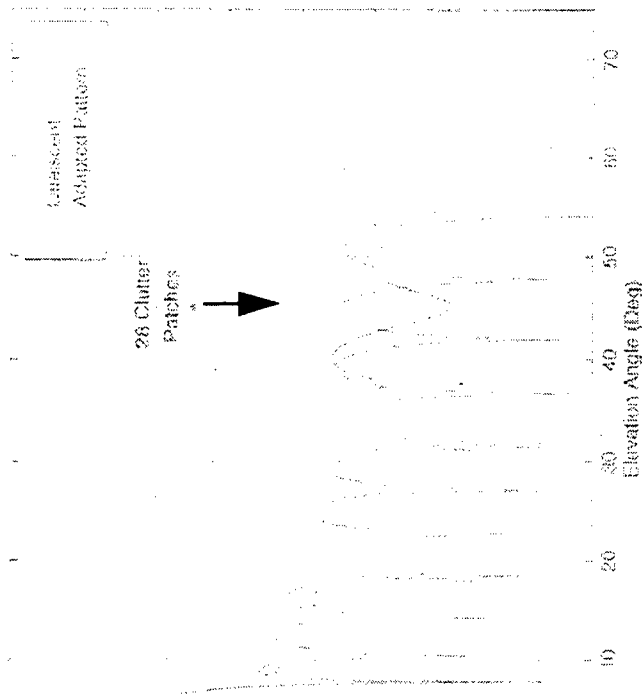


12 Adaptive Phases
Constant Amplitude Clutter Model

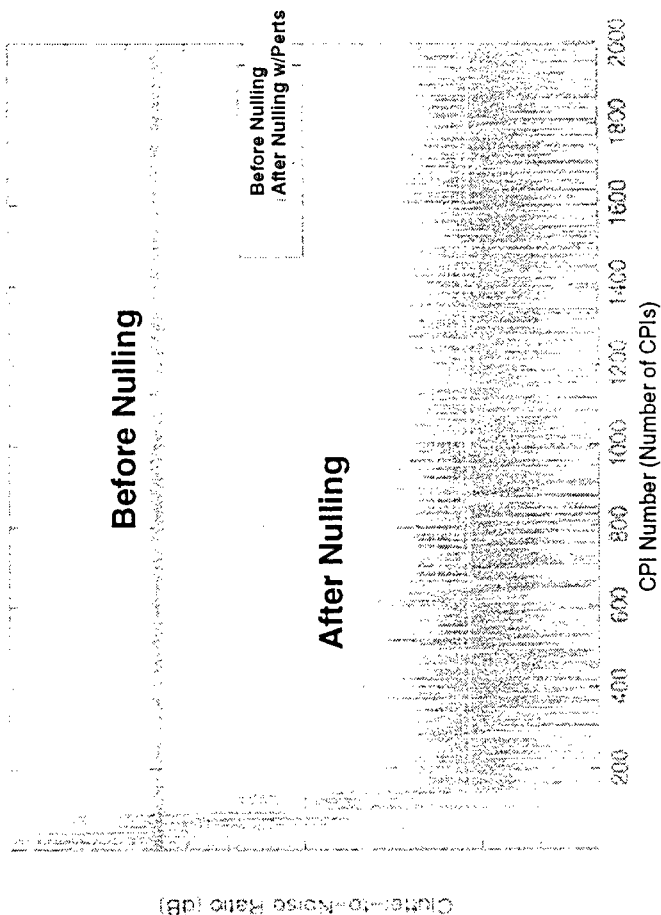
MITRE

Performance of Phase Perturbation Algorithm On Non-Rotating Elliptical Planar Array; Power Minimized in Doppler Bin 12

One Way Antenna Patterns (Nulling in Doppler Bin 12)



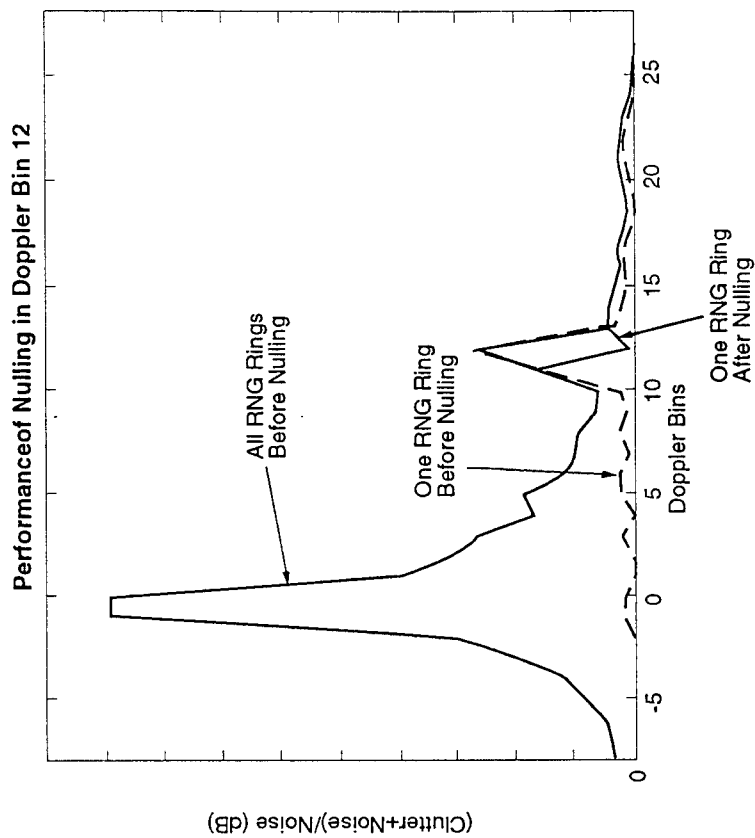
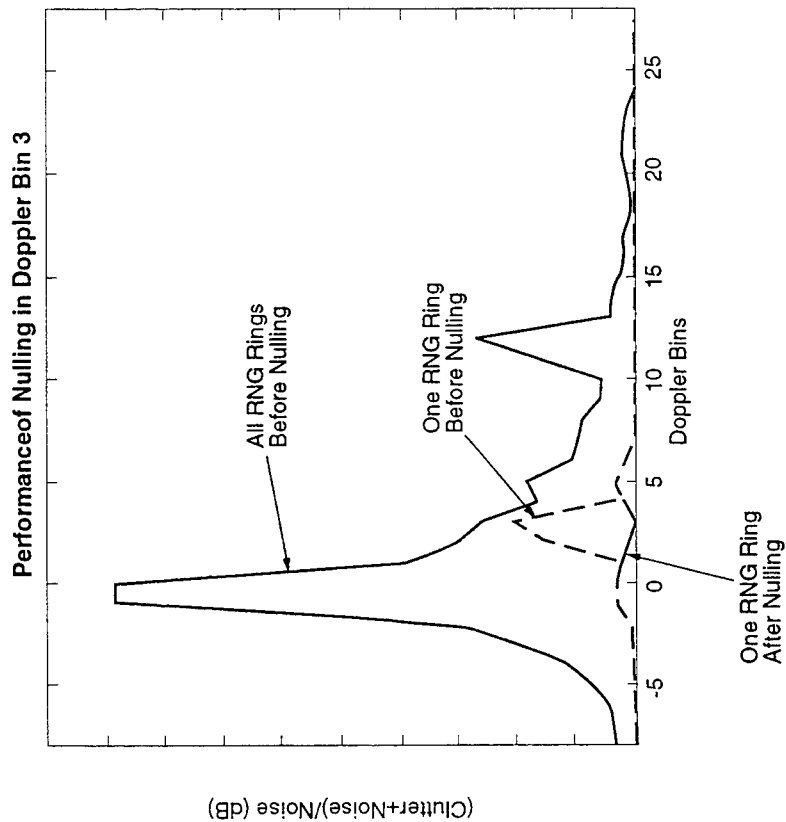
Performance Without Rotation: Nulling in Doppler Bin 12



12 Adaptive Phases
Constant Amplitude Clutter Model

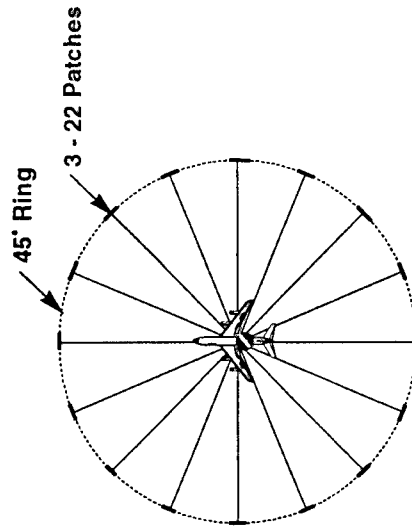
MITRE

Clutter Plus Noise-to-Noise Ratio in Doppler Bins Before and After Nulling



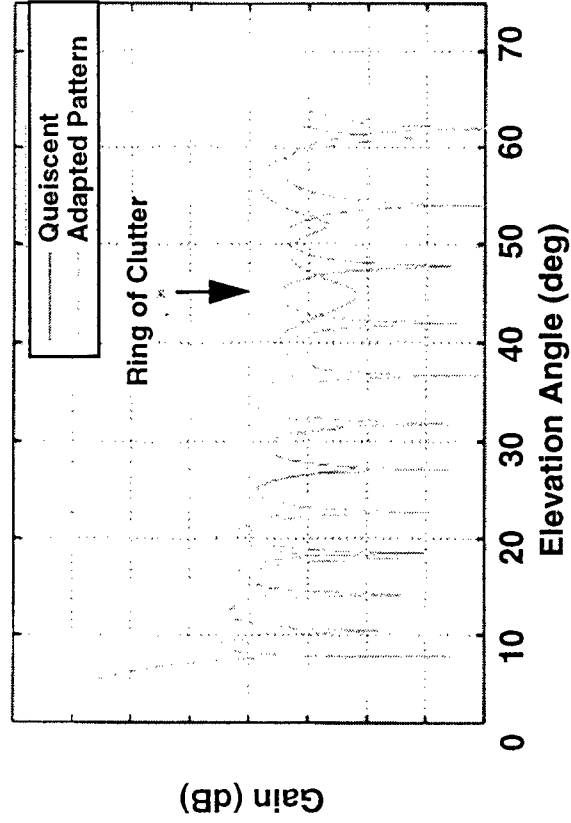
MITRE

Phase Perturbation Algorithm Performance on Rotating Elliptical Planar Array; Constant Amplitude, Random Phase RCS Model

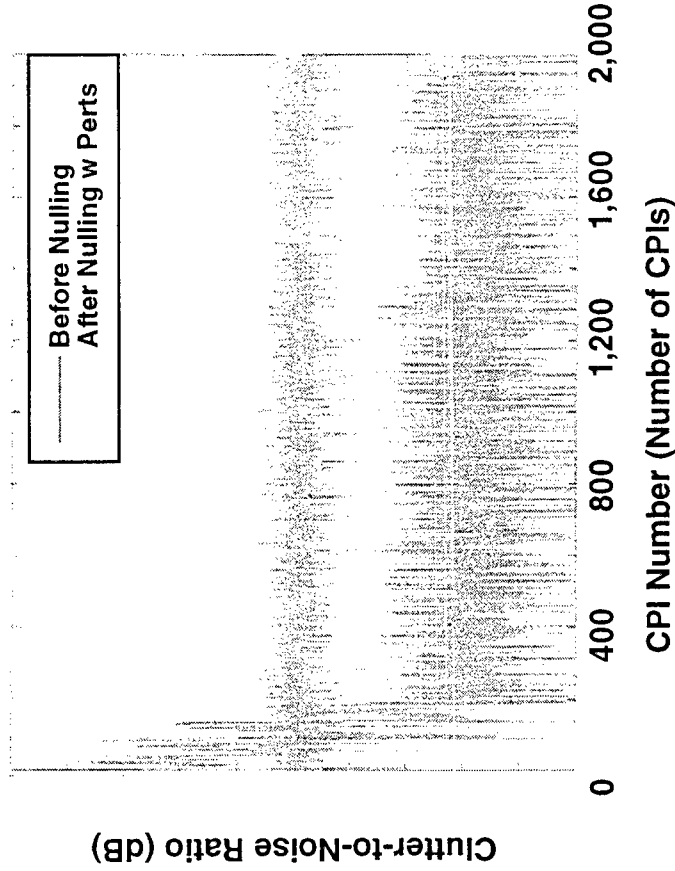


16 Look Directions

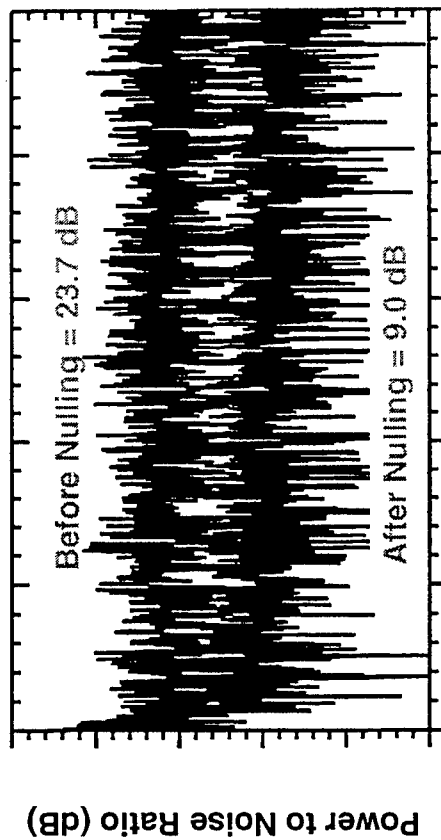
One Way Antenna Patterns



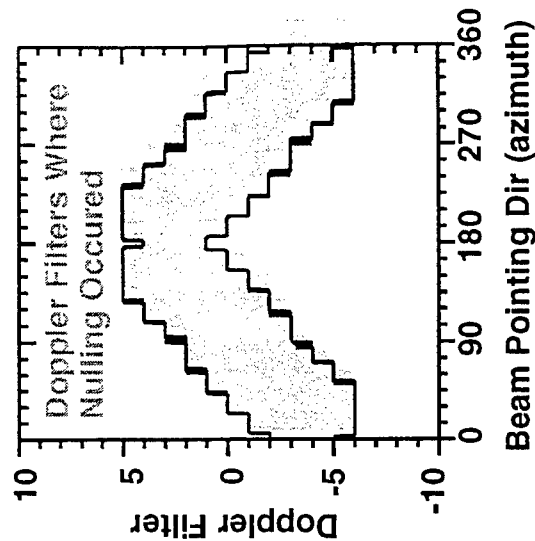
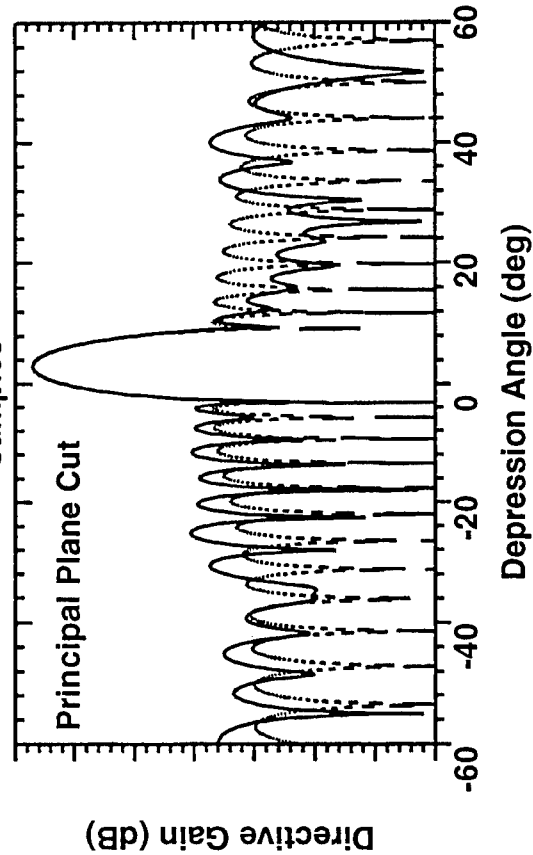
Performance With Rotation



Phase Perturbation Algorithm Performance on Rotating Rectangular Planar Array; Random Amplitude, Random Phase RCS Model



0 2,000 4,000 6,000 8,000 10,000



28X160 ELEM 2-DIM ARRAY
14 ADAPTIVE PHASES
ROTATION RATE = 0.36 DEG/SAMPLE
WT STEP SIZE = 0.15/GMAX
INITIAL PERT AMPLITUDE = 0.4
720 EQUAL SPACED PATCHES/RING
NUMBER OF RINGS = 5
EL SPREAD OF RINGS = 15-30 DEG
AZ WINDOW LIMITED TO 10 DEG
SURROUNDING MAINLOBE
NULLING OCCURS IN 5-7 DOPPLER
FILTERS AS ANTENNA ROTATES

Issues

- Algorithm stability in real world nonstationary environment (rotating/translating antenna)
- Amplitude statistics of clutter RCS
- Degrees of freedom only available in elevation plane, yet significant clutter can appear over 1-2 sidelobes in azimuth
- Finite number of available degrees-of-freedom
 - Two phase weights needed to make one complex weight
 - Multiple complex weights needed to null one sidelobe
 - Implementing fully adaptive array requires use of constraint in beam pointing direction. Constraint analysis for phase-only perturbation algorithm, to our knowledge, does not exist
- Tracking particular sidelobes through Doppler filters as antenna rotates and direction of zero Doppler changes

Summary

- Presented a low-cost phase-only perturbation canceller (without modifying antenna) to minimize clutter and improve low velocity target detection
- Computer simulations of stationary elliptical planar array and rotating rectangular planar arrays
 - Predicts that phase perturbation algorithm can be used to null sidelobe clutter, in particular Doppler cells in a stationary environment, and lower principal plane elevation sidelobes
 - Requires only measurements of the power in the Doppler filters
- Results suggest adaptive (spatial-only) nulling using phase perturbation or other adaptive techniques (e.g., genetic or simulated annealing) may be able to lower principal plane sidelobes and improve low velocity target detection in airborne radars

References

- Phase-Only Perturbation Algorithms
 - Davis, R. M., “Least Mean Square Phase-Only Adaptive Algorithms,” IEEE Antennas and Propagation Society International Symposium 1996, Volume 2
 - Davis, R. M., “Phase-Only LMS and Perturbation Adaptive Algorithms,” *IEEE Transactions AES*, to be published January 1998
- Complex Perturbation Algorithms
 - Cantoni, A., “Application of Orthogonal Perturbation Sequences to Adaptive Beamforming,” *IEEE Trans. on Antennas and Propagation*, AP-28, No. 2, March 1980
 - Davis, R. M., D. C. Farden, and J. S. Sher, “A Coherent Perturbation Algorithm,” *IEEE Trans. on Antennas and Propagation*, p. 45, No. 3, March 1986
 - Ivandich, S., and A. Cantoni, “Performance Analysis of Narrowband Adaptive Arrays Using Projected Perturbation Sequences, *IEEE Trans. on Antennas and Propagation*, Vol. 41, No. 5, May 1993

An Efficient Implicit Interference Subspace Removal Technique for STAP

S.U. Pillai, Y.L. Kim, and J.R. Guerci

Dept. of Electrical Engineering
Polytechnic University
Six Metrotech Center
Brooklyn, New York 11201
tel: (718) 260-3732
fax: (718) 260-3906
email: pillai@arma.poly.edu

Abstract A new technique for removing dominant interference eigenvectors is presented which does not require that an eigendecomposition be performed—as is the case with the eigencanceler method. Similar to eigen-based cancellation techniques, the resulting space-time pattern is formed by subtracting from the quiescent steering vector, a weighted sum of interference eigenvectors. However, the subtraction is accomplished implicitly, without having to directly estimate the interference eigenvectors. Instead, a subspace projection is formed in the data domain which typically has a dimension an order of magnitude smaller than the total available number of degrees-of-freedom for the space-time array. This new method is ideally suited for nonstationary clutter environments, where only a small sample support is available for the adaptive training set, and where a premium is placed on computational overhead. A detailed analytical comparison between the proposed technique and existing eigen and non-eigen based constrained interference removal techniques is presented. Also, experimental results are presented based on both synthetic and recorded data sets originating from the Mountaintop radar.

An Efficient Implicit Interference Subspace Removal Technique for STAP[†]

S. U. Pillai, Y. L. Kim and J. R. Guerci

Polytechnic University
Dept. of Electrical Engineering
Six Metrotech Center
Brooklyn, New York 11201
jguerci@radar.poly.edu

[†]Supported, in part, by a grant from the Office of Naval Research (ONR)

Outline

- Background and motivation
- Derivation of Implicit Subspace Removal (ISR) technique
- Analytical properties of ISR
- Eigen-based interpretation of ISR
- Application to both synthetic and measured data sets
- Summary and discussion

Motivation and Background

- Highly nonstationary (heterogeneous) AND “strong” clutter interference
- Very insufficient sample support for full DOF processing (typically $MN/10$)
- Desire less complex implementation than eigen-based techniques
 - Yet retain excellent “robustness” properties of eigen-based techniques
 - Achieve order of magnitude or better reduction in computational load

Derivation of Implicit Subspace Removal (ISR) Technique

- Sample snapshot covariance matrix with limited sample support

$$\hat{R}_k = \frac{1}{k} \sum_{i=1}^k \mathbf{x}_i \mathbf{x}_i^* = \frac{1}{k} Y_k Y_k^*$$

where Y_k is of size $NM \times k$, and is defined by

$$Y_k = [\mathbf{x}_1, \mathbf{x}_2, \dots, \mathbf{x}_k]$$

- We assume that (out of neccesity) $k < NM$ (usually $k \ll NM$) \rightarrow Thus \hat{R}_k is singular.
- Consider the nonsingular diagonally loaded auxillary $NM \times NM$ matrix \hat{R}_ϵ :

$$\begin{aligned} \hat{R}_\epsilon &= \hat{R}_k + \epsilon I_{MN} \\ &= \frac{1}{k} Y_k Y_k^* + \epsilon I_{MN}. \end{aligned}$$

Derivation of ISR Technique (Cont.)

- To obtain an expression for \hat{R}_ϵ^{-1} recall the matrix identity:

$$[P^{-1} + MQ^{-1}M^*]^{-1} = P - PM[M^*PM + Q]^{-1}M^*P$$

letting $P \triangleq \frac{1}{\epsilon}I_{MN}$, $Q \triangleq kI_k$, and $M \triangleq Y_k$ we obtain

$$\boxed{\hat{R}_\epsilon^{-1} = \frac{1}{\epsilon}[I_{MN} - Y_k(Y_k^*Y_k + \epsilon kI_k)^{-1}Y_k^*]} \quad (1)$$

- Recall that SML space-time weights are obtained from $\hat{\mathbf{w}}_k \propto \hat{R}_k^{-1}\mathbf{a}_t$, thus $\frac{1}{\epsilon}$ factor in (1) is superfluous
- **Theorem 1:** Assuming that the $k \times k$ matrix $(Y_k^*Y_k)^{-1}$ exists, then $\lim_{\epsilon \rightarrow 0} \epsilon \hat{R}_\epsilon^{-1} < \infty$ and is given by

$$\boxed{\lim_{\epsilon \rightarrow 0} \epsilon \hat{R}_\epsilon^{-1} = [I_{MN} - Y_k(Y_k^*Y_k)^{-1}Y_k^*] \triangleq \Phi_k} \quad (2)$$

$$\boxed{\hat{\mathbf{w}}_k = \Phi_k \mathbf{a}_t = \mathbf{a}_t - Y_k(Y_k^*Y_k)^{-1}Y_k^*\mathbf{a}_t} \quad (3)$$

Properties of ISR Technique

Properties of Φ_k :

- Only a $k \times k$ matrix inversion required to form Φ_k (plus two $(MN \times k)$ by $(k \times k)$ matrix multiplies)
 - No SVD required
 - Diagonal loading requires $MN \times MN$ matrix inversion
- Φ_k is a projection matrix, i.e., $\Phi_k^2 = \Phi_k$
- Φ_k is NOT a Moore-Penrose or generalized inverse
- $\hat{\mathbf{w}}_k = \Phi_k \mathbf{a}_t$ is not a minimum norm eigencanceler
- $\Phi_k(Y_k Y_k^*) = \emptyset$
 - Thus, Φ_k projects \mathbf{a}_t into the orthogonal complement of the space spanned by $Y_k Y_k^*$
 - Therefore, the choice of k and training support is crucial
 - Choose training samples with “strong” interference (interference dominated subspace)

Eigen-Based Interpretation of ISR Technique

- For comparison purposes, assume that the full DOF exact covariance R_c is available. The optimum set of weights is given by $\mathbf{w}_o = R_c^{-1} \mathbf{a}_t$, or

$$\mathbf{w}_o = \mathbf{a}_t - \sum_{i=1}^{MN-1} \left(1 - \frac{\mu_{\min}}{\mu_i} \right) (\mathbf{u}_i^* \mathbf{a}_t) \mathbf{u}_i$$

$$R_c = \sum_{i=1}^{MN} \mu_i \mathbf{u}_i \mathbf{u}_i^*$$

- Assume that R_c has only k dominant vectors such that

$$\mu_{k+1} = \mu_{k+2} = \dots = \mu_{\min} = \sigma^2$$

$$R_c = U \begin{bmatrix} \tilde{\mu}_1 & & \\ & \tilde{\mu}_2 & \\ & & \dots \\ & & & \tilde{\mu}_k \end{bmatrix} U + \sigma^2 I$$

where $\tilde{\mu}_i \triangleq \mu_i - \sigma^2$, $i = 1 \rightarrow k$ and $U \triangleq [\mathbf{u}_1, \mathbf{u}_2, \dots, \mathbf{u}_k]$.

Eigen-Based Interpretation of ISR Technique (Cont.)

- Therefore

$$\mathbf{w}_o = \mathbf{a}_t - \sum_{i=1}^k \left(1 - \frac{\mu_{\min}}{\mu_i}\right) (\mathbf{u}_i^* \mathbf{a}_t) \mathbf{u}_i = \mathbf{a}_t - \sum_{i=1}^k p_i \mathbf{u}_i$$

$$p_i = \left(1 - \frac{\mu_{\min}}{\mu_i}\right) (\mathbf{u}_i^* \mathbf{a}_t) = \frac{\tilde{\mu}_i}{\tilde{\mu}_i + \sigma^2} (\mathbf{u}_i^* \mathbf{a}_t)$$

which, in general, is NOT strictly a subspace removal (projection)

- By comparison, it can be shown that if k in Y_k matches above k then

$$\hat{\mathbf{w}}_k = \Phi_k \mathbf{a}_t = \mathbf{a}_t - \sum_{i=1}^k c_i \mathbf{u}_i$$

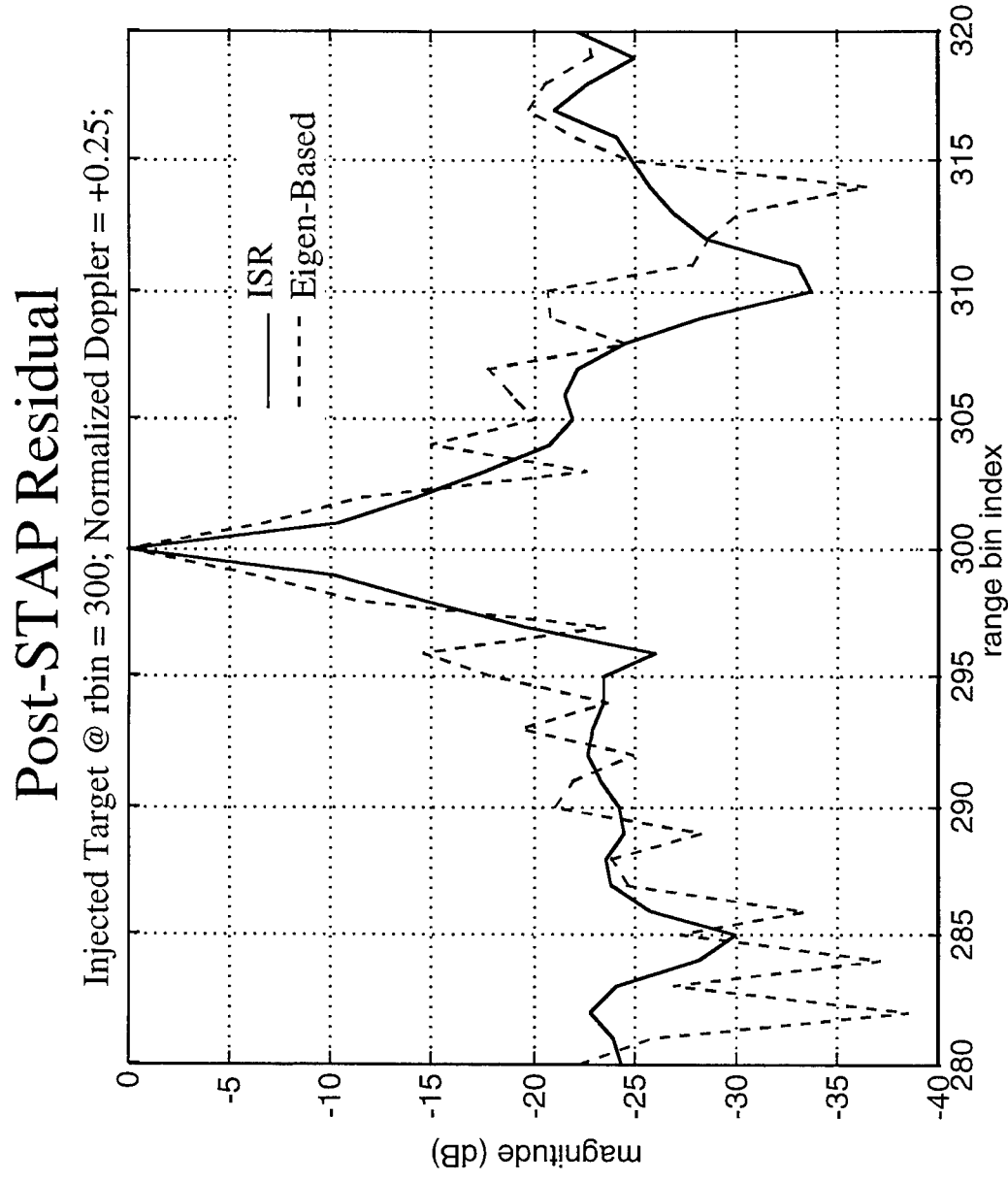
$$c_i = \sum_{j=1}^k \frac{\rho_j d_j}{\rho_j + \sigma^2} s_{i,j}$$

where the $\{c_i\}$ must satisfy: $\Phi_k^2 = \Phi_k$ and $\Phi_k(Y_k Y_k^*) = \emptyset$.

- Thus, in the above case, the ISR technique is “structurally” equivalent to the optimum beamformer.

Application to Mountain Top Data Set

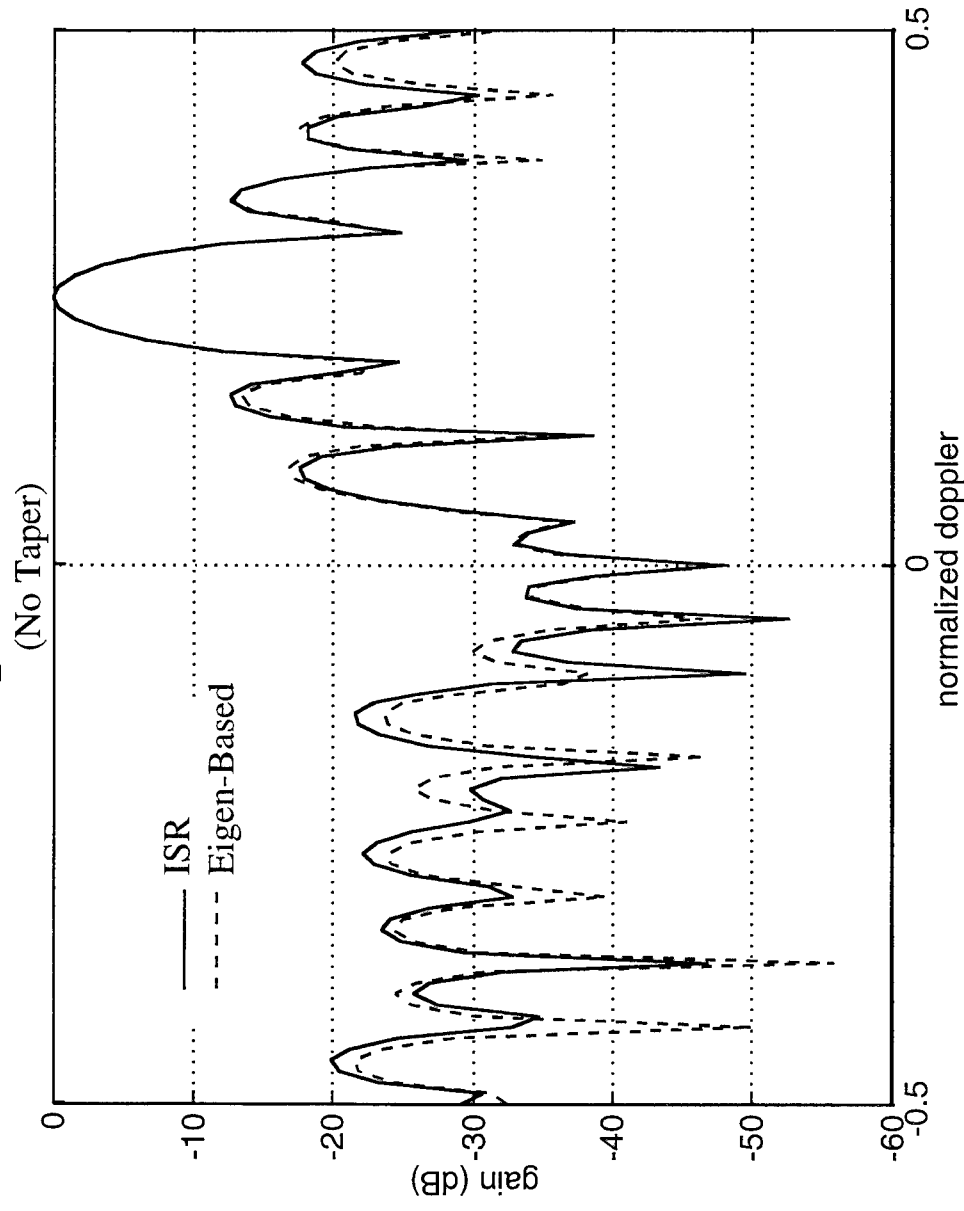
- IDPCA65v1 data set (40 range bin symmetric support; 30 principal eigenvectors)



Application to Mountain Top Data Set

- IDPCA65v1 data set (40 range bin symmetric support; 30 principal eigenvectors)

Adapted Patterns

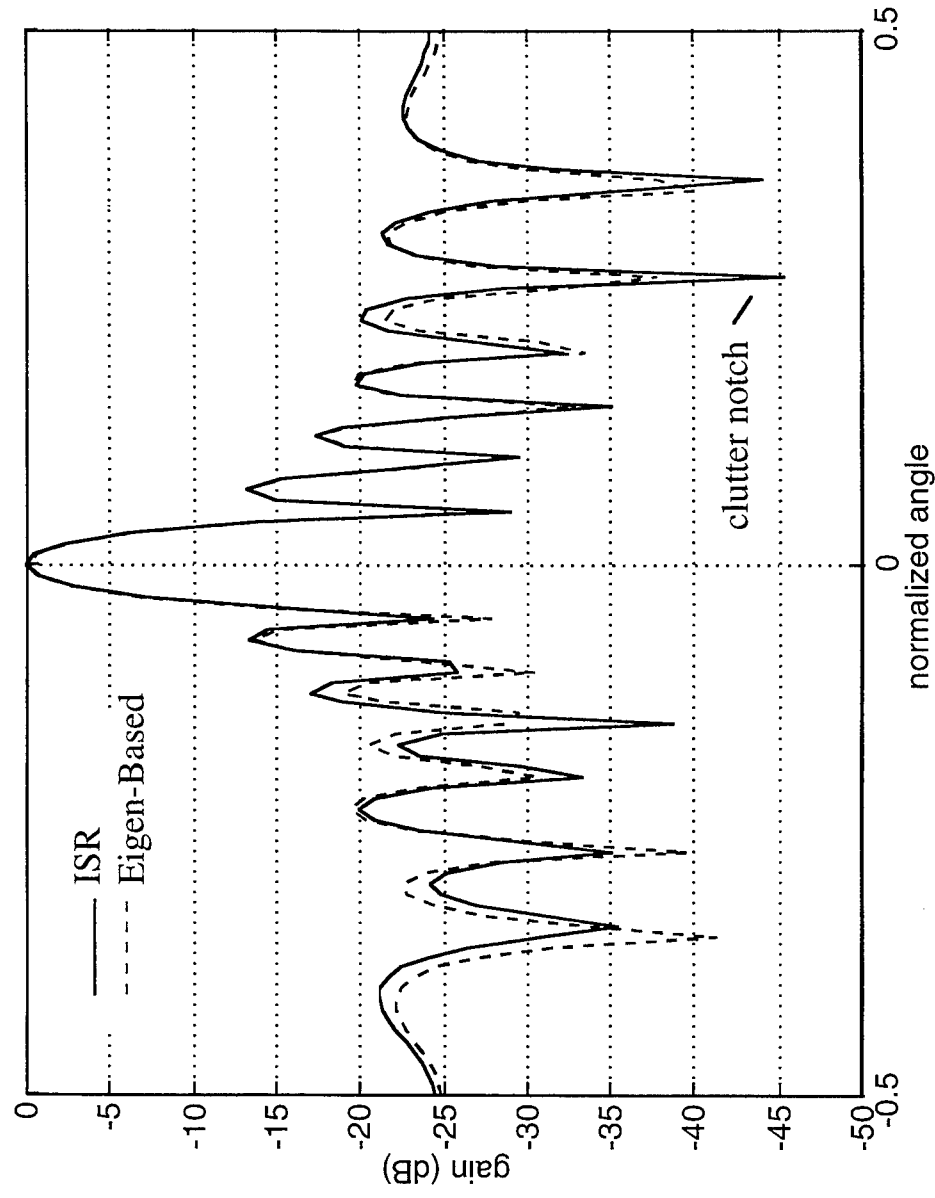


Application to Mountain Top Data Set

- IDPCA65v1 data set (40 range bin symmetric support; 30 principal eigenvectors)

Adapted Patterns

(No Taper)



Summary and Conclusions

- Introduced an implicit subspace removal (ISR) technique applicable to strong and highly nonstationary (heterogeneous) interference environments
- Substantially less complex than eigen-based techniques (or diagonal loading) for most implementations
 - Yet shares a “structural” similarity to eigen-based methods
- Application to both synthetic and measured data sets shows performance is essentially equivalent to eigen-based techniques
- More definitive testing required to delineate regions favorable to an ISR implementation
- Requires the development of an integrated CACFAR back-end (Post-ISR-STAP detection)

Session IV

Terrain Scattered Interference

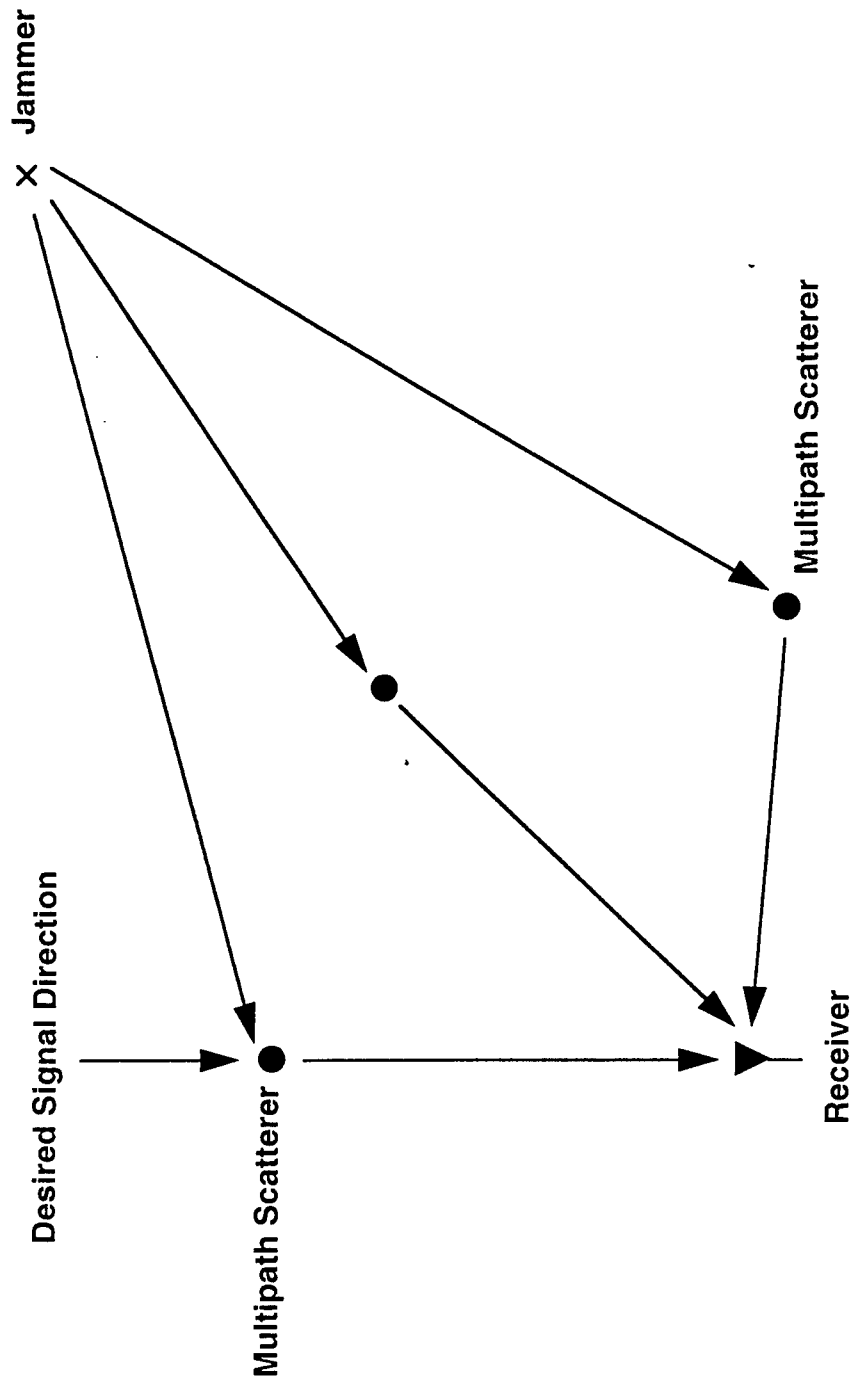
R. L. Fante

MITRE Corporation
Bedford, MA 01730

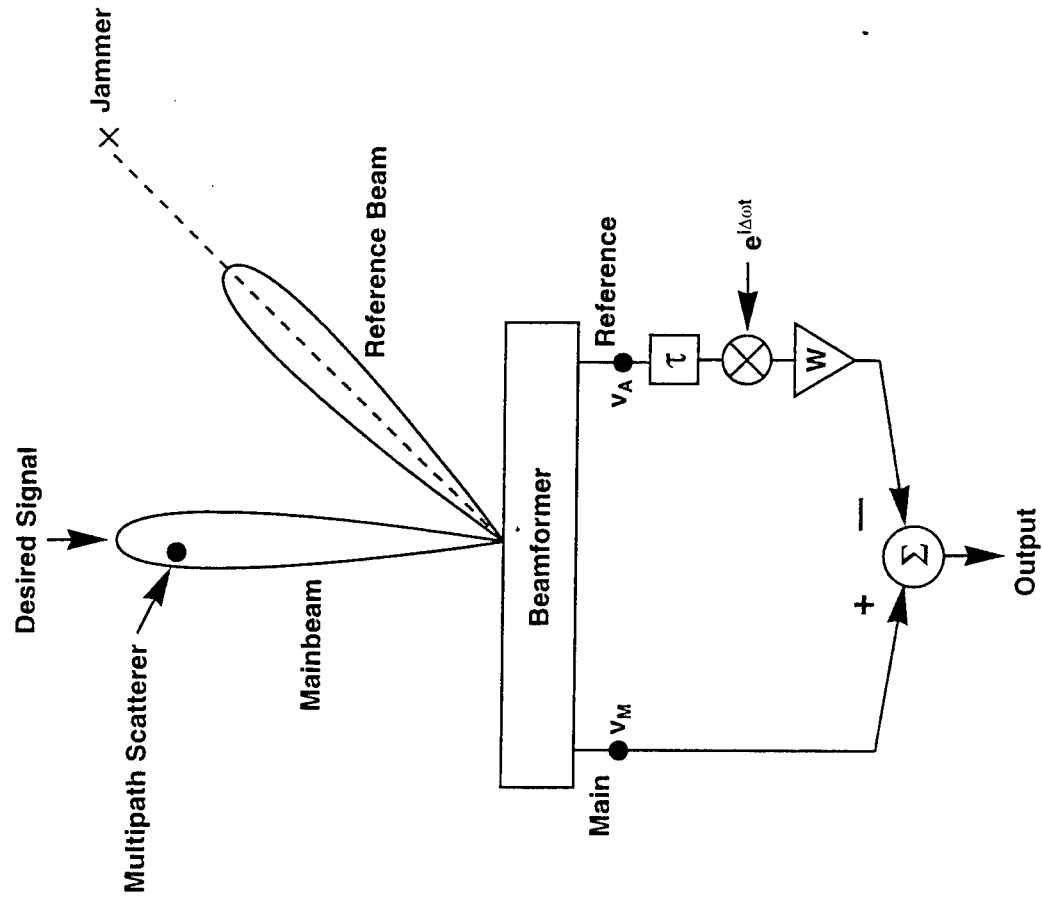
Terrain Scattered Interference

Jammer multipath influences performance of radar, navigation (GPS) and communications systems. Therefore, ideas presented on TSI have broad application.

Spatial Nulls Alone are Insufficient for Jammer Multipath

**MITRE**

Reference Beam is One Cancellation Approach



Need Both Delay and Doppler Correction

$$v_M(t) = s(t) + A J(t - \tau_1) e^{j\omega_1 t} + n_1(t)$$

$$v_A(t) = J(t - \tau_2) e^{j\omega_2 t} + n_2(t)$$

$$\text{Output} = v_M(t) - W v_A(t - \tau) e^{j\Delta\omega t}$$

Jammer cancellation if

$$W = A, \tau = \tau_1 - \tau_2$$

$$\Delta\omega = \omega_1 - \omega_2$$

$$\text{Output power after cancellation} = |s|^2 + \sigma^2(1 + |W|^2)$$

Without Doppler Correction Weight Must be Continually Updated

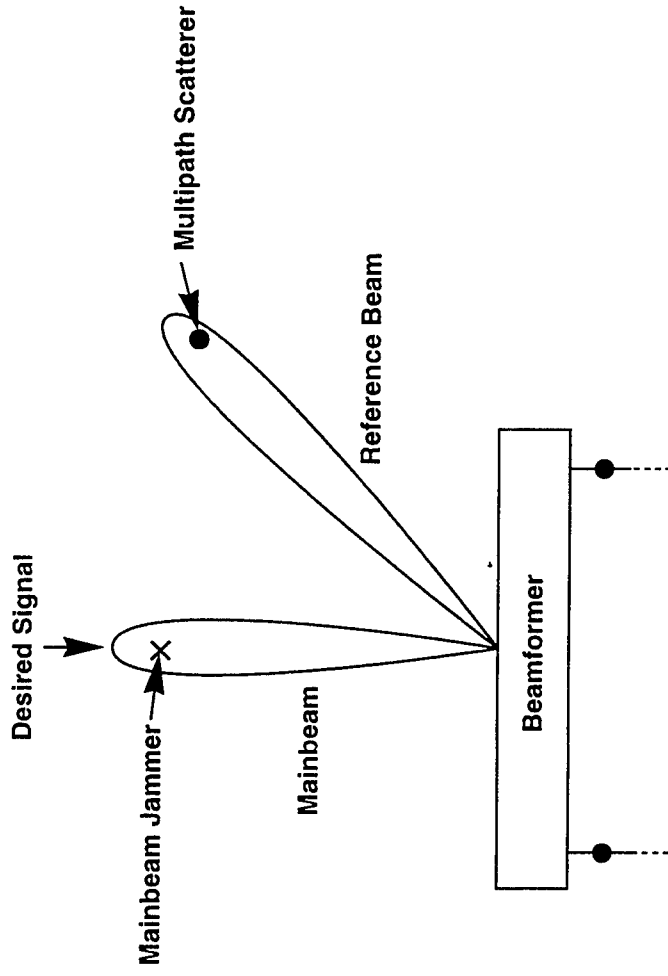
$$\text{Output Jammer Voltage} = 2A J(t - \tau_1) e^{i(\frac{\omega_1 + \omega_2}{2})t} \sin\left(\frac{\omega_1 - \omega_2}{2}\right)t$$

Jammer multipath cancelled at $t = 0$, but degrades thereafter.
Therefore, must update every Δt seconds

$$\Delta t \ll \frac{2}{|\omega_1 - \omega_2|}$$

However, what is effect of time-varying weight on Doppler processing?

Reference Beam Also Appropriate if Jammer/ Multipath Interchanged



Paper #4 (Kogan) addresses case when multipath scatterer is the ground

Paper #5 (Coutts) shows how multipath can be used to determine jammer location

Session IV:

TERRAIN SCATTERED INTERFERENCE

R. Fante, Chair

- **Multi-Channel Airborne Bistatic Radar Data Collection and Analysis J. Arnts**
- **Signal Modulation in Pulse-By-Pulse Adaptive Nulling Systems D. Rabideau**
- **On the Use of Terrain Scattered Interference for Mainbeam Jammer Suppression S. Kogon**
- **3-D Emitter Localization Using Out-of-Plane Multipath .. S. Coutts**

Multi-Channel Airborne Bistatic Radar Data Collection

James Arnts and David Fenner

Northrop Grumman Corporation
Baltimore, MD 21230

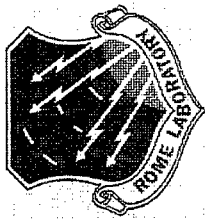
Lee Moyer and Douglas Page

Technology Service Corporation
Trumbull, CT 06611

Ralph Kohler, David Mokry and Mike Little

Rome Laboratory
Rome, NY 13441-4514

Abstract A bistatic radar concept has been postulated as an approach for extending the surveillance range against low observable targets. This advanced surveillance concept would employ a receive-only radar on a UAV operating with existing radar systems such as the E-3 AWACS. The receive-only system would fly closer to the FEBA and therefore have a signal-to-noise advantage over the long standoff range monostatic system. This advantage, however, comes with a penalty in that it must operate in a significantly more complex clutter environment. Bistatic radar data was acquired for Rome Laboratory using the multi-channel LBand MCARM system as the receiver and the Tethered Aerostat Radar System (TARS) at Horse shoe Beach, FL as the transmitter. The primary goal of the test was to emulate the advanced bistatic surveillance concept operating with either a high PRF or low PRF waveform in test geometries which produced both pseudo monostatic, as well as wide bistatic angle geometries. A Moving-Target Simulator (MTS) was located in the test scene. The MTS emulated targets having various Doppler frequencies and amplitudes and which fell within the ground clutter spectrum. The acquired bistatic MCARM data was processed by both conventional (i.e., MTI and Doppler filtering) and Space-Time Adaptive Processing (STAP) techniques. The STAP concepts included both pre-Doppler and postDoppler algorithms. A comparison was made to determine the optimal allocation of the available degrees-of-freedom in time, azimuth, and elevation for the STAP algorithms. The MTS provided calibrated Doppler tones from which a quantitative assessment of the algorithms' performance could be made. It was shown that a significant improvement in the signal-to-clutter ratio could be achieved under stressing clutter conditions. Multi-channel data which was taken in 1995 and which is available for developing STAP algorithms for advanced bistatic systems will be covered. Preliminary results obtained by applying several STAP algorithms will also be presented.



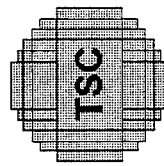
ASAP
'97

MULTI-CHANNEL AIRBORNE BISTATIC RADAR DATA COLLECTION

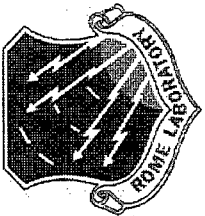
JAMES ARNTS AND DAVID FENNER
NORTHROP GRUMMAN CORPORATION

LEE MOYER AND DR. DOUGLAS PAGE
TECHNOLOGY SERVICE CORPORATION

RALPH KOHLER, DAVID MOKRY AND MICHAEL LITTLE
ROME LABORATORY



Technology Service
Corporation



ASAP
'97

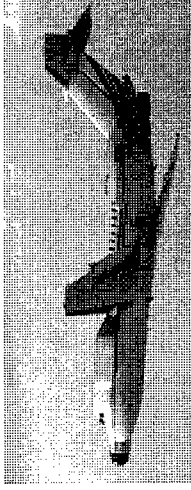
INTRODUCTION

Horseshoe Beach
TARS Aerostat



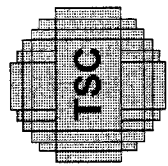
Bistatic Transmitter

RL/Northrop Grumman
BAC1-11 MCARM



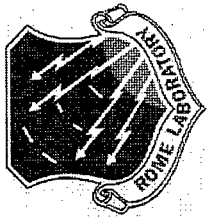
Bistatic Receiver

- MULTI-CHANNEL BISTATIC RADAR DATA HAS BEEN COLLECTED TO SUPPORT STAP ALGORITHM DEVELOPMENT
 - USAF TETHERED AEROSTAT RADAR SYSTEM (TARS) WAS TRANSMITTER
 - ROME LABORATORY/NORTHROP GRUMMAN MULTI-CHANNEL AIRBORNE RADAR MEASUREMENTS (MCARM) SYSTEM WAS RECEIVER
- BISTATIC COLLECTION EXPERIMENT USED:
 - HORSESHOE BEACH, FLORIDA AEROSTAT SITE
 - GAINESVILLE, FLORIDA BAC1-11 BASING AND FLIGHT ROUTES
- DATA COLLECTION PERFORMED FROM 13 MAY TO 21 MAY, 1995
- EFFORT PERFORMED UNDER AIR FORCE ROME LABORATORY CONTRACT NUMBER F30602-92-C-0161



Technology Service
Corporation

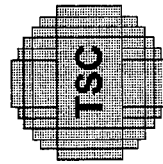
NORTHROP GRUMMAN



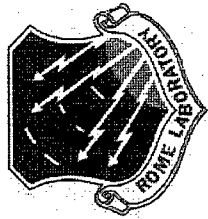
**ASAP
'97**

ROME LAB PROGRAM OBJECTIVES

- **CONDUCT A QUICK-REACTION EXPERIMENT TO SUPPORT KEY ROME LABORATORY PROGRAMS**
- **COLLECT BISTATIC CLUTTER DATA**
 - **SUPPORT DEVELOPMENT OF BISTATIC STAP ALGORITHMS**
 - **PROVIDE PSEUDO-MONOSTATIC TO WIDE BISTATIC ANGLE DATA**
 - **0 TO 150 DEGREES**
- **PROVIDE CALIBRATED TARGET-IN-CLUTTER DATA**
- **EVALUATE BISTATIC CLUTTER DATA**
 - **DEVELOP BISTATIC CLUTTER MODELS**
 - **ESTIMATE IMPACT OF HOT CLUTTER**



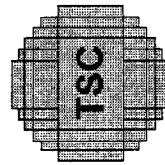
TSC
Technology Service
Corporation



ASAP
'97

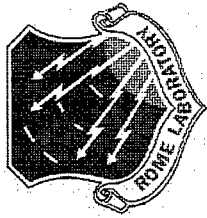
PRESENTATION OBJECTIVES

- DESCRIBE THE BISTATIC DATA COLLECTION EXPERIMENT
- DISCUSS A REPRESENTATIVE DATA SAMPLE
- PRESENT A LISTING OF THE DATA AVAILABLE IN THE ARCHIVES



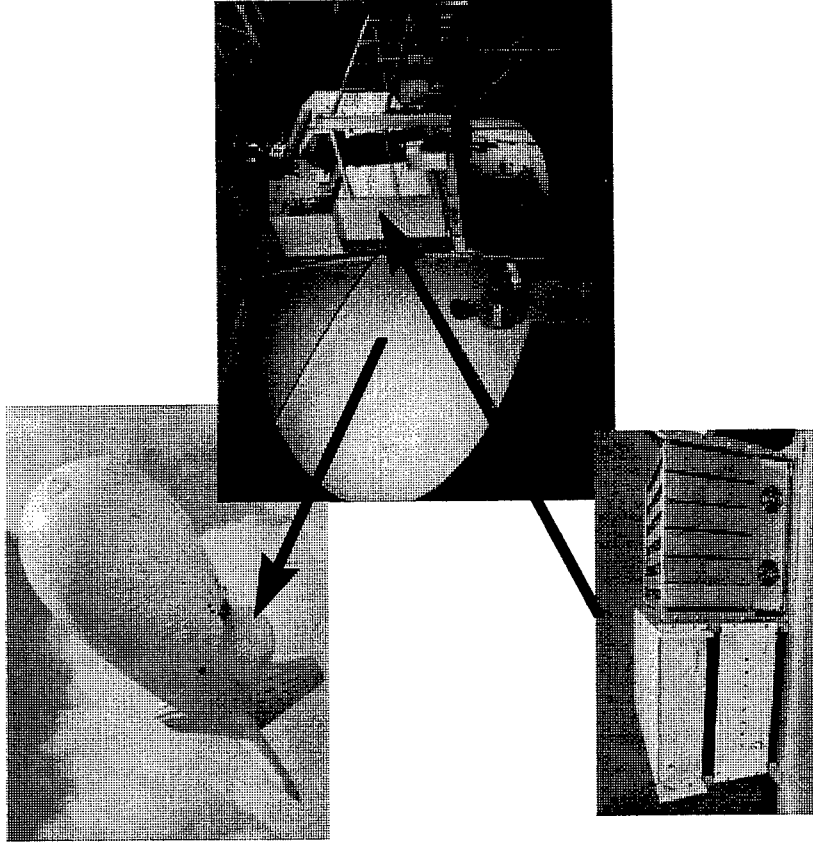
Technology Service
Corporation

ANTHONY GRUMMAN



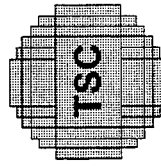
MODIFIED TARS RADAR PROVIDED IN-FLIGHT-PROGRAMMABLE LOW AND HIGH PRF WAVEFORMS

ASAP
'97



MCARM STALOWFG
integrated with TARS
for bistatic tests

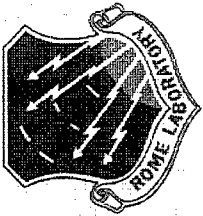
- **TARS TRANSMITTER**
 - L-BAND (1215-1350 MHz)
 - 30 kW PEAK POWER
 - 1.2 kW AVERAGE POWER
- **TARS ANTENNA**
 - 25 FEET BY 13 FEET
 - 35 dBi GAIN
 - 2.2° AZIMUTH BEAMWIDTH
 - SHAPED ELEVATION BEAM
 - 5 RPM ROTATION RATE
- **IN-FLIGHT PROGRAMMABLE WAVEFORMS**
 - FREQUENCIES: 1240/1250/1260/1270 MHz
 - PULSEWIDTHS: 0.8 TO 204.8 μ sec
 - INTER-PULSE PERIODS: 1.6 μ sec TO 52.4 msec
 - LINEAR FM AND UNMODULATED PULSES



Technology Service
Corporation

NOTE: DETAILED PARAMETERS ARE PROVIDED AT END OF PRESENTATION

ADDITIONAL CHANNELS

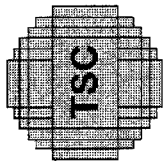


**ASAP
'97**

BISTATIC DATA WAS COLLECTED USING TWO DIFFERENT WAVEFORMS

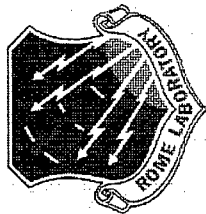
- **HIGH PRF WAVEFORM**
 - 1.6 μ sec PULSEWIDTH
 - 0.8 MHz BANDWIDTH
 - 23.1 kHz PRF
 - NO MODULATION ON PULSE
 - 27 RANGE GATES
 - 2048 PULSE RECORDS

- **LOW PRF WAVEFORM**
 - 14.4 μ sec PULSEWIDTH (UNCOMPRESSED)
 - 0.8 MHz BANDWIDTH
 - 312 Hz PRF
 - LFM MODULATION
 - 2000 RANGE GATES
 - 32 PULSE RECORDS



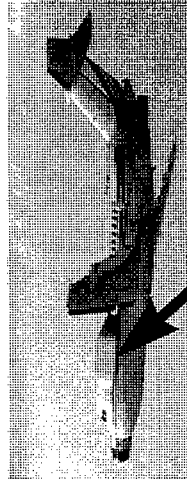
TSC
Technology Service
Corporation

NOTHING CHANGING

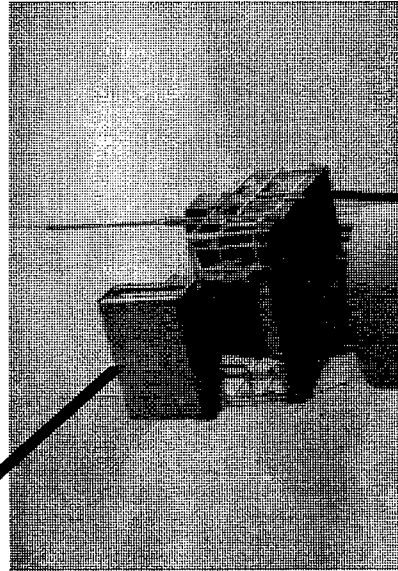


MCARM BISTATIC RECEIVER COLLECTED WIDEBAND DIGITAL DATA

ASAP
'97

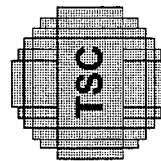


Northrop Grumman
Airborne Surveillance
Technology Testbed
(BAC1-11)



MCARM Array at
Antenna Test Range

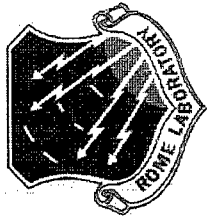
- ANTENNA
 - L-BAND PHASED ARRAY
 - 6 FEET X 4 FEET
 - 16 COLUMNS
 - 8 ROWS (4 UPPER + 4 LOWER)
 - 16 COLUMNS X 2 ELEVATION PORTS
- RECEIVER
 - 24 DIGITAL RECEIVERS
 - 11 COLUMNS BY 2 ROWS USED FOR BISTATIC DATA COLLECTION
 - RF Σ AND OMNI CHANNELS
 - OPERATED IN PASSIVE MODE
- DATA COLLECTION
 - DCRSi RECORDED
 - 24 CHANNELS
 - ~0.1 SEC OF DATA EVERY 12 SECONDS
 - CUED TO RECORD AS TARS BEAM PASSED OVER MULTI-TARGET SIMULATOR



Technology Service
Corporation

NOTE: DETAILED PARAMETERS ARE PROVIDED AT END OF PRESENTATION

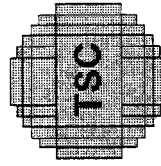
NOTATION: CHANGES



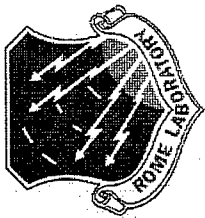
MULTI-TARGET SIMULATOR (MTS) PRODUCED TARGET-LIKE SIGNALS IN RADAR CLUTTER RETURN

**ASAP
'97**

- SUPPLIED AND OPERATED BY ROME LABORATORY
- PROVIDES FLEXIBLE, DIGITALLY SYNTHESIZED TONES
- ALLOWS TRIGGERED AND NON-TRIGGERED OPERATION
- GPS-SITED NEAR GAINESVILLE TO SUPPORT BISTATIC TESTS
- CALIBRATED SIGNAL AMPLITUDES
- TWO REFERENCE TONES
 - 0 Hz DOPPLER AT 0 dB
 - +462.9 Hz DOPPLER AT 0 dB
- FIVE PAIRS OF TONES POSITIONED SYMMETRICALLY ABOUT ZERO-DOPPLER FREQUENCY
 - 46.3 Hz SEPARATION
 - MONOTONICALLY DECREASING BY 6 dB PER TONE
 - LOWEST TONE -30 dB BELOW REFERENCE TONES
- MTS POWER: 23 dBm (maximum)
- MTS ANTENNA GAIN: 12 dB

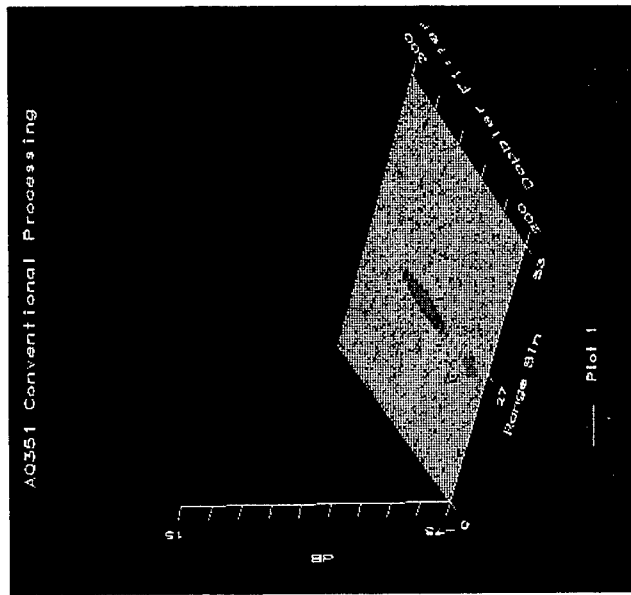


Technology Service
Corporation

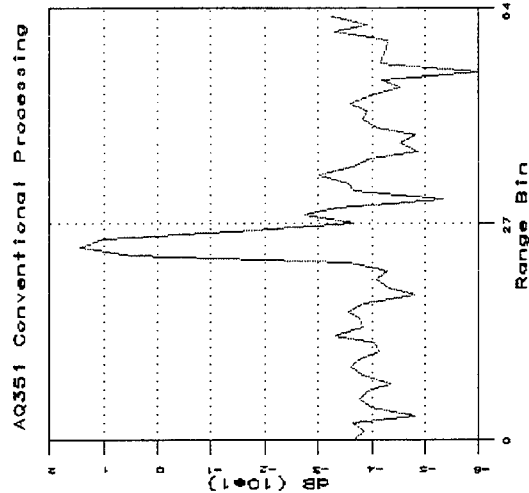


ASAP
'97

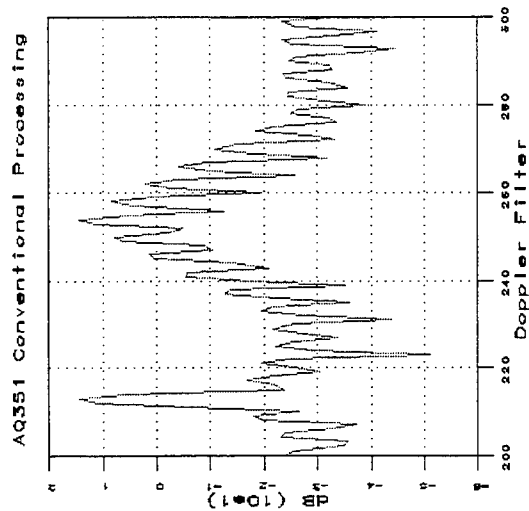
MTS SIGNAL CHARACTERISTICS



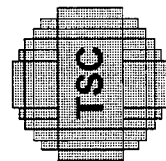
RANGE-DOPPLER PLOT



RANGE PROFILE
(CLEAR TONE)

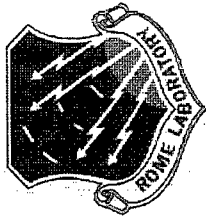


DOPPLER PROFILE



Technology Service
Corporation

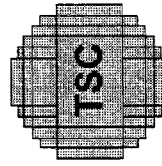
NORTHROP GRUMMAN



**ASAP
'97**

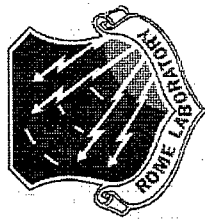
FIVE BISTATIC DATA ACQUISITIONS WERE PERFORMED

- **LOCAL BALTIMORE CHECKOUT FLIGHT: MAY 9, 1995**
- **FLY-BY ENROUTE TO GAINESVILLE: MAY 15, 1995**
- **FIRST OFFICIAL BISTATIC FLIGHT: MAY 16, 1995**
- **SECOND OFFICIAL BISTATIC FLIGHT: MAY 20, 1995**
- **THIRD OFFICIAL BISTATIC FLIGHT: MAY 21, 1995**



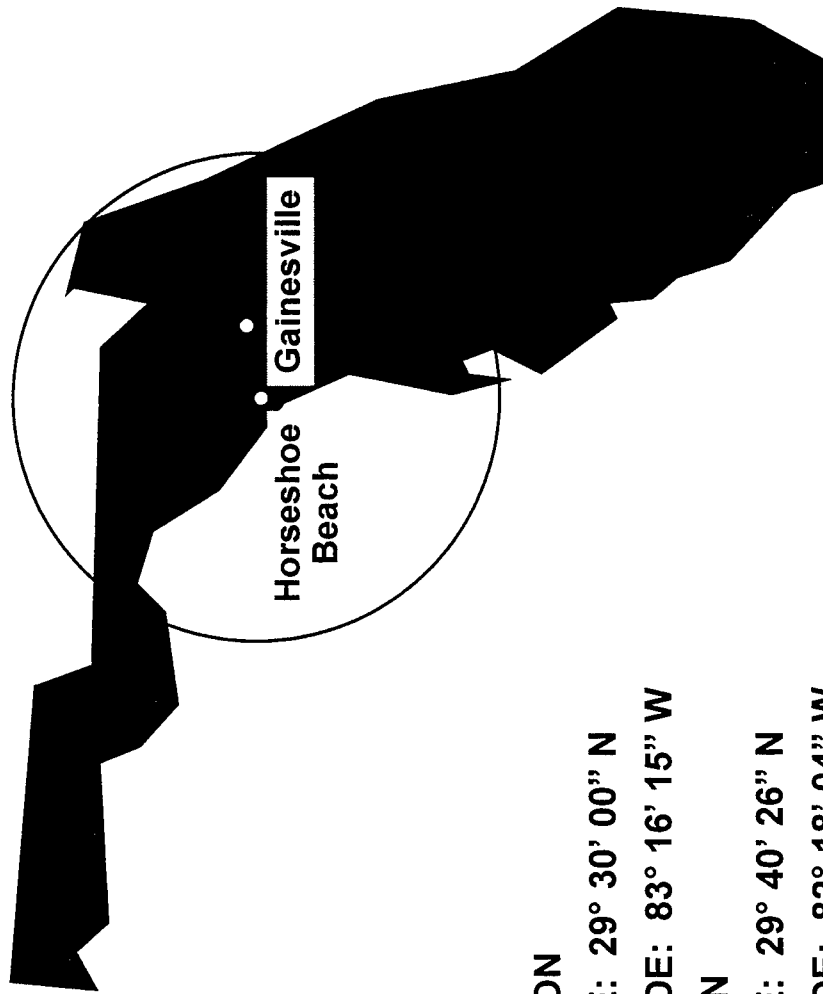
**Technology Service
Corporation**

NORTHROP GRUMMAN



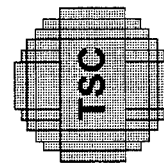
ASAP
'97

HORSESHOE BEACH, FLORIDA AEROSTAT SITE GAINESVILLE, FLORIDA MCARM BASING



- TARS LOCATION
 - LATITUDE: 29° 30' 00" N
 - LONGITUDE: 83° 16' 15" W
- MTS LOCATION
 - LATITUDE: 29° 40' 26" N
 - LONGITUDE: 82° 18' 04" W

- AEROSTAT AT NOMINALLY 10 KFT ALTITUDE FOR BISTATIC TESTS
- BAC1-11 FLEW AT 10 KFT ALTITUDE

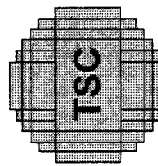


Technology Service
Corporation



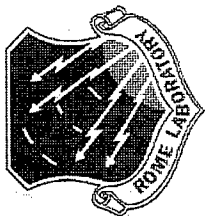
ASAP
'97

PROGRAM ROAD MAP



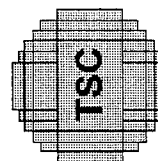
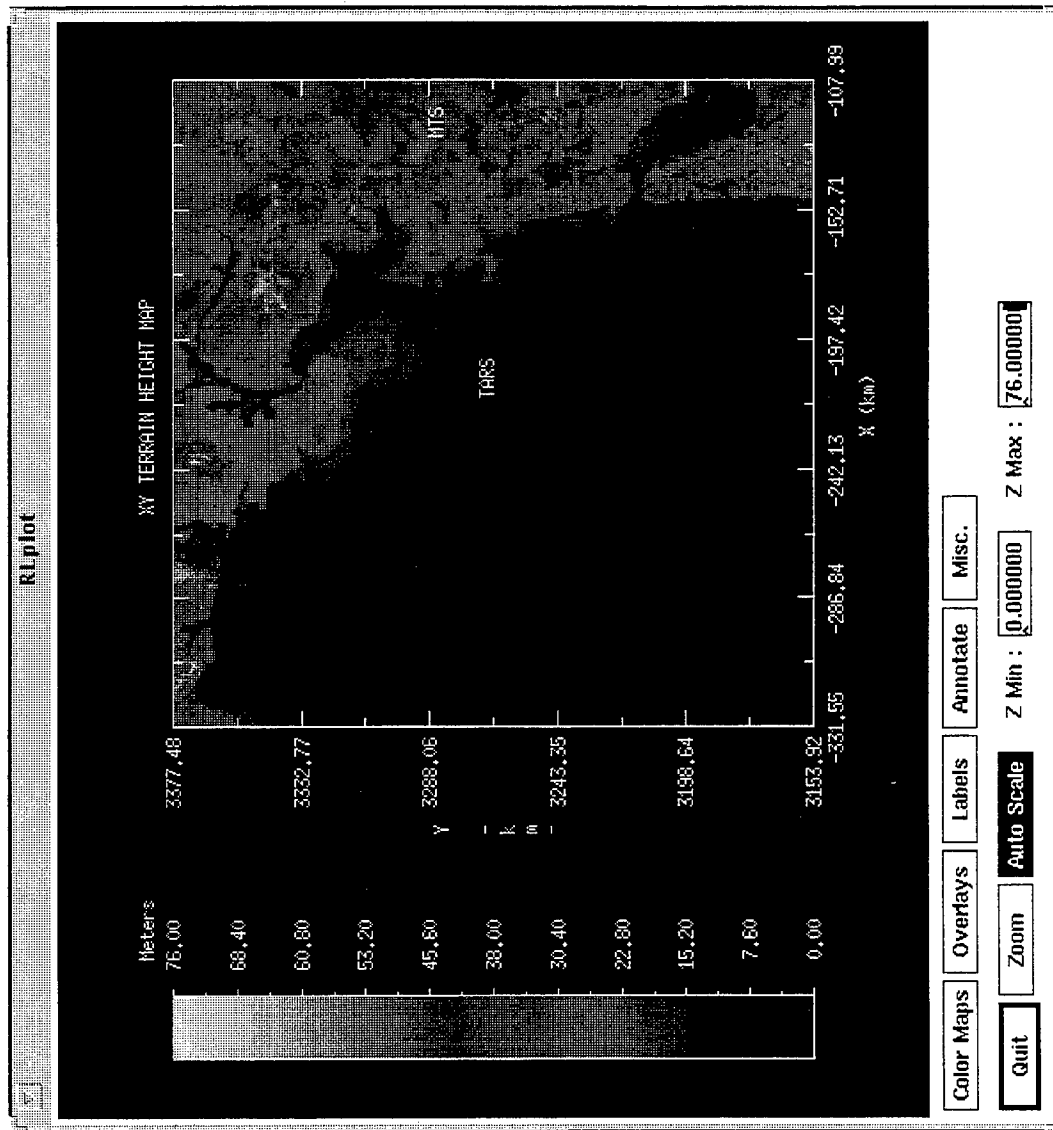
Technology Service
Corporation

NORTHROP GRUMMAN



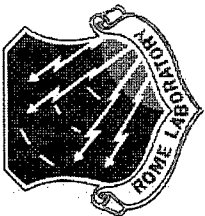
ASAP
'97

TOPOGRAPHIC MAP OF BISTATIC TEST AREA



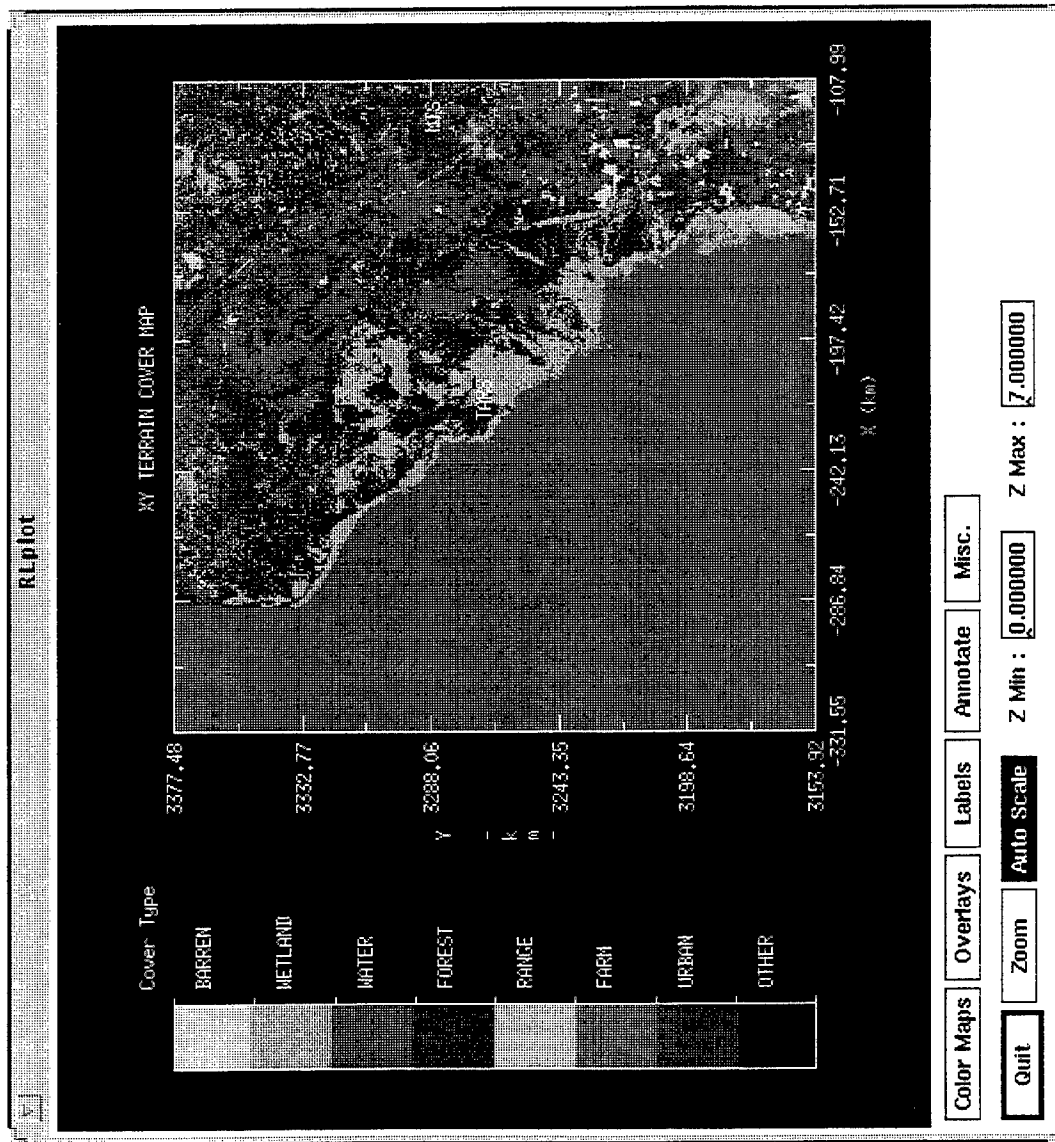
Technology Service
Corporation

ASAP '97



ASAP
'97

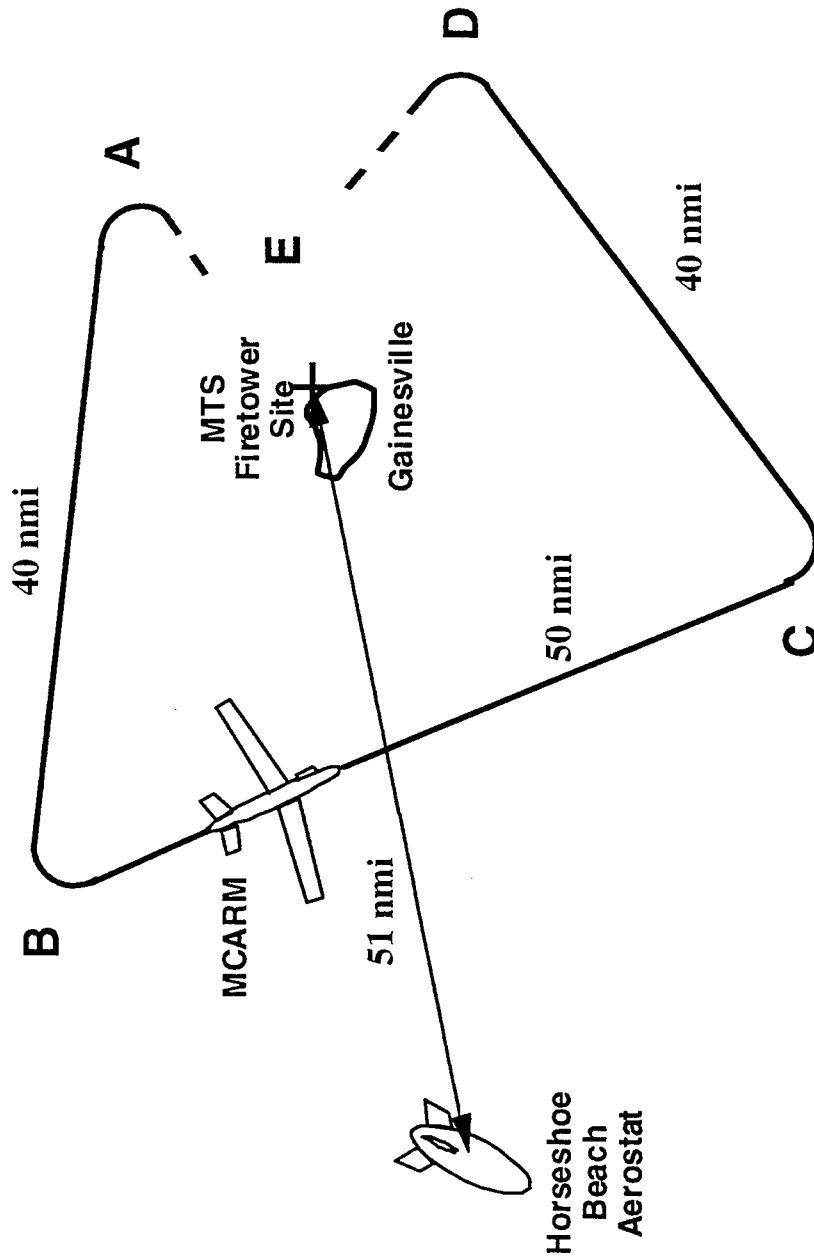
LAND COVER MAP OF BISTATIC TEST AREA





BISTATIC CLUTTER AND TARGET DATA COLLECTION SCENARIO (CONTAINS URBAN CLUTTER FROM GAINESVILLE)

ASAP
'97

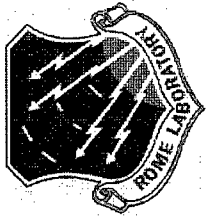


- MULTIPLE DATA COLLECTION PASSES MADE BETWEEN POINTS B AND C
- ONE B-TO-C PASS MADE NEARER GAINESVILLE



Technology Service
Corporation

NORTHROP GRUMMAN

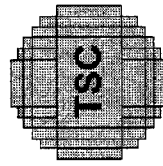


ASAP
'97

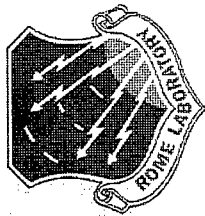
SAMPLE DATA PARAMETERS (MCARM FLIGHT 8, ACQUISITION 109)

RANGE FROM MTS TO TARS (km/nmi)	95/51
RANGE FROM MTS TO MCARM (km/nmi)	63/34
RANGE FROM TARS TO MCARM (km/nmi)	53/29
BISTATIC ANGLE AT MTS LOCATION (deg)	30
BEAM SQUINT ANGLE (deg)	39.8
AIRCRAFT CRAB ANGLE (deg)	1.5
AIRCRAFT VELOCITY (m/s / kts)	110/214
CLUTTER DOPPLER FREQUENCY AT MAINLOBE PEAK (Hz)	291

- NOMINAL ACQUISITION 109 GEOMETRY DEPICTED ON PREVIOUS CHART

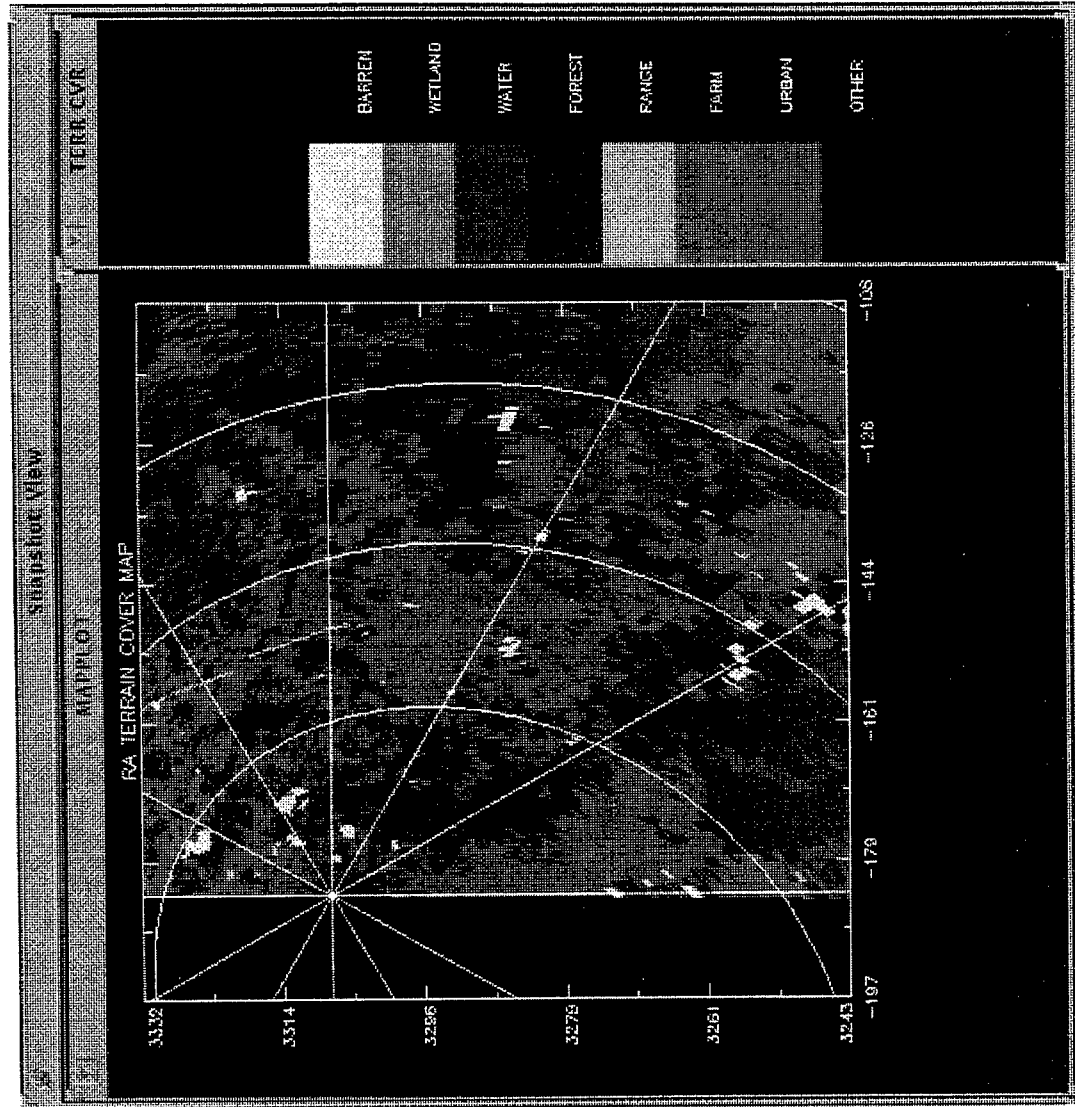


Technology Service
Corporation

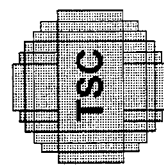


LAND COVER FOR ACQUISITION 109

ASAP
'97

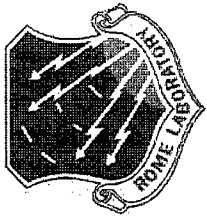


- DISTANCE IN KILOMETERS
- ELLIPSES SPACED BY THREE RANGE AMBIGUITIES



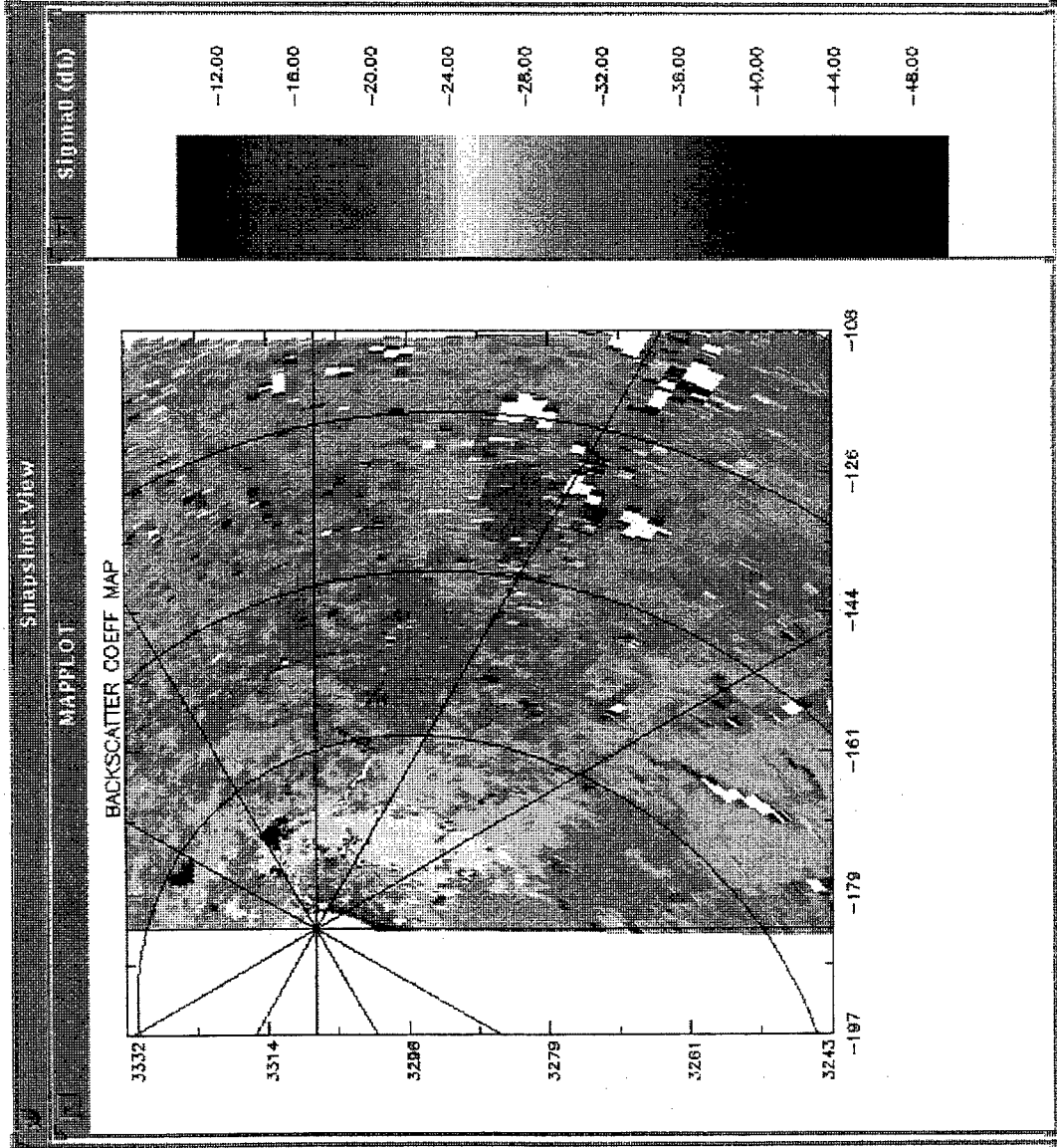
Technology Service
Corporation

ADDITIONAL CHANGES

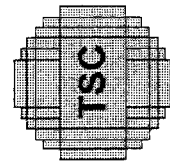


ESTIMATED σ^0 VALUES FOR ACQUISITION 109

ASAP
'97

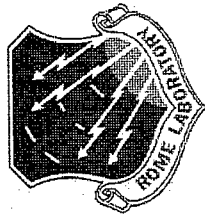


- DISTANCE IN KILOMETERS
- ELLIPSES SPACED BY THREE RANGE AMBIGUITIES



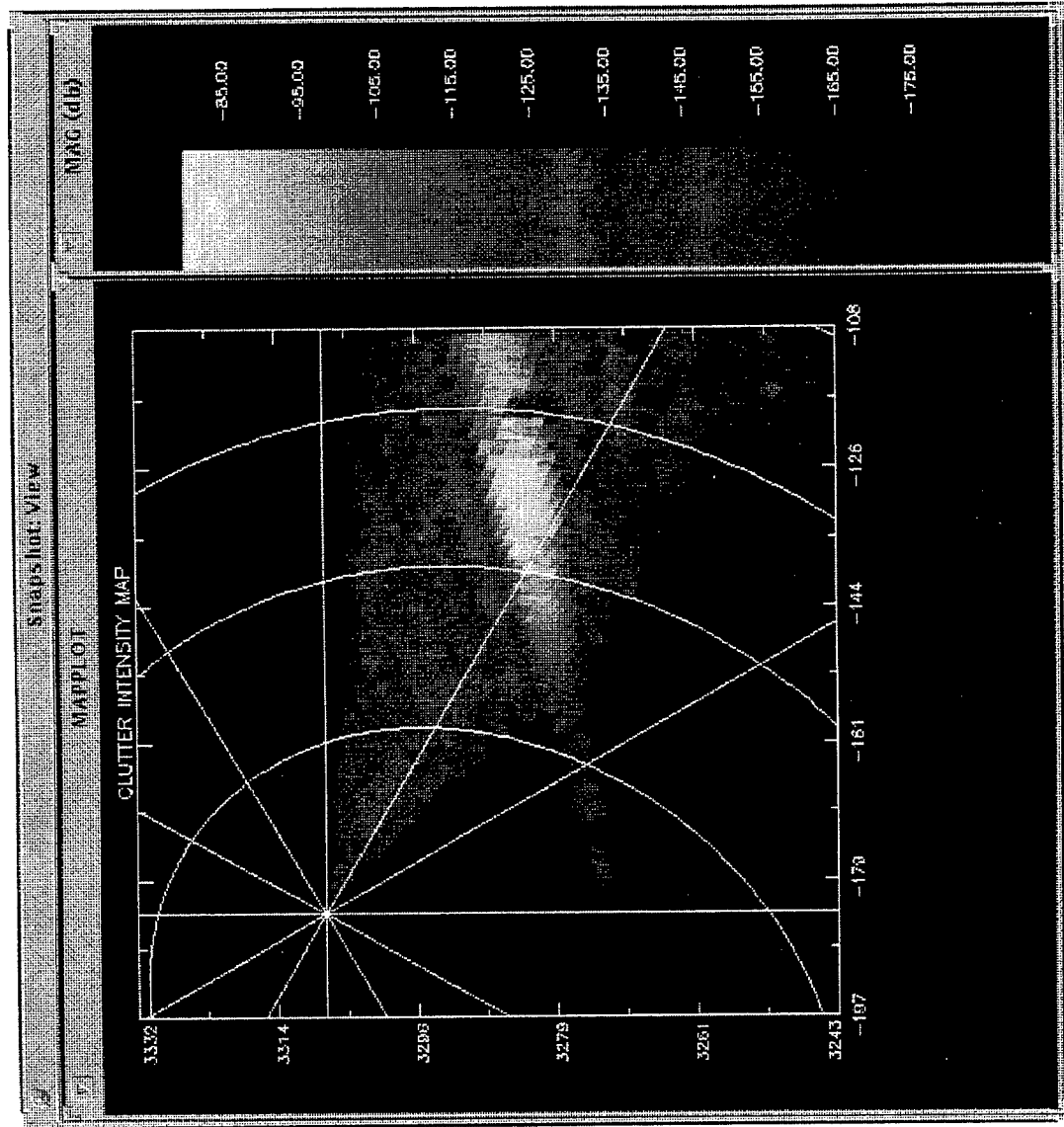
Technology Service
Corporation

NOTHING BUT GRUMMAN

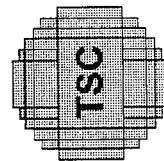


ESTIMATED CLUTTER STRENGTH FOR ACQUISITION 109

ASAP
'97

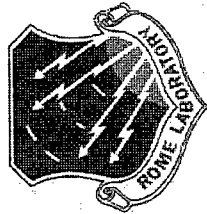


- DISTANCE IN KILOMETERS
- ELLIPSES SPACED BY THREE RANGE AMBIGUITIES



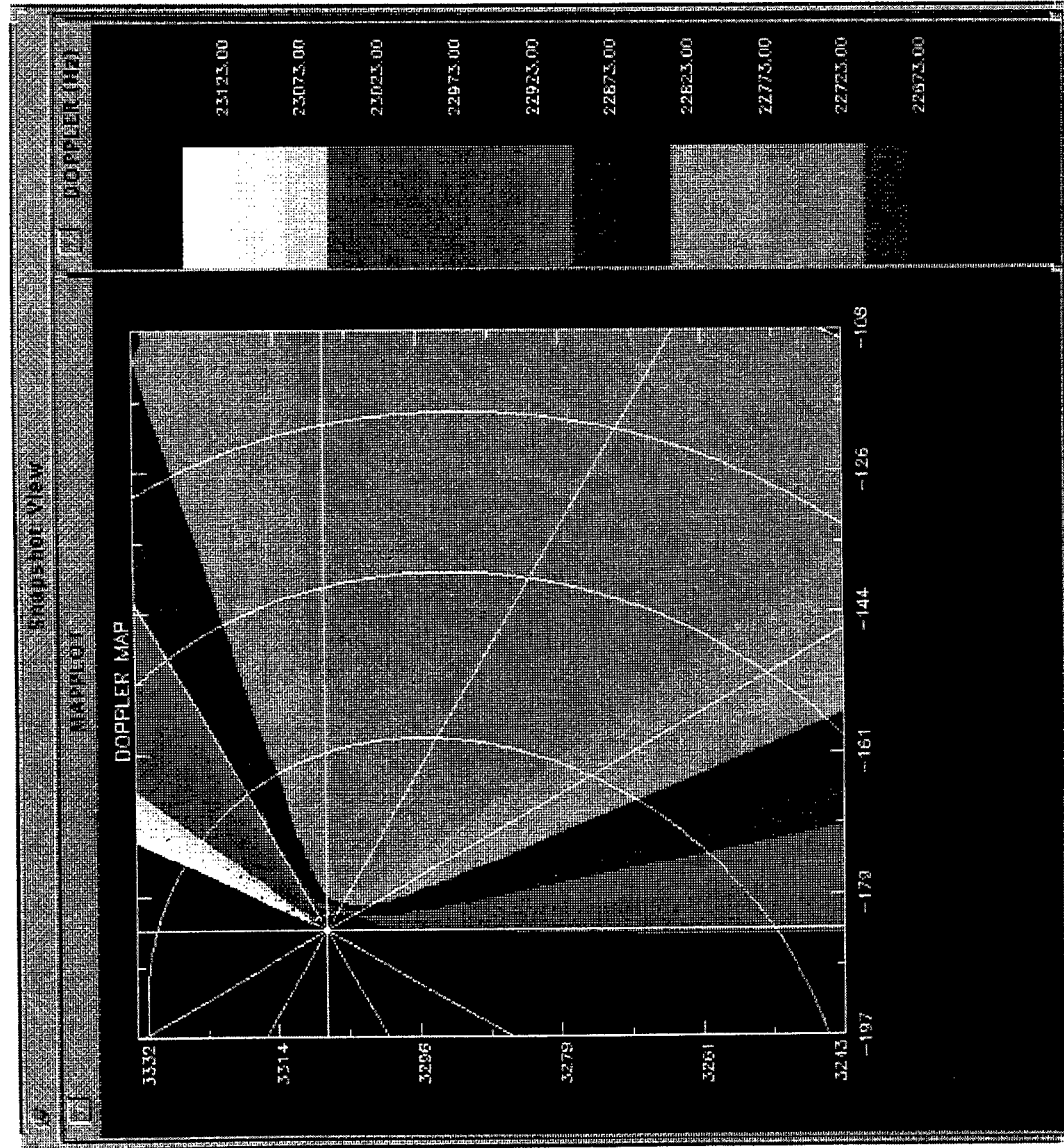
Technology Service
Corporation

ACQUISITION 109

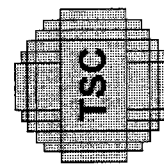


CLUTTER DOPPLER FREQUENCY FOR ACQUISITION 109

ASAP
'97

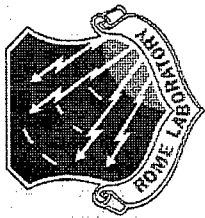


- DISTANCE IN KILOMETERS
- ELLIPSES SPACED BY THREE RANGE AMBIGUITIES



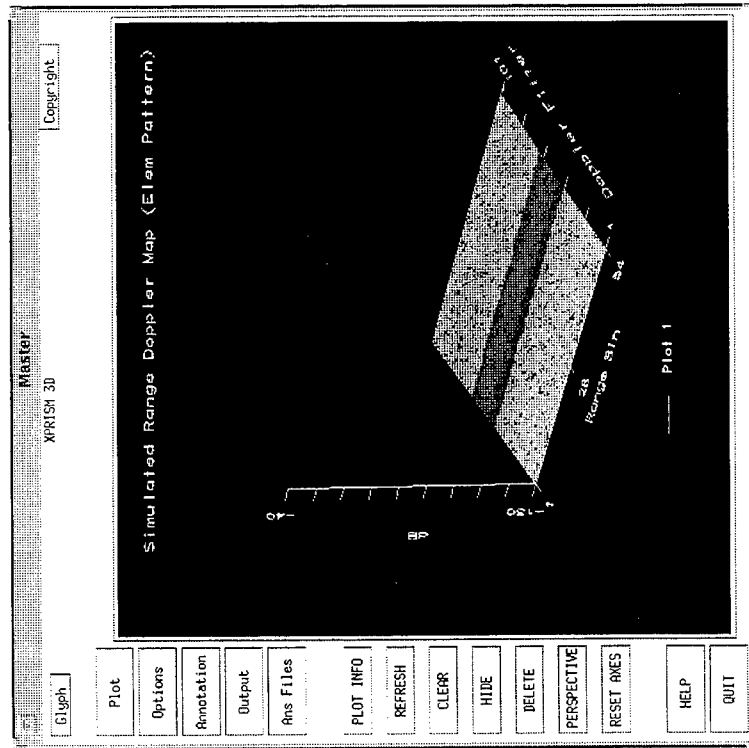
Technology Service
Corporation

NOTHING CHANGING

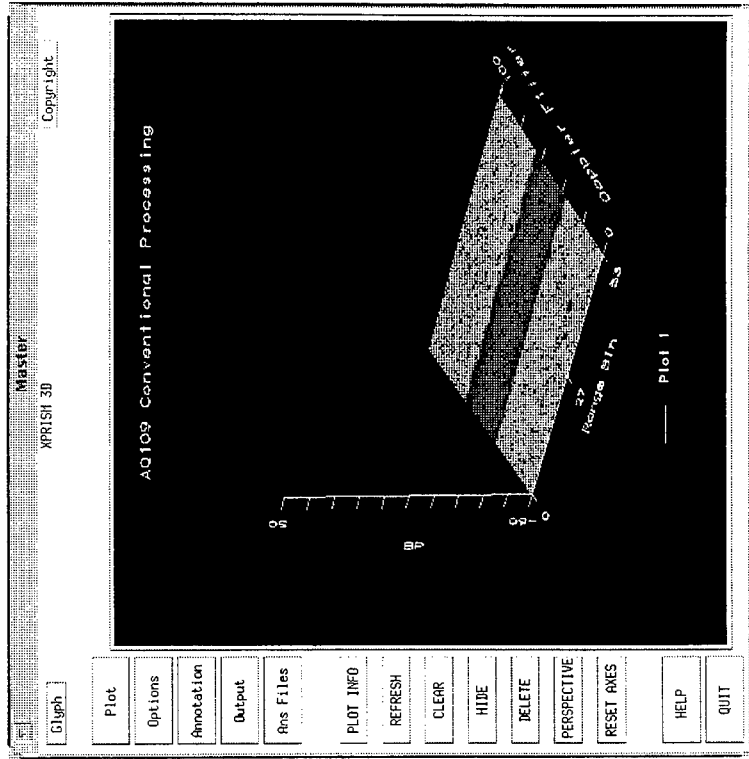


RANGE AMBIGUOUS CLUTTER RETURN FOR ACQUISITION 109

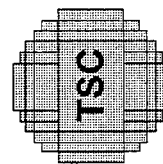
ASAP
'97



SIMULATED DATA

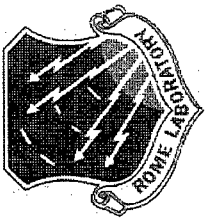


COLLECTED DATA



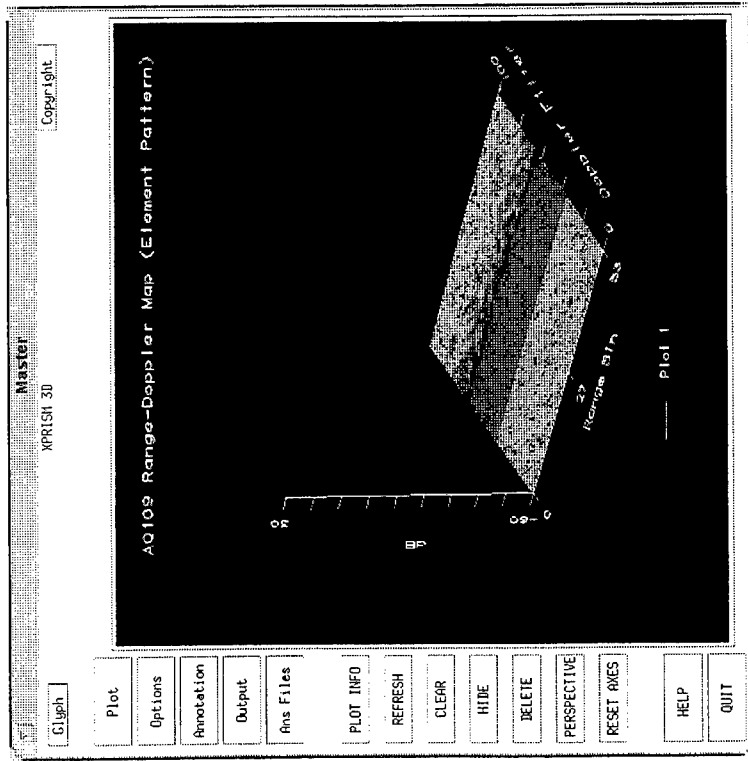
Technology Service
Corporation

NOTHING BUT THE BEST

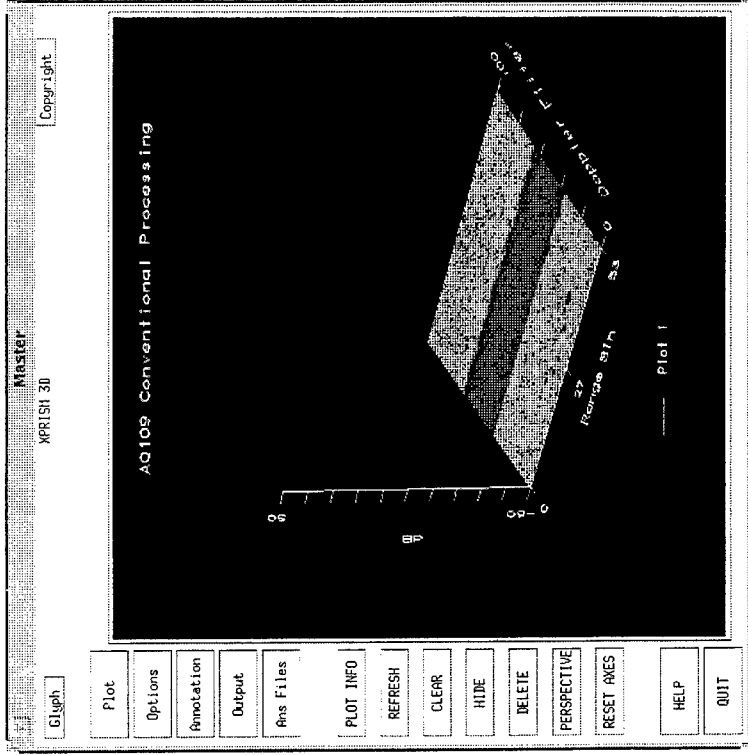


ASAP
'97

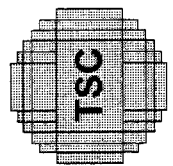
COMPARISON OF CLUTTER SPECTRA FOR ACQUISITION 109



INDIVIDUAL ELEMENT

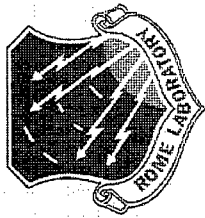


CONVENTIONAL BEAMFORMING
(60 dB TAYLOR WEIGHTING)



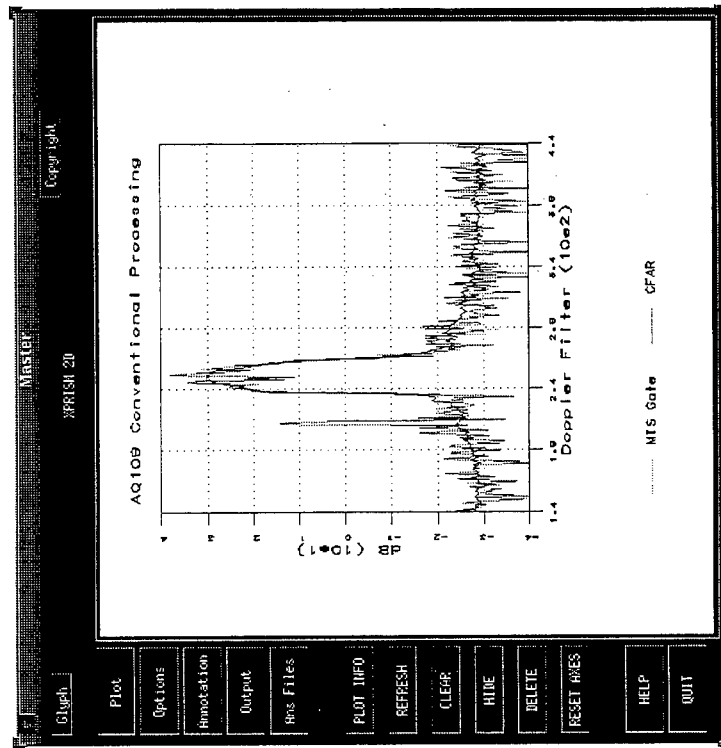
Technology Service
Corporation

ACQUISITION 109

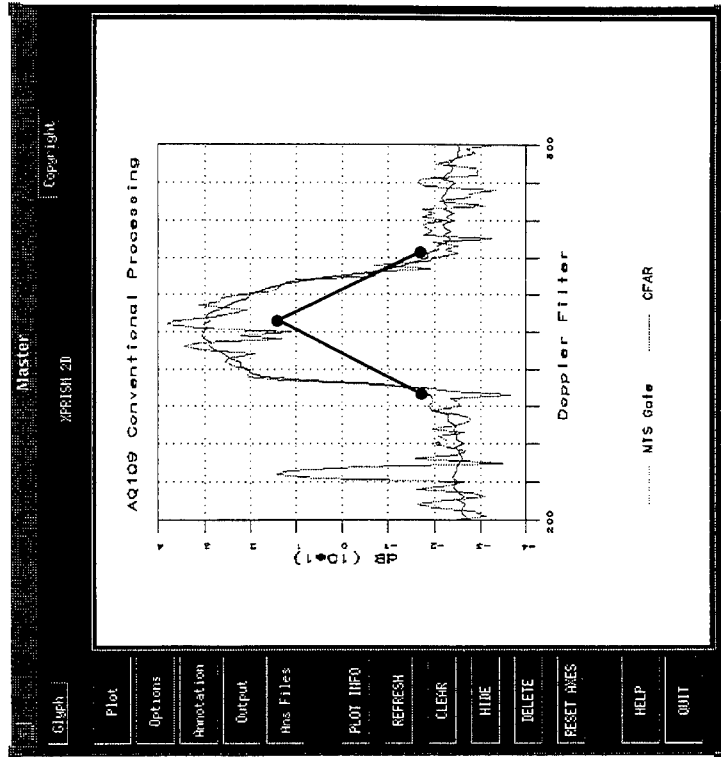


DOPPLER SPECTRUM FOR ACQUISITION 109

ASAP
'97

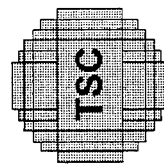


PRINCIPAL CLUTTER EXTENT



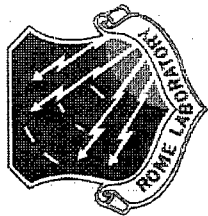
EXPANDED SCALE

NOTE: RED IS RANGE GATE CONTAINING MTS.
BLUE IS AVERAGE OF RANGE GATES CONTAINING ONLY CLUTTER.
TRIANGLE SHOWS MTS TONE LOCATIONS



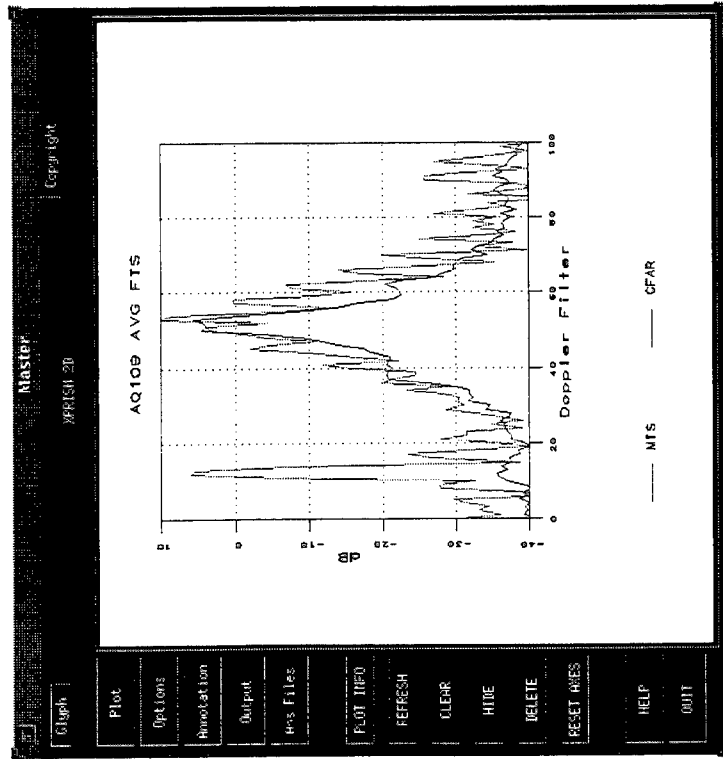
Technology Service
Corporation

NORTHROP GRUMMAN

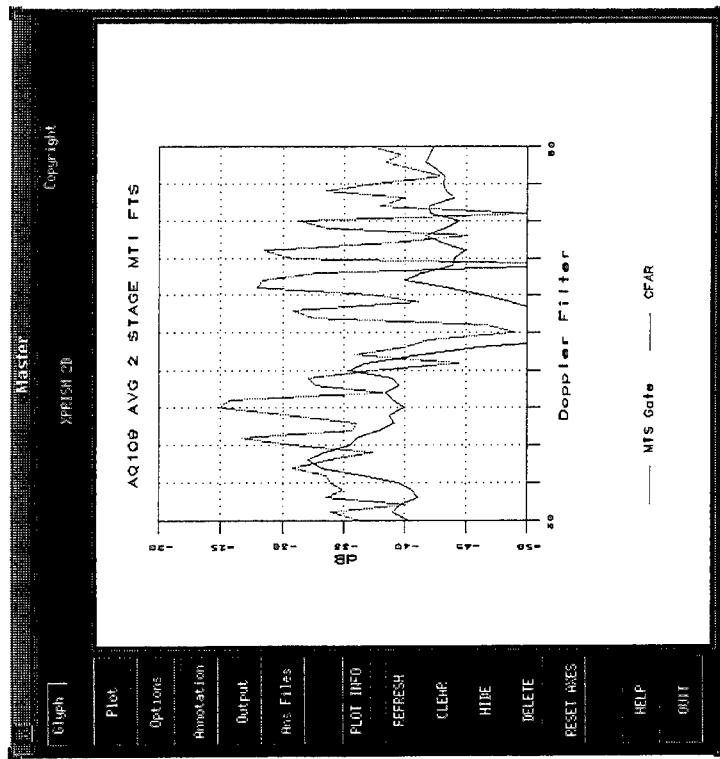


SPACE-TIME ADAPTIVE PROCESSING REVEALS MTS TONE LOCATIONS (POST-DOPPLER ADAPTIVE PROCESSING EXAMPLE)

ASAP
'97

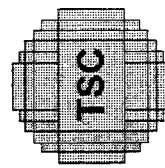


FULL MTS SPECTRUM

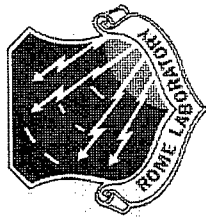


EXPANDED VIEW
(2-STAGE MTI FILTERING)

NOTE: RED IS RANGE GATE CONTAINING MTS.
BLUE IS AVERAGE OF RANGE GATES CONTAINING ONLY CLUTTER.

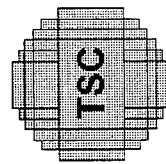
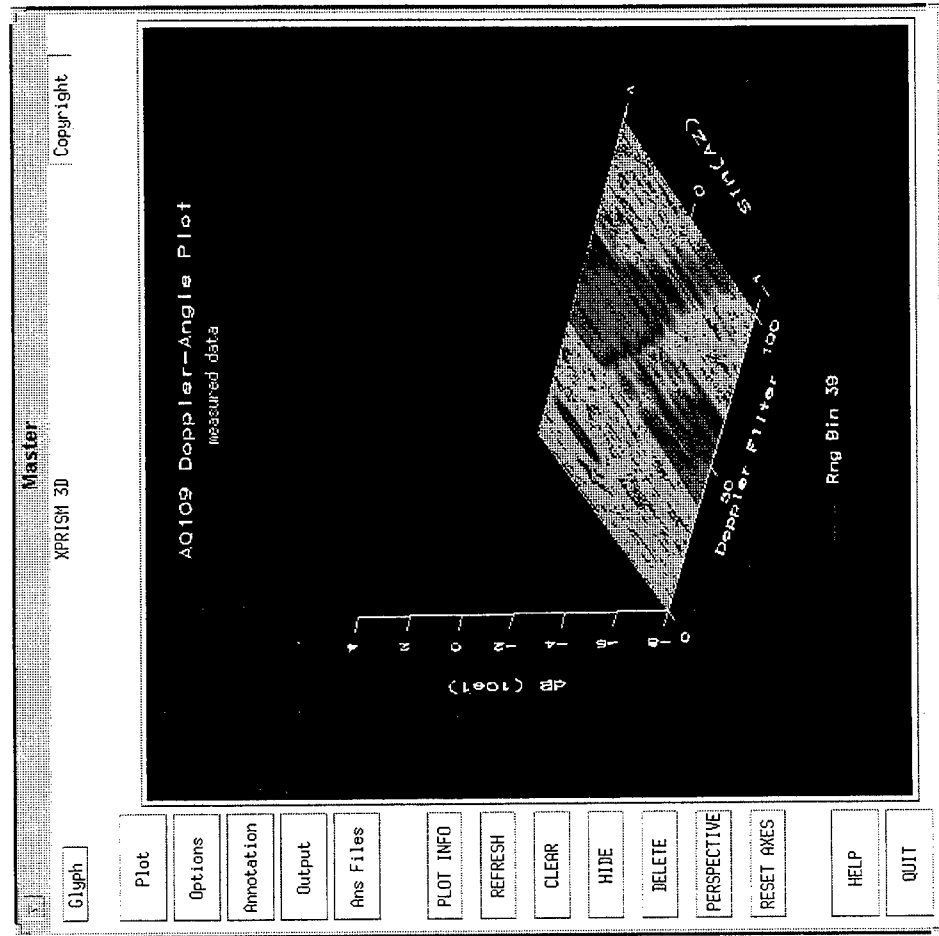


NORTHROP GRUMMAN



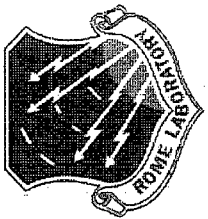
ASAP
'97

DOPPLER-ANGLE PLOT OF MTS RANGE GATE FOR ACQUISITION 109



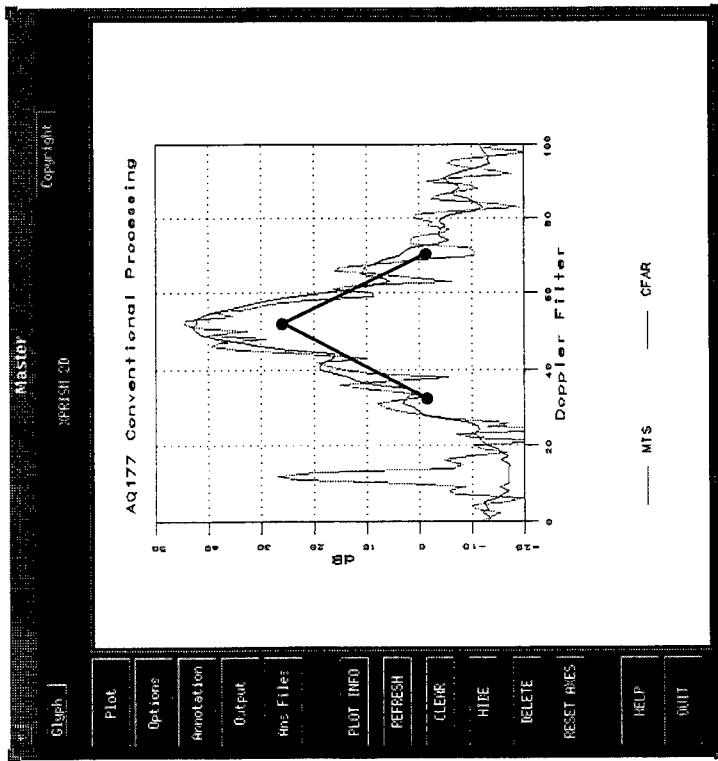
Technology Service
Corporation

ANTHONY CHAMMAN



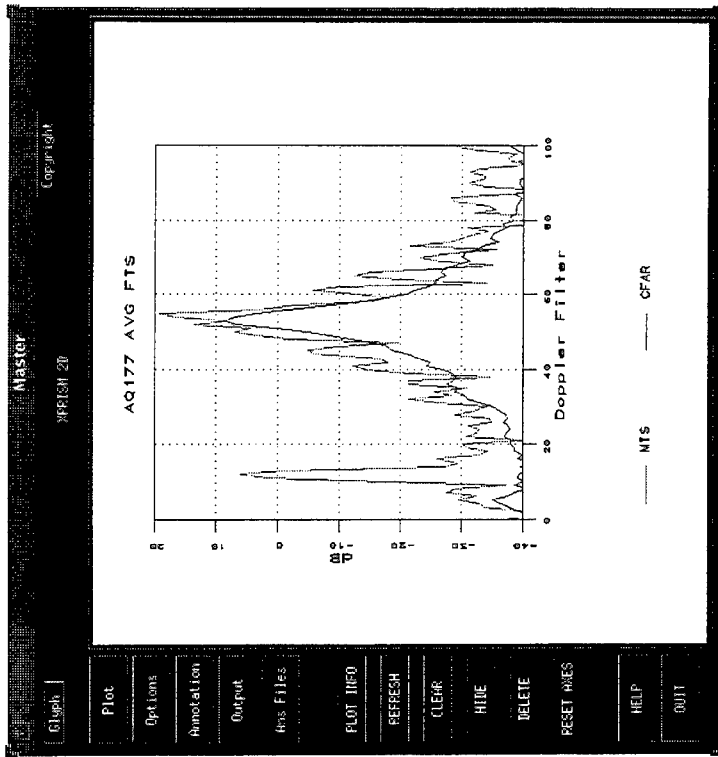
ASAP
'97

CLUTTER SPECTRUM FOR PSEUDO-MONOSTATIC GEOMETRY

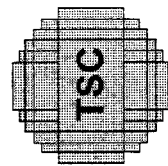


CONVENTIONAL PROCESSING

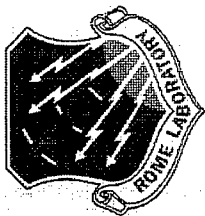
**NOTE: RED IS RANGE GATE CONTAINING MTS.
BLUE IS AVERAGE OF RANGE GATES CONTAINING ONLY CLUTTER.
TRIANGLE SHOWS MTS TONE LOCATIONS**



POST-DOPPLER STAP



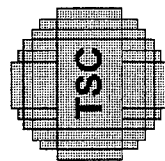
Technology Service
Corporation



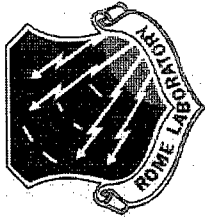
A VARIETY OF BISTATIC DATA IS AVAILABLE IN THE ROME LABORATORY LIBRARY

ASAP
'97

DATA TYPE	PRF	TARS	MTS	RNG TO MTS	FLT NO.
PSEUDO-MONOSTATIC	HI	ON	ON	LONG	8
PSEUDO-MONOSTATIC	HI	ON	ON	LONG	9
MTS CALIBRATION	HI	OFF	ON	N/A	8
MTS CALIBRATION	HI	OFF	ON	N/A	8
MTS CALIBRATION	HI	OFF	ON	N/A	9
WIDE BISTATIC ANGLES	HI	ON	ON	N/A	8
WIDE BISTATIC ANGLES	HI	ON	ON	N/A	8
WIDE BISTATIC ANGLES	HI	ON	ON	N/A	9
PSEUDO-MONOSTATIC	LO	ON	ON	LONG	10
MTS CALIBRATION	LO	OFF	ON	N/A	10
WIDE BISTATIC ANGLES	LO	ON	ON	N/A	10
WIDE BISTATIC ANGLES	LO	ON	ON	N/A	10
PSEUDO-MONOSTATIC	HI	ON	ON	SHORT	8
PSEUDO-MONOSTATIC	HI	ON	ON	SHORT	9
CLUTTER (2 SEC NON-TRIG)	HI	ON	ON	LONG	9
CLUTTER (2 SEC NON-TRIG)	LO	ON	ON	LONG	9



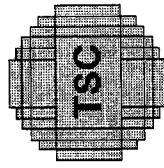
TSC
Technology Service
Corporation



ASAP
'97

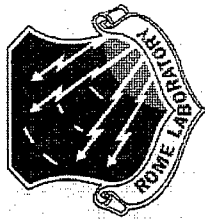
CONCLUSIONS

- THE BISTATIC MCARM DATA COLLECTION EFFORT HAS SUCCESSFULLY ACQUIRED THE FIRST AIRBORNE MULTI-CHANNEL BISTATIC RADAR DATA
- SUMMARY OF PROGRAM ACCOMPLISHMENTS:
 - MODIFIED AEROSTAT FOR HIGH PRF OPERATION WITH REMOTE OPERATION
 - OPERATED MCARM AND BAC 1-11 FROM REMOTE BASE
 - SUCCESSFULLY DEPLOYED AND OPERATED MTS FOR CALIBRATED TARGETS
 - SUCCESSFULLY TRIGGERED DATA ACQUISITIONS
 - ANALYZED MULTI-CHANNEL DATA BETWEEN FLIGHTS
 - ACQUIRED ALL PLANNED DATA
 - ACQUIRED ADDITIONAL NON-PLANNED DATA (SHORT RANGE AND NON-TRIGGERED)
 - PROCESSED DATA WITH STAP ALGORITHMS TO EXTRACT TARGETS FROM CLUTTER



Technology Service
Corporation

NORTHROP GRUMMAN



DETAILED BISTATIC SYSTEM PARAMETERS

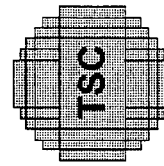
ASAP
'97

TARS BISTATICS PARAMETERS

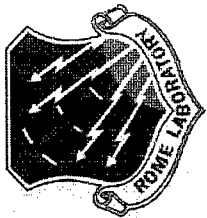
PARAMETER	UNITS	VALUE
ANTENNA GAIN	dBi AT 1300 MHz	34.5
POLARIZATION		VERTICAL
AZIMUTH BEAMWIDTH	DEGREES	2.2 AT 1215 MHz
AZIMUTH PATTERN		SEE APPENDIX B
ELEVATION PATTERN		SEE APPENDIX B
ANTENNA ROTATION RATE	RPM	5 ± 5%
TRANSMIT LOSS	dB	0.4
FREQUENCY	MHz	1240
FREQUENCY STABILITY	ppm	±1 x 10 ⁻⁷

MEASURED TARS BISTATICS PARAMETERS

PARAMETER	UNITS	VALUE
TRANSMIT POWER	kW PEAK	31.5 (flt 10) 18.1 (flt 8 & 9)
PULSEWIDTH (HIGH PRF)	μsec	1.5
IPP (HIGH PRF)	μsec	43
PULSEWIDTH (LOW PRF)	μsec	14
IPP (LOW PRF)	μsec	2850
TRANSMIT RISETIME	nsec	500
TRANSMIT FALLTIME	nsec	<400
ANTENNA TILT ANGLE	deg	-1
FREQUENCY STABILITY	ppm	±1 x 10 ⁻⁷



Technology Service
Corporation



ASAP
'97

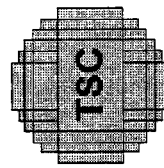
DETAILED BISTATIC SYSTEM PARAMETERS (CONCL'D)

BISTATIC TEST WAVEFORMS

WF	PW (CLKS)	PRF (CLKS)	MOD	PW (μ sec)	PRF (kHz)	DUTY FACTOR	REMARKS
HIPRF	2	54	NONE	1.6	23.1	0.037	
LOPRF	18	4000	LFM	14.4	0.312	0.0045	DOWN CHIRP

MCARM BISTATICS PARAMETERS

PARAMETER	UNITS	VALUE
SYSTEM NOISE FIGURE	dB	3.6 (INCLUDES REC LOSSES)
A/D RATE	MHz	5 (OFFSET BASEBAND) 1.25 AFTER DIGITAL I/Q
GATE WIDTH	μ sec	0.8
NOISE BANDWIDTH	MHz	0.83
PC RATIO		18:1 (LOW PRF ONLY)
PC SIDELOBES	dB	30 (LOW PRF ONLY)
ANTENNA SIZE	dB	11 x 8 (22 CHANNELS)
ANTENNA GAIN*	dBi	22.3 AT 1270 MHz
AZIMUTH BW*	deg	11.1 AT 1270 MHz
ELEVATION BW	deg	11.9
ELEVATION SIDELOBES	dB	-20
ELEVATION POINTING	deg	-5
POLARIZATION		VERTICAL
FREQUENCY	MHz	1240
FREQUENCY STABILITY	ppm	$\pm 1 \times 10^{-7}$
* WITH UNIFORM TAPER IN AZIMUTH. STAP WEIGHTING WILL DETERMINE FINAL TAPER LOSS AND AZIMUTH BEAMWIDTH.		



Technology Service
Corporation

Signal Modulation in Pulse-by-Pulse Adaptive Nulling Systems

Daniel J. Rabideau

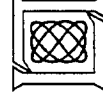
MIT Lincoln Laboratory
244 Wood Street
Lexington, MA 02173-9108
tel: (617) 981-2892
email: danr@ll.mit.edu

Abstract Due to radar and jammer motion, the process by which an airborne jammer's energy is scattered off the terrain and into the receiver is continually changing. As a result, rapid weight updates have been proposed as a way to maintain interference suppression throughout a coherent processing interval. In fact, it has been suggested that the weights be re-computed on each pulse. In this presentation, we examine the effect of the "pulse-by-pulse" adaptive beamforming for hot clutter mitigation on other signals (e.g., targets or monostatic clutter) that may be present in the data. Two effects are examined in detail: random signal modulations induced by finite sample sizes and non-random signal modulations induced by the signals' coherence. In the first of these, overall signal localization in Doppler is degraded due to random fluctuations in the adaptive beam patterns (resulting from the use of estimated covariance matrices). Increased training set sizes or design constraints are effective at restoring localization performance. In the second effect, the coherence of the multipath interference gives rise to more predictable signal modulations. Unfortunately, these modulations cause the clutter ridge to expand within the angle-Doppler plane, requiring more adaptive degrees of freedom and more sophisticated STAP algorithms to reject. In this paper, we present an analytical model for both effects. We also compare and contrast these effects to the previously reported "clutter leakage" phenomena. Finally, we will discuss several techniques that might be employed to reduce the performance loss associated with these effects.

SIGNAL MODULATION IN PULSE-BY-PULSE ADAPTIVE NULLING SYSTEMS

**DANIEL J. RABIDEAU
LINCOLN LABORATORY
MASSACHUSETTS INSTITUTE OF TECHNOLOGY**

1997 ADAPTIVE SENSOR ARRAY PROCESSING WORKSHOP



JOINT MITIGATION ARCHITECTURES

• FOUR ARCHITECTURES FOR JOINT TSI & CLUTTER MITIGATION ...

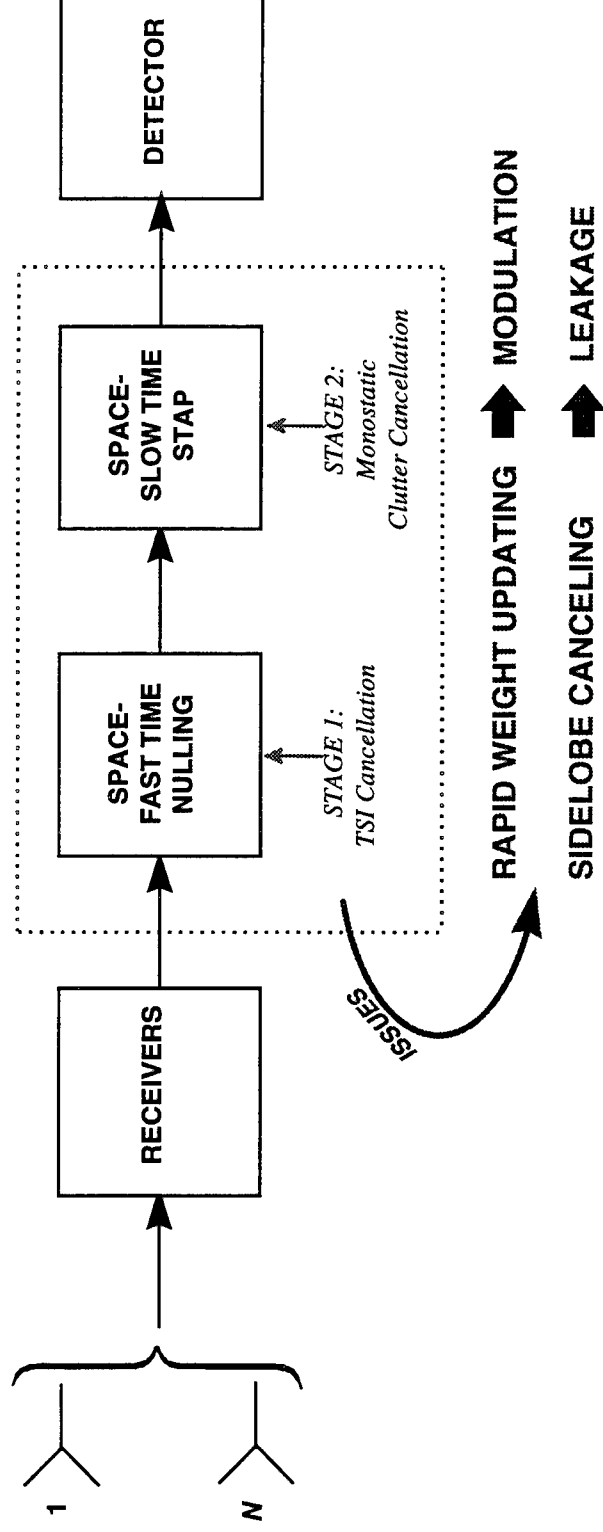
- 3D STAP
- 2D STAP
- FULL BEAM SPACE SIDELOBE CANCELLER
- SELECTED-AUX SIDELOBE CANCELLER

} COMBINED TSI & CLUTTER NULLING

OFTEN NOT FEASIBLE
... LOTS OF DOFS
... BIG TRAINING SETS

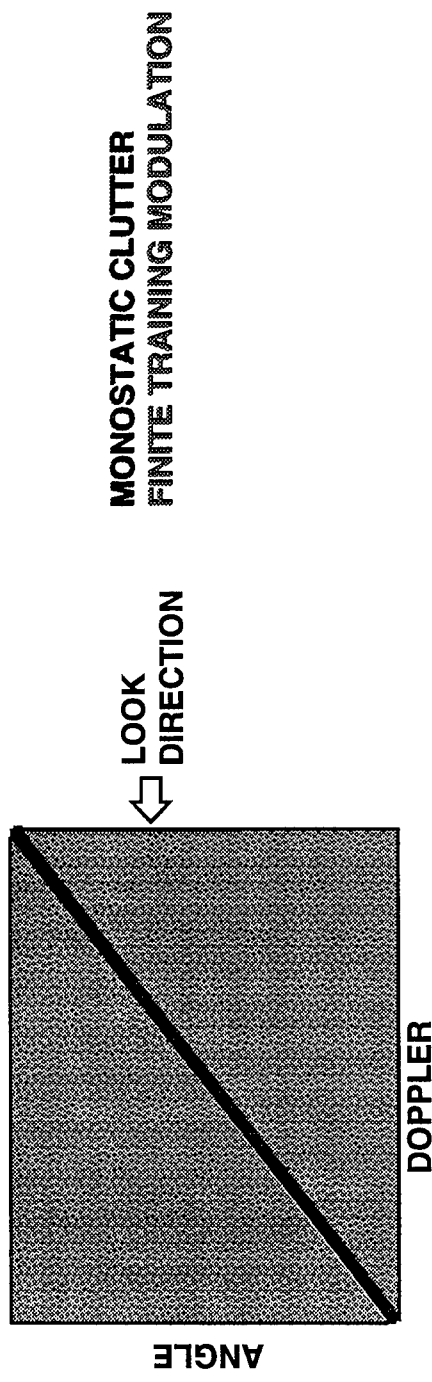
CASCADED
ARCHITECTURES

CASCADED ADAPTIVE INTERFERENCE CANCELLER



OUTLINE

- INTRODUCTION
- **RANDOM SIGNAL MODULATIONS**
 - MODEL FOR ADAPTIVE SIDELOBE LEVELS
 - WHAT CAN WE DO ABOUT IT?



- COHERENCE INDUCED MODULATIONS
- SIDELOBE CANCELLER CLUTTER LEAKAGE
- CONCLUSIONS



MODULATIONS DUE TO FINITE SAMPLES (1)

- WEIGHTS = QUIESCENT + RANDOM:

$$w_i^d = w_{quiescent,i}^d + C t_i$$

$$w_{quiescent}^d = \frac{R_{ideal}^{-1} d}{d^H R_{ideal}^{-1} d}$$

- SIDELOBES = QUIESCENT + RANDOM:

$$w_a^H v_a^d = g + C \cdot t$$

$$g = w_{quiescent}^H v_a$$

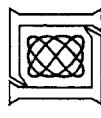
- COLLECT WEIGHTS COMPUTED ON EACH PULSE:

$$W = \begin{bmatrix} w_1 & \dots & w_P \end{bmatrix}$$

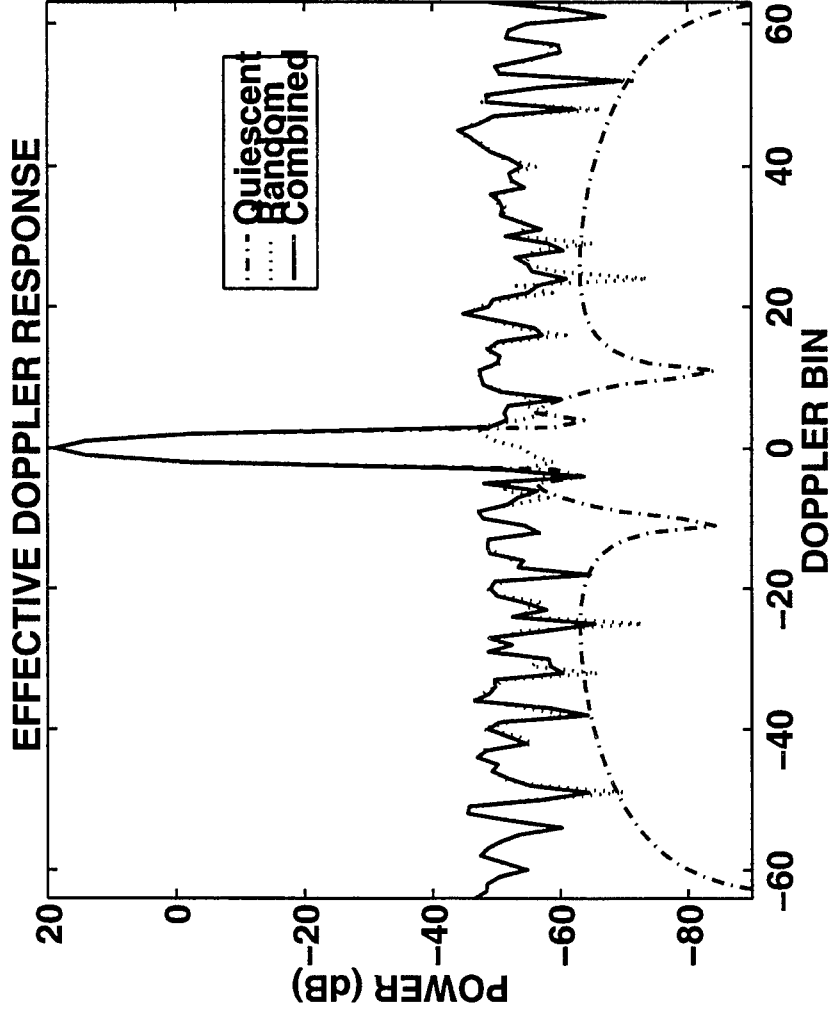
- APPLY TO HYPOTHETICAL TARGET (OR CLUTTER DISCRETE) AT $v_d \otimes v_a$:

$$v_d^d \circ (W^H v_a) = g v_d + C \cdot v_d \circ \begin{bmatrix} t_1 \\ \vdots \\ t_P \end{bmatrix}$$

QUIESCENT
RANDOM



MODULATION DUE TO FINITE SAMPLES (2)

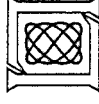
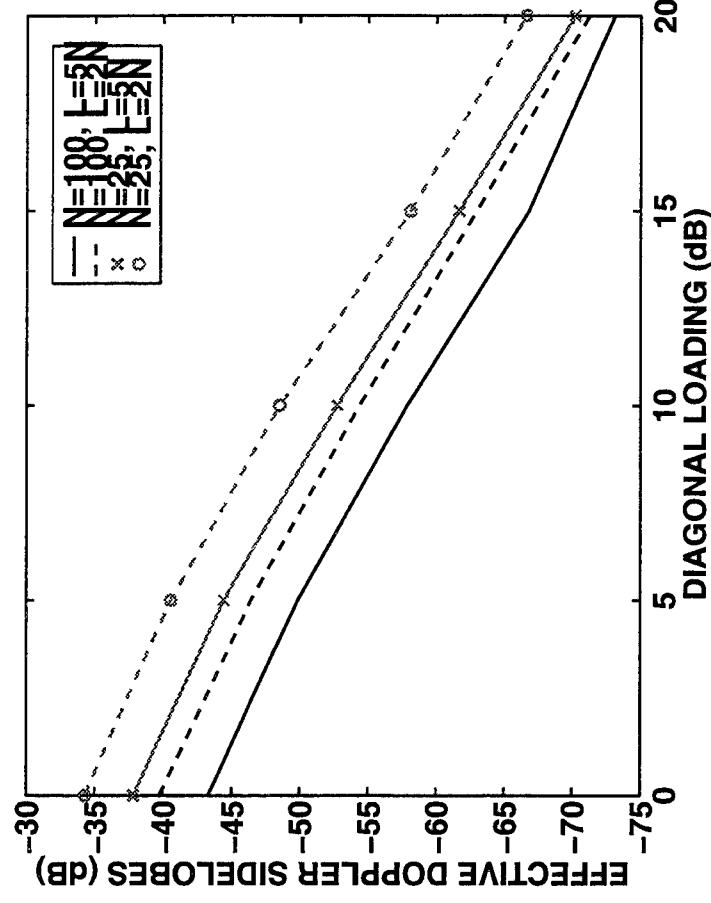
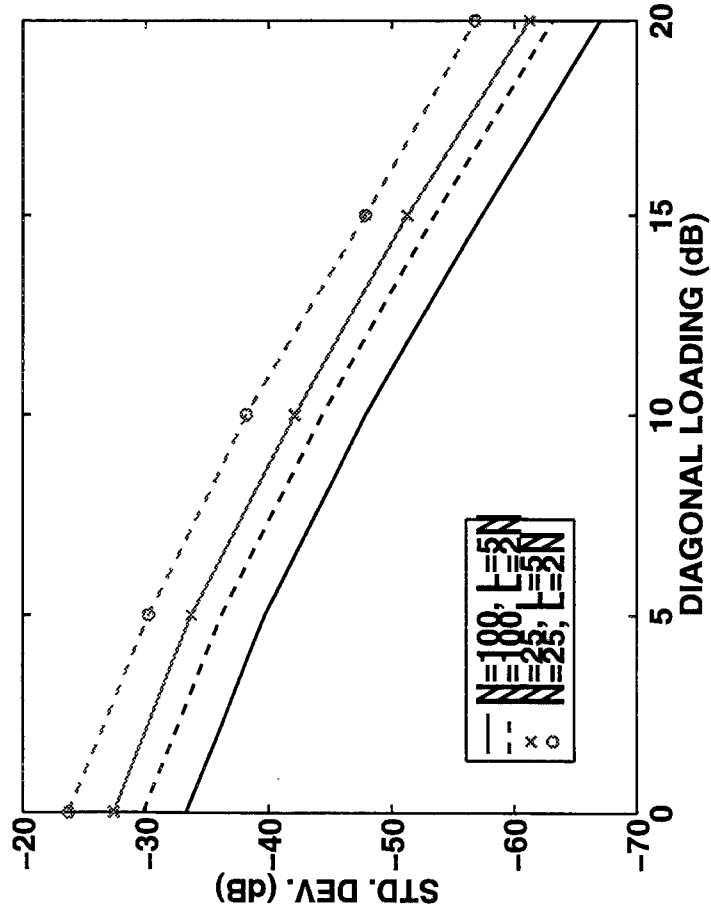


- RANDOM COMPONENT REDUCES OVERALL ABILITY TO LOCALIZE SIGNALS

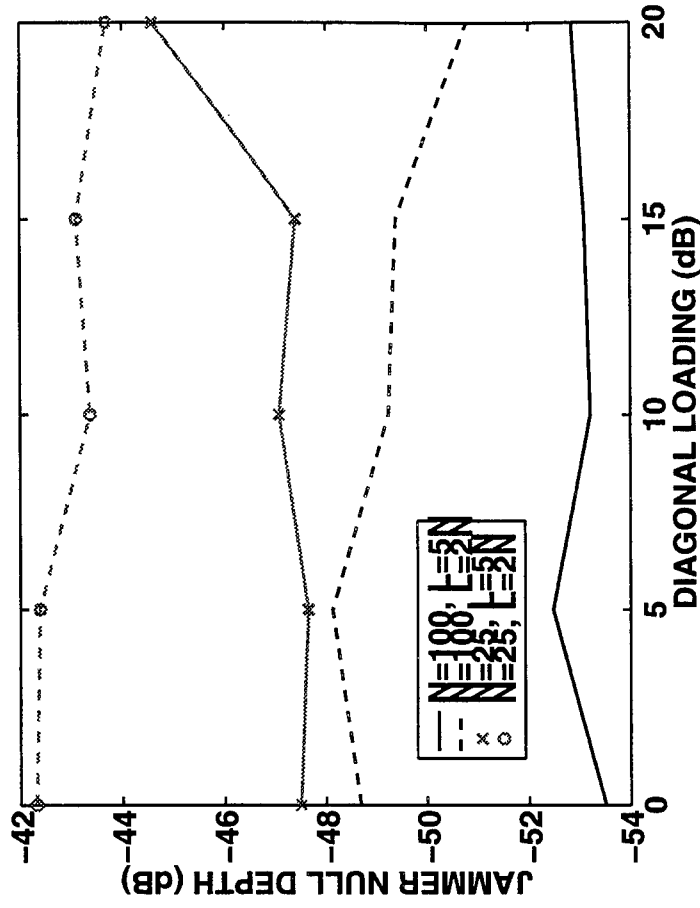
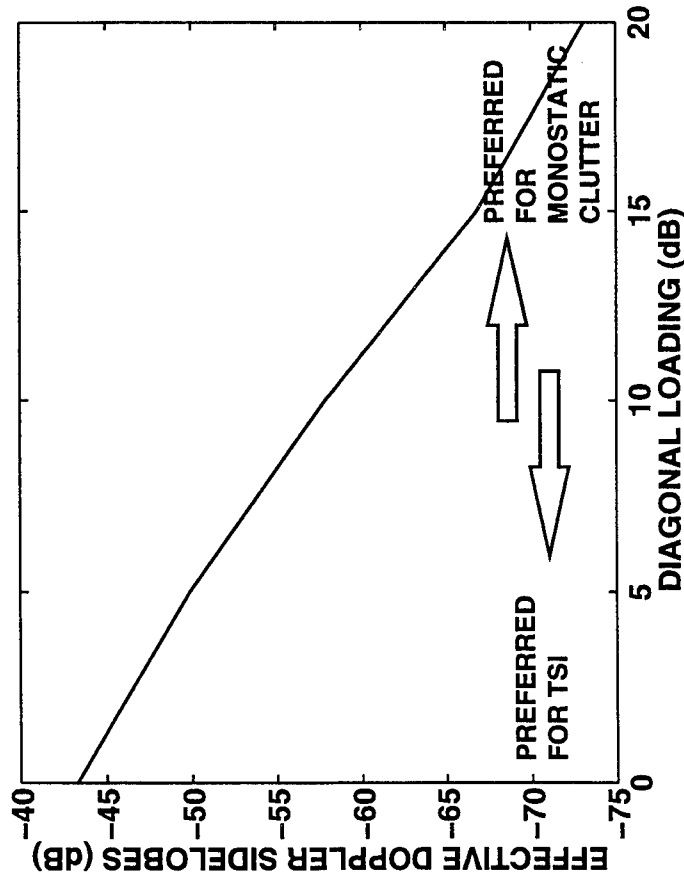


WHAT CAN WE DO ABOUT IT?

- USE BIGGER TRAINING SET ...
 - FREQUENTLY NOT POSSIBLE
- CAREFUL BEAM SUB-SELECTION
 - TRAINING SET IS EFFECTIVELY ENLARGED
- CONSTRAINED FILTER DESIGN ...



DIAGONAL LOADING TRADEOFF ...



- ABILITY TO LOCALIZE SIGNAL IS ENHANCED BY LOADING

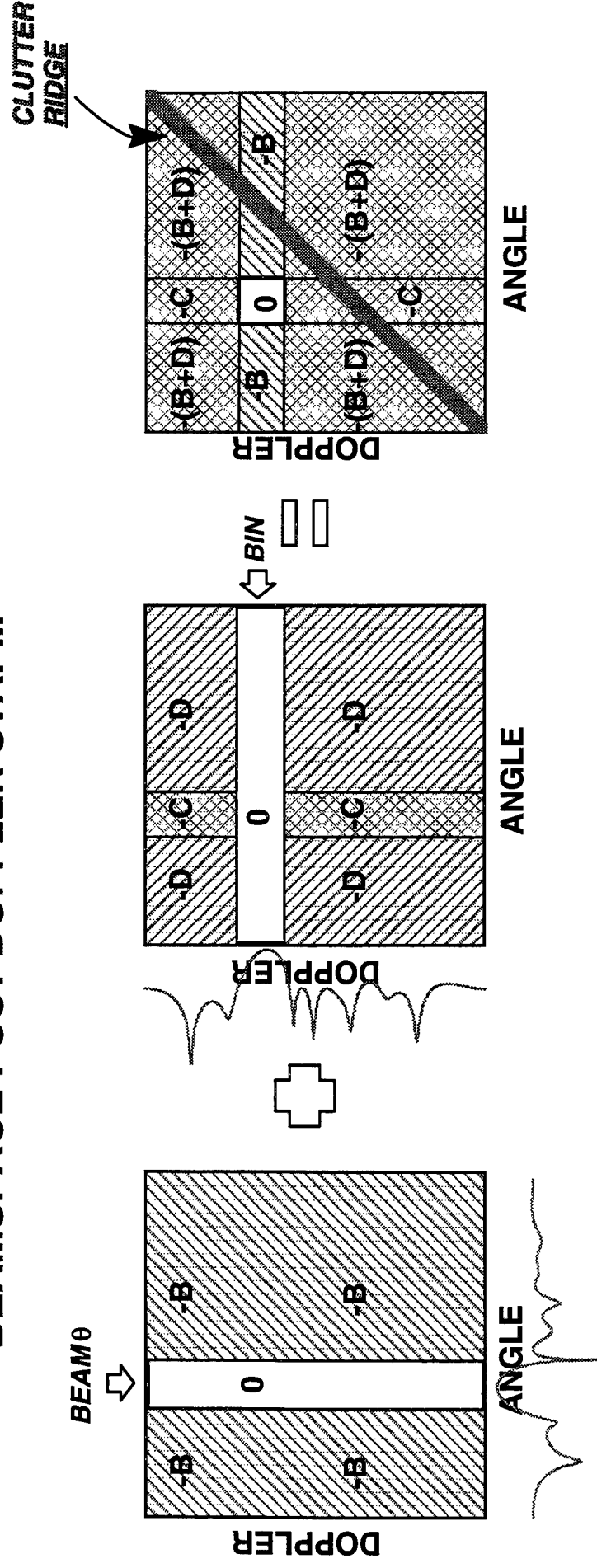
... BUT WEAKER JAMMERS MAY NOT BE CANCELED

- UPSIDE: JAMMER NULL DEPTH IS RELATIVELY INSENSITIVE TO LOADING!

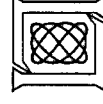


HOW MUCH DIAGONAL LOADING?

- BEAMSPACE POST DOPPLER STAP...

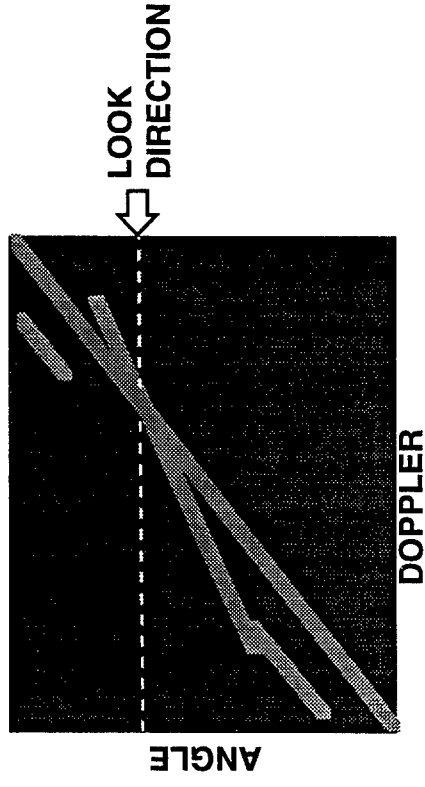


- CHOOSE CONSTRAINT TO ACHIEVE COMBINED ANGLE AND DOPPLER REJECTION LEVELS WHICH HANDLE EXPECTED INTERFERENCE



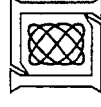
OUTLINE

- INTRODUCTION
- RANDOM SIGNAL MODULATIONS
- ➔ • **COHERENCE INDUCED MODULATIONS**
 - MODEL FOR ADAPTIVE SIDELOBE LEVELS
 - EFFECT ON CLUTTER
 - WHAT CAN WE DO ABOUT IT?

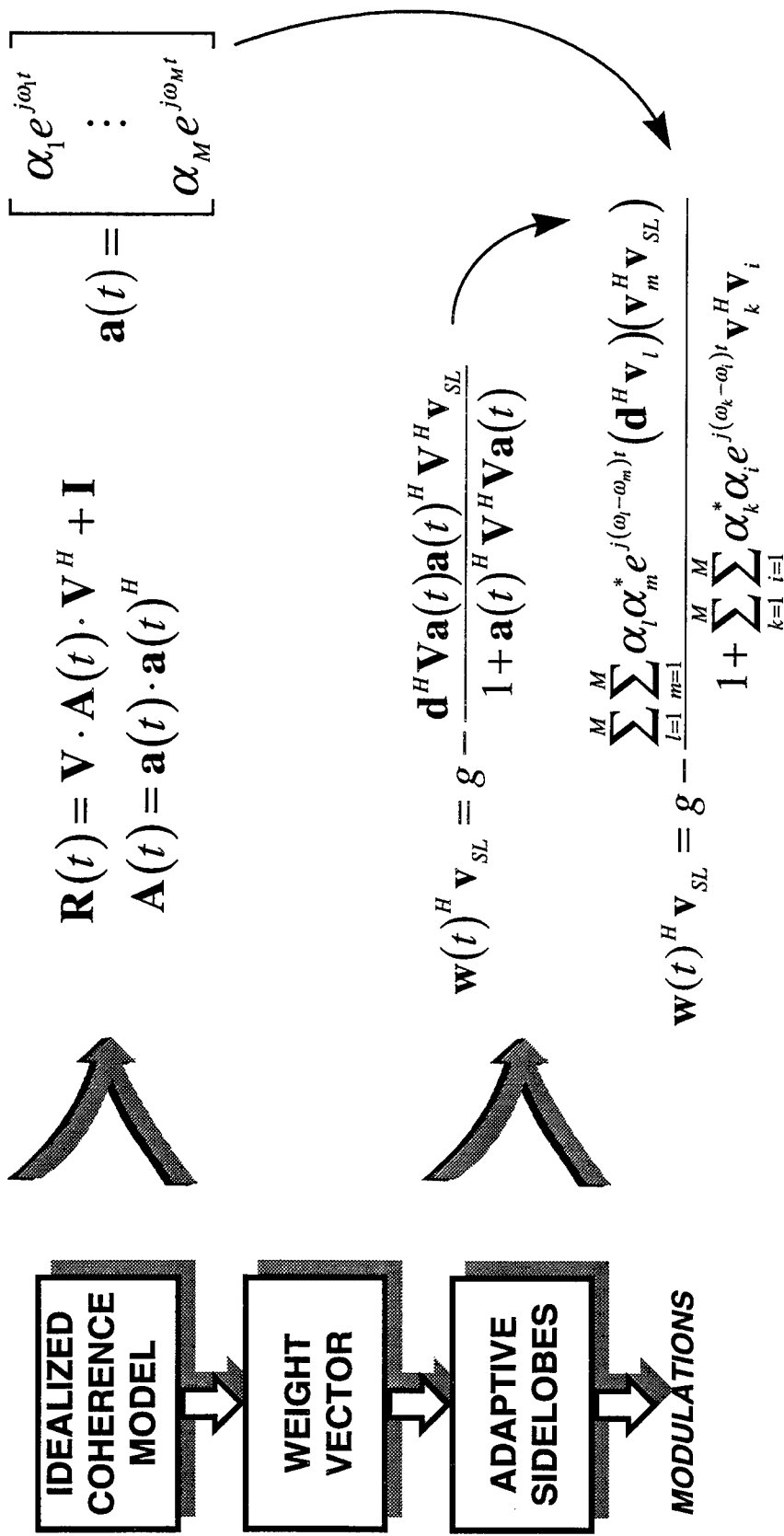


MONOSTATIC CLUTTER
COHERENCE MODULATIONS

- **SIDELOBE CANCELLER CLUTTER LEAKAGE**
- **CONCLUSIONS**



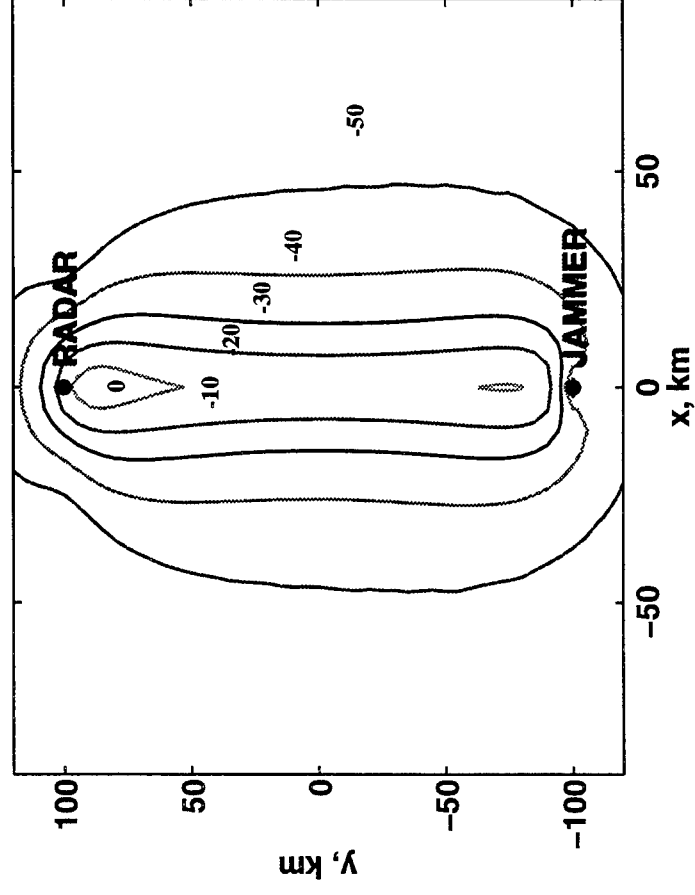
MODULATIONS DUE TO COHERENT JAMMING



BEAMFORMER OUTPUT IS SUM OF MODULATED TERMS

EXAMPLE: HOT CLUTTER

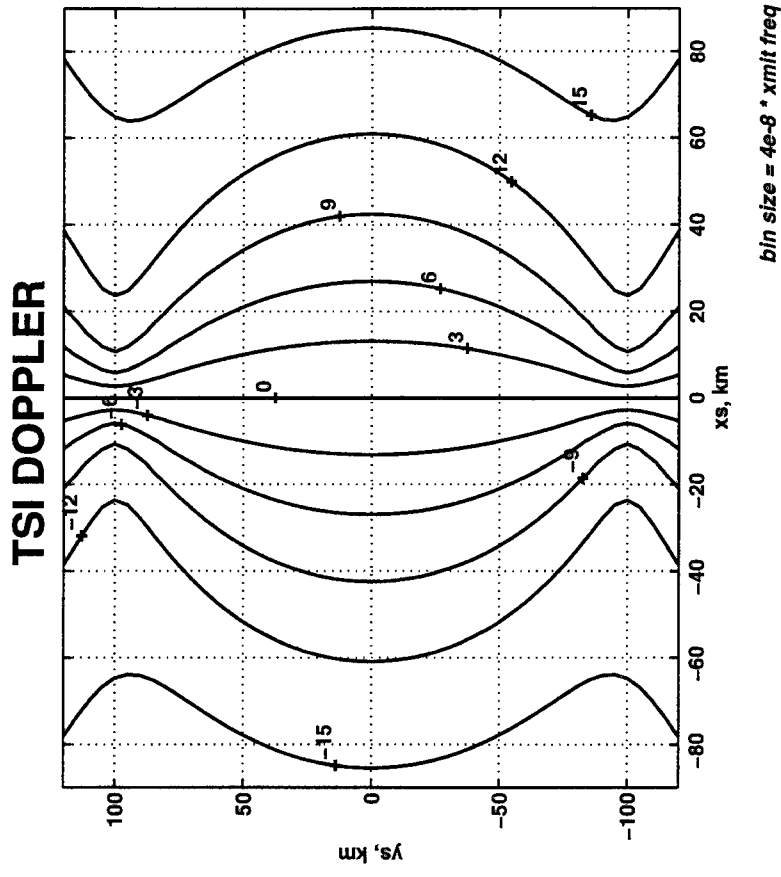
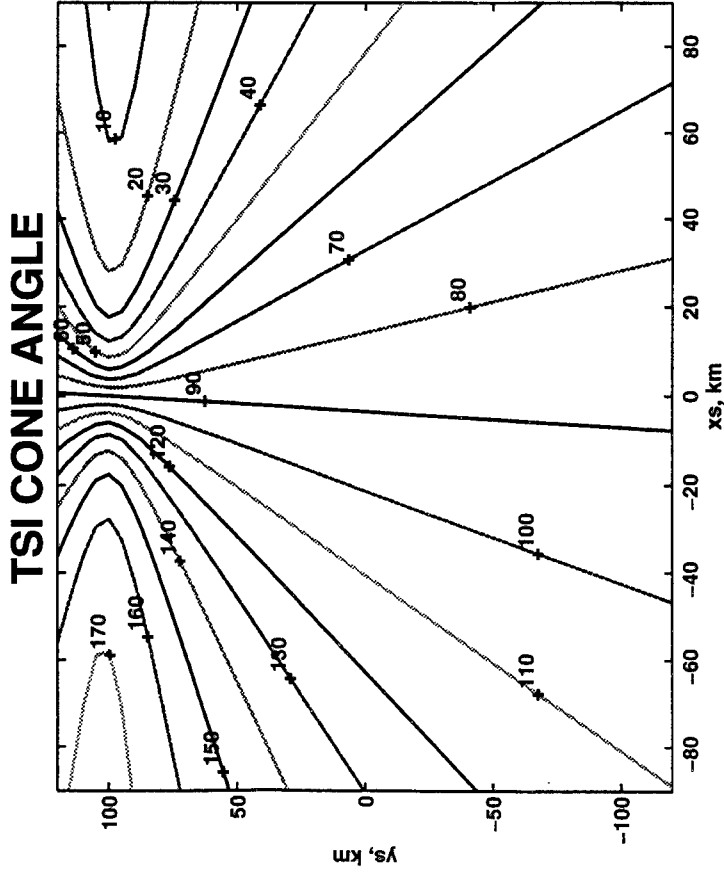
RECEIVED TSI POWER:



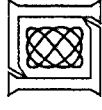
- TSI STRONGEST UNDER PLATFORMS AND ALONG SPECULAR RIDGE



TSI CONE ANGLE & DOPPLER CONTOURS



- FOR EACH CONE ANGLE, TSI SPREADS IN DOPPLER
- THE SPREAD IS SMALL WITHIN THE DOMINANT SCATTERING REGION

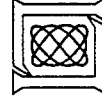


SIGNAL MODULATION DUE TO TSI

$$\mathbf{w}(t)^H \mathbf{v}_{SL} = g - \frac{\sum_{l=1}^M \sum_{m=1}^M \alpha_l \alpha_m^* e^{j(\omega_l - \omega_m)t} (\mathbf{d}^H \mathbf{v}_l) (\mathbf{v}_m^H \mathbf{v}_{SL})}{1 + \sum_{k=1}^M \sum_{i=1}^M \alpha_k^* \alpha_i e^{j(\omega_k - \omega_i)t} \mathbf{v}_k^H \mathbf{v}_i}$$

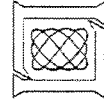
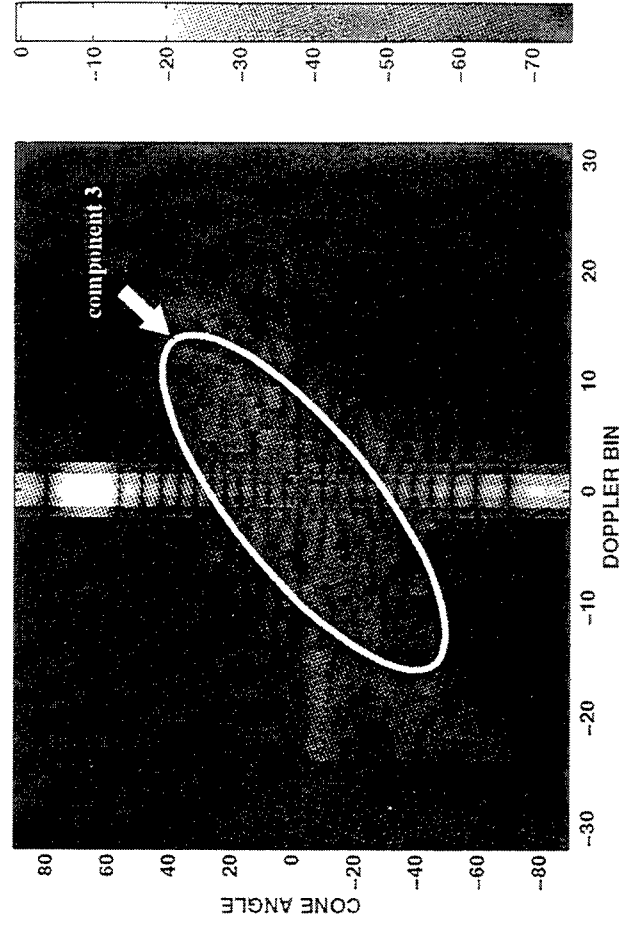
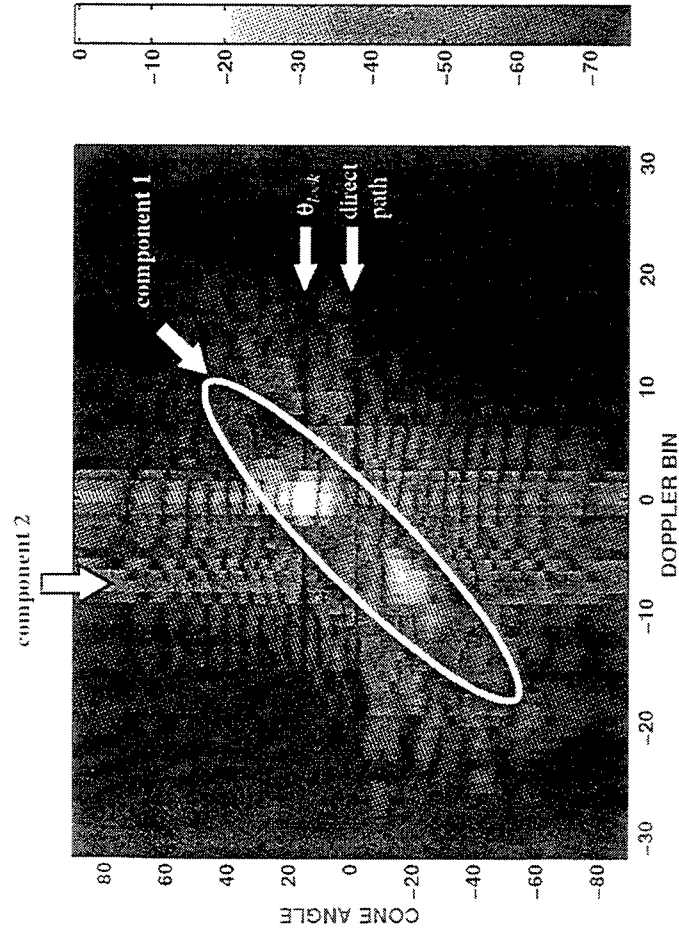
- DENOMINATOR DOMINATED BY DC COMPONENTS
- NUMERATOR IS SUM OF MANY MODULATION TERMS
 - RELATIVELY FEW DOMINANT TERMS:

Principal Component	Region		Approximate $\mathbf{w}^H \mathbf{v}_{SL}$	Modulation Description (in Angle Doppler Plane)
1	1	1	$g - \alpha_{look} \alpha_{SL}^* e^{j(\omega_{look} - \omega_{SL})t}$	Modulation follows a curve which passes through the look direction
2	1	2	case 1: $g - \alpha_{look} \alpha_1^* e^{j(\omega_{look} - \omega_{direct})t}$ case 2: $g - \alpha_{look} \alpha_{SL}^* e^{j(\omega_{look} - \omega_{SL})t}$	Vertical Line Same as component 1
3	2	1	case 1: $g - \alpha_{look} \alpha_1^* e^{j(\omega_{direct} - \omega_{SL})t}$ case 2: $g - \alpha_{look} \alpha_{SL}^* e^{j(\omega_{look} - \omega_{SL})t}$	Curve passing through direct path direction Same as component 1

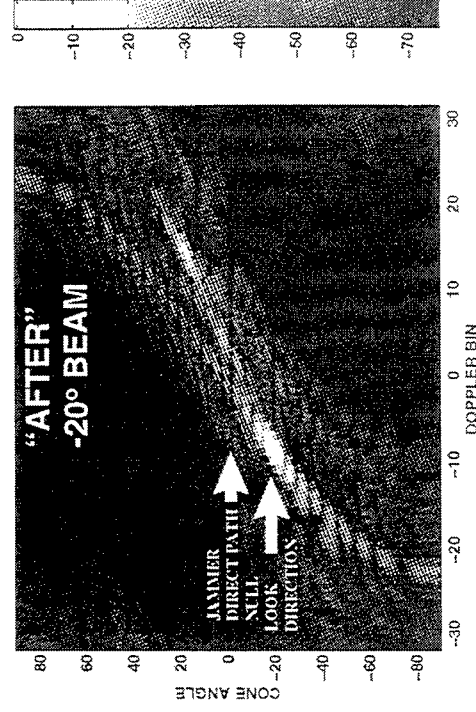
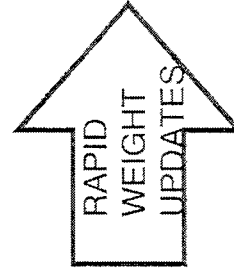
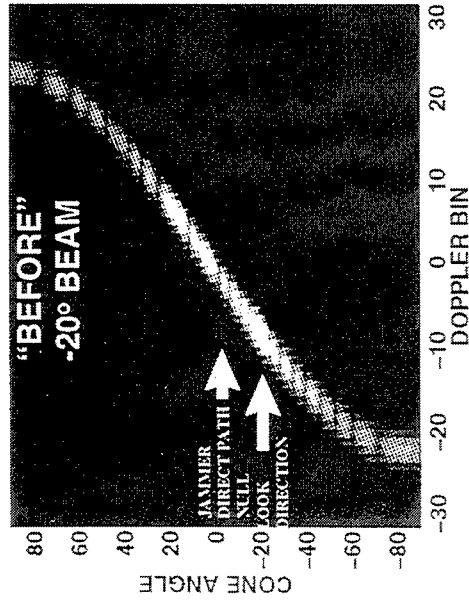
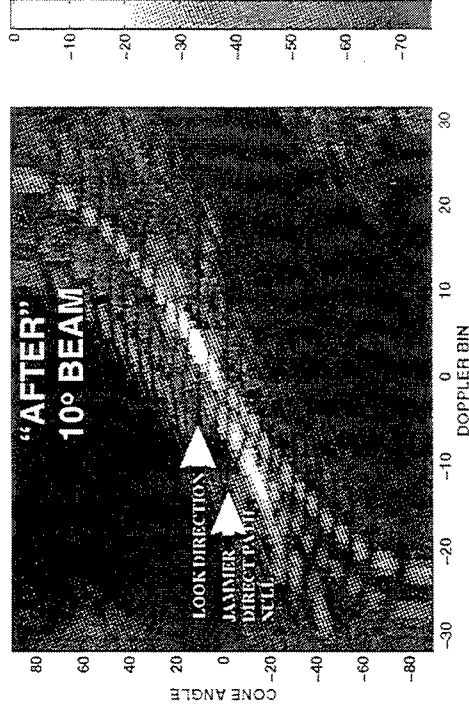
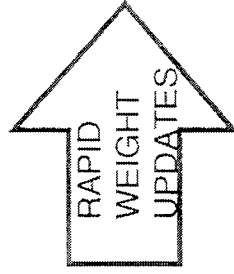
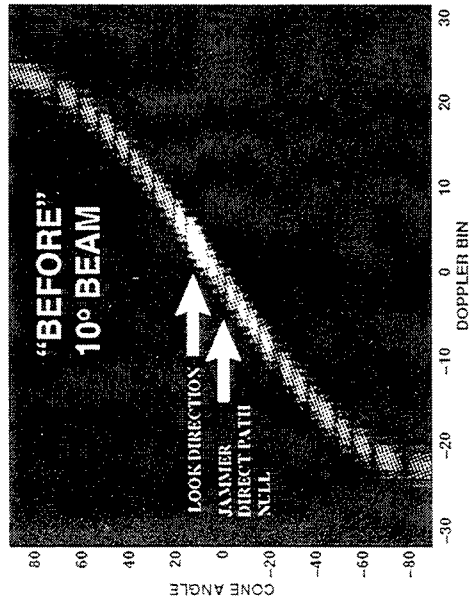


MODEL VALIDATION

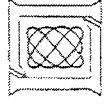
- 25 ELEMENT, 64 PULSE ULA SIMULATION
- COMPUTE OUTPUT SPECTRUM FOR A 0Hz SIGNAL AS ITS SOURCE ANGLE VARIES FROM -90 to 90 DEG.



EFFECT ON MONOSTATIC CLUTTER RIDGE



MODULATED CLUTTER VARIES FROM BEAM TO BEAM
 - MUST REVISE "POINT BEAM" STAP ALGORITHMS



WHAT CAN WE DO ABOUT IT?

- 3 POSSIBLE APPROACHES
- 

1. AVOID IT ...

... 3D STAP

- ISSUES: COMPLEXITY, TRAINING, TARGET MODULATION
- ... LESS FREQUENT WEIGHT UPDATING

2. REDUCE IT ...

... PARTIAL BEAMSPACE TRANSFORMS

... ANTI-SPREADING FILTERS

... TAPERED STEERING VECTORS

3. DEAL WITH IT...

... EIGEN-NULLING

... DETACHED-BIN STAP

... NEW TARGET CLUSTERING ALGORITHMS

- USE PREDICTED MODULATION POSITIONS

} MONOSTATIC CLUTTER
CANCELLATION



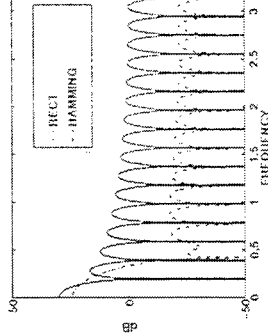
LESS FREQUENT WEIGHT UPDATING

Q: WHAT IF WE UPDATE LESS FREQUENTLY?

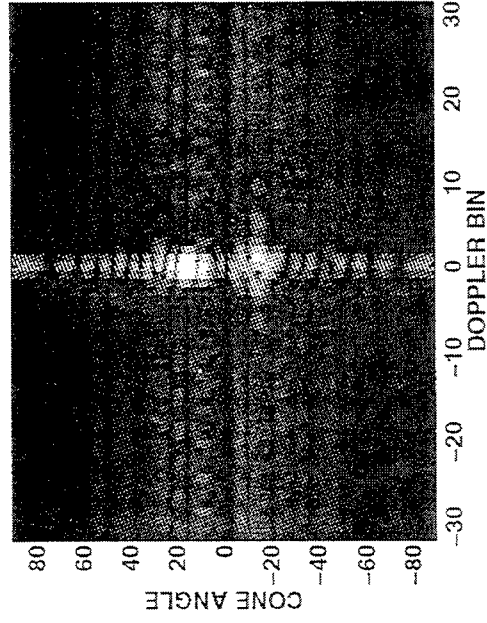
- E.G., WEIGHTS UPDATED ONLY ON PULSES {0, PRF/f₀, ... M} ==> "SAMPLE & HOLD"

A: ALIASING

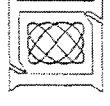
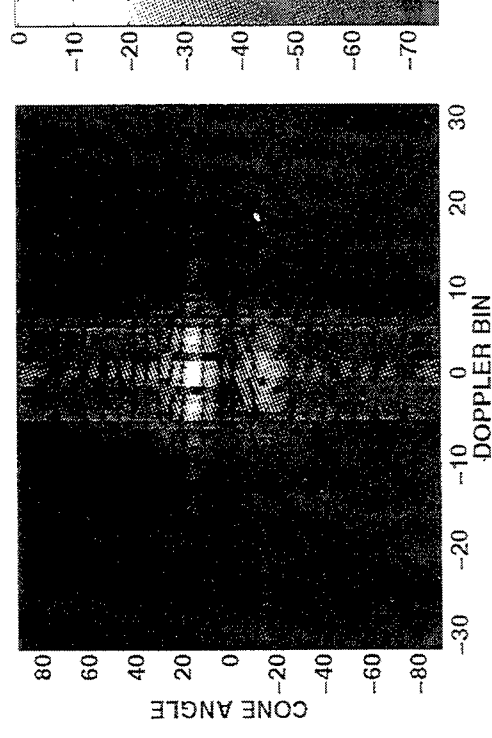
- MODULATED SIGNAL COMPONENTS WHICH ARE OUTSIDE $\pm .5f_0$ WILL ALIAS.
 - MUST FULLY CANCEL MONO-CLUTTER WITHIN SAME SUBCPI TO PREVENT IT FROM ALIASING (E.G., PRE-DOPPLER STAP)
- ALIASED COMPONENTS HAVE A SINC ENVELOPE



UNTAPERED SUBCPIs

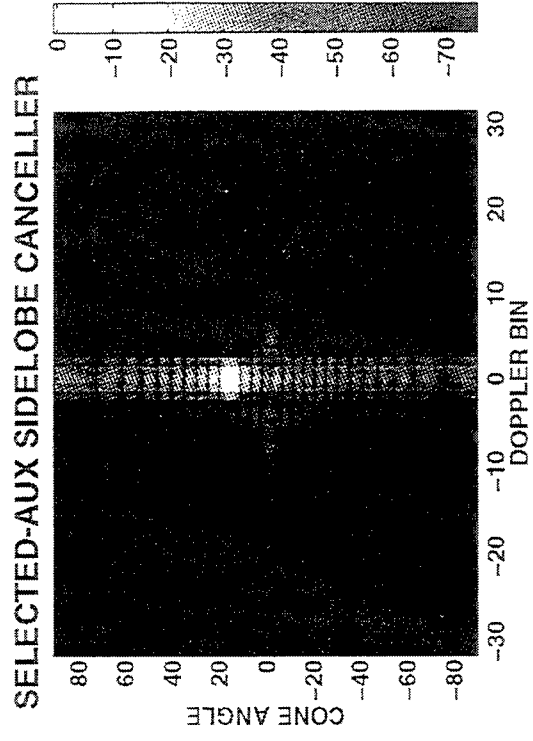
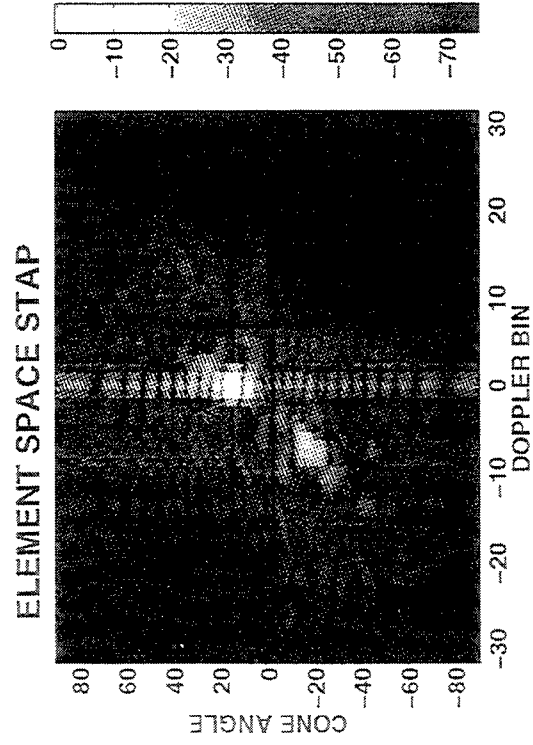
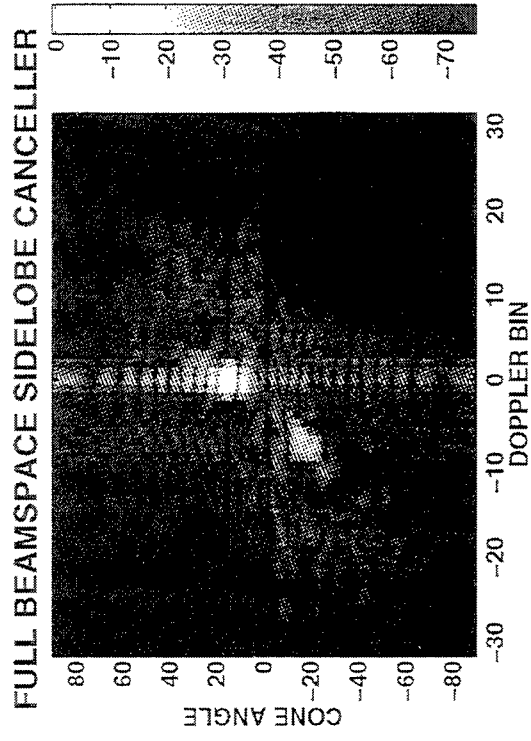


TAPERED SUBCPIs

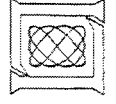


... EFFECT OF TAPER ON SUBSEQUENT STAP ???

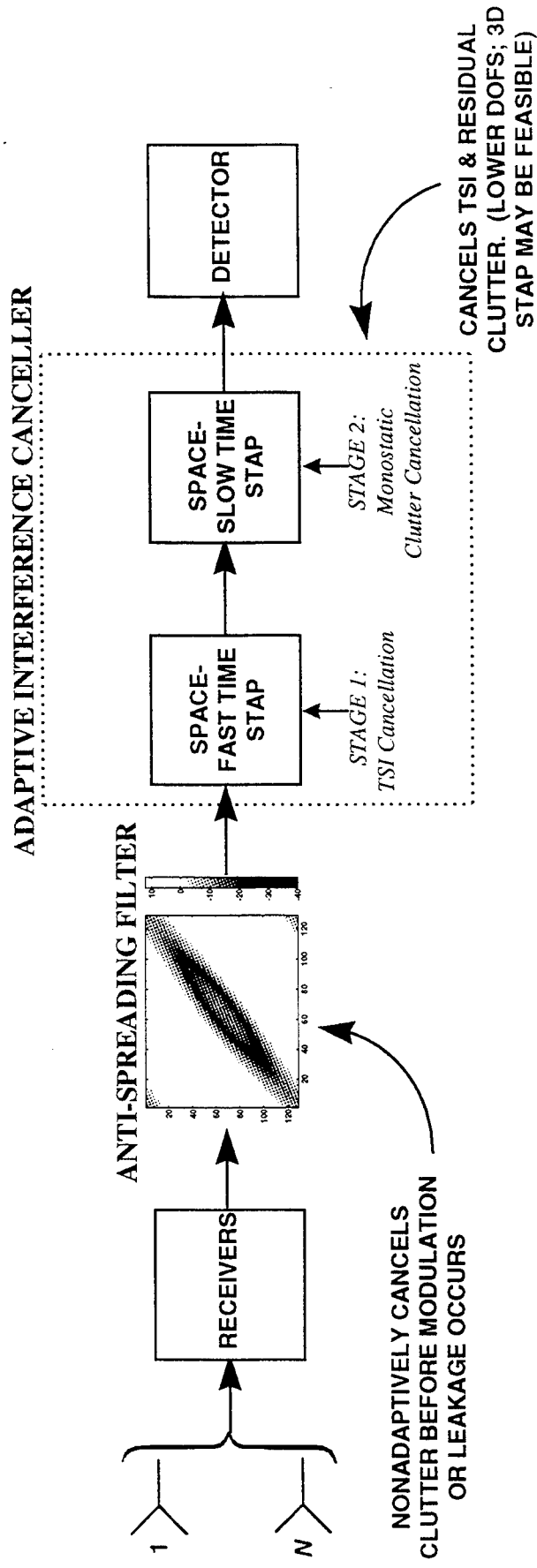
COMPARISON OF CANDIDATE ARCHITECTURES



USING A PARTIAL BEAMSPACE HELPS CONTROL MODULATIONS



NONADAPTIVE “ANTI-SPREADING” FILTERS

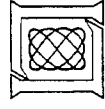


• TSI ARCHITECTURES WITH FULL SPATIAL ADAPTIVITY:

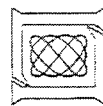
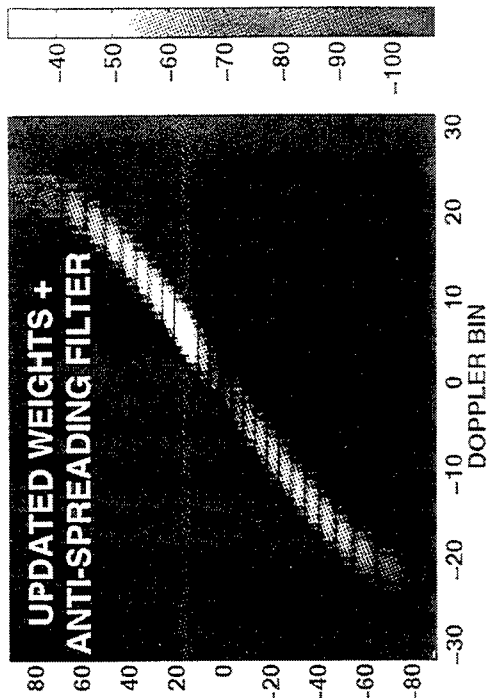
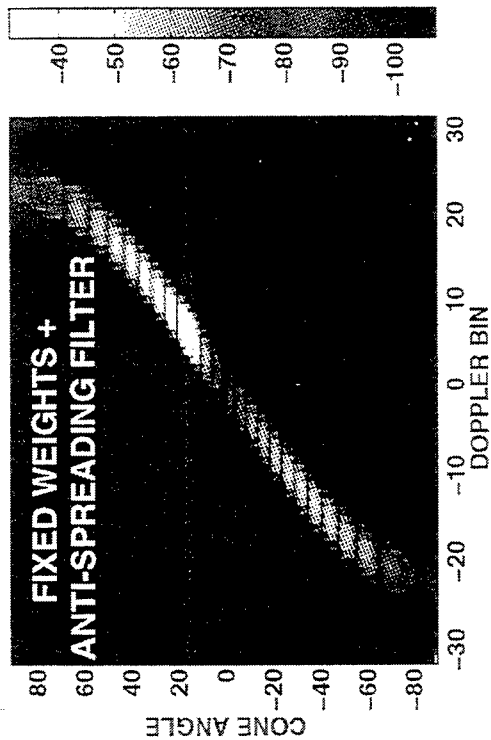
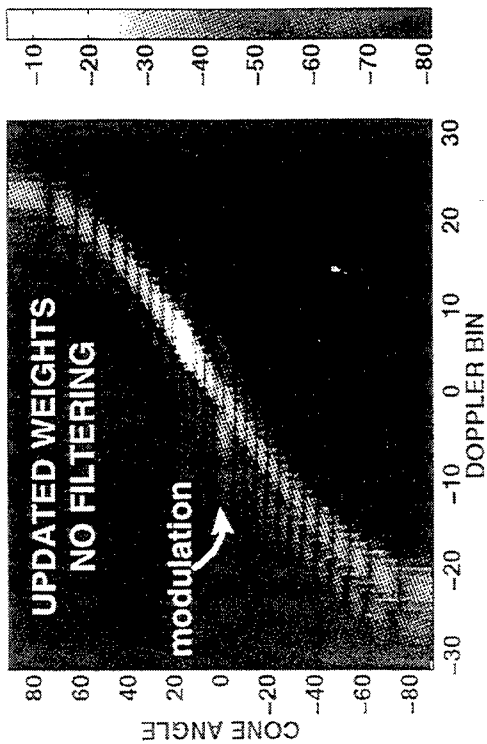
- MODULATIONS AT MANY ANGLES
- USE 2D FIR FILTER
 - E.G. ELLIPTIC FILTERS (McCielllan 96)
 - WIDEN NOTCH VIA CASCADED CONCENTRIC ELLIPTICAL FILTERS
 - USE TRANSMIT PATTERN AS A WEIGHTING IN THE FILTER DESIGN

• TSI ARCHITECTURES WITH PARTIAL SPATIAL ADAPTIVITY (CSLC):

- MODULATIONS AT SELECT ANGLES
- SEVERAL ALGORITHM CHOICES ...
 - 2D FIR NOTCH FILTERS
 - SPATIAL-ONLY FILTERS



PERFORMANCE OF ANTI-SPREADING FILTER

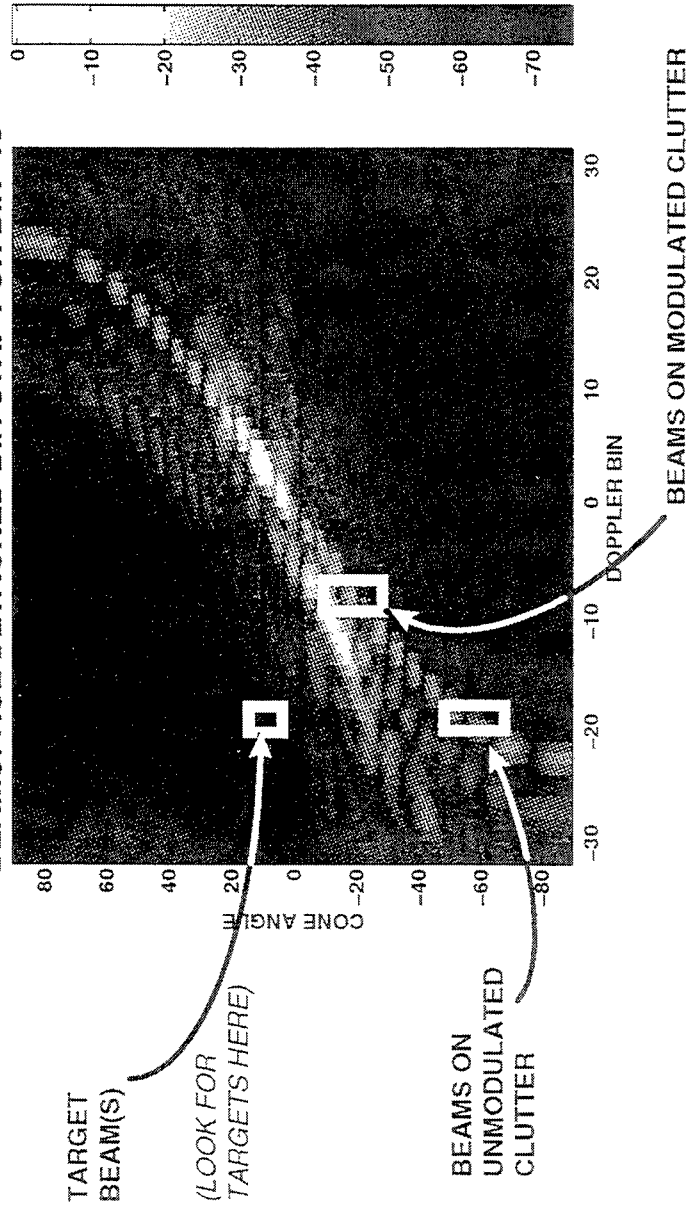


ANTI-SPREADING FILTER REDUCES
MODULATED CLUTTER

REVISED STAP STRATEGIES

- OBJECTIVE: DIMENSION REDUCING TRANSFORMS WHICH "CAPTURE" MODULATED CLUTTER IN THE COVARIANCE MATRIX
 - PROBLEM: MODULATED CLUTTER VARIES FROM BEAM TO BEAM
- SOME APPROACHES ...
 - EIGEN NULLING
 - BEAMSPACE "DETACHED" BIN STAP
 - USES BEAMS POINTED AT THE CLUTTER PRESENT IN TARGET'S BEAM/BIN (BUT NOT NECESSARILY FROM NEAR THE TARGET'S BIN)

BEAMSPACE DETACHED BIN STAP FOR BIN -18

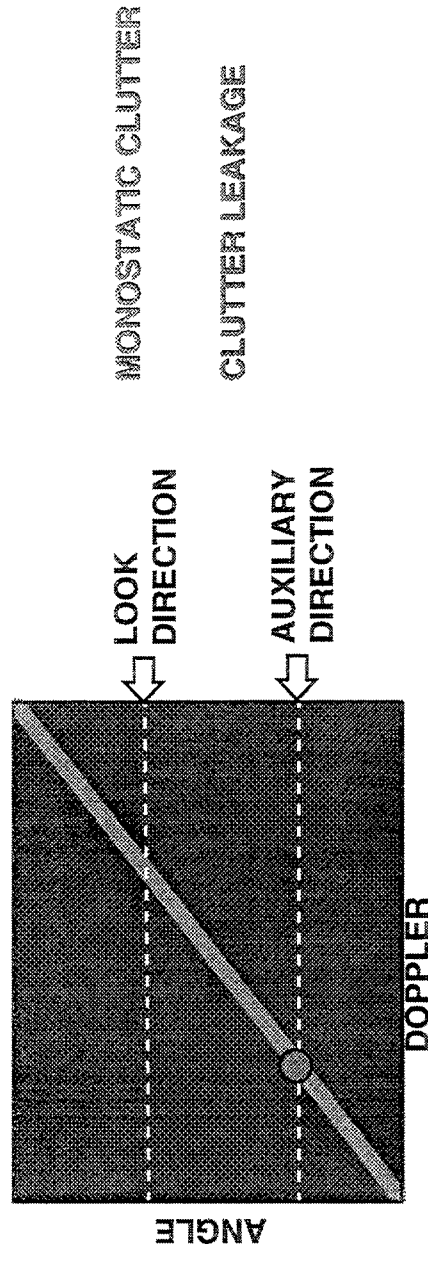


OUTLINE

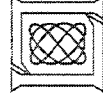
- INTRODUCTION/ PROBLEM STATEMENT
- RANDOM SIGNAL MODULATION
- COHERENCE INDUCED MODULATION



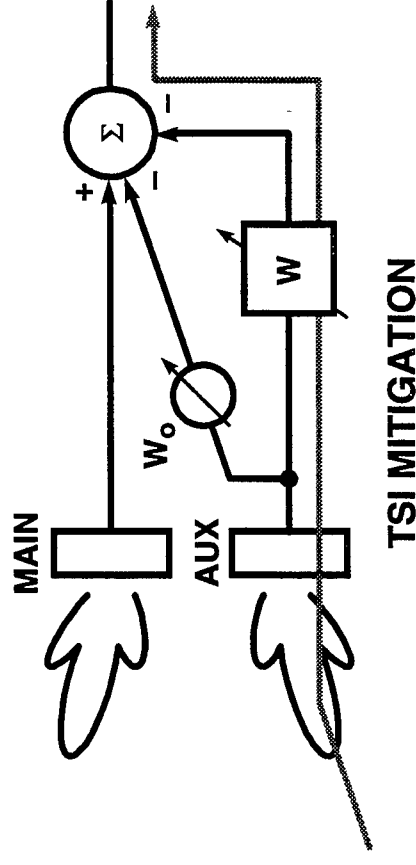
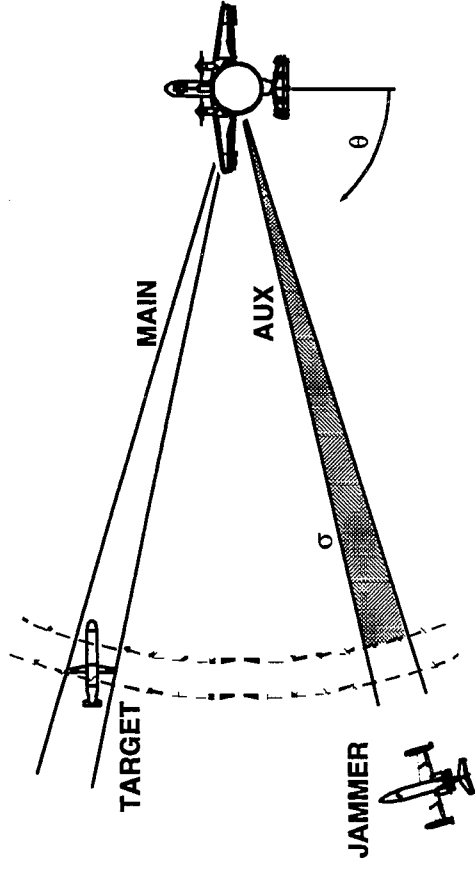
- **SIDELobe CANCELLER CLUTTER LEAKAGE**
 - MODEL
 - WHAT CAN WE DO ABOUT IT?



- CONCLUSIONS

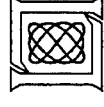


SIDELOBE CANCELLER CLUTTER LEAKAGE



- FOR SIDELOBE CANCELLERS, CLUTTER FROM AUX BEAM “LEAKS” INTO MAIN BEAM

- FIXED SLC WEIGHTS ==> “CLUTTER LEAKAGE”
 - GABEL RL-TIM 96
- UPDATED SLC WEIGHTS ==> SPECIAL CASE OF MODULATION
 - THE “LEAKAGE” IS MODULATED



LEAKAGE CONTROL

- PROBLEM: LARGE WEIGHTS IN LEAKAGE PATH ALLOW CLUTTER TO PASS FROM AUX BEAM TO MAIN BEAM
- METHODS OF CONTROL ...

1. GET MAXIMUM INTERFERENCE POWER IN AUX BEAM
2. CONSTRAINED FILTER DESIGN: $\min_{\mathbf{w}} E\left\{\left|\mathbf{t}_{main}^H \mathbf{x} - \mathbf{w}^H \mathbf{T}_{aux}^H \mathbf{x}\right|^2\right\}$ subject to $|w_i| \leq \xi$

Penalty Function Approach:

$$\min_{\mathbf{w}} E\left\{\left|\mathbf{t}_{main}^H \mathbf{x} - \mathbf{w}^H \mathbf{T}_{aux}^H \mathbf{x}\right|^2 + c\|\mathbf{w}\|^2\right\}$$

$$\min_{\mathbf{w}} \left\{ \mathbf{w}^H \mathbf{T}_{aux}^H \mathbf{R} \mathbf{t}_{main} + \mathbf{t}_{main}^H \mathbf{R} \mathbf{T}_{aux} \mathbf{w} + \mathbf{w}^H (\mathbf{T}_{aux}^H \mathbf{R} \mathbf{T}_{aux} + c\mathbf{I}) \mathbf{w} \right\}$$

$$\mathbf{w} = (\mathbf{T}_{aux}^H \mathbf{R} \mathbf{T}_{aux} + c\mathbf{I})^{-1} \mathbf{T}_{aux}^H \mathbf{R} \mathbf{t}_{main}$$

Beamspace Aux.
Correlation Matrix

Beamspace Cross
Correlation Vector

Penalty Term ...

N.b. This is NOT Diagonal Loading!

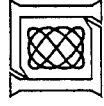
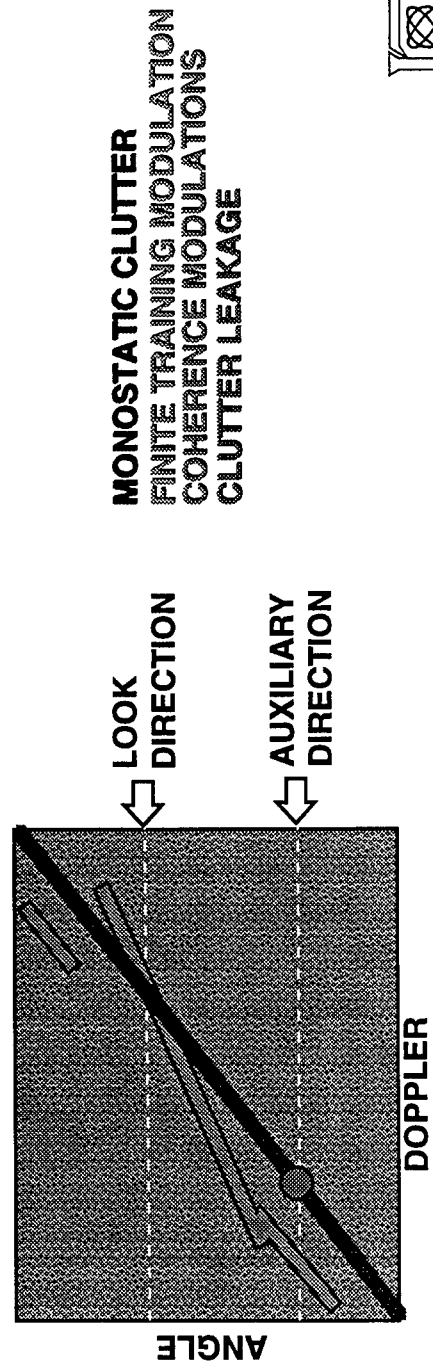


OUTLINE

- INTRODUCTION
- RANDOM SIGNAL MODULATION
- COHERENCE INDUCED MODULATION
- SIDELobe CANCELLER CLUTTER LEAKAGE

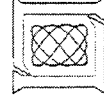
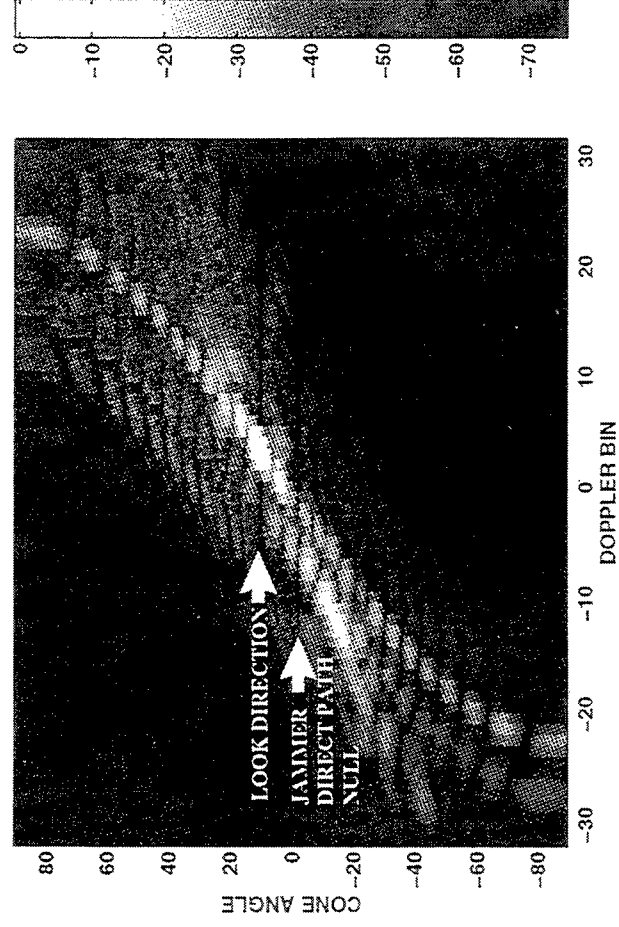


- CONCLUSIONS



CONCLUSION

- **BAD THINGS HAPPEN WHEN TSI WEIGHTS ARE UPDATED ...**
 - CLUTTER AND SIGNALS ARE MODULATED
 - SMALLER VISIBLE REGION
 - SIDELobe TARGETS ARE A BIGGER PROBLEM
- **PROGRESS HAS BEEN MADE ...**
 - PHENOMENOLOGY IS UNDERSTOOD
 - EFFECT ON SEVERAL TSI ARCHITECTURES IS QUANTIFIED
 - POTENTIAL SOLUTIONS IDENTIFIED => RESULTS PROMISING!



PROBLEMS ... SOLUTIONS?

PROBLEM	TSI MITIGATION	EFFECT	SOME OPTIONS
LEAKAGE	SIDELOBE CANCELLER	BLIND DOPPLERS	- CAREFUL BEAM SELECTION - FILTER CONSTRAINTS
RANDOM MODULATIONS	RAPID WEIGHT UPDATING	DEGRADED SIDELOBES	- "BIGGER" TRAINING SET - FILTER CONSTRAINTS
COHERENCE MODULATIONS	RAPID WEIGHT UPDATING	MODULATED CLUTTER RIDGE	- PARTIAL BEAMSPACE - ANTI-SPREADING FILTER



On the Use of Terrain Scattered Interference for Mainbeam Jammer Suppression

Stephen M. Kogon and E. Jeff Holder

Georgia Tech Research Institute
Georgia Institute of Technology
Atlanta, GA 30332-0800

Douglas B. Williams

Georgia Institute of Technology, School of ECE
Atlanta, GA 30332-0250

Abstract The presence of jammers within the mainbeam of a radar receiver presents a particularly challenging adaptive processing problem. In some instances, the interference can still be mitigated via null steering, provided the target and the jamming source do not share the same azimuth angle. However, when the angular separation of the target and the jammer becomes too small, the two are essentially spatially colocated. In this case, spatial nulling techniques will cancel the target in their attempt to suppress the jammer. The current approach to this problem is a technique known as "burn-through," which exploits the temporal coherence of target returns by integrating over long periods of time. This coherent integration increases the target signal-to-noise ratio, while the jammer does not experience this gain since it lacks temporal correlation. However, large pulse lengths increase the occupancy of the radar resource period and, as a result, decrease the number of targets the radar can track. In addition, in airborne systems the maximum pulse repetition frequency the radar is able to support is reduced, creating possible velocity ambiguities. We propose the use of space-time adaptive processing (STAP) methods to combat the mainbeam jammer problem. Typically, the jammer transmitter has a broad transmit beam with high sidelobe levels. As a result, the jammer signal is transmitted over large angular regions which can produce terrain reflections. These potential multipath signals are incident on the radar receiver and can be exploited to achieve mainbeam jammer suppression while maintaining gain on the target. Even modest suppression decreases the pulse length required for burn-through. The proposed strategy is the converse of that used for terrain scattered interference (TSI) mitigation, which uses the jammer direct-path signal to remove TSI. Target extraction results with a mainbeam jammer are presented with experimental data collected as part of the DARPA/Navy Mountaintop program.

ON THE USE OF TERRAIN SCATTERED INTERFERENCE FOR MAINBEAM JAMMER SUPPRESSION

**STEPHEN KOGON AND JEFF HOLDER
GEORGIA TECH RESEARCH INSTITUTE**

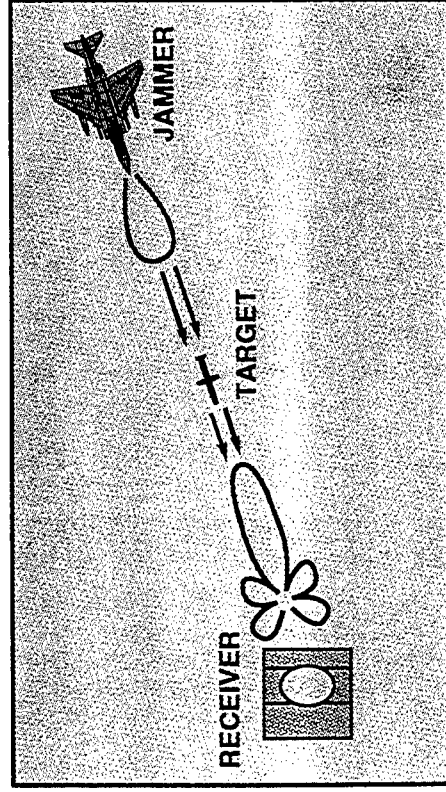
**DOUGLAS WILLIAMS
GEORGIA TECH, SCHOOL OF ECE**

OUTLINE

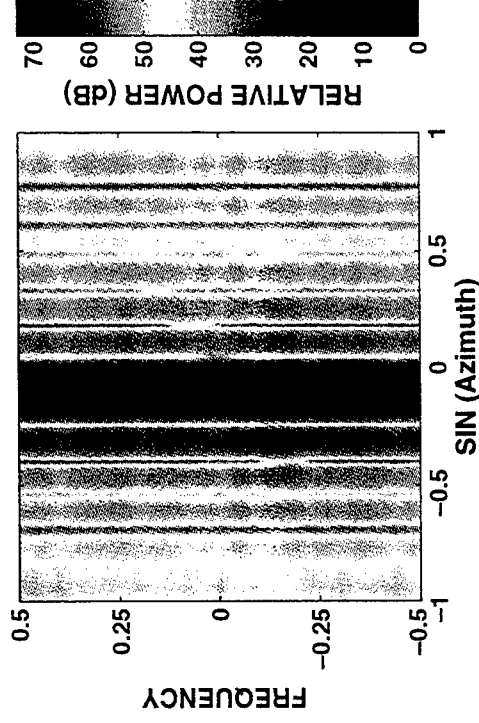
- **MAINBEAM JAMMER INTERFERENCE**
- **SUPPRESSION USING FULLY ADAPTIVE STAP**
- **MOUNTAINTOP EXPERIMENTAL RESULTS**
- **SUMMARY**

PROBLEM STATEMENT

SCENARIO



SPACE-TIME POWER SPECTRUM

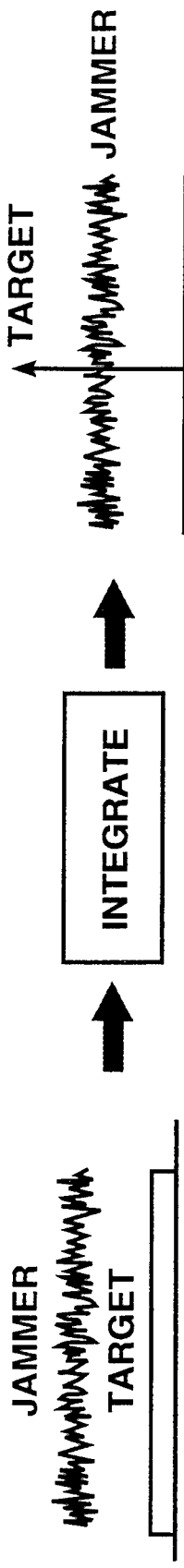


- JAMMER AND TARGET ARE ESSENTIALLY CO-LOCATED
(Separation < Beamwidth / 10)
- ADAPTIVE SPATIAL NULLING IN MAINBEAM IS NOT POSSIBLE

GOAL: LOOK DIRECTLY INTO JAMMER TO EXTRACT
POTENTIAL TARGETS

BURN-THROUGH METHODS

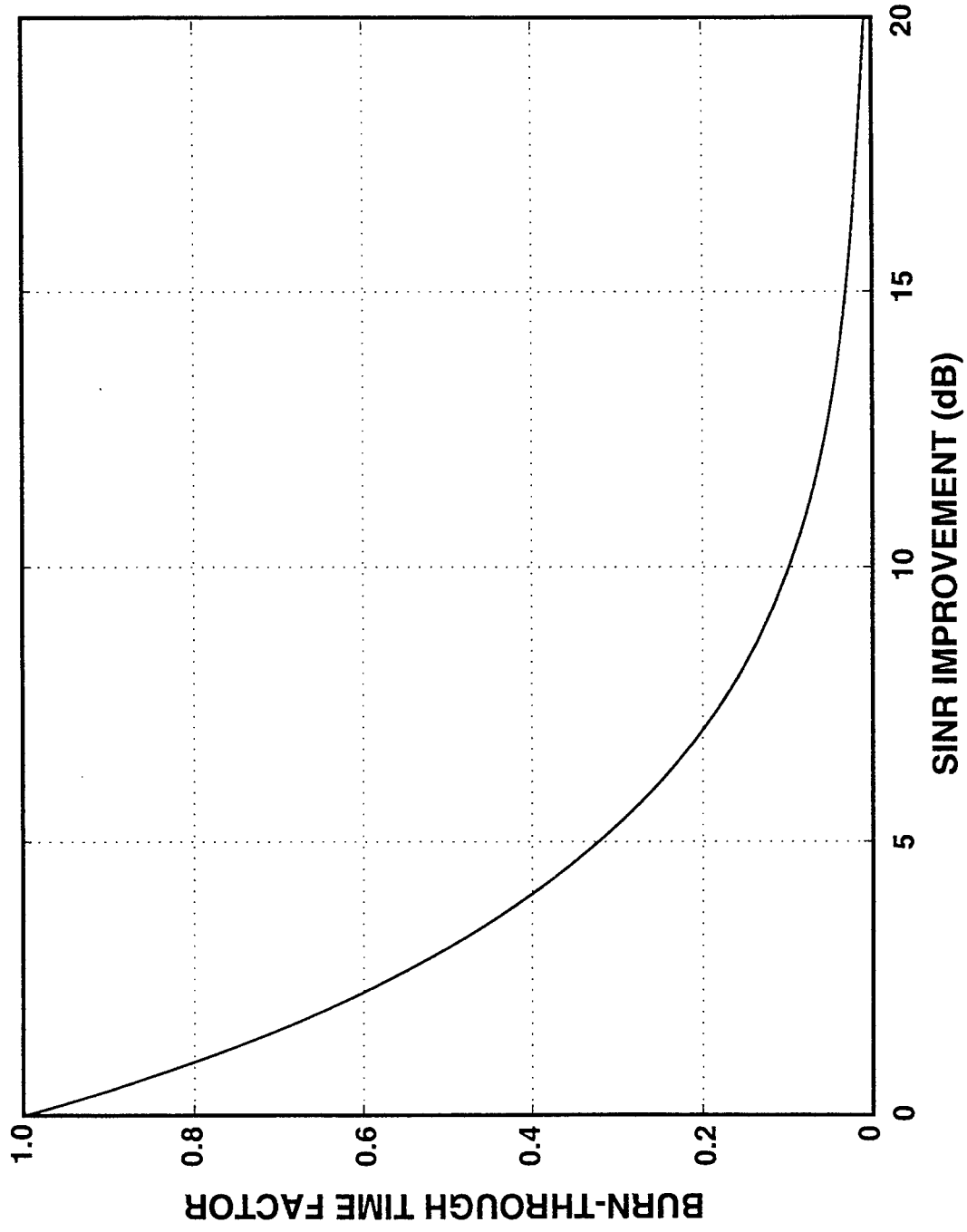
- CONCEDE PRESENCE OF A MAINBEAM JAMMER (No Mitigation)
- USE LARGE DURATION RADAR SIGNAL AND TEMPORALLY INTEGRATE TARGET RETURNS TO IMPROVE OVERALL SINR



DRAWBACKS

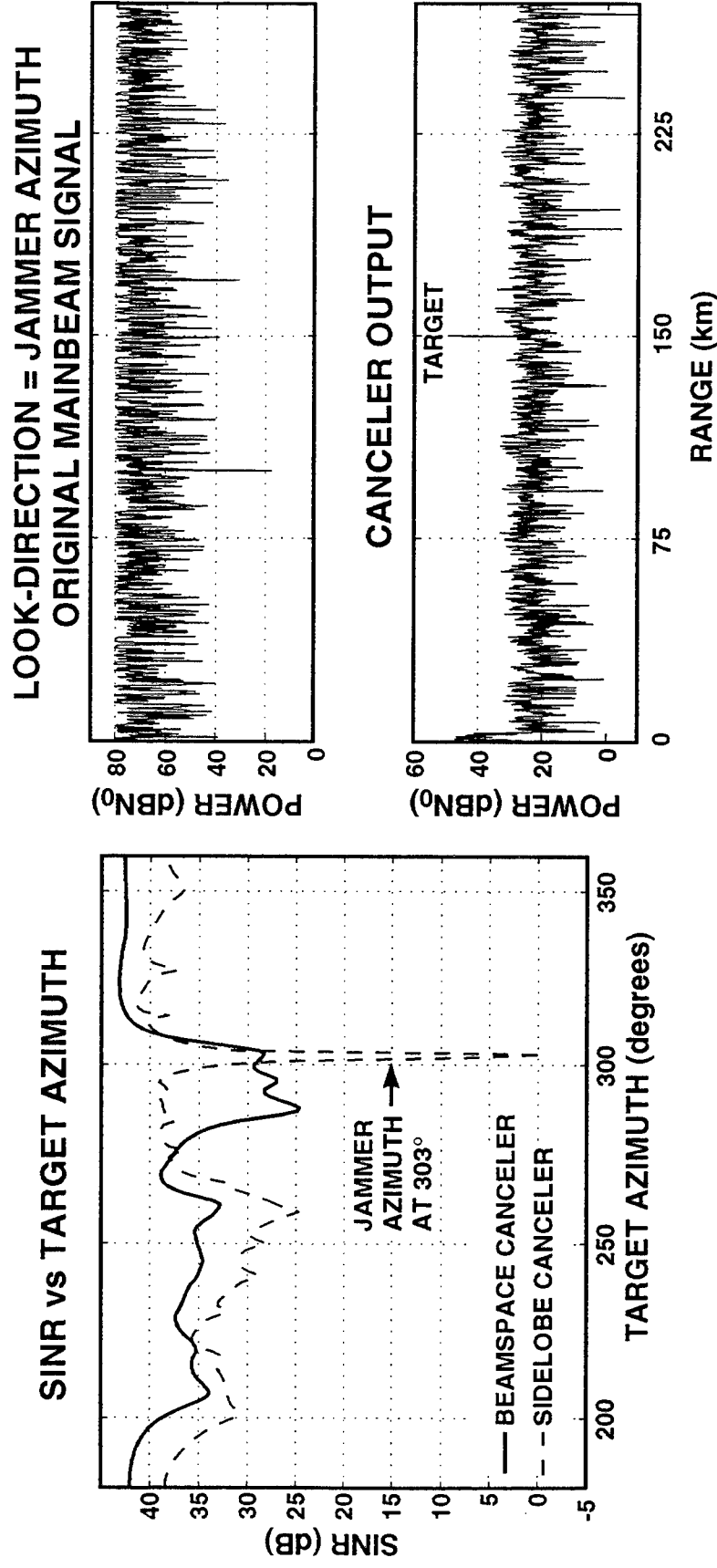
- DECREASED NUMBER OF SURVEILLANCE SECTORS AND/OR TARGET TRACKS
- DECREASED MINIMUM DETECTABLE VELOCITY FOR AIRBORNE SYSTEMS

BURN-THROUGH TIME SAVINGS



- INTERFERENCE SUPPRESSION PROVIDES SUBSTANTIAL BURN-THROUGH SAVINGS

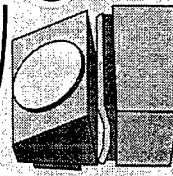
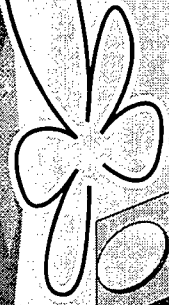
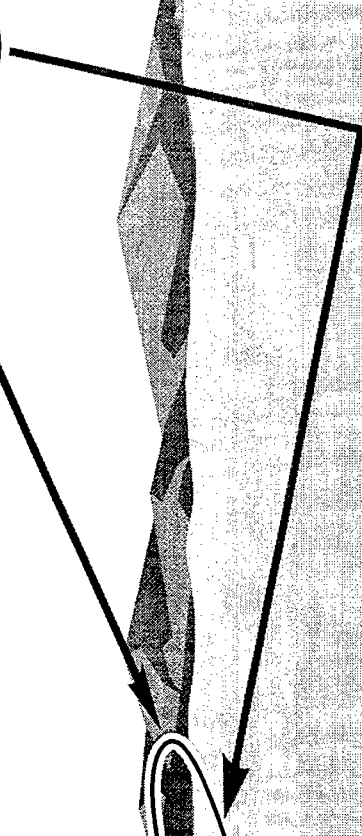
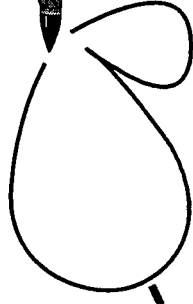
TSI MITIGATION FROM ASAP '96



- DEMONSTRATED THE ABILITY OF STAP TO EXTRACT TARGETS, EVEN AT THE JAMMER DIRECT-PATH AZIMUTH (i.e. Mainbeam Jammer)

SPACE-TIME CANCELLATION: THE CONCEPT

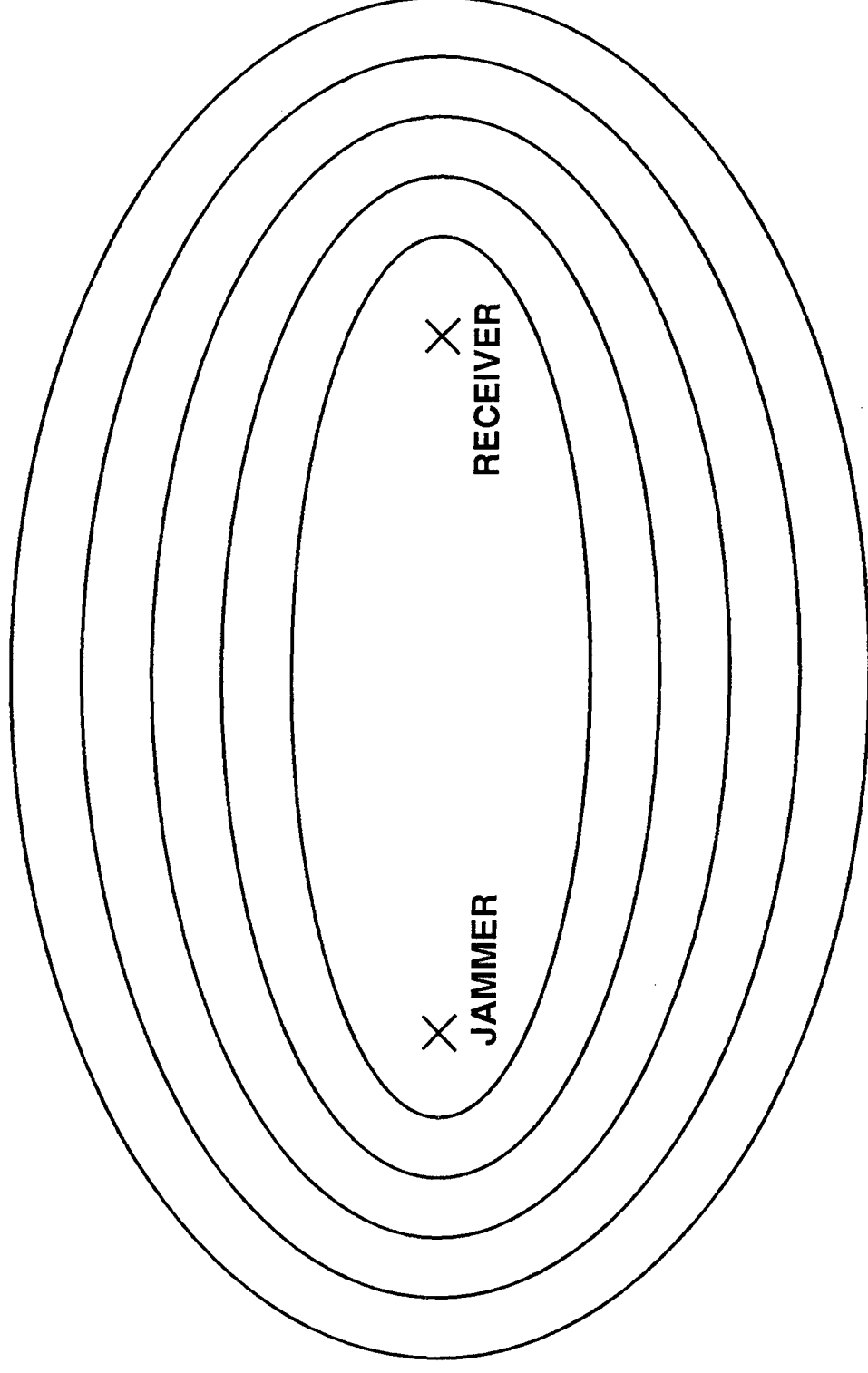
MAINBEAM
JAMMER



RECEIVER

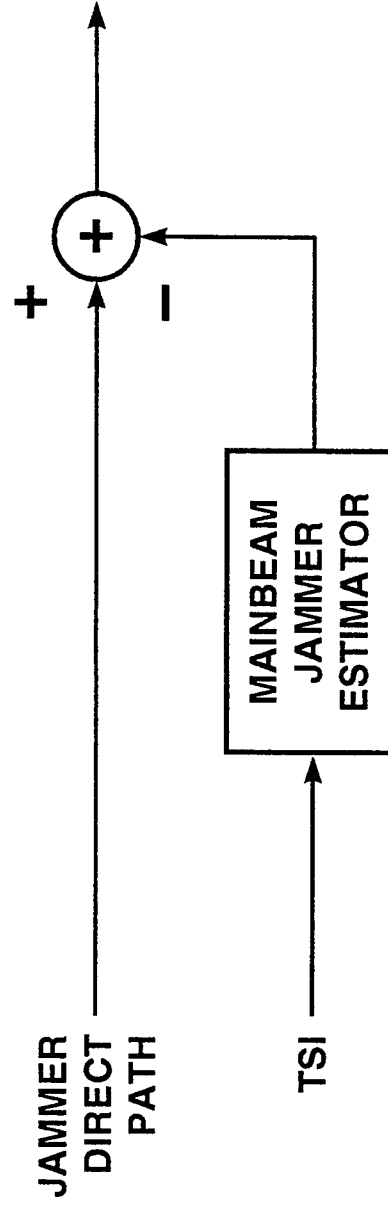
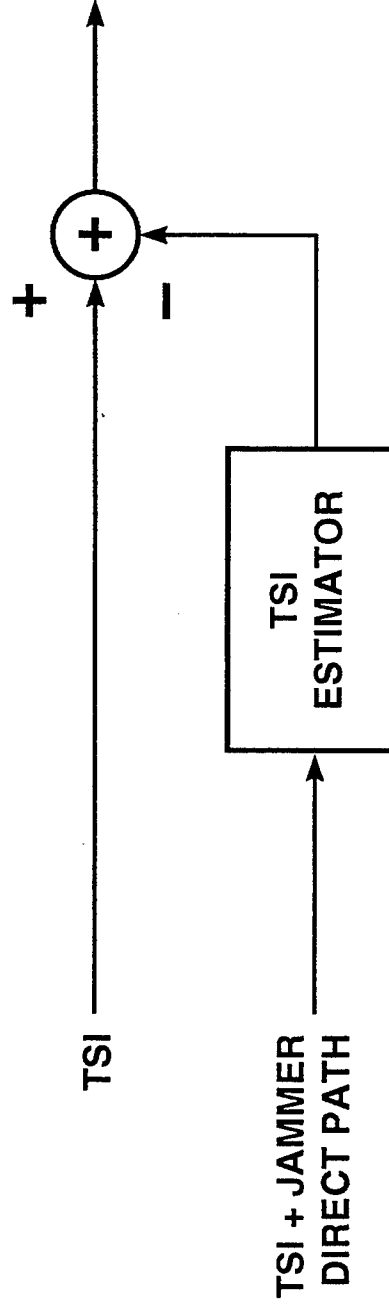
- JAMMER TRANSMITS WITH LARGE MAINLOBE AND HIGH SIDELOBES
- DIFFERENT DELAYS FROM JAMMER TO RECEIVER FOR JAMMER DIRECT-PATH AND MULTIPATH SIGNALS
- JAMMER MULTIPATH MADE UP OF MANY REFLECTIONS, ALL WITH DIFFERENT DELAYS TO THE RECEIVER

COHERENCE THROUGH MULTIPATH



- **RADAR RECEIVER BANDWIDTH RESULTS IN COHERENT INTERFERENCE AT VARIOUS TAPPED DELAYS (Within Bistatic Iso-Delay Contours)**

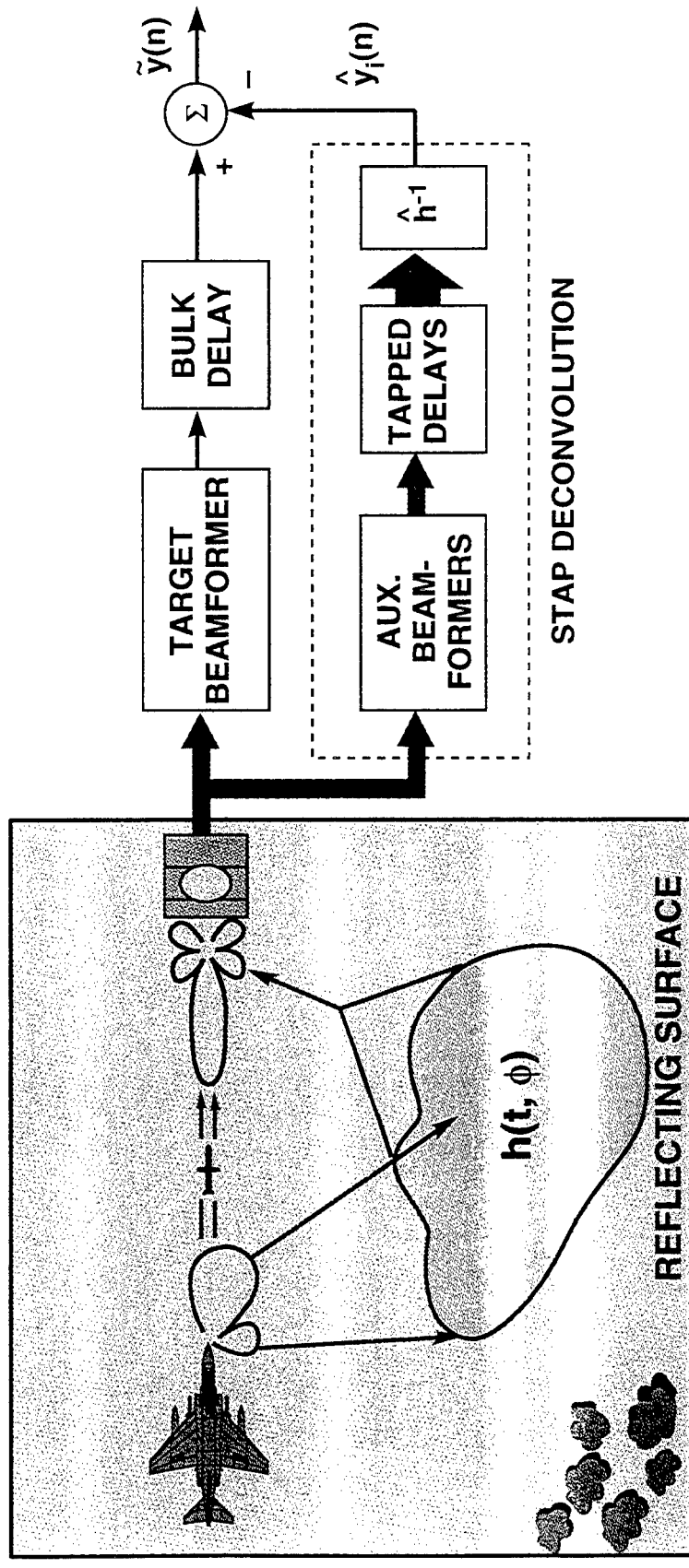
DUAL TO TSI MITIGATION



- DIRECT-PATH AND TSI ARE COHERENT (Same Source)

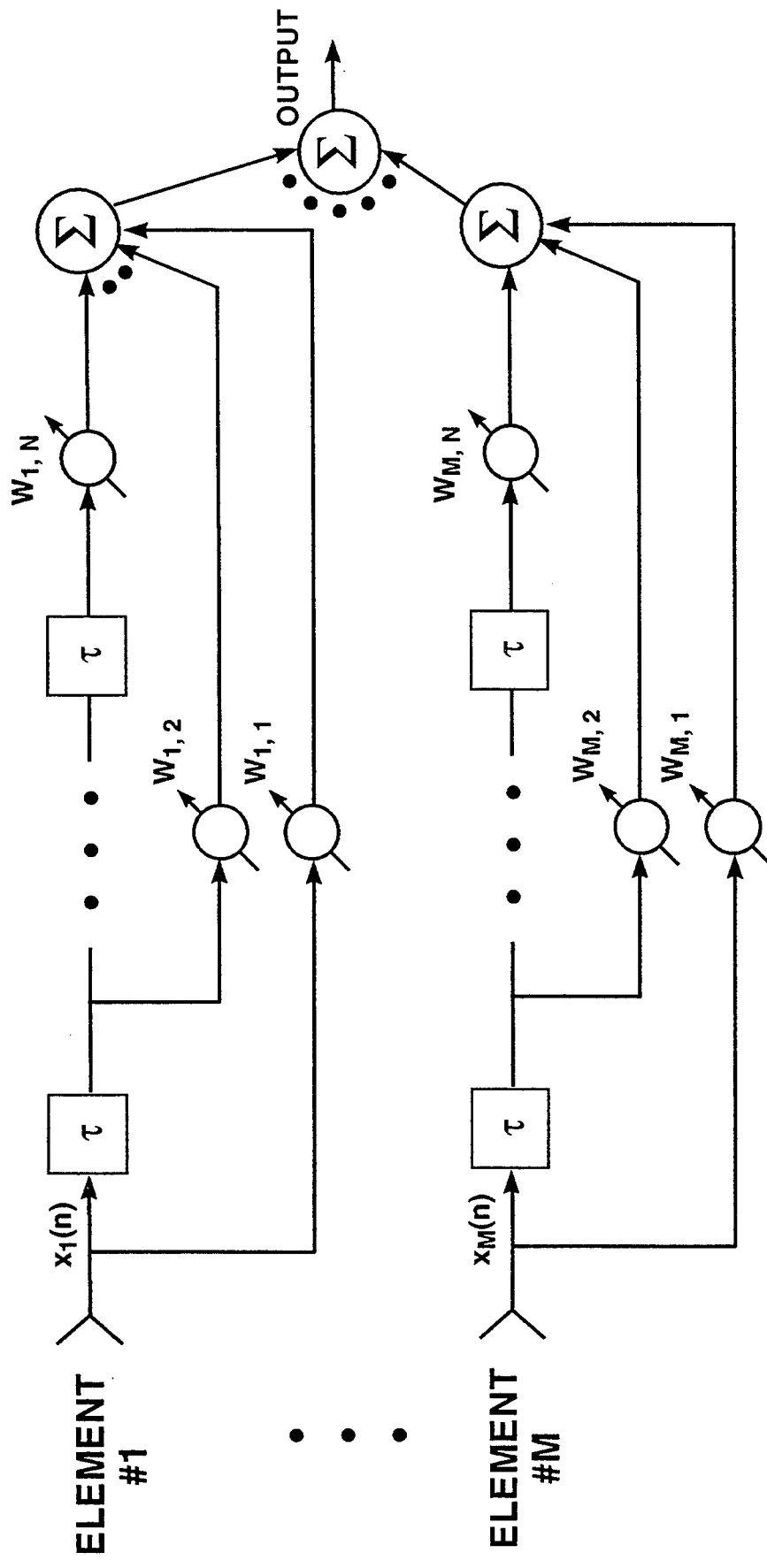
- EXPLOIT COHERENCE FOR CANCELLATION

MAINBEAM JAMMER CANCELLATION



- EXPLOIT JAMMER MULTIPATH REFLECTIONS USING AUXILIARY BEAMS
- ESTIMATE MAINBEAM JAMMER WITH ADAPTIVE DECONVOLUTION FILTER
- BULK DELAY AND TAPPED DELAY LINES COMPENSATE FOR DIFFERENCES IN PROPAGATION PATHS

CONSTRAINED ELEMENT SPACE ADAPTIVE CANCELER

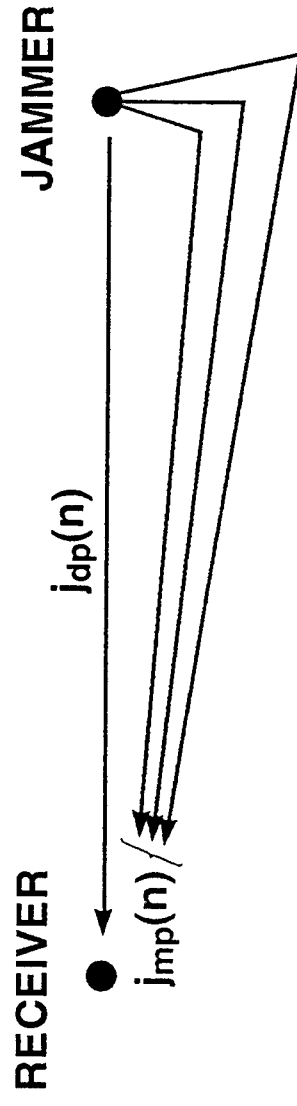


- LINEARLY CONSTRAINED MINIMUM VARIANCE (LCMV) ADAPTIVE WEIGHTS
- CONSTRAINTS:
 - DISTORTIONLESS RESPONSE IN LOOK-DIRECTION, LAG_N
 - ZERO RESPONSE IN LOOK-DIRECTION AT ALL OTHER LAGS

SIGNAL MODEL

• SPACE-TIME RETURNS

$$x(n) = \underbrace{j_{dp}(n)}_{\text{JAMMER DIRECT-PATH}} + \underbrace{j_{mp}(n)}_{\text{JAMMER MULTIPATH}} + \underbrace{e(n)}_{\text{THERMAL NOISE}}$$



• SPACE-TIME COVARIANCE MATRIX

$$R_x = \underbrace{v_i v_i^H}_{\text{JAMMER}} + \underbrace{I_{MN}}_{\text{THERMAL NOISE}}$$

$$v_i = \sum_k \alpha_k v_k$$

SPACE-TIME STEERING VECTORS \rightarrow \sum_k α_k v_k \leftarrow AMPLITUDES

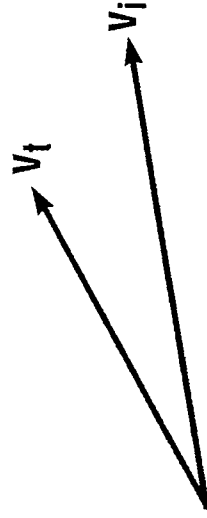
ADAPTIVE PROCESSING GAIN

$$\xi_{\zeta} = \frac{\text{SINR}_{\text{out}}}{\text{SINR}_{\text{in}}} \approx \underbrace{\text{JNR}_{\text{in}}}_{\substack{\uparrow \\ \text{DIRECT} \\ \text{PATH}}} \underbrace{\left(1 - \frac{|v_i^H v_t|^2}{v_i^H v_i} \right)}_{\substack{\text{SINR LOSS} \\ \text{TARGET SPACE-TIME STEERING VECTOR}}} \quad \text{OVERALL INTERFERENCE}$$

• $v_i \neq v_t \Rightarrow$ CANCELLATION

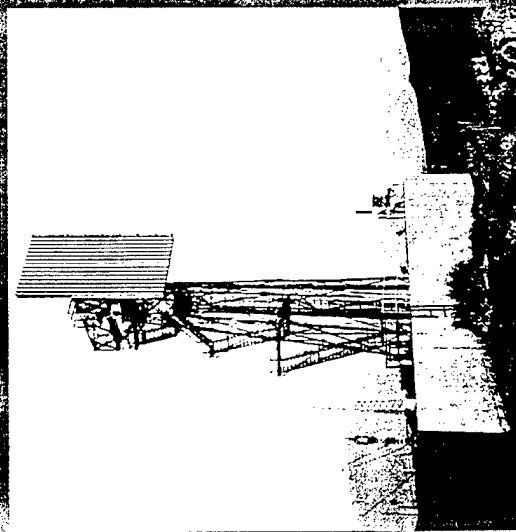
• $v_i = v_t \Rightarrow$ NO CANCELLATION
(Multipath Not Present)

• $v_i \perp v_t \Rightarrow$ COMPLETE CANCELLATION

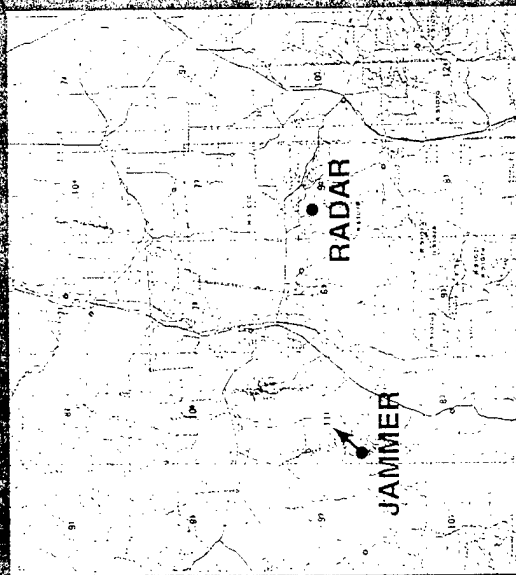


MOUNTAINTOP EXPERIMENT

(File = hot 6067v1 mat)



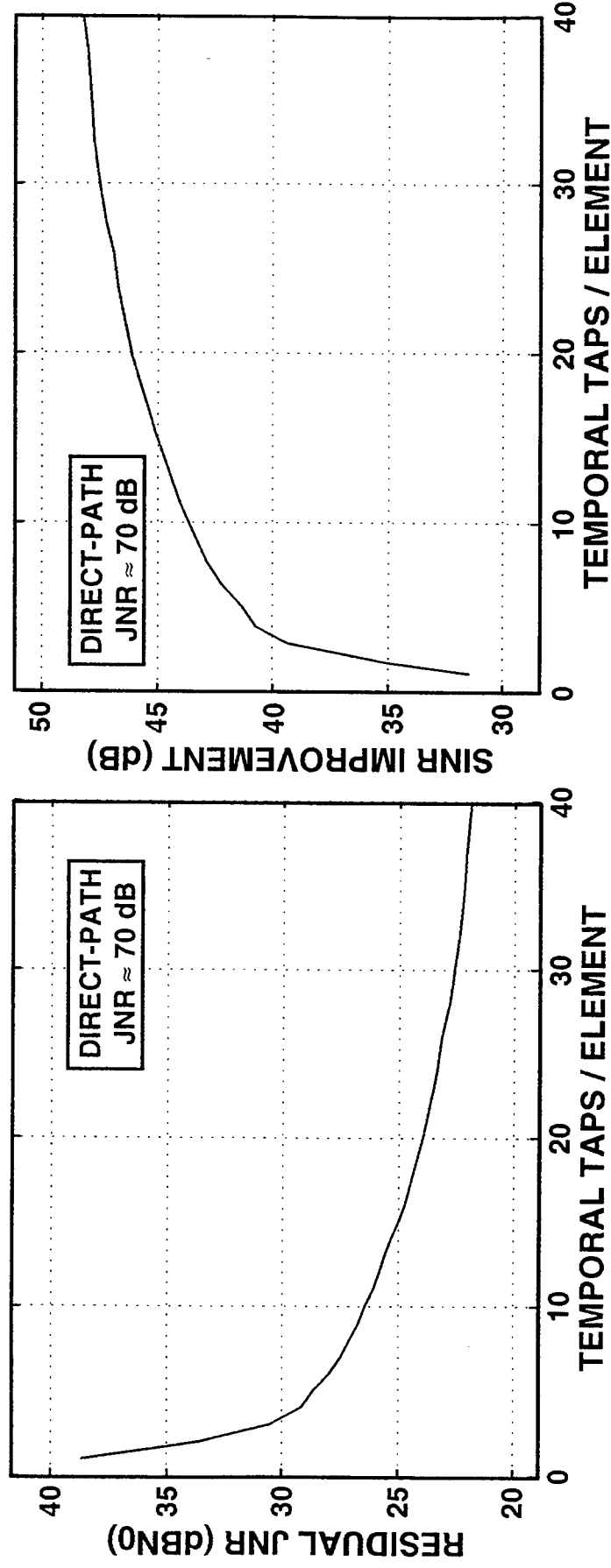
- 14 ELEMENT UNIFORM LINEAR ARRAY



- JAMMER AZIMUTH $\theta = 268^\circ$
- MAINBEAM JNRN₀ ≈ 70 dB
- MULTIPATH JNRN₀ ≈ 50 dB

300076-211

CANCELLATION PERFORMANCE MAINBEAM DIRECTLY AT JAMMER AZIMUTH

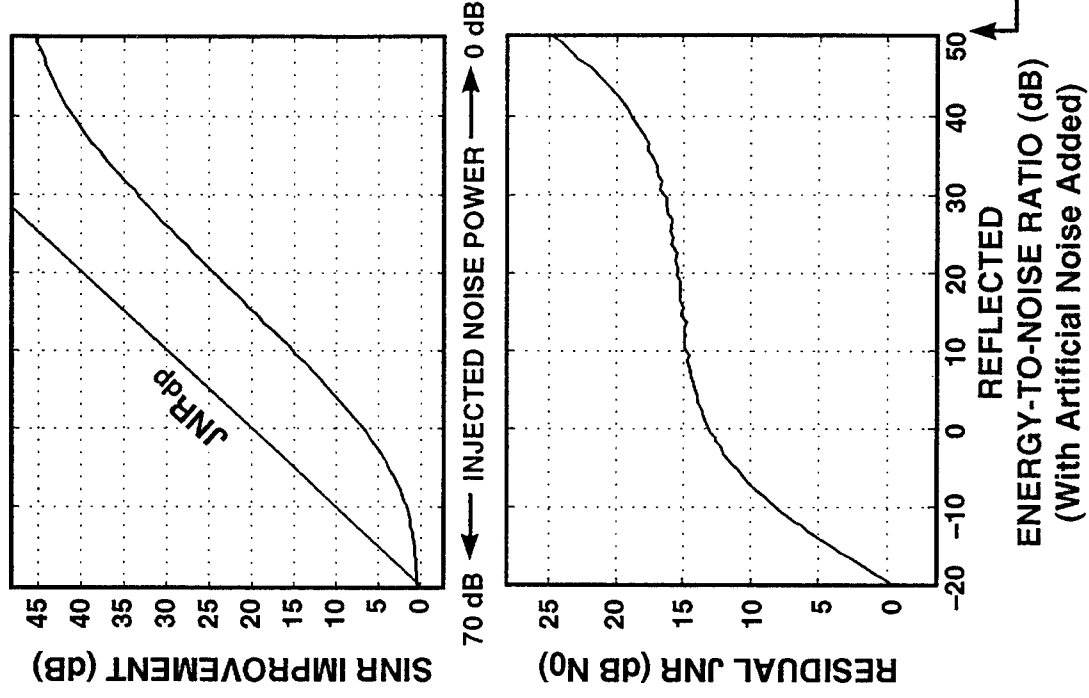
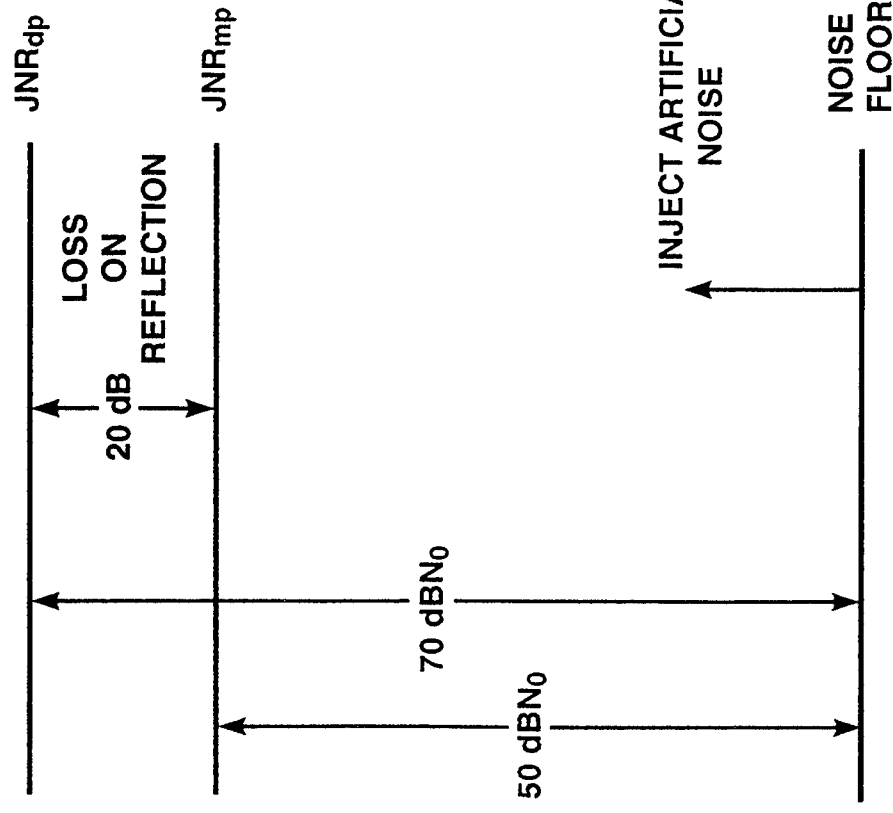


- SIGNIFICANT CANCELLATION POSSIBLE EVEN WITH ZERO DELAY
(1 Temporal Tap)

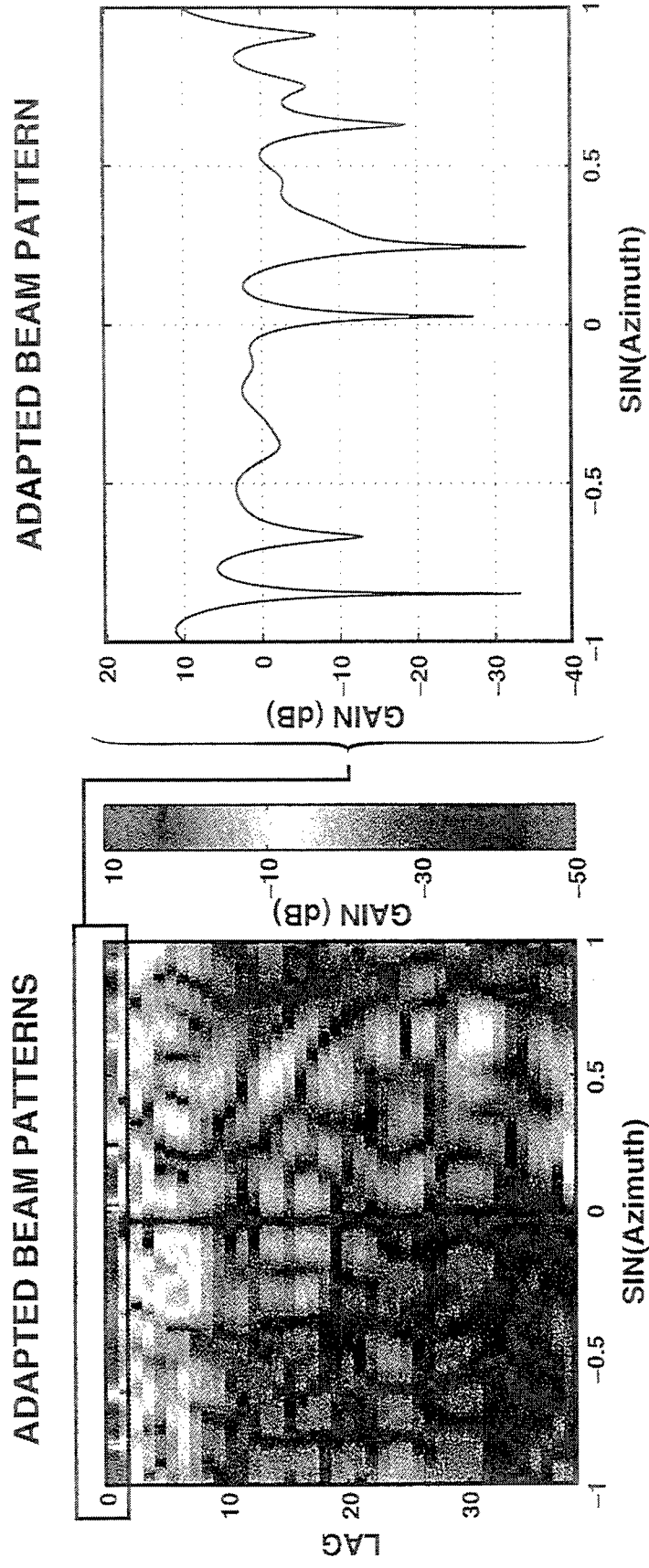
EXPERIMENTAL RESULTS

MULTIPATH REFLECTION POWER

- INJECT NOISE TO REDUCE EFFECTIVE REFLECTED ENERGY



CANCELER BEAM PATTERNS



- HIGH SIDELOBES DUE TO GAIN COMPENSATION FOR LOSS ON REFLECTION
- RESPONSE MAY RESULT IN ANGLE ACCURACY DEGRADATION
- USE PERIODIC FULL BURN-THROUGHS FOR REACQUISITION OF TARGET ANGLE

REDUCTION IN BURN-THROUGH TIMES

- MOUNTAINTOP DATA: (70 dB Direct-Path Jammer)

PROCESSING	SINR IMPROVEMENT	BURN-THROUGH TIME
NON-ADAPTIVE	0 dB	T_0
SPATIALLY ADAPTIVE (1 Temp. Tap)	32 dB	$\frac{T_0}{1600}$
STAP (20 Temp. Taps)	47 dB	$\frac{T_0}{50,000}$

➔ ADAPTIVE PROCESSING ALLOWS FOR SIGNIFICANT BURN-THROUGH TIME SAVINGS

SUMMARY

- **MAINBEAM JAMMER CANCELLATION WHILE MAINTAINING GAIN ON TARGET DEMONSTRATED WITH EXPERIMENTAL DATA**
- **CONSIDERABLE SAVINGS IN BURN-THROUGH TIMES AS A RESULT OF ADAPTIVE PROCESSING**
- **BURN-THROUGH TIME SAVINGS RESULTS IN:**
 - **REDUCTION IN RADAR RESOURCE OCCUPANCY**
 - **INCREASE IN NUMBER OF TARGET TRACKS POSSIBLE**

3-D Emitter Localization Using Out-of-Plane Multipath

Scott D. Coutts

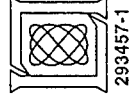
MIT Lincoln Laboratory
244 Wood Street
Lexington, MA 02173-9108
tel: (617) 981-5789
email: scoutts@ll.mit.edu

Abstract The ability to estimate the range, heading, and velocity of an airborne emitter by a single passive receiver using out-of-plane multipath was demonstrated at the 1996 ASAP Workshop. Progress on this topic has been made in several areas. First, the maximum likelihood estimator that is based on a homogeneous clutter assumption was expanded to include emitter altitude estimation. The Cramer-Rao lower bounds were determined and jammer localization results using Mountaintop data collected at White Sands Missile Test Range are presented. The second major area of progress is the design of an estimator based on an inhomogeneous clutter assumption. This approach uses correlation techniques to obtain time-difference-of-arrival (TDOA), and frequency-difference-of-arrival (FDOA) estimates for the emitter direct-path signal and the delayed and Doppler shifted replicas reflected by some number of dominant scatterers. The TDOA and FDOA estimates were combined with emitter and scatterer azimuth estimates to form a minimum-variance unbiased estimator of emitter location parameters. The covariance of the emitter parameter estimates was determined and localization results using Mountaintop field data are presented. Comparisons of both the inhomogeneous and the homogeneous estimation approaches are presented along with localization results from several Mountaintop jamming scenarios. Localization performance versus emitter power was studied by artificially increasing the noise floor of the Mountaintop data sets. Similarly, performance versus signal bandwidth was studied by using lowpass filters to reduce the bandwidth of the Mountaintop data. Pulsed and self-correlated emitter waveforms were also considered.

3-D EMITTER LOCALIZATION USING OUT-OF-PLANE MULTIPATH

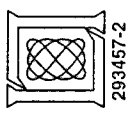
**SCOTT D. COUTTS
MIT LINCOLN LABORATORY**

13 MARCH 1997

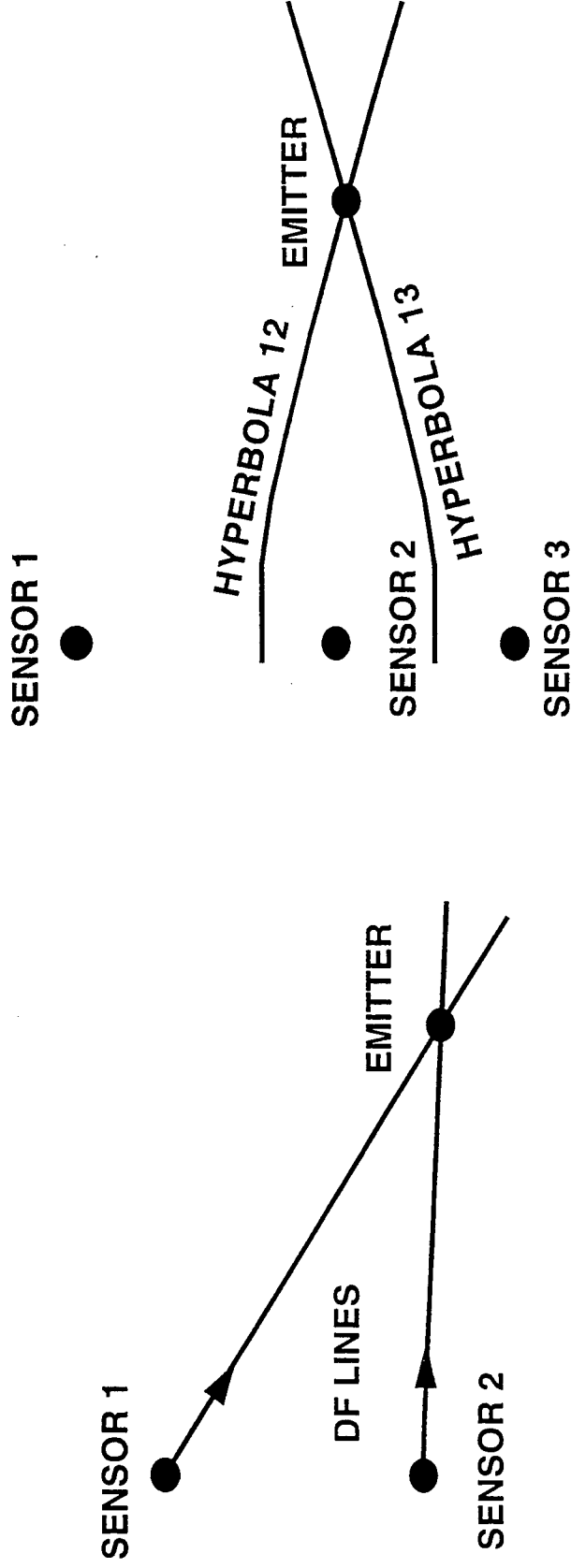


OUTLINE

- INTRODUCTION
- PROBLEM FORMULATION
- DEMONSTRATION USING MOUNTAINTOP FIELD DATA
- SUMMARY

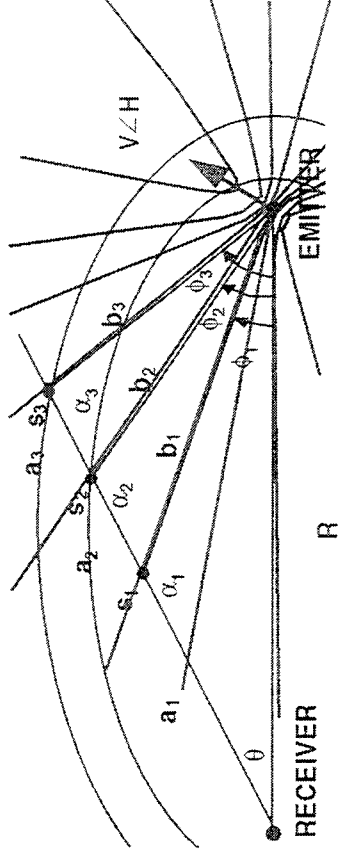
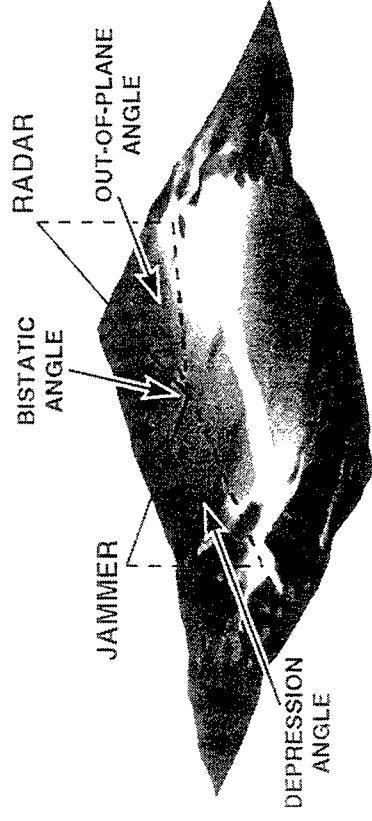


COMMON LOCALIZATION METHODS



- TRIANGULATION USING MULTIPLE SENSORS
 - SINGLE SENSOR CAN USE SEQUENTIAL ANGLE MEASUREMENTS
- TIME DIFFERENCE OF ARRIVAL (TDOA)
 - CROSS-CORRELATION USED TO ESTIMATE DIFFERENTIAL TIME DELAYS FOR WIDELY SPACED SENSORS
- OUT-OF-PLANE MULTIPATH IS A SINGLE-SENSOR TECHNIQUE

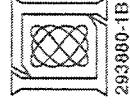
LOCALIZATION USING OUT-OF-PLANE MULTIPATH



- (Measure Emitter Azimuth)
- EACH SCATTERING POINT s_i DEFINES A TRIANGLE
- MEASURE ANGLE ϕ_i AND DELAY $D_i = a_i + b_i - R$ AND RELATIVE DOPPLER ω_i
- ANGLE ϕ_i IS RELATED TO DOPPLER ω_i
 - TWO ANGLES AND DELAY D_i SOLVE TRIANGLE
- MINIMUM OF 3 SCATTERERS REQUIRED TO ESTIMATE 3 EMITTER PARAMETERS (R, H, V)

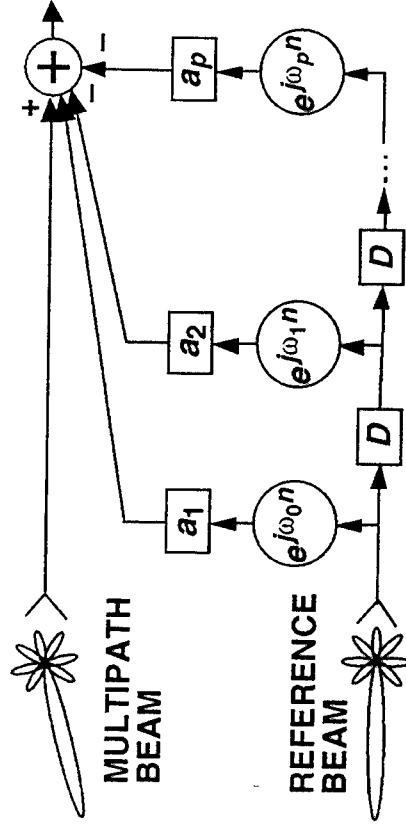
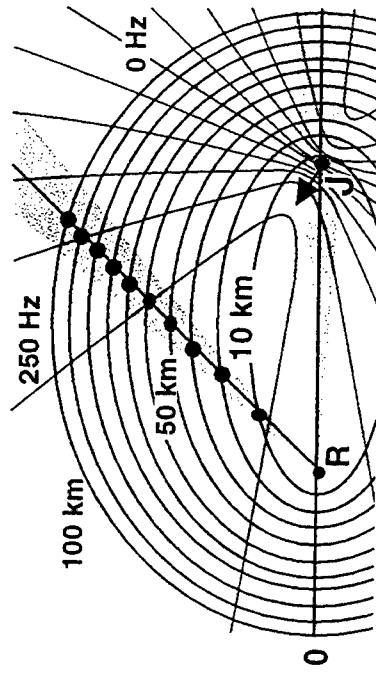
OUTLINE

- INTRODUCTION
- PROBLEM FORMULATION
 - PARAMETER ESTIMATION MODELS FOR HOMOGENEOUS AND INHOMOGENEOUS CLUTTER
 - ALTITUDE ESTIMATION
 - STATISTICAL FORMULATION FOR INHOMOGENEOUS CLUTTER
- DEMONSTRATIONS USING MOUNTAINTOP FIELD DATA
- SUMMARY



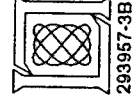
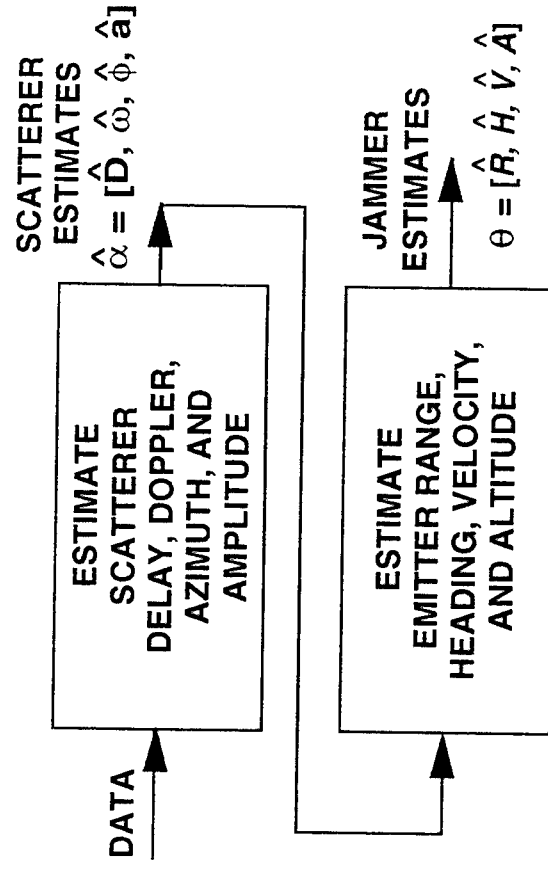
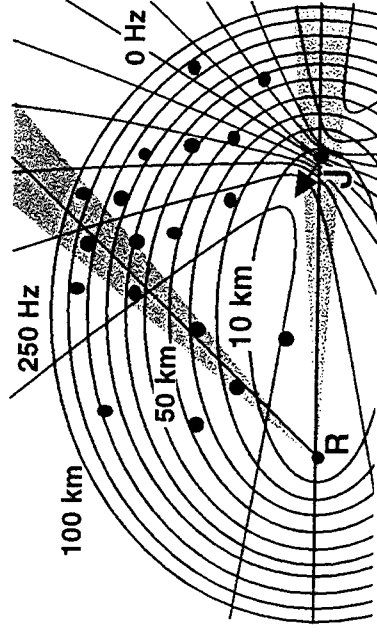
TWO CLUTTER MODELS AND ESTIMATION APPROACHES

HOMOGENEOUS CLUTTER MODEL



- SCATTERING DELAY AND AZIMUTH ARE INDEPENDENT VARIABLES
- DOPPLER COMPUTED FOR EACH TRAIL PARAMETER SET
- ESTIMATE COMPLEX AMPLITUDE

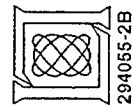
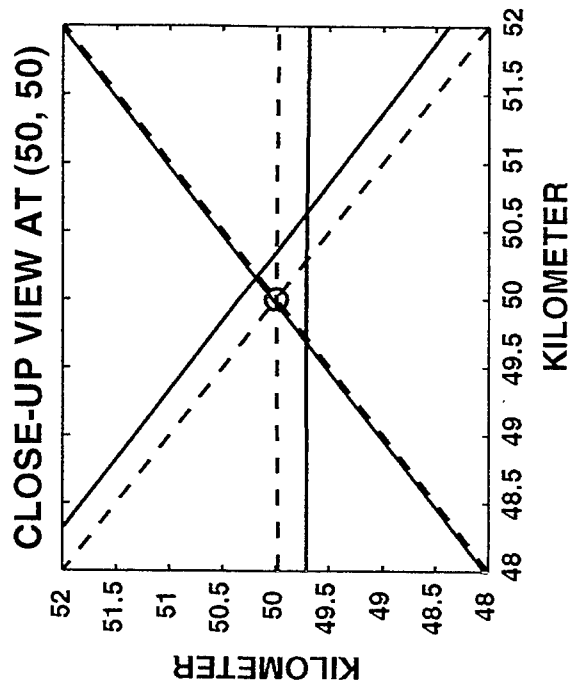
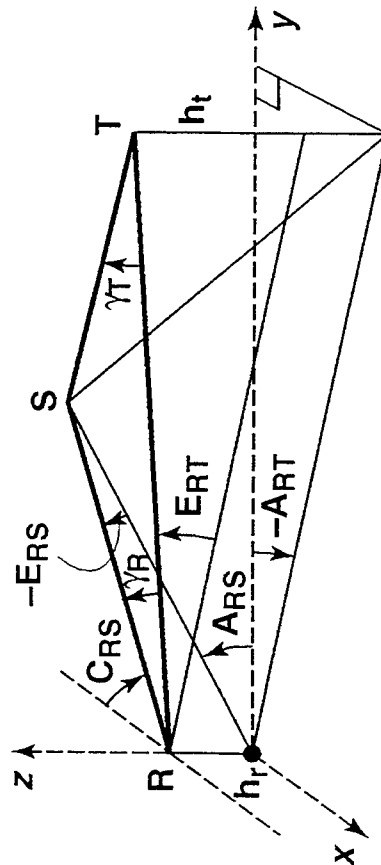
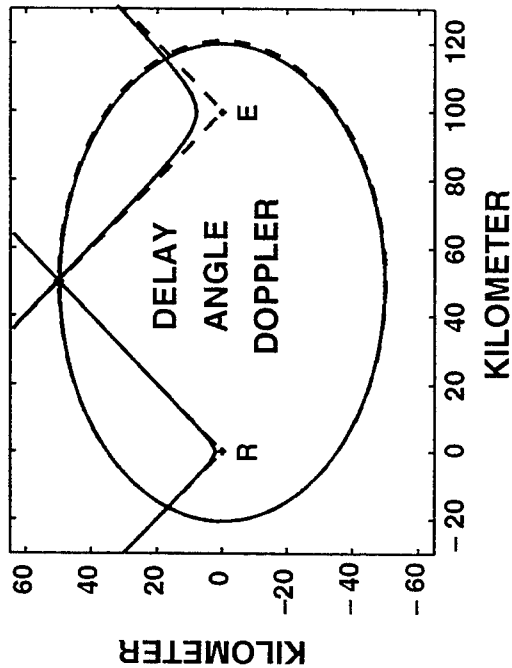
INHOMOGENEOUS CLUTTER MODEL



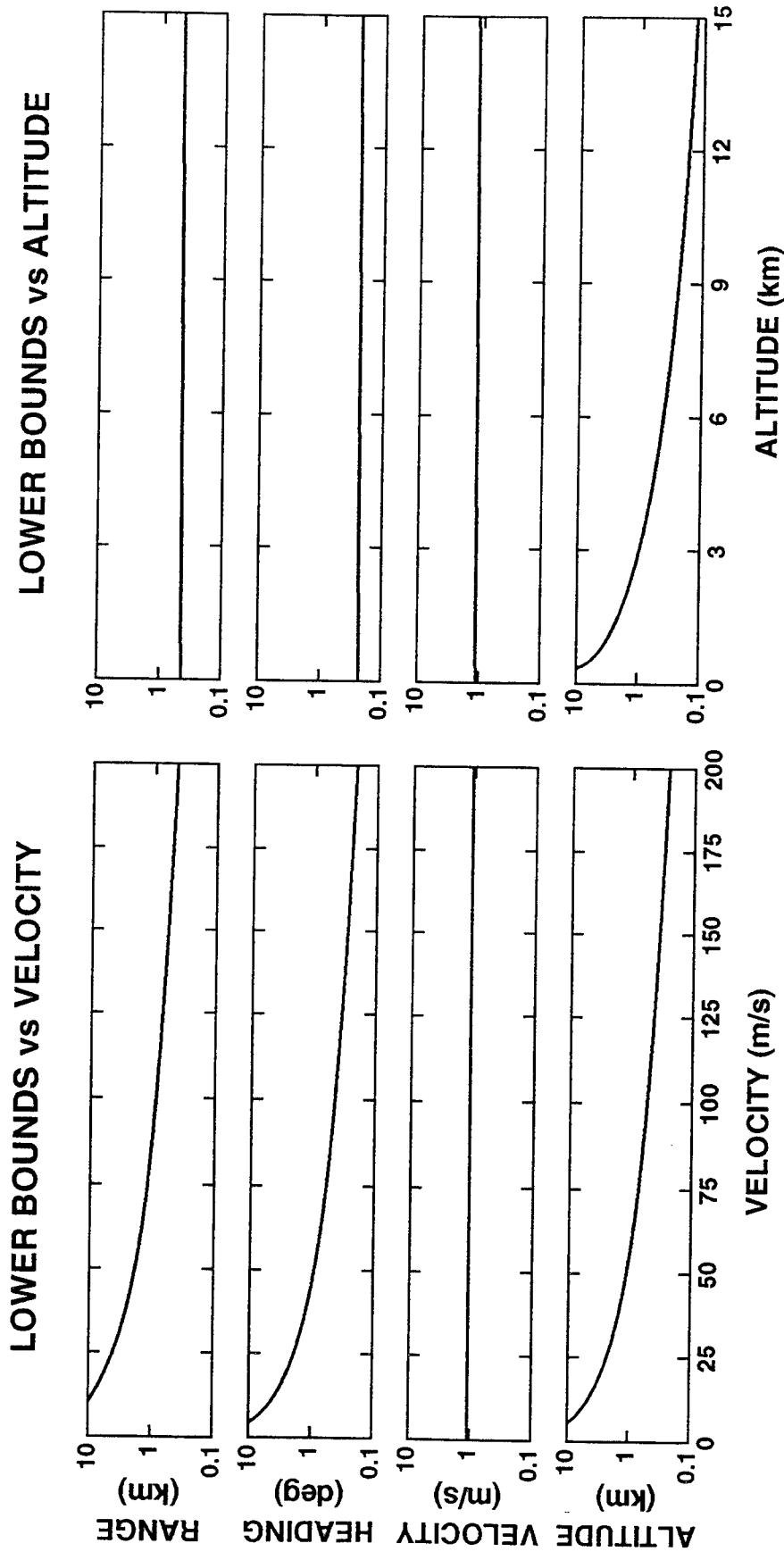
ESTIMATION OF ALTITUDE

- FUNCTIONS OF ALTITUDE
 - CONICAL ANGLES
 - HYPERBOLIC DOPPLER CONTOURS
 - ELLIPSOIDAL DELAY CONTOURS

CONTOURS FOR ALTITUDES OF 0 (--) AND 8 km (—)



CRAMER-RAO LOWER BOUNDS RMS ESTIMATION ERROR

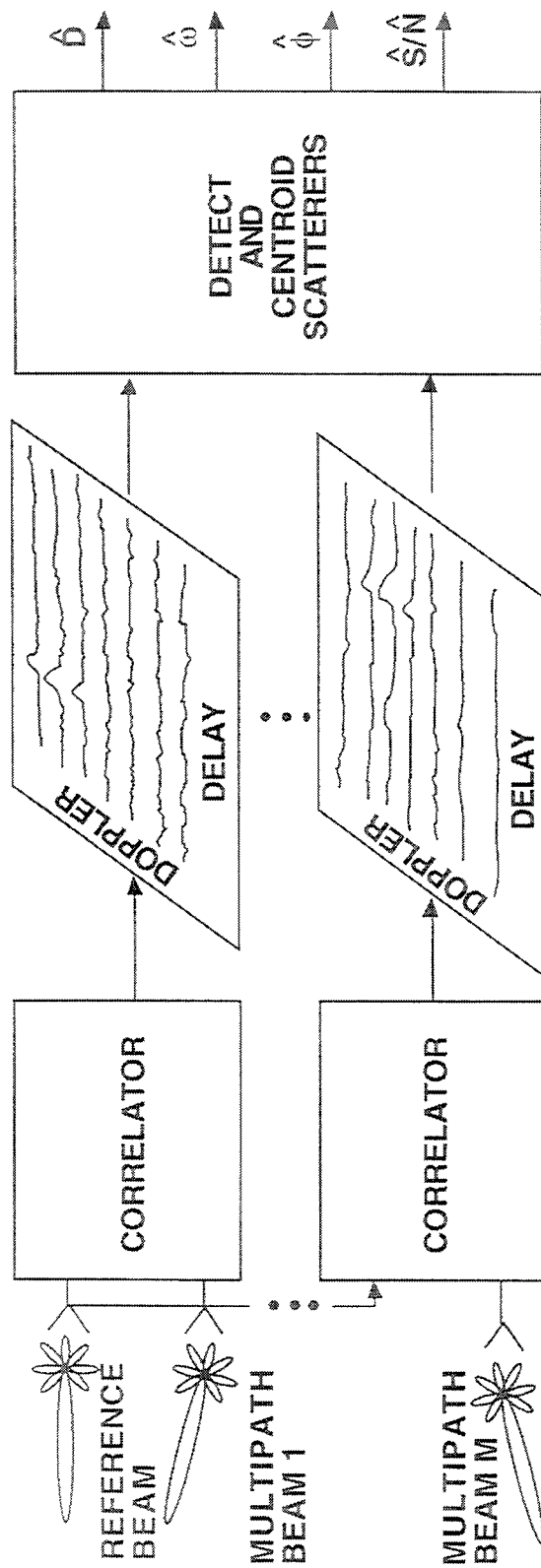


SCENARIO: $R = 100$ km, $H = 90$ deg, $V = 200$ m/s FILTER LENGTH = 50, TAP SPACING = $5\mu\text{s}$,
JNR = 0 dB PER SAMPLE, 10 k SAMPLES, SINGLE BEAM AZIMUTH = 30 deg.

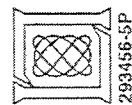
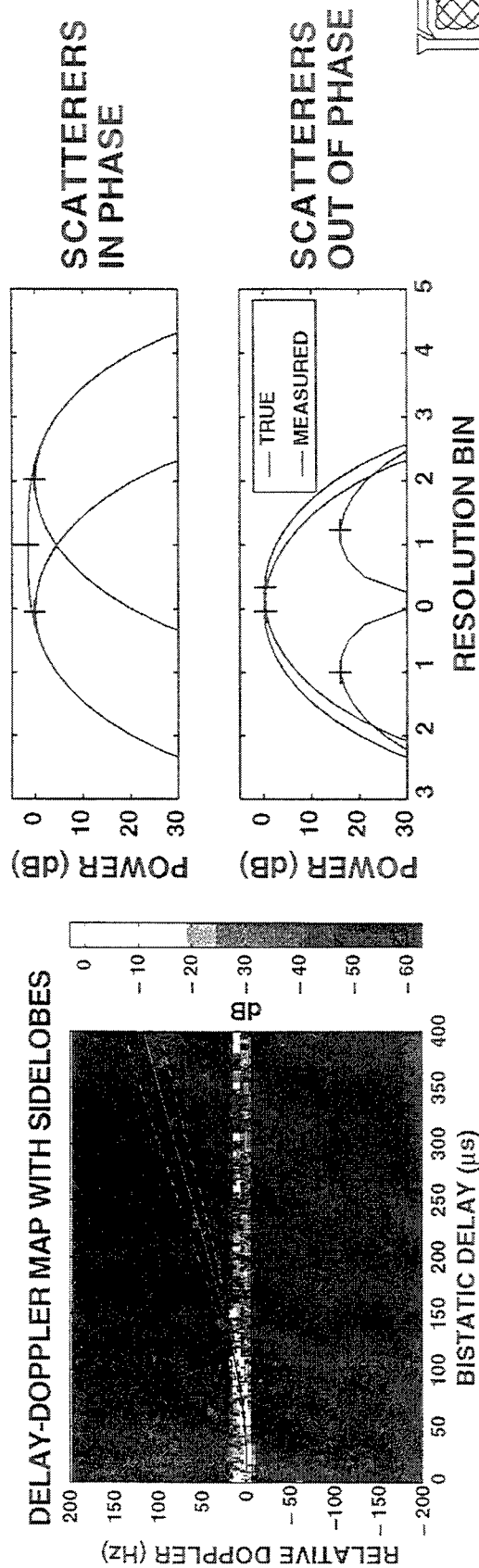


293456-4B

INHOMOGENEOUS CLUTTER MODEL

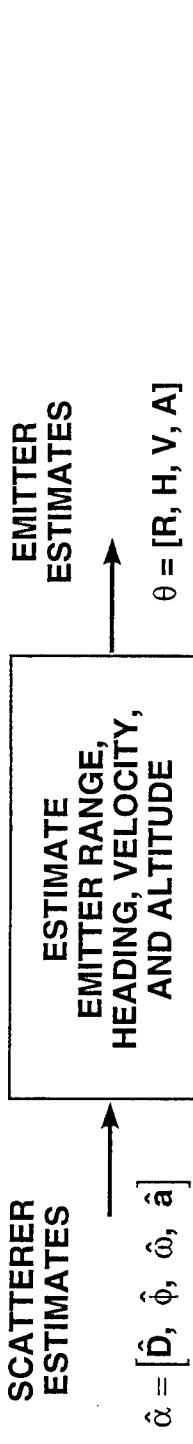


ERRORS INTRODUCED BY COHERENCE



293456-5P

ESTIMATOR FOR INHOMOGENEOUS MODEL



$$\begin{aligned}\hat{\omega}_i &= g(\theta, \alpha_i) + e_{\omega i}, \quad \text{USING TAYLOR SERIES: } \hat{\omega}_i \equiv g(\theta, \hat{\alpha}_i) + \delta_{\alpha i 1} g'_{\alpha i 1}(\theta, \hat{\alpha}_i) + \delta_{\alpha i 2} g'_{\alpha i 2}(\theta, \hat{\alpha}_i) + e_{\omega i} \\ &\equiv g(\theta_0, \hat{\alpha}_i) + \delta_{\theta 1} g'_{\theta 1}(\theta_0, \hat{\alpha}_i) + \delta_{\theta 2} g'_{\theta 2}(\theta_0, \hat{\alpha}_i) + \delta_{\theta 3} g'_{\theta 3}(\theta_0, \hat{\alpha}_i) + \delta_{\theta 4} g'_{\theta 4}(\theta_0, \hat{\alpha}_i) \\ &\quad + [\delta_{\alpha i 1} g'_{\alpha i 1}(\theta_0, \hat{\alpha}_i) + \delta_{\alpha i 2} g'_{\alpha i 2}(\theta_0, \hat{\alpha}_i) + e_{\omega i}]\end{aligned}$$

$$A\delta = z - n \quad \delta = [A^T R_n^{-1} A]^{-1} A^T R_n^{-1} z \quad R_n = R_\omega + H^T R_\alpha H$$

$$z = \hat{\omega} - g(\theta_0, \hat{\alpha}) \quad R_\alpha = \begin{bmatrix} R_D & 0 \\ 0 & R_\phi \end{bmatrix} \quad H = \begin{bmatrix} H_D \\ H_\phi \end{bmatrix}$$

$$R_\omega = \begin{bmatrix} \sigma_{\omega 1}^2 & 0 & 0 & 0 \\ 0 & \sigma_{\omega 2}^2 & 0 & 0 \\ 0 & 0 & \sigma_{\omega 3}^2 & 0 \\ 0 & 0 & 0 & \sigma_{\omega p}^2 \end{bmatrix} \quad R_D = \begin{bmatrix} \sigma_{D1}^2 & 0 & 0 & 0 \\ 0 & \sigma_{D2}^2 & 0 & 0 \\ 0 & 0 & \sigma_{D3}^2 & 0 \\ 0 & 0 & 0 & \sigma_{Dp}^2 \end{bmatrix} \quad R_\phi = \begin{bmatrix} \sigma_{\phi 1}^2 & 0 & 0 & 0 \\ 0 & \sigma_{\phi 2}^2 & 0 & 0 \\ 0 & 0 & \sigma_{\phi 3}^2 & 0 \\ 0 & 0 & 0 & \sigma_{\phi p}^2 \end{bmatrix}$$

- CONTRIBUTION OF EACH SCATTERER WEIGHTED BY:
 - SNR THROUGH R_θ , R_D , AND R_ϕ (Taken from CRLB for Mountaintop)
 - GRADIENT OF FUNCTION g WRT θ (Matrix A) AND α (Matrix H)
- ESTIMATOR CLASSIFIED AS BEST LINEAR UNBIASED ESTIMATOR (BLUE), MAXIMUM LIKELIHOOD ESTIMATOR (MLE), AND MINIMUM VARIANCE UNBIASED (MVU) ESTIMATOR

SOLUTION AND MONTE-CARLO SIMULATION

- PERFORM COARSE LS SEARCH TO DETERMINE θ_0

- DETERMINE ESTIMATE

$$\delta = [A^T R_n^{-1} A]^{-1} A^T R_n^{-1} z$$

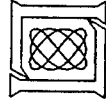
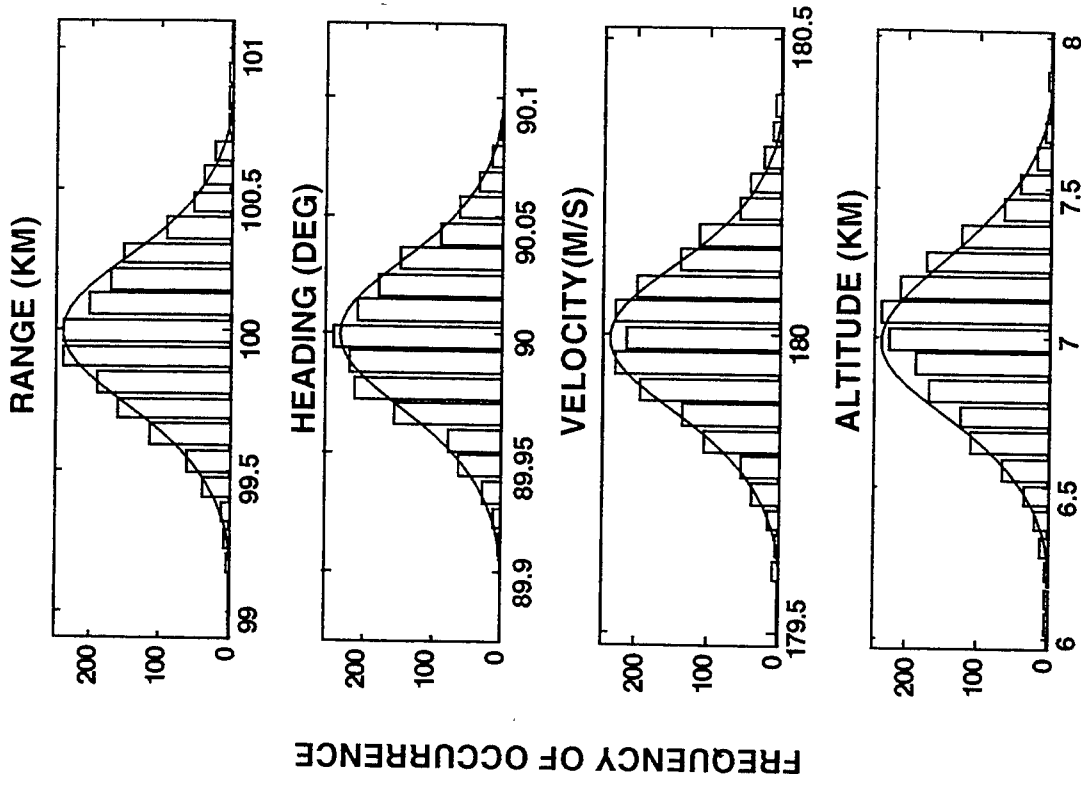
- ITERATE $\theta_0 \leftarrow \theta_0 + \delta$

- PARAMETER COVARIANCE

$$R_\theta = [A^T R_n^{-1} A]^{-1}$$

- PARAMETERS FOR MONTE-CARLO SIMULATIONS

- 20 SCATTERERS WITH 10 dB SNR
- 1800 TRIALS
- RESULTS GAUSSIAN, UNBIASED AND MATCH CRLB



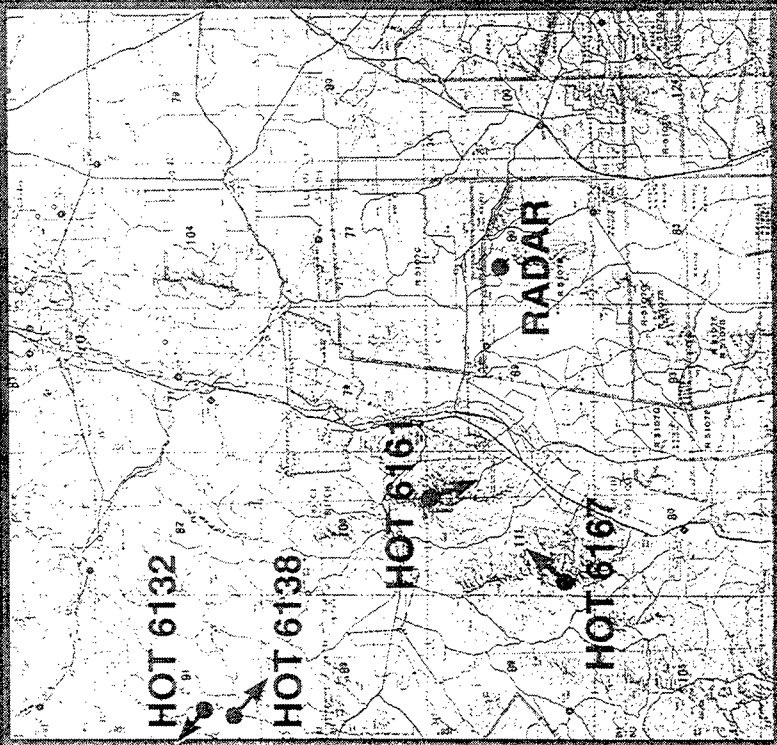
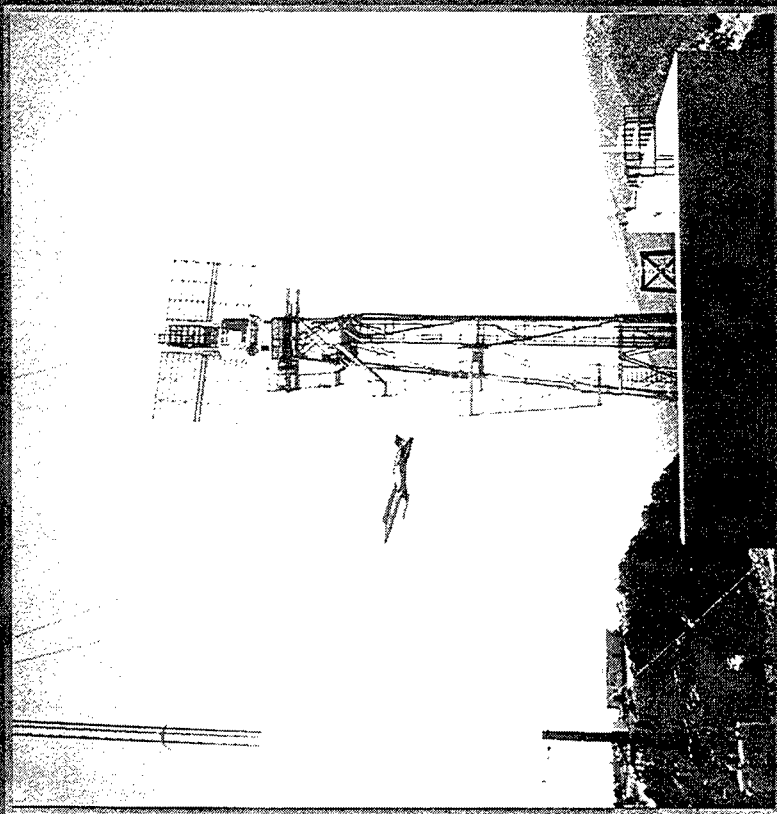
293957-2

OUTLINE

- INTRODUCTION
- PROBLEM FORMULATION
- DEMONSTRATION USING MOUNTAINTOP FIELD DATA
 - ESTIMATOR FOR HOMOGENEOUS MODEL
 - ESTIMATOR FOR INHOMOGENEOUS MODEL
 - REDUCED EMITTER POWER AND BANDWIDTH CASES
 - EXTENSIONS TO BASIC RESULTS
- SUMMARY



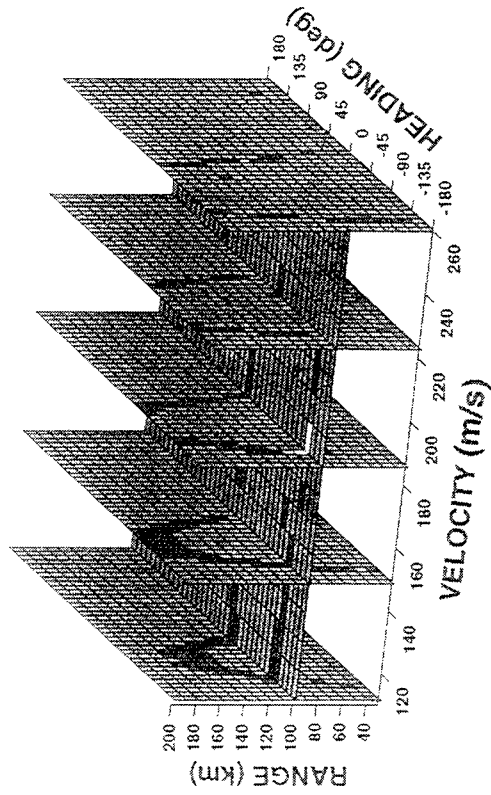
MOUNTAINTOP RADAR AT WSMR



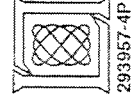
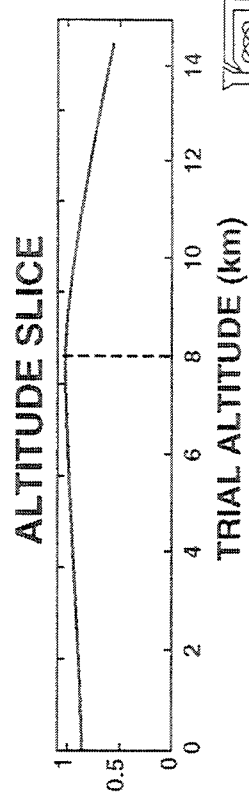
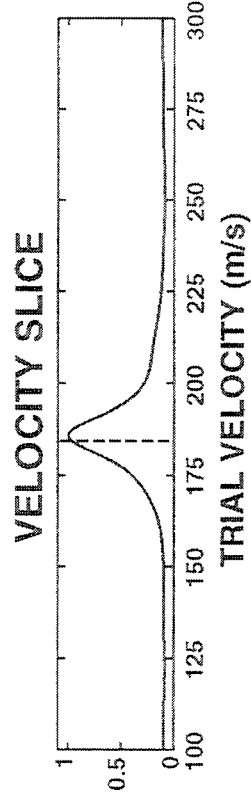
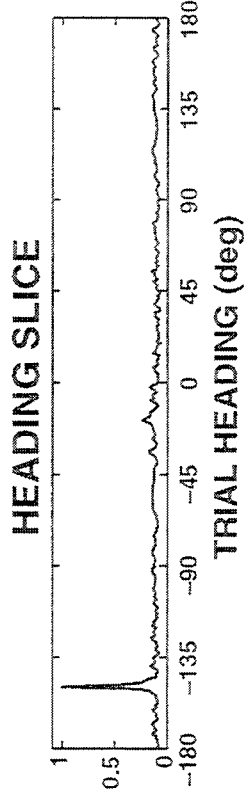
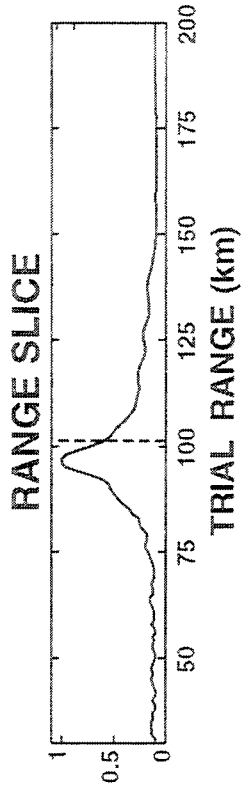
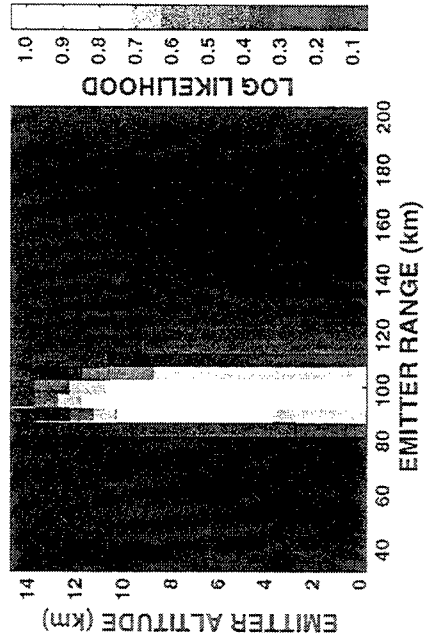
4-D LOG-LIKELIHOOD FUNCTION

MOUNTAINTOP DATA SET HOT6067

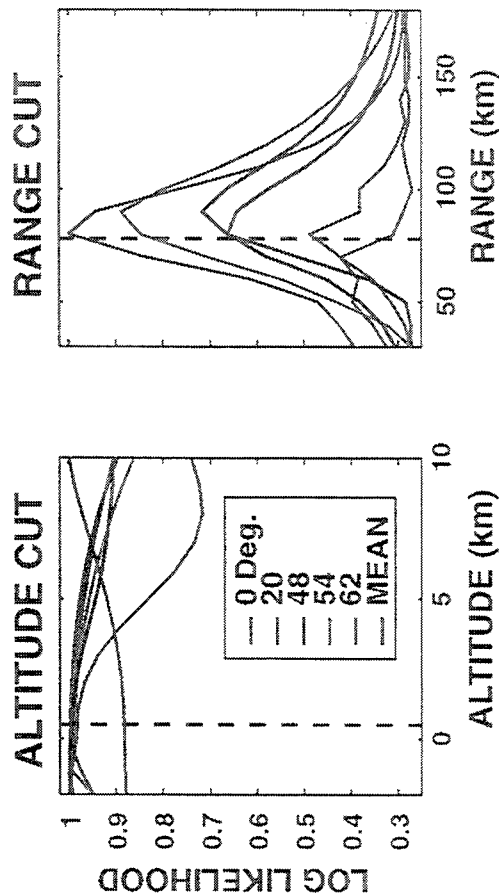
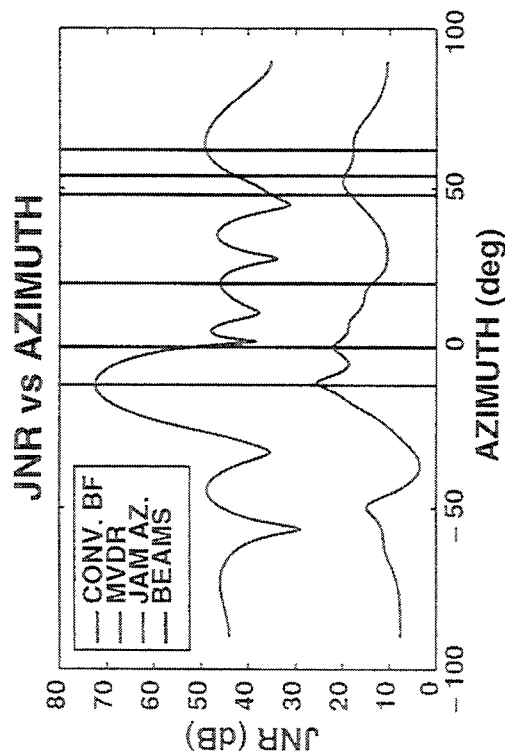
VELOCITY SLICES



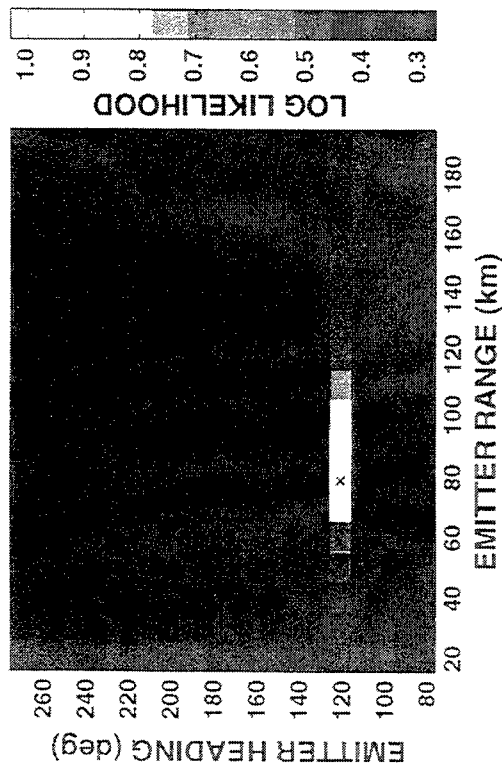
RANGE-ALTITUDE SLICE



MULTIPLE BEAM LOCALIZATIONS MILLIGAN GULCH HOT6161 (Low-altitude Runs)



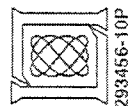
RANGE-VELOCITY SLICE



NUMERICAL RESULTS

EMITTER PARAMETER	TRUE VALUE	ESTIMATED VALUE	ERROR
RANGE (km)	78.3	83.0	6%
HEADING (deg)	121.8	122.1	0.25%
VELOCITY (m/s)	134.3	139.1	3.6%
ALTITUDE (km)	0.5	0	-

- EACH BEAM PRODUCED PEAKS
NEAR TRUE JAMMER PARAMETERS
- ALTITUDE ESTIMATED SUCCESSFULLY

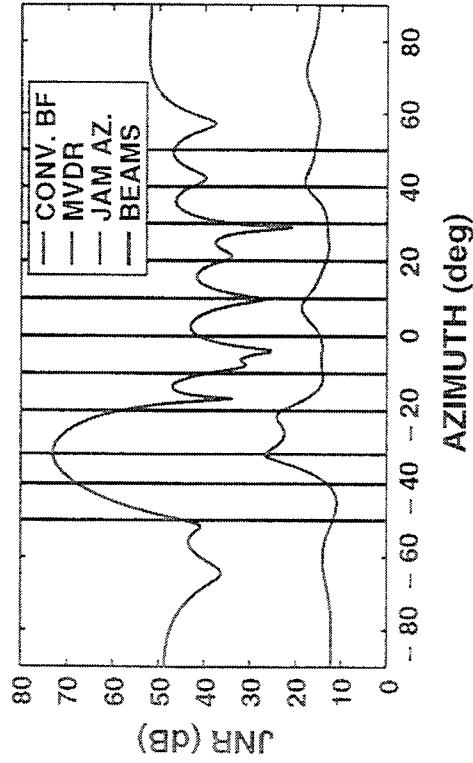


293456-10P

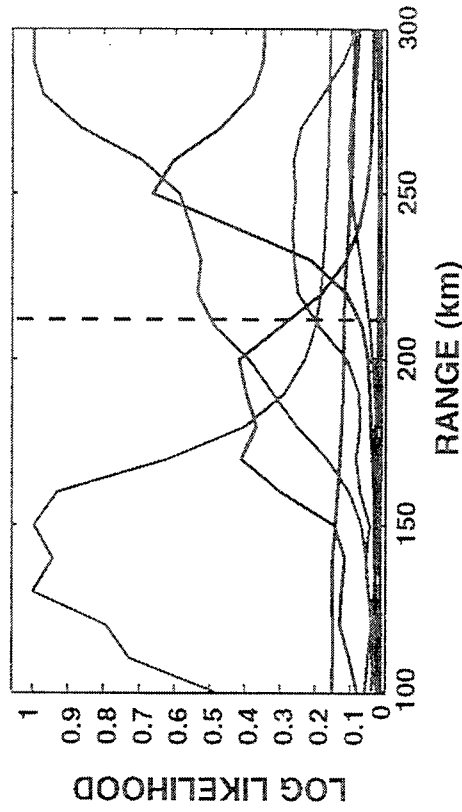
MULTIPLE BEAM LOCALIZATIONS (cont.)

SOCORRO PEAK HOT6132 – FIRST ATTEMPT UNSUCCESSFUL

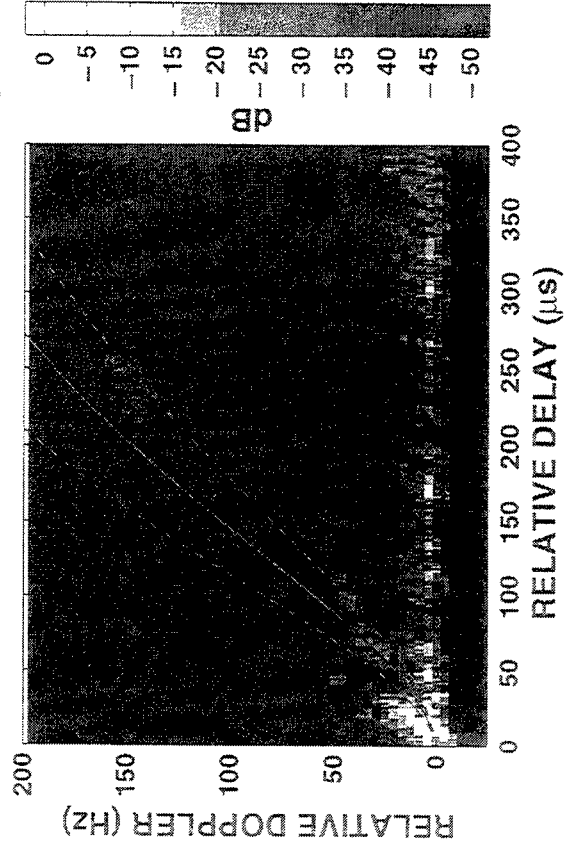
JNR vs AZIMUTH



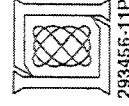
RANGE CUTS



DELAY-DOPPLER MAP (-60 deg)



- SEVERAL PEAKS 125-250 km
 - TRUE RANGE IS 212 km
- LOCALIZATION TECHNIQUE FAILED TO PRODUCE SINGLE UNAMBIGUOUS RESULT
 - TOO MUCH DOPPLER SPREAD IN 'FAT' ANTENNA BEAMS
 - COULD ADJUST MODEL PARAMETERS
- REEXAMINE WITH INHOMOGENEOUS MODEL

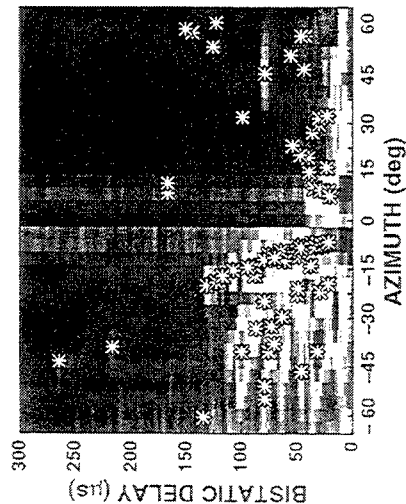


293455-11P

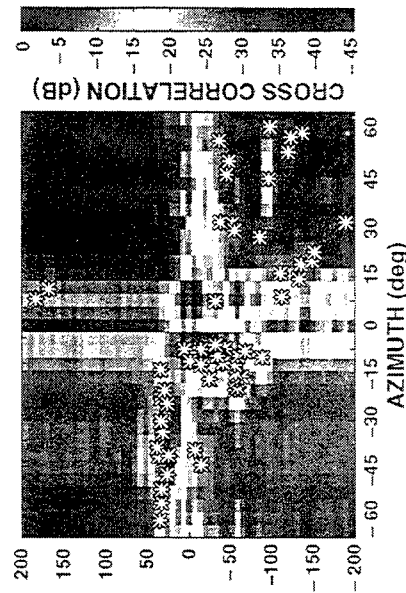
ESTIMATOR FOR INHOMOGENEOUS CLUTTER MODEL

MOUNTAINTOP DATA SET HOT6067

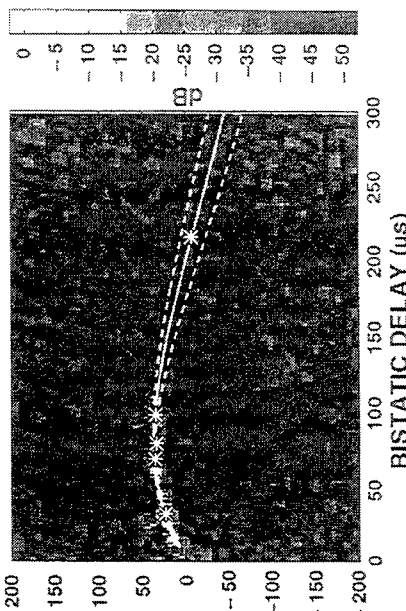
CORRELATION vs TIME



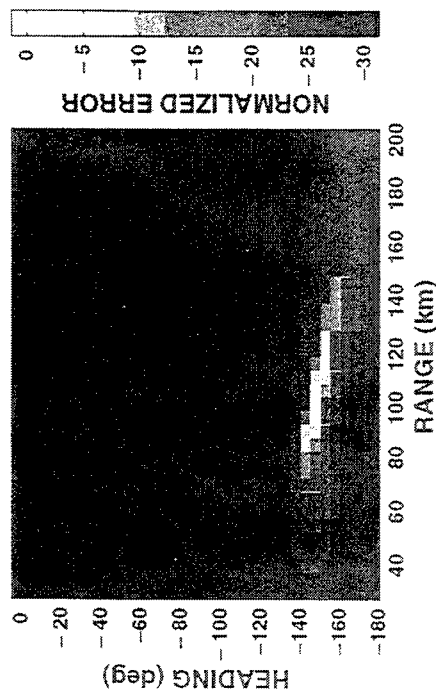
CORRELATION vs DOPPLER



DELAY - DOPPLER MAP AT -40 DEG.



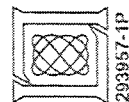
COARSE SEARCH



NUMERICAL RESULTS

EMITTER PARAMETER	TRUE VALUE	3-D ESTIMATE ERROR	4-D ESTIMATE ERROR	ERROR IN TERMS OF CRLB
RANGE (km)	101.7	-0.6	0.1	0.5σ
HEADING (deg)	-147.2	0.1	0.2	8σ
VELOCITY (m/s)	184.5	-6.8	-5.3	19σ
ALTITUDE (km)	8	-	1.2	8σ

- EXCELLENT PERFORMANCE
- NOT EXPECTED TO MATCH CRLB

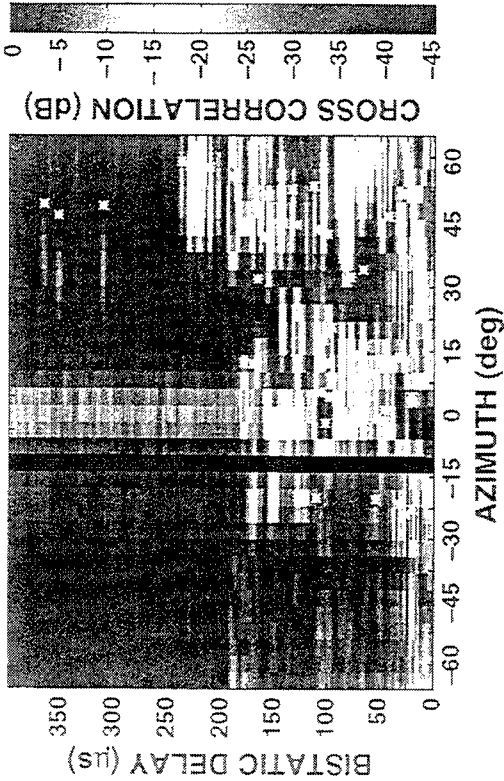


293957-1P

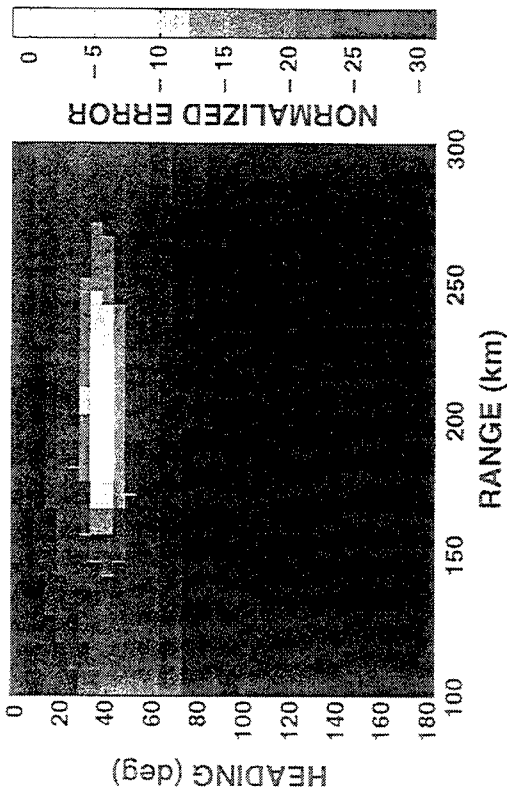
ADDITIONAL DEMONSTRATIONS

INHOMOGENEOUS CLUTTER MODEL

CORRELATION vs TIME (6161)



COARSE SEARCH (6132)



ESTIMATES FOR HOT6161 (Milligan Gulch)

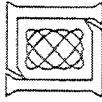
EMITTER PARAMETER	TRUE VALUE	3-D ESTIMATE ERROR	4-D ESTIMATE ERROR	ERROR IN TERMS OF CRLB
RANGE (km)	78.3	-1.0	0.2	1.7 σ
HEADING (deg)	121.8	0.1	0.2	12 σ
VELOCITY (m/s)	134.3	1.1	0.6	7.5 σ
ALTITUDE (km)	0.5	-	-1.2	10 σ

ESTIMATES FOR HOT6161 (Socorro Peak)
(Failed using homogeneous model)

EMITTER PARAMETER	TRUE VALUE	3-D ESTIMATE ERROR	4-D ESTIMATE ERROR	ERROR IN TERMS OF CRLB
RANGE (km)	211.9	-0.4	9.3	60 σ
HEADING (deg)	-36.2	-0.3	-0.5	100 σ
VELOCITY (m/s)	142.1	2.5	9.7	80 σ
ALTITUDE (km)	8	-	12.8	160 σ

- ESTIMATOR FOR INHOMOGENEOUS MODEL
SUCCESSFULLY LOCALIZED ALL DATA SETS

- RANGE ERRORS SMALLER THAN HOMOG. MODEL
- ALTITUDE ERRORS LARGER THAN HOMOG. MODEL



293456-13P

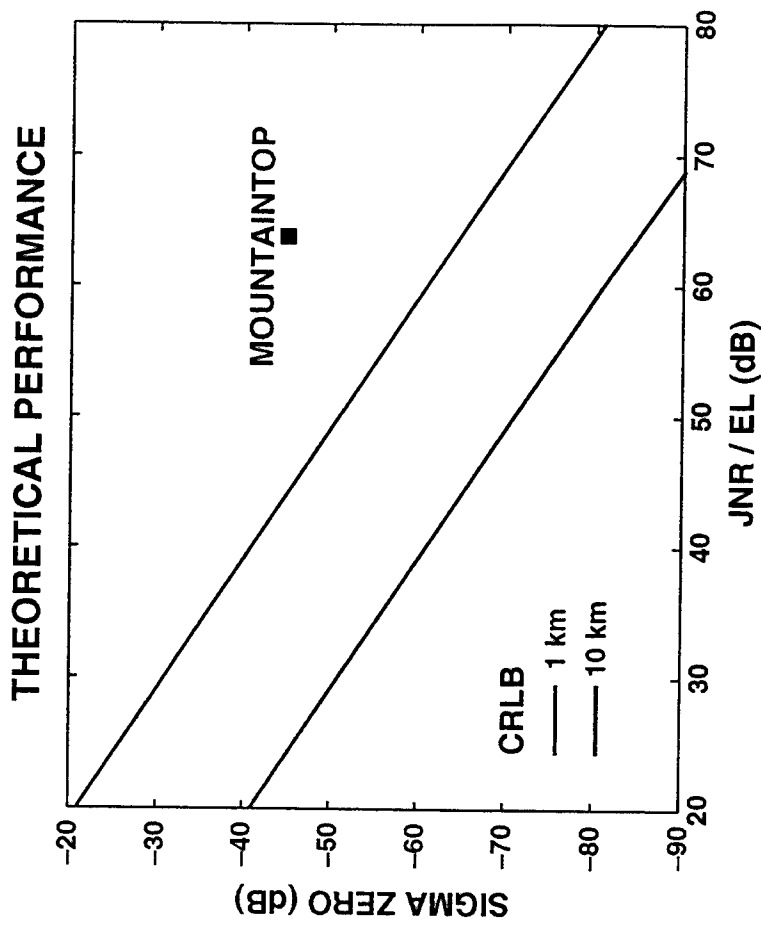
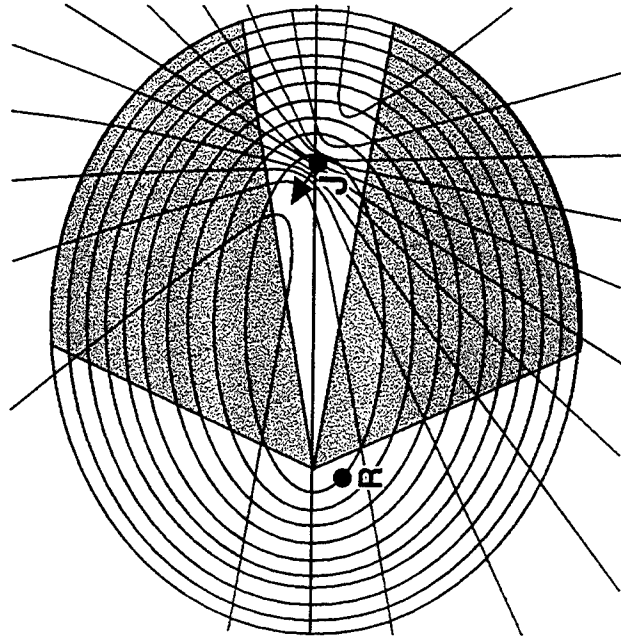
OUTLINE

- INTRODUCTION
- PROBLEM FORMULATION
- DEMONSTRATION USING MOUNTAINTOP FIELD DATA
 - ESTIMATOR FOR HOMOGENEOUS MODEL
 - ESTIMATOR FOR INHOMOGENEOUS MODEL
 - REDUCED EMITTER POWER AND BANDWIDTH CASES
 - EXTENSIONS TO BASIC RESULTS
- SUMMARY



LOCALIZATION PERFORMANCE vs EMITTER POWER

- MOUNTAIN JAMMER POWER WAS 700 W (ERP) IN 200 kHz
 - 60 – 65 dB JNR/ELEMENT

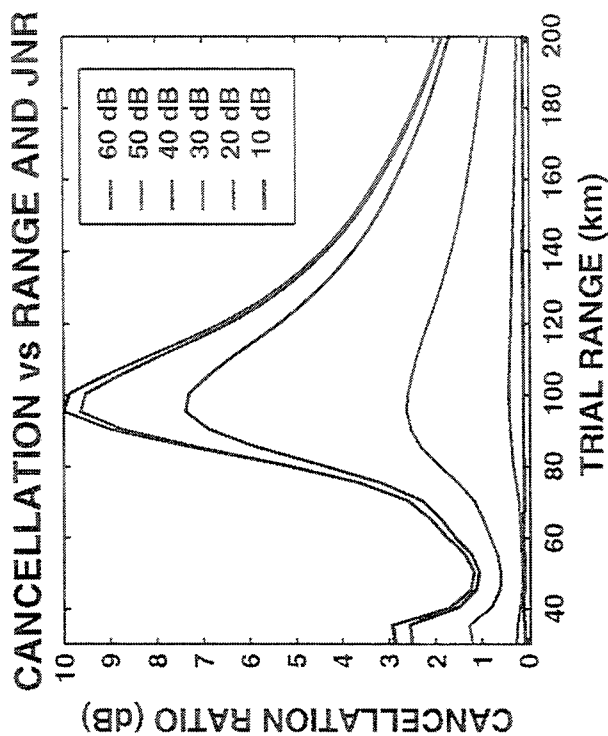
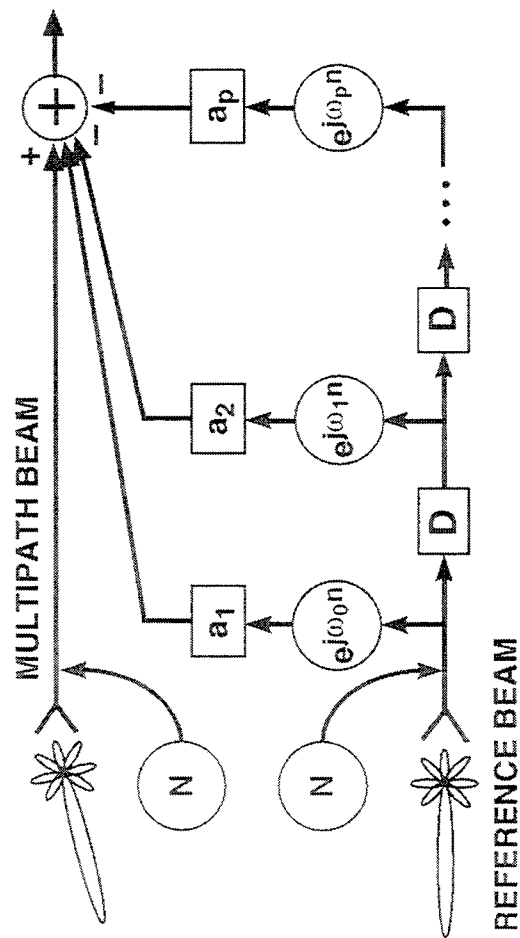


SCENARIO: R = 100 km, H = 90 deg, V = 200 m/s FILTER LENGTH = 50, TAP SPACING = 5 μ s,
10 k SAMPLES, 12 BEAMS

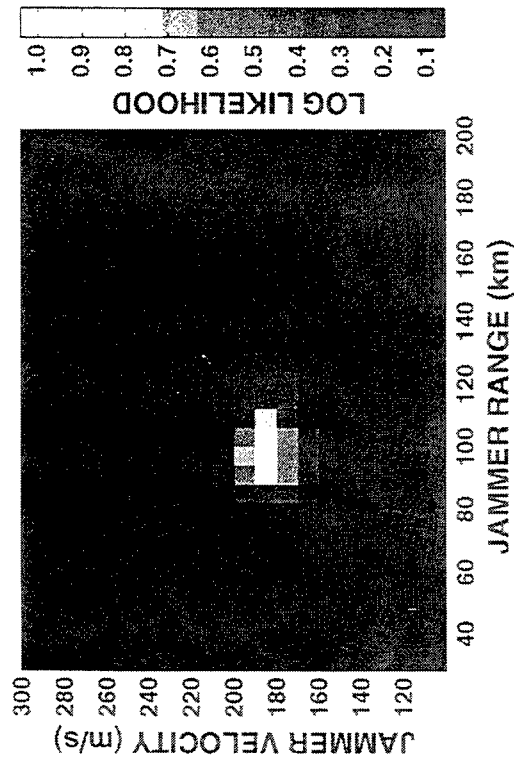
LOCALIZATION OF HOT6067 WITH NOISE ADDED

(Homogeneous Clutter Model)

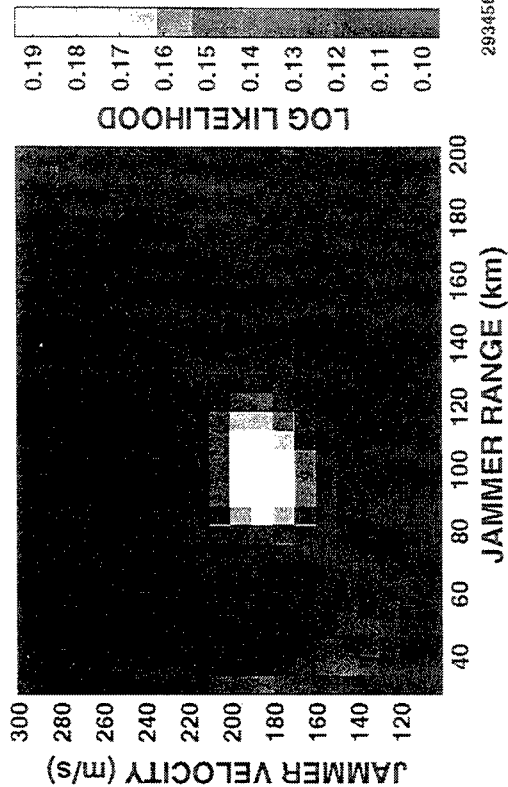
INJECT NOISE TO REDUCE JNR



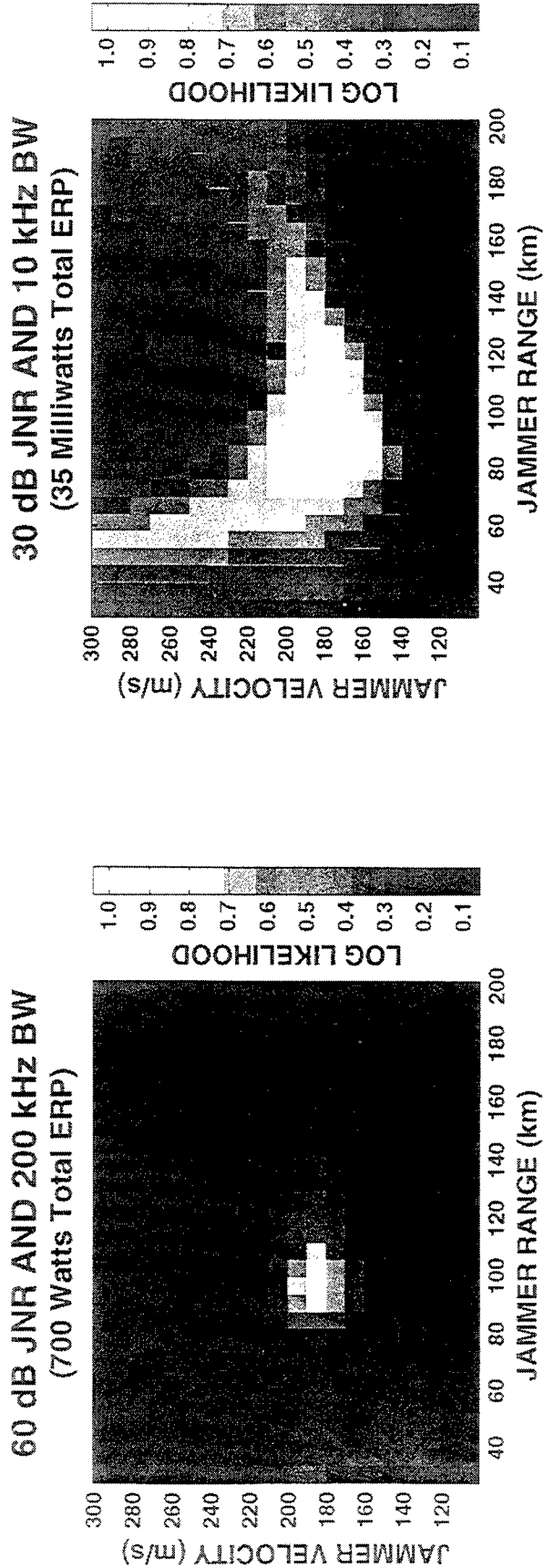
RANGE-VELOCITY CUT FOR 60 dB JNR



RANGE-VELOCITY CUT FOR 30 dB JNR



EMITTER BANDWIDTH REDUCED TO 10 KHZ (Homogeneous Clutter Model)

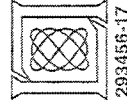
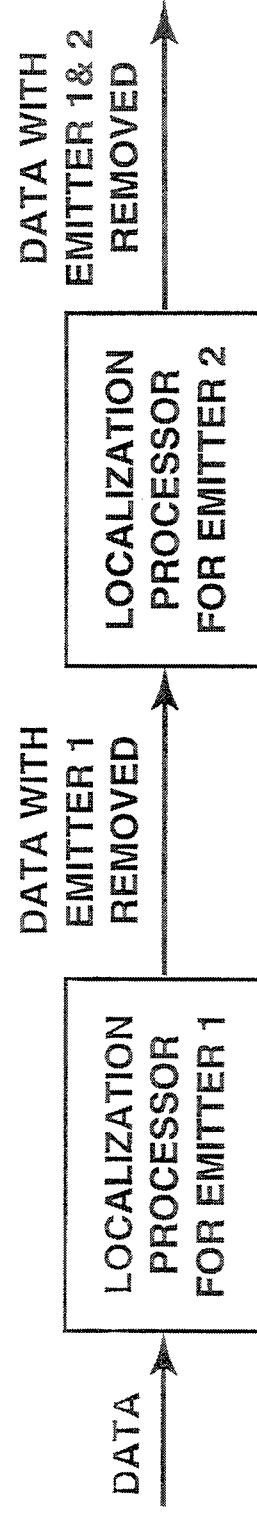


RESULTS USING ESTIMATOR FOR INHOMOGENEOUS CLUTTER

PARAMETER	TRUE VALUE	60 dB JNR 200 kHz BW		20 dB JNR 200 kHz BW		30 dB JNR 20 kHz BW	
		4-D EST.	CRLB σ	4-D EST.	CRLB σ	4-D EST.	CRLB σ
RANGE (km)	101.7	101.8	0.18	94.0	1.47	78.8	10.7
HEADING (deg)	-147.2	-147.0	0.022	-146	0.33	-141	3.1
VELOCITY (m/s)	184.5	179.2	0.22	175	3.4	130	19.2
ALTITUDE (km)		9.2	0.16	10.9	0.25	-	-
# SCATTERS		67		36		6	

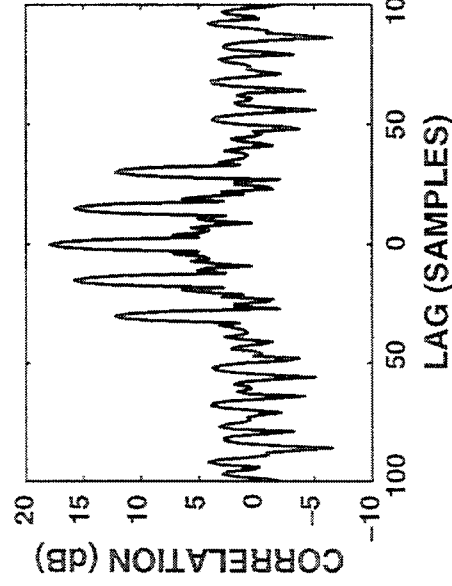
EXTENSIONS TO BASIC RESULTS

- SELF-CORRELATED EMITTER WAVEFORMS
 - USED TO GENERATE LOCALIZATION “GHOSTS”
SIMULATED BY INTRODUCING CORRELATION TO DATA SETS
- PULSED EMITTER WAVEFORMS
 - LOCALIZATION OF RADAR TRANSMITTERS
USE DATA FROM MOUNTAINTOP MAPPING EXPERIMENTS
- MULTIPLE EMITTERS
 - SIMULATE BY COMBINING DATA SETS
 - USE A SERIAL APPROACH WHICH LOCALIZES WHILE REMOVING
TERRAIN SCATTERED INTERFACE

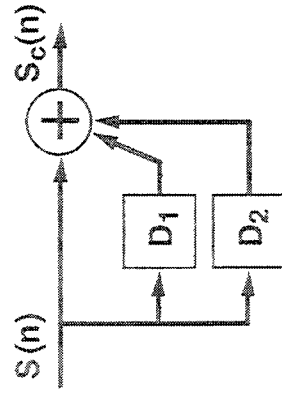
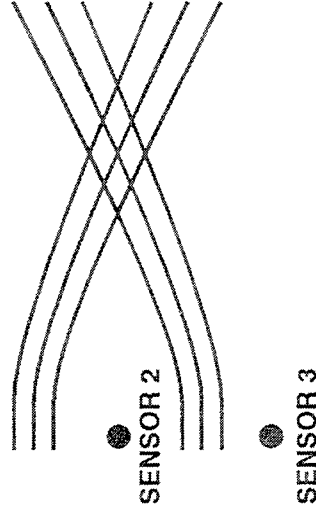


SELF-CORRELATED WAVEFORMS MAY BE USED TO IMPEDE JAMMER LOCALIZATION

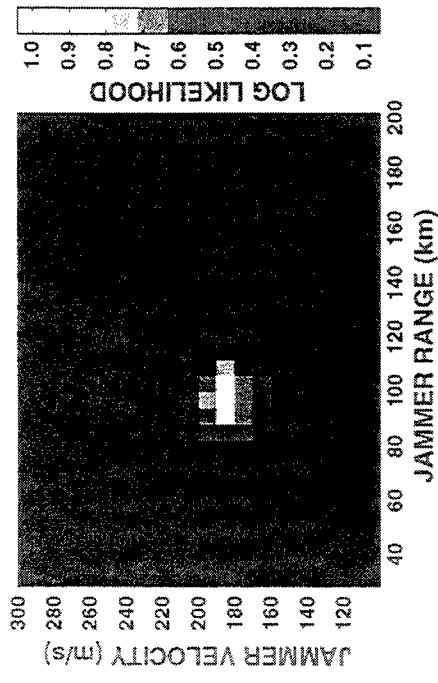
JAMMER AUTOCORRELATION



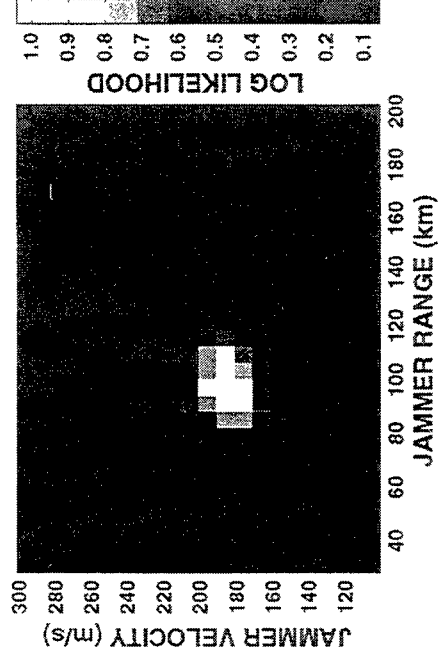
SENSOR 1 CORRELATION GENERATES
MULTIPLE FALSE EMITTER
LOCATIONS (Ghosts)



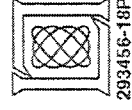
LIKELIHOOD WITH NO CORRELATION



LIKELIHOOD WITH CORRELATION

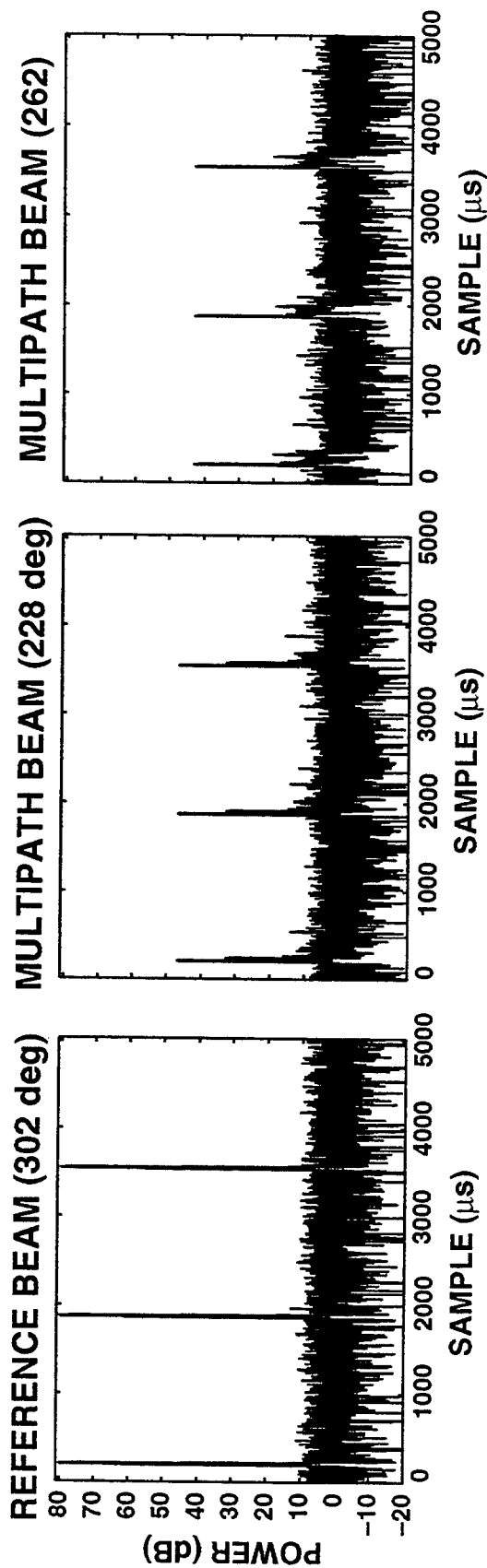


- NO FALSE TARGETS GENERATED
- CORRELATION SHOWS UP AS AN INCREASE IN NOISE POWER

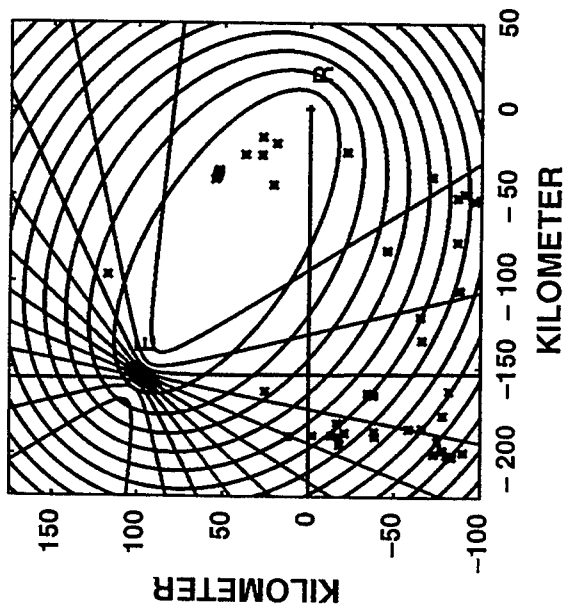


293456-18P

PULSED WAVEFORM (HOT6138) **REPRESENTS PASSIVE LOCALIZATION OF RADAR TRANSMITTER**



DETECTED SCATTERERS



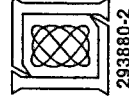
ESTIMATES

EMITTER PARAMETER	TRUE VALUE	3-D ESTIMATE ERROR	4-D ESTIMATE ERROR	ERROR IN TERMS OF CRLB
RANGE (km)	183.3	-9.0	-7.9	10σ
HEADING (deg)	143.5	-1.2	-0.3	4.2σ
VELOCITY (m/s)	191.5	-9.3	-19.0	29σ
ALTITUDE (km)	8	-	-3.75	3σ



SUMMARY

- **MOVING EMITTERS PASSIVELY LOCALIZED**
 - RANGE, HEADING, VELOCITY, ALTITUDE (and Azimuth)
- **FORMULATION FOR HOMOGENEOUS AND INHOMOGENEOUS CLUTTER**
 - CRAMER-RAO BOUNDS AND MONTE-CARLO SIMULATIONS
- **DEMONSTRATED USING MOUNTAINTOP DATA**
 - REDUCED EMITTER POWER
 - REDUCED EMITTER BANDWIDTH
 - SELF-CORRELATED AND PULSED WAVEFORMS
- **POSSIBLE FUTURE WORK**
 - STUDY ADDITIONAL SCENARIOS
 - USE OVER OCEAN
 - OTHER FREQUENCIES, WAVEFORMS
 - MULTIPLE EMITTERS
 - MOVING RECEIVER
 - FURTHER DEVELOP AND REFINE LOCALIZATION TECHNIQUES



SESSION V: DETECTION AND ESTIMATION (U)

GAMMA: A Fast Adaptive Parameter Estimation Algorithm for Multidimensional Arrays

Gary F. Hatke

MIT Lincoln Laboratory

244 Wood Street

Lexington, MA 02173-9108

tel: (617) 981-3364

email: hatke@ll.mit.edu

Abstract The problem of adaptive detection using multidimensional array structures, such as planar arrays, polarization diverse arrays, and space-time arrays, has been discussed thoroughly in the literature. Various sub-optimal methods have been proposed to decrease the computation of the optimal detection test statistic. However, the problem of estimating the parameters of the detected signal in an efficient manner has only recently been addressed. Specifically, when the dimensionality of the target parameters becomes larger than two, there have been no algorithms proposed which do not require a computationally intensive manifold search for parameter estimation. This talk introduces a method for adaptively estimating signal parameters in the presence of non-white noise. The technique couples the multidimensional rooting aspects of elimination theory with a generalized form of adaptive monopulse to produce an algorithm which can estimate a signal parameter set of arbitrary dimension. The algorithm projects the error vector between the measured whitened steering vector and a candidate whitened steering vector taken from a multivariate polynomial manifold onto a space which has dimension equal to the number of unknown parameters to be estimated. Hence, the elements of the error vector constitute a set of multivariate polynomial equations which have a finite set of homogeneous solutions, one of which corresponds to the desired solution. Simulation results are shown for a simple planar array used to estimate target azimuth, elevation, and polarization state of the target. In all cases, comparison of the simulation results with Cramer-Rao bounds for estimate uncertainty show that the new estimator, although generally sub-optimal, achieves the lower bound.

GAMMA: A FAST ADAPTIVE PARAMETER ESTIMATION ALGORITHM FOR MULTI-DIMENSIONAL ARRAYS *

**GARY F. HATKE
MIT LINCOLN LABORATORY**

***This work was sponsored by the Defense Advanced Research Projects Agency under Air Force Contract F-19628-95-C-0002. Opinions, interpretations, conclusions and recommendations are those of the author and are not necessarily endorsed by the Defense Advanced Research Projects Agency.**

GFH

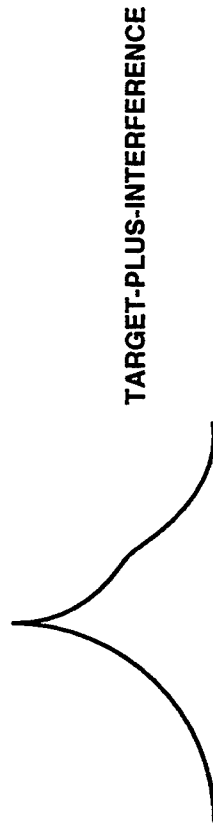
OUTLINE

- ADAPTIVE PARAMETER ESTIMATION
- ERROR PROJECTION METHOD
- SIMULATION RESULTS
- CONCLUSIONS



ADAPTIVE DIRECTION ESTIMATION

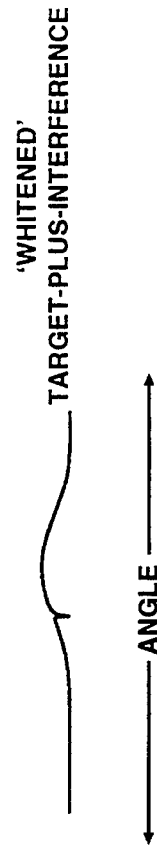
- PROCESSOR ESTIMATES
TARGET-PLUS-INTERFERENCE,
INTERFERENCE ONLY
COVARIANCE MATRICES



- PROCESSOR 'WHITENS'
TARGET-PLUS-INTERFERENCE
WITH INTERFERENCE ONLY
COVARIANCE MATRIX

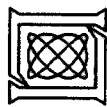


- PROCESSOR SEARCHES OVER
'WHITENED' STEERING VECTORS
FOR BEST MATCH TO DATA



SUBSPACE REQUIREMENTS

- WHITENING NULLS SPACE ALIGNED WITH INTERFERENCE
 - TARGET PARAMETER INFORMATION WILL BE LOST IN SUBSPACE ALIGNED WITH INTERFERENCE
- FOR ACCURATE PARAMETER ESTIMATION, ENOUGH 'DEGREES OF FREEDOM' MUST BE LEFT AFTER NULLING
 - FOR K UNKNOWN PARAMETERS, A K DIMENSIONAL SPACE MUST BE INTERFERENCE-FREE
 - ALL PARAMETERS MUST BE OBSERVABLE IN THE INTERFERENCE-FREE SPACE



OUTLINE

- ADAPTIVE PARAMETER ESTIMATION

⇒ ERROR PROJECTION METHOD

- SIMULATION RESULTS

- CONCLUSIONS



OPTIMIZATION METRICS

- FOR HIGH JNR, OPTIMAL DF METRIC BECOMES:

$$\arg \max_{\vec{\theta}} \frac{\vec{v}(\vec{\theta})^H \mathbf{R}_I^{-\frac{1}{2}} \mathbf{R}_x \mathbf{R}_I^{-\frac{1}{2}} \vec{v}(\vec{\theta})}{\vec{v}(\vec{\theta})^H \mathbf{R}_I^{-\frac{1}{2}} \mathbf{R}_I^{-\frac{1}{2}} \vec{v}(\vec{\theta})}$$

- DEFINE A *WHITENED STEERING VECTOR* AS $\mathbf{R}_I^{-\frac{1}{2}} \vec{v}(\vec{\theta})$;
WHITENED COVARIANCE MATRIX AS $\mathbf{R}_I^{-\frac{1}{2}} \mathbf{R}_x \mathbf{R}_I^{-\frac{1}{2}}$

- WHITENED COVARIANCE MATRIX CAN BE APPROXIMATED AS SCALED OUTER PRODUCT OF ITS PRINCIPAL EIGENVECTOR, \vec{a}_w
- ALTERNATE FORM OF DF METRIC CAN BE WRITTEN:

$$\arg \min_{\vec{\theta}, \alpha} \|\alpha \mathbf{R}_I^{-\frac{1}{2}} \vec{v}(\vec{\theta}) - \vec{a}_w\|^2$$



MINIMIZING PROJECTED ERROR NORM

- CONSIDER THE OPTIMIZATION METRIC FOR THE M DIMENSIONAL VECTOR θ :

$$\arg \min_{\theta, \alpha} \left\| \alpha R_I^{-\frac{1}{2}} \vec{v}(\vec{\theta}) - \vec{a}_w \right\|^2$$

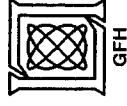
- PROJECT ERROR VECTOR $\alpha R_I^{-\frac{1}{2}} \vec{v}(\vec{\theta}) - \vec{a}_w$ ONTO AN $M + 1$ DIMENSIONAL SUBSPACE

$$P \left(\alpha R_I^{-\frac{1}{2}} \vec{v}(\vec{\theta}) - \vec{a}_w \right)$$

- DRIVING PROJECTED ERROR VECTOR TO ZERO GIVES $M + 1$ EQUATIONS IN $M + 1$ UNKNOWN $(\vec{\theta}, \alpha)$

- SIMULTANEOUS SOLUTION COMPUTABLE DEPENDING ON FUNCTIONAL DEPENDENCE OF $\vec{v}(\vec{\theta})$ ON θ

POLYNOMIAL DEPENDENCE DESIRED



FINDING BEST PROJECTION MATRIX

- MATRIX P SHOULD BE CHOSEN TO MAXIMIZE SENSITIVITY TO THE PARAMETERS $\vec{\theta}$ AND α
- CONSIDER ERROR INDUCED BY SMALL PERTURBATION FROM TRUE VALUE $\vec{\theta}^*$, α^* :

$$P \left(\alpha^* R_I^{-\frac{1}{2}} \vec{v}(\vec{\theta}^*) + \alpha^* R_I^{-\frac{1}{2}} \frac{\partial \vec{v}(\vec{\theta}^*)}{\partial \theta_i} \Delta \theta_i - \vec{a}_w \right) = P \left(\alpha^* R_I^{-\frac{1}{2}} \frac{\partial \vec{v}(\vec{\theta}^*)}{\partial \theta_i} \Delta \theta_i \right)$$

- FOR BEST SENSITIVITY TO ANY $\Delta \theta_i$ OR $\Delta \alpha$,

$$\left\| P R_I^{-\frac{1}{2}} \frac{\partial \vec{v}(\vec{\theta}^*)}{\partial \theta_i} \right\| = \left\| R_I^{-\frac{1}{2}} \frac{\partial \vec{v}(\vec{\theta}^*)}{\partial \theta_i} \right\|, \quad \left\| P R_I^{-\frac{1}{2}} \vec{v}(\vec{\theta}^*) \right\| = \left\| R_I^{-\frac{1}{2}} \vec{v}(\vec{\theta}^*) \right\|$$

- CHOOSE P TO PROJECT ONTO SPAN OF

$$R_I^{-\frac{1}{2}} \frac{\partial \vec{v}(\vec{\theta}^*)}{\partial \theta_1}, \dots, R_I^{-\frac{1}{2}} \frac{\partial \vec{v}(\vec{\theta}^*)}{\partial \theta_M}, R_I^{-\frac{1}{2}} \vec{v}(\vec{\theta}^*)$$



IMPLEMENTATION OF PROJECTION MATRIX

- IF TARGET PARAMETERS KNOWN APPROXIMATELY:
 - TARGET CAN BE ASSUMED EFFECTIVELY AT BORESIGHT IF INTERFERENCE IS NOT AT BORESIGHT
- IF NO PARAMETER INFORMATION AVAILABLE, OPTIMAL PROJECTION MATRIX CAN BE ESTIMATED
 - GOOD ESTIMATE OF $R_I^{-\frac{1}{2}} \vec{v}(\vec{\theta}^*)$ AVAILABLE IN \vec{a}_w
 - $\frac{\partial \vec{v}(\vec{\theta}^*)}{\partial \theta_i} = D_i \vec{v}(\vec{\theta}^*)$, WHERE D_i IS DEPENDENT ONLY ON ARRAY GEOMETRY
 - USE $R_I^{-\frac{1}{2}} D_i R_I^{\frac{1}{2}} \vec{a}_w$ AS ESTIMATE OF $R_I^{-\frac{1}{2}} \frac{\partial \vec{v}(\vec{\theta}^*)}{\partial \theta_i}$
- AFTER ESTIMATE OF $\vec{\theta}$ OBTAINED, PARTIAL DERIVATIVE VECTORS CAN BE RE-CALCULATED USING PARAMETER KNOWLEDGE



ARRAY MANIFOLD CHARACTERIZATION

- (MULTIVARIATE) POLYNOMIAL ARRAY MANIFOLD CHARACTERIZATION DESIRED
 - ARRAYS OF IDENTICAL GRIDDED ELEMENTS SATISFY THIS CONSTRAINT GLOBALLY
- ARBITRARY ARRAY MANIFOLDS CAN BE CHARACTERIZED LOCALLY AS POLYNOMIALS
 - GENERATE TAYLOR SERIES EXPANSION IN DIRECTION PARAMETERS AROUND SOME POINT
 - MANIFOLD IS LOCALLY DESCRIBED BY POLYNOMIALS IN $\vec{\Delta\theta}$
 - EXPANSION VECTORS IMPLY A BEAMSPACE IMPLEMENTATION, WHERE NUMBER OF BEAMS \propto CONVERGENCE AREA, POLYNOMIAL DEGREE



TAYLOR SERIES EXPANSION MANIFOLD

4 ELEMENT SQUARE ARRAY

$$z = e^{2ju_1} \quad w = e^{2ju_2} \quad \xrightarrow{\quad} \quad v(z,w) = \begin{bmatrix} zw & z & w & 1 \end{bmatrix}$$

$$V(u_1, u_2) = \begin{bmatrix} e^j(u_1 + u_2) \\ e^j(u_1 - u_2) \\ e^j(u_2 - u_1) \\ e^{-j}(u_1 + u_2) \end{bmatrix}$$

STEERING VECTOR

**TAYLOR SERIES
EXPANSION MANIFOLD
(AROUND $u_1 = 0, u_2 = 0$)**

$\Delta u_1 = a \quad \Delta u_2 = b \quad \longrightarrow \quad V(a,b) =$

$$\Delta u_1 = a \quad \Delta u_2 = b \quad \longrightarrow \quad V(a,b) =$$

$V(a,b) =$

(AROUND $u_1 = 0, u_2 = 0$)

$$M = \begin{bmatrix} -1 & 1 & 1 & -1 \\ -j & -j & j & -j \\ -j & j & j & -j \\ 1 & 1 & 1 & 1 \end{bmatrix} \quad M^{-1}V(a,b) = \begin{bmatrix} ab & b & a & 1 \end{bmatrix}$$

'MONOPULSE' BEAMFORMER

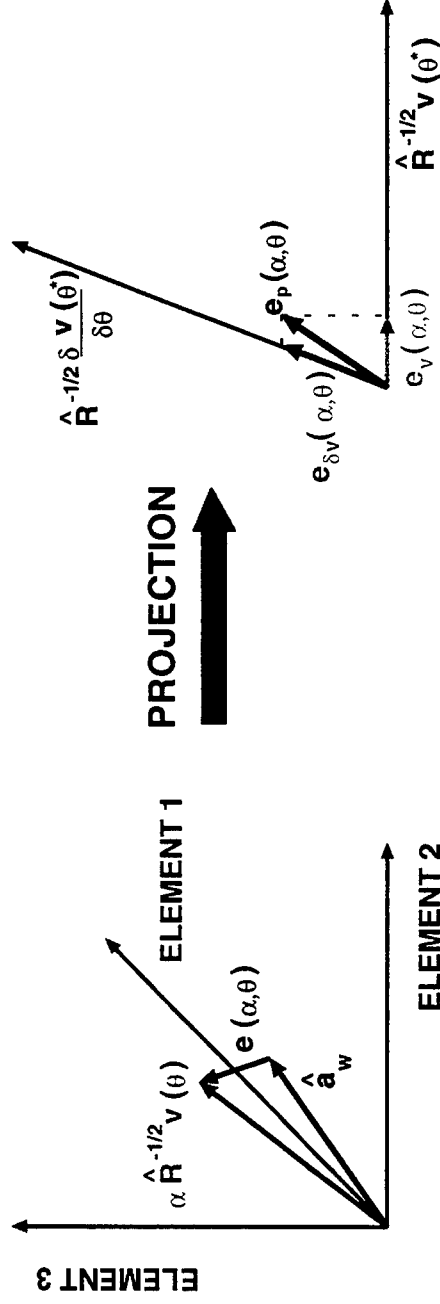
$$M V(a, b) =$$

***GAMMA*: GENERALIZED ADAPTIVE MULTIDIMENSIONAL MONOPULSE ALGORITHM**

- JOINTLY ESTIMATES TARGET PARAMETERS FOR TARGETS IN SPATIALLY COHERENT JAMMING ENVIRONMENTS
- APPLICABLE TO VIRTUALLY ALL ARRAY TYPES (SPACE-TIME, PLANAR, DUAL POLARIZED, ETC.)
- AVOIDS ARRAY MANIFOLD SEARCH COMPLEXITY
- PROVIDES NEARLY-ML PARAMETER ESTIMATES



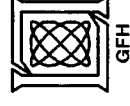
ERROR PROJECTION EXAMPLE (THREE ELEMENT CASE)



ERROR VECTOR IN
ELEMENT SPACE

PROJECTED
ERROR VECTOR

OPTIMIZATION EQUATIONS:
$$\begin{cases} | \hat{e}_{\delta v}(\alpha, \theta) | = 0 \\ | \hat{e}_v(\alpha, 0) | = 0 \end{cases}$$



OUTLINE

- ADAPTIVE PARAMETER ESTIMATION
- ERROR PROJECTION METHOD

⇒ SIMULATION RESULTS

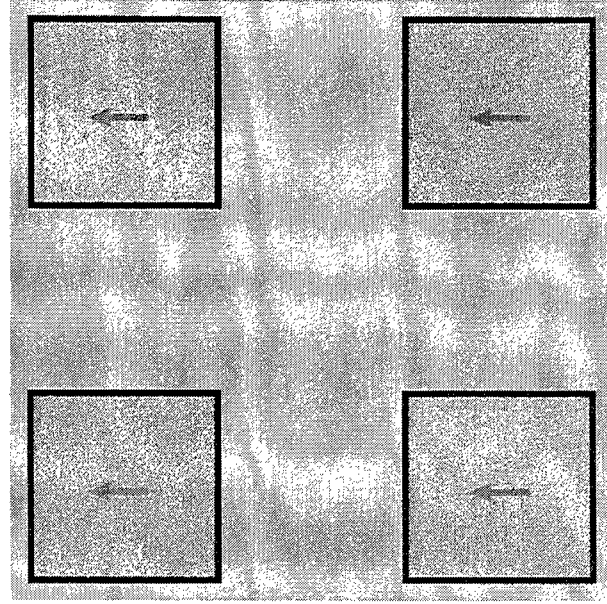
- CONCLUSIONS



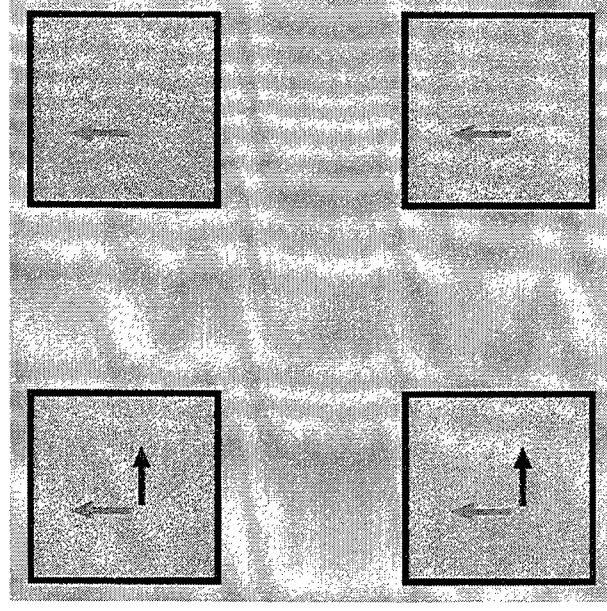
SIMULATION ARRAY TOPOLOGIES

SQUARE ARRAYS

4 CHANNEL V-POL
ARRAY

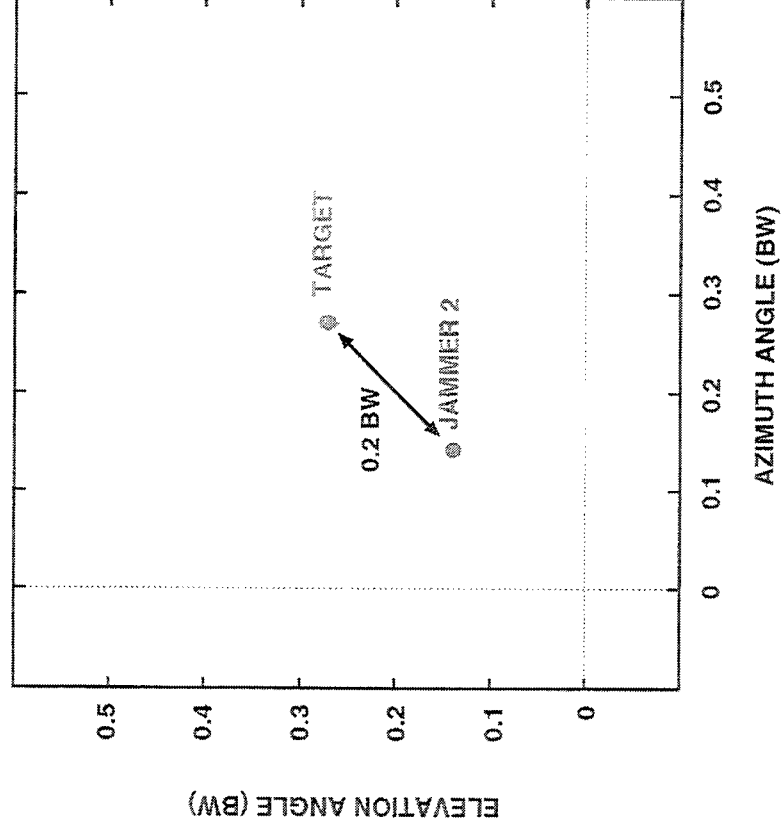


6 CHANNEL DUAL-POL
ARRAY



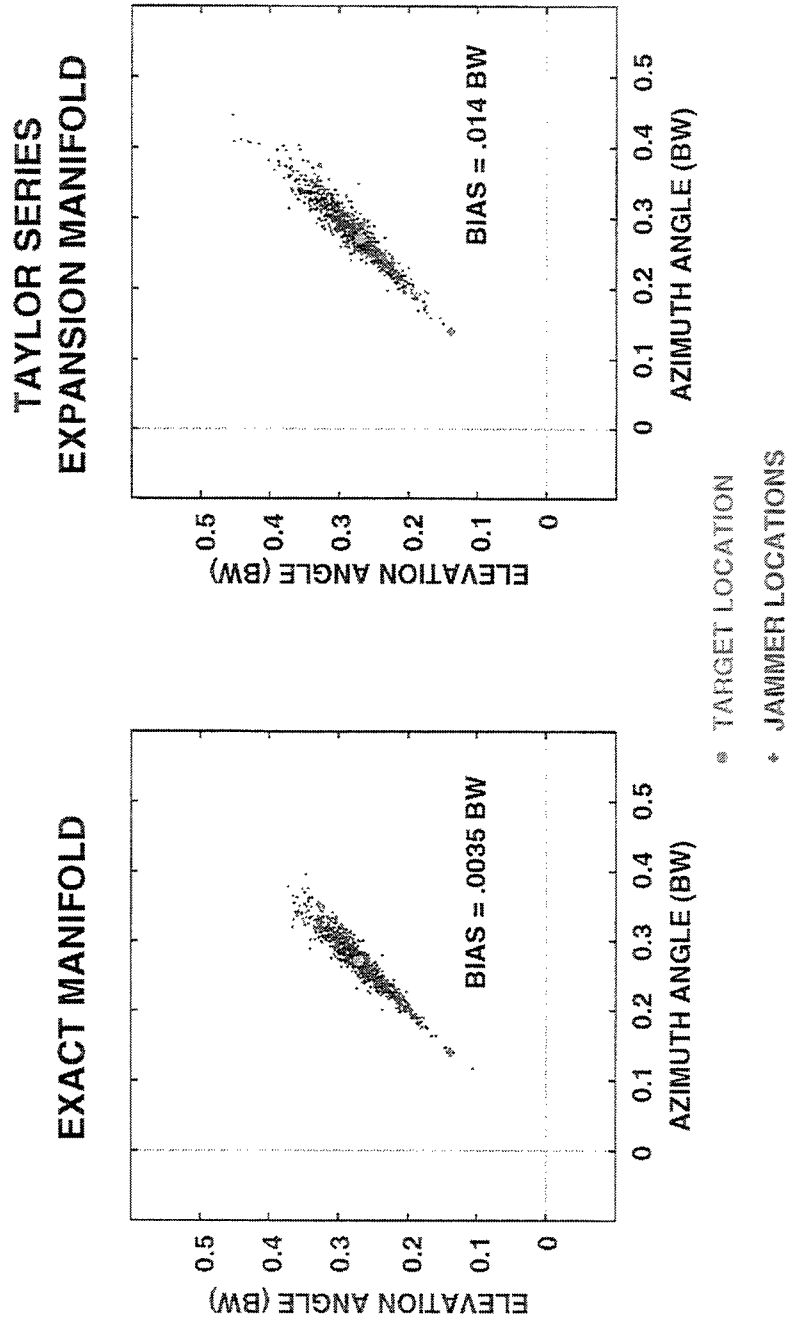
SIMULATION SOURCE LOCATIONS

ONE JAMMER SCENARIO, SINGLE POL ARRAY



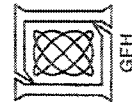
GAMMA DIRECTION ESTIMATION

4 CHANNEL VERTICAL POLARIZATION ARRAY



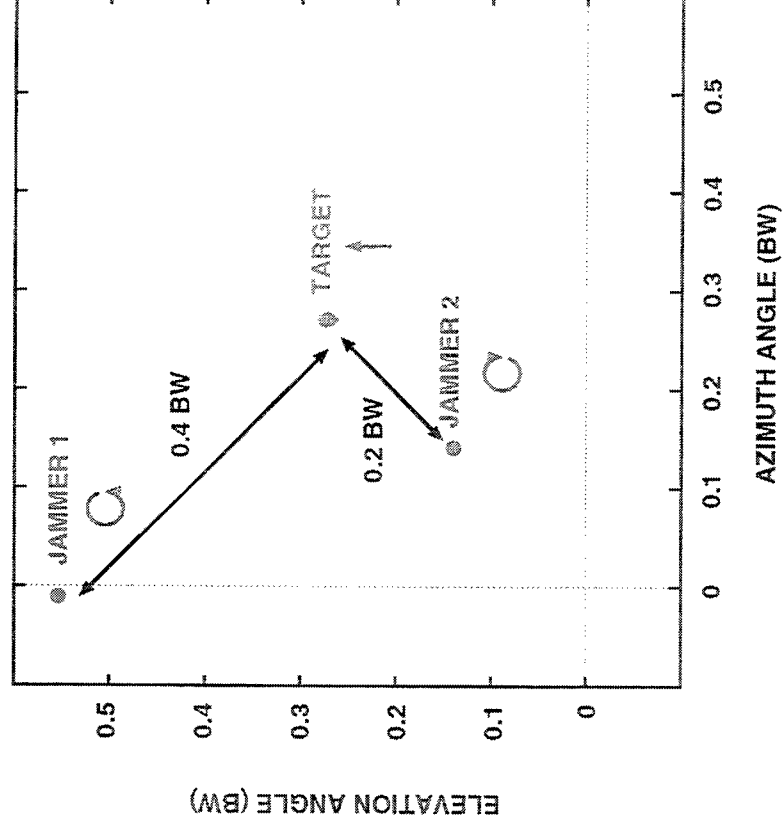
50 dB JNR
20 dB SNR
40 INTERFERENCE ONLY LOOKS
10 TARGET LOOKS (10:1 PDI*)

* PDI = POST-DOPPLER INTEGRATION



SIMULATION SOURCE LOCATIONS

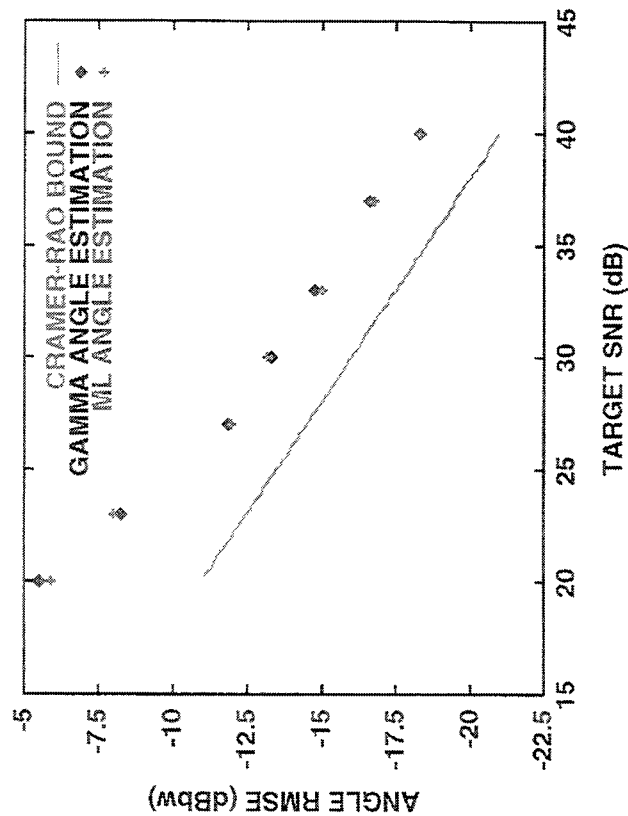
TWO JAMMER SCENARIO, DUAL POL ARRAY



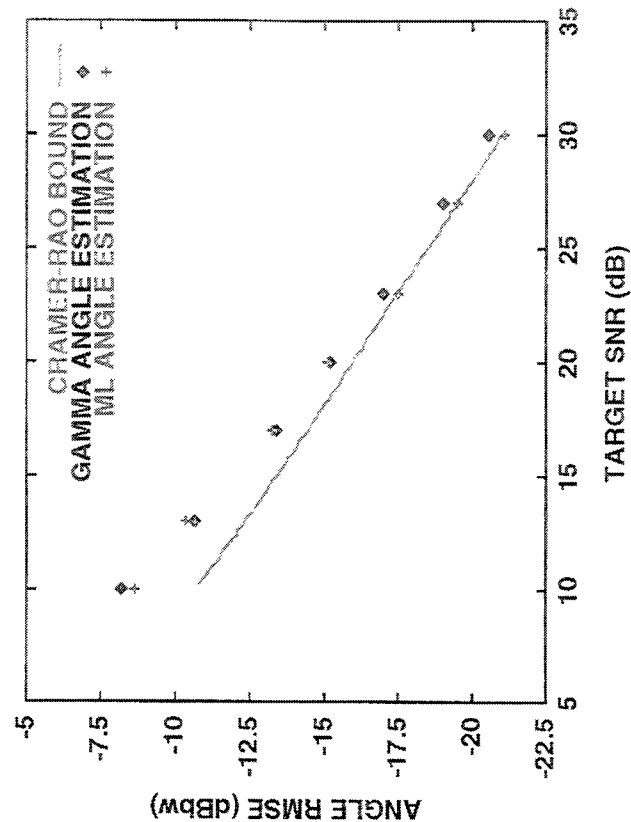
GAMMA DF ACCURACY

6 CHANNEL DUAL POLARIZATION ARRAY

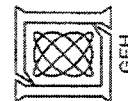
1 TARGET LOOK (1:1 PDI)



10 TARGET LOOKS (10:1 PDI)



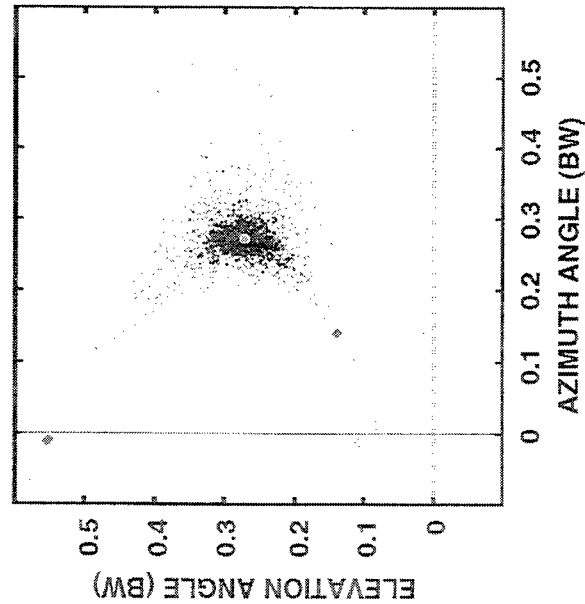
2 JAMMERS
50 dB JNR PER JAMMER
40 INTERFERENCE ONLY LOOKS



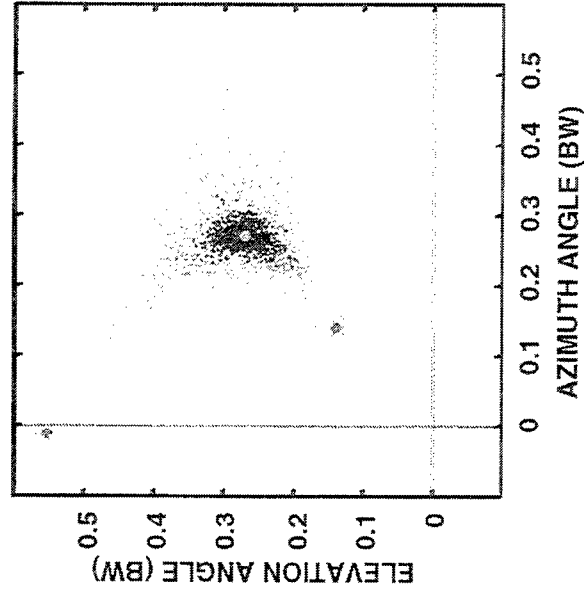
GAMMA DIRECTION ESTIMATION

6 CHANNEL DUAL POLARIZATION ARRAY

GAMMA
PARAMETER ESTIMATION



ML
PARAMETER ESTIMATION



* TARGET LOCATION
* JAMMER LOCATIONS

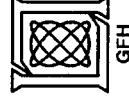
50 dB JNR
40 INTERFERENCE ONLY LOOKS
10 TARGET LOOKS (10:1 PDI)

20 dB SNR 13 dB SNR



CONCLUSIONS

- A NEW ALGORITHM, *GAMMA*, HAS BEEN DERIVED FOR ADAPTIVE PARAMETER ESTIMATION FROM MULTI-DIMENSIONAL ARRAYS
 - GENERALIZED MONOPULSE FRAMEWORK USED TO GENERATE MULTIVARIATE POLYNOMIAL SYSTEM OF EQUATIONS
 - REQUIRES NO ARRAY MANIFOLD SEARCH
 - CAN BE APPLIED TO ARBITRARY ARRAY TOPOLOGIES
 - GIVES NEARLY ML PARAMETER ESTIMATES



Statistical Analysis of Clutter Editing Adaptive Detection Algorithm

Christ D. Richmond

MIT Lincoln Laboratory
244 Wood Street
Lexington, MA 02173-9108
tel: (617) 981-5954
email: christ@ll.mit.edu

Abstract An adaptive detection algorithm known as clutter editing (CLED) was recently proposed as a means of overcoming the high probability of false alarm (PFA) rate associated with the adaptive matched filter (AMF) detector in the presence of undemulled clutter and/or clutter discretes. The AMF is known to be a constant false alarm rate (CFAR) detector under the assumptions of homogeneous clutter with complex Gaussian statistics. In practice, the inhomogeneity of radar clutter (especially in airborne radar systems), and the resulting difficulties in estimating the data covariance matrix significantly mitigate the AMF's inherent CFAR property. The CLED adaptive detection algorithm attempts to remedy this situation. Essentially, this algorithm can be described as a two-stage adaptive sequential detection consisting of a first stage AMF detection followed by a second stage detector known as an adaptive coherence estimator (ACE). The ACE statistic provides a measure of the correlation between the test cell and the assumed target array response vector in a whitened space. Only those range-Doppler test cells that survive both detection thresholdings are declared as target bearing. This present analysis of the CLED algorithm assumes the traditional complex Gaussian statistics in a homogeneous clutter environment. In particular, we provide exact novel closed form expressions for the resulting probability of detection (PD) and PFA of the CLED adaptive detection algorithm and demonstrate that (1) the CLED has a higher or commensurate PD for a given PFA than both the AMF and the ACE, (2) the CLED has a lower or commensurate PFA for a given PD than both the AMF and the ACE, (3) the CLED has an overall performance which is commensurate with the benchmark generalized likelihood ratio test (GLRT), and (4) the CLED is computationally more efficient than a straight GLRT.

STATISTICAL ANALYSIS OF CLUTTER EDITING ADAPTIVE DETECTION ALGORITHM

CHRIST D. RICHMOND

FIFTH ANNUAL ASAP WORKSHOP 14 MARCH 1997



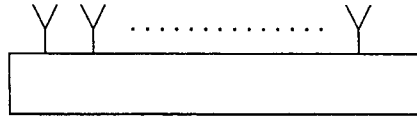
OUTLINE

- **ADAPTIVE DETECTION**
- **CLUTTER EDITING ALGORITHM (CLED)**
- **PERFORMANCE OF CLED**
 - **HOMOGENEOUS CLUTTER**
 - **NON-HOMOGENEOUS CLUTTER**
- **CLOSING REMARKS**



ADAPTIVE DETECTION PROBLEM

ARRAY



TEST CELL:

$$H_0: \mathbf{x} = \mathbf{n}$$

$$H_1: \mathbf{x} = \mathbf{S} \mathbf{v} + \mathbf{n}$$

$$\text{cov}(\mathbf{x}) = \mathbf{R}$$

● TWO UNKNOWNNS: \mathbf{R} & \mathbf{S}

● USE NOISE ONLY TRAINING SET:

$$\mathbf{x}_1, \mathbf{x}_2, \dots, \mathbf{x}_L$$

$$\text{cov}(\mathbf{x}_i) = \mathbf{R}, \quad i = 1, 2, \dots, L$$

CLASSICAL ASSUMPTIONS:

- ALL DATA COMPLEX GAUSSIAN
- TRAINING SAMPLES HAVE SAME COVARIANCE AS TEST CELL
(HOMOGENEOUS CLUTTER CASE)



ADAPTIVE DETECTION ALGORITHMS

- ADAPTIVE MATCHED FILTER

(AMF) ROBEY (1992), REED (1974)

$$t_{AMF} = \frac{|v^H \hat{R}^{-1} x|^2}{v^H \hat{R}^{-1} v}$$

- GENERALIZED LIKELIHOOD

RATIO TEST (GLRT) KELLY (1986)

$$t_{GLRT} = \frac{t_{AMF}}{1 + x^H \hat{R}^{-1} x}$$

- ADAPTIVE COHERENCE

ESTIMATOR (ACE)

CONTE (1996), SCHARF (1996)

$$t_{ACE} = \frac{t_{AMF}}{x^H \hat{R}^{-1} x} \quad (NEW)$$

- CLUTTER EDITING ALGORITHM

(CLED) KREITHEN, BARANOSKI (1996)

$$f(t_{AMF}, t_{ACE}) \quad (NEW)$$

$$\hat{R} = x_1 x_1^H + x_2 x_2^H + \dots + x_L x_L^H \leftarrow$$

SAMPLE COVARIANCE



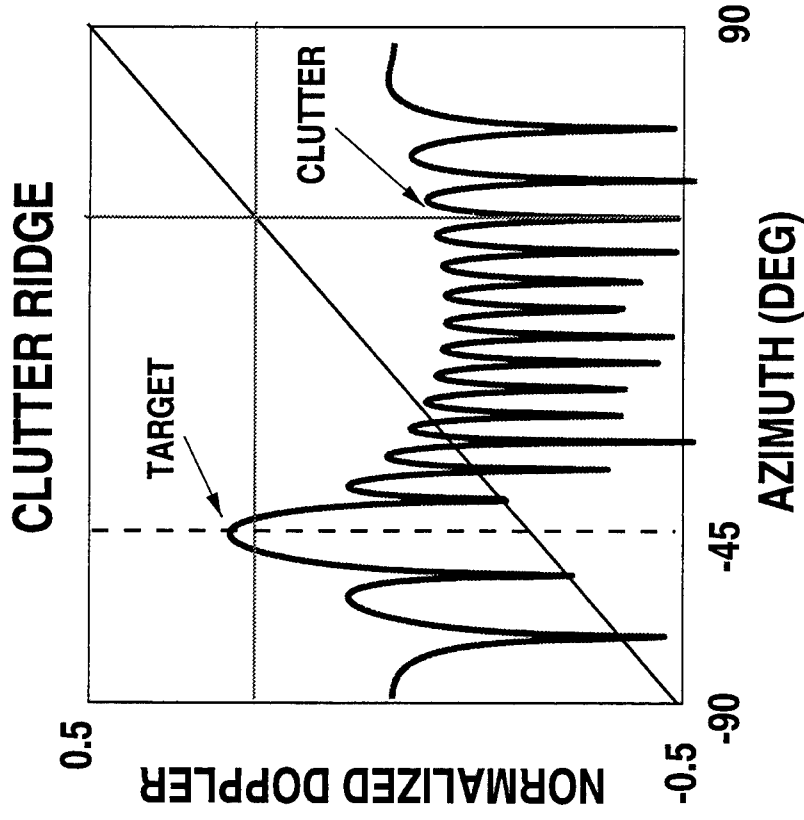
PRACTICAL ISSUES: THE AMF

- **AMF COMPUTATIONALLY ATTRACTIVE: LINEAR FILTER**
- **AMF IS AN ADAPTIVE BEAMFORMER**
 - PROVIDES A MEASURE OF POWER PRESENT IN TARGET DIRECTION
- **COVARIANCE MISMATCH BETWEEN TRAINING SET & TEST CELL**
 - ARTIFACT OF NON-HOMOGENEITY
 - UNDERNULLLED CLUTTER CAN RESULT IN HIGH PFA



THE AMF & CLUTTER DISCRETES

- INHOMOGENEITY CAN LEAD TO UNDERNULLED CLUTTER
- UNDERNULLED CLUTTER CAN RESULT IN HIGH AMF PFA
- CLED ALGORITHM ATTEMPTS TO REMEDY THIS PROBLEM



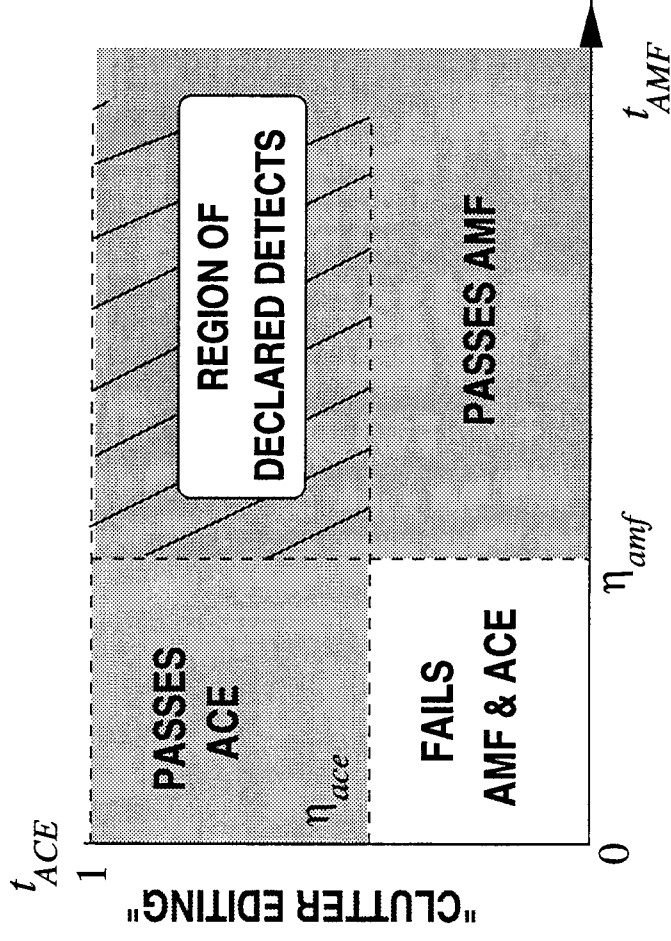
OUTLINE

- **ADAPTIVE DETECTION**
- **CLUTTER EDITING ALGORITHM (CLEd)**
- **PERFORMANCE OF CLEd**
 - **HOMOGENEOUS CLUTTER**
 - **NON-HOMOGENEOUS CLUTTER**
- **CLOSING REMARKS**



CLED DETECTION ALGORITHM

2-D ADAPTIVE DETECTOR



STEP 1: TARGET PRESENT?

$$t_{AMF} > \eta_{amf}$$

POWER IN TARGET
DIRECTION

STEP 2: CLUTTER EDITING

$$t_{AMF} > \eta_{ace} * \mathbf{x}^H \hat{\mathbf{R}}^{-1} \mathbf{x}$$

POWER IN TARGET
DIRECTION

TOTAL POWER FROM
ALL DIRECTIONS



OUTLINE

- **ADAPTIVE DETECTION**
- **CLUTTER EDITING ALGORITHM (CLED)**
- **PERFORMANCE OF CLED**
 - **HOMOGENEOUS CLUTTER**
 - THEORETICAL RESULTS**
 - NUMERICAL RESULTS**
 - **NON-HOMOGENEOUS CLUTTER**
- **CLOSING REMARKS**



DISTRIBUTIONS OF DETECTORS

- RECALL THAT PD OF CLED IS

$$PD_{CLED} = Pr(t_{ACE} > \eta_{ace}, t_{AMF} > \eta_{amf})$$

- DEFINE THE FOLLOWING

$$\tilde{t}_{GLRT} \triangleq t_{GLRT}/(1 - t_{GLRT}) \quad \tilde{t}_{ACE} \triangleq t_{ACE}/(1 - t_{ACE})$$

$$\delta_\beta = \sqrt{\beta_{K,N-1}} \cdot |S| \cdot \sqrt{\mathbf{v}^H \mathbf{R}^{-1} \mathbf{v}} \quad K \triangleq L - N + 2$$

- IT CAN BE SHOWN THAT

Distributions of Adaptive Detectors

$$\begin{aligned} \tilde{t}_{GLRT} &\stackrel{d}{=} F_{1,K-1}(\delta_\beta) \\ t_{AMF} &\stackrel{d}{=} F_{1,K-1}(\delta_\beta)/\beta_{K,N-1} \\ \tilde{t}_{ACE} &\stackrel{d}{=} F_{1,K-1}(\delta_\beta)/(1 - \beta_{K,N-1}) \end{aligned}$$



PD & PFA OF CLED ALGORITHM

● DEFINE THE QUANTITY

$$\gamma(\eta_{ace}, \eta_{amf}) \triangleq \frac{\eta_{ace}}{\eta_{ace} + \eta_{amf}(1 - \eta_{ace})}, \quad 0 \leq \gamma(\eta_{ace}, \eta_{amf}) \leq 1$$

● IT CAN BE SHOWN THAT

$$PD_{CLED} = \int_0^{\gamma(\eta_{ace}, \eta_{amf})} P_\beta d\beta \cdot PD_{ACE|\beta} + \int_{\gamma(\eta_{ace}, \eta_{amf})}^1 P_\beta d\beta \cdot PD_{AMF|\beta}$$

$$PFA_{CLED} = \int_0^{\gamma(\eta_{ace}, \eta_{amf})} P_\beta d\beta \cdot PFA_{ACE|\beta} + \int_{\gamma(\eta_{ace}, \eta_{amf})}^1 P_\beta d\beta \cdot PFA_{AMF|\beta}$$



PD & PFA OF CLED ALGORITHM

● DEFINE THE QUANTITY

$$\gamma(\eta_{ace}, \eta_{amf}) \triangleq \frac{\eta_{ace}}{\eta_{ace} + \eta_{amf}(1 - \eta_{ace})}, \quad 0 \leq \gamma(\eta_{ace}, \eta_{amf}) \leq 1$$

● IT CAN BE SHOWN THAT

$$PD_{CLED} = \int_0^{\gamma(\eta_{ace}, \eta_{amf})} P_{\beta} d\beta \cdot PD_{ACE|\beta} + \int_{\gamma(\eta_{ace}, \eta_{amf})}^1 P_{\beta} d\beta \cdot PD_{AMF|\beta}$$

$$PFA_{CLED} = \int_0^{\gamma(\eta_{ace}, \eta_{amf})} P_{\beta} d\beta \cdot PFA_{ACE|\beta} + \int_{\gamma(\eta_{ace}, \eta_{amf})}^1 P_{\beta} d\beta \cdot PFA_{AMF|\beta}$$



PD & PFA OF CLED ALGORITHM

- DEFINE THE QUANTITY

$$\gamma(\eta_{ace}, \eta_{amf}) \triangleq \frac{\eta_{ace}}{\eta_{ace} + \eta_{amf}(1 - \eta_{ace})}, \quad 0 \leq \gamma(\eta_{ace}, \eta_{amf}) \leq 1$$

$$\eta_{ace} = 0$$

- IT CAN BE SHOWN THAT

$$PD_{CLED} = \int_0^{\gamma(\eta_{ace}, \eta_{amf})} P_{\beta} d\beta \cdot PD_{ACE|\beta} + \int_{\gamma(\eta_{ace}, \eta_{amf})}^1 P_{\beta} d\beta \cdot PD_{AMF|\beta}$$



$$PFA_{CLED} = \int_0^{\gamma(\eta_{ace}, \eta_{amf})} P_{\beta} d\beta \cdot PFA_{ACE|\beta} + \int_{\gamma(\eta_{ace}, \eta_{amf})}^1 P_{\beta} d\beta \cdot PFA_{AMF|\beta}$$





PD & PFA OF CLED ALGORITHM

- DEFINE THE QUANTITY

$$\gamma(\eta_{ace}, \eta_{amf}) \triangleq \frac{\eta_{ace}}{\eta_{ace} + \eta_{amf}(1 - \eta_{ace})}, \quad 0 \leq \gamma(\eta_{ace}, \eta_{amf}) \leq 1$$

$$\eta_{amf} = 0$$

- IT CAN BE SHOWN THAT

$$PD_{CLED} = \int_0^{\gamma(\eta_{ace}, \eta_{amf})} P_{\beta} d\beta \cdot PD_{ACE|\beta} + \int_{\gamma(\eta_{ace}, \eta_{amf})}^1 P_{\beta} d\beta \cdot PD_{AMF|\beta}$$

ACE AMF

0 0

$$PFA_{CLED} = \int_0^{\gamma(\eta_{ace}, \eta_{amf})} P_{\beta} d\beta \cdot PFA_{ACE|\beta} + \int_{\gamma(\eta_{ace}, \eta_{amf})}^1 P_{\beta} d\beta \cdot PFA_{AMF|\beta}$$

ACE AMF

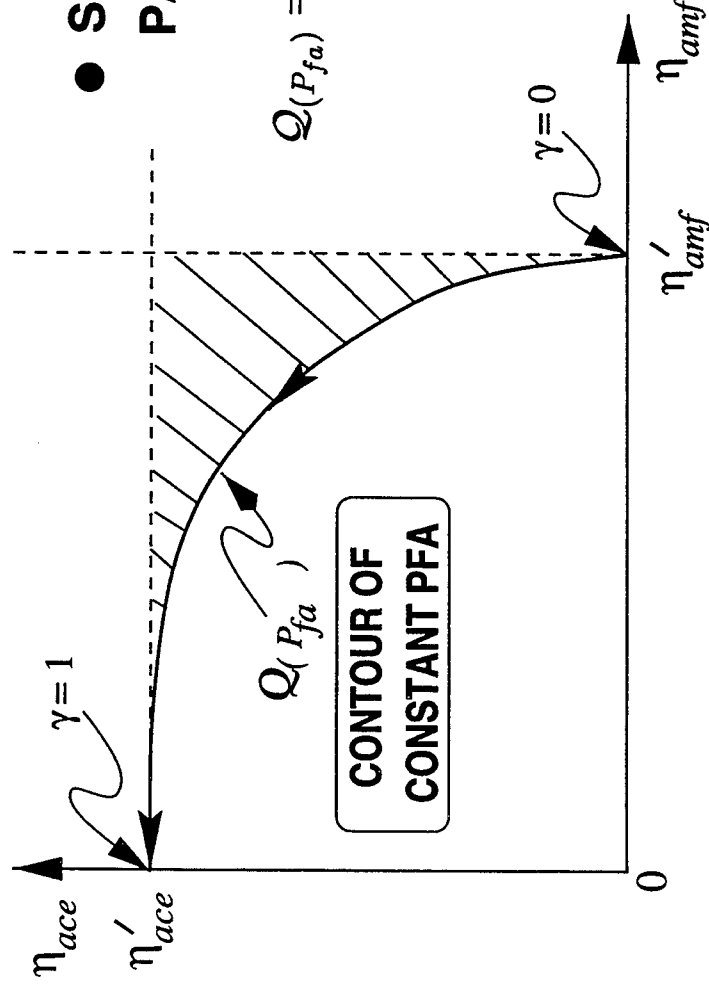
0 0



CLED CONTOUR OF CONSTANT PFA

- SET OF ALL THRESHOLD PAIRS YIELDING SAME PFA:

$$\mathcal{Q}(P_{fa}) = \{(\eta_{ace}, \eta_{amf}) \mid \text{PFA}_{CLED} = P_{fa}\}$$



Endpoints of $\mathcal{Q}(P_{fa})$ are given by $(\eta'_{ace}, 0)$ and $(0, \eta'_{amf})$:

$$\text{PFA}_{ACE} = \Pr(t_{ACE} > \eta'_{ace} | H_0) = P_{fa}$$

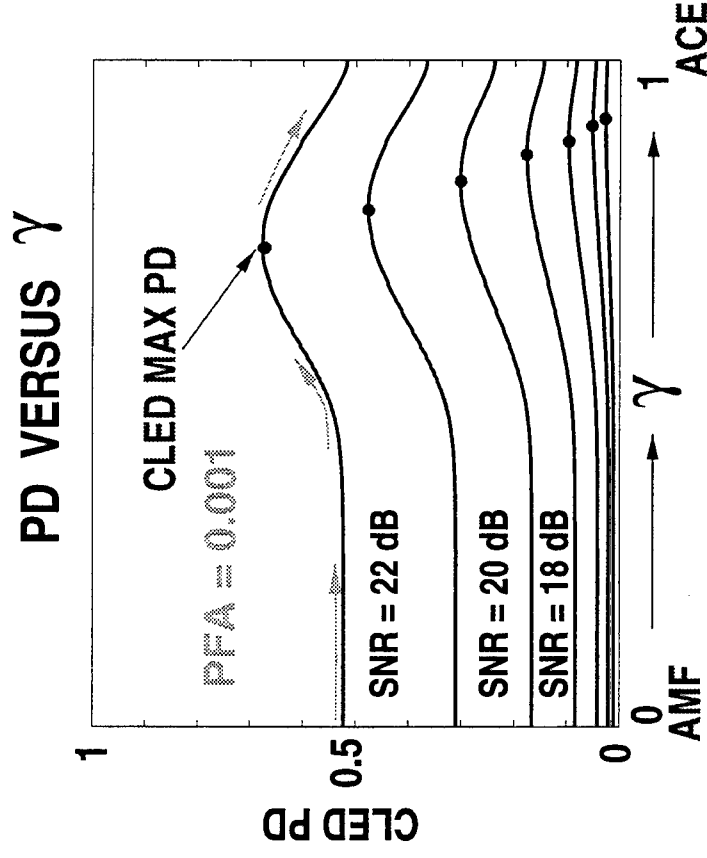
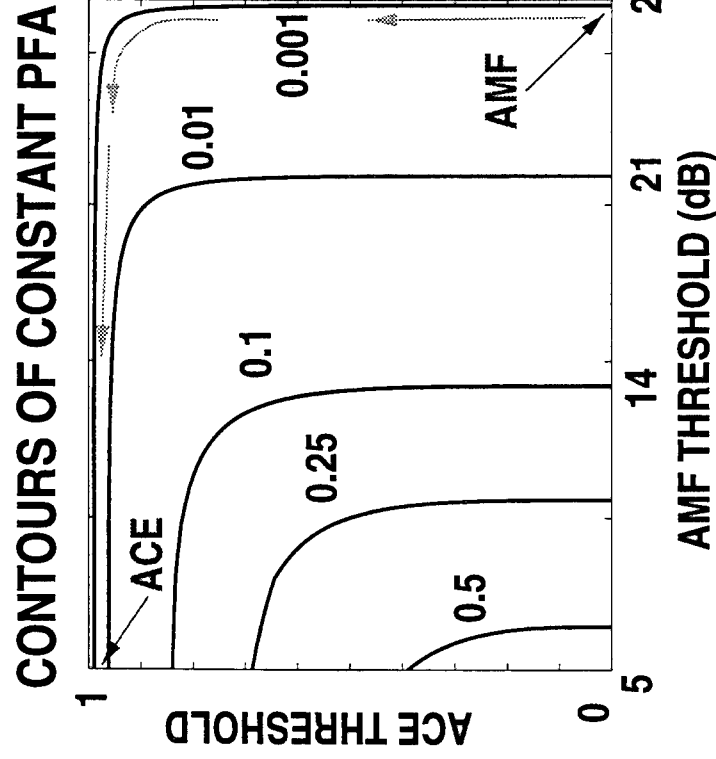
$$\text{PFA}_{AMF} = \Pr(t_{AMF} > \eta'_{amf} | H_0) = P_{fa}.$$



NUMERICAL RESULTS FOR CLED

-ARRAY OF $N = 4$ ELEMENTS

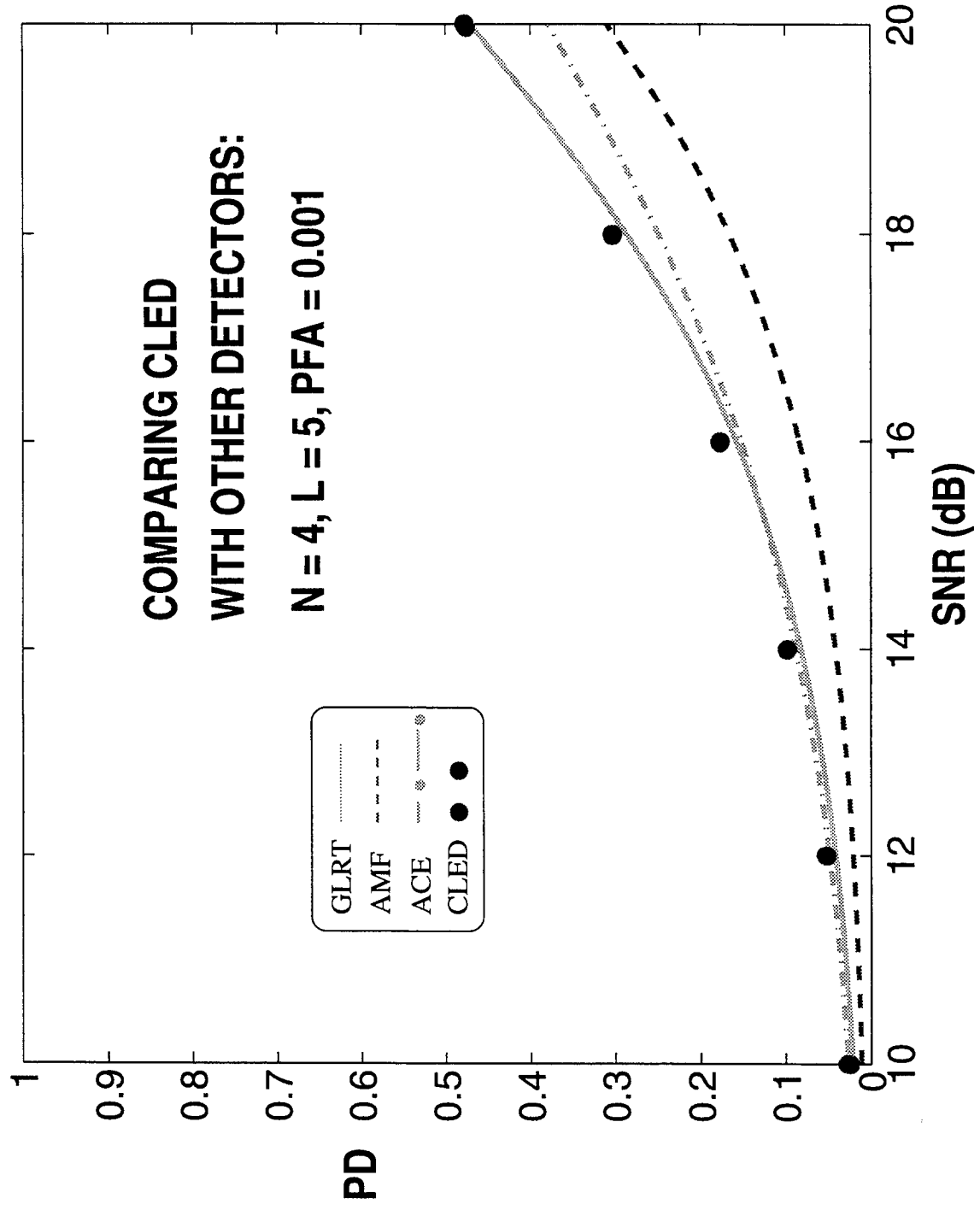
-TRAINING SET OF SIZE $L = 5$ SAMPLES



NUMERICAL RESULTS FOR CLED

COMPARING CLED
WITH OTHER DETECTORS:

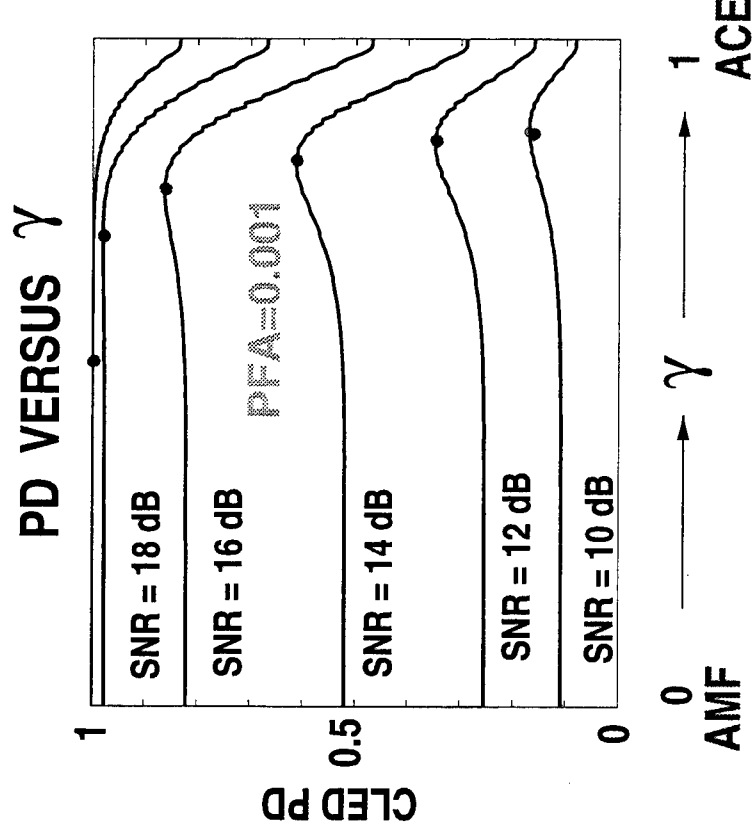
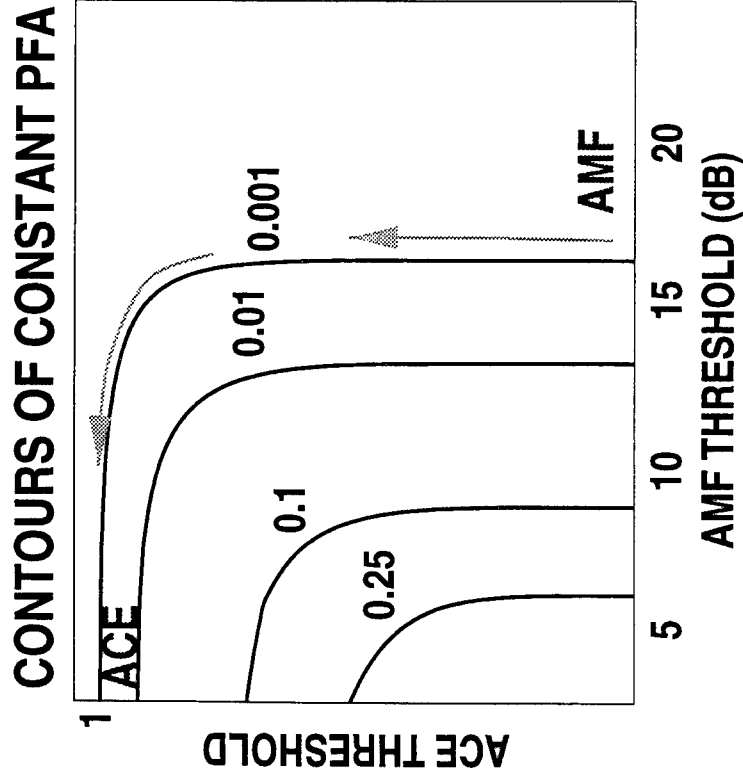
$N = 4, L = 5, PFA = 0.001$



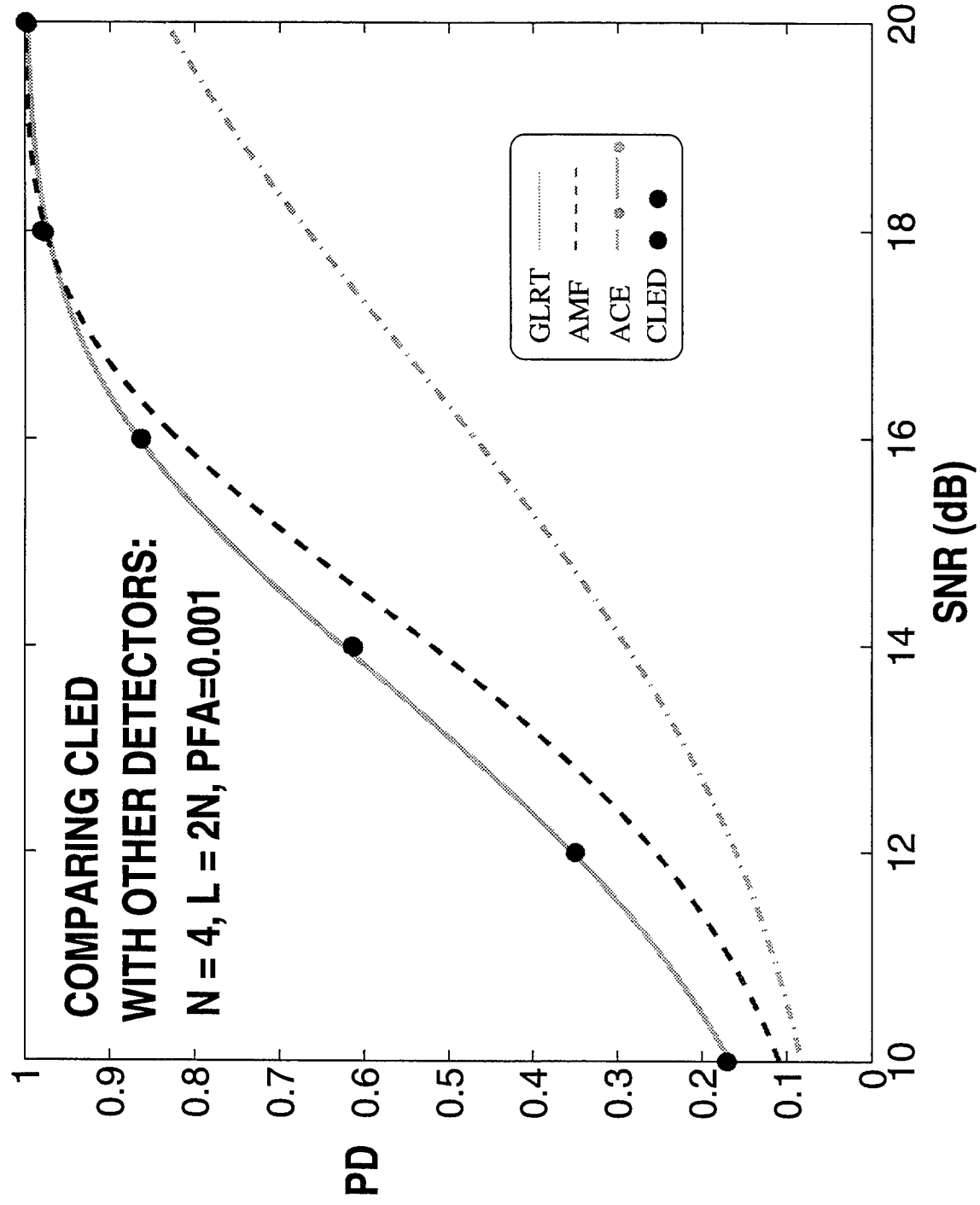
NUMERICAL RESULTS FOR CLED

-ARRAY OF $N = 4$ ELEMENTS

-TRAINING SET OF SIZE $L = 2N$ SAMPLES



NUMERICAL RESULTS FOR CLED



OUTLINE

- **ADAPTIVE DETECTION**
- **CLUTTER EDITING ALGORITHM (CLEd)**
- **PERFORMANCE OF CLEd**
 - **HOMOGENEOUS CLUTTER**
 - **NON-HOMOGENEOUS CLUTTER**
- **CLOSING REMARKS**

THEORETICAL RESULTS

NUMERICAL RESULTS



INHOMOGENEITY: COVARIANCE MISMATCH

- SHALL ASSUME

-HOMOGENEOUS NOISE ONLY TRAINING SET

$$\mathbf{x}_1, \mathbf{x}_2, \dots, \mathbf{x}_L \quad \text{cov}(\mathbf{x}_i) = \mathbf{R}, \quad i = 1, 2, \dots, L$$

-COVARIANCE MISMATCHED TEST CELL

$$\text{cov}(\mathbf{x}) = \mathbf{R}_T$$

- NICE THEORETICAL RESULTS POSSIBLE IF

$$\bar{\mathbf{R}}^{-1} \mathbf{v} = \lambda \bar{\mathbf{R}}_T^{-1} \mathbf{v}$$



DISTRIBUTIONS OF DETECTORS / PD & PFA

- DEFINE THE FOLLOWING

$$\tilde{\delta}_\beta = \left[\frac{\beta}{\beta(\lambda - 1) + 1} \right] \cdot |S| \cdot \sqrt{\mathbf{v}^H \mathbf{R}^{-1} \mathbf{v}} \quad \text{where} \quad \mathbf{R}^{-1} \mathbf{v} = \lambda \cdot \mathbf{R}_T^{-1} \mathbf{v}$$

- IT CAN BE SHOWN THAT

Distributions of Adaptive Detectors

$$\begin{aligned} \tilde{t}_{GLRT} &\stackrel{d}{=} F_{1,K-1}(\tilde{\delta}_\beta) \cdot [\beta(\lambda - 1) + 1] \\ t_{AMF} &\stackrel{d}{=} F_{1,K-1}(\tilde{\delta}_\beta) \cdot \left[(\lambda - 1) + \frac{1}{\beta} \right] \\ \tilde{t}_{ACE} &\stackrel{d}{=} F_{1,K-1}(\tilde{\delta}_\beta) \cdot \left[\frac{\lambda\beta}{1-\beta} + 1 \right] \end{aligned}$$

- PDF OF β DEPENDS ON EIGENVALUES OF $\mathbf{R}^{-1/2} \mathbf{R}_T \mathbf{R}^{-1/2}$

- PD & PFA EXPRESSIONS SIMILAR



NUMERICAL RESULTS FOR CLED

-ARRAY OF $N=4$ ELEMENTS

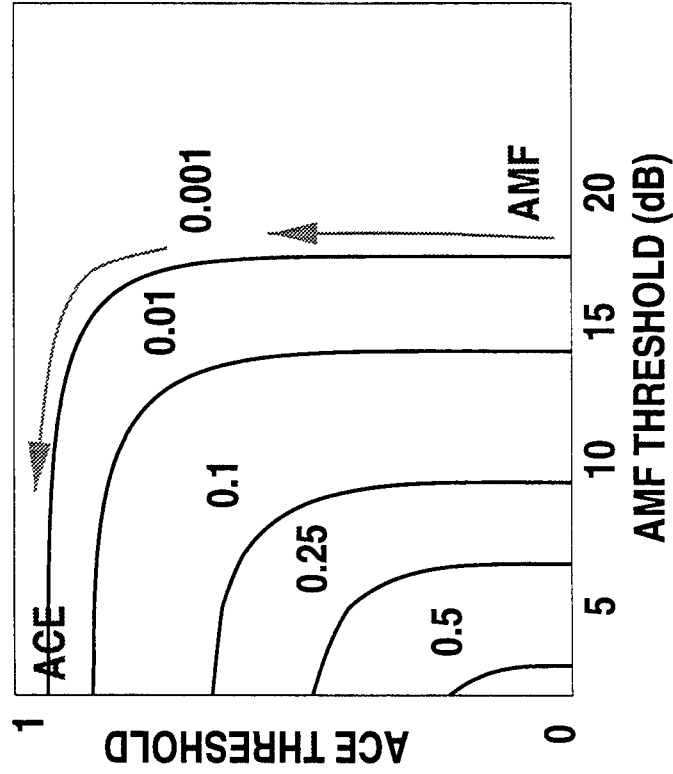
-TRAINING SET OF SIZE $L=2N$ SAMPLES

$$\mathbf{R}_T = \mathbf{R} + \sigma_J^2 \mathbf{q} \mathbf{q}^H \quad \text{WHERE} \quad \mathbf{v}^H \mathbf{R}^{-1} \mathbf{q} = 0$$

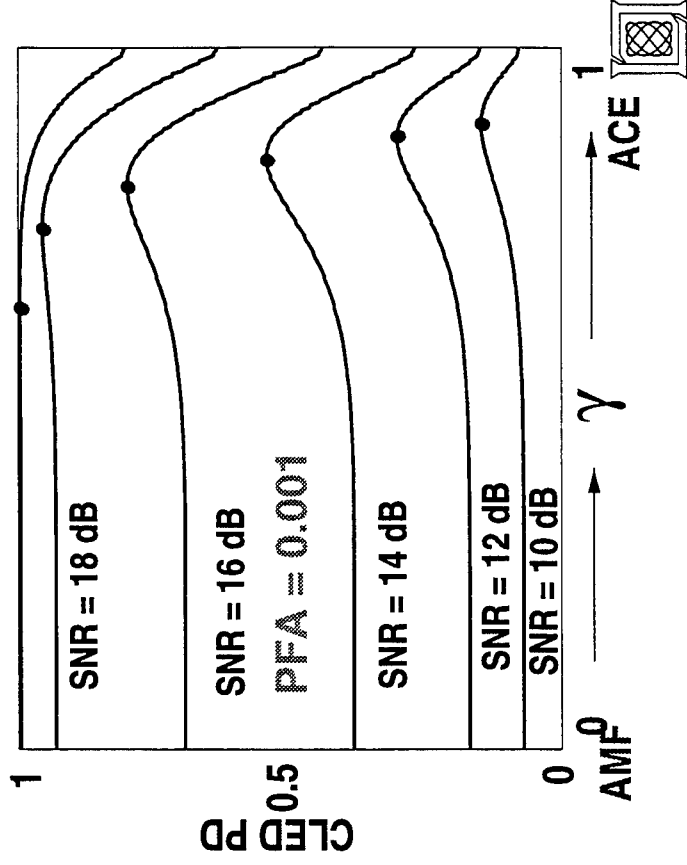
$$\sigma_J^2 = 15 \text{ dB}$$

← RELATIVE TO NOISE FLOOR

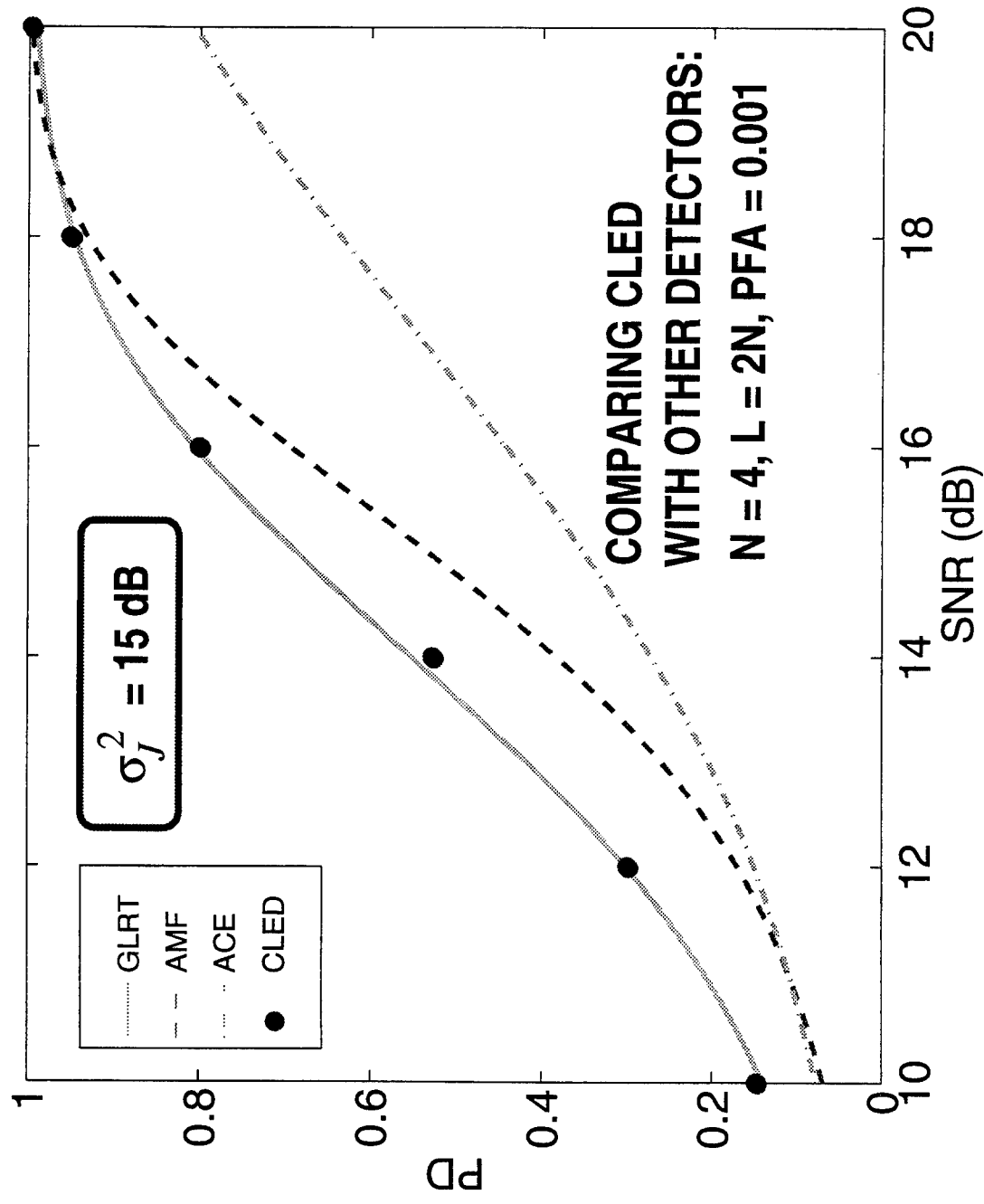
CONTOURS OF CONSTANT PFA



PD VERSUS γ



NUMERICAL RESULTS FOR CLED



NUMERICAL RESULTS FOR CLED

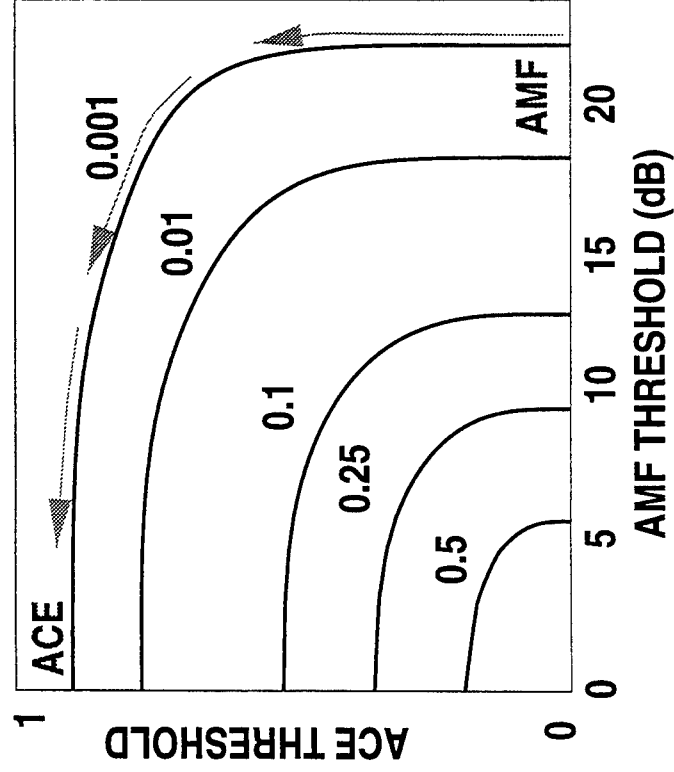
-ARRAY OF $N=4$ ELEMENTS

-TRAINING SET OF SIZE $L=2N$ SAMPLES

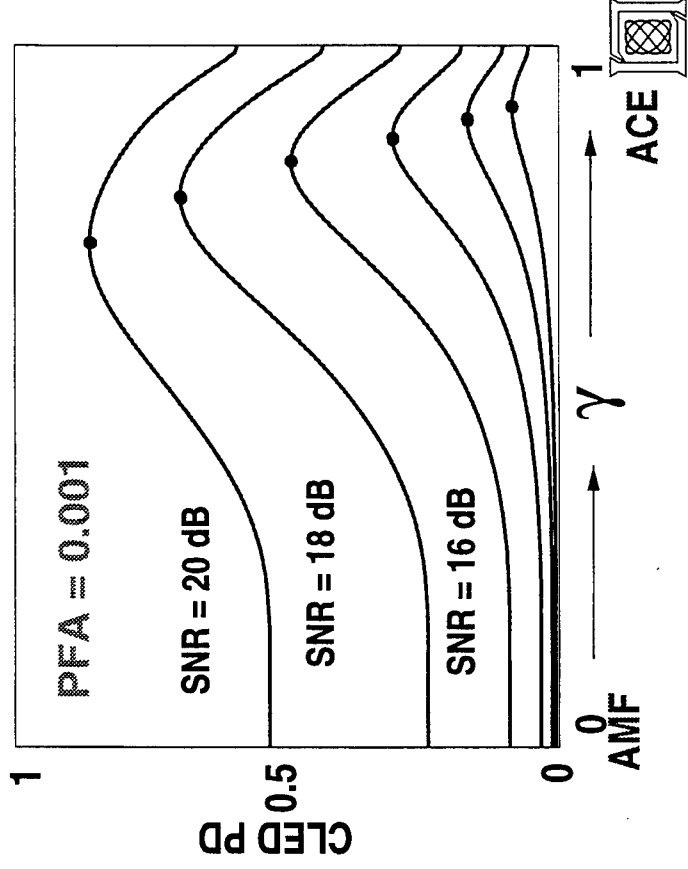
$$\mathbf{R}_T = \mathbf{R} + \sigma_J^2 \mathbf{q} \mathbf{q}^H \quad \text{WHERE} \quad \mathbf{v}^H \mathbf{R}^{-1} \mathbf{q} = 0$$

$$\sigma_J^2 = 25 \text{ dB}$$

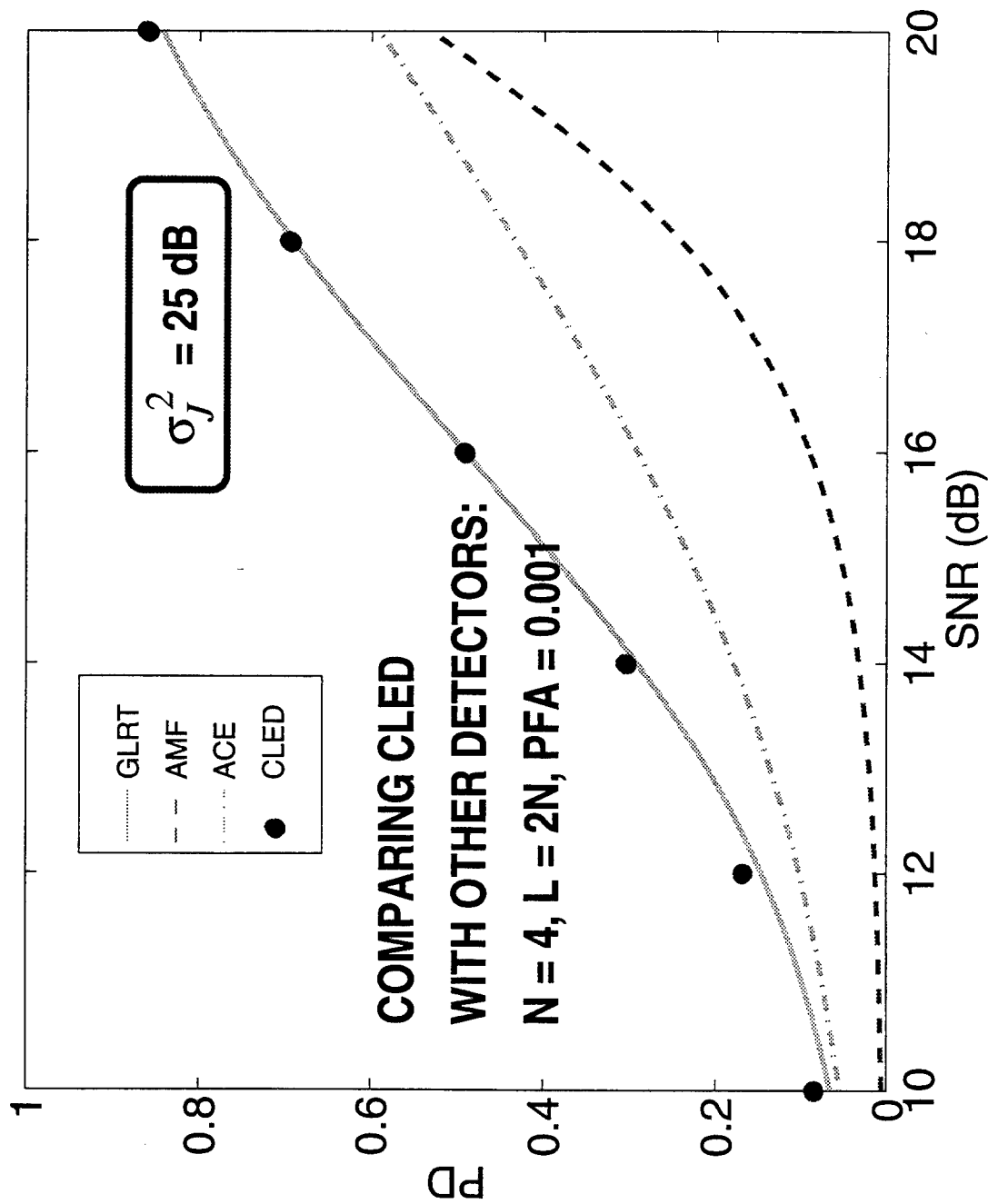
CONTOURS OF CONSTANT PFA



PD VERSUS γ



NUMERICAL RESULTS FOR CLED



NUMERICAL RESULTS FOR CLED

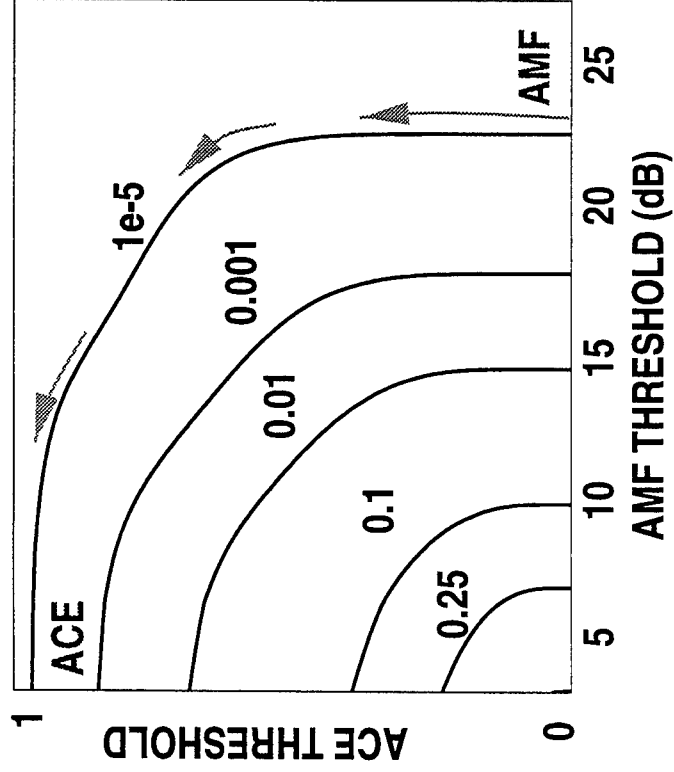
-ARRAY OF $N=4$ ELEMENTS

-TRAINING SET OF SIZE $L=3N$ SAMPLES

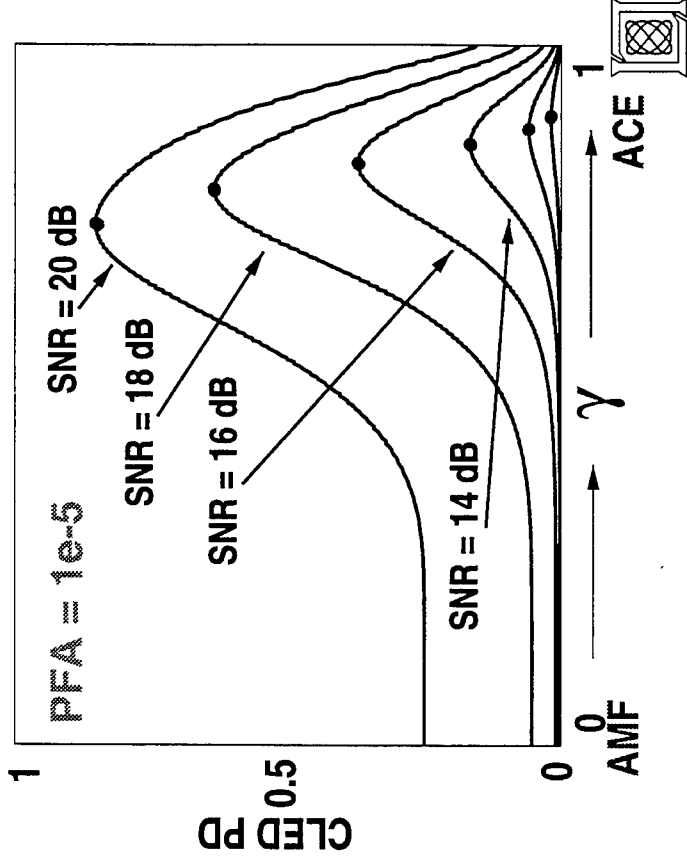
$$\mathbf{R}_T = \mathbf{R} + \sigma_J^2 \mathbf{q} \mathbf{q}^H \quad \text{WHERE} \quad \mathbf{v}^H \mathbf{R}^{-1} \mathbf{q} = 0$$

$$\sigma_J^2 = 25 \text{ dB}$$

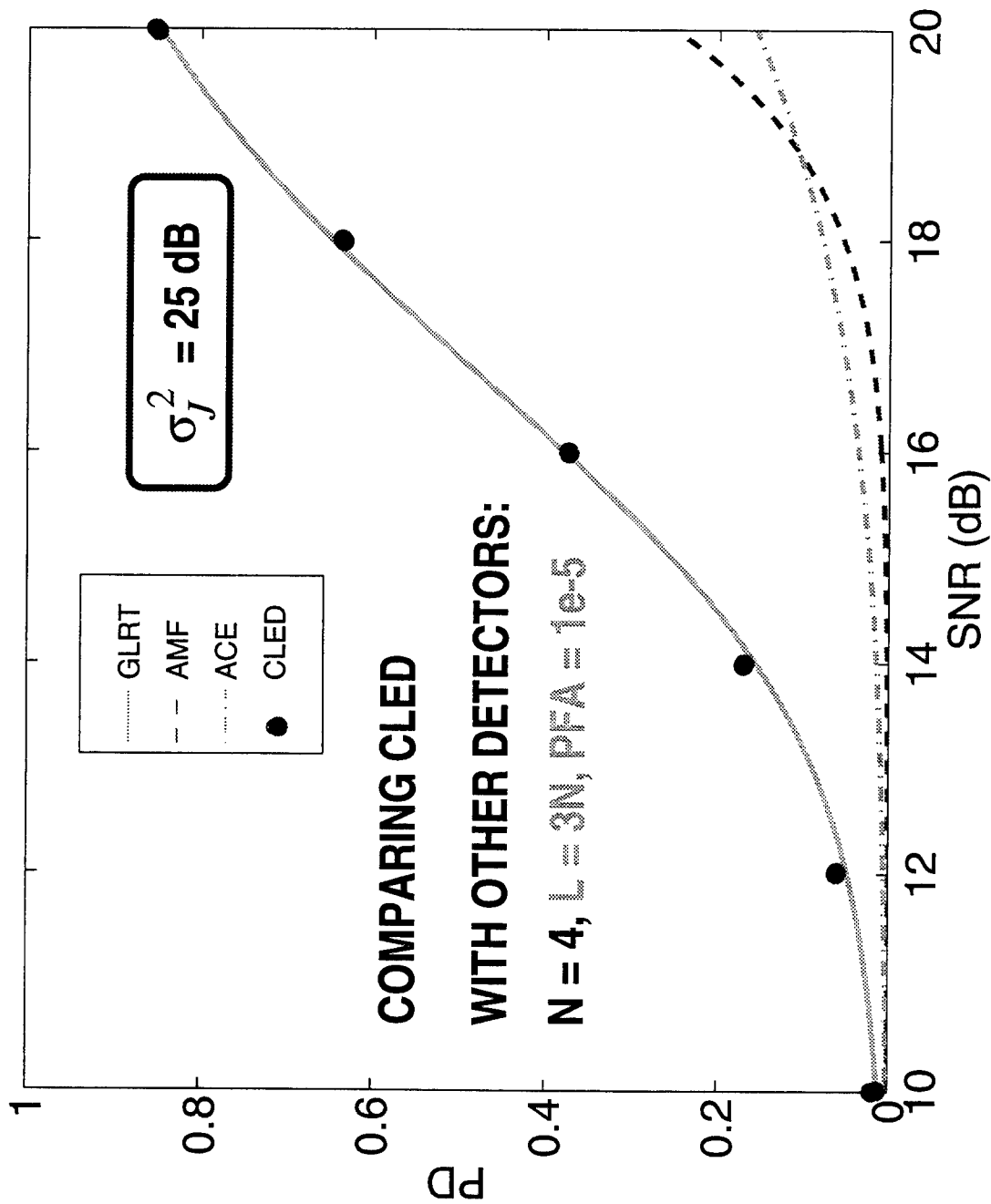
CONTOURS OF CONSTANT PFA



PD VERSUS γ



NUMERICAL RESULTS FOR CLED



CLOSING REMARKS

- **FLEXIBILITY IN CLED THRESHOLD CHOICES ALLOW:**
 - MAXIMIZATION OF RESULTING PD
 - SIDELOBE TARGET SENSITIVITY REGULATION
- **AS GOOD AS OR BETTER THAN AMF OR ACE**
- **PERFORMANCE COMMENSURATE WITH GLRT**
- **COMPUTATIONALLY MORE EFFICIENT THAN GLRT
WITH ADJUSTABLE SENSITIVITY TO SIDELOBE TARGETS**

*** TRUE IN BOTH HOMOG. & NON-HOMOG. CLUTTER**



Adaptive Detection Performance in Non-Ideal Conditions

Steven Smith

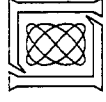
MIT Lincoln Laboratory
244 Wood Street
Lexington, MA 02173-9108
tel: (617) 981-3106
email: stsmith@ll.mit.edu

Abstract Adaptive filtering affects radar system detection performance in a variety of ways. If enough ideal assumptions are made, namely independent, identically distributed Gaussian samples used in the AMF, GLRT, or ACE detectors, then closed form detection statistics are obtainable. However, it is easy to find examples where each or all of these assumptions fails to hold. For example, pre-Doppler STAP coherently combine adaptive outputs determined from overlapping data sets, i.e., the assumption of independence is invalid. Furthermore, clutter is notoriously inhomogeneous in range; if training samples are drawn from that dimension, then the assumption of identically distributed data is invalid (up to a scale factor). Finally, all closed-form analysis of standard adaptive detectors involves the Wiener equation $w = R^{-1}v$; however, diagonal loading is oftentimes used for sidelobe control, which seems impervious to closed-form analysis. These oft encountered issues raise the following interesting questions: Do pre- and post-Doppler STAP algorithms exhibit the same detection performance given fixed sample support and degrees of freedom? What can be said about the detection performance of the AMF, GLRT, ACE, and CLED detectors in the presence of an inhomogeneous scale factor in range? How does diagonal loading affect the detection performance of pre- and post-Doppler STAP algorithms? This talk will answer these questions using Monte Carlo analysis, possible alternate simplifying assumptions, and comparison to previous closed-form analysis.

ADAPTIVE DETECTOR PERFORMANCE IN NON-IDEAL CONDITIONS

**STEVEN T. SMITH
LINCOLN LABORATORY
MASSACHUSETTS INSTITUTE OF TECHNOLOGY**

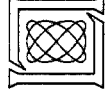
1997 ASAP WORKSHOP



970313-0

OUTLINE

- INTRODUCTION
- NON-IDEAL SCENARIOS
- NON-IDEAL DETECTOR PERFORMANCE
- CONCLUSIONS

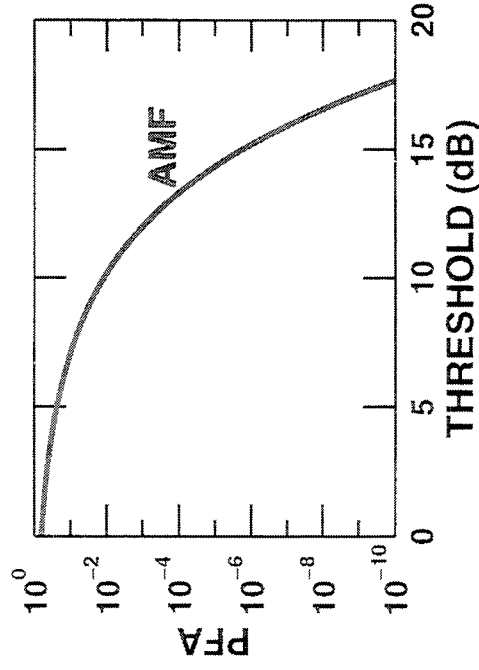


IDEAL ADAPTIVE DETECTORS

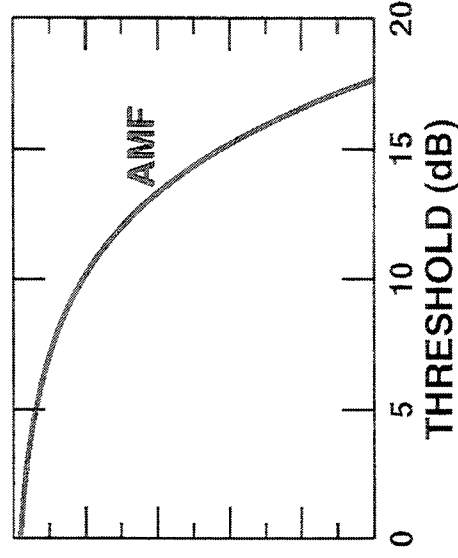
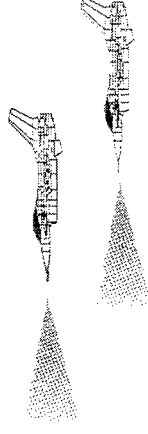
THE BEST OF ALL POSSIBLE WORLDS

- INDEPENDENT IDENTICALLY DISTRIBUTED DATA
- CONSTANT FALSE ALARM RATE
- CLOSED FORM STATISTICS

NO INTERFERENCE



INTERFERENCE



FALSE ALARM RATE INDEPENDENT
OF INTERFERENCE SCENARIO

IDEAL ADAPTIVE DETECTORS

ALL HAVE CFAR PROPERTY

$$\begin{array}{ll} H_0: & z = n \quad \text{NOISE-ONLY} \\ H_1: & z = b v + n \quad \text{SIGNAL-PLUS-NOISE} \end{array}$$

- ADAPTIVE MATCHED FILTER (AMF)

$$AMF = \frac{|v^H \hat{R}^{-1} z|^2}{v^H \hat{R}^{-1} v} \underset{H_0}{\overset{H_1}{\gtrless}} \text{THRESHOLD}$$

$$\hat{R} = \frac{1}{K} \sum_{k=1}^K n_k n_k^H$$

- GENERALIZED LIKELIHOOD RATIO TEST (GLRT)

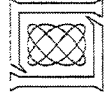
$$GLRT = \frac{AMF}{K^{-1} + z^H \hat{R}^{-1} z} \underset{H_0}{\overset{H_1}{\gtrless}} \text{THRESHOLD}$$

- ADAPTIVE COHERENCE ESTIMATOR (ACE)

$$ACE = \frac{AMF}{z^H \hat{R}^{-1} z} \underset{H_0}{\overset{H_1}{\gtrless}} \text{THRESHOLD}$$

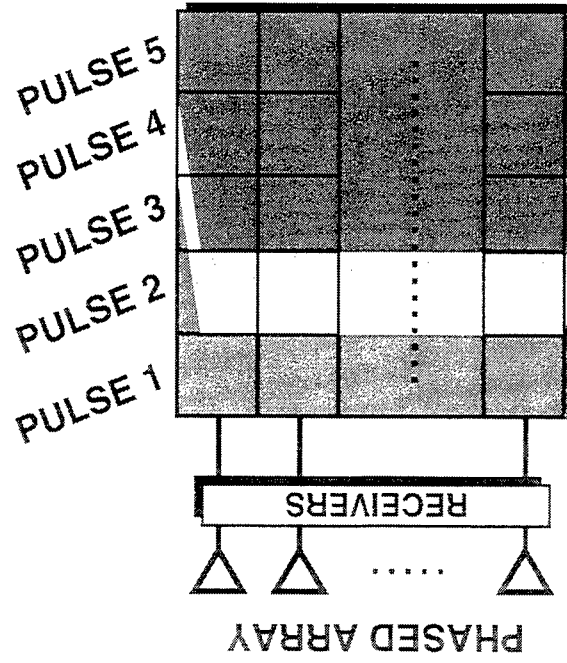
OUTLINE

- INTRODUCTION
- NON-IDEAL SCENARIOS
 - PRE-DOPPLER STAP
 - DIAGONAL LOADING
 - INHOMOGENEOUS CLUTTER
- NON-IDEAL DETECTOR PERFORMANCE
- CONCLUSIONS



PRE-DOPPLER STAP

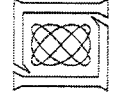
ADAPT SEPARATELY ON SUB-CPIs / DOPPLER FILTER



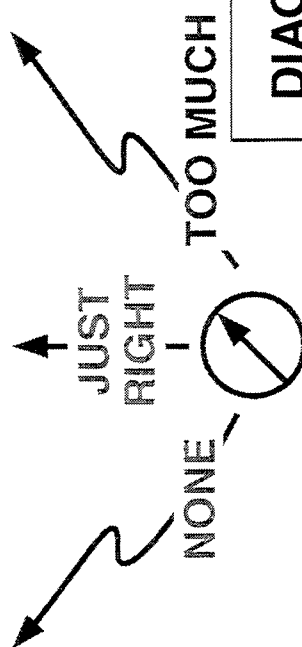
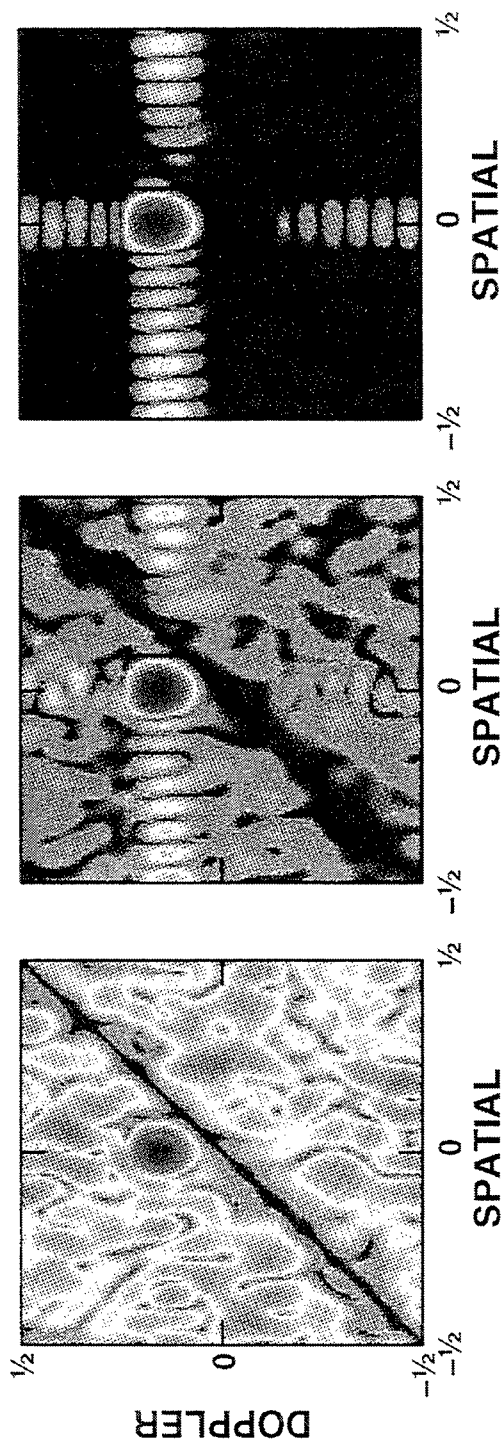
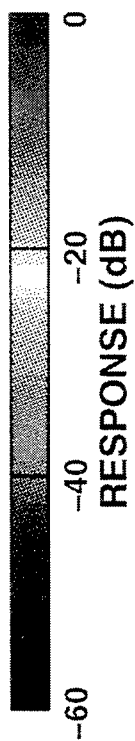
DOPPLER BIN OUTPUT = $w^H z$ = COHERENT COMBINATION OF SEVERAL DEPENDENT ADAPTIVE OUTPUTS

$$\text{SINR} = \frac{|w^H z|^2}{w^H \hat{R}_w w} \neq \frac{|v^H \hat{R}^{-1} z|^2}{v^H \hat{R}^{-1} v} = \text{AMF}$$

PRE-DOPPLER STAP DETECTION PERFORMANCE IS NOT GIVEN BY KNOWN RESULTS



DIAGONAL LOADING



**DIAGONALLY LOADED
PERFORMANCE IS
NOT GIVEN BY
KNOWN RESULTS**

**DIAGONAL
LOADING
LEVEL**

• **DON'T USE**

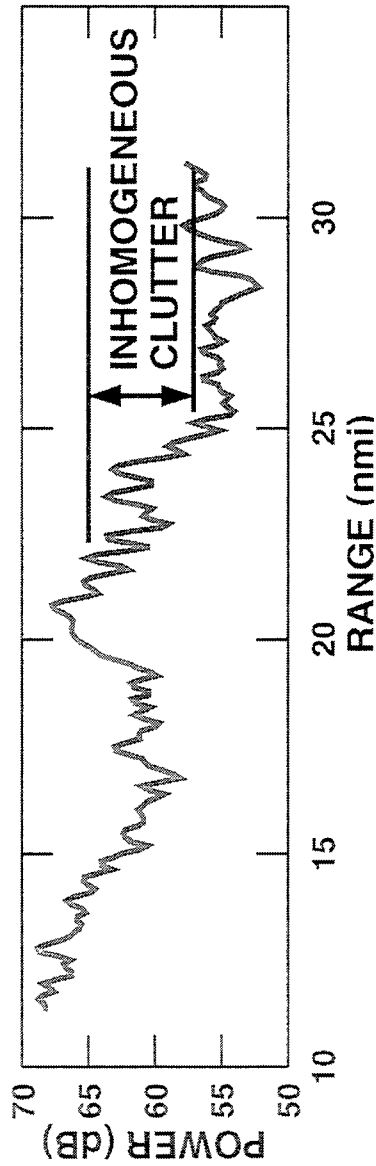
$$w = \hat{R}^{-1}v$$

• **USE**

$$w = (\hat{R} + \delta I)^{-1}v$$

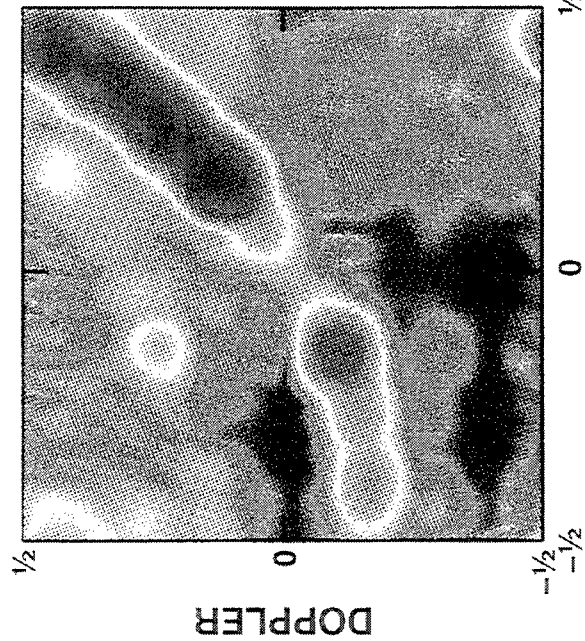
INHOMOGENEOUS CLUTTER

MOUNTAINTOP DATA

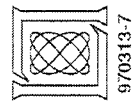
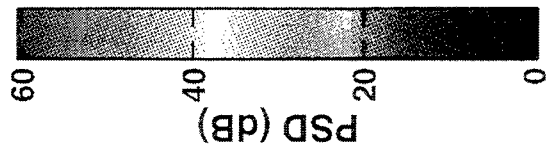
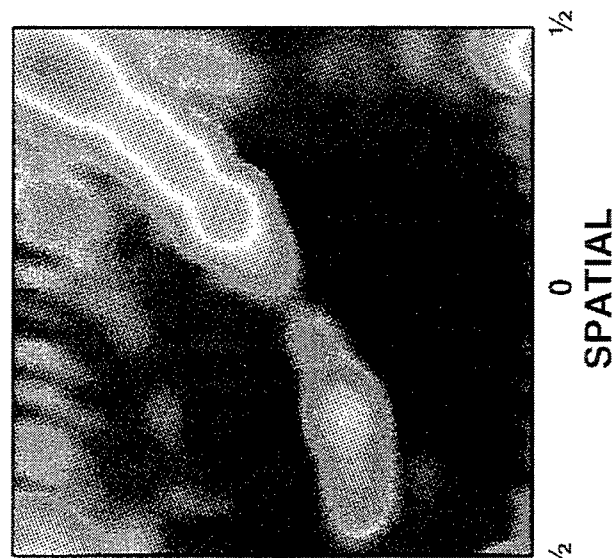


**KNOWN RESULTS
DO NOT APPLY**

10–15 nmi

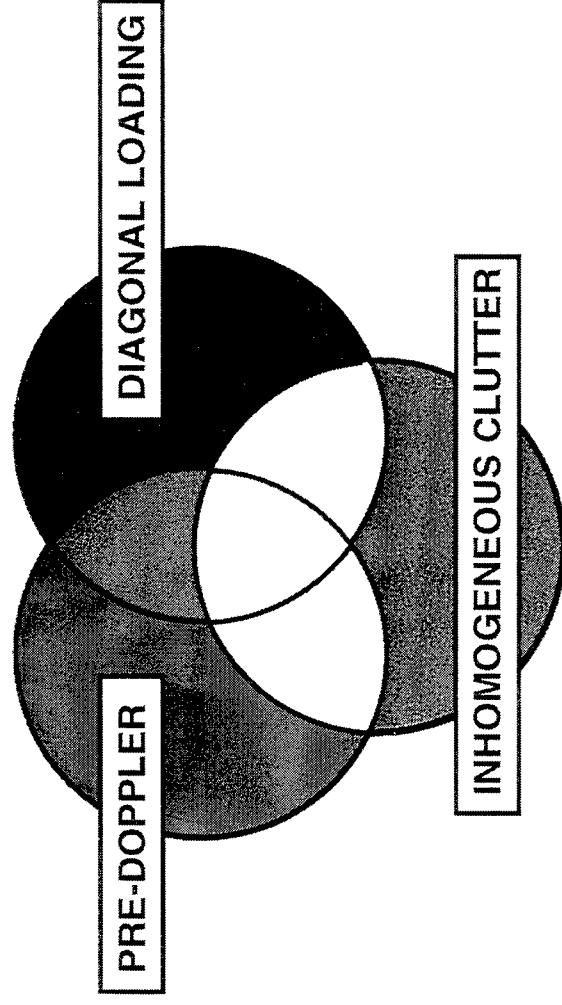


25–30 nmi

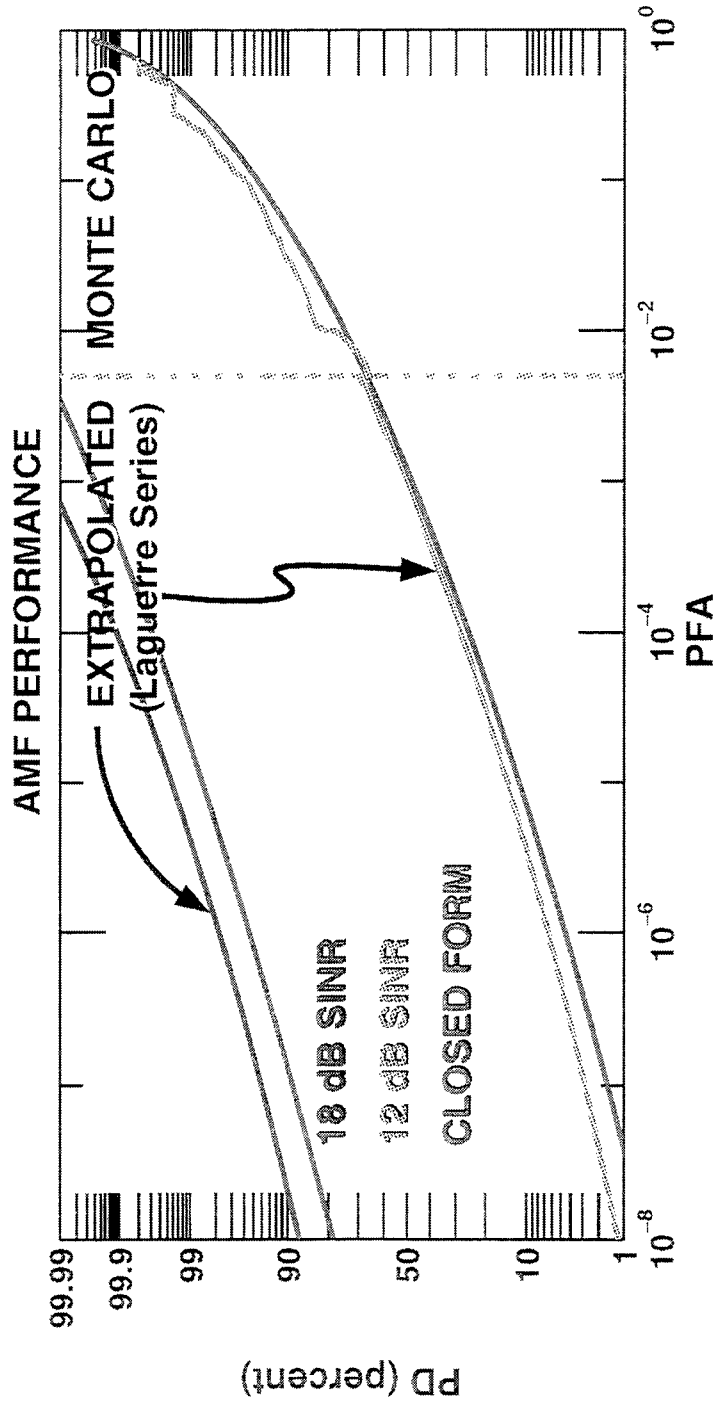


OUTLINE

- INTRODUCTION
- NON-IDEAL SCENARIOS
- NON-IDEAL DETECTOR PERFORMANCE
- CONCLUSIONS

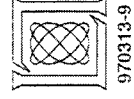


MONTE CARLO ANALYSIS



TOTAL TIME*:	PFA = 10^{-10}	10^{-6}	10^{-2}
POST-DOPPLER	2,500 years	1/4 year	1/4 hr
PRE-DOPPLER	80,000 years	8 years	8 hr
*1000 TRIALS / 54 DOF / 3 x DOF SAMPLE SUPPORT			

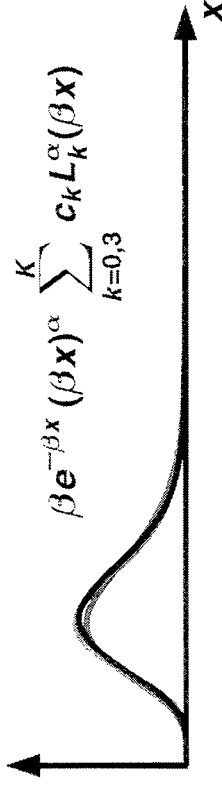
EXTRAPOLATE TO RADAR-SIZED PFAS



970313-9

LAGUERRE SERIES EXTRAPOLATION

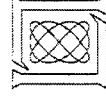
- ASSUMPTION: UNKNOWN STATISTICS APPROXIMATED BY LAGUERRE SERIES
- JUSTIFICATION: APPROXIMATION HOLDS FOR MANY KNOWN STATISTICS



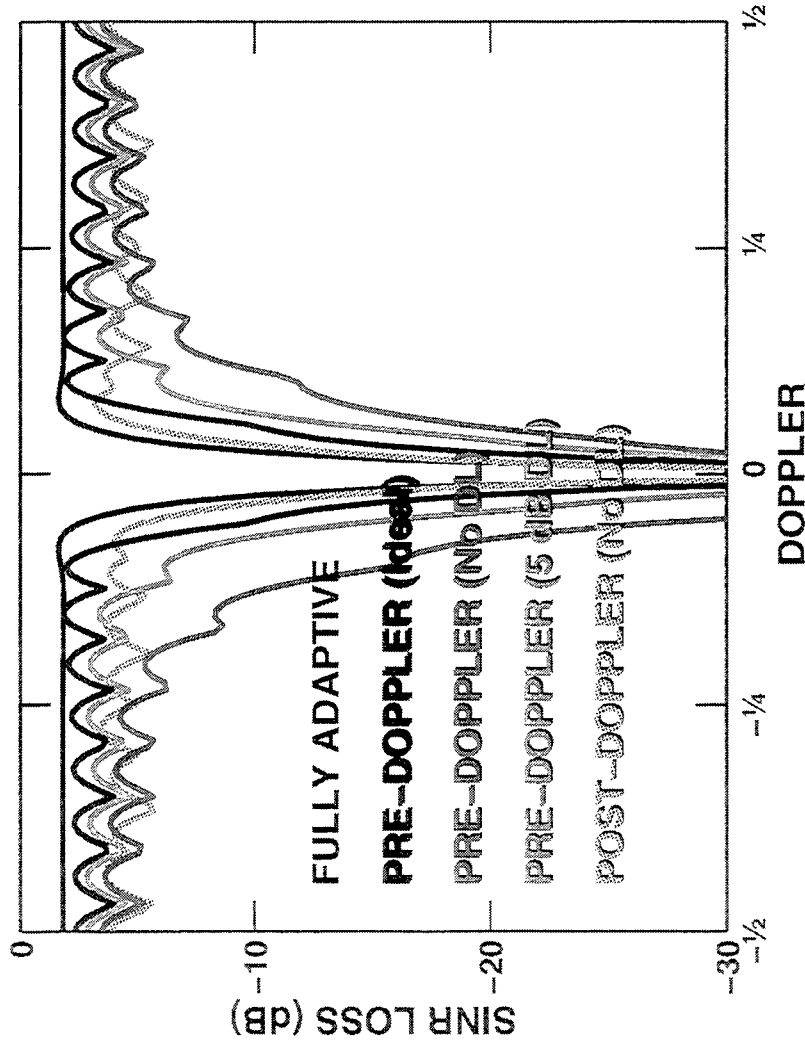
DETERMINE: α, β, c_k
 USING: ν_1, ν_2, \dots

- DETERMINE PARAMETERS FROM ESTIMATED MOMENTS:

$$\alpha = \frac{\hat{\nu}_1^2}{\hat{\sigma}^2} - 1 \quad \beta = \frac{\hat{\nu}_1}{\hat{\sigma}^2} \quad c_0 = \frac{1}{\Gamma(\alpha + 1)}$$



SINR LOSS PERFORMANCE



WEIGHT NOISE
DEGRADES
PRE-DOPPLER
PERFORMANCE

TWO SOLUTIONS:

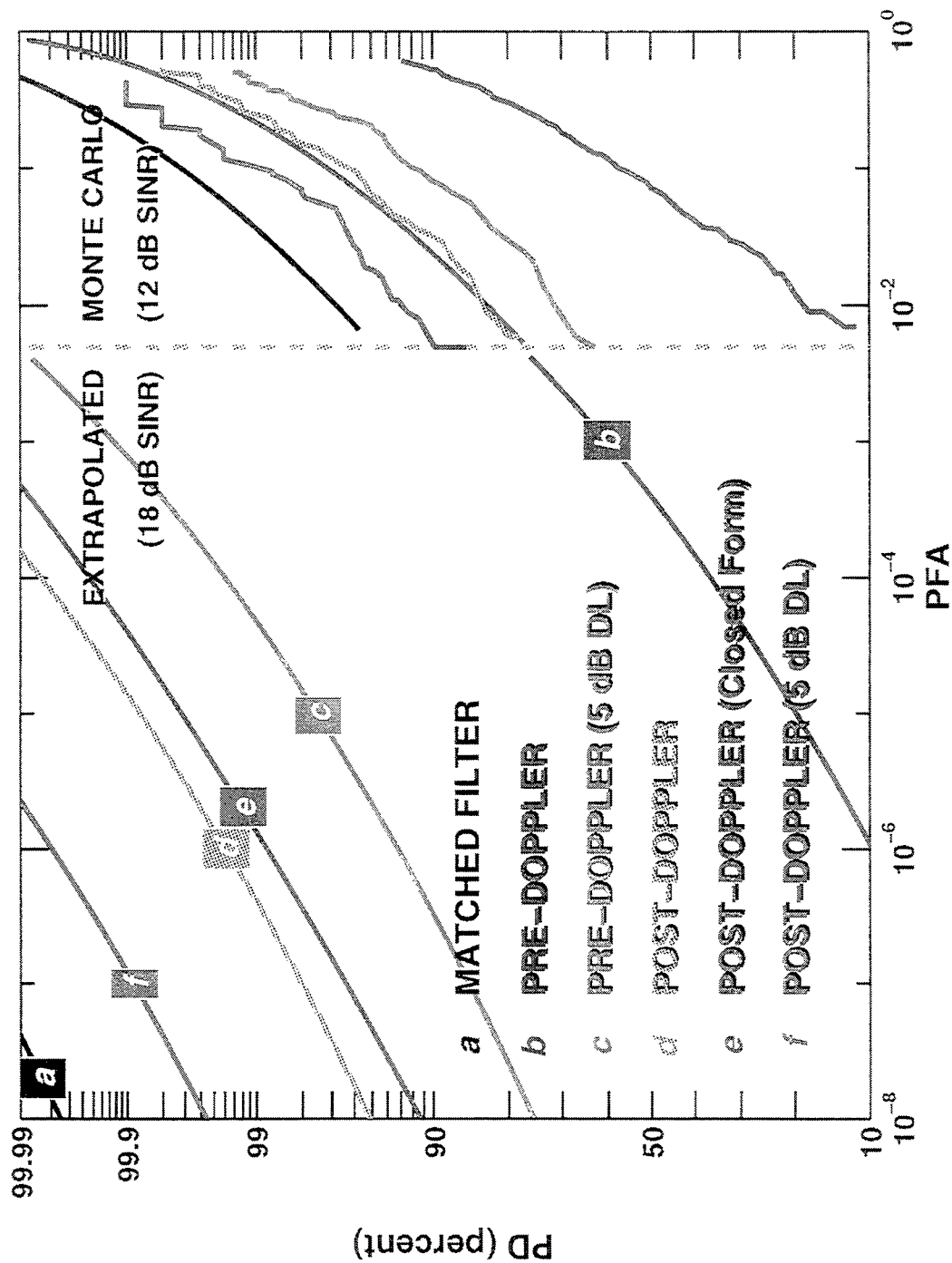
- DIAGONAL
LOADING
(Ward)
- OPTIMUM
TAPERING
(Baranowski)

$$\text{SINR LOSS} = \frac{\text{ADAPTIVE SINR}}{\text{NONADAPTIVE SINR}} = \frac{|w^H v|^2}{w^H R w} / \frac{v^H v}{v^H v}$$

40 dB CNR
40 dB CHEBYSHEV DOPPLER TAPER
30 dB CHEBYSHEV SPATIAL TAPER

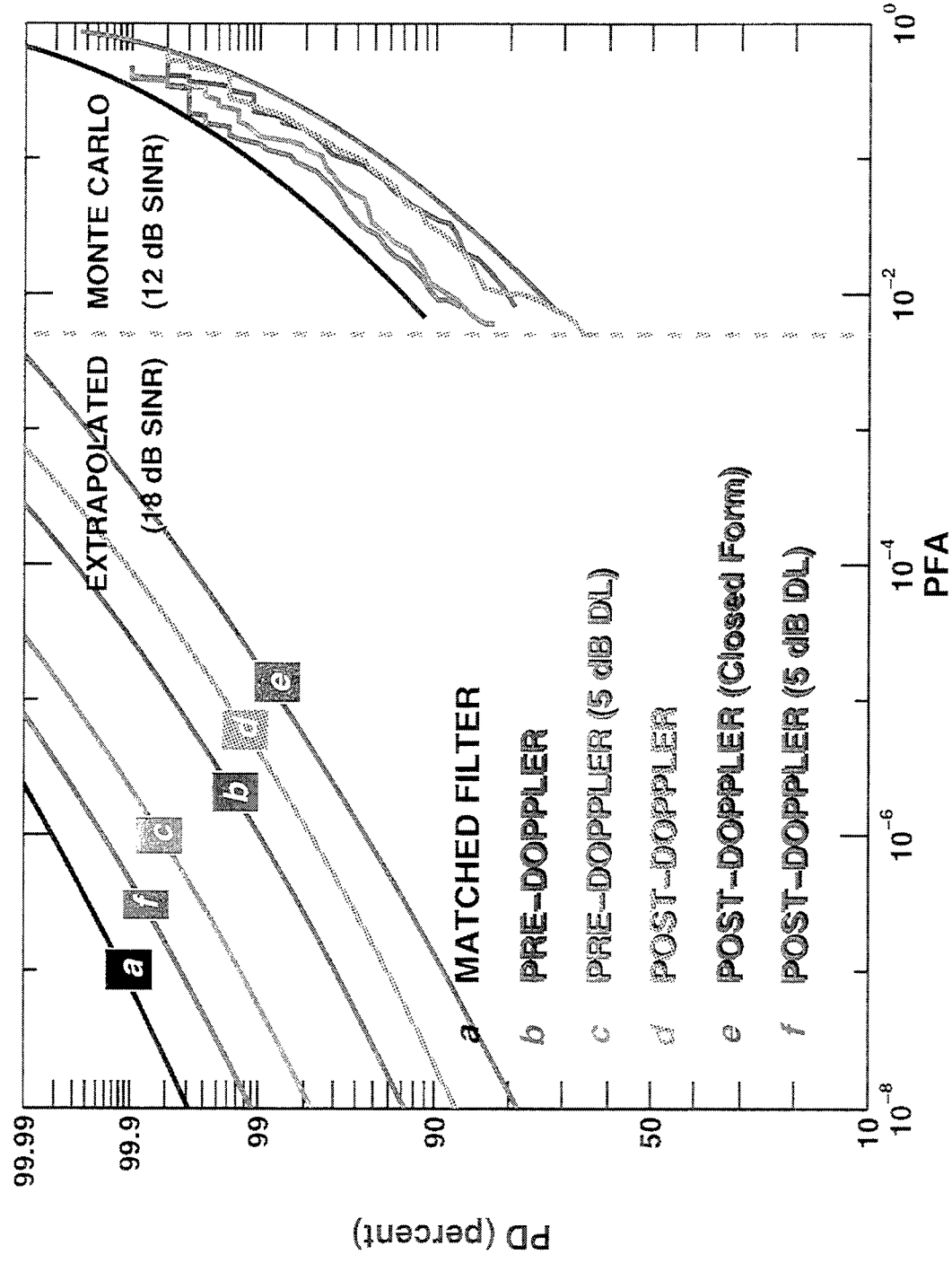
PRE- vs. POST-DOPPLER RECEIVER CHARACTERISTICS

3×18 DOF / 3×DOF SAMPLE SUPPORT / DOPPLER BIN 2



PRE- vs. POST-DOPPLER RECEIVER CHARACTERISTICS

3×18 DOF / $3 \times$ DOF SAMPLE SUPPORT / DOPPLER BIN 9



PREDICTED vs. MEASURED PERFORMANCE

18 dB SINR TARGET

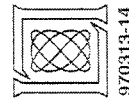
	DOPPLER BIN 2			DOPPLER BIN 9		
	SINR (dB)	PD† (%)	PD‡ (%)	SINR (dB)	PD† (%)	PD‡ (%)
PRE-DOPPLER	8.8	2.0	1.9	14.4	91.9	92.6
PRE-DOPPLER (5 dB DL)	13.5	75.9	75.5	15.1	98.2	97.7
POST-DOPPLER	14.8	96.5	94.9	14.1	88.4	87.1
POST-DOPPLER (5 dB DL)	15.9	99.8	99.5	15.2	98.5	99.1

PFA = 10⁻⁸

† PREDICTED WITH MATCHED FILTER AND MEAN SINR

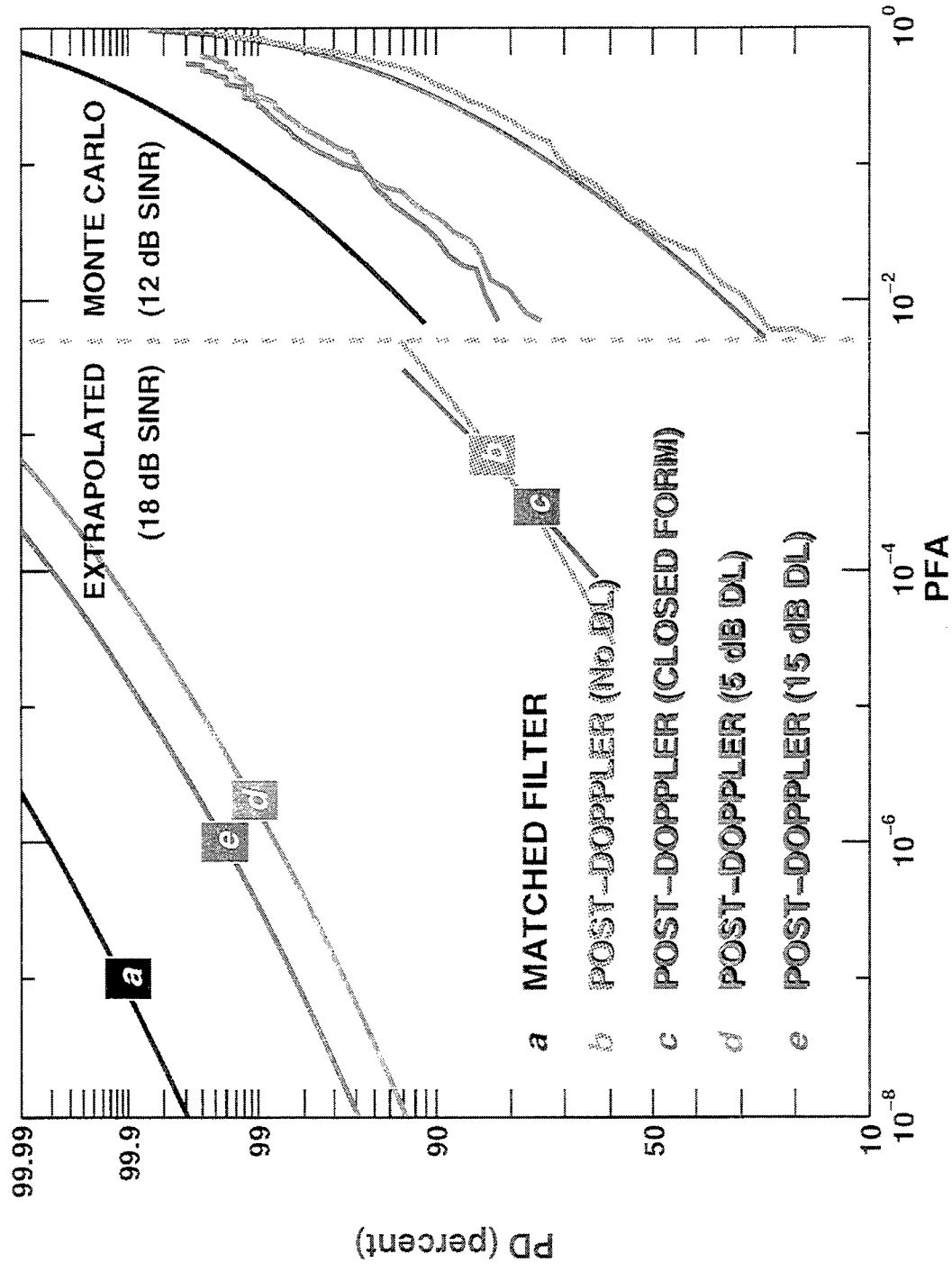
‡ MEASURED WITH MONTE CARLO EXTRAPOLATION

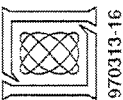
DETECTION PERFORMANCE PREDICTED BY
MATCHED FILTER AND SINR LOSS



DIAGONAL LOADING RECEIVER CHARACTERISTICS

POST-DOPPLER / $1.5 \times \text{DOF}$ TRAINING DATA / DOPPLER BIN 9

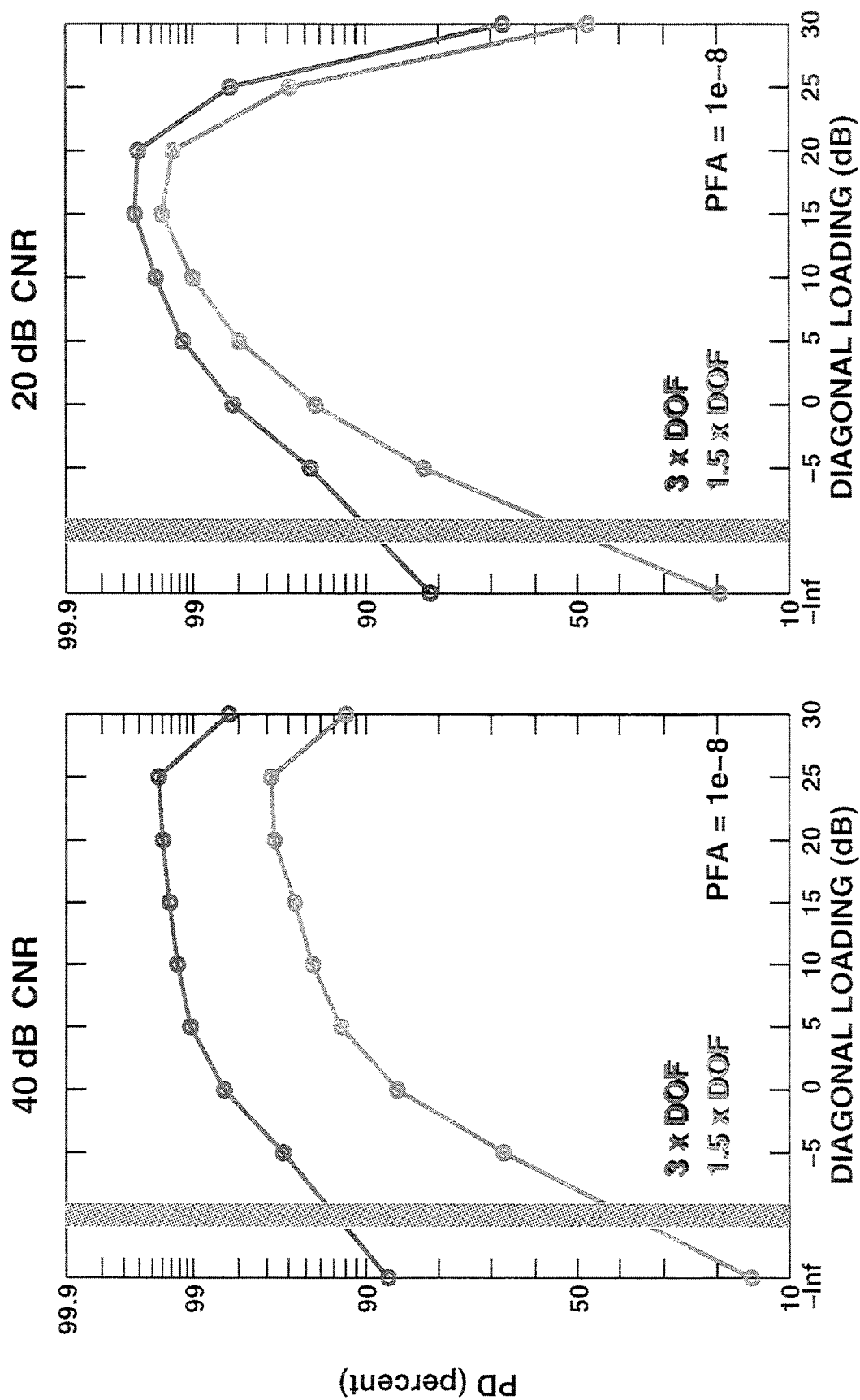




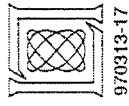
970313-16

PD vs. DIAGONAL LOADING

POST-DOPPLER / 18 dB SINR / DOPPLER BIN 9



INHOMOGENEOUS CLUTTER MODEL



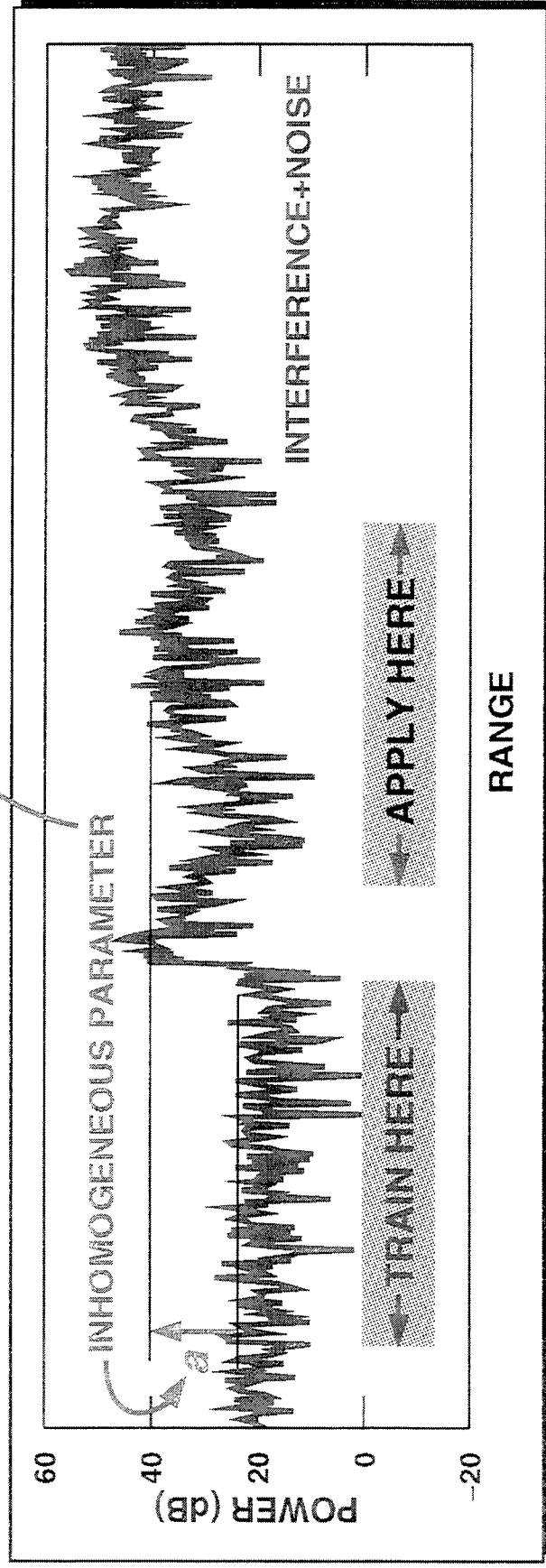
970313-17

TRAINING AND APPLICATION
REGIONS HAVE DIFFERENT
STATISTICS

UNKNOWN DETECTION
PERFORMANCE

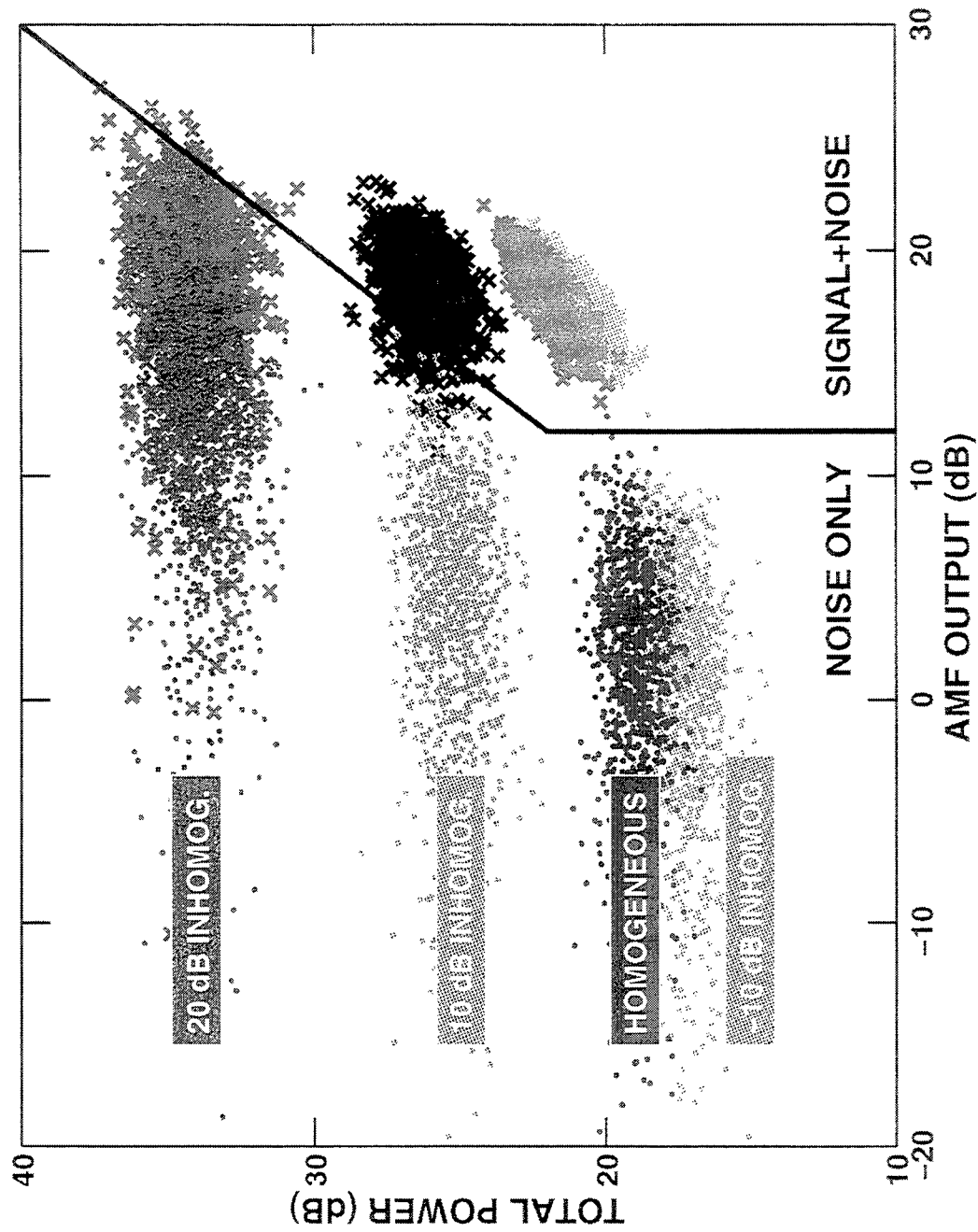
TRAIN: $z = n_0$; $E[n_0 n_0^H] = I + a R_c = R_0$

APPLY: $z = bv + n_1$; $E[n_1 n_1^H] = I + R_c = R_1$



CLUTTER EDITING WITH INHOMOGENEOUS CLUTTER

POST-DOPPLER / 18 dB SINR / 3×DOF TRAINING DATA



CONCLUSIONS

- **PREDICTED DETECTION PERFORMANCE OF SEVERAL NON-IDEAL ADAPTIVE SCENARIOS**
- **PRE-DOPPLER ACHIEVES COMPARABLE PERFORMANCE TO POST-DOPPLER**
 - **BUT ... PRE-DOPPLER VERSION OF GLRT AND ACE NOT KNOWN**
- **DIAGONAL LOADING IMPROVES PERFORMANCE**
- **CLUTTER EDITING IMPROVES PERFORMANCE USING INHOMOGENEOUS CLUTTER MODEL**

POSTER SESSION II: EMBEDDED COMPUTING

Seeker Algorithm and Architecture Study

Masahiro Arakawa and Robert A. Ford

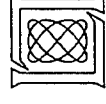
MIT Lincoln Laboratory
244 Wood Street
Lexington, MA 02173-9108
tel: (617) 981-4906
email: masa@ll.mit.edu

Abstract Missile seekers today must operate against increasingly elusive targets. These targets have inherently low radar signatures, operate at low altitudes, offering terrain masking and clutter, have variable flight paths, and employ countermeasures. Maintaining tracking performance despite these difficulties requires sophisticated signal processing. To improve their detection and tracking capabilities, seekers often use multiple modes. These multiple modes typically have many algorithmic commonalities. In this study, we explored the possibility of developing one processor architecture to handle both space-time adaptive processing (STAP) in the radar mode and single- and dual-frame image processing in the infrared (IR) mode. Specifically, we targeted commercial off-the-shelf (COTS) technology to reduce cost and technology insertion lag time, and parallel processors to exploit parallelism in the algorithms. Although a relaxation of the latency constraints on the signal processor makes coarse grain solutions possible, our analysis indicates that an investment commitment in miniaturization is necessary to close the gap between the processing densities available with state-of-the-art COTS parallel processors and the missiles' severe form factor requirements.

SEEKER ALGORITHM AND ARCHITECTURE STUDY

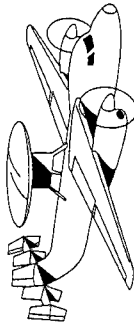
MASAHIRO ARAKAWA AND ROBERT A. FORD
MIT LINCOLN LABORATORY

MARCH 13, 1997



SEEKER MISSILE ENVIRONMENT

AEW RADAR

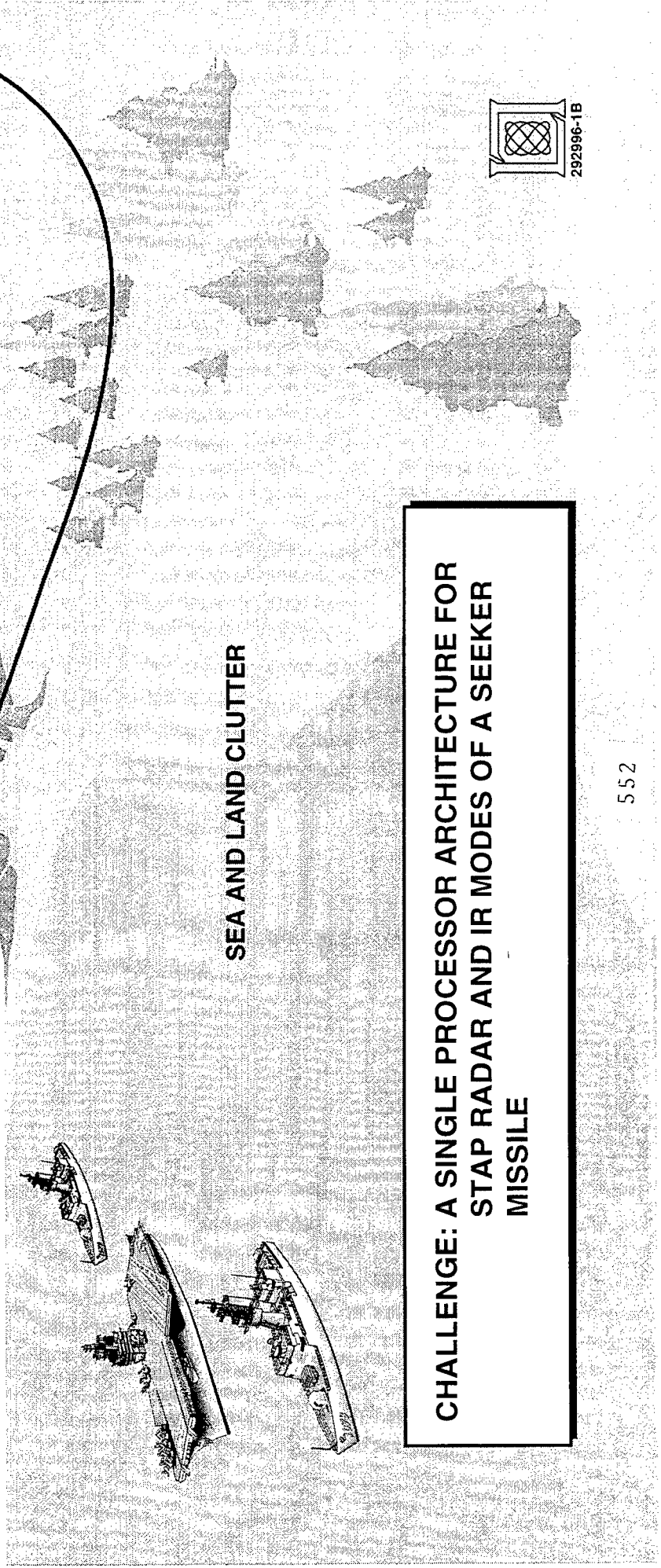


SEEKER

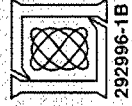
TARGET



SEA AND LAND CLUTTER



CHALLENGE: A SINGLE PROCESSOR ARCHITECTURE FOR
STAP RADAR AND IR MODES OF A SEEKER
MISSILE



292996-1B

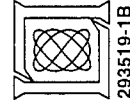
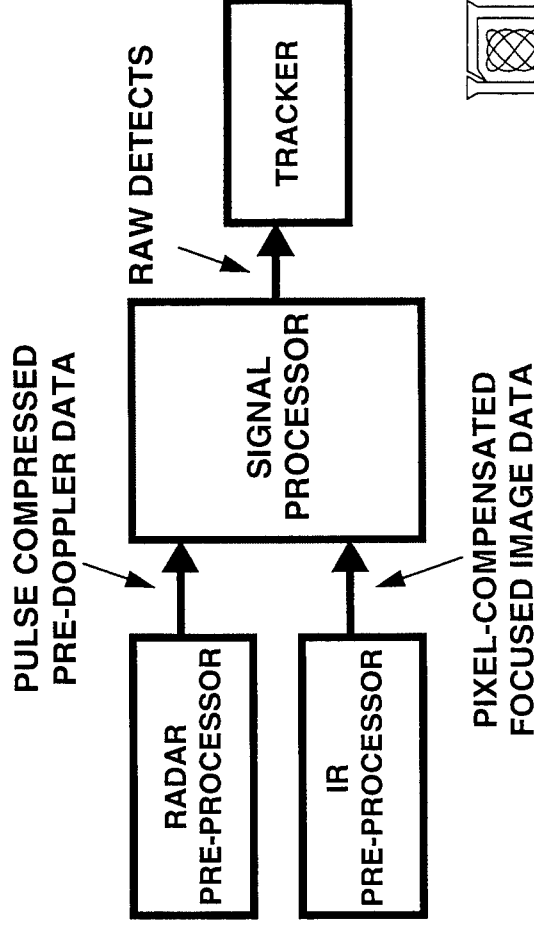
GOALS

- ANALYZE COMPUTATIONAL REQUIREMENTS OF STAP AND IR ALGORITHMS
 - COMPUTATIONAL KERNELS
 - DEGREES OF PARALLELISM
 - PROCESSING THROUGHPUT, LATENCY, MEMORY, AND I/O REQUIREMENTS
- GENERATE CANDIDATE ALGORITHM-TO-ARCHITECTURE MAPPINGS
 - FINE vs. COARSE GRAIN
 - PROCESSOR PERFORMANCE AND SCALABILITY
 - COMMUNICATION PATTERNS
 - COMMUNICATION TO COMPUTATION RATIO

SEEKER CHARACTERISTICS

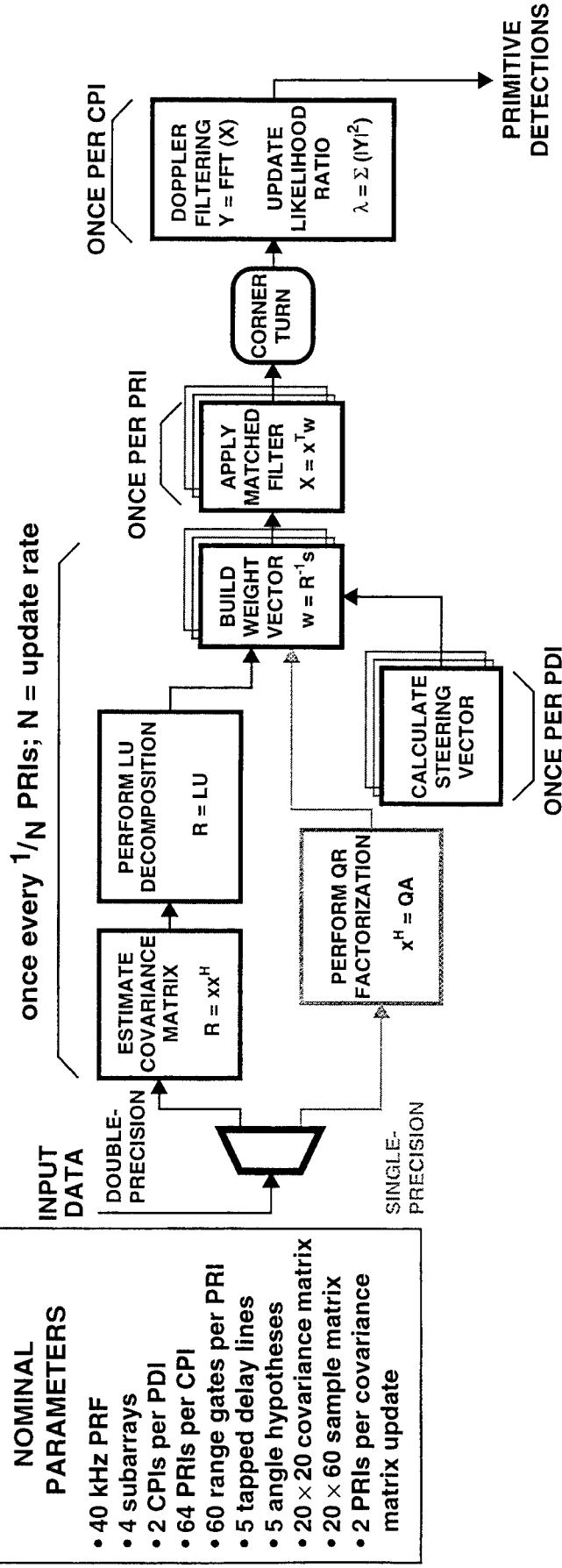
	PLATFORM		
	A	B	C
VOLUME (in ³)	355	150	64
WEIGHT (lbs)	11.5	3.6	2.4
POWER (W)	220	55	32
Gflop/s per ft ³ *	74	176	412

* ASSUMING 30% EFFICIENCY

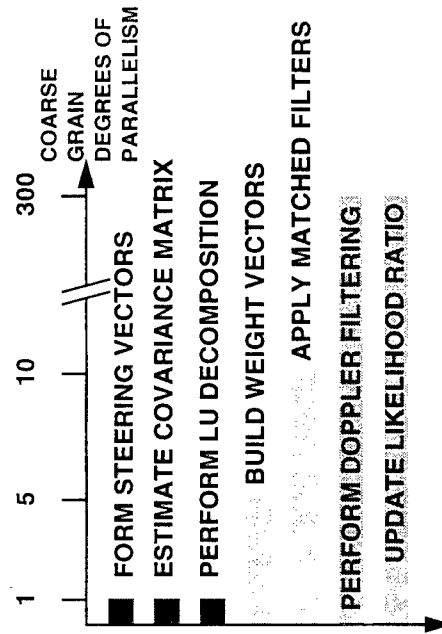


293519-1B

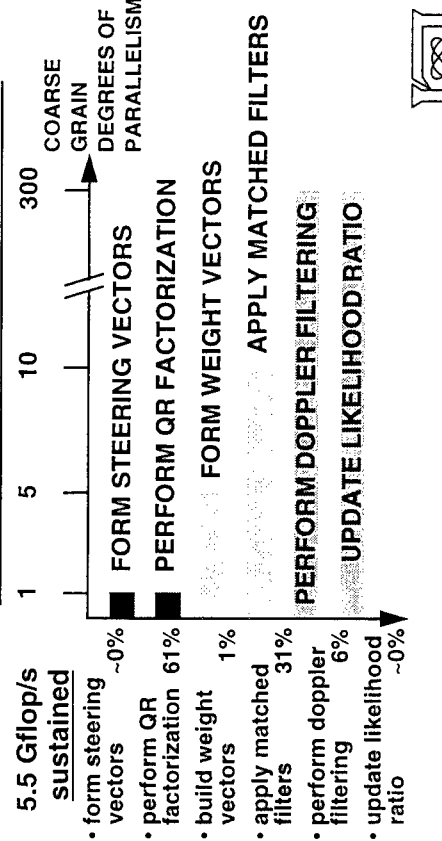
STAP ALGORITHM



LU METHOD: DOUBLE-PRECISION

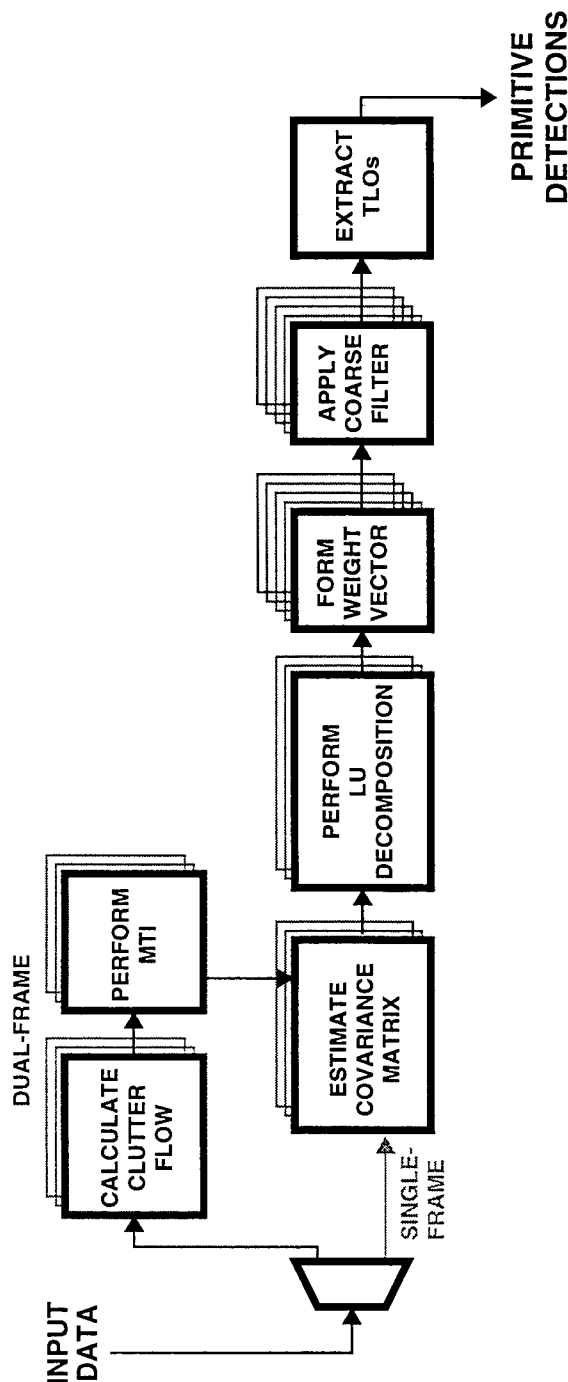


QR METHOD: SINGLE-PRECISION

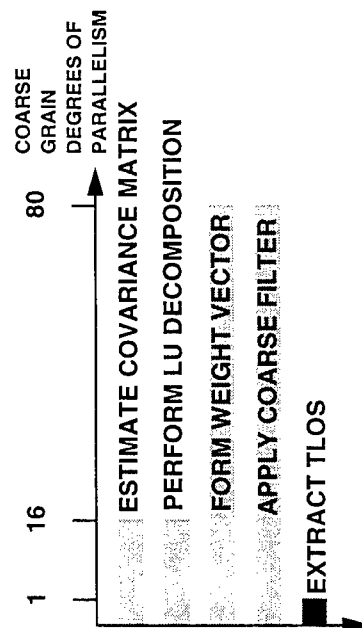


IR ALGORITHM

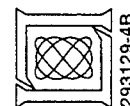
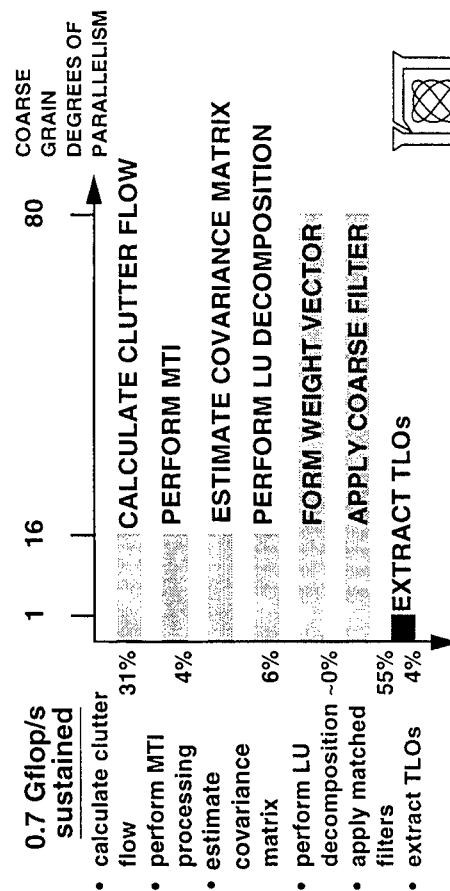
- NOMINAL PARAMETERS**
- 256 × 256 pixels per frame
 - 4 × 4 tiles per frame
 - 64 × 64 pixels per tile
 - 25 × 25 covariance matrix
 - 25 × 169 sample matrix
 - 5 coarse filters
 - 5 × 5 pixels per coarse filter
 - 200 pre-TLOs
 - 20 TLOs
 - 80 Hz frame update rate (single-frame mode)
 - 20 Hz frame update rate (dual-frame mode)



SINGLE-FRAME MODE



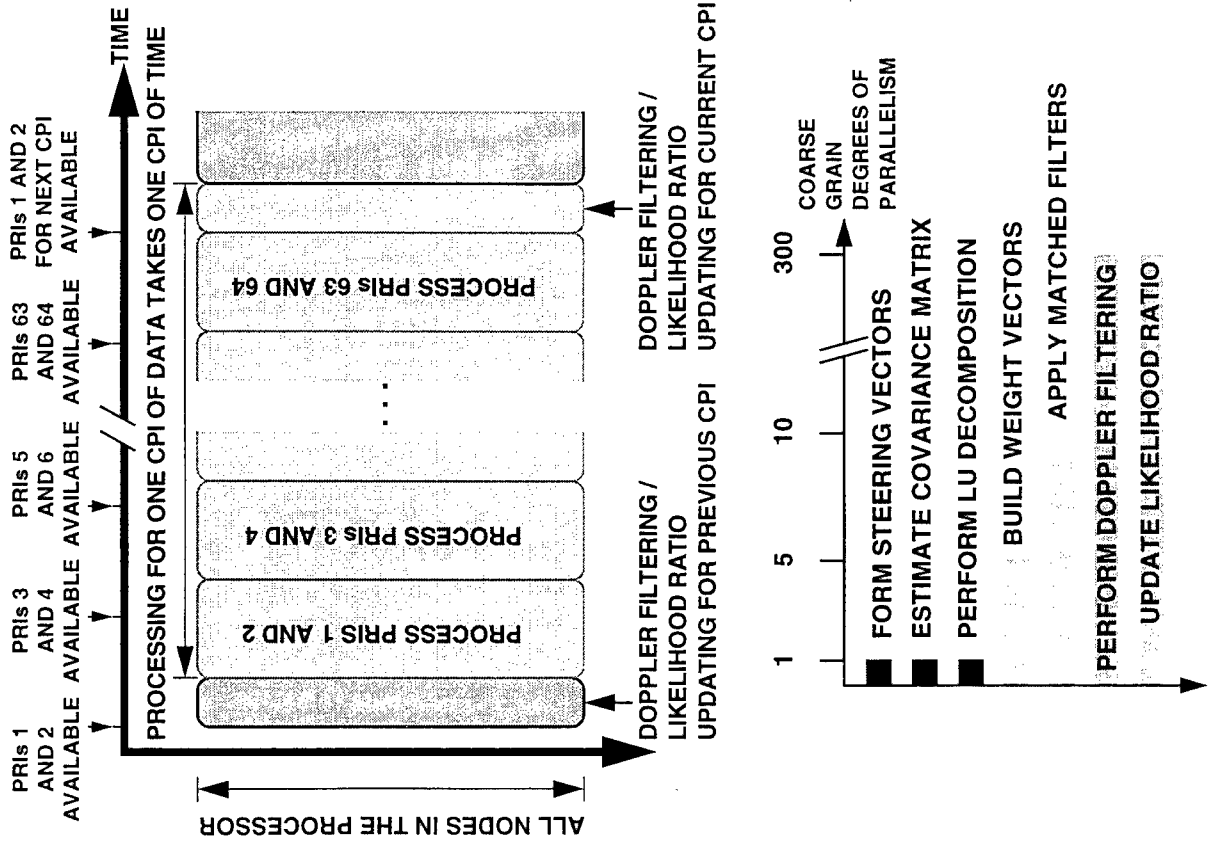
DUAL-FRAME MODE



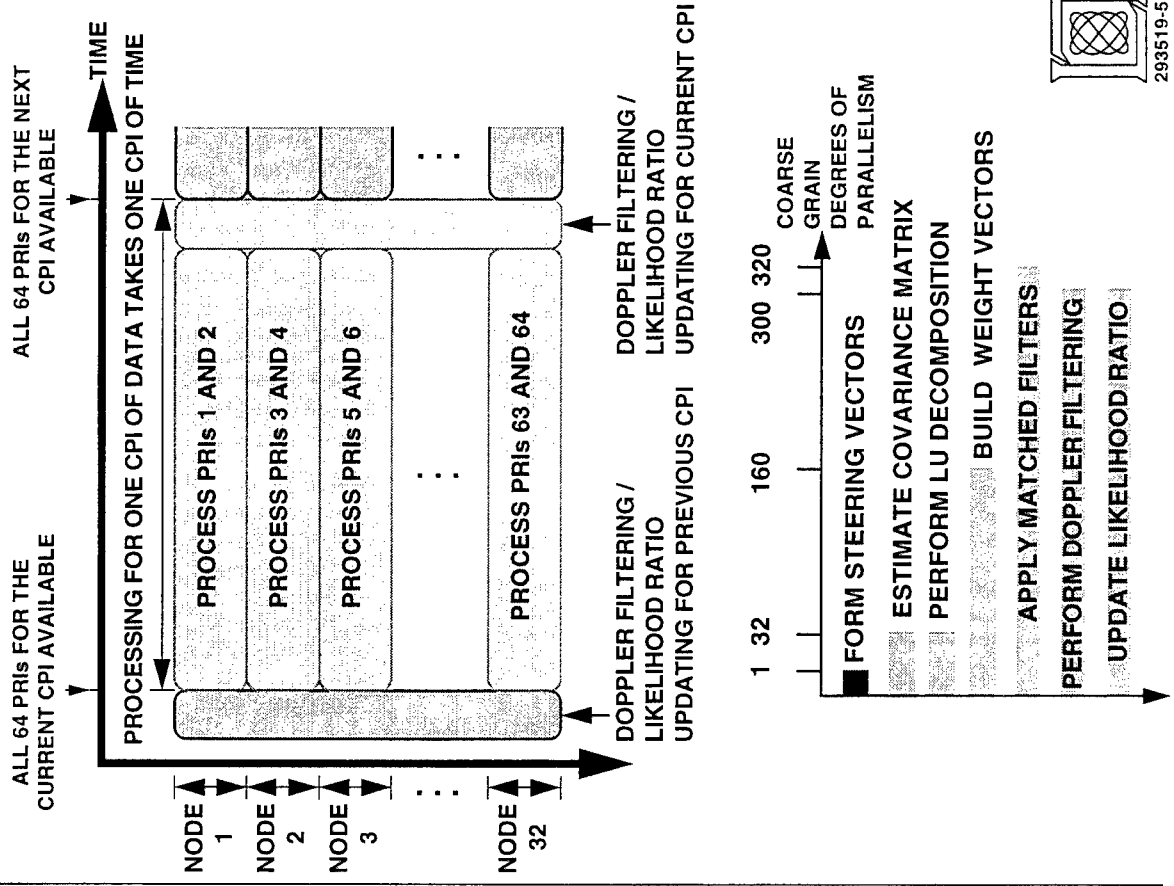
293129-4B

LATENCY VS EFFICIENCY

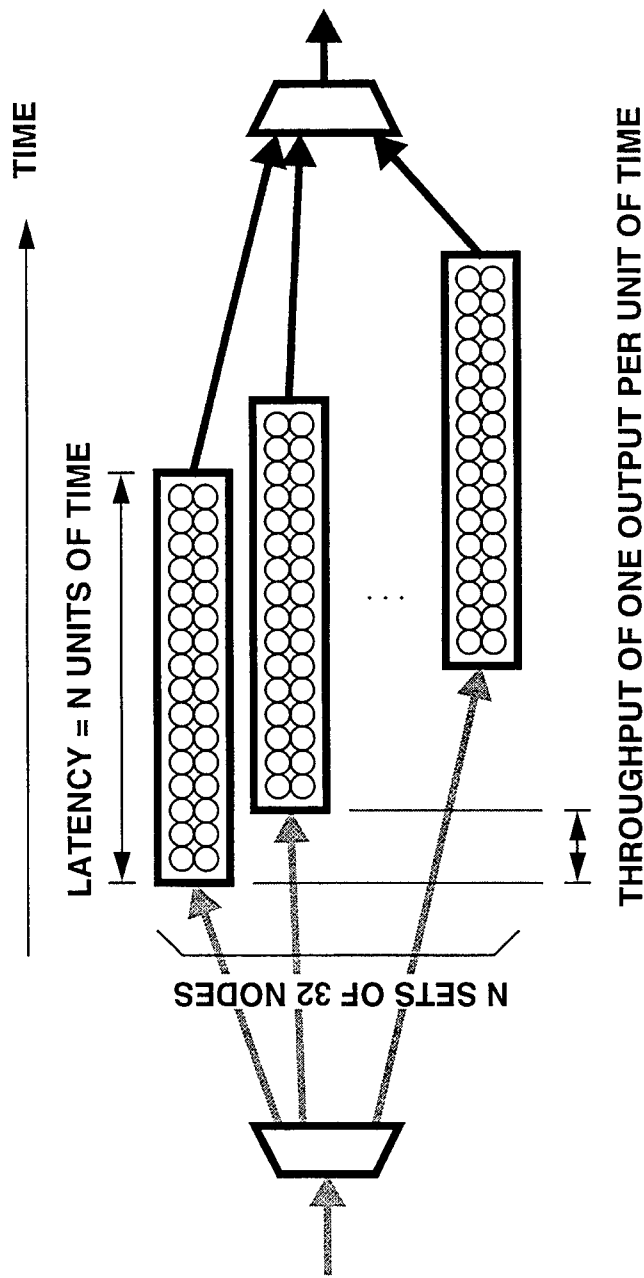
ORIGINAL STAP TIMELINE



RELAXED LATENCY STAP TIMELINE



RECOMMENDED MAPPING

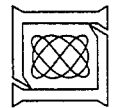


COARSE GRAIN MAPPINGS

- STAP: ONE COARSE GRAIN DEGREE OF PARALLELISM PER NODE
 4.6 Gflop/s SUSTAINED (LU METHOD)
 32N NODES \rightarrow $143/N$ Mflop/s SUSTAINED
 30% EFFICIENCY ASSUMED \rightarrow $477/N$ Mflop/s PEAK
- IR: ONE COARSE GRAIN DEGREE OF PARALLELISM (ONE TILE) PER TWO NODES
 1.8 Gflop/s SUSTAINED (SINGLE-FRAME MODE)
 32N NODES \rightarrow $56/N$ Mflop/s SUSTAINED
 30% EFFICIENCY ASSUMED \rightarrow $185/N$ Mflop/s PEAK

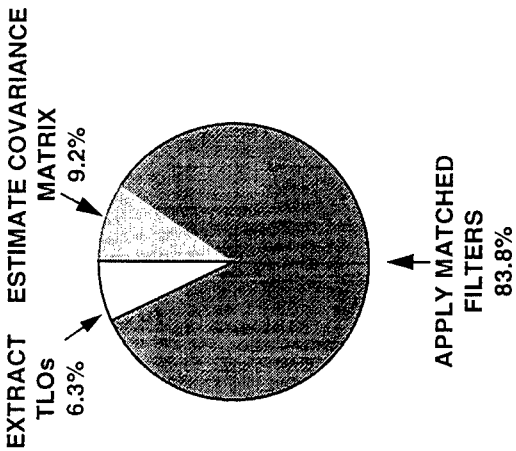
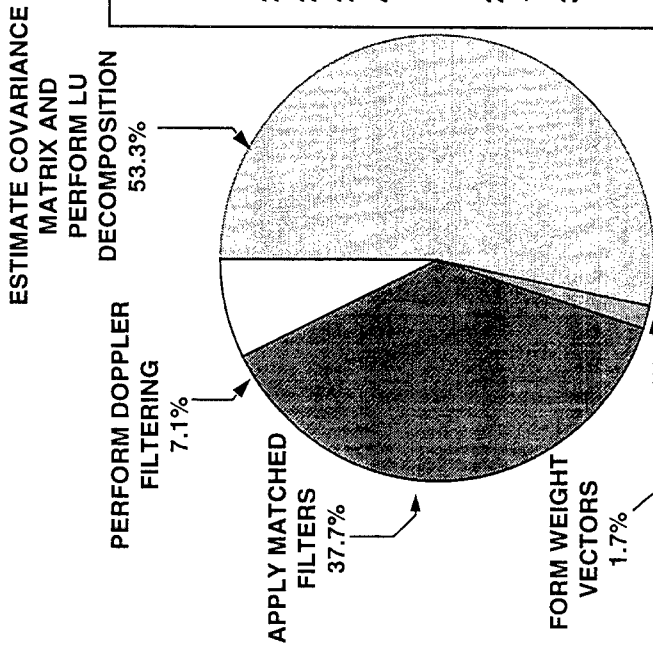
DEFINITIONS

- ONE UNIT OF TIME =
 ONE CPI OF TIME OR
 ONE FRAME UPDATE INTERVAL
- ONE OUTPUT =
 TARGETS FROM ONE CPI OF DATA OR
 TLOs FROM ONE SET OF FRAMES



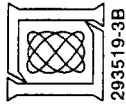
293129-6B

COMMON ARCHITECTURE



Algorithm Comparison			
STAP	covariance matrix estimation	IR	
20 × 20	covariance matrix size	25 × 25	
20 × 60	sample matrix size	20 × 169	
2.0 Gflop/s	sustained throughput	0.16 Gflop/s	
44%	fraction of total workload	9%	
STAP	weight application	IR	
20 (1-D)	kernel size	5 × 5 (2-D)	
1.7 Gflop/s	sustained throughput	1.4 Gflop/s	
38%	fraction of total workload	84%	

	DSP-BASED SYSTEMS	RISC-BASED SYSTEMS
PER-NODE THROUGHPUT	AVERAGE	GOOD
DOUBLE-PRECISION NATIVE		YES
COMMUNICATION NETWORK	AVERAGE	GOOD
FORM FACTOR REQUIREMENT		



293519-3B

SUMMARY AND RECOMMENDATIONS

- **STAP AND IR ALGORITHMS CAN BE HOSTED ON A SINGLE ARCHITECTURE**
 - COMMON COMPUTATIONAL KERNELS INCLUDE COVARIANCE ESTIMATION, LU DECOMPOSITION, MATCHED FILTER APPLICATION
 - NATURAL PARALLELISM IN ALGORITHMS LEND TO PARALLEL IMPLEMENTATIONS
- **MAPPINGS WITH MANY COARSE GRAIN DEGREES OF PARALLELISM REALIZED**
 - ALLOW USE OF PROCESSORS WITH LOWER PER-NODE THROUGHPUT
 - RESULT IN LESS COMPLEX AND MORE EFFICIENT SOFTWARE
- **NEED INVESTMENT IN MINIATURIZATION OF COTS PROCESSORS**
 - ONE TO TWO ORDERS OF MAGNITUDE BETWEEN TODAY'S COTS PROCESSORS AND SEEKER FORM FACTOR REQUIREMENTS
- **EXTEND ARCHITECTURE STUDY WITH BENCHMARK MEASUREMENTS**



Processing Considerations and Performance Results for a Real-Time STAP Flight Demonstration

Russell Brown, Richard Linderman, and Mark Linderman

Rome Laboratory
Rome, NY 13441-4514
tel: (315) 330-4437
fax: (315) 330-2528
email: brownr@rl.af.mil

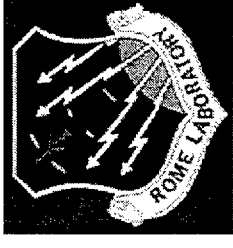
John Samson and David Grimm

Honeywell Corporation

Arnold Bramson, Bruce Havlicsek, and Robert Warta

Northrop Grumman Corporation

Abstract Space-Time Adaptive Processing (STAP) presents a challenge to digital signal processors which are required to operate in real time. Available processing hardware, given limits on size, weight and power, must achieve a substantial percentage of its peak operating capacity to perform this task which involves careful attention to programming details. This paper discusses a real-time demonstration of STAP clutter suppression in the May 1996 Real Time Multichannel Airborne Radar Measurement (RT-MCARM) flight demonstration program. The system collected and processed IF sampled data from 16 phased array radar receiver channels, performing Doppler processing, adaptive clutter cancellation, pulse compression, and formation of multiple receive beams within an intentionally broadened transmit beam. Selective PRI stagger was implemented in Doppler regions of strong clutter to provide increased cancellation. An efficient method of adaptation with variable beam constraints was developed, which allows preservation of target phase across boundaries between range intervals with differing clutter statistics. In addition to improved angle estimation compared to unconstrained adaptive processing, the constraint makes it possible to perform pulse compression after beamforming thereby reducing the computational requirements. Rome Laboratory STAP algorithms were ported and mapped by Honeywell and Rome Laboratory to the Rugged Touchstone processor, a rugged COTS product derived from the Intel Paragon High Performance Computer. These algorithms were implemented using two different mapping approaches and compared with a mainbeam clutter suppression technique hosted on an onboard Mercury Computer.

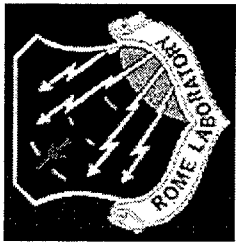


Processing Considerations and Performance Results for a Real-Time STAP Flight Demonstration

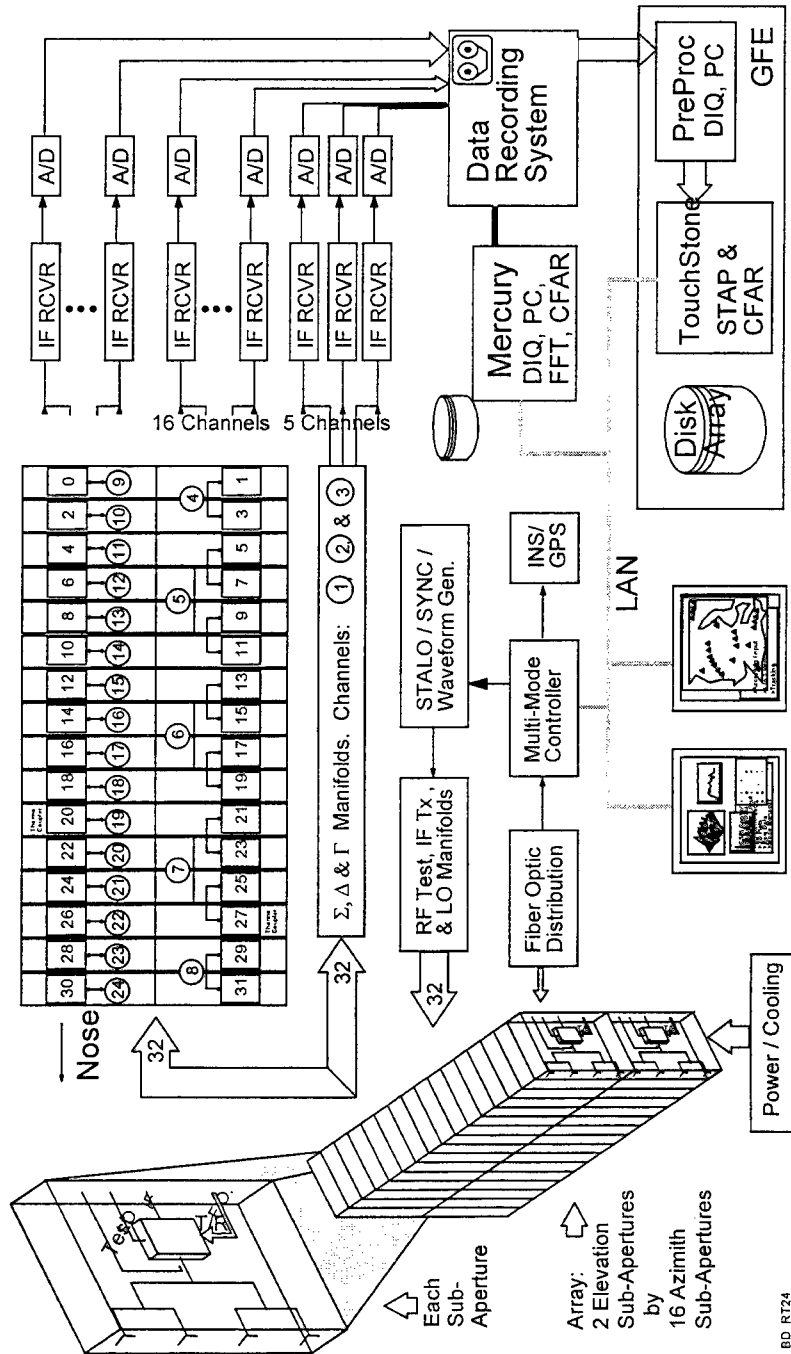
**Russell Brown, Richard Linderman,
Mark Linderman, Michael Little
Rome Laboratory**

**John Samson, David Grimm
Honeywell Corp.**

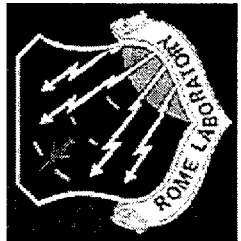
**Arnold Bramson, Bruce Havlicsek, Robert Warta
Northrop Grumman Corp.**



RTMCARM System Configuration

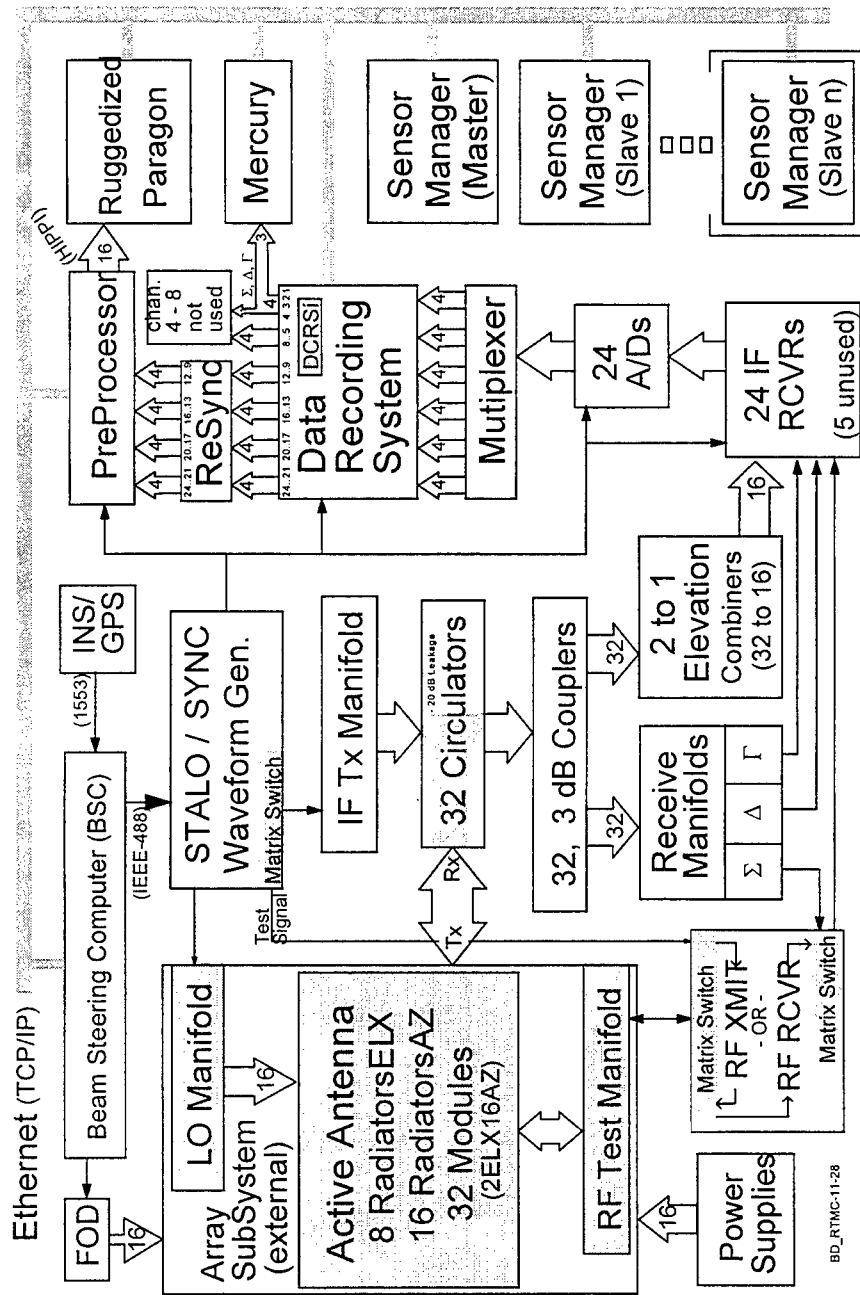


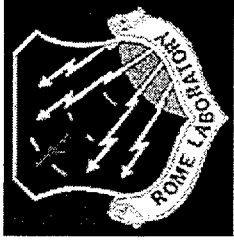
BD RT24



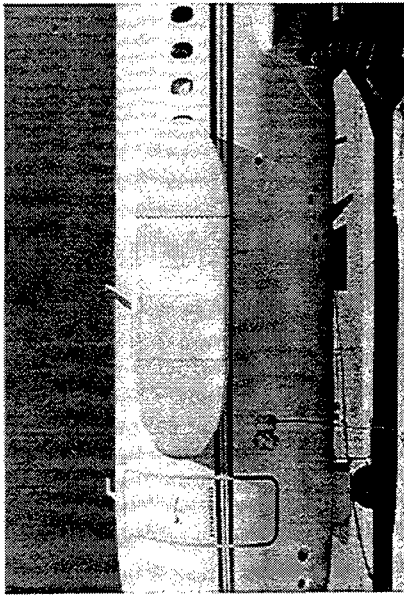
RTMCARM

System Block Diagram

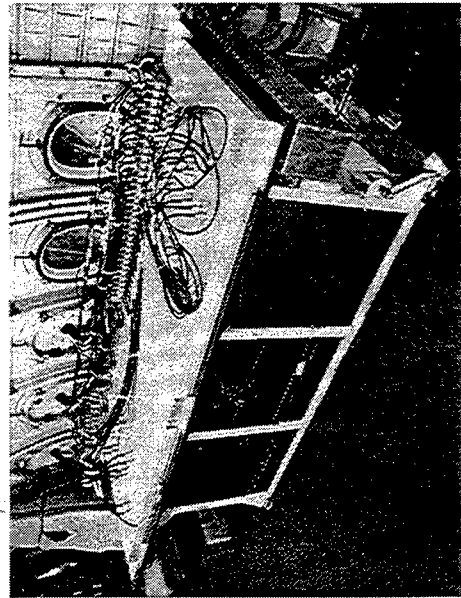




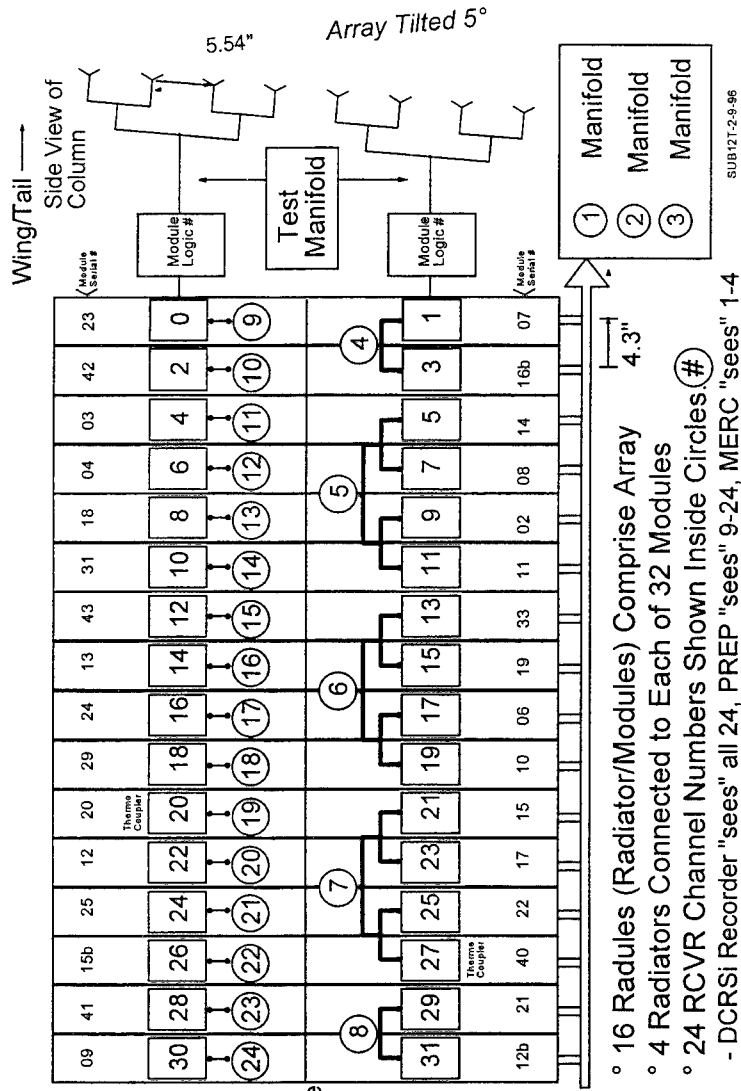
RTMCARM Array Configuration



Nose

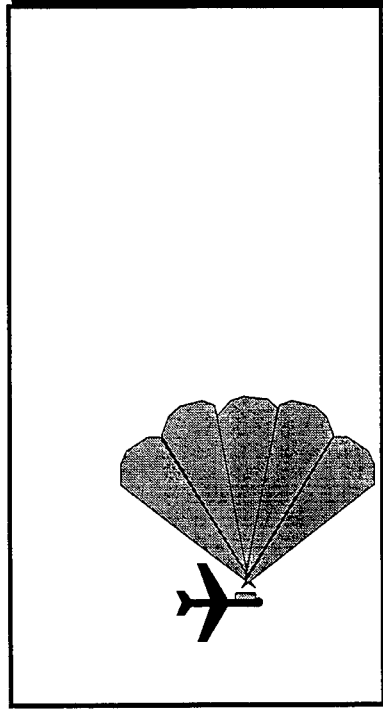
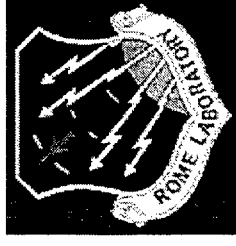


Antenna Sub-Apertures & RCVR Channels (RTMCARM)



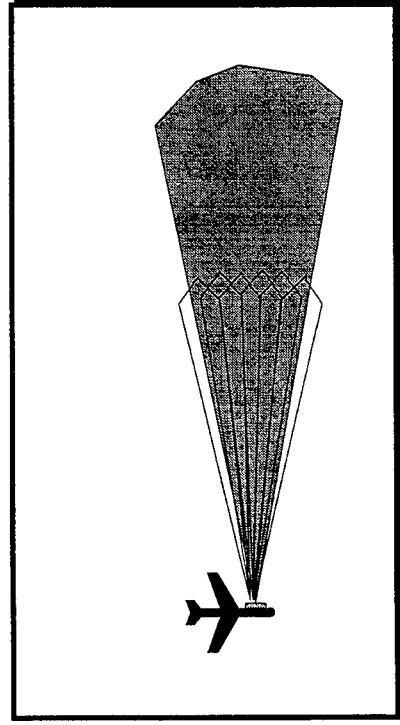


Surveillance Volume Coverage



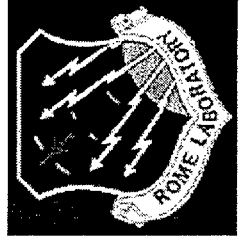
Transmit Beams

- 0, +20, -20, +40, -40 degrees to broadside
- Nominal 25 degree 3dB beamwidth=> 100 deg coverage
- However relies on STAP to cancel higher sidelobe clutter
- Each CPI looks in different direction
- 10 hertz CPI rate implies volume coverage in 0.5 secs

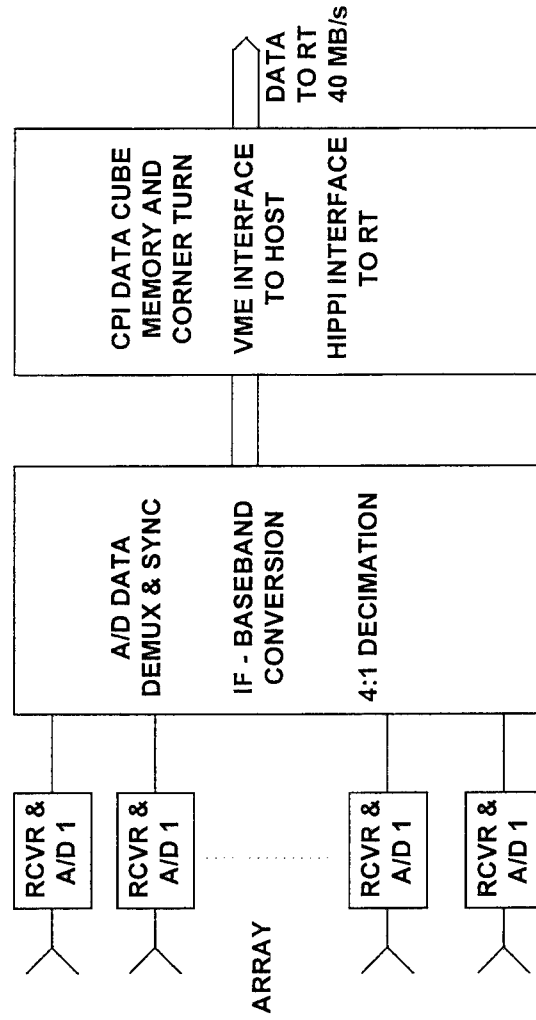
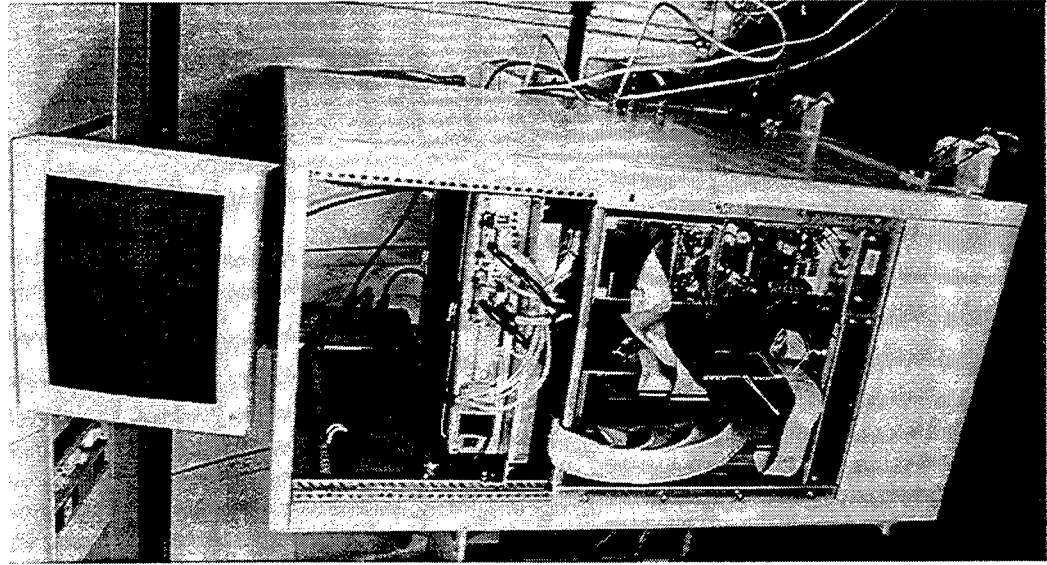


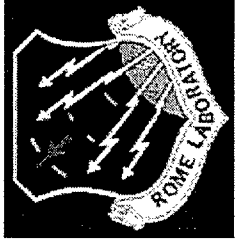
Receive Beams

- Six Adaptive Rx Beams per Tx Beam
- Nominal 8 degree 3dB beamwidth (some taper)
- Overlapped 50% to cover 20 degrees
- Only "Soft" Beam shape constraints

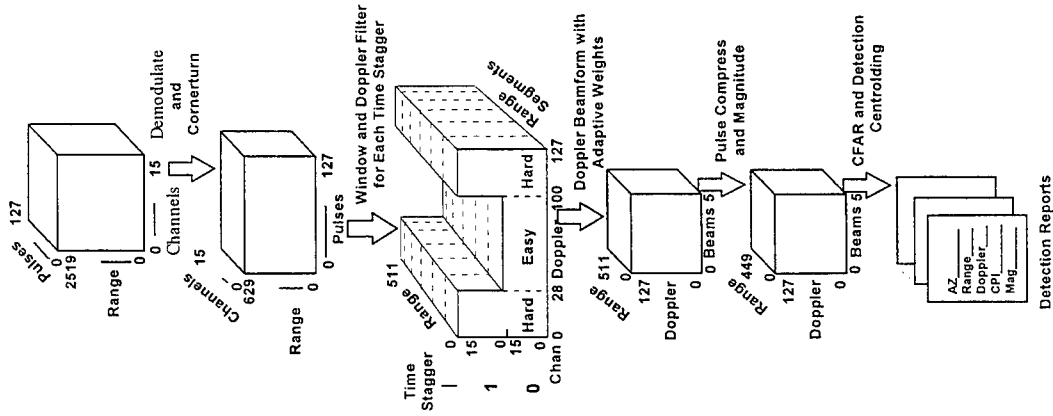


Data Acquisition System





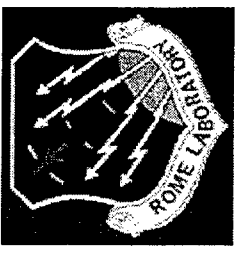
RTMCARM Processing Chain



- Doppler space segmented into easy and hard bins
- Post Doppler adaptive beamforming used for easy bins
- PRI-staggered post Doppler for hard bins in each of 6 range segments
- Pulse compression across range segments
- Sliding window CFAR
- Centroided detection outputs

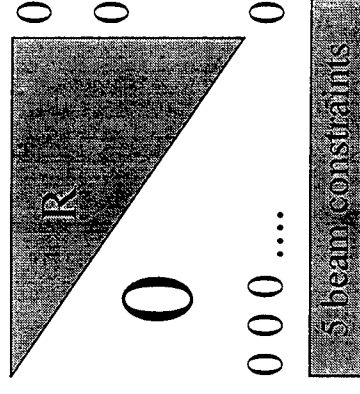


Weight Computation Process



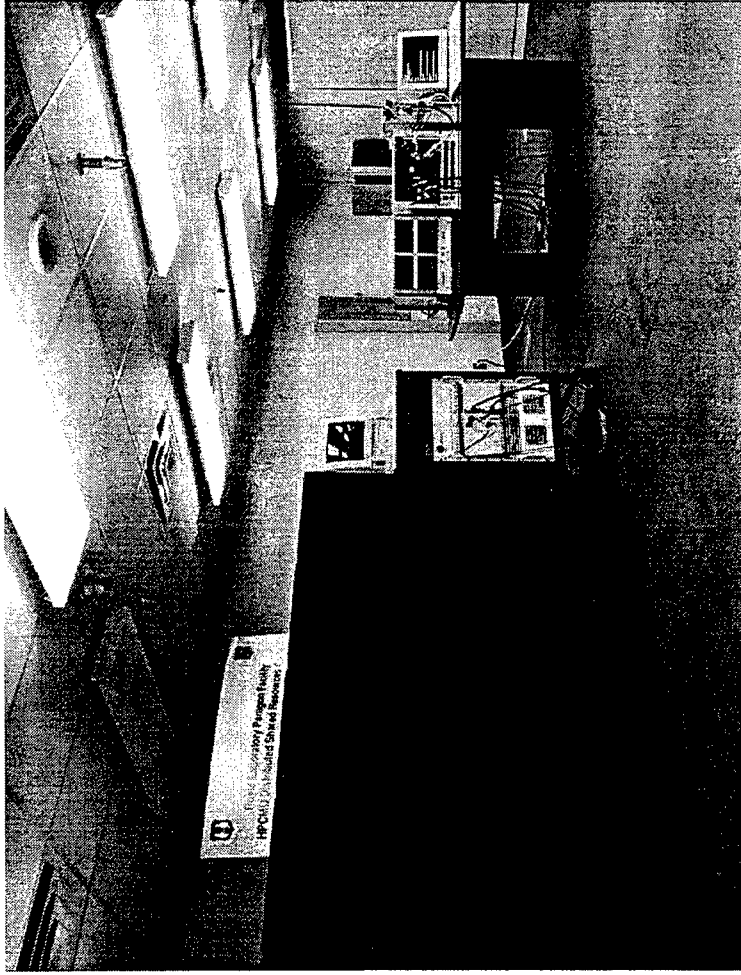
Block Update to QR Factorization

- 32x32 R matrix augmented to 38x33
- 5 beam constraint equations per beam
- Reorthogonalized to R'
- Backsolved for weights
- R'[33,33] is residual





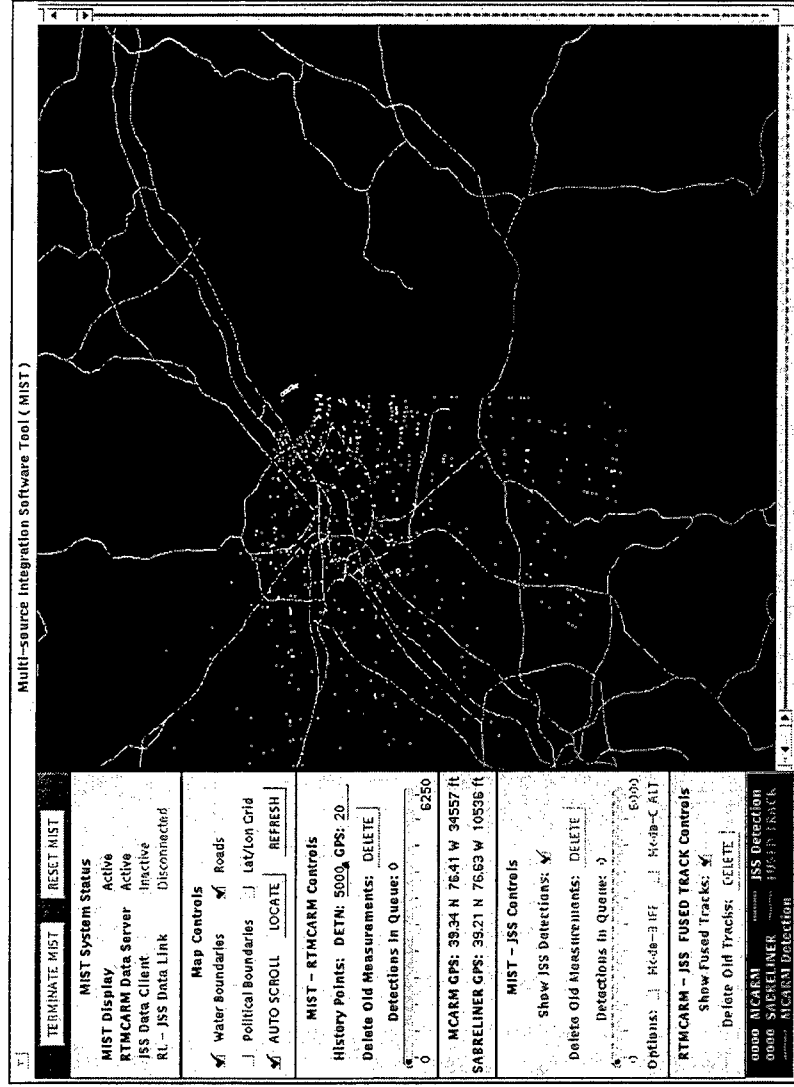
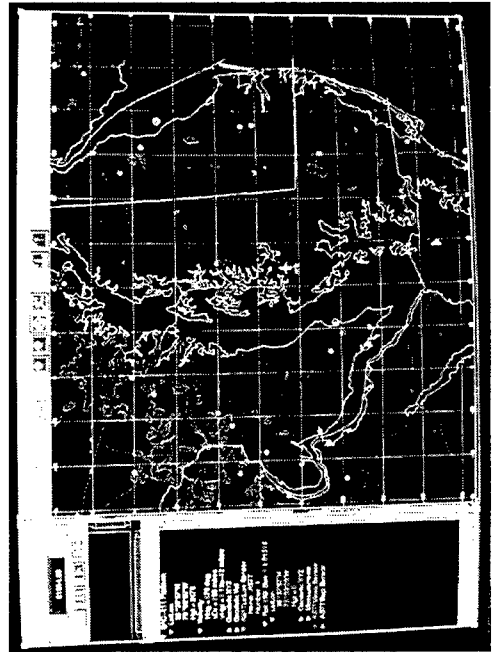
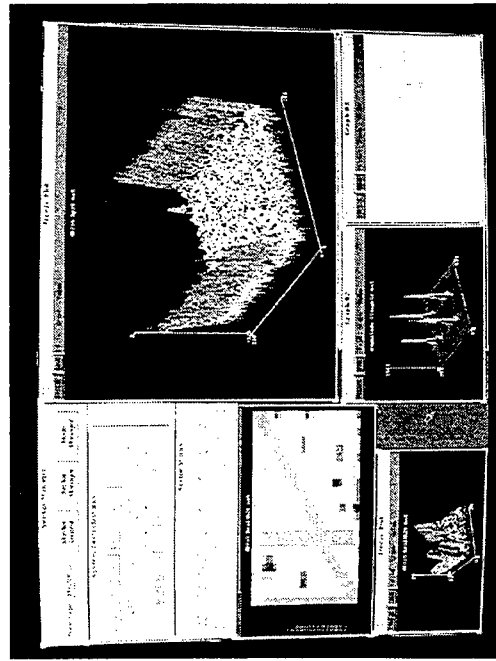
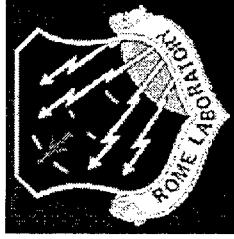
Real Time Algorithm Development



- 96 GFlops Paragon (on left) used for algorithm development and timing
- Ported to 7.5 GFlops Ruggedized Touchstone racks (on table on right) without problem
- Paragon fed Touchstone with recorded MCARM airborne data at real time rates across HiPPI cables



Inflight Data Display





Conclusions



- **STAP implemented in Real Time using embedded High Performance Computer onboard aircraft with 16 channel phased array**
- **100 degree surveillance volume coverage approximately every half second at peak rate**
- **Beam shapes constrained while canceling clutter with PRI-staggered post Doppler and Post Doppler adaptive beamforming algorithms**

Automated Application Synthesis for High-Performance Sensor Array Processing

***William J. Kostis, Gary E. Adams,
Robert C. Durie, and Adam W. Bojanczyk***

Cornell University
School of Electrical Engineering
Ithaca, NY 14853

Abstract Development of high-performance radar and sonar signal processing applications continues to be a daunting task. Performance optimization, code reusability, and algorithm verification are each goals requiring a substantial effort in software engineering. In this paper, we describe our Parallel Program Factory (PPF), a development system designed to address these issues. An illustrative example application is taken from Space-Time Adaptive Processing (STAP). Achieving optimal application performance for a variety of problem sizes requires careful choices of both algorithms and, indeed, particular implementations of these computational "modules." The communication demands imposed by the data distribution requirements of each implementation further complicates the task. For example, it may be beneficial to use a data distribution that is inefficient for one module in order to increase the performance of another, more compute-intensive task. These relationships are of particular interest as the performance of many complex signal processing applications can be communication-limited. While applications may be portable across distributed memory platforms, performance frequently is not. Our approach relies upon libraries of performance benchmarks and models for each computational module implementation on each platform. Similar data is maintained for all data distribution modules. The top level application description can be specified using the Khoros dataflow environment. An application designer need only select the sequence of computational modules for the PPF to assemble a near-optimal software solution for the designated problem size and platform. In this way, machine performance characteristics, complex data distributions, and the effects of memory hierarchy are all shielded from the developer. In addition, a near optimal solution for a different problem size or platform can be generated automatically.

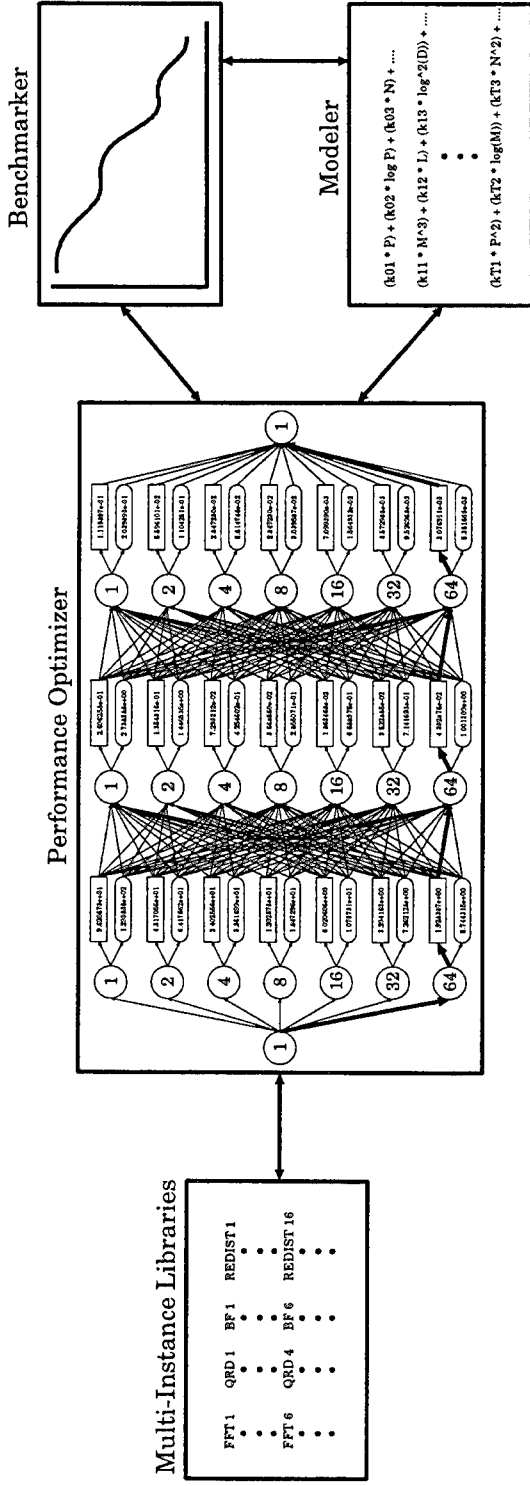
Automated Application Synthesis for High-Performance Sensor Array Processing

William J. Kostis, Gary E. Adams, Robert C. Durie, and Adam W. Bojanczyk

School of Electrical Engineering
Cornell University
Ithaca, NY 14853

- Goals of Parallel Program Development
 - Algorithm verification
 - Code reusability
 - Performance optimization
 - *Portable performance*
- Approach: Parallel Program Factory (PPF)
 - Multi-Instance Libraries
 - Benchmarking
 - Performance modeling
 - Pre-compiler/optimizer

Parallel Program Factory



A complete application synthesis environment providing:

- Efficient, algorithmic-level implementation
- Detailed performance information
- Cross-platform performance portability

Multi-Instance Libraries

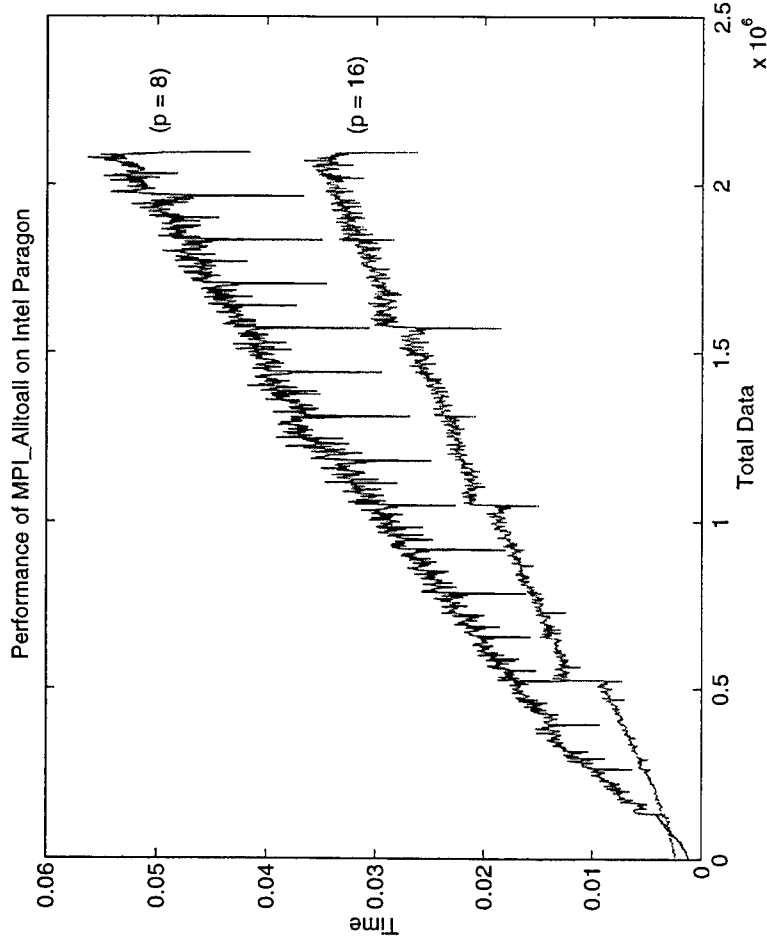
Multi-Instance Library: Modules can have more than one implementation

- Modules can operate on different data distributions
- Can have different implementations, i.e. convolution vs. FFT-Multiply-IFFT

A Multi-Instance Library contains:

- Executables (LAPACK, Custom)
- Data redistribution routines (e.g. Transpose, Divide, Scatter/Gather)
- Set of influencing parameters (e.g. # of processors, data size, blocking params.)
- Performance models
- Routines to generate arguments for benchmarking

Benchmarking



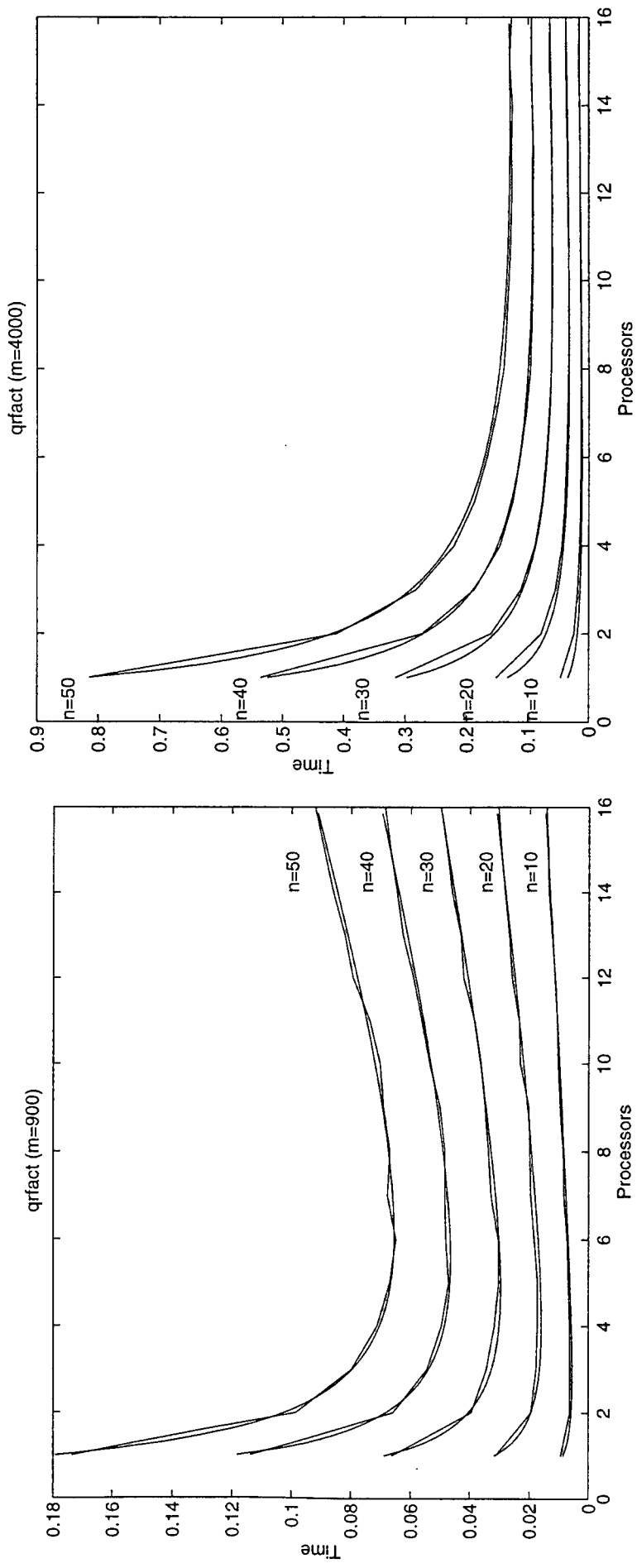
- Automatic benchmarking for all legal sets of influencing parameters
- Portable: Intel Paragon, IBM SP2, others in the future
- Debugging mode to assist in code development

Modeling

- Generate accurate polynomial models with minimal user intervention
 - Fully automatic: select polynomial and compute coefficients
 - Specify set of possible terms: generate final polynomial and coefficients
 - Specify polynomial: generate coefficients only
- Piecewise models required for modeling cache effects, paging, etc.
- Terms of the form $X^i \log(Y)$
- Pseudo-variables: $\text{power2}(X)$, $\text{ceil}(X)$, $\text{floor}(X)$
- Models based on 2-norm minimization

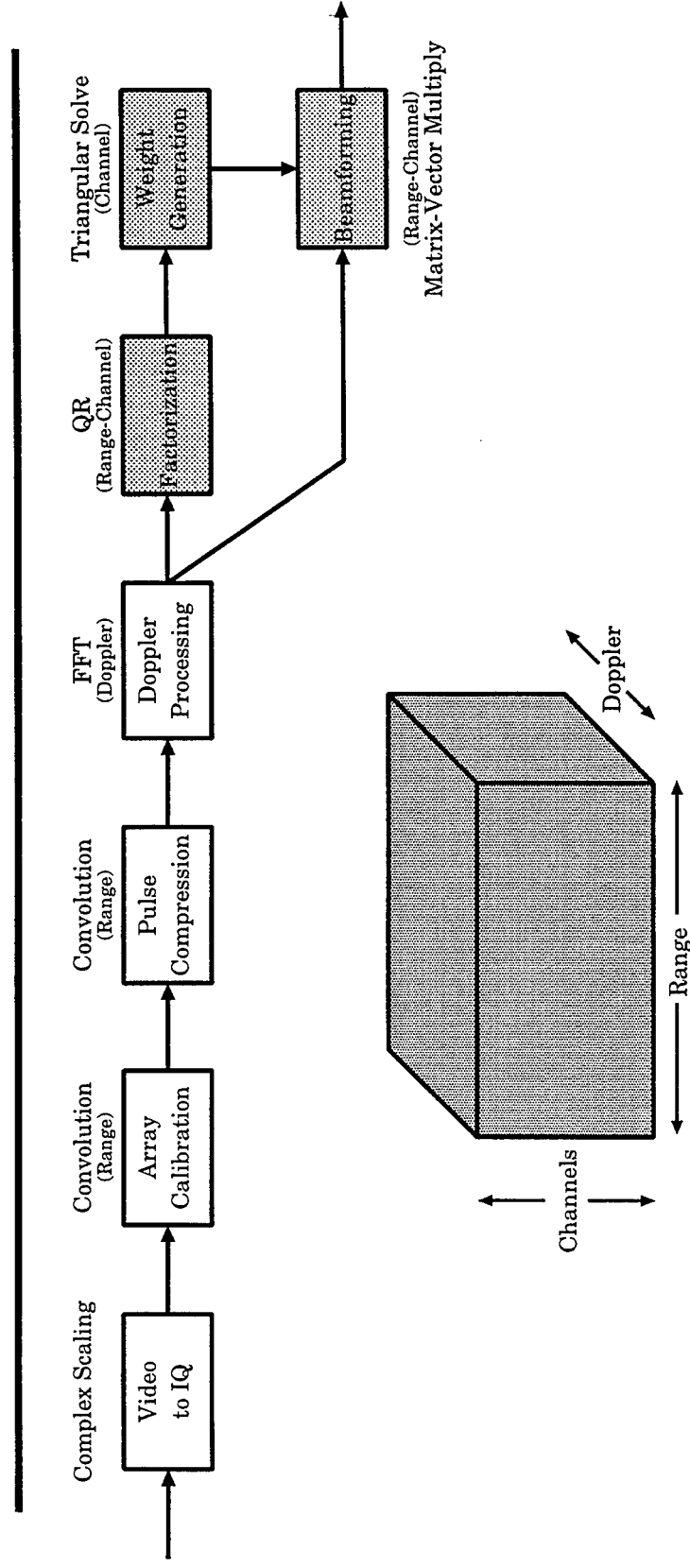
Modeling Example

Modeling QR Factorization using benchmark data



$$\text{Model: } K_1 \frac{MN^2}{P} + K_2 \frac{N^3}{P} + K_3 NP + K_4 N^2$$

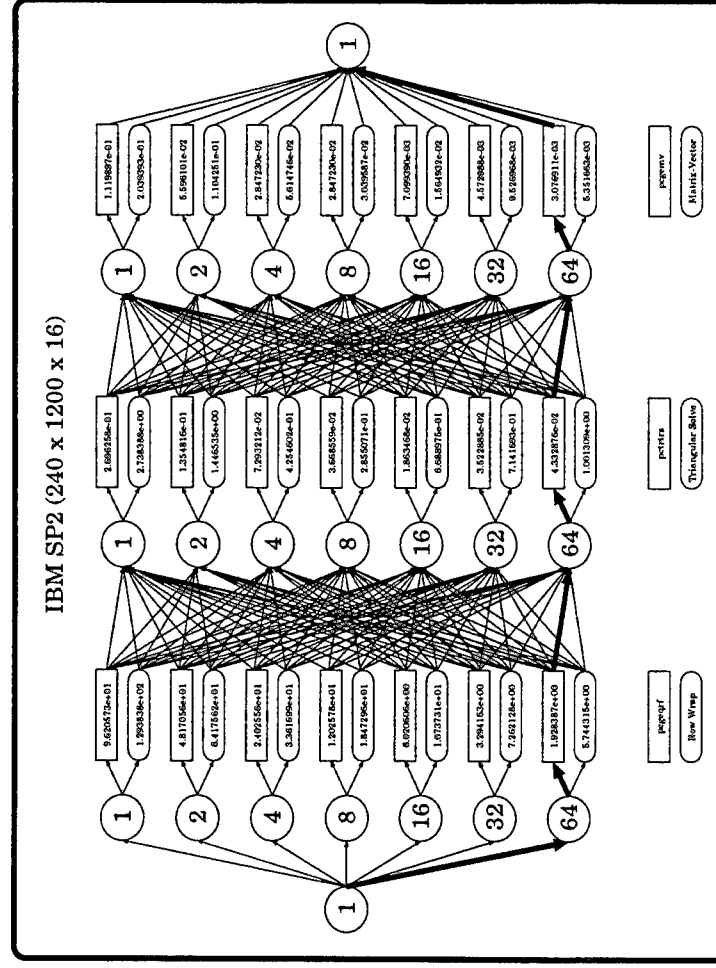
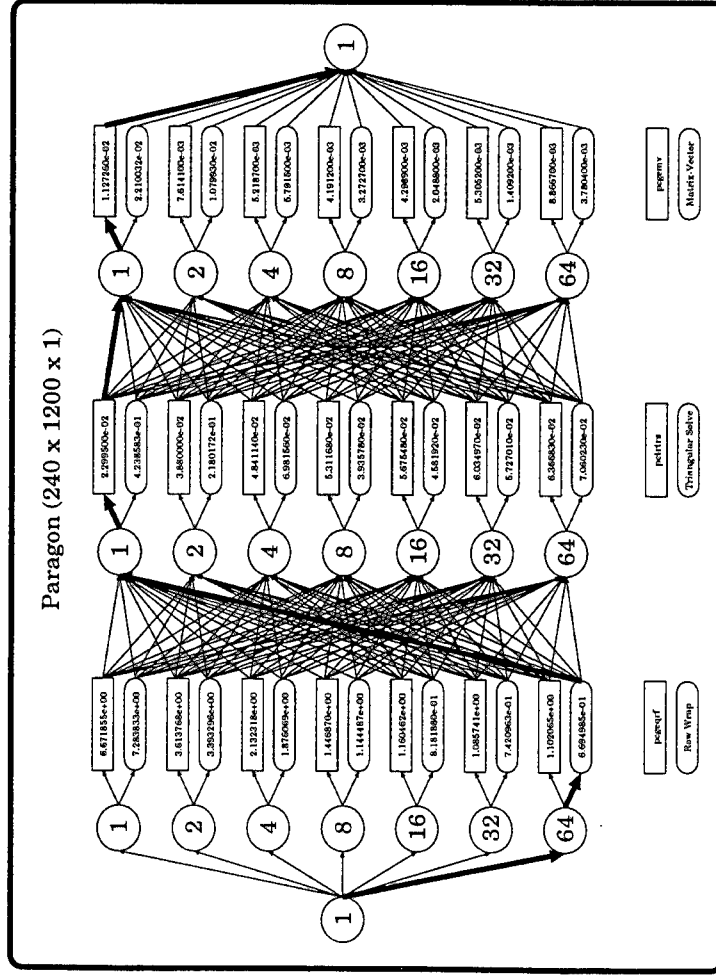
Space-Time Adaptive Processing Example



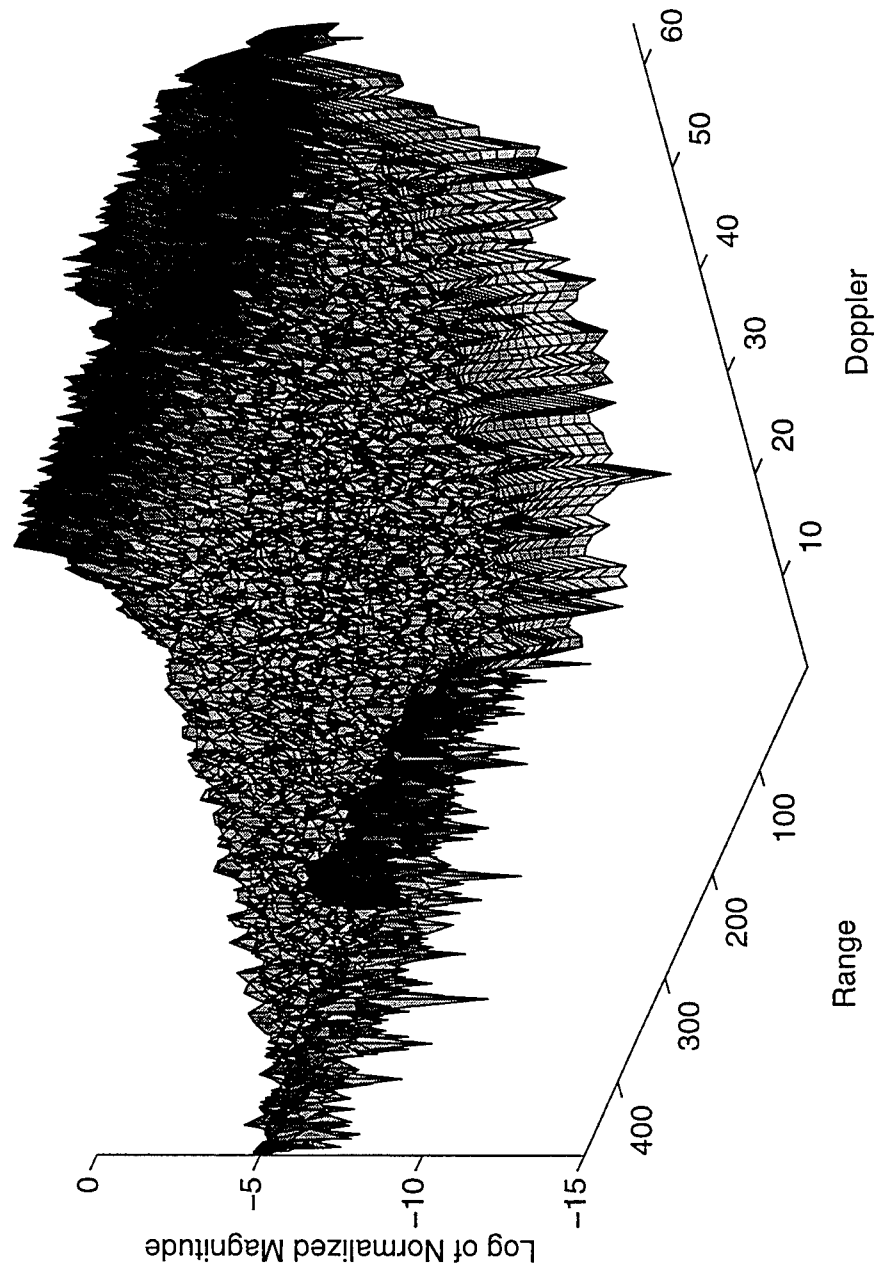
Differing data distributions at various algorithmic steps necessitate:

- Multiple implementations of computational modules
- Flexible data redistribution modules
- Formal method of module selection that yields optimal performance

Example Optimizations



Example STAP Output



Future Enhancements

- Better piecewise models, pseudo-variables
- Fully-automatic application synthesis
- Real-time task management
 - List of tasks and priorities
 - Resource constraints
 - Select best sequence of implementations for each task
- Add alternative input formats to libraries
 - MATLAB source
 - Khoros

Automated Application Synthesis for High-Performance Sensor Array Processing

William J. Kostis, Gary E. Adams, Robert C. Durie,
and Adam W. Bojanczyk

School of Electrical Engineering
Cornell University
Ithaca, NY 14853

Development of high-performance radar and sonar signal processing applications continues to be a daunting task. Performance optimization, code reusability, and algorithm verification are each goals requiring a substantial effort in software engineering. In this paper, we describe our Parallel Program Factory (PPF), a development system designed to address these issues. An illustrative example application is taken from Space-Time Adaptive Processing (STAP).

Achieving optimal application performance for a variety of problem sizes requires careful choices of both algorithms and, indeed, particular implementations of these computational "modules". The communication demands imposed by the data distribution requirements of each implementation further complicates the task. For example, it may be beneficial to use a data distribution that is inefficient for one module in order to increase the performance of another, more compute-intensive task. These relationships are of particular interest as the performance of many complex signal processing applications can be communication-limited. Lastly, while applications may be portable across distributed memory platforms, performance frequently is not.

Our approach relies upon libraries of performance benchmarks and models for each computational module implementation on each platform. Similar data is maintained for all data distribution modules. The top level application description can be specified using the Khoros dataflow environment. An application designer need only select the sequence of computational modules for the PPF to assemble a near-optimal software solution for the designated problem size and platform. In this way, machine performance characteristics, complex data distributions, and the effects of memory hierarchy are all shielded from the developer. In addition, a near optimal solution for a different problem size or platform can be generated automatically.

Data Remapping Techniques for High-Performance Embedded Signal Processing Applications

Viktor K. Prasanna

University of Southern California
Department of Electrical Engineering
3740 McClintock Avenue, EEB 200
Los Angeles, CA 90089-2562
email: prasanna@ganges.usc.edu

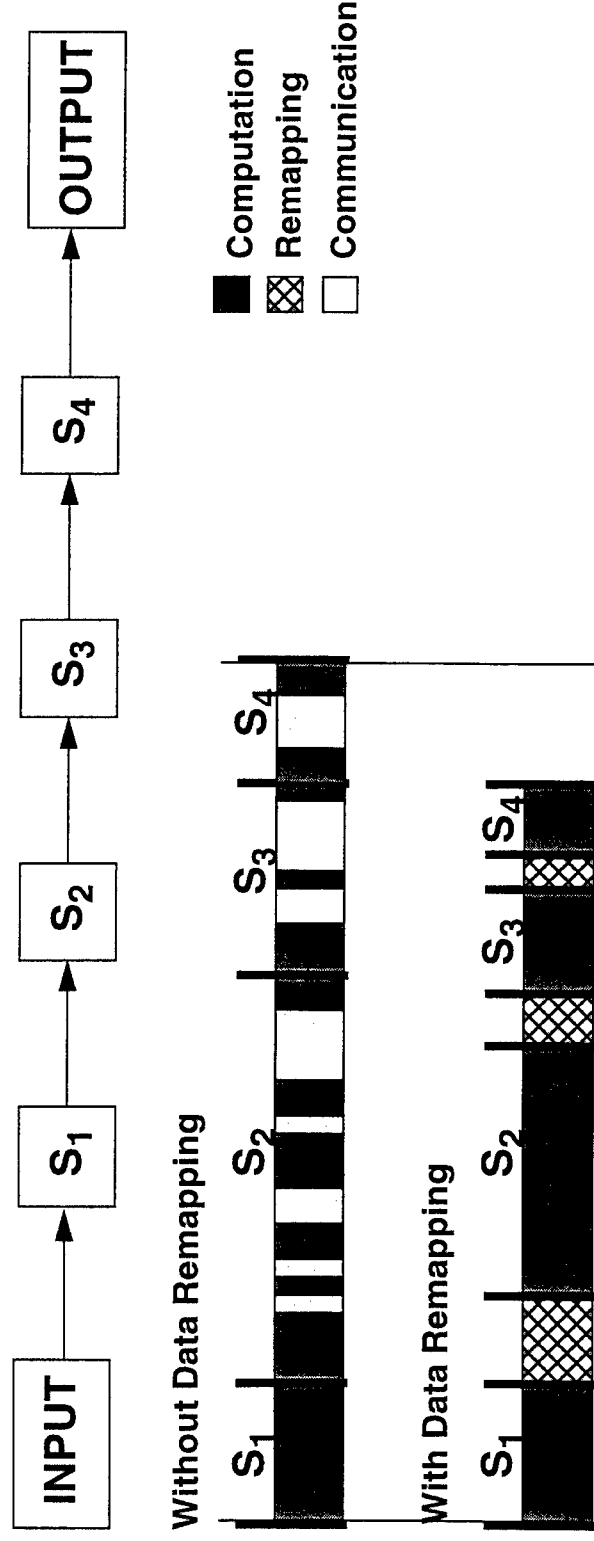
Abstract Embedded signal processing applications such as STAP, SAR, ATR, Sonar among others consist of a number of stages in which data is accessed along different axes as the computation proceeds. For these applications, we first develop a unified methodology using run time data remapping between stages to realize scalable performance in using HPC technology. We then present new techniques to solve the classic run time data redistribution problem. For the $Cyclic(X)$ to $Cyclic(KX)$ distribution, problem we show new indirect techniques that perform the mapping using ceiling $\log K + 2$ steps. Previous approaches take as much as K steps. All the data transfers are performed in a conflict-free manner and the index computation at the nodes can be performed in a distributed fashion with simple modulo computations. The corner turn operation and the data cube access between Doppler processing and beamforming in STAP are special cases of the above data redistribution problem. Using our approach we show efficient algorithms for several related redistribution problems arising in throughput oriented implementations of signal processing applications. Interstage data movement operations that arise in using HPC platforms for STAP, SAR, ATR, and Sonar applications can be modelled by the above data redistribution problem. Using our techniques for redistribution, we show scalable parallel algorithms and implementations for STAP, SAR, ATR, and universal beamforming in Sonar applications on IBM SP-2 and Cray T3D. Experimental results are shown using MITRE and MIT LL STAP benchmarks and Sonar benchmarks from NUWC. For corner turn and SAR image formation, we show implementations that reduce the number of compute nodes by 40% compared with earlier implementations. These implementations have been performed using the Message Passing Interface (MPI) and C and are portable.

Data Remapping Techniques for High-performance Embedded Signal Processing Applications

Viktor K. Prasanna
University of Southern California
prasanna@usc.edu

Data Remapping

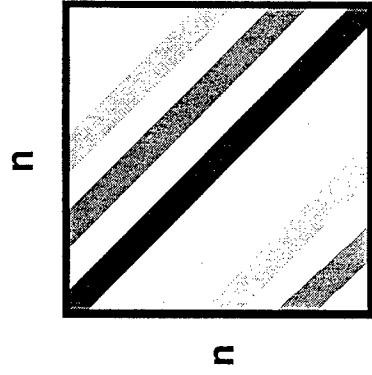
Communication Overheads in Multi-Stage Signal Processing Applications



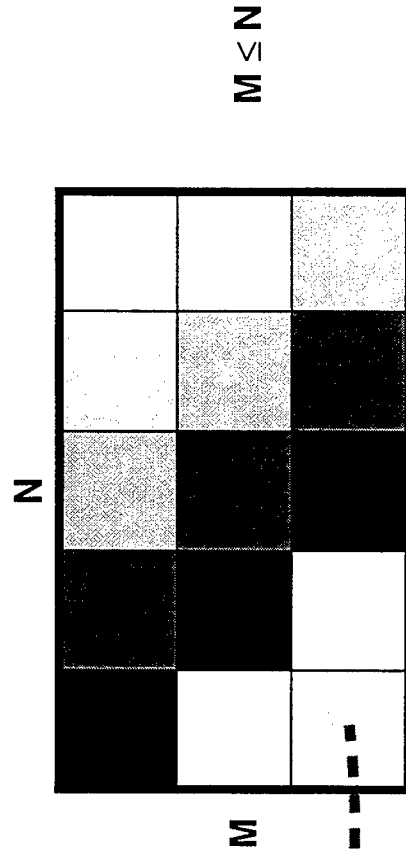
Benefits of Data Remapping

- Maximizes Data Locality
 - Allows Predictable, Controlled Communication Patterns
 - Scalable Performance
- ➔ Data remapping must be used when the benefits exceed the overheads of remapping

Circulant Matrix



Generalized Circulant Matrix



Diagonal elements are the same

No. of distinct elements = n or N

All the elements of row 0 are distinct

Every row has distinct elements.

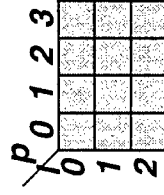
Definition of Generalized Circulant Matrix

$$C = \begin{bmatrix} C_0 & C_1 & C_2 & \dots & C_{N-1} \\ C_{N-1} & C_0 & C_1 & \dots & C_{N-2} \\ C_{N-2} & C_{N-1} & C_0 & \dots & C_{N-3} \\ \dots & \dots & \dots & \dots & \dots \\ C_{N-M+1} & C_{N-M+2} & C_{N-M+3} & \dots & C_{N-M} \end{bmatrix}$$

$$C_j = \begin{bmatrix} c^{(j)}_0 & c^{(j)}_1 & c^{(j)}_2 & \dots & c^{(j)}_{n-1} \\ c^{(j)}_{n-1} & c^{(j)}_0 & c^{(j)}_1 & \dots & c^{(j)}_{n-2} \\ c^{(j)}_{n-2} & c^{(j)}_{n-1} & c^{(j)}_0 & \dots & c^{(j)}_{n-3} \\ \dots & \dots & \dots & \dots & \dots \\ c^{(j)}_{n-1} & c^{(j)}_{n-2} & c^{(j)}_{n-3} & \dots & c^{(j)}_0 \end{bmatrix}$$

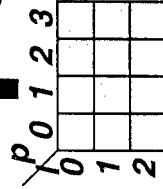
Our Communication Schedule for Redistribution

Generalized
Circulant Matrix



Row Transformation

Transformation



Initial DPT

Direct
Indirect
Hybrid
Multi-phase

Column

Transformation



Final DPT

Initial Column Transformation: Local Data Rearrangement
Row Transformation: Reorganize Communication Patterns
Final Column Transformation: Local Data Rearrangement

Communication Schedule using a Generalized Circulant Matrix(1)

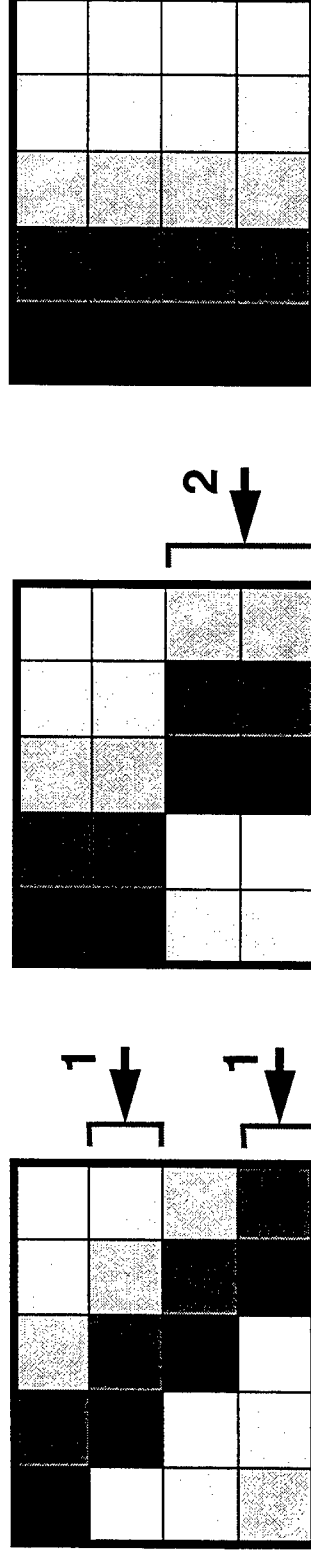
Recursive Alignment of Diagonal Elements into a Vertical Line

Communication Events Reorganization

Log Steps \longrightarrow Minimize Start-up Costs

Cyclic Shift

Strided Communication Pattern
Applicable to arbitrary K and P values
Contention Free



Communication Schedule using a Generalized Circulant Matrix (2)

Generalized Circulant Matrix provides a Uniform Framework
for a class of Contention Free Communication Schedules

1. **Direct Schedule** → **Minimal Transmission Costs**
i-th row of DPT = i-th communication event (step)
2. **Indirect Schedule** → **Minimal Startup Costs**
Combine and Forward through Intermediate Nodes
3. **Hybrid Schedule** → **Flexible Trade-off between
Startup Costs and Transmission Costs**
Combination of Direct and Indirect Schedules

**Direct and Indirect Schedules
can be viewed as special cases of Hybrid Schedule.**

Cyclic(x) \rightarrow Cyclic(Kx) over P processors

Communication Events Reorganization Theorem:

For all K and P , the Destination Processor Table can be transformed into a Generalized Circulant Matrix.

Communication Scheduling Theorem :

Using the Destination Processor Table in a Generalized Circulant Matrix form, we can perform the redistribution via

- (1) Indirect Schedule in $\lceil \log_2 K \rceil + 2$ communication steps,
- (2) Direct Schedule in K communication steps,
- (3) Hybrid Schedule

in a **contention free** manner.

Index Set Computation Theorem :

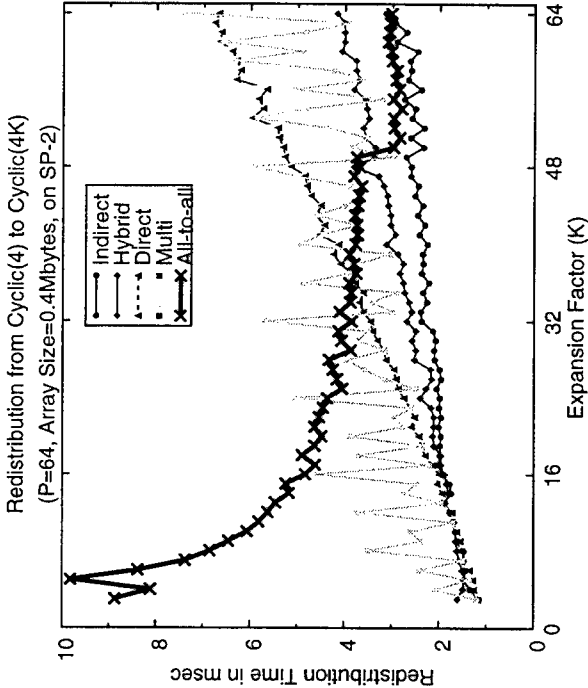
The index sets can be efficiently computed in a distributed way by exploiting the periodicity arising from modular K and P systems .

Our Data Remapping Techniques

Redistribution Cyclic(x) to Cyclic(Kx)		Contention Free Schedule	
	Direct Schedule	Hybrid Schedule	Indirect Schedule
Number of Communication Steps	K	$d + \lceil K/2^d \rceil$	$\lceil \log_2 K \rceil + 2$

MPI All-to-all Communication Primitives?

☐ Not Efficient when K is small



Experimental Results

Cray T3D

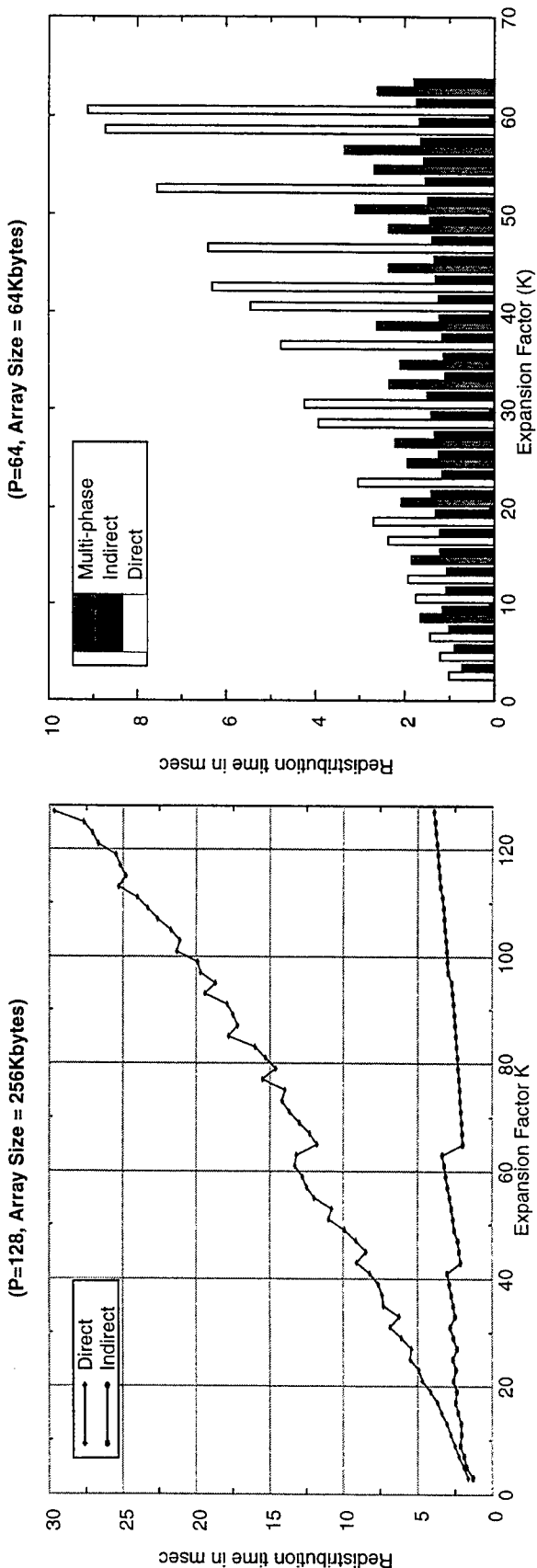
Redistribution from Cyclic(2) to Cyclic(2K)

Direct Excessive Start-up Costs (∞ K)

Indirect Reduces Start-up Costs ($\propto \log_2 K$)

Multi-phase Effective only when K is a Composite Number

Total Message Size is large (Compared with Indirect Schedule)

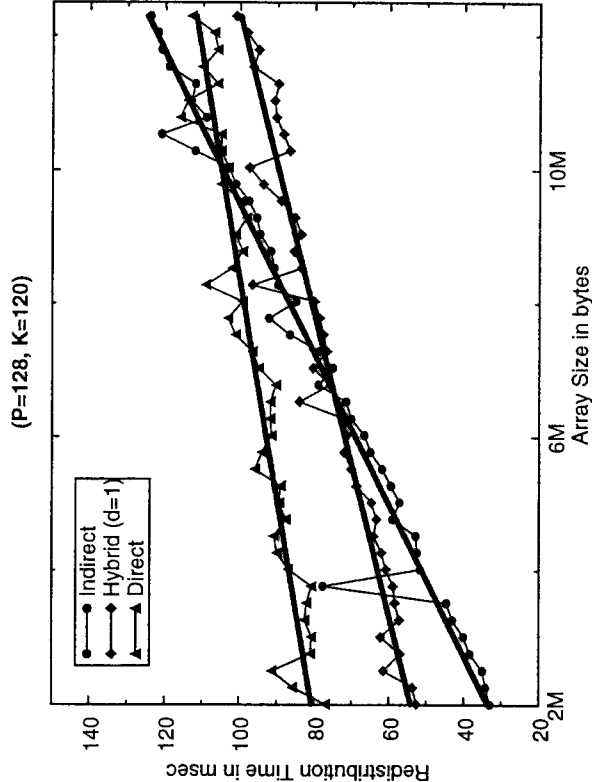
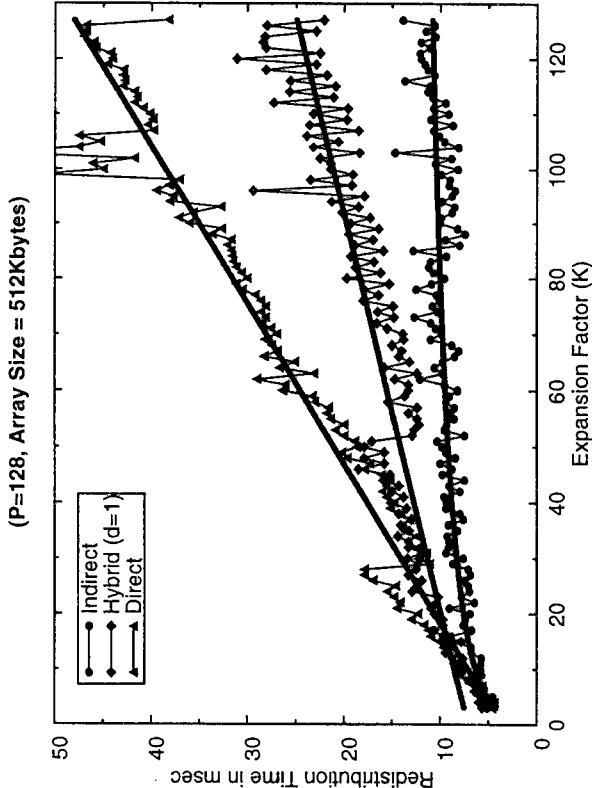


Experimental Results

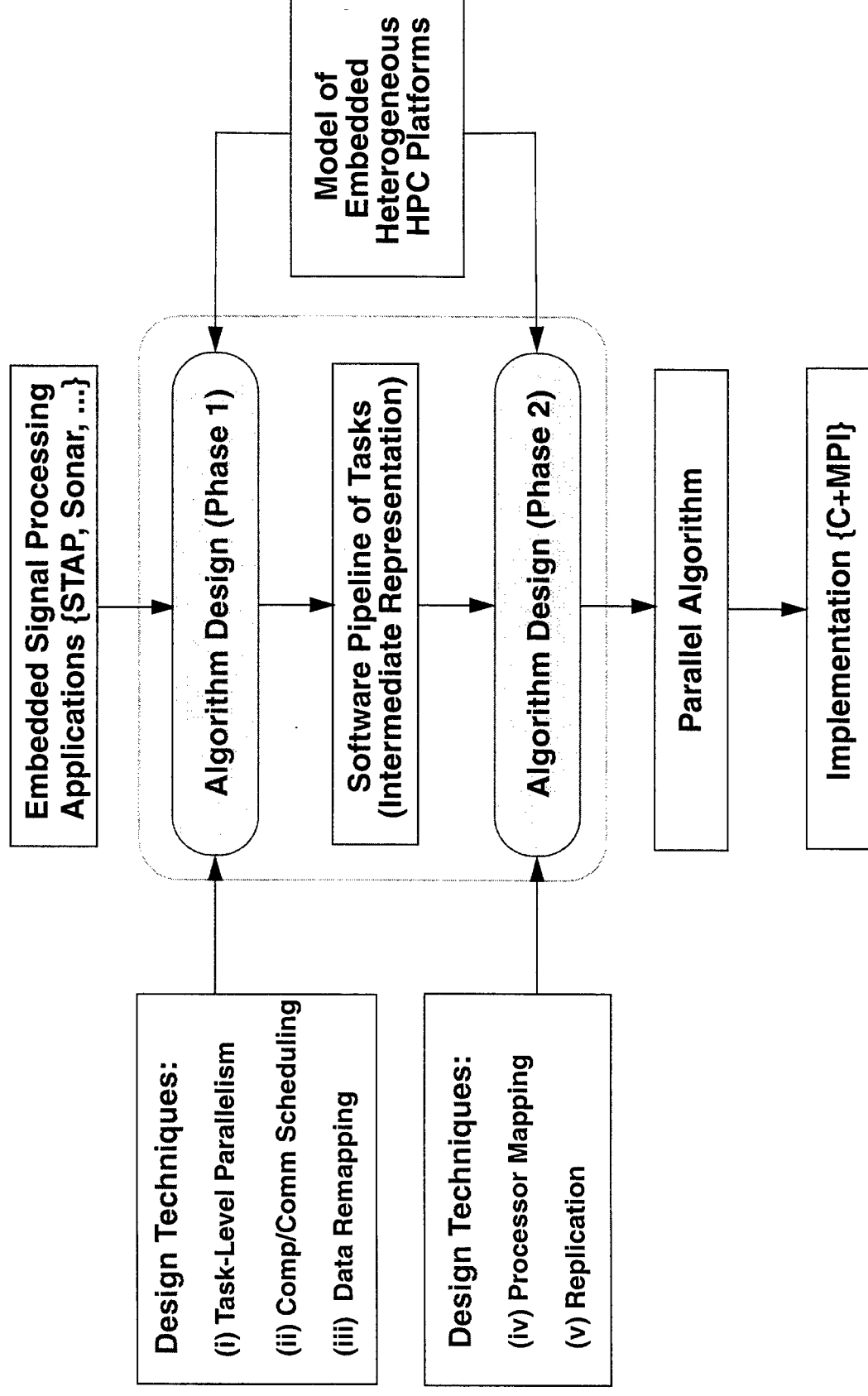
IBM SP-2

Redistribution from Cyclic(4) to Cyclic(4K)

- | | |
|----------|--|
| Direct | Excessive Start-up Costs ($\propto K$) |
| Indirect | Reduces Start-up Costs ($\propto \log_2 K$) |
| Hybrid | Flexible Trade-off between Start-up Costs and Transmission Costs |



Our Parallel Algorithm Design Methodology



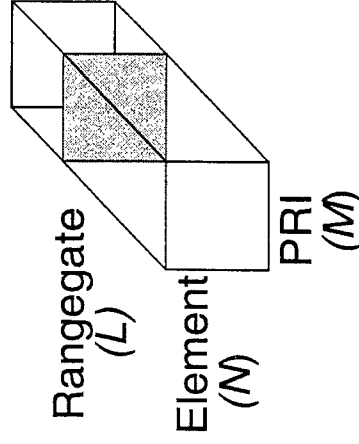
□ Performance Measures: Latency, Throughput, Processor Utilization, Efficiency, etc.

Example: Throughput Oriented Radar Implementation

Parallel Algorithm Design and Implementation for Beam Space Post Doppler STAP

□ Beam Space Post Doppler (BSPD) STAP

Data Cube Accumulated in One CPI:



Processing Stages:

- (i) Data Input
- (ii) Beam Forming
- (iii) Doppler Processing
- (iv) Weight Computation / Application:
Takes the Most Computation Time

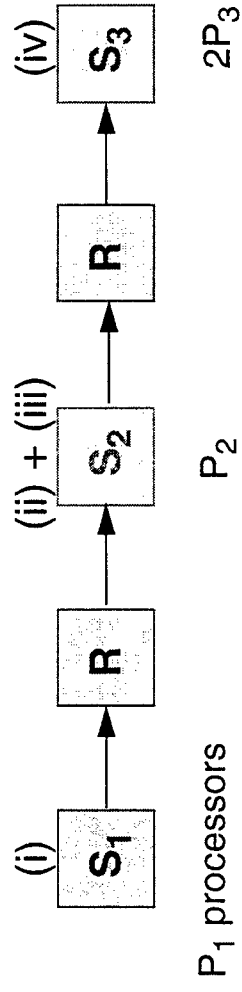
Problem Size Chosen: 12 (N) X 64 (M) X 576 (L)

□ A Parallel Algorithm for BSPD STAP

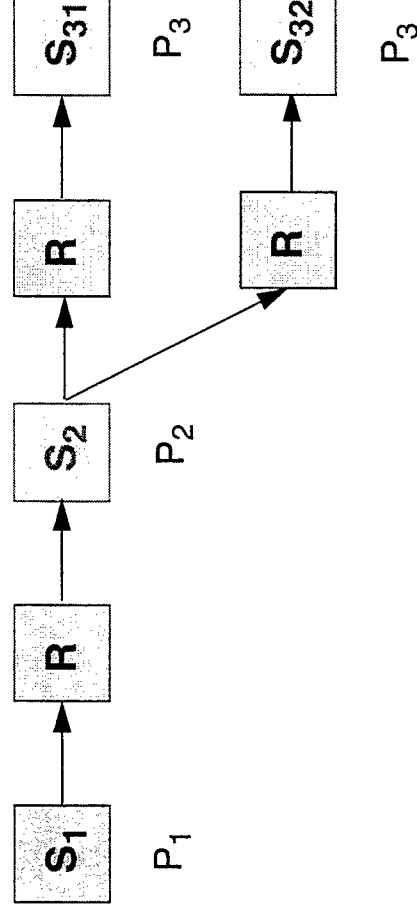
- Exploiting task level parallelism to schedule computation / communication
- Efficient data remapping between stages
- Mapping software pipeline of tasks onto processors
- Replication of software pipeline stages considered in processor mapping

Replication of pipeline stages

(i) Mapping without replication

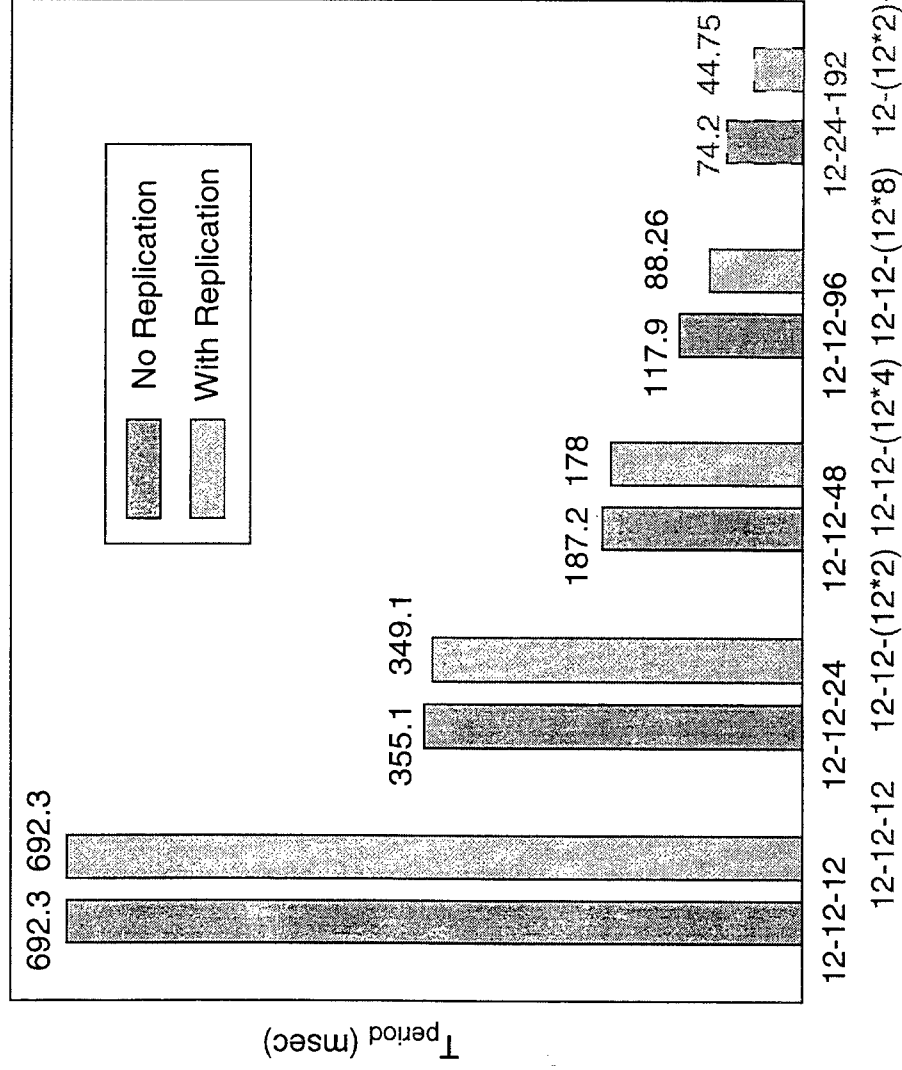


(ii) Mapping with replication: replicating S_3 two times



Experimental Results on IBM SP-2

- Code written using C and MPI ---> Portable
- Experimental results on 120 nodes, projected results on 228 nodes

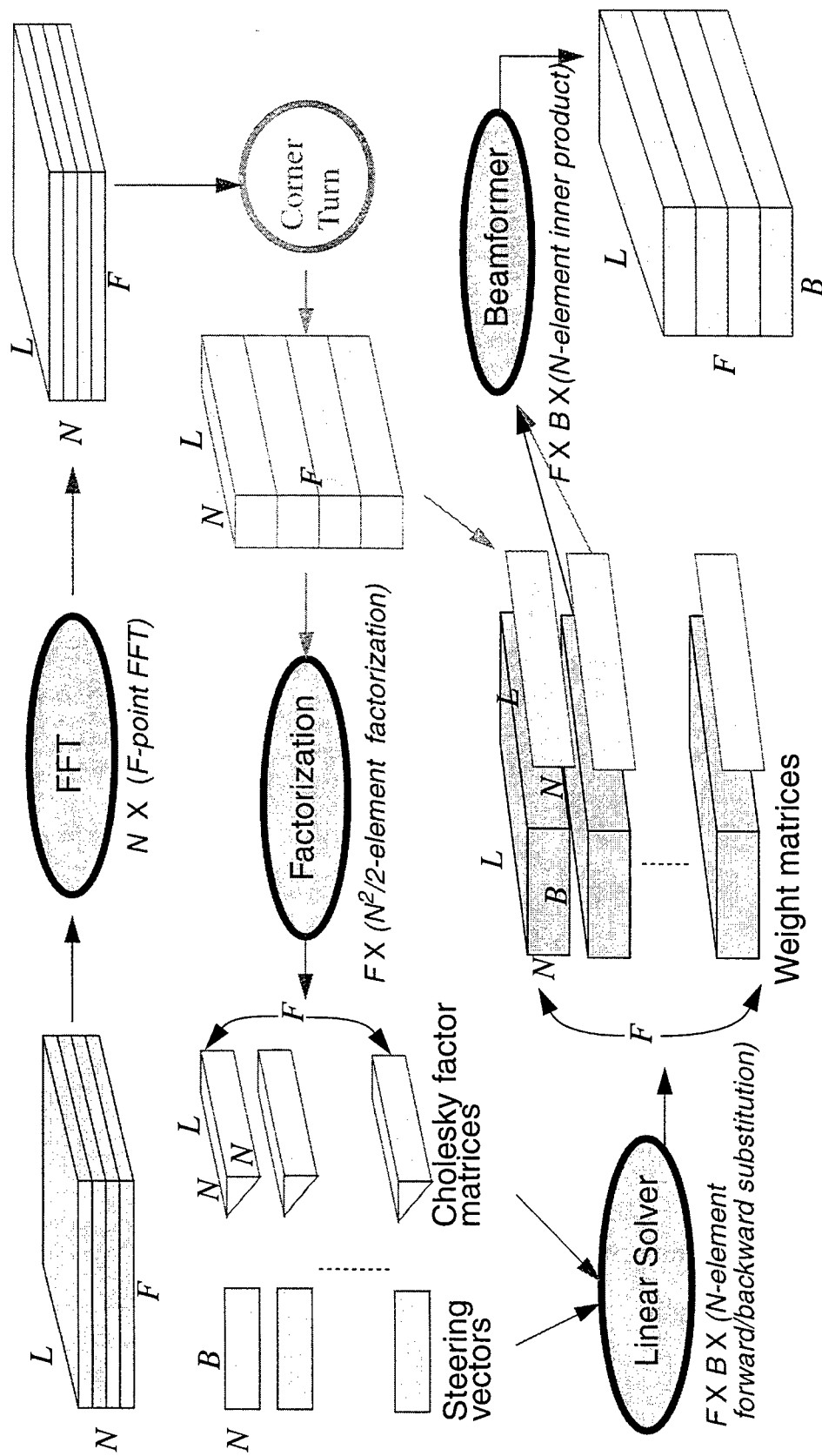


Number of Outputs
per Second

Processor Assignment	Without Replication	With Replication
12+12+12	1.44	1.44
12+12+24	2.82	2.86
12+12+48	5.34	5.62
12+12+96	8.48	11.20
12+24+192	13.48	22.35

Processor Mapping With and Without Replication: S₁ - S₂ - S₃

Implementation of a Plane-wave Minimum Variance Distortionless Response (MVDR) Sonar Beamformer [NUWC Sonar benchmark]



N : no of sensors (channels) B : no. of beams in a particular frequency
 F : no. of frequency bins L : no. of iterations

Features of the MVDR ABF

(Based on the classification of the ABF techniques)

Narrow-band	Broad-band
Fully adaptive	Partially adaptive
Element (data) space	Beam space
Time domain	Frequency domain
Recursive estimation	Block estimation

Computational Complexity and Degree of Parallelism

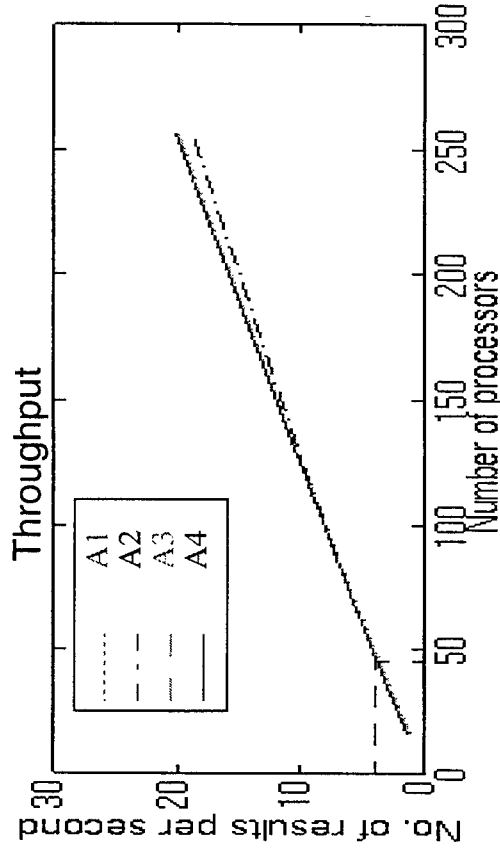
N : no of sensors B : no. of beams per bin
 F : no. of bins L : no. of iterations

Processing stage	Computational complexity	Degree of parallelism (DoP)	Comments
FFT	$NF \log_2 F$	N	
Factorization	$33N^2F$	F	Cholesky factorization reduces complexity of matrix inversion from $O(N^3)$ to $O(N^2)$
Linear Solver	$8N^2FB$	FB	
Beamformer	$8N^2FB$	FB	

Experimental Results on SP2

$N=64$, $F=256$, $B=8$
Total number of beams=2048

Processing Stage	Complexity (per iteration)	DoP
FFT	0.13 MFLOP	64
Factorization	34 MFLOP	256
Linear Solver	671.1 MFLOP	2048
Beamformer	671.1 MFLOP	2048



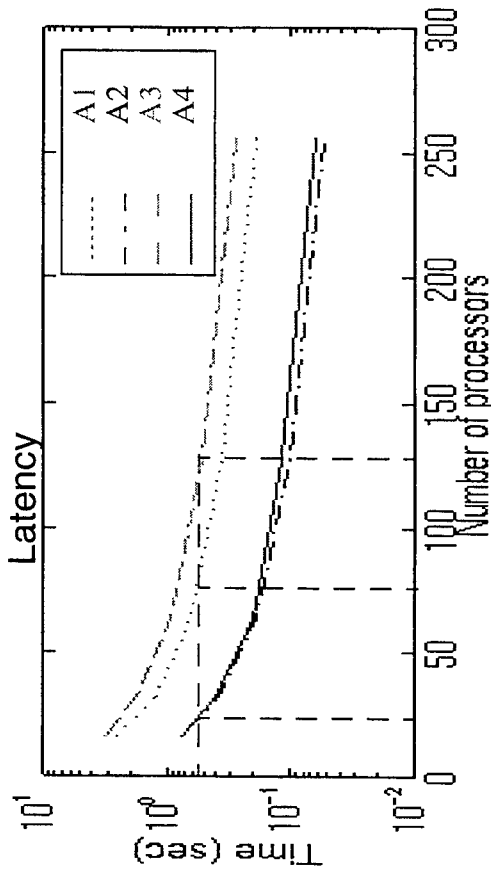
Four software pipelines

A1: Linear software pipeline

A2: Feedback software pipeline

A3: Linear software pipeline
with replicated modules

A4: General software pipeline

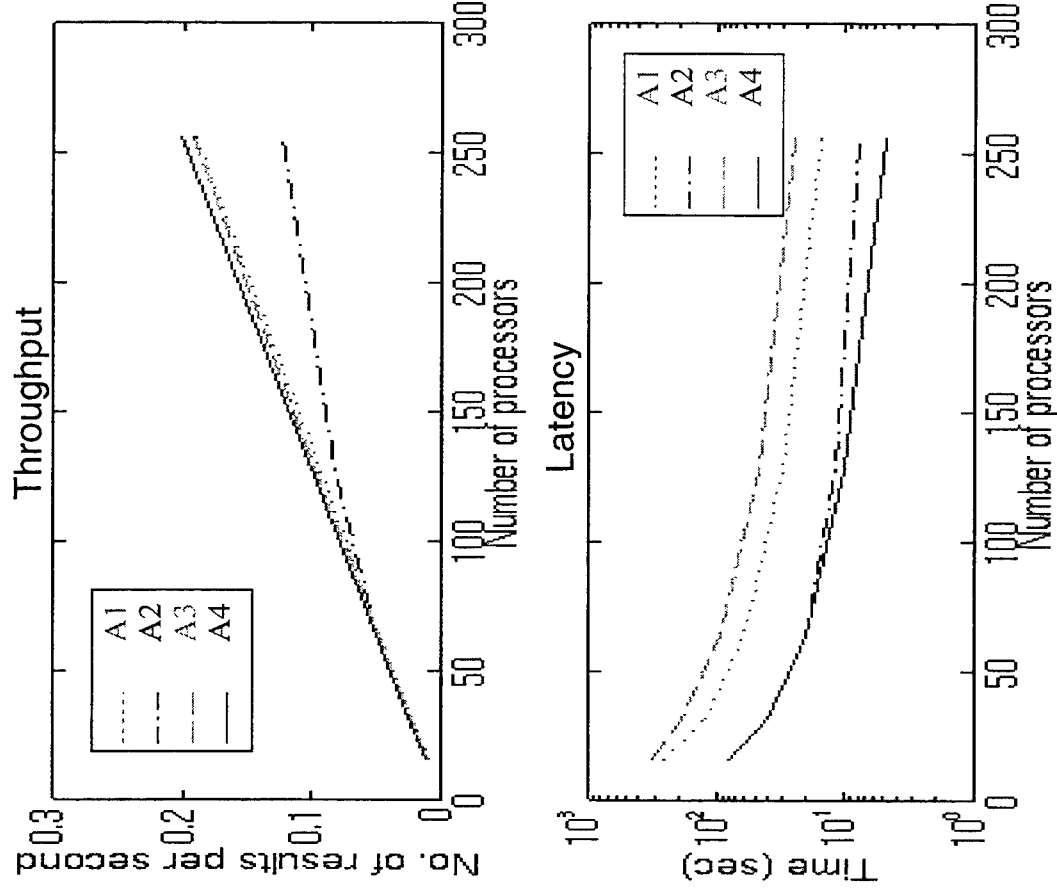


Experimental Results on T3D

$N=1024$, $F=64$, $B=8$.

Total number of beams=512

Processing stage	Complexity (per iteration)	DoP
FFT	0.39 MFLOP	1024
Factorization	2.21 GFLOP	64
Linear Solver	4.30 GFLOP	512
Beamformer	4.30 GFLOP	512



Digital Radar Receiver

William S. Song

MIT Lincoln Laboratory
244 Wood Street
Lexington, MA 02173-9108
tel: (617) 981-4693
email: song@ll.mit.edu

Abstract MIT Lincoln Laboratory has developed an experimental all digital radar receiver for the airborne surveillance applications such as the airborne E-2C UHF radar. The all-digital radar receiver directly samples the radio frequency (RF) input and performs the baseband downconversion and in-phase/quadrature signal generation in the digital domain. The direct RF sampling eliminates much of the mixers, filters, and other analog circuitry in the receiver. The component count reduction is also expected to reduce the receiver size, weight, and cost significantly. In order to meet the 65 GOPS per channel computational throughput requirements of digital down-conversion, a very high performance signal processor chip-set has been developed using CMOS bit-level systolic array cell architecture.

DIGITAL RADAR RECEIVER

WILLIAM S. SONG

DIVISION 10
AIR DEFENSE TECHNOLOGY
MASSACHUSETTS INSTITUTE OF TECHNOLOGY
LINCOLN LABORATORY

THIS WORK WAS SPONSORED BY DARPA UNDER AIR FORCE CONTRACT F19628-95-C0002.
OPINIONS, INTERPRETATIONS, CONCLUSIONS AND RECOMMENDATIONS ARE THOSE OF
THE AUTHOR AND ARE NOT NECESSARILY ENDORSED BY THE UNITED STATES AIR FORCE.



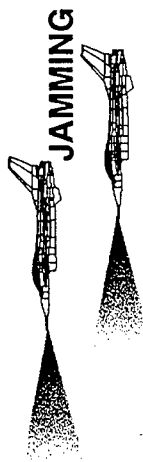
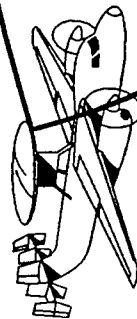
OUTLINE

- ● INTRODUCTION
- DIGITAL RECEIVER CONCEPT
- HARDWARE DEVELOPMENT
- TECHNOLOGY DEMONSTRATION PLAN
- SUMMARY

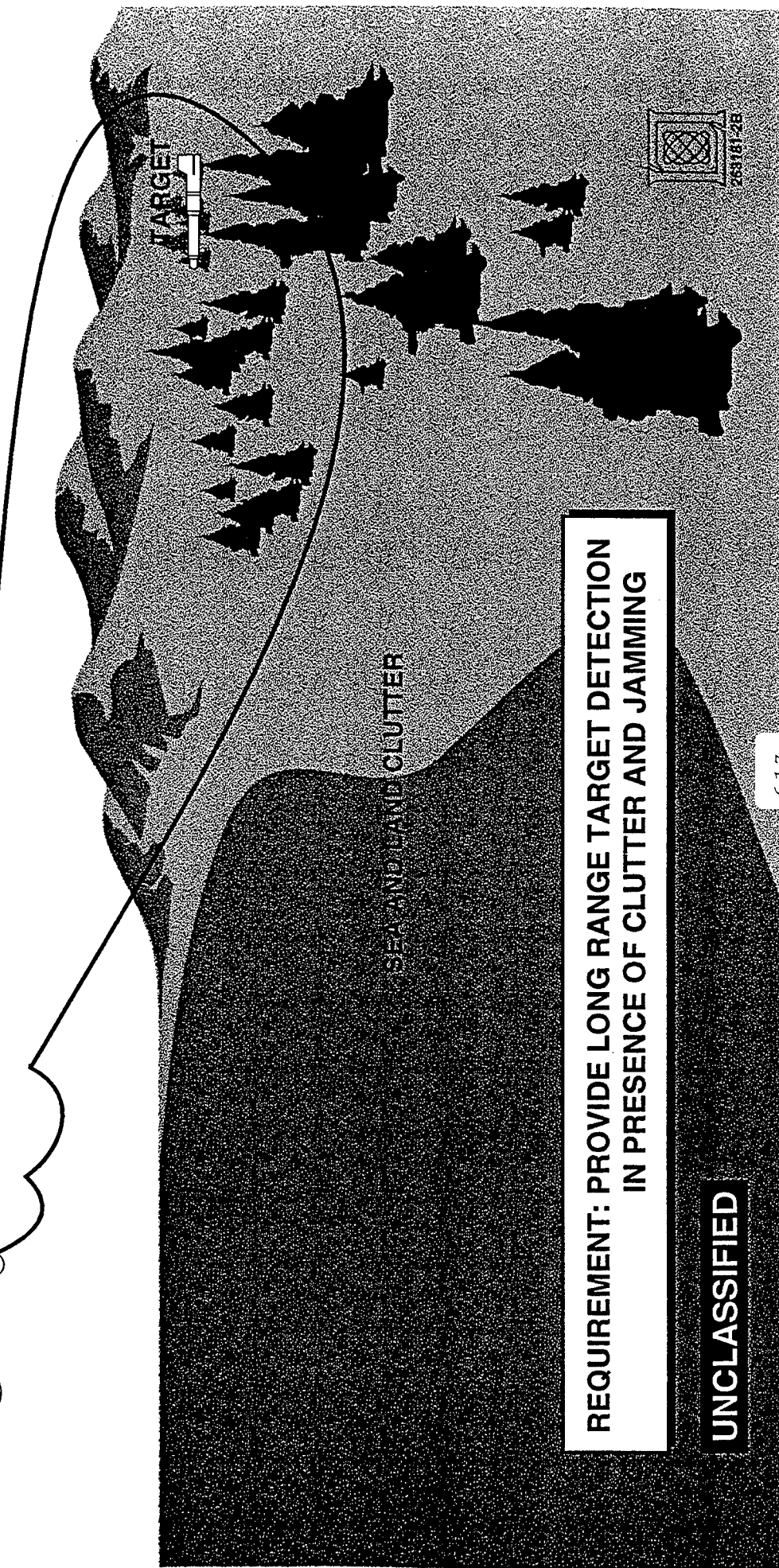
UNCLASSIFIED

AIRBORNE EARLY WARNING (AEW) RADAR ENVIRONMENT

AEW RADAR



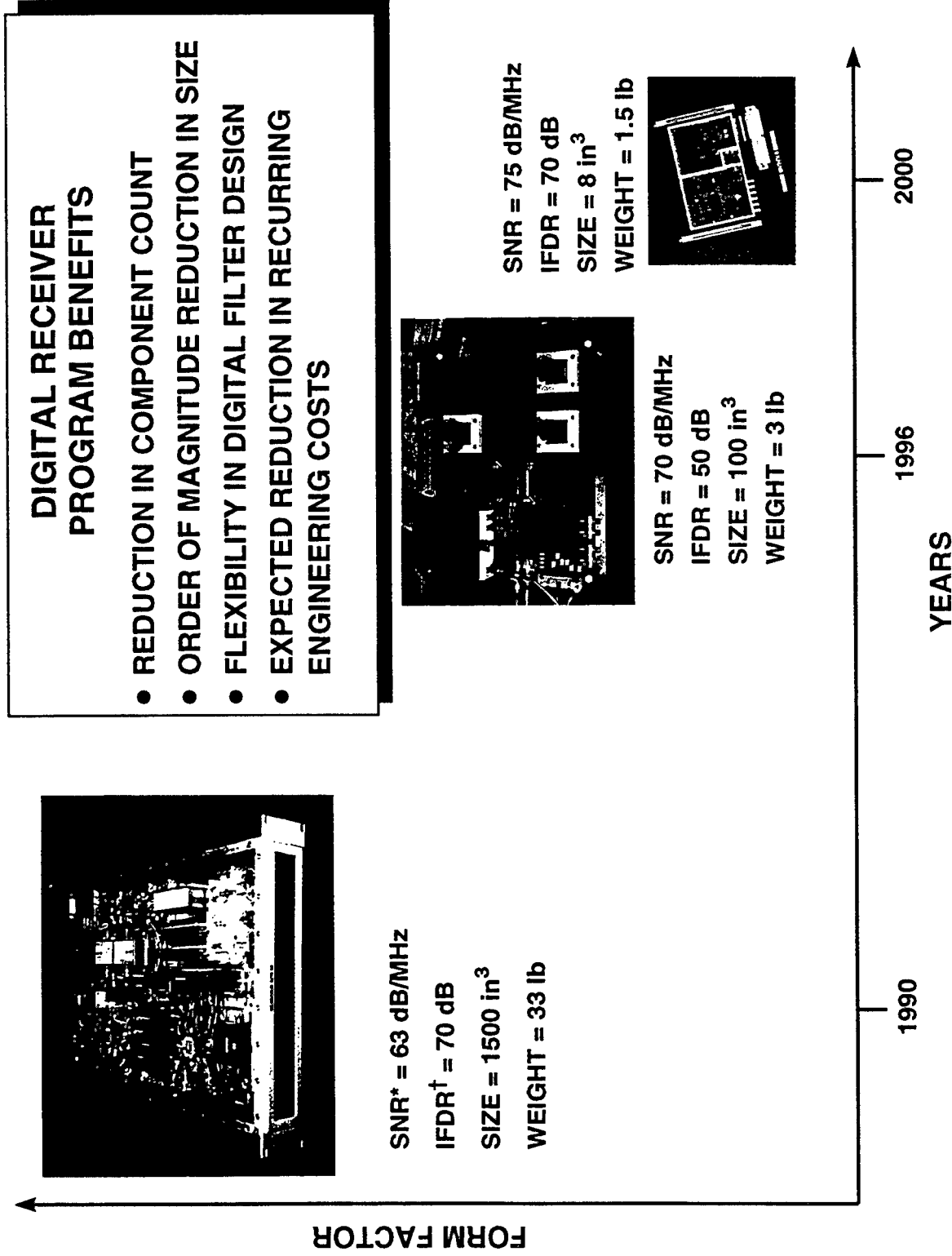
JAMMING



REQUIREMENT: PROVIDE LONG RANGE TARGET DETECTION
IN PRESENCE OF CLUTTER AND JAMMING

UNCLASSIFIED

RADAR RECEIVER TECHNOLOGY EVOLUTION



*SIGNAL-TO-NOISE RATIO

†INTERMOD FREE DYNAMIC RANGE



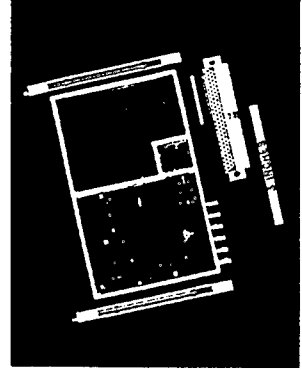
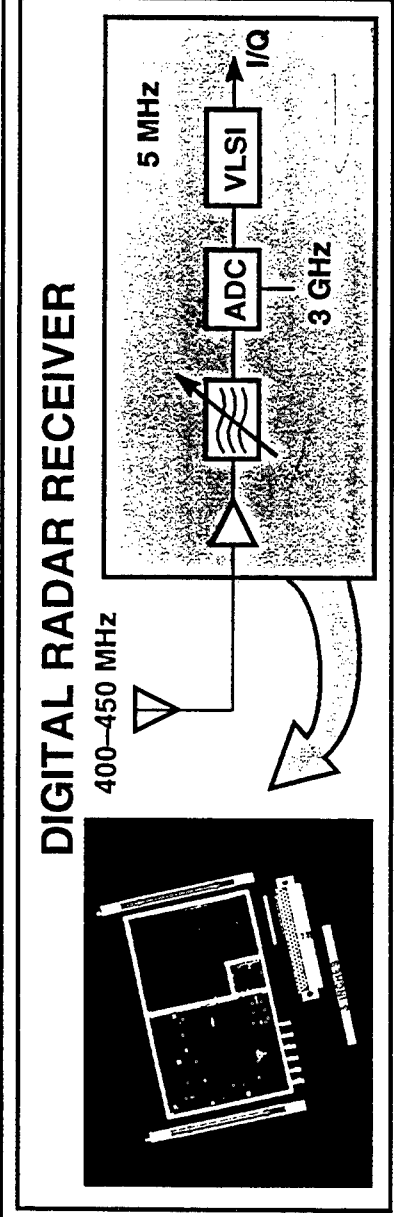
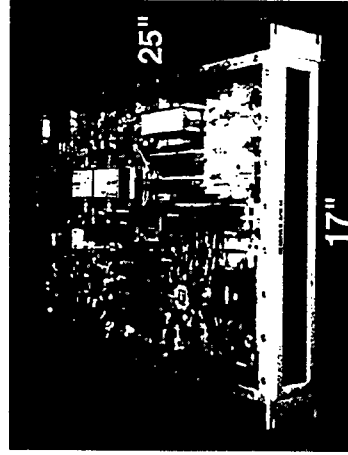
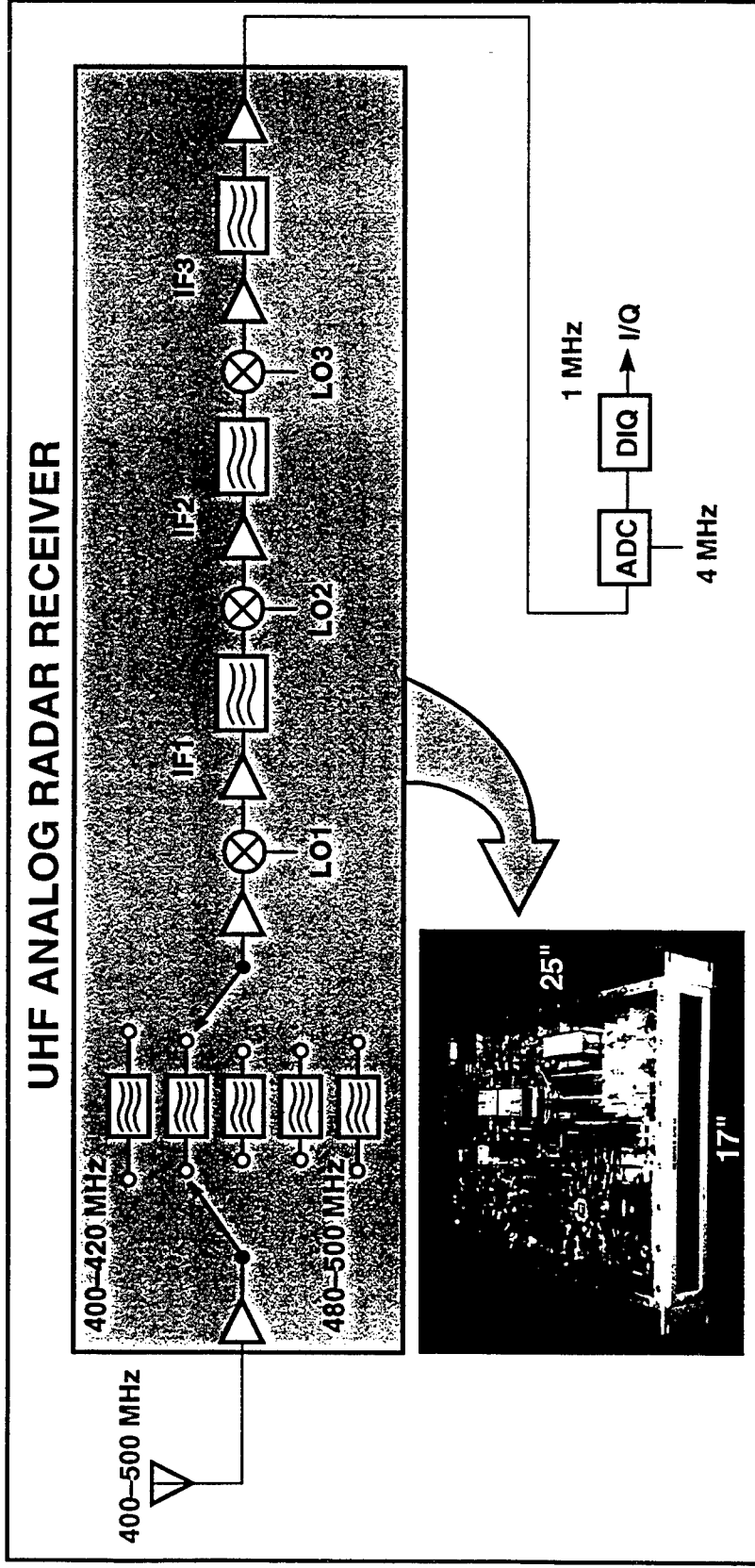
293003-1P

OUTLINE

- INTRODUCTION
- ➔ • DIGITAL RECEIVER CONCEPT
- HARDWARE DEVELOPMENT
- TECHNOLOGY DEMONSTRATION PLAN
- SUMMARY

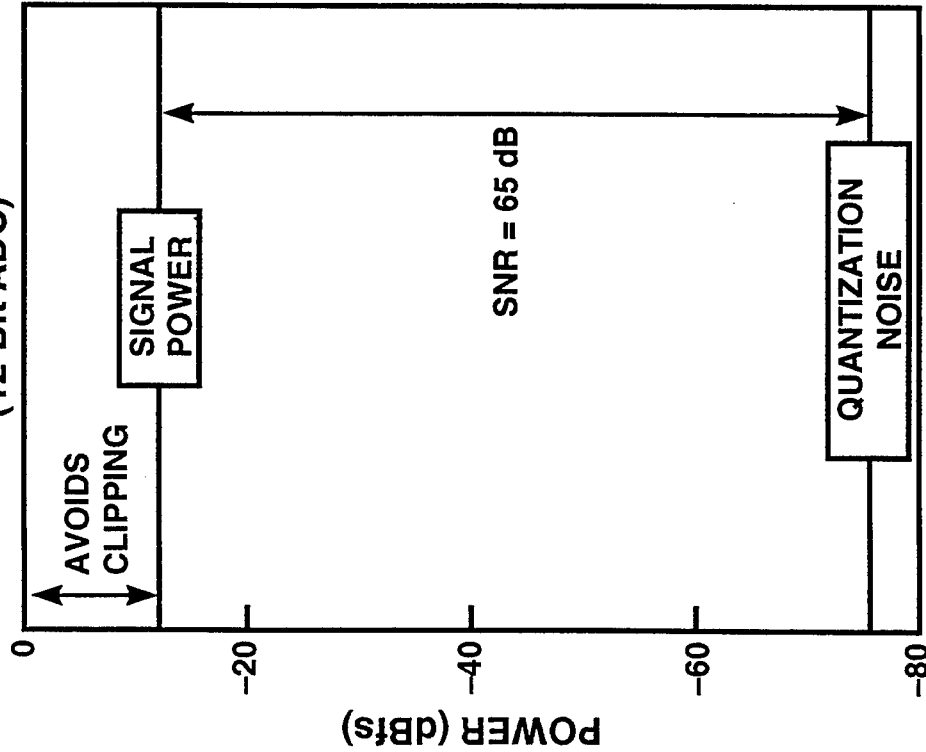


ANALOG AND DIGITAL RECEIVER ARCHITECTURES



ADC DYNAMIC RANGE

EXAMPLE
(12-Bit ADC)



SIGNAL-TO-QUANTIZATION NOISE

DEFINITIONS:

n = NUMBER OF TOTAL ADC BITS

$SNR = 10 \cdot \log_{10} (\text{Signal Power} / Q)$

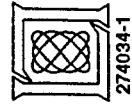
A_{max} = ADC FULL SCALE = $4 \cdot \text{SIGNAL AMPLITUDE}$
(4 Factor Avoids Clipping)

Q = QUANTIZATION NOISE POWER

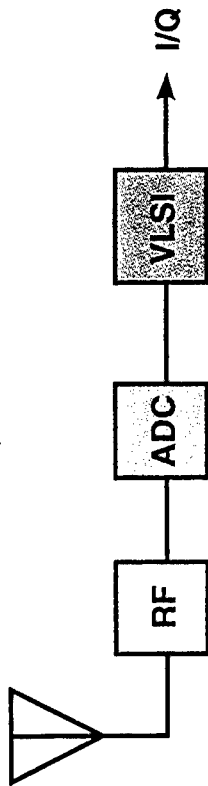
REQUIRED ADC WORDLENGTH:

$$2^{n-1} \geq A_{\text{max}}$$

$$n \geq SNR / 6 + 1.2$$



DYNAMIC RANGE GAIN

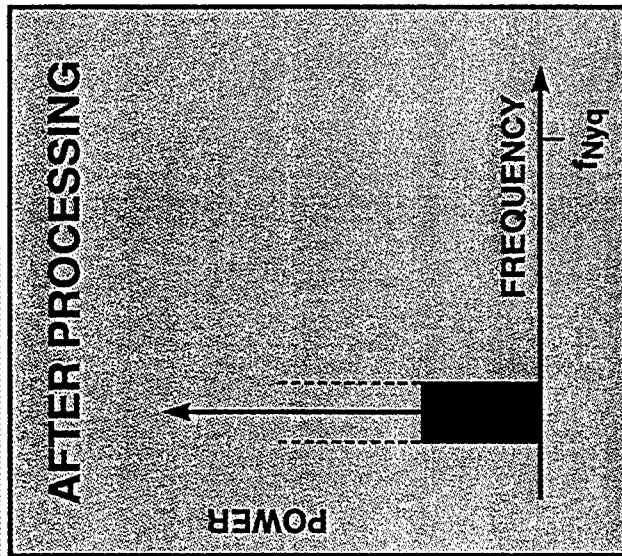
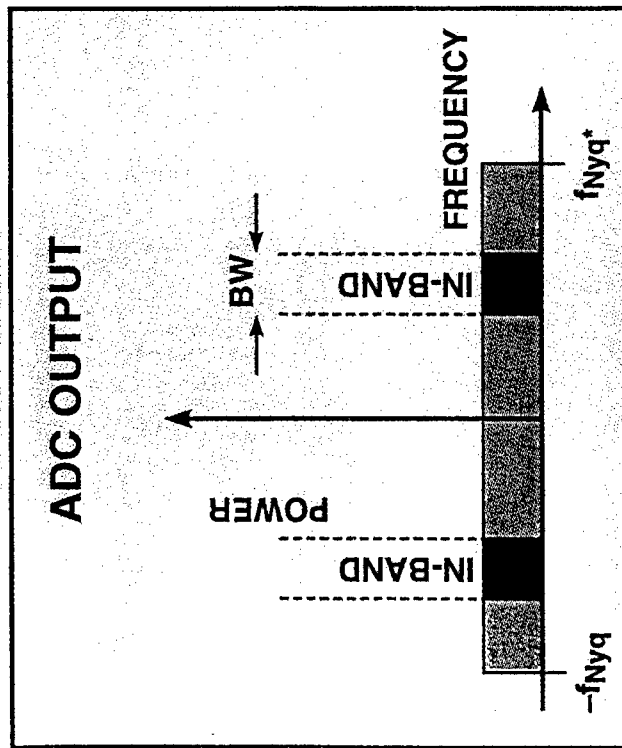


● SIGNAL-TO-NOISE RATIO GAIN

$$\text{SNR GAIN} = F_{\text{Nyquist}} / \text{BW}$$

EXAMPLE:

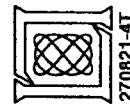
F_s	=	3000	MHz
BW	=	5	MHz
SNR GAIN	=	25	dB
BITS GAINED	=	4	BITS



IN-BAND A/D
QUANTIZATION
NOISE AND
SPURS†

OUT-OF-BAND
A/D QUANTIZATION
NOISE AND SPURS

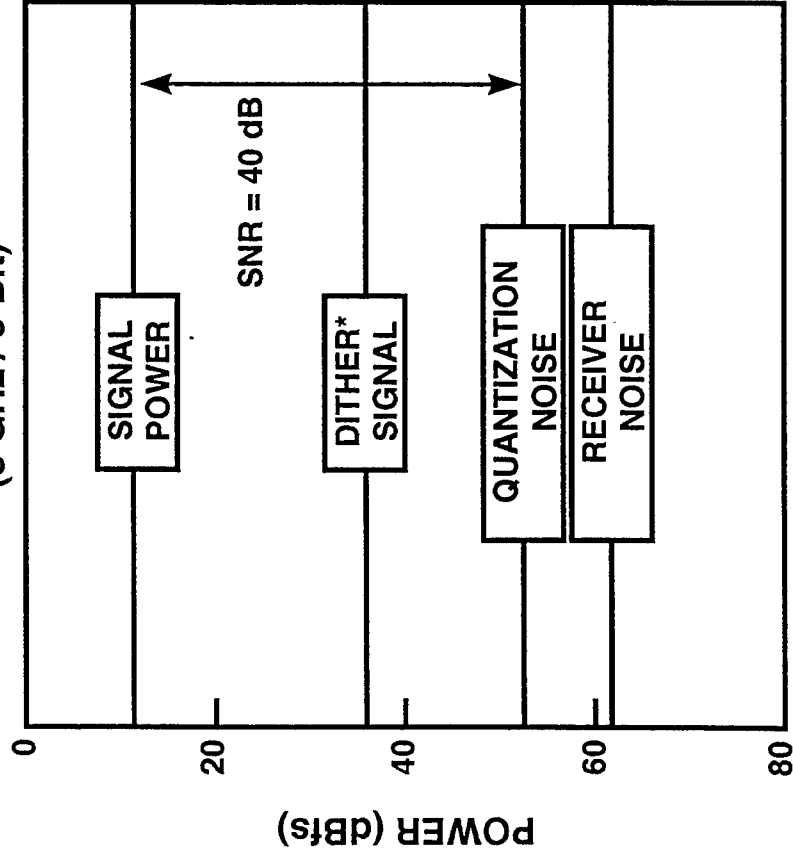
* NYQUIST FREQUENCY
† IN-BAND SPURS INCLUDE INTERMODS



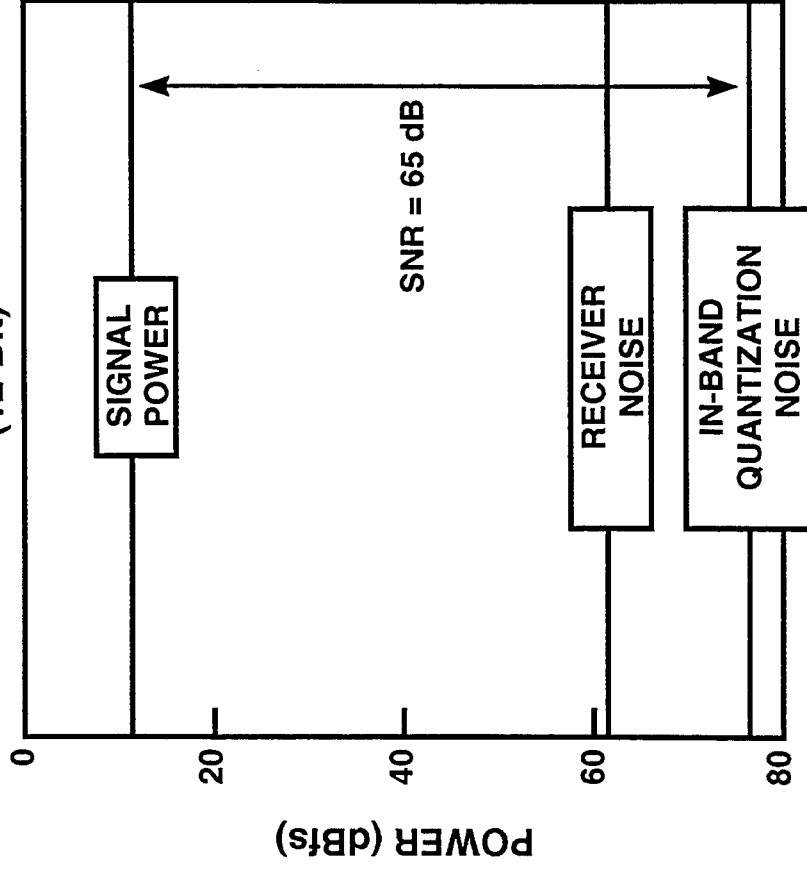
270821-4T

SIGNAL-TO-NOISE GAIN

HIGH-SPEED ADC
(3 GHz / 8-Bit)



AFTER VLSI PROCESSING
(12-Bit)



*DITHER SIGNAL

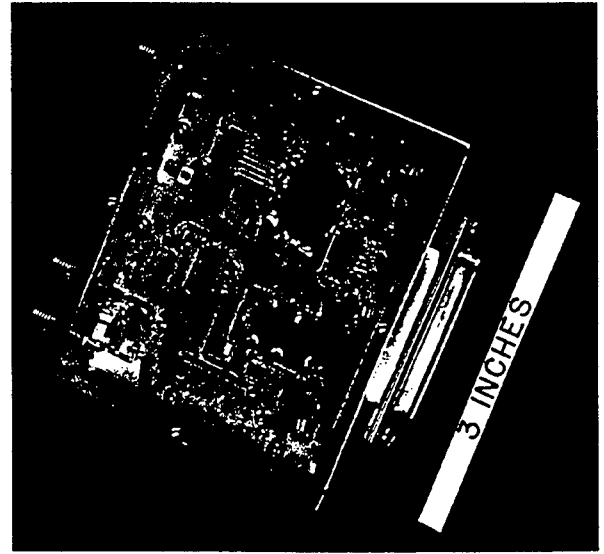
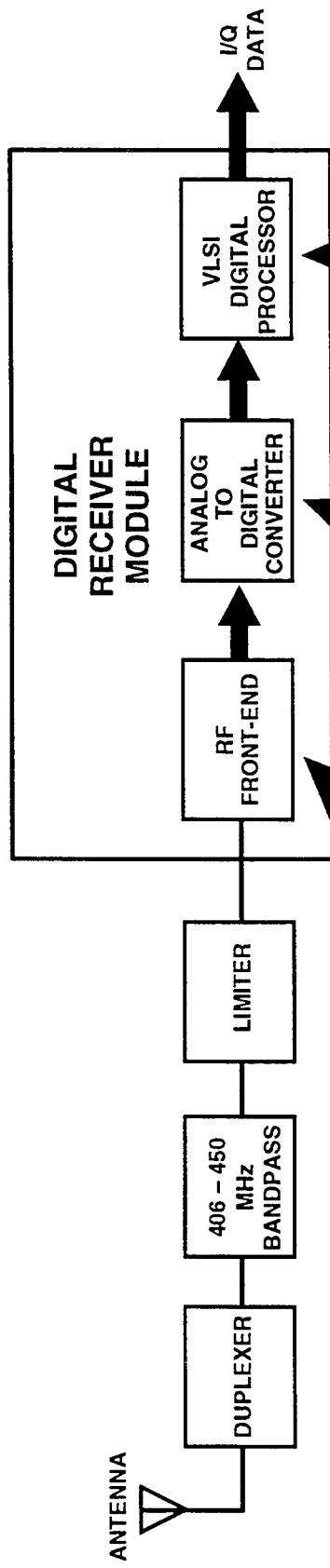
- NECESSARY TO TOGGLE LOW-ORDER BITS
- PRESENT OUTSIDE SIGNAL BAND
- FILTERED OUT IN VLSI PROCESSING



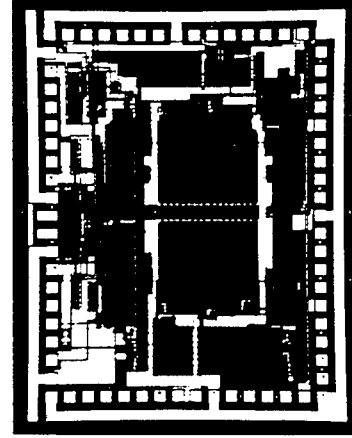
OUTLINE

- INTRODUCTION
- DIGITAL RECEIVER CONCEPT
- ➔ • HARDWARE DEVELOPMENT
- TECHNOLOGY DEMONSTRATION PLAN
- SUMMARY

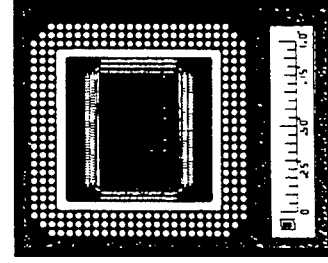
DIGITAL RECEIVER HARDWARE TECHNOLOGY



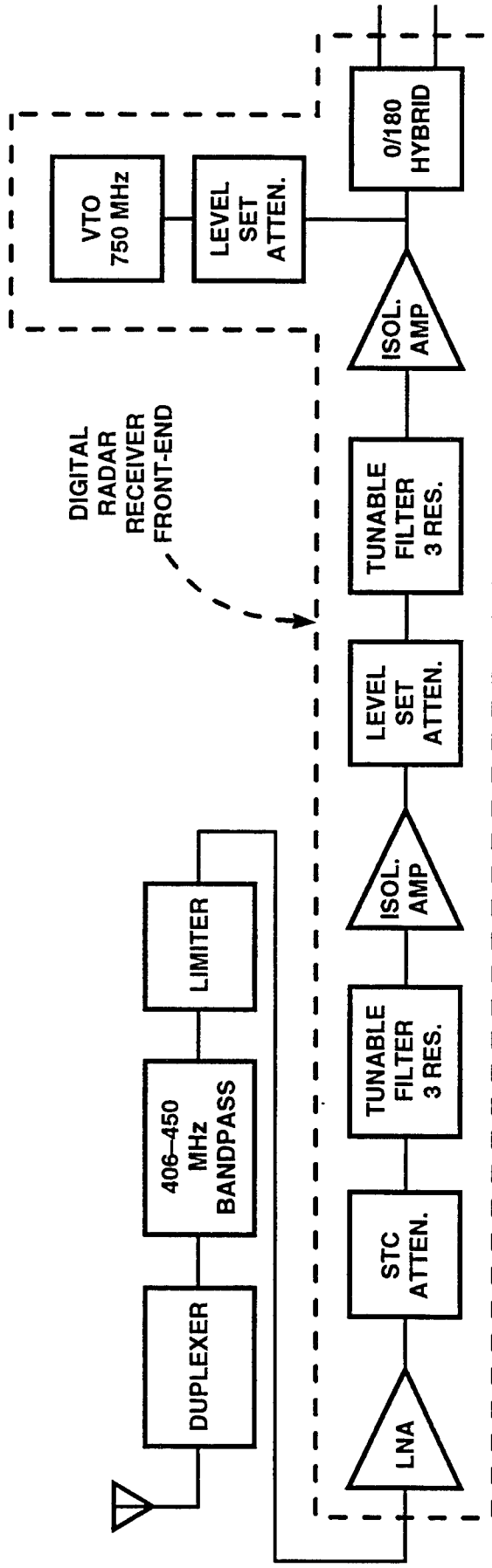
8-BIT 3-GSPS* ADC



*** BILLION SAMPLES PER SECOND**



FRONT-END RF HARDWARE

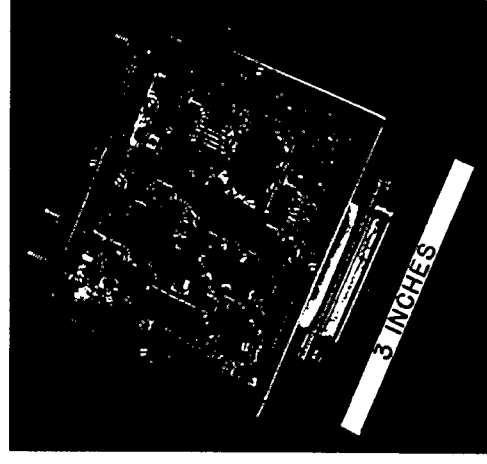


PERFORMANCE CHARACTERISTICS

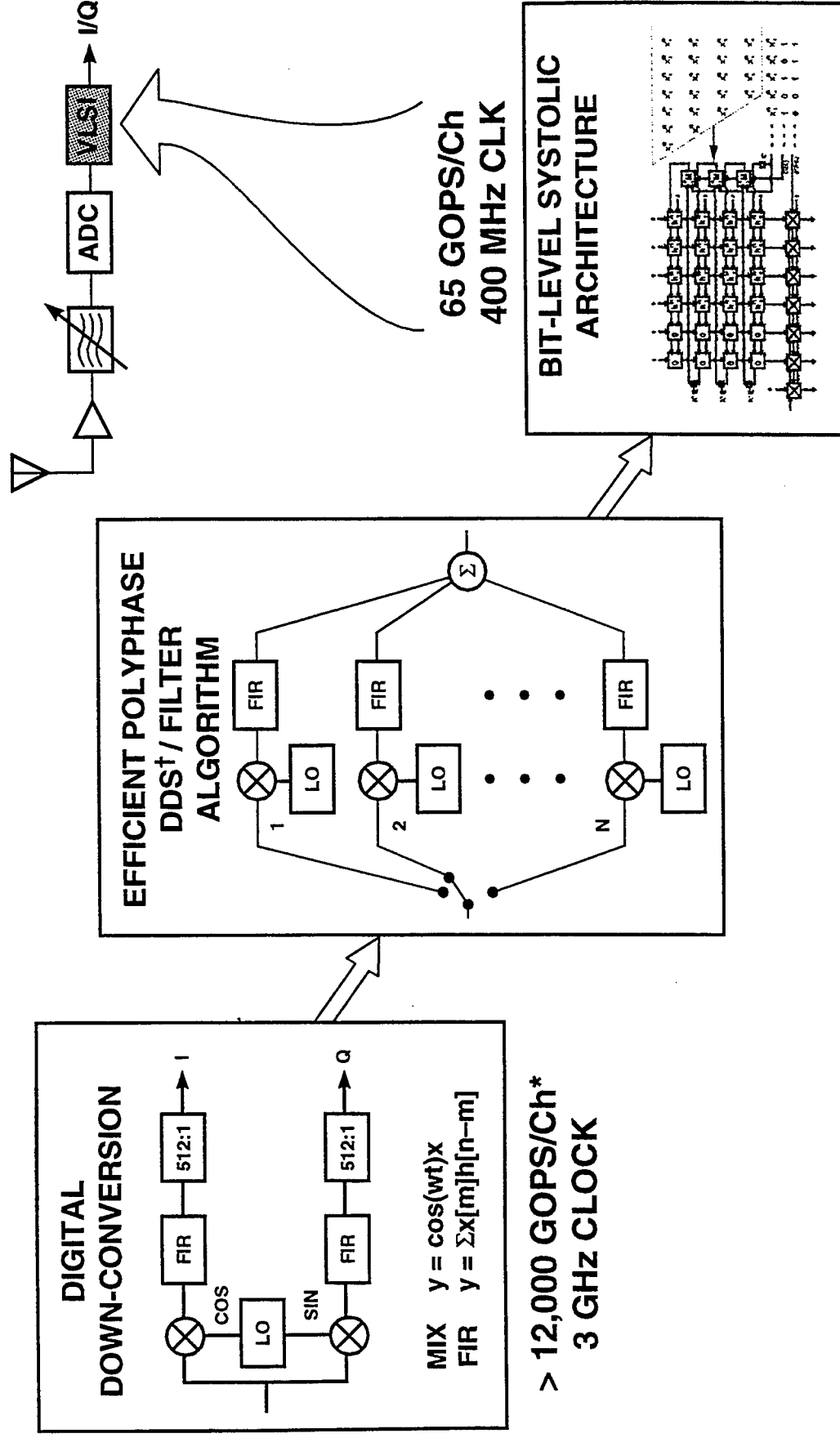
GAIN = 45 dB

INTERMOD FREE DYNAMIC RANGE = 75 dB

NOISE FIGURE = 1.3 dB



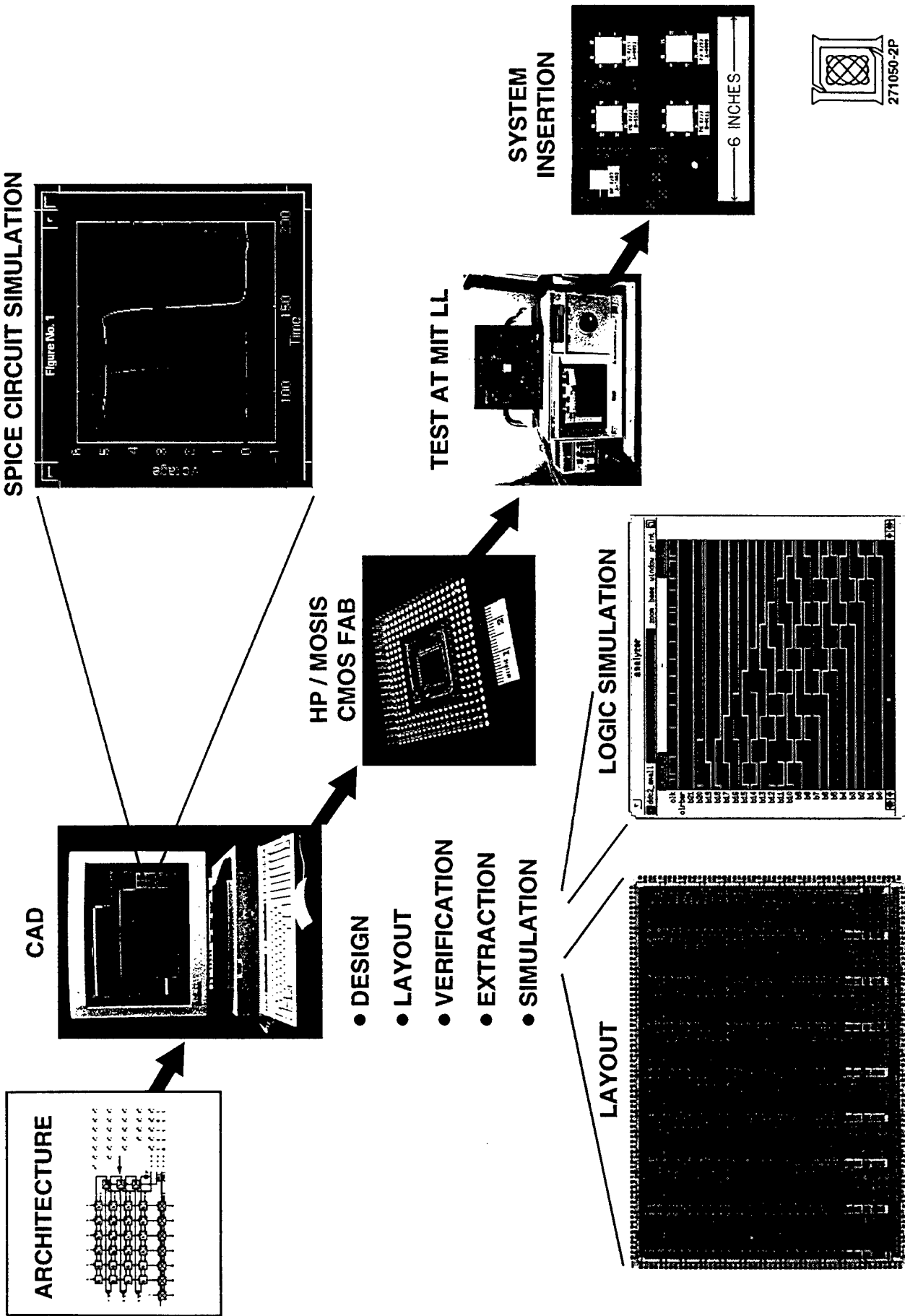
VLSI DOWN-CONVERSION ALGORITHM OPTIMIZATION AND ARCHITECTURE MAPPING



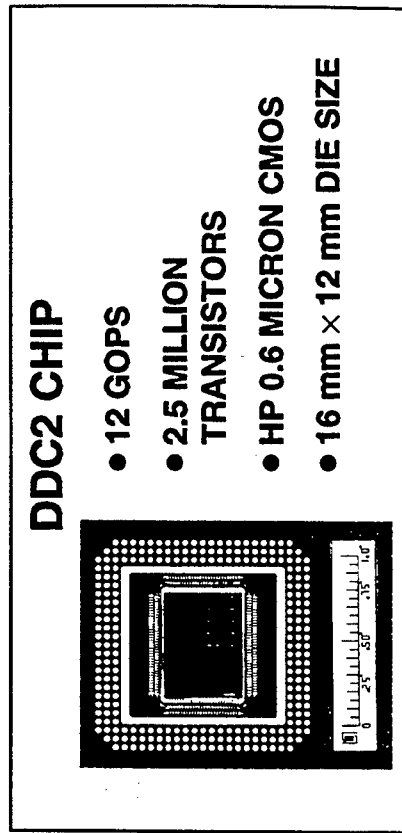
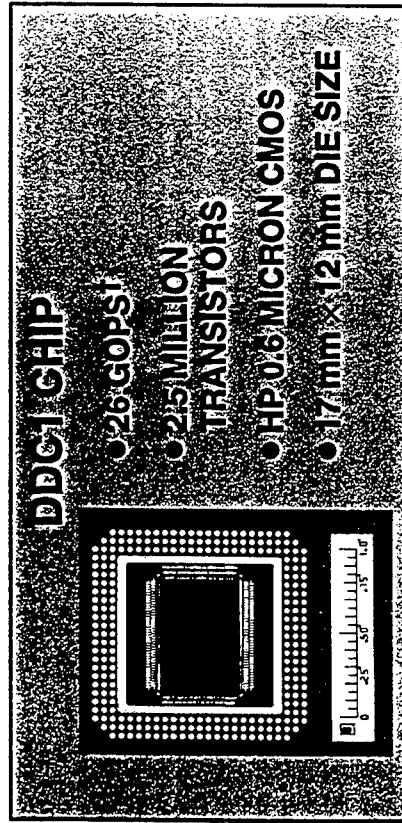
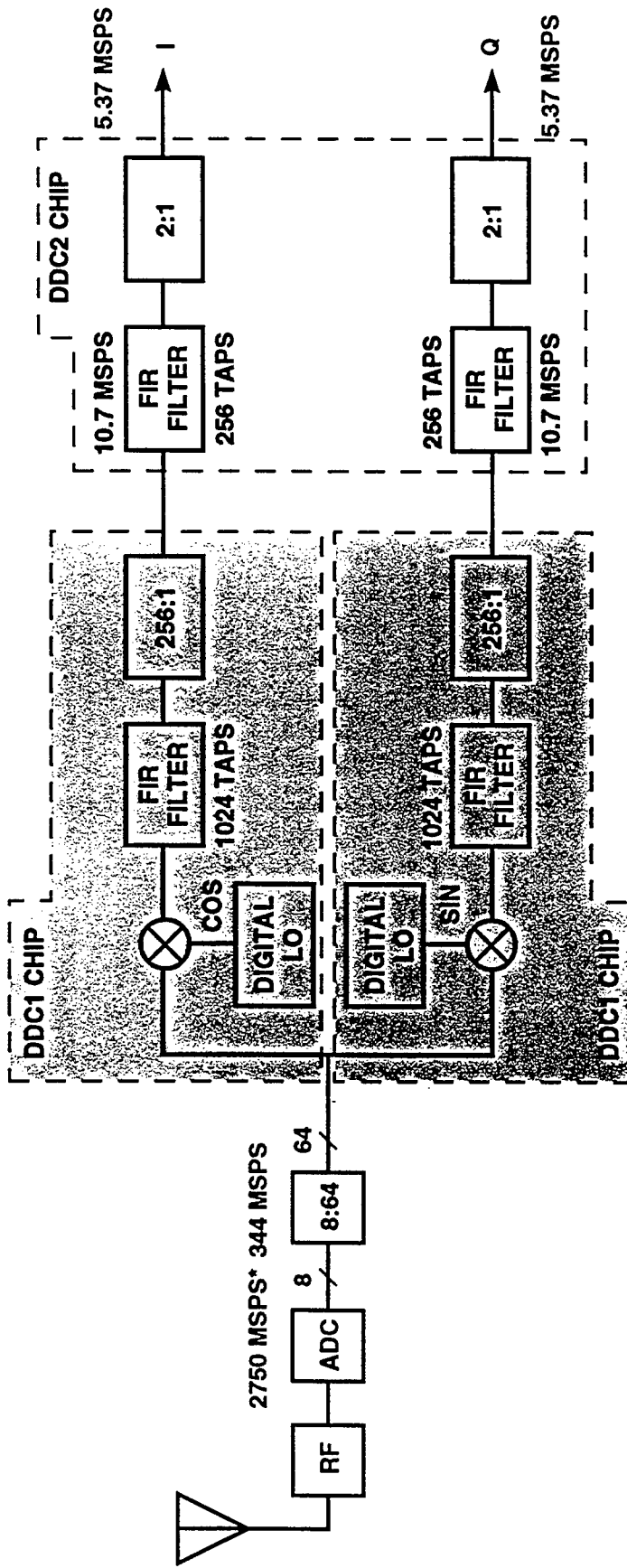
* BILLION OPERATIONS PER CHANNEL
† DIRECT DIGITAL SYNTHESIS



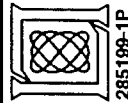
DIGITAL RADAR RECEIVER CHIP-SET DEVELOPMENT METHODOLOGY



DIGITAL RECEIVER VLSI CHIP-SET



* MEGA-SAMPLES PER SECOND
† GIGA-OPERATIONS PER SECOND

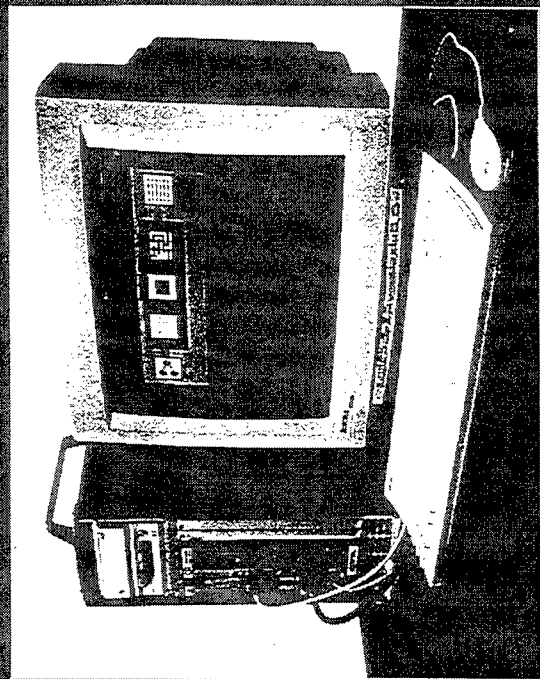
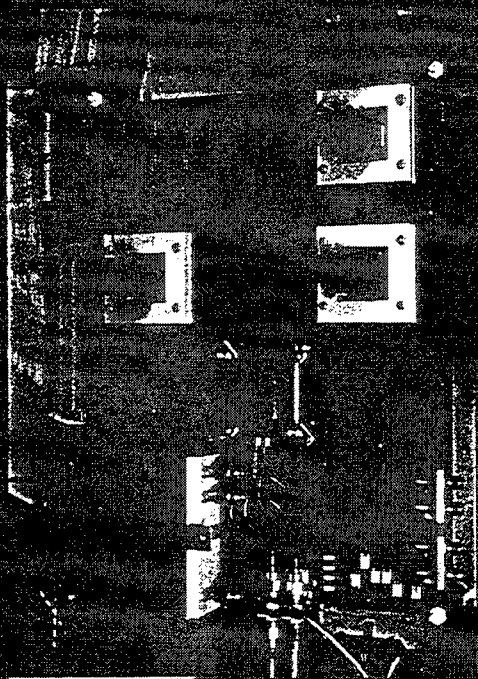
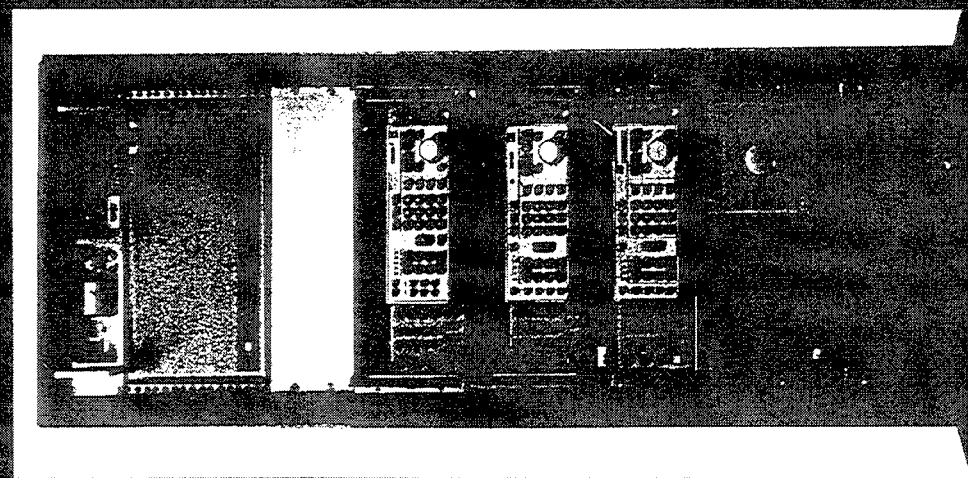


OUTLINE

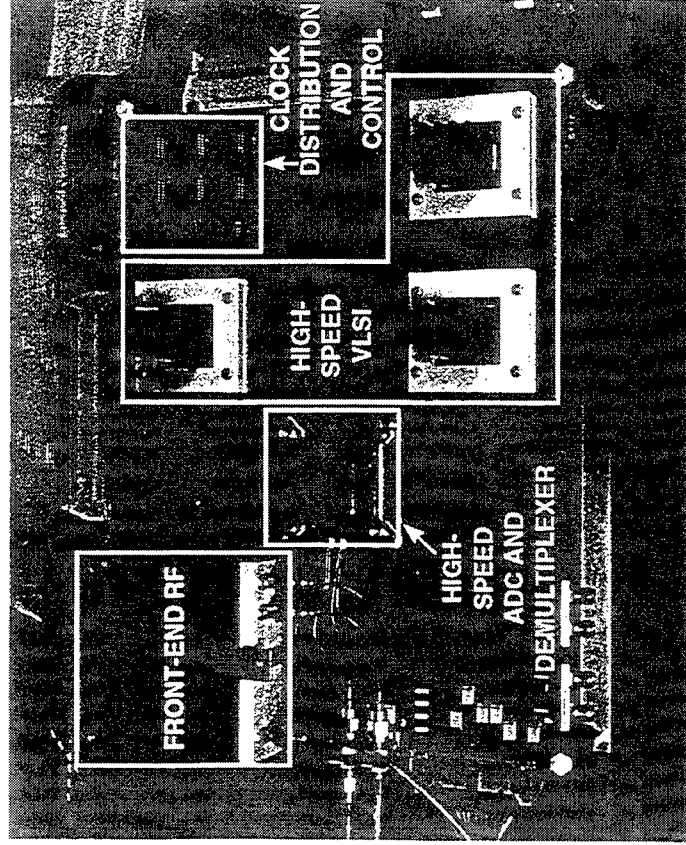
- INTRODUCTION
- DIGITAL RECEIVER CONCEPT
- HARDWARE DEVELOPMENT
- ➡ ● TECHNOLOGY DEMONSTRATION PLAN
 - BREADBOARD HARDWARE DEMONSTRATION
 - MINIATURIZED RADAR RECEIVER
 - MOUNTAINTOP DEMONSTRATION
- SUMMARY



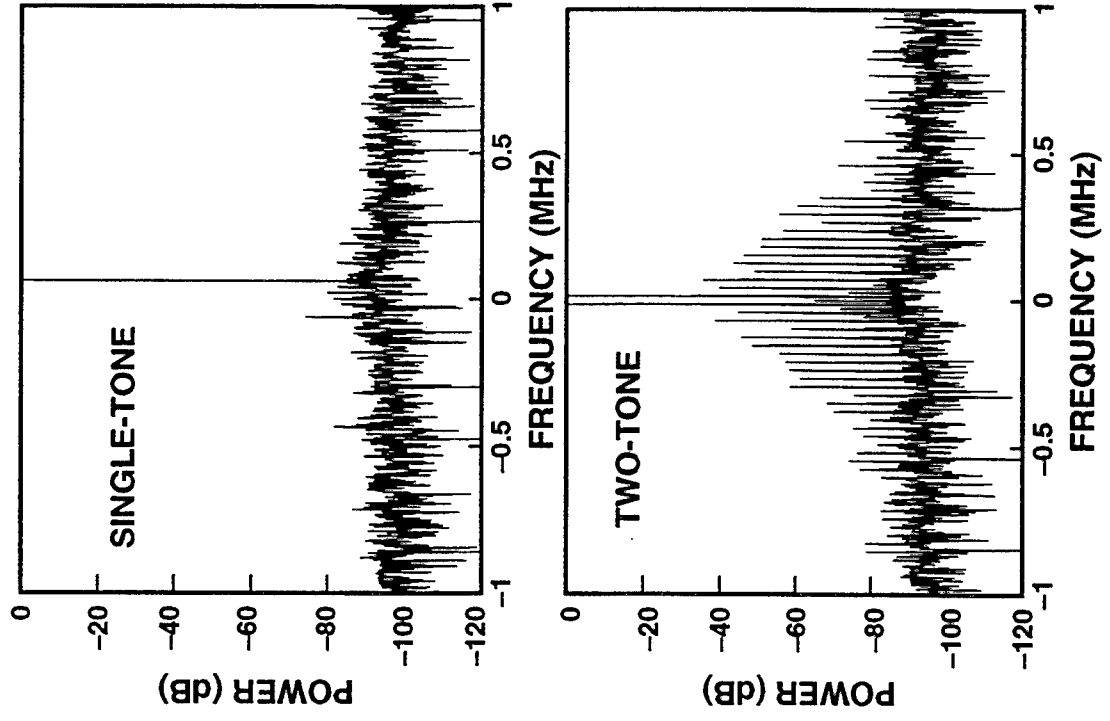
DIGITAL RADAR BREADBOARD DEMONSTRATION



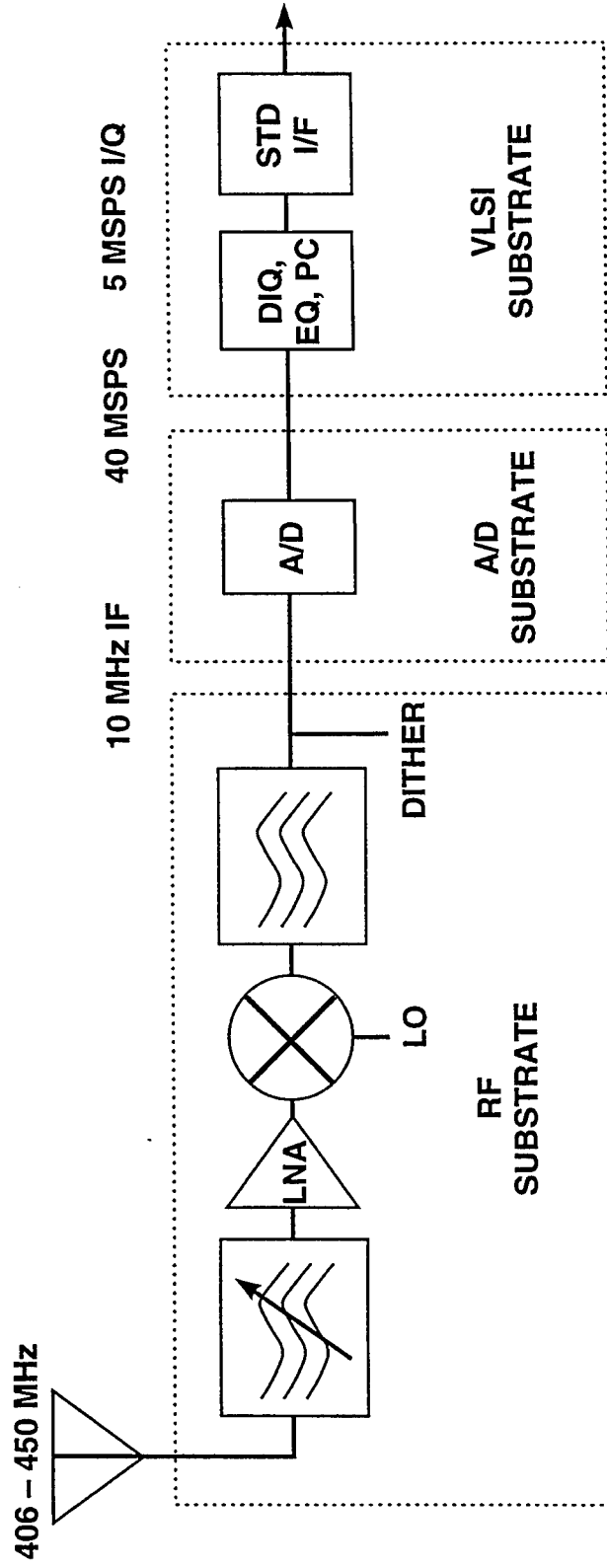
DIGITAL RECEIVER DEMONSTRATION RESULTS



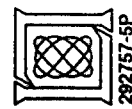
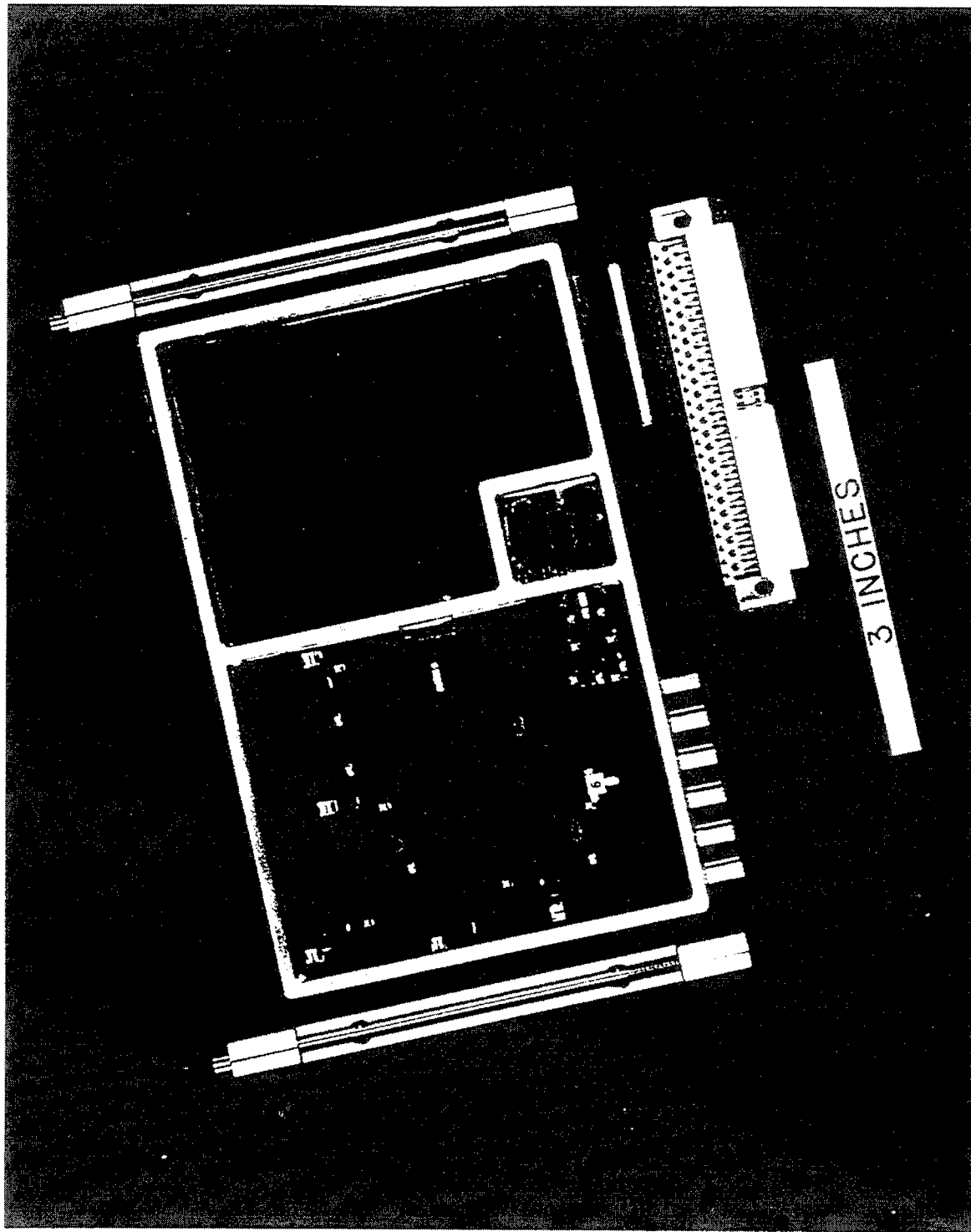
DIGITAL RECEIVER TEST RESULTS



MINIATURIZED DIGITAL RECEIVER ARCHITECTURE

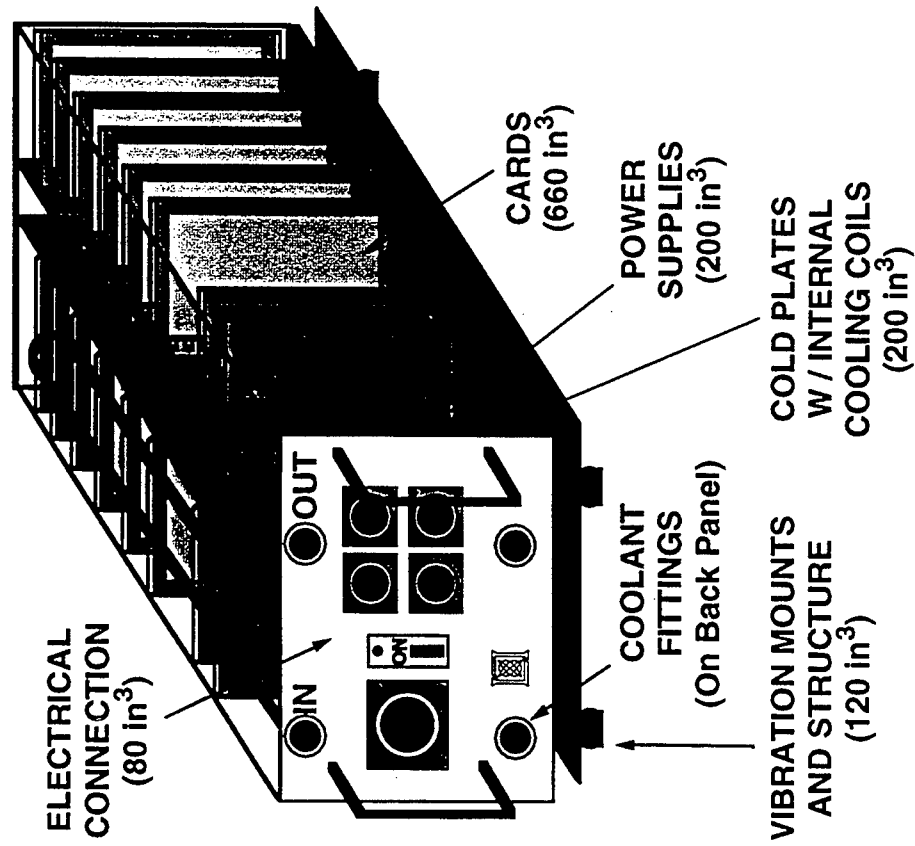


MINIATURIZED DIGITAL RECEIVER MODULE DESIGN

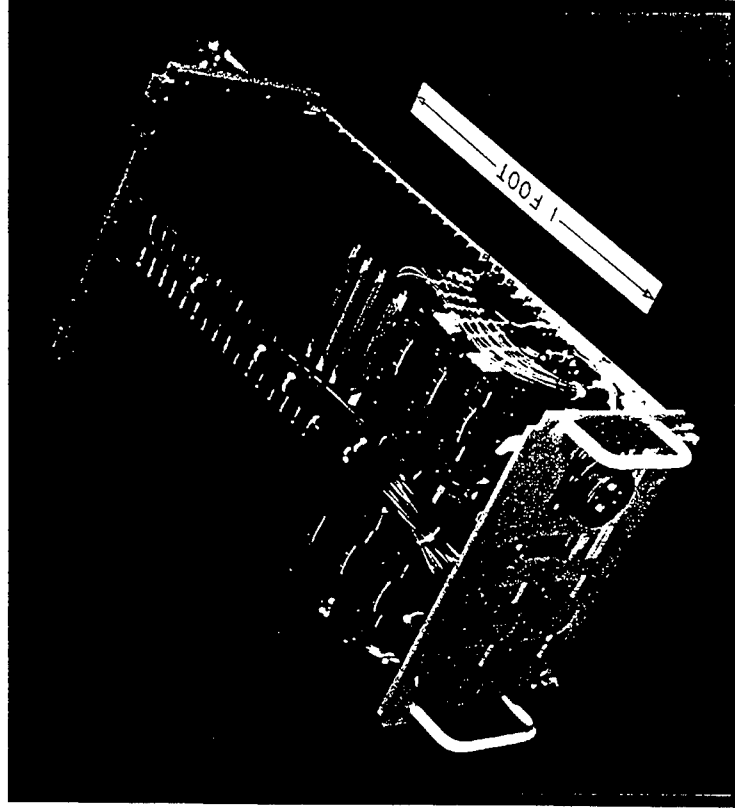


DIGITAL RECEIVER CHASSIS DESIGN

CONCEPT



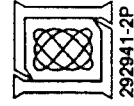
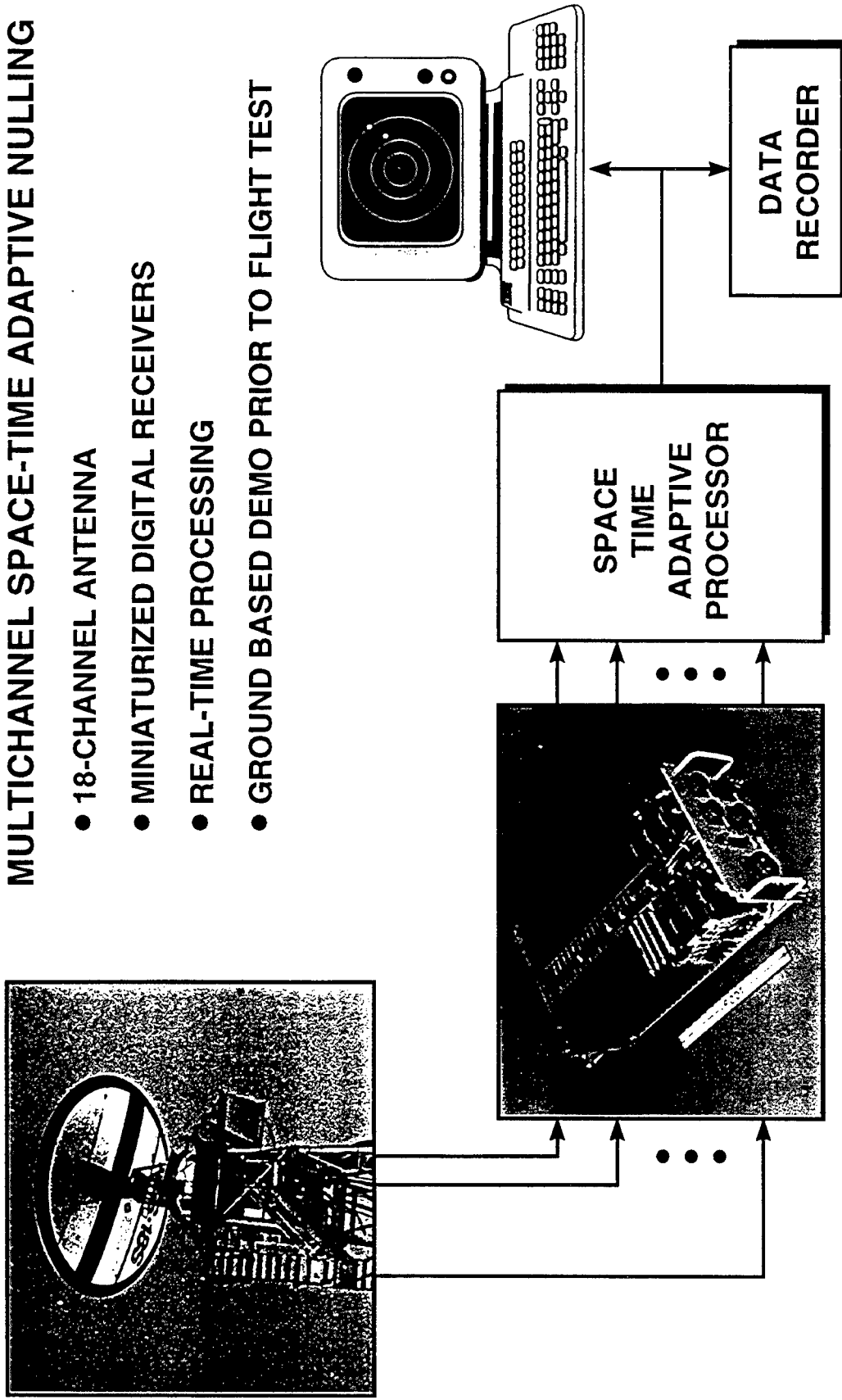
MOCKUP



MOUNTAINTOP SYSTEM DEMONSTRATION

MULTICHANNEL SPACE-TIME ADAPTIVE NULLING

- 18-CHANNEL ANTENNA
- MINIATURIZED DIGITAL RECEIVERS
- REAL-TIME PROCESSING
- GROUND BASED DEMO PRIOR TO FLIGHT TEST



SUMMARY

- **MODERN ADAPTIVE RADARS REQUIRE MANY RECEIVER CHANNELS**
 - **DIGITAL RADAR RECEIVER OFFERS SIGNIFICANT SIZE AND WEIGHT REDUCTIONS**
- **DIGITAL RECEIVER PROTOTYPE BREADBOARD DEMONSTRATED**
- **TECHNOLOGY INNOVATIONS**
 - **DOWN-CONVERSION ALGORITHM / ARCHITECTURE**
 - **OPTIMIZED SCALABLE BIT-LEVEL SYSTOLIC CELL LIBRARY**
- **MINIATURIZED DIGITAL RECEIVER UNDER DEVELOPMENT**
 - **32 CHANNEL MOUNTAINTOP DEMONSTRATION PLANNED**



SESSION VI: SONAR AND UNDERWATER ACOUSTICS II (U)

Reduced Complexity Receivers for Time-Dispersive Digital Communication Channels

M. Stojanovic and J.G. Proakis

Northeastern University
Department of Electrical and Computer Engineering
360 Huntington Avenue
Boston, MA 02115
tel: (617) 373-4429
fax: (617) 373-8970

Abstract This paper treats the problem of signal demodulation in a digital communication system that employs a large receiver array in the transmission of data through a time-dispersive channel, such as an underwater acoustic channel. In general, severely time-spread communication channels require long equalizers to combat intersymbol interference. With spatial diversity, the receiver performance may be limited by its complexity due to factors such as noise enhancement, slower tracking of time variations in the channel characteristics, and increased sensitivity to numerical errors. To alleviate these problems, a beamforming interpretation of the optimal diversity combining method is exploited. The resulting receiver consists of a many-to-few coherent spatial pre-combiner followed by a reduced complexity multichannel equalizer. Its performance is studied on experimental underwater acoustic data demonstrating capability to fully exploit spatial variability of multipath channels while keeping the complexity at minimum, thus allowing efficient use of large receiver arrays.

**REDUCED COMPLEXITY RECEIVERS
FOR
TIME-DISPERSIVE DIGITAL
COMMUNICATION CHANNELS**

**John G. Proakis
and
Milica Stojanovic
Department of Electrical and Computer Engineering
360 Huntington Avenue
Boston, Massachusetts 02115**

PROBLEM DEFINITION

- Reduce the size of adaptive filters, but keep multichannel processing gain.
- Investigate the role of beamforming in optimal combining and equalization.

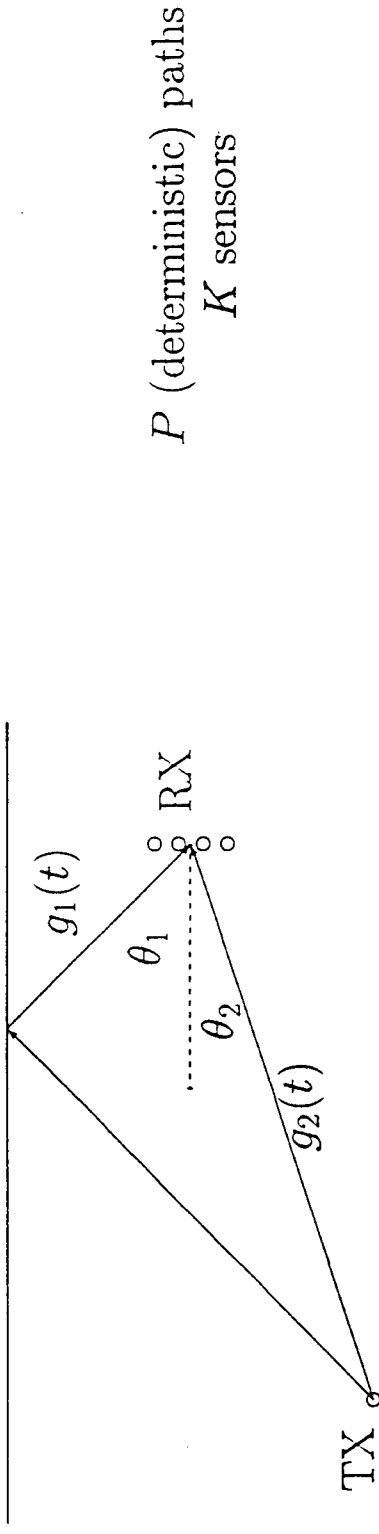
OVERVIEW

- Propagation model and the optimal receiver.
- Adaptive combiners based on optimal beamforming and diversity combining.
- A practical receiver: reduced-complexity multichannel DFE.
- Experimental performance results.

MOTIVATION

- Communications over time-varying multipath channels.
- Example: underwater acoustic channels.
- Spatial signal combining offers:
 - robustness to fading
 - reduction of ISI.
- Two approaches:
 - diversity combining
 - beamforming.
- High complexity of adaptive diversity combining causes:
 - noise enhancement
 - stability problems with fast algorithms.

PROPAGATION MODEL

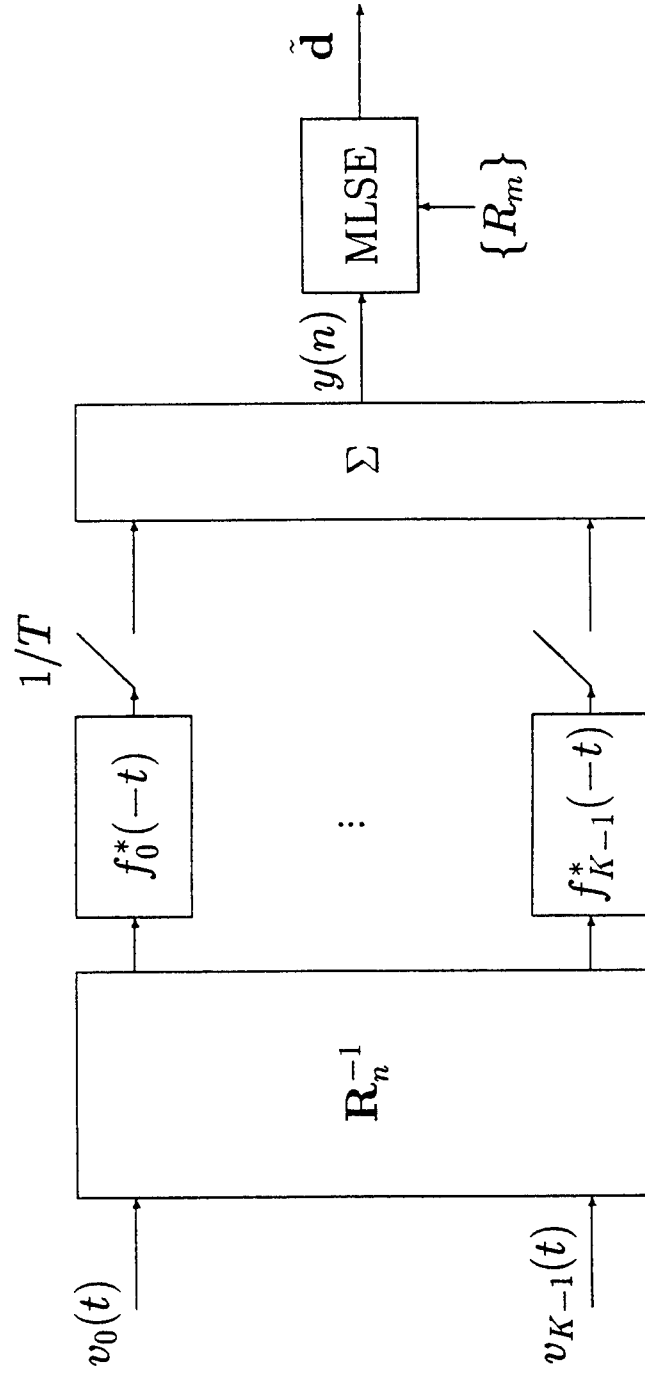


- $\mathbf{g}(t)$: vector of P path responses
- $\mathbf{f}(t) = \Phi \mathbf{g}(t)$: vector of K channel responses
- Φ : $K \times P$ array transformation matrix
- received signal vector:

$$\mathbf{v}(t) = \Phi \sum_n d(n) \mathbf{g}(t - nT) + \mathbf{n}(t) = \sum_n d(n) \mathbf{f}(t - nT) + \mathbf{n}(t).$$

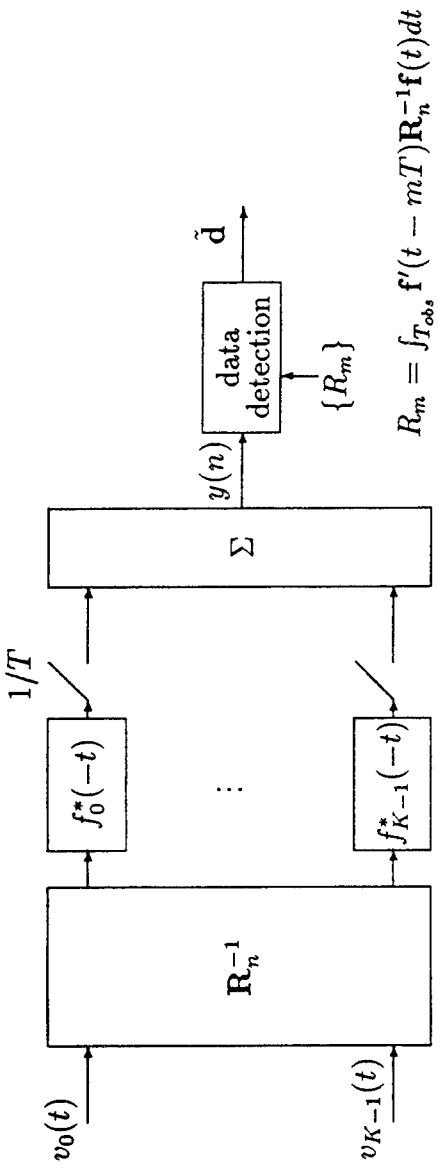
OPTIMAL (ML) MULTICHANNEL RECEIVER

$$\mathbf{v}(t) = \sum_n d(n) \mathbf{f}(t - nT) + \mathbf{n}(t), \quad \mathbf{n} \sim N(\mathbf{0}, \mathbf{R}_n)$$



$$\mathbf{R}_m = \int_{T_{\text{obs}}} \mathbf{f}'(t - mT) \mathbf{R}_n^{-1} \mathbf{f}(t) dt$$

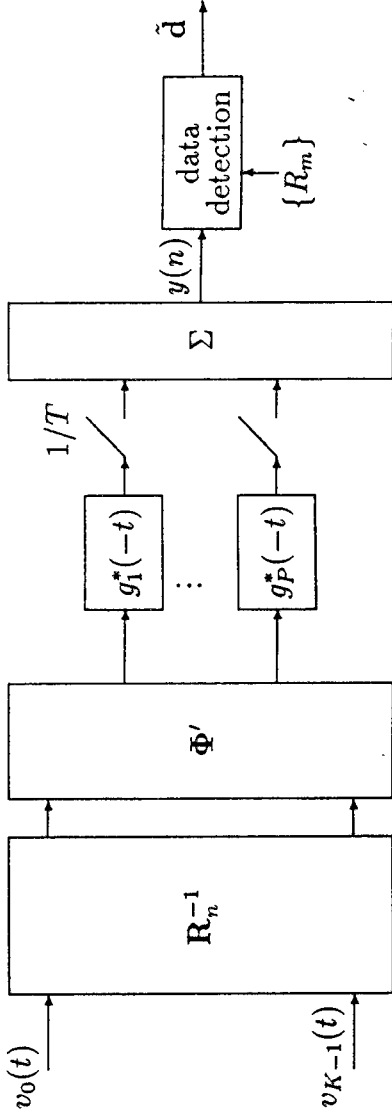
OPTIMAL COMBINER AS A BEAMFORMER



General structure of the optimal receiver.

spatial distribution:

$$\mathbf{f}(t) = \Phi \mathbf{g}(t)$$

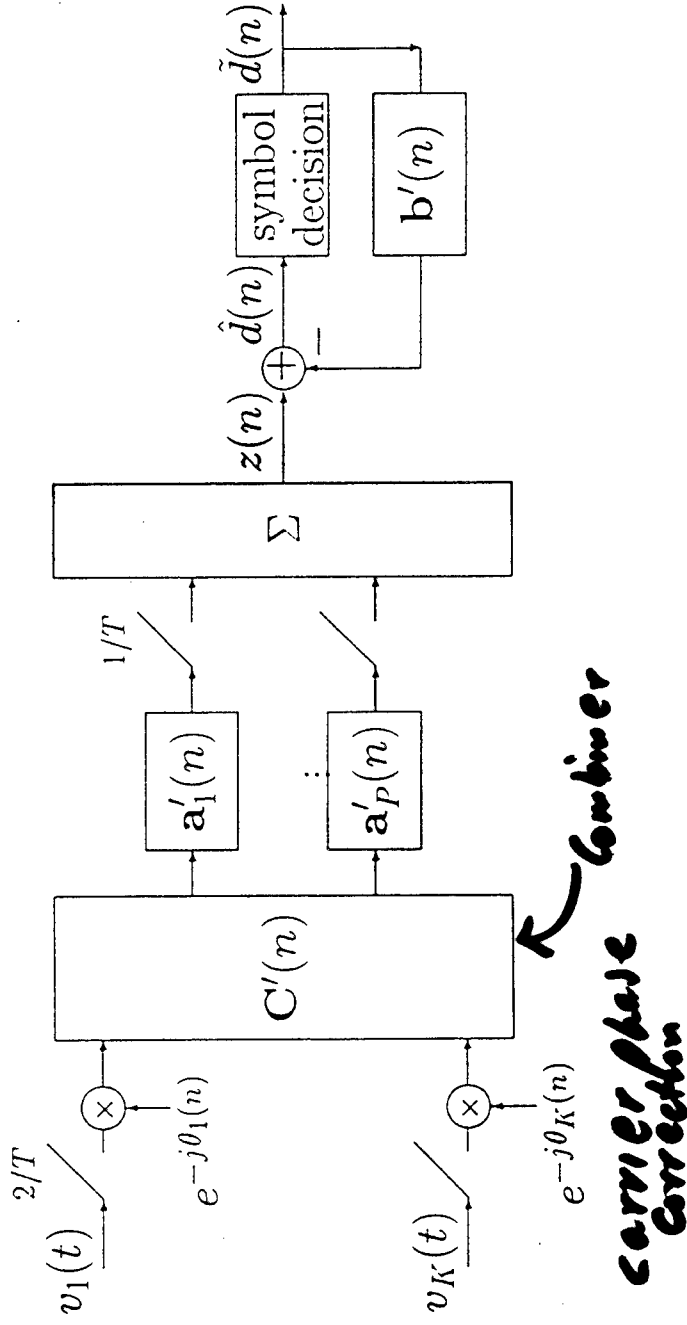


Optimal beamformer Φ : no spatial signal separation.

REDUCED-COMPLEXITY MULTICHANNEL EQUALIZATION

- Two classes of adaptive implementations:
 1. full-complexity K -channel equalizer
 2. $K \times P$ 'beamformer' and reduced-complexity P -channel equalizer.
- Narrow-band case: equal performance if reduced number of channels to be equalized \geq number of propagation paths.
- Broad-band case: optimal performance of reduced-complexity receiver ensured by joint optimization of combiner, equalizer.

REDUCED-COMPLEXITY MULTICHANNEL DFE



- Optimization of combiner not constrained on the knowledge of Φ : joint MMSE solution for combiner, equalizer.
- Receiver algorithm:
 - second-order multichannel DPLL
 - double RLS for combiner, equalizer.

RECEIVER ALGORITHM

- Adaptive algorithm : second-order multichannel DPLL, RLS.
- Computational complexity :
 - numerically stable fast RLS (Slock and Kailath, '91)
 $\sim 10 N$
 - periodic update
- Receiver functions:
 - temporal processing (implicit diversity):
joint Doppler and multipath synchronization in each
branch
 - spatial processing (explicit diversity):
coherent maximal ratio type combining

UNDERWATER ACOUSTIC EXPERIMENT

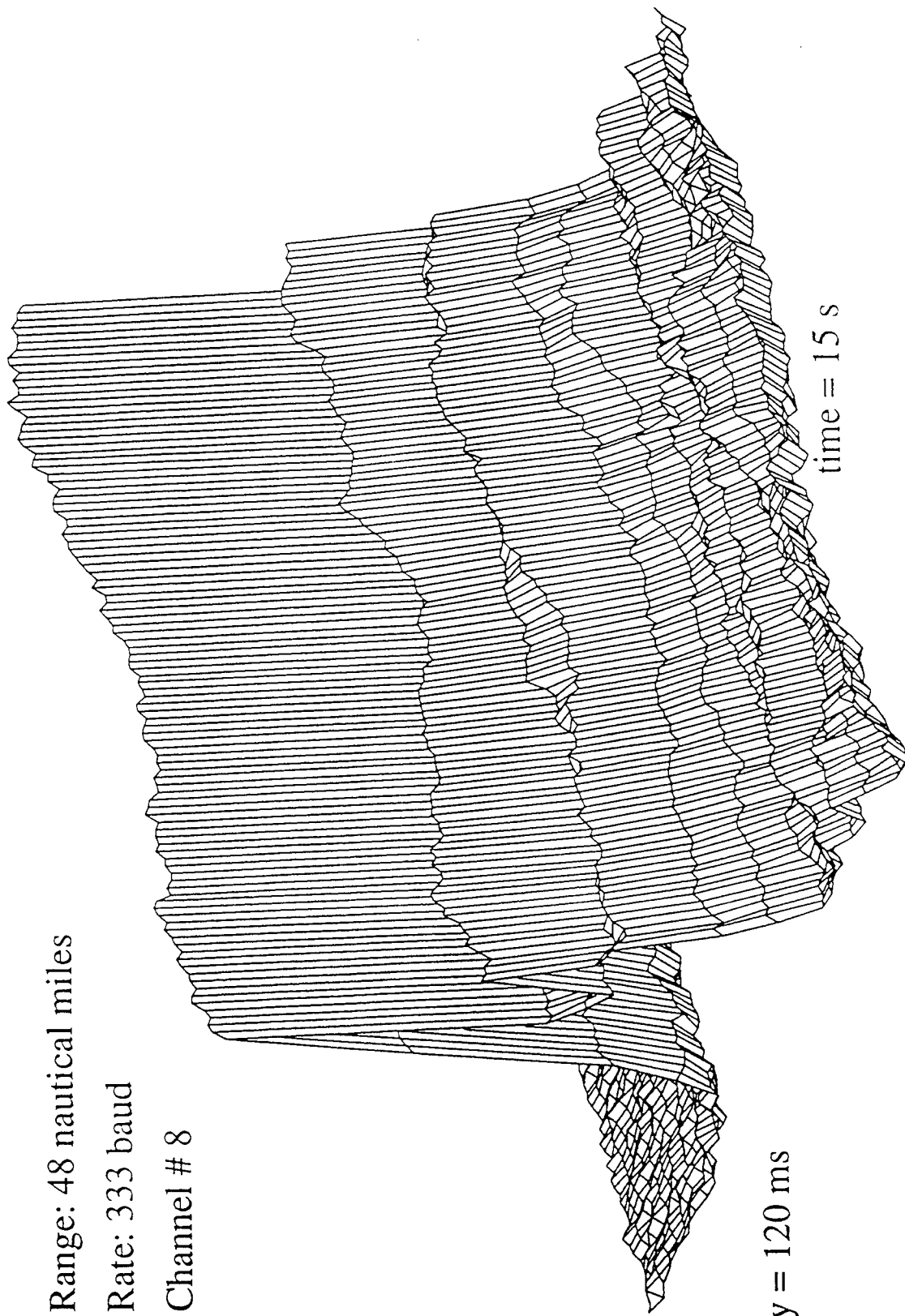
- New England Continental Shelf, May 1992.
- transmitter: 1 kHz carrier
- receiver: 20 sensors, omnidirectional
- range: ~ 50 nautical miles
- data rates: ≤ 2000 bits per second (QPSK, 8-PSK)
- channel: ~ 100 ms dispersion (1-3 significant arrivals).

SHALLOW WATER

Range: 48 nautical miles

Rate: 333 baud

Channel # 8

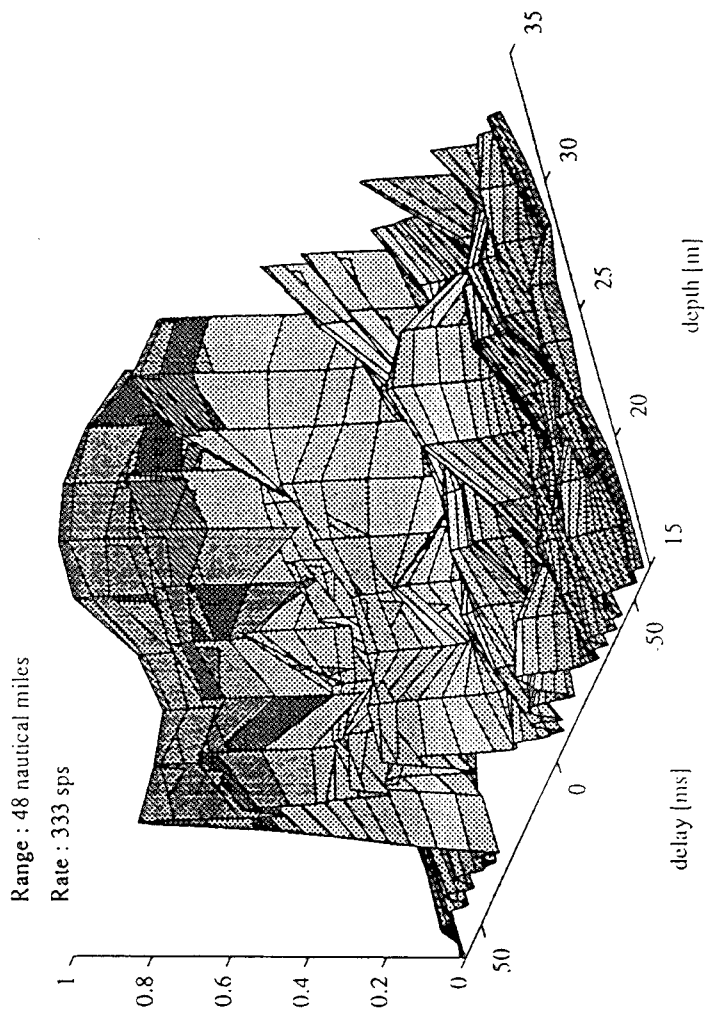


delay = 120 ms

time = 15 s

RLS estimation

Long-Range Shallow Water Channels



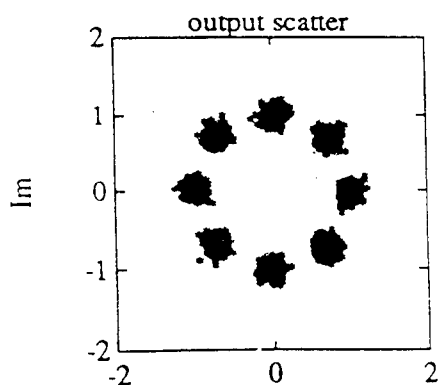
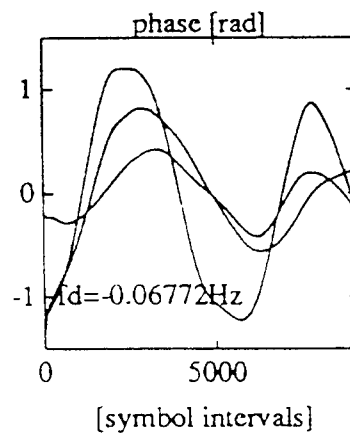
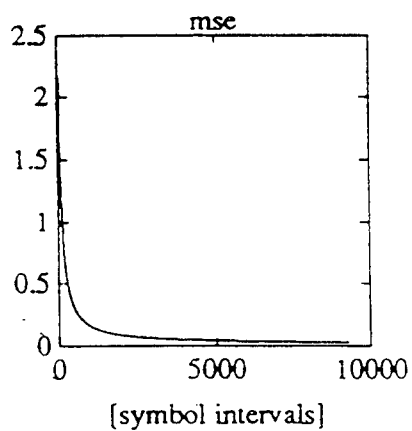
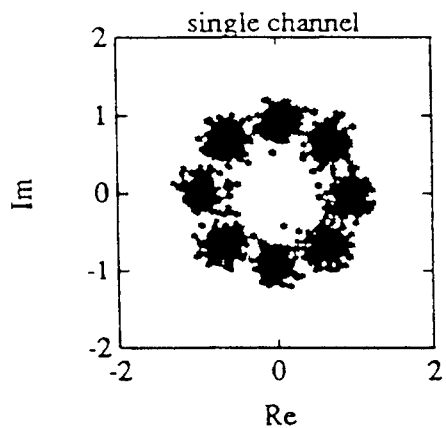
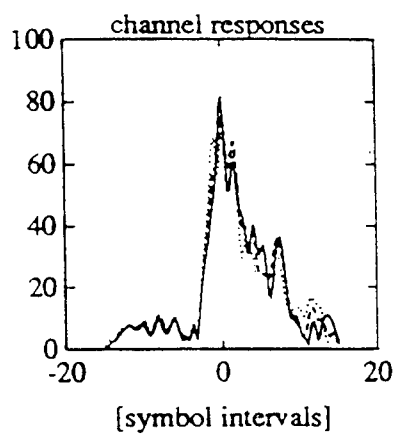
instantaneous
channel state information receiver depths

Range: 48 nautical miles

Rate: 500 symbols per second; 8-PSK

Channel # 2,4,6

SNR_{in}~20.99 dB



receiver parameters:

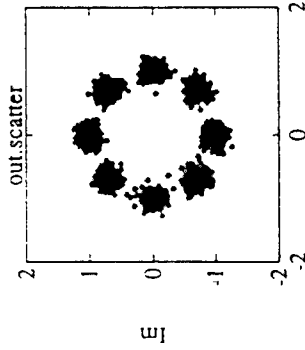
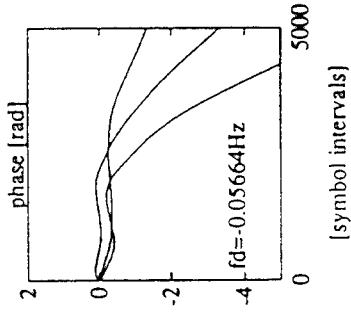
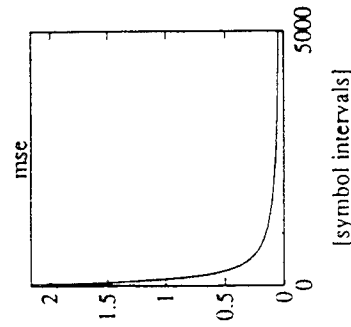
$N=60$ $M=60$ $f.f.=0.998$

$Kf1=0.0005$ $Kf2=5e-05$

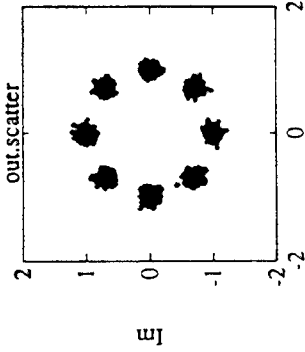
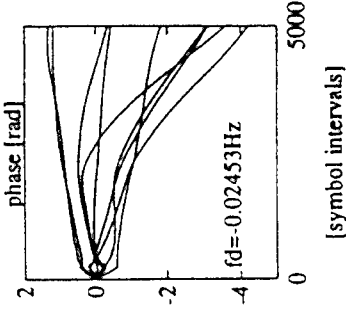
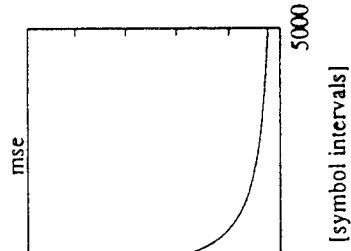
$Pe \sim 0.01075$

SNR_{out}~20.47dB/17.2dB

Experimental Results



$K=3$
 $L=0.998$
 $N=60$ $M=60$
 $Kf1=0.0005$ $Kf2=5e-05$
 $Pe \sim 0$
 $SNR_{out} \sim -19.41dB$



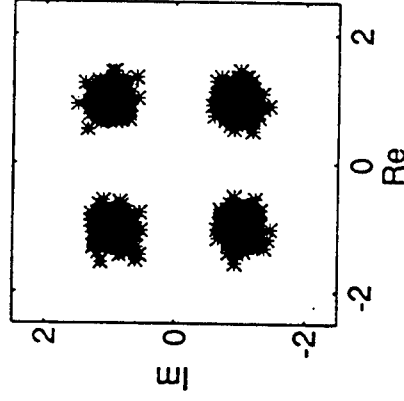
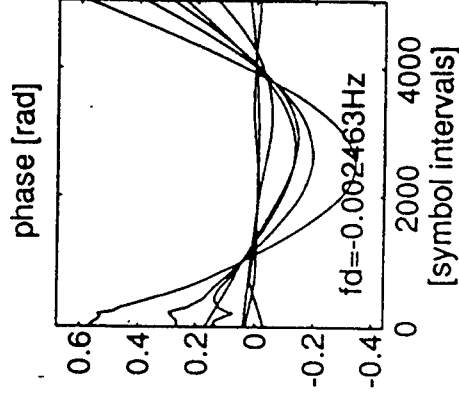
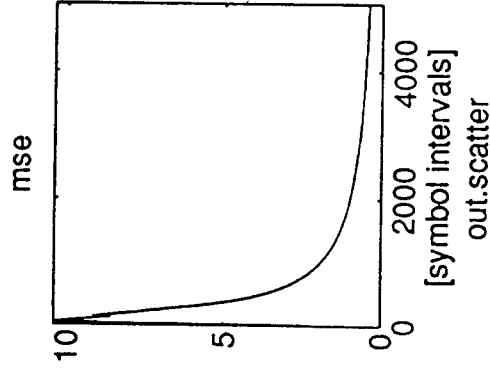
$K=10$ $P=3$
 $L1=0.99$ $L2=0.998$
 $N=60$ $M=60$
 $Kf1=0.0005$ $Kf2=5e-05$
 $Pe \sim 0$
 $SNR_{out} \sim -21.46dB$

Range=48 nautical miles, Rate=500 sps, 8-PSK.

→ performance
 almost insensitive
 to the choice of
 no channels

- this is the best case performance with 3 channels;
 cases could be found where the 3 channels were so "good"
 the algorithm wouldn't operate in decision-directed mode
 - adding the fourth channel results in virtually the same performance.

PERFORMANCE RESULTS



receiver parameters : 1000 sps

$N=80$ ($T/2$) $M=100$

$K=7$ $P=3$

$L_e=0.998$ $L_c=0.99$

$Kf_1=0.0001$ $Kf_2=1e-05$

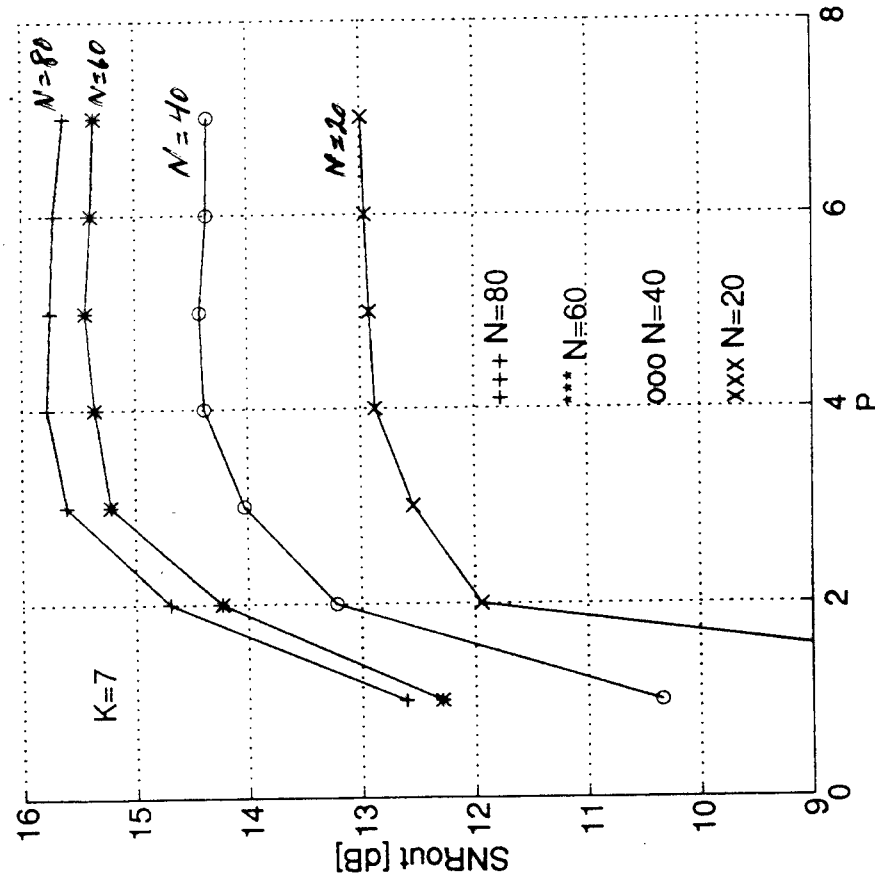
$P_e \sim 0$

$SNR_{out} \sim 15.66dB$

$R = 1000$ band
 $M =$ length of
 feedback
 filter

- 2 dB better than full-complexity 3-channel receiver
- insensitive to the choice of input channels

SUMMARY OF PERFORMANCE RESULTS



M=100

- saturation at $P > 3$: no need to further increase complexity.

CONCLUSIONS

- Beamforming interpretation of optimal combiner leads to reduction in complexity of adaptive multichannel receivers.
- Reduced complexity is achieved at no cost in performance.
- Spatial diversity of multipath is fully exploited without significantly increasing the receiver complexity.
- Keeping the complexity at minimum:
 - avoids noise enhancement
 - provides efficient use of fast algorithms.
- Experimental results demonstrate:
 - eliminated sensitivity to the choice of receiver position
 - spatial diversity gain over same size K -channel receiver
 - negligible increase in computational complexity with additional input channels

SESSION VII: ADVANCED APPLICATIONS (U)

Fast Approximate Subspace Tracking

D.W. Tufts, E.C. Real¹, and J.W. Cooley²

University of Rhode Island
Department of Electrical Engineering
Kingston, RI 02881
email: tufts@ele.uri.edu

¹Sanders, A Lockheed Martin Company
PTP2-A001, P.O. Box 868
Nashua, NH 03061-0868
email: real@rocket.sanders.com

²University of Rhode Island
Department of Electrical Engineering
Kingston, RI 02881
email: cooley@ele.uri.edu

Abstract A new fast and accurate algorithm for tracking singular values, singular vectors and the dimension of the signal subspace through an overlapping sequence of data matrices is presented. The accuracy of the algorithm approaches that of the Prony-Lanczos (PL) method [1] with speed and accuracy superior to both the PAST and PASTd algorithms [2] for moderate to large size problems. The algorithm is described for the special case of changes to two columns of the matrix prior to each update of principle singular vectors and values; although the approach is not limited to two column updates. Comparisons of speed and accuracy are made with the algorithms named above. Specifically, we introduce a new algorithm for efficiently tracking the principle singular values and the associated left (or right) singular vectors of successive data matrices formed from observations of a nonstationary signal in non-stationary noise. The dimension of the signal subspace is tracked simultaneously with the singular values and vectors. The ability to do this accurately and in real time is a critical requirement of many signal processing applications in areas such as radar, sonar, communications, pattern recognition, and speech processing.

Dr. D. W. Tufts

Department Of Electrical Engineering
University Of Rhode Island
Kingston, RI 02881

E. C. Real

Signal Processing Center Of Technology
Sanders, A Lockheed Martin Company
Nashua, NH 03061-0868

Dr. J. W. Cooley

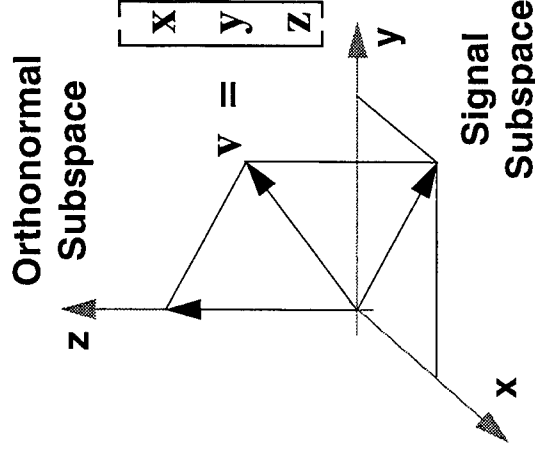
Department Of Electrical Engineering
University Of Rhode Island
Kingston, RI 02881

- **Introduction**
- **Statement of the problem**
- **Theoretical development**
- **The FAST algorithm**
- **Some examples**
- **Conclusions**

- The FAST algorithm is an accurate and efficient algorithm for tracking singular values and their associated singular vectors through a sequence of overlapping matrices.
- The accuracy is achieved by preserving that component of the matrix perturbation that lies in the orthogonal subspace from update to update.
- The speed is achieved by replacing a larger approximation matrix A with a much smaller approximation B , which is computationally easier to deal with.
- Faster versions of the FAST algorithm exist which trade accuracy for speed.

- **Signal subspace/orthonormal subspace decomposition:**

This signal processing point of view decomposes a measurement vector into one component that lies in a signal subspace and another that lies in an orthonormal subspace. This decomposition is typically accomplished via an eigen or SVD analysis.



- **Subspace tracking:**

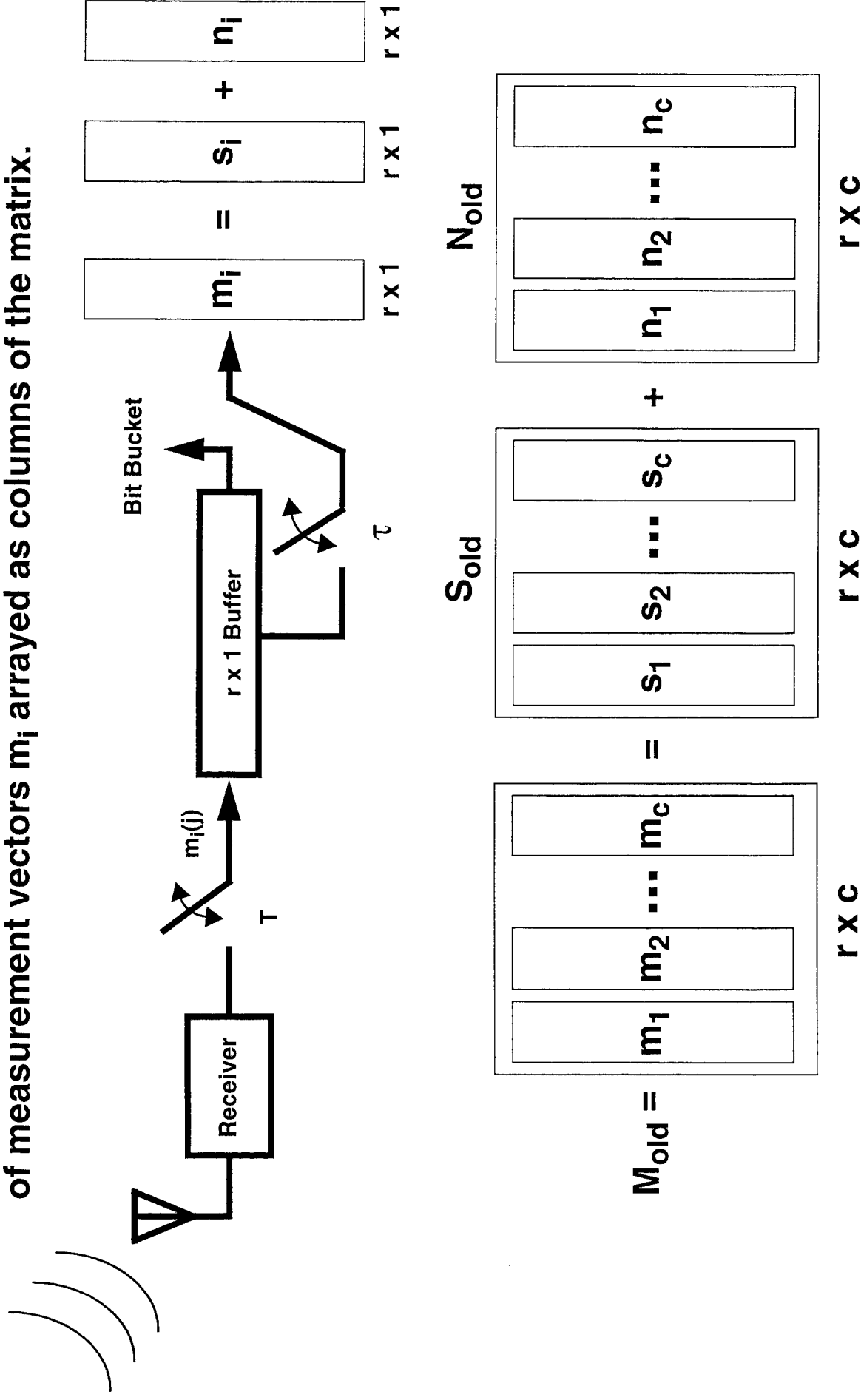
In subspace tracking, the components of non-stationary measurement vectors that lie in the signal or orthonormal subspace are tracked through a sequential series of measurements.

- **Technologies which employ subspace tracking:**

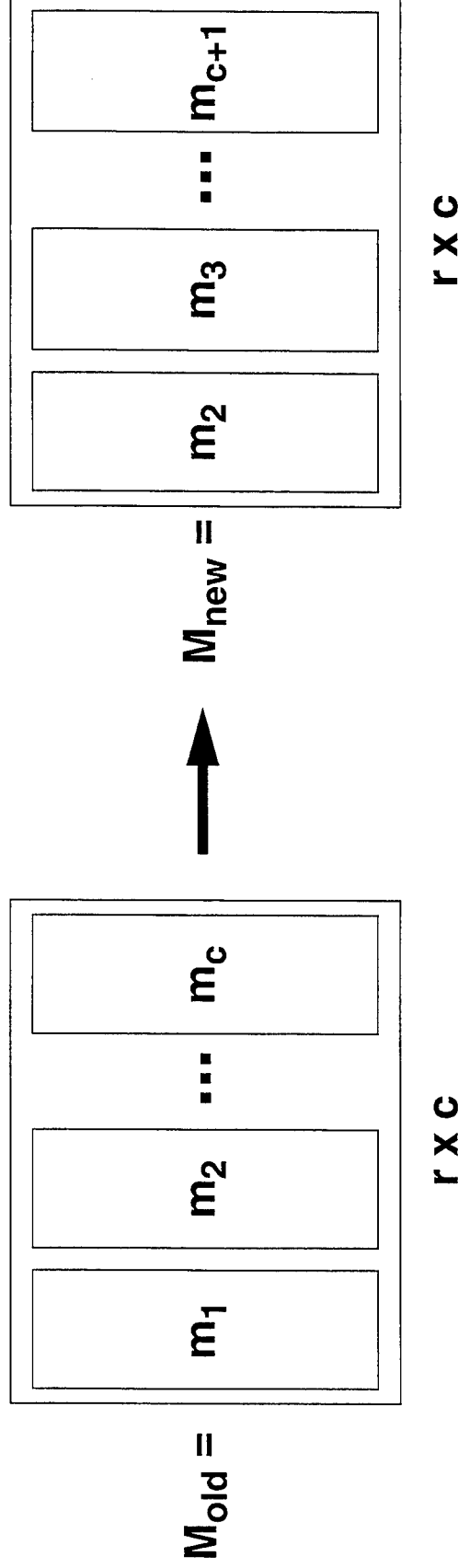
Subspace tracking is used in signal processing areas such as:

- RADAR and SONAR:** Fluctuating targets, clutter suppression.
- Speech processing:** Formant tracking, clutter suppression.
- Array processing:** Beamforming, adaptive nulling.
- Image processing:** Signal enhancement, clutter suppression.

- Suppose we have an r by c data matrix M_{old} composed from a sequence of measurement vectors m_i arrayed as columns of the matrix.



- Suppose now that we have a new measurement vector available to us m_{c+1} and with it we update M_{old} . In doing this we keep the row and column size constant by removing the oldest column vector m_1 .



- The objective is to track the principal singular values and associated left singular vectors of the corresponding signal matrix as it makes the transition from S_{old} to S_{new} . This process is complicated by the fact that the signal is measured in the presence of noise.

- We develop the theory behind the FAST algorithm in two steps.

Step One:

- Develop a low rank matrix A that is appropriate for tracking the singular values and singular vectors of a rank k signal matrix measured in the presence of noise.
- The matrix A is a reduced rank version of the data matrix M_{new} , but one that has the same number of rows and columns.

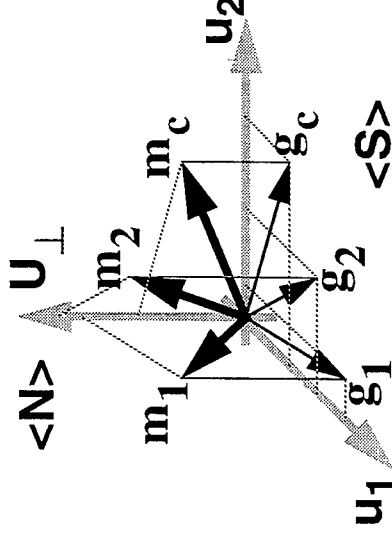
Step Two:

- Construct a smaller matrix B which has the same k principal singular values and associated left singular vectors as A and track this matrix.
- It is in this step that the major computational advantage is gained.

- In choosing to track the k principal singular values and vectors, we have also chosen an associated “noise level”, namely the squared Frobenius norm error in the approximation of M_{old} by $U_{old}^H M_{old}$:

$$E_{old} = \|M_{old} - U_{old} U_{old}^H M_{old}\|_F^2$$

$$E_{old} = \sum_{j=1}^c \|m_j - g_j\|^2$$



- We wish an approximation to M_{new} which is at least this good. One matrix which meets this requirement is:

$$A = \begin{bmatrix} U_{old} & q \end{bmatrix} \begin{bmatrix} a_2 & a_3 & \dots & a_c & a_{(c+1)} \\ 0 & 0 & \dots & 0 & b \end{bmatrix}$$

where we define

$$a_i = U_{old}^H m_i \quad z = m_{(c+1)} - U_{old} a_{(c+1)}$$

$$b = \|z\|$$

$$q = z/b$$

$$A = \begin{bmatrix} U_{\text{old}} & q \end{bmatrix} \begin{bmatrix} a_2 & a_3 & \dots & a_c & a_{(c+1)} \\ 0 & 0 & \dots & 0 & b \end{bmatrix}$$

- Two attributes of the matrix **A** are worthy of note.

- 1) The first $c+1$ columns of **A** are the same as the last $c+1$ columns of the approximation to M_{old} :

$$U_{\text{old}}^H U_{\text{old}} M_{\text{old}} = U_{\text{old}} \begin{bmatrix} a_1 & a_2 & \dots & a_c \end{bmatrix}$$

- 2) The last column of **A** is the same as the last column of M_{new} since:

$$M_{\text{new}} = \begin{bmatrix} m_2 & m_3 & \dots & m_c & m_{c+1} \end{bmatrix}$$

and

$$m_{c+1} = U_{\text{old}} a_{c+1} + bq$$

- In words, the matrix A is a better approximation to M_{new} than the matrix $U_{\text{old}}^H M_{\text{old}}$ is to M_{old} , because every column in M_{old} is approximated while the last column in M_{new} is not.
- To see this we compare the Frobenius norms of the corresponding error matrices.

$$E_{\text{old}} = \left\| M_{\text{old}} - U_{\text{old}} U_{\text{old}}^H M_{\text{old}} \right\|_F^2$$

$$E_{\text{new}} = \left\| M_{\text{new}} - A \right\|_F^2$$

$$E_{\text{old}} = \sum_{j=1}^c \|m_j - g_j\|^2$$

$$E_{\text{new}} = \sum_{j=2}^c \|m_j - g_j\|^2 + \|m_{(c+1)} - m_{(c+1)}\|^2$$

0

Therefore

$$E_{\text{new}} \leq E_{\text{old}}$$

$$A = \begin{bmatrix} U_{\text{old}} & q \end{bmatrix} \underbrace{\begin{bmatrix} a_2 & a_3 & \dots & a_c & a_{(c+1)} \\ 0 & 0 & \dots & 0 & b \end{bmatrix}}_E$$

- To reduce the computational load, we now replace the r by c matrix A by an r by $k+1$ matrix B , defined as follows:

$$B = \begin{bmatrix} U_{\text{old}} & q \end{bmatrix} E E^H = \begin{bmatrix} U_{\text{old}} & q \end{bmatrix} F$$

where like terms are the same as in the equation for A .

- Notice that the columns of B lie in the same space as those of A , and that the matrix $\begin{bmatrix} U_{\text{old}} & q \end{bmatrix}$ is unitary.

$$\mathbf{B} = \begin{bmatrix} \mathbf{U}_{\text{old}} & \mathbf{q} \end{bmatrix} \mathbf{E} \mathbf{E}^H = \begin{bmatrix} \mathbf{U}_{\text{old}} & \mathbf{q} \end{bmatrix} \mathbf{F}$$

- The left singular vectors of \mathbf{F} are the left singular vectors of \mathbf{E} .
- The singular values of \mathbf{F} are the squares of the singular values of \mathbf{E} .
- Therefore, we can now compute the singular values and left singular vectors of \mathbf{A} as follows.

- First we form the SVD of the matrix \mathbf{F} as $\mathbf{F} = \mathbf{U}_{\mathbf{F}} \Sigma_{\mathbf{F}} \mathbf{V}_{\mathbf{F}}^H$.
- The matrix \mathbf{B} can then be written as $\mathbf{B} = \begin{bmatrix} \mathbf{U}_{\text{old}} & \mathbf{q} \end{bmatrix} \mathbf{U}_{\mathbf{F}} \Sigma_{\mathbf{F}} \mathbf{V}_{\mathbf{F}}^H$.
- The left singular vectors of \mathbf{B} are computed as $\mathbf{U}_{\mathbf{B}} = \begin{bmatrix} \mathbf{U}_{\text{old}} & \mathbf{q} \end{bmatrix} \mathbf{U}_{\mathbf{F}}$.
- And the singular values are computed as $\Sigma_{\mathbf{B}} = \Sigma_{\mathbf{F}}^{1/2}$.

- The left singular values and vectors of \mathbf{B} are the same as those of \mathbf{A} .

- In words, the k principal singular values of Σ_B and the associated columns of U_B will approximate the k principal singular values and vectors of M_{new} .

- These are computed efficiently now because, given U_{old} and q from a previous iteration, the only SVD required is that of the matrix F , and the matrix F is only of size $k+1$ by $k+1$, where k is typically a small number in comparison to r or c .

An SVD is required
of this matrix only.

$$B = \begin{bmatrix} U_{\text{old}} & q \end{bmatrix} F = \begin{bmatrix} r \times (k+1) \\ (k+1) \times (k+1) \end{bmatrix} \begin{bmatrix} U_{\text{old}} & q \end{bmatrix} F$$

- The steps of the FAST algorithm are given below.

Step (0) Initialize. First obtain an initial estimate of the k principal singular values and associated left singular vectors of the starting data matrix M . One way to do this is to compute the SVD of M , and from it extract the required k principal singular values and construct the matrix U_{old} as above.

Step (1) Obtain the next data vector $m_{(c+1)}$, and compute $a_i = U_{old}^H m_i$ for $i = 2, 3, \dots, (c+1)$.

Step (2) Compute $z = m_{(c+1)} - U_{old} a_{(c+1)}$.

Step (3) Compute $b = \|z\|$.

Step (4) Compute $q = z/b$.

Step (5) Form the E matrix

$$E = \begin{bmatrix} a_2 & a_3 & \dots & a_c & a_{(c+1)} \\ 0 & 0 & \dots & 0 & b \end{bmatrix}$$

Step (6) Compute the matrix $F = EE^H$.

Step (7) Compute the SVD of $F = U_F \Sigma_F V_F^H$.

Step (8) Using U_{old} , q and U_F , update U_{old} by replacing its columns with the principal singular vectors of $U_B = \begin{bmatrix} U_{old} & q \end{bmatrix} U_F$.

Step (9) Update the existing singular values by replacing them with the square roots of the principal singular values of Σ_F .

Step (10) Update the data vectors m_i by setting $m_i = m_{i+1}$, $i = 1, 2, \dots, c$ and return to Step (1).

Parameters Of Experiment 1

Parameter	Value
Radian frequency 1 (constant)	$2\pi/3$
Radian frequency 2 (constant)	$4\pi/5$
Noise standard deviation (real and imaginary)	0.1
Number of rows of M	64
Number of columns of M	8
Number of singular values/vectors tracked	2
Beta value (for PASTd algorithm)	0.95

Statistics For Largest Singular Value Estimate

Algorithm	Mean Error	Standard Deviation
PL	-0.07047	0.2386
PAST	-5.581	7.283
PASTd	-3.785	8.932
FAST	-0.5896	0.8188

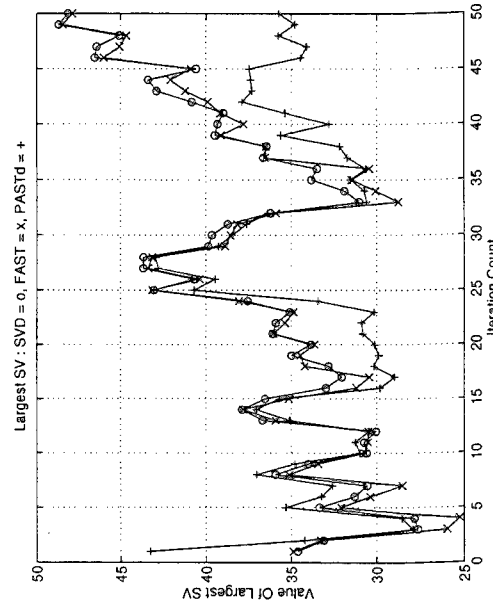
Statistics For 2nd Largest Singular Value Estimate

Algorithm	Mean Error	Standard Deviation
PL	-0.1848	1.038
PAST	7.124	4.988
PASTd	6.413	4.153
FAST	0.843	1.166

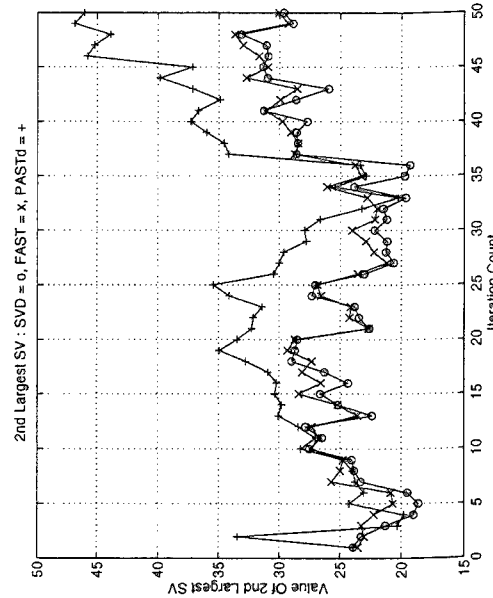
Speed Improvements Over A Standard SVD

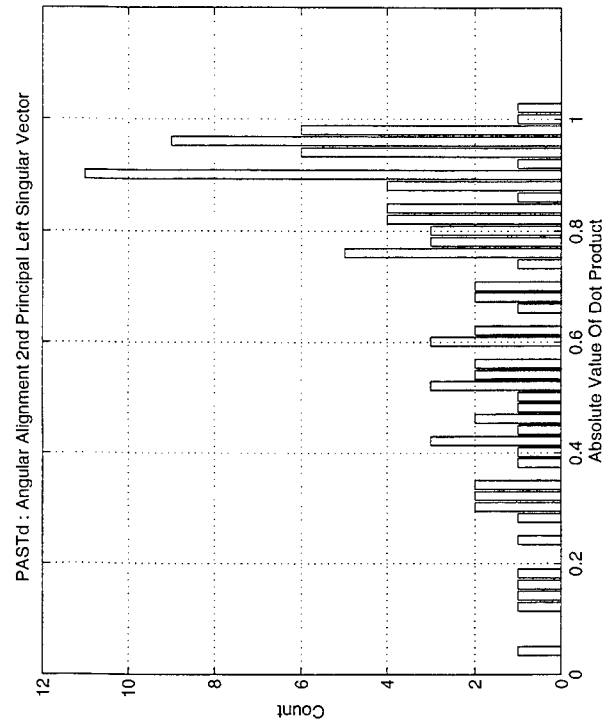
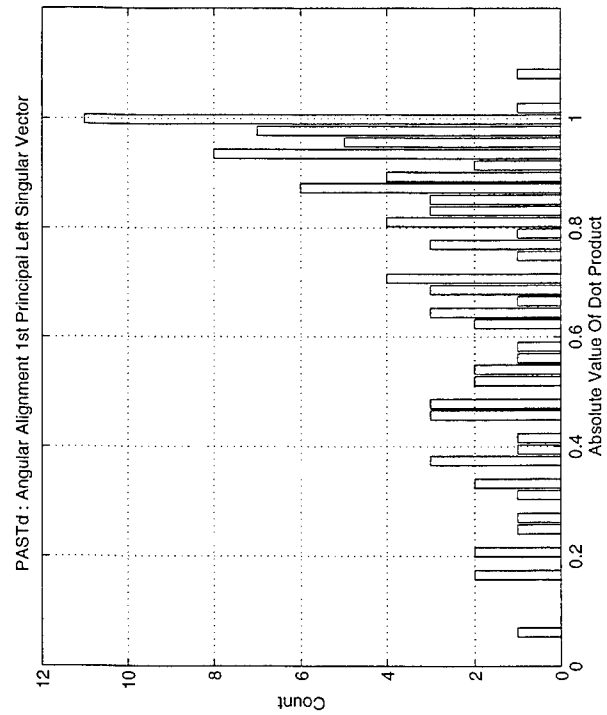
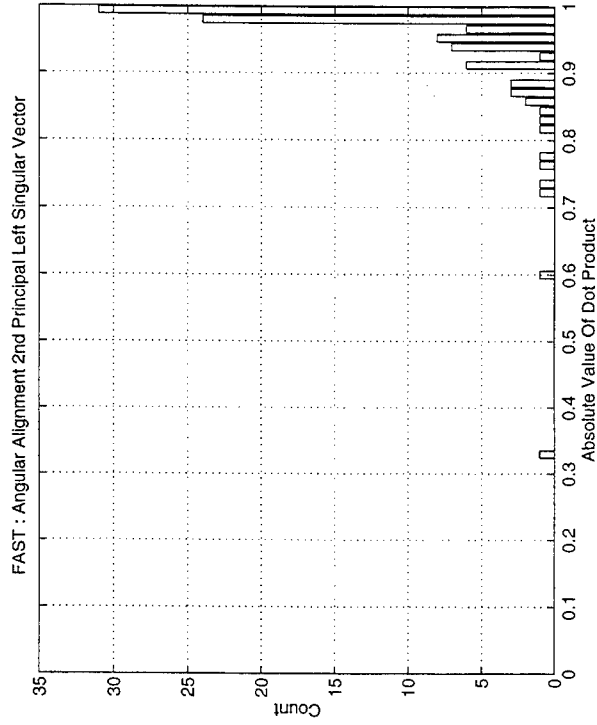
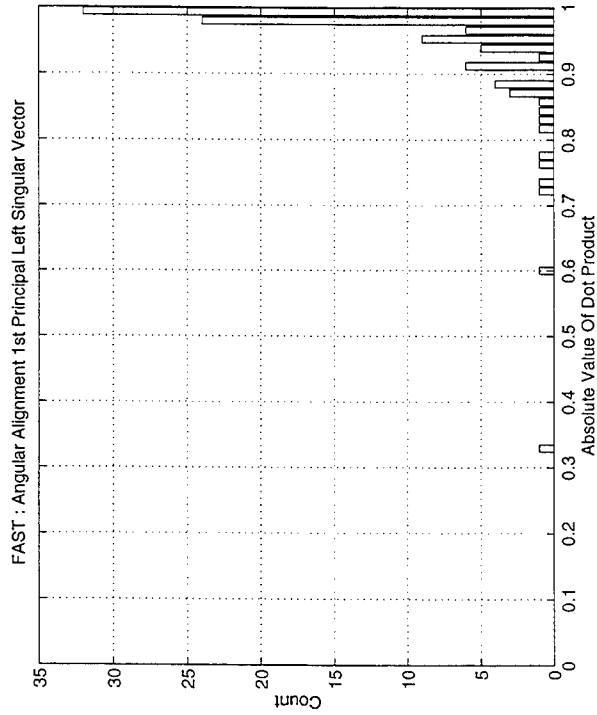
Algorithm	Mean Speed Up
PL	1.7553
PAST	1.7571
PASTd	1.7541
FAST	39.4356

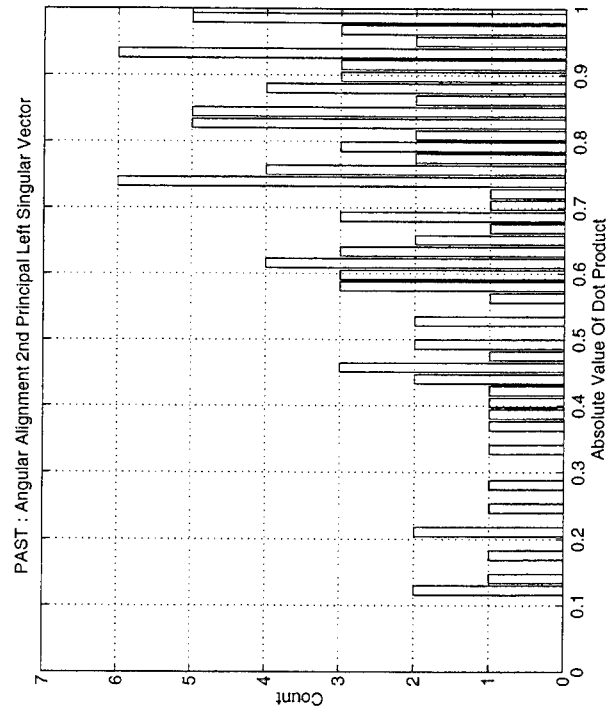
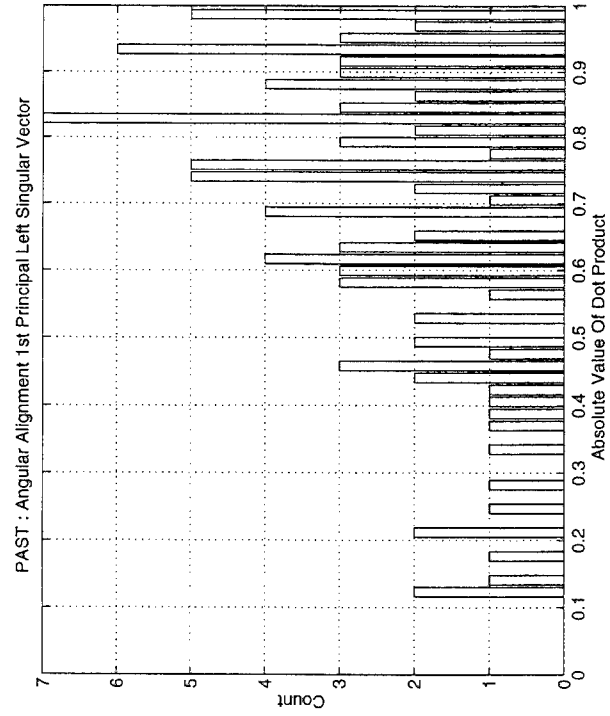
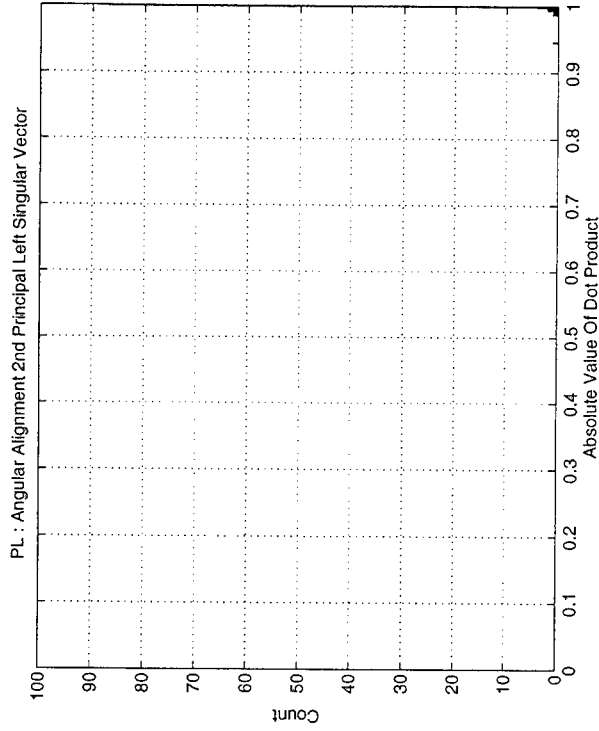
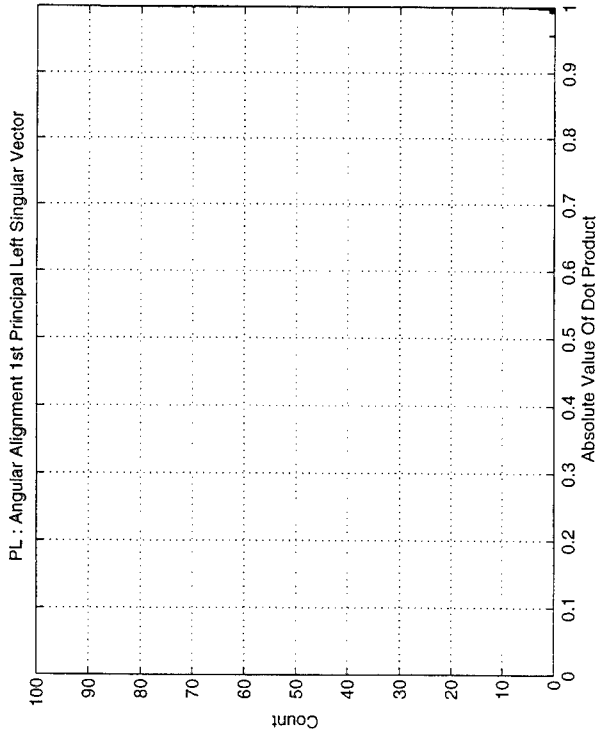
A comparison of the trace of the largest singular value computed by the SVD over 50 iterations vs. the estimate of it from the various algorithms indicated.



A comparison of the trace of the second largest singular value computed by the SVD over 50 iterations vs. the estimate of it from the various algorithms indicated.



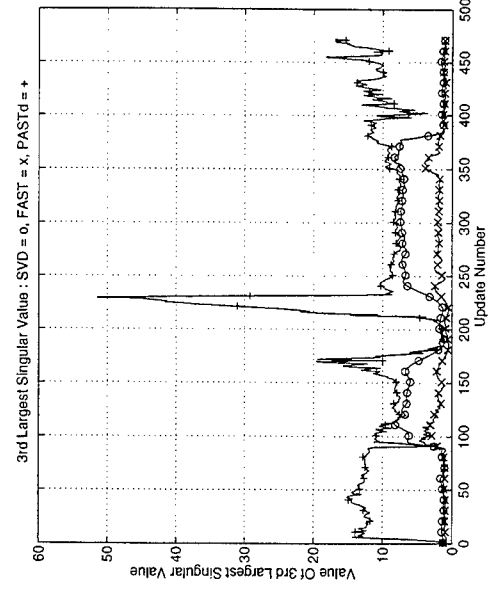
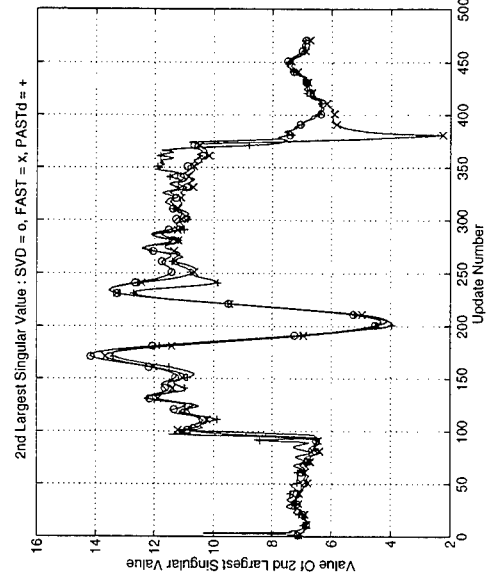
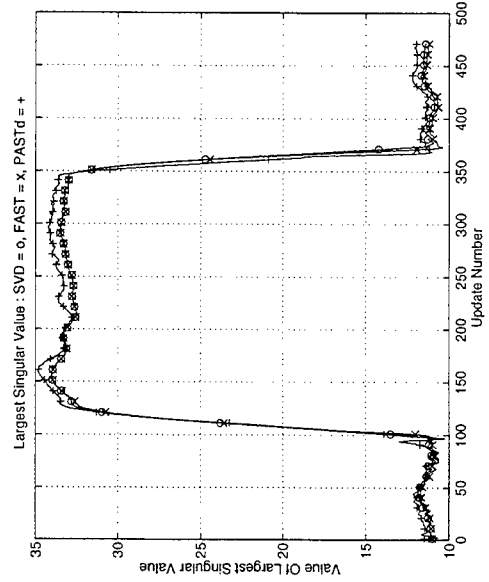
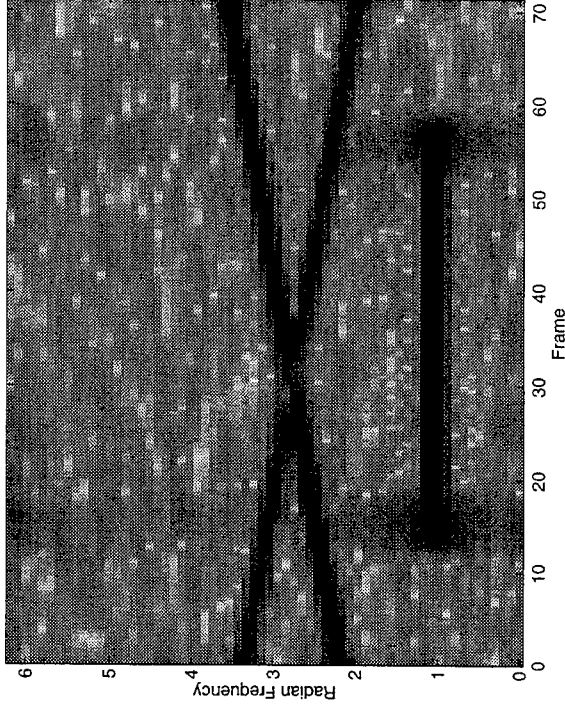




Parameters Of Experiment 3

Parameter	Value
Radian frequency 1 (start)	$2\pi/3$
Change in radian frequency 1 per sample	$\pi/2048$
Radian frequency 2 (start)	$5.5\pi/5$
Change in radian frequency 2 per sample	$-\pi/2048$
Radian frequency 3 (constant)	$\pi/3$
Noise standard deviation (real and imaginary)	0.05
Number of rows of M	20
Number of columns of M	20
Number of singular values/vectors tracked	2
Beta value (for PASTd algorithm)	0.6

Spectrogram Of Example 3 Data



Statistics For Largest Singular Value Estimate

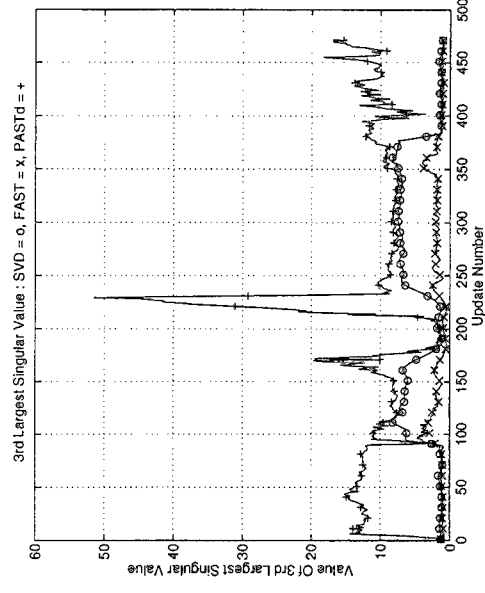
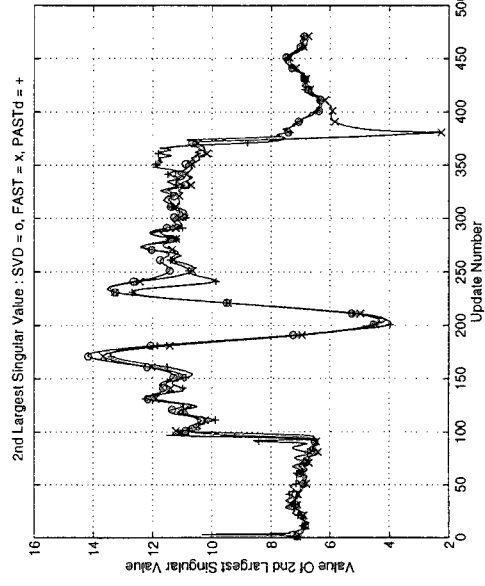
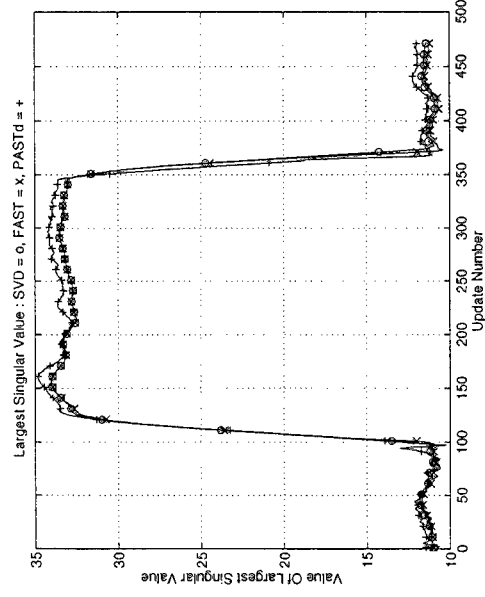
Algorithm	Mean Error	Standard Deviation	RMS Error
PL	-2.599e-3	0.02568	0.5602
PAST	0.8293	11.59	252.1
PASTd	0.2261	0.9293	20.76
FAST	-0.1457	0.2851	6.951

Statistics For 2nd Largest Singular Value Estimate

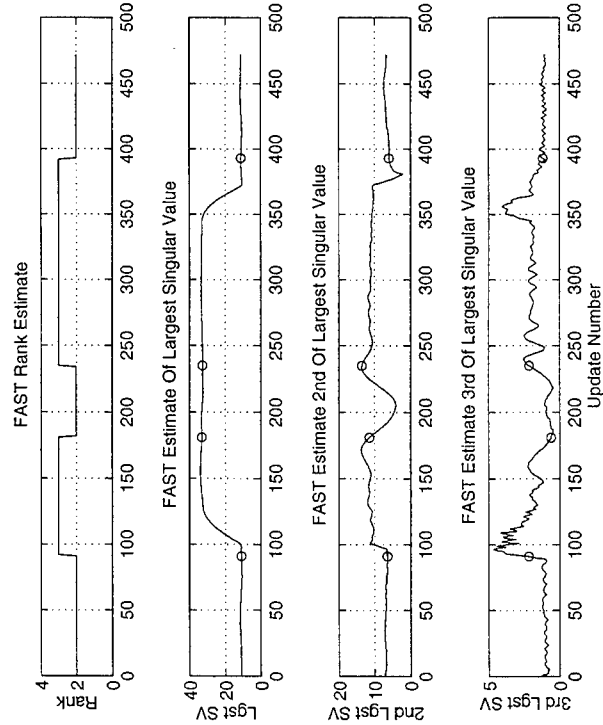
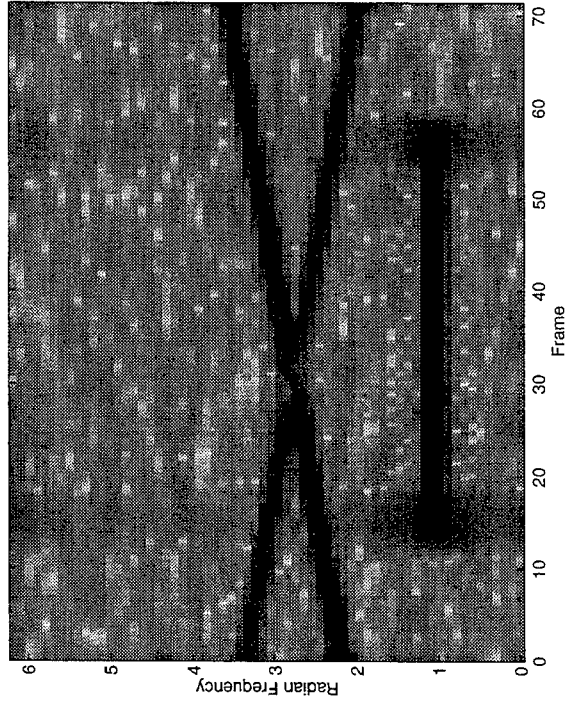
Algorithm	Mean Error	Standard Deviation	RMS Error
PL	-0.03544	0.2137	4.701
PAST	-4.215	4.366	131.8
PASTd	-0.08441	0.6364	13.93
FAST	-0.3378	0.5803	14.58

Statistics For 3rd Largest Singular Value Estimate

Algorithm	Mean Error	Standard Deviation	RMS Error
PL	-0.2750	0.7470	17.2783
PAST	1.4859	1.5737	46.99
PASTd	6.3841	7.0191	206.0
FAST	-2.4954	2.2363	72.76



Spectrogram Of Example 3 Data

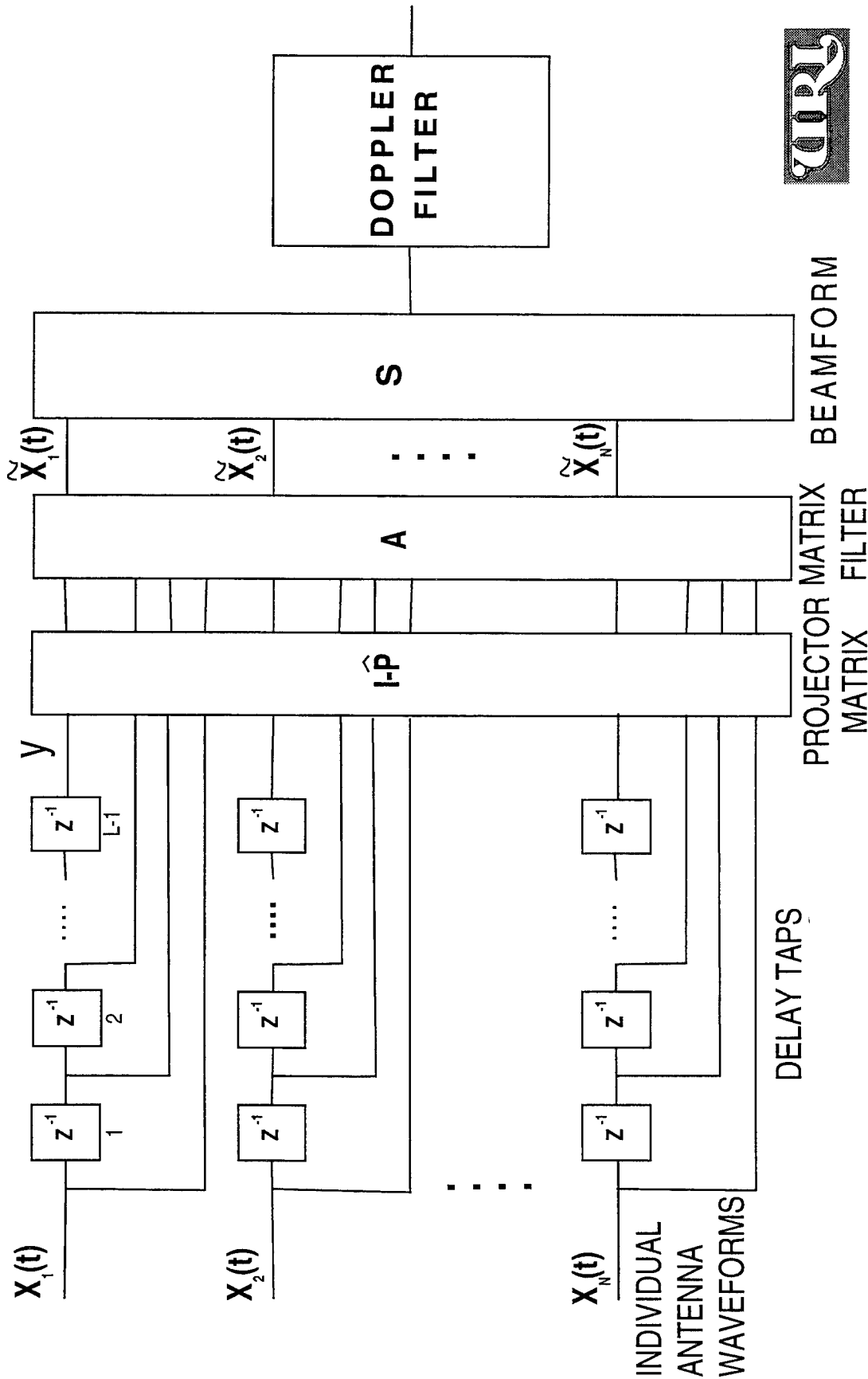


Speed Improvements Over A Standard SVD

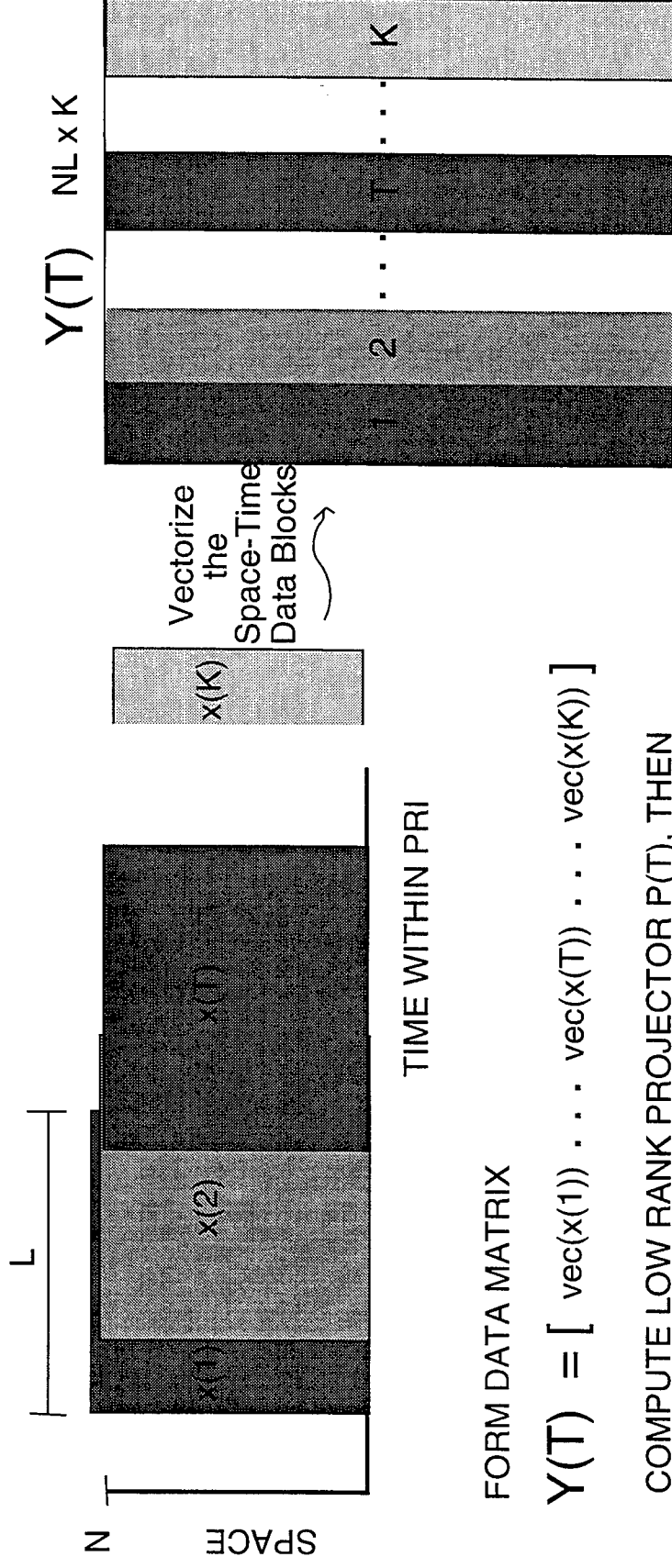
Algorithm	Mean Speed Up
PL	3.8129
PAST	4.8523
PASTd	4.8410
FAST	35.8031

VECTORIZED SPACE TIME PCI (VST/PCI)

VECTORIZED SPACE-TIME PCI (VST/PCI) (PLOT A BELOW)



SLIDING WINDOW UPDATE METHOD



FORM DATA MATRIX

$$Y(T) = [\text{vec}(x(1)) \quad \dots \quad \text{vec}(x(T)) \quad \dots \quad \text{vec}(x(K))]$$

COMPUTE LOW RANK PROJECTOR $P(T)$, THEN

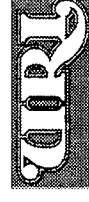
$\tilde{X}(T) = A P(T) \text{VEC}(T)$. WHERE A IS A MATRIX FILTER, SPACE-TIME \rightarrow SPACE

$\tilde{X}(T)$ IS THE "CLEANED" SNAPSHOT AT TIME T .

SLIDE WINDOWS FOR NEW MATRIX

$$Y(T+1) = [\text{vec}(x(2)) \quad \dots \quad \text{vec}(x(T+1)) \quad \dots \quad \text{vec}(x(K+1))]$$

USE SVD UPDATE ALGORITHM TO COMPUTE $P(T+1)$, THEN $\tilde{X}(T+1)$.





SLIDING WINDOW METHOD

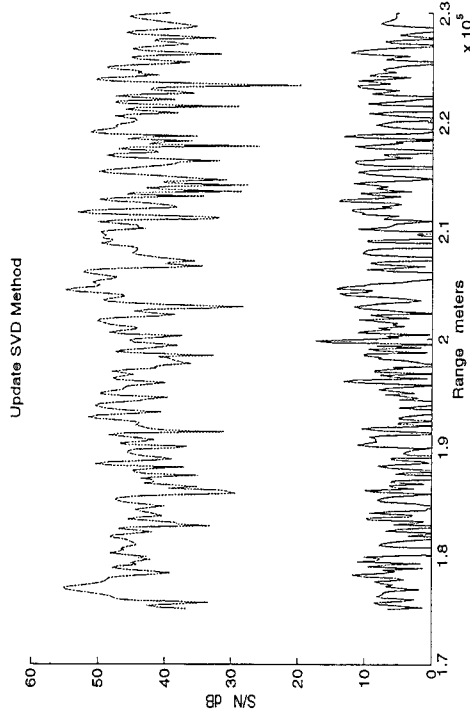
SLIDING WINDOW METHOD REDUCES RESIDUAL AT 225 Km

AIRBORNE JAMMER - RIO043
1 PULSE 40 TAPS
INJECTED TARGET 28dB SNR at 200 Km,
150Hz, BROADSIDE

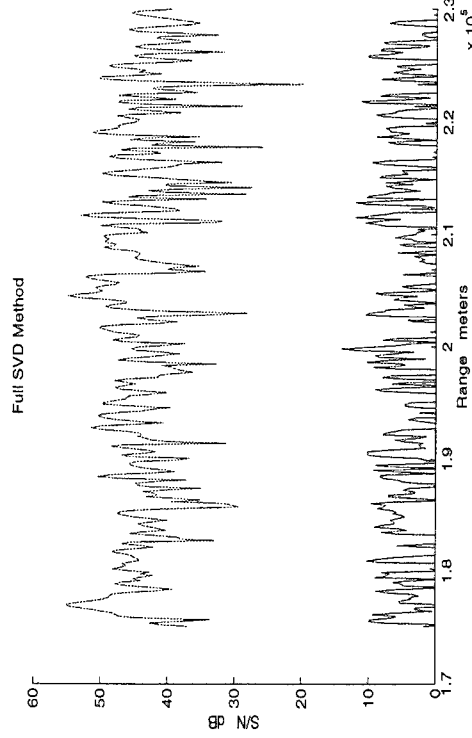
Table 1: COMPUTATION MATLAB FLOPS

	VST/PCI	SVD UPDATE	SVD FULL
MATLAB FLOPS	8.3E09	3.9E11	3.3E12

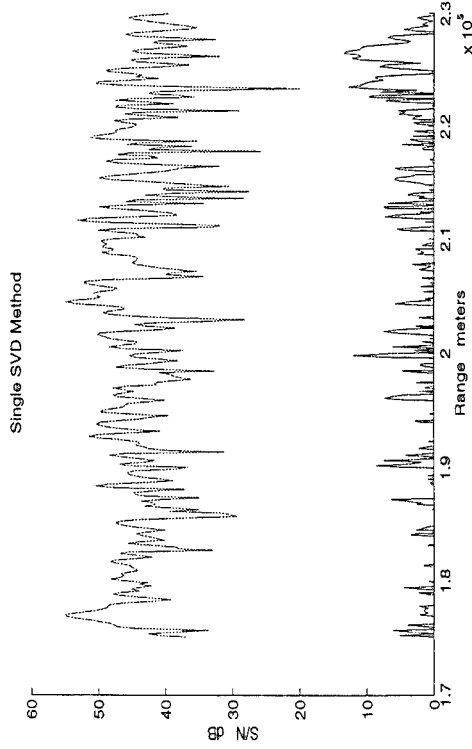
SLIDING WINDOW PCI w/SVD UPDATE



SLIDING WINDOW PCI w/FULL SVD



VST/PCI



- The FAST algorithm is an accurate and efficient algorithm for tracking singular values and their associated singular vectors through a sequence of overlapping matrices.
- The accuracy is achieved by preserving that component of the matrix perturbation that lies in the orthogonal subspace from update to update.
- The speed is achieved by replacing a larger approximation matrix A with a much smaller approximation B , which is computationally easier to deal with.
- Faster versions of the FAST algorithm exist which trade accuracy for speed.

STAP in Wireless Communications: Performance Analysis

A.M. Haimovich and A. Shah

New Jersey Institute of Technology
Center for Communications and Signal Processing
Department of E.C.E.

University Heights, Newark, NJ 07102-2982

Abstract In wireless communications, degrees of freedom provided by space-time processing can be used to combat both fading and interferences. In this presentation we are concerned with spatial processing and STAP in a Rayleigh channel model with cochannel interference. STAP is applicable to both narrowband (TDMA), and wideband (CDMA) communications. With TDMA, temporal degrees of freedom are applied to equalization in addition to their role in interference cancellation, while in CDMA, temporal processing is also used for diversity. While couched in terms of a specific multiple access method, the analysis is quite generic and may be extended to the other method. For narrowband communications, new closed-form expressions are presented for the distribution of the signal-to-noise and interference ratio (SNIR), and for bounds on the error probability for spatial processing in a Rayleigh channel with multiple cochannel interferences. Reduced-rank methods are studied for their ability to provide better performance through improved statistical stability. Finally, STAP is analyzed with respect to the rejection of narrowband interferences in CDMA communications. This situation arises either when narrowband communications share the spectrum with the CDMA signal, or when the interferences are intentional. The conventional approach to rejecting narrowband interferences in direct sequence spread spectrum signals, has been to whiten the received signal containing the interference prior to spread spectrum demodulation. In this presentation it is shown that STAP is much more robust with respect to the interference bandwidth. New closed-form expressions are obtained that characterize the performance of STAP in rejecting narrowband interferences in CDMA communications.

**STAP IN WIRELESS COMMUNICATIONS:
PERFORMANCE ANALYSIS**

A.M. HAIMOVICH & A. SHAH

**CENTER FOR COMMUNICATIONS AND SIGNAL PROCESSING
NEW JERSEY INSTITUTE OF TECHNOLOGY**

ASAP'97

OVERVIEW

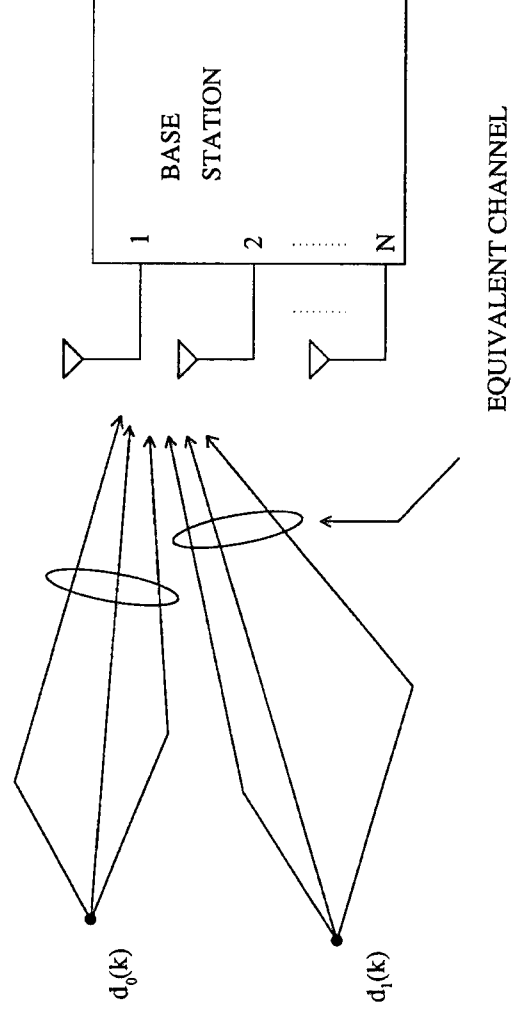
- STAP IN WIRELESS COMMUNICATIONS: CHANNEL AND SIGNAL MODELS
- STUDY CASE: OVERLAY INTERFERENCE REJECTION
- RECEIVER ARCHITECTURES:
 - TIME/TIME
 - SPACE/TIME
- INTERFERENCE RANK CASES: $L = 1$, $L \leq$ STAP DIM., $L >$ STAP DIM
- FINITE SAMPLE EFFECTS
- NUMERICAL RESULTS
- CONCLUSIONS & FUTURE WORK

STAP APPLICATIONS IN WIRELESS

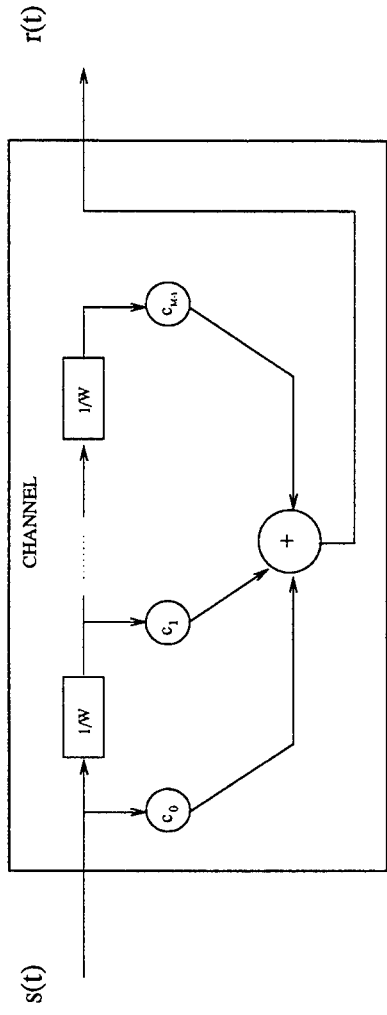
- MULTIPATH FADING
 - SPATIAL DIVERSITY - ANTENNAS SEPARATION $\gg \lambda/2$
 - FREQUENCY DIVERSITY - TDL FILTER, TAP SPACING = MP SPREAD TIME
- NARROWBAND INTERFERENCE REJECTION IN WIDEBAND COMMUNICATIONS (OVERLAY)
 - TIME-TIME VS. SPACE-TIME ARCHITECTURE
- CDMA - FREQUENCY SELECTIVE CHANNEL
 - REJECTION OF COCHANNEL INTERFERENCE+MP MITIGATION
- TDMA - FLAT CHANNEL
 - REJECTION OF COCHANNEL INTERFERENCE+MP MITIGATION+EQUALIZATION

CHANNEL MODEL

- SPATIAL CHANNEL MODEL

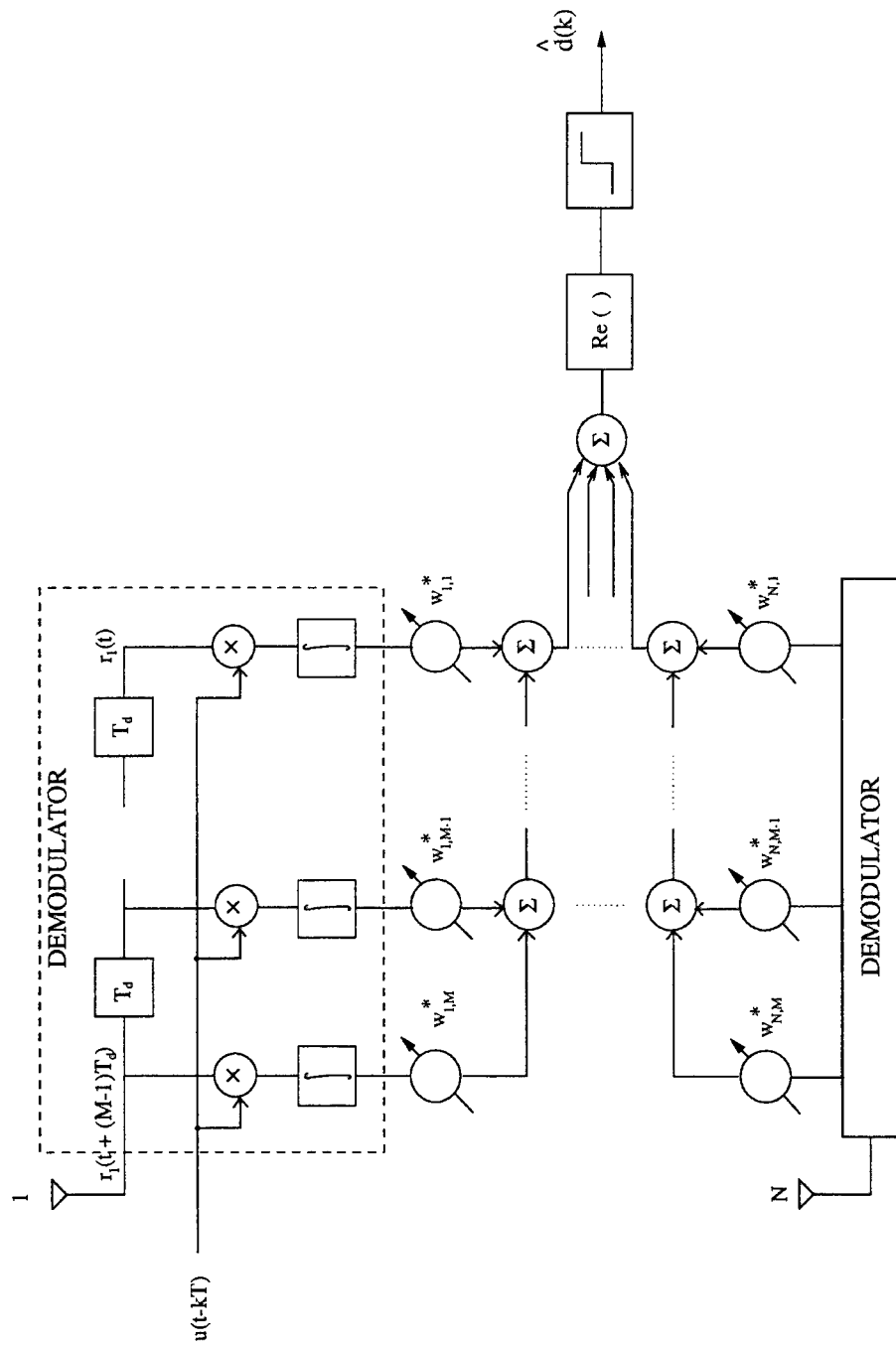


- FREQUENCY SELECTIVE CHANNEL



- CHANNEL INPUT: $s(t) = \sqrt{\mathcal{E}} \sum_k d(k)u(t - kT)$, CHANNEL OUTPUT:
 $R(t) = \sqrt{\mathcal{E}} \sum_k d(k)\mathbf{c}_0^T \mathbf{u}(t - kT)$
- STACK N SPATIAL CHANNELS AND M FREQUENCY CHANNELS TO
 GENERATE $NM \times 1$ CHANNEL VECTOR \mathbf{c}
- RAYLEIGH FADING: CHANNEL VECTOR IS RANDOM $\text{CN}[\mathbf{0}, \mathbf{I}]$

SPACE-TIME ARCHITECTURE



SIGNAL MODEL

- GENERIC SIGNAL MODEL FOR SPACE-TIME PROCESSING (N ANTENNAS, M TAP DELAYS) WHICH APPLIES TO THE FOLLOWING CASES:
 - FREQUENCY-SELECTIVE CHANNEL WITH CCI
 - FREQUENCY-SELECTIVE CHANNEL WITH OVERLAY NB INTERFERENCE
 - FLAT CHANNEL WITH ISI
- AFTER DEMODULATION, AT THE INPUT OF SIGNAL PROCESSOR FOR DETECTION

$$\mathbf{r}(k) = d_0(k)\sqrt{\mathcal{E}}\mathbf{c}_0 + \sum_{\ell=1}^L d_{\ell}(k)\sqrt{\mathcal{P}_{\ell}}\mathbf{c}_{\ell} + \mathbf{v}(k)$$

- BINARY DATA, IID CHANNELS $\mathbf{c}_{\ell} \sim \text{CN}[\mathbf{0}, \mathbf{I}]$, SLOW FADING (CONSTANT OVER PROCESSING INTERVAL), WGN $\mathbf{v}(k) \sim \text{CN}[\mathbf{0}, N_o\mathbf{I}]$

OVERLAY INTERFERENCE MODEL

- FREQUENCY-SELECTIVE CHANNEL MODEL, TAP SPACING $T_d = 1/W$, M TAPS
- OVERLAY FRACTIONAL BANDWIDTH $= p$ (ACTUAL BW $= pW/2$)
- DEMODULATION PRODUCTS

$$j_{nm}(k) = \langle j_n(t + mT_d), u(t - kT) \rangle$$

- FORM $NM \times 1$ STACKED VECTOR $\mathbf{j}(k)$. THE MATRIX $E[\mathbf{j}(k)\mathbf{j}^H(k)]$ HAS L PRINCIPAL EIGENVALUES

$$L = p(M - 1) + 1$$

- KARHUNEN-LOEVE DECOMPOSITION

$$\mathbf{j}(k) = \sum_{k=1}^L \alpha(k) \mathbf{q}_k$$

- OVERLAY MODEL IS EQUIVALENT TO MULTIPLE CCI MODEL

STAP PARADIGMS

- DIVERSITY PROCESSING ONLY \Rightarrow MAXIMUM RATIO COMBINER
- DIVERSITY+CCI REJECTION \Rightarrow OPTIMUM COMBINER
- \mathbf{R} = INTERFERENCE+NOISE COVARIANCE MATRIX
- BER FOR BINARY MODULATION, SINGLE CHANNEL ($N = 1$, $M = 1$),
CONDITIONED ON THE CHANNEL, NO CCI ($L = 0$)

$$\mathbf{w} = \mathbf{R}^{-1} \mathbf{c}_0$$

$$P_e = Q\left(\sqrt{2\mu_0}\right) < e^{-\mu_0}$$

$$\mu_0 = |c_0|^2 \gamma_0 = |c_0|^2 \mathcal{E} N_o^{-1}.$$

- AVERAGE OVER FADING, μ_0 HAS EXPONENTIAL DISTRIBUTION
WITH PARAMETER γ_0^{-1} , $f(\mu_0) = \gamma_0^{-1} e^{-\mu_0/\gamma_0}$,

$$P_e < (1 + \gamma_0)^{-1}$$

RANK-ONE INTERFERENCE

- SPATIAL DIVERSITY + RAKE (TOTAL OF NM INDEPENDENT PATHS), $\mu_0 = \|\mathbf{c}_0\|^2 \gamma_0$, $f(\mu_0) = \Gamma^{-1}(NM) \gamma_0^{-NM} \mu_0^{-(NM-1)} e^{-\mu_0/\gamma_0}$,
 $E[\mu_0] = NM \gamma_0$

$$P_e < (1 + \gamma_0)^{-NM}$$
- EFFECTIVE SNR, $\mu_0 = \mathcal{E} \mathbf{c}_0^H \mathbf{R}^{-1} \mathbf{c}_0$
- P.D.F. OF μ_0 FOR SINGLE INTERFERENCE - (also Bogachev&Kiselev 1980, Winters 1984)

$$f(\mu_0) = \Gamma^{-1}(NM) \gamma_1^{-1} \gamma_0^{-(NM-1)} \mu_0^{NM-1} e^{-\mu_0/\gamma_1} {}_1F_1[N-1, N; (\gamma_1^{-1} - \gamma_0^{-1}) \mu_0]$$

$$\gamma_1 = \mathcal{E}(\lambda_1 + N_o)^{-1}, \lambda_1 \text{ IS THE PRINCIPAL EIGENVALUE}$$

- BOUND ON BER FOR ARBITRARY INR

$$P_e < (1 + \gamma_1)(1 + \gamma_0)^{-(NM-1)}$$

INTERFERENCE RANK $L < NM$

- SNR, $\mu_0 = \mathcal{E} \mathbf{c}_0^H \mathbf{R}^{-1} \mathbf{c}_0$
- FADING MODEL ASSUMED FOR DESIRED SIGNAL, BUT NOT FOR INTERFERENCE
- SINCE $L < NM$, INTERFERENCE IS CANCELED AND FADING HAS LITTLE EFFECT
- FOR \mathbf{R} OF RANK L ,

$$\mathbf{c}_0^H \mathbf{R}^{-1} \mathbf{c}_0 = \sum_{n=1}^L (\lambda_n + N_o)^{-1} |\mathbf{c}_0^H \mathbf{q}_n|^2 + N_o^{-1} \sum_{n=L+1}^N |\mathbf{c}_0^H \mathbf{q}_n|^2$$

- EIGENVECTORS FORM A UNITARY TRANSFORMATION
- SNR P.D.F. FOR L EQUAL EIGENVALUES $\lambda_1, \gamma_1 = \mathcal{E} (\lambda_1 + N_o)^{-1}$

$$f(\mu_0) = \Gamma^{-1}(NM) \gamma_1^{-L} \gamma_0^{-(NM-L)} \mu_0^{NM-L} e^{-\mu_0/\gamma_1} {}_1F_1[N-L, N; (\gamma_1^{-1} - \gamma_0^{-1}) \mu_0]$$

BER $L < NM$

- BER BOUND FOR INTERFERENCE WITH L EQUAL PRINCIPAL EIGENVALUES

$$P_e < (1 + \gamma_1)^{-L} (1 + \gamma_0)^{-(NM-L)}$$

- ASYMPTOTIC PDF, $\text{INR} \rightarrow \infty$ ($\gamma_1 \rightarrow 0$) \Rightarrow GAMMA DISTRIBUTION WITH PARAMETERS $NM - L$ AND γ_0^{-1} :

$$f(\mu_0) = \Gamma(NM - L, \gamma_0^{-1}) = \Gamma^{-1}(NM - L) \gamma_0^{-(NM-L)} \mu_0^{NM-L-1} e^{-\mu_0/\gamma_0}$$

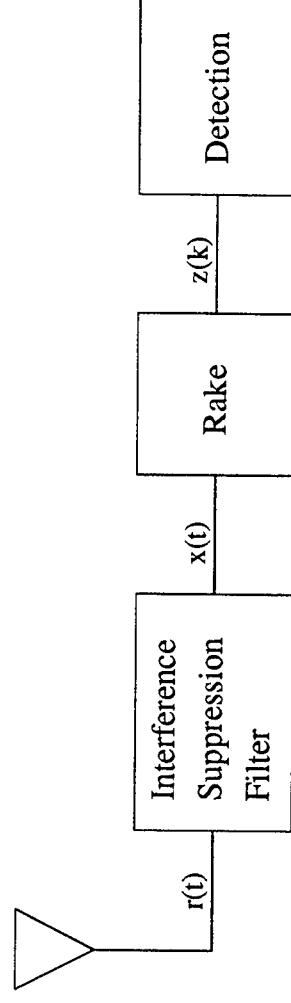
- BER BOUND FOR LARGE INR

$$P_e < (1 + \gamma_0)^{-(NM-L)}$$

- LOSS OF L DOF, EQUIVALENT TO SYSTEM WITH $(NM - L)$ DIVERSITY
- FOR $\text{INR} \rightarrow \infty$, SIMILAR RESULT BY Winters, Salz, Gitlin 1994 BASED ON MSE ARGUMENT

TIME-TIME PROCESSING

- TIME-TIME ADAPTIVE PROCESSING (TTAP) AS AN ALTERNATIVE TO STAP
- COMPARISON BETWEEN TTAP AND STAP ARCHITECTURES
- TTAP IMPLEMENTED BY A PEF FOLLOWED BY A RAKE



- IT CAN BE SHOWN (Haimovich, Shah 1997) THAT PEF WITH Q TAPS REJECTS OVERLAY AT COST OF NOISE GAIN $= (1 - L/Q)^{-1}$. PEF-RAKE COMBINATION ACTS AS AN M DIVERSITY RECEIVER (M IS THE NUMBER OF TAPS IN THE FREQUENCY SELECTIVE CHANNEL) WITH AN INPUT NOISE OF $N_o (1 - L/Q)^{-1}$.

TTAP SNR PERFORMANCE

- IN THE ABSENCE OF INTERFERENCE, SNR AT RAKE OUTPUT

$$\mu_0 = \mathcal{E} N_o^{-1} \sum_{m=0}^{M-1} |c_m|^2$$

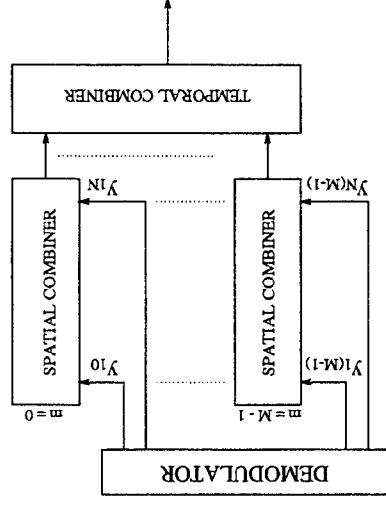
- EFFECTIVE SNR, WITH INTERFERENCE, AT PEF-RAKE OUTPUT

$$\mu_0 = \mathcal{E} N_o^{-1} (1 - L/Q) \sum_{m=0}^{M-1} |c_m|^2$$

- SNR DISTRIBUTION $\mu_0 \sim \Gamma \left(M, [\mathcal{E} N_o^{-1} (1 - L/Q)]^{-1} \right)$

CASCADE STAP

- ALTERNATIVE ARCHITECTURE TO JOINT-DOMAIN STAP
- APPLICABLE TO CDMA WITH LONG CODES
- SPATIAL PROCESSING FOLLOWED BY RAKE



- SINGLE OVERLAY INTERFERENCE OF RANK L WITH $\text{INR} \rightarrow \infty$,

$$f(\mu_0) = \Gamma((N-1)M, \gamma_0^{-1}) = \Gamma^{-1}((N-1)M) \gamma_0^{-(N-1)M} \mu_0^{(N-1)M-1} e^{-\mu_0/\gamma_0}$$

PERFORMANCE COMPARISONS MEAN SNR

- MEAN SNR $E[\mu_0]$ WITH $\gamma_0 = \varepsilon N_o^{-1}$ AND $\text{INR} \rightarrow \infty$, FOR TTAP AND STAP
- RANK L OVERLAY INTERFERENCE

ARCHIT.	CONFIG.	$E[\mu_0]$
	$NM = 1, L = 0$	γ_0
STAP	$NM > 1, L = 0$	$NM\gamma_0$
STAP	$NM > 1, L = 1$	$(NM - 1)\gamma_0$
TTAP	$M > 1, 0 \leq L \leq Q$	$M(1 - L/Q)\gamma_0$
CAS	$NM > 1, 1 \leq L \leq M$	$(N - 1)M\gamma_0$
STAP	$NM > 1, 0 \leq L \leq NM$	$(NM - L)\gamma_0$

- PERFORMANCE ORDERING

$$\overline{\mu_{0\text{STAP}}} \geq \overline{\mu_{0\text{CAS}}} \geq \overline{\mu_{0\text{TTAP}}}$$

PERFORMANCE COMPARISONS AVERAGE BER

- BOUND ON AVERAGE BER
- BASED ON $Q(\sqrt{2\mu}) < e^{-\mu}$, WITH $\gamma_0 = \mathcal{E}N_o^{-1}$, AND $\text{INR} \rightarrow \infty$

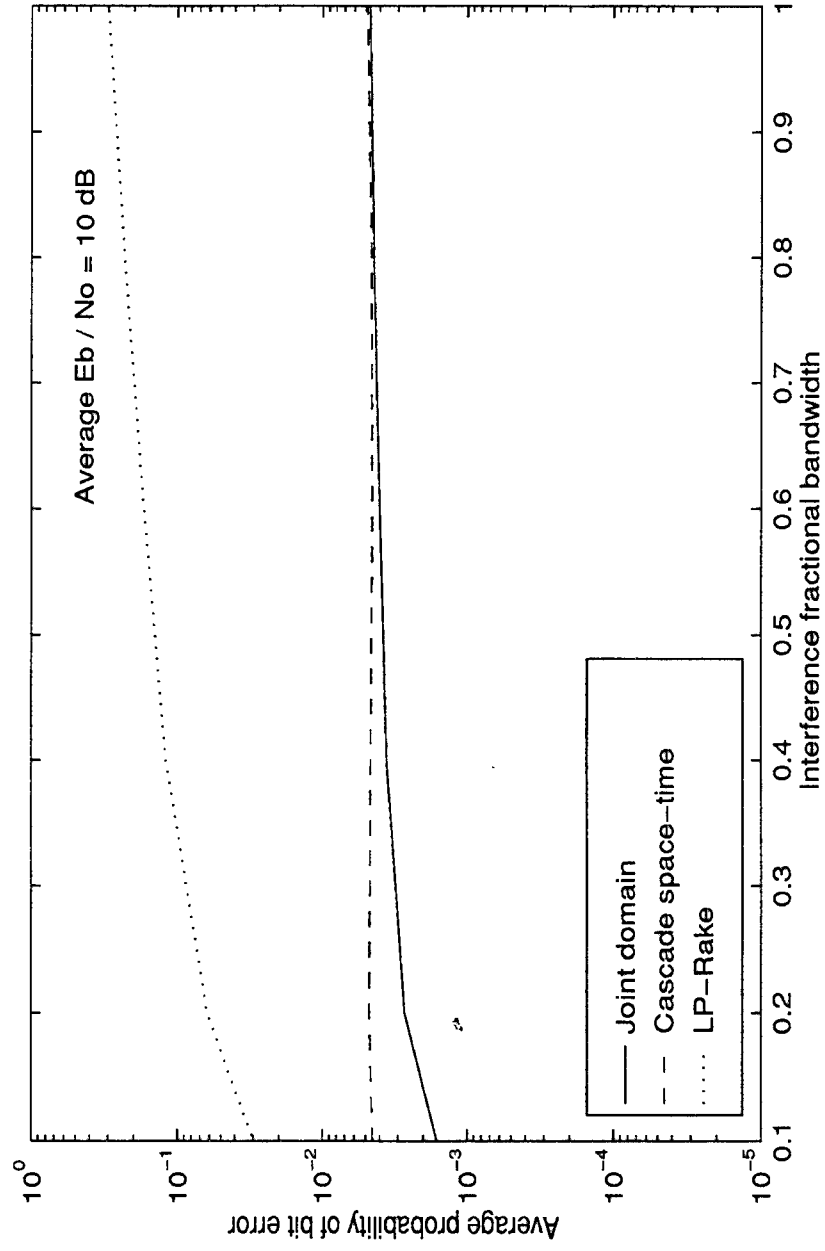
ARCHIT.	CONFIG.	BER BOUND
	$NM = 1, L = 0$	$(1 + \gamma_0)^{-1}$
STAP	$NM > 1, L = 0$	$(1 + \gamma_0)^{-NM}$
STAP	$NM > 1, L = 1$	$(1 + \gamma_0)^{-(NM-1)}$
TTAP	$M > 1, 0 \leq L \leq Q$	$(1 + (1 - L/Q)\gamma_0)^{-M}$
CAS	$NM > 1, 1 \leq L \leq M$	$(1 + \gamma_0)^{-(N-1)M}$
STAP	$NM > 1, 0 \leq L \leq NM$	$(1 + \gamma_0)^{-(NM-L)}$

- COMPARATIVE PERFORMANCE

$$P_{e,\text{STAP}} \leq P_{e,\text{CAS}} \leq P_{e,\text{TTAP}}$$

EFFECT OF INTERFERENCE BW

- BER FOR BPSK OVERLAY INTERFERENCE



SIGNAL MODEL FOR $L > N$

- SIGNAL MODEL: N = ANTENNA ELEMENTS, L = NUMBER OF CCI
- SINCE NUMBER OF DOF IS LESS THAN NUMBER OF ANTENNAS, COMPLETE CANCELLATION OF CCI IS NOT POSSIBLE
- CLEARLY AN INTERFERENCE LIMITED SYSTEM; IGNORE NOISE IN SIGNAL MODEL

$$\mathbf{r}(t) = \sqrt{\mathcal{E}} s_0(t) \mathbf{c}_0 + \sqrt{\mathcal{P}} \sum_{k=1}^L s_k(t) \mathbf{c}_k$$

BINARY DATA $s_0(t)$, $s_k(t) = \pm \psi(t)$, $\psi(t)$ UNIT ENERGY WAVEFORM, $s_0(t)$ DESIRED SIGNAL, $s_k(t)$ CCI, IID CHANNELS $\mathbf{c}_0, \mathbf{c}_k \sim \text{CN}[\mathbf{0}, \mathbf{I}_N]$, SLOW FADING (CONSTANT OVER PROCESSING INTERVAL)

- DUE TO HIGHLY NON-LINEAR NATURE OF P_e CURVE, SMALL SNR IMPROVEMENT MAY ENTAIL SIGNIFICANT P_e REDUCTION
- CASE OF PRACTICAL INTEREST FOR WIRELESS WHERE EACH CELL IS SURROUNDED BY OTHER CELLS

PERFORMANCE FOR $L > N$

- SNR

$$\mu_0 = \frac{\mathcal{E} \left| \mathbf{w}^H \mathbf{c}_0 \right|^2}{\mathbf{w}^H \mathbf{R} \mathbf{w}}$$

$$\mathbf{R} = \mathcal{P} \sum_{k=1}^L \mathbf{c}_k \mathbf{c}_k^H$$

- IT CAN BE SHOWN THAT FOR A RAYLEIGH CHANNEL (Shah, Haimovich 1997):

- MAXIMAL RATIO COMBINING SNR PDF (F DISTRIBUTION)

$$f(\mu_0) = \frac{\Gamma(L+N)}{\Gamma(L)\Gamma(N)} \gamma^L \frac{\mu_0^{N-1}}{(\gamma + \mu_0)^{L+N}}$$

$$\gamma = \mathcal{E}/\mathcal{P}, \text{ SIR PER CHANNEL}$$

- MEAN SNR

$$E[\mu_0] = \frac{N}{L} \gamma$$

- FADING CCI: \mathbf{R}/\mathcal{P} HAS A COMPLEX WISHART DISTRIBUTION
 $\mathbf{C}\mathbf{W}_N(\boldsymbol{\Sigma}, L), \boldsymbol{\Sigma} = E[\mathbf{c}_k \mathbf{c}_k^H] = \mathbf{I}_N$

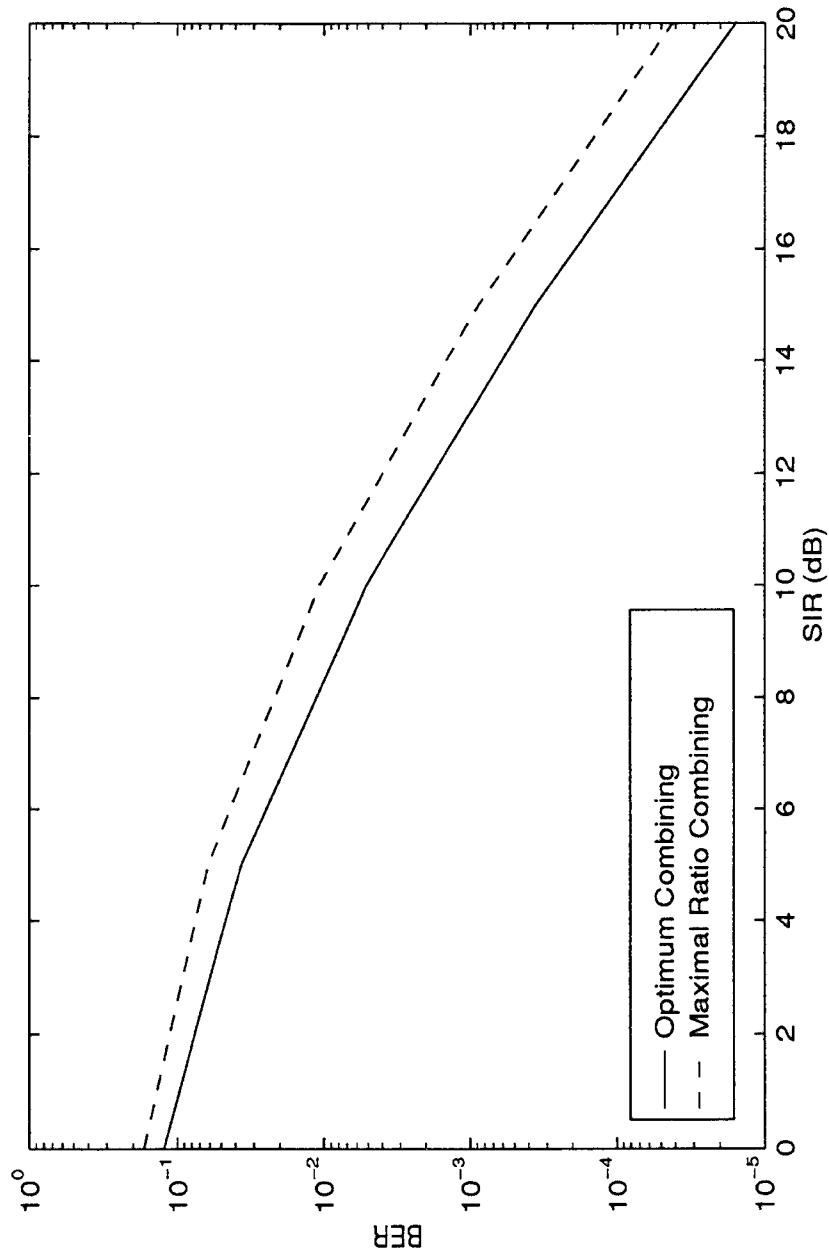
– PDF OF SNR

$$f(\mu_0) = \frac{\Gamma(L+1)}{\Gamma(L+1-N)\Gamma(N)} \gamma^{L+1-N} \frac{\mu_0^{N-1}}{(\gamma + \mu_0)^{L+1}}$$

– MEAN SNR

$$E[\mu_0] = \frac{N}{L-N} \gamma$$

BER CURVES FOR $L > N$



SIGNAL MODEL FOR FINITE SAMPLE EFFECTS

- N ANTENNA ARRAY, $L = 1$ CCI, K DATA VECTORS AVAILABLE TO TRAIN THE ARRAY (EX: IN TDMA 14 SYMBOLS)
- INTERFERENCE+NOISE TRAINING VECTOR $\mathbf{x}(k)$

$$\mathbf{R} = E \left[\mathbf{x}(k) \mathbf{x}(k)^H \right] = \mathcal{P} \mathbf{c}_1 \mathbf{c}_1^H + N_o \mathbf{I}$$

- SIGNAL MODEL $\mathbf{x}(k) \sim \text{CN}[\mathbf{0}, \mathbf{R}]$ (GAUSSIAN ASSUMPTION)
- SMI

$$\mathbf{w} = \hat{\mathbf{R}}^{-1} \mathbf{c}_0$$

ESTIMATE $\hat{\mathbf{R}} = 1/K \sum_{k=1}^K \mathbf{x}(k) \mathbf{x}(k)^H$, VECTOR \mathbf{c}_0 ASSUMED KNOWN

- EIGENCANCELER WEIGHT VECTOR

$$\mathbf{w} = (\mathbf{I} - \hat{\mathbf{q}}_1 \hat{\mathbf{q}}_1^H) \mathbf{c}_0$$

\mathbf{q}_1 IS PRINCIPAL EIGENVECTOR OF $\hat{\mathbf{R}}$

CSNR ANALYSIS

- CONDITIONED SNR (CSNR)
- BER AVERAGED OVER THE FADING CHANNEL AND OVER ρ

$$\rho = \frac{|\mathbf{w}^H \mathbf{c}_0|^2}{\mathbf{w}^H \mathbf{R} \mathbf{w}} \frac{1}{\mathbf{c}_0^H \mathbf{R}^{-1} \mathbf{c}_0}$$

$$P_e = \int_0^\infty \int_0^1 P(e | \rho, \mu_0) f(\rho) f(\mu_0) d\mu_0 d\rho$$

- BER BOUND $P(e | \rho, \mu_0) = Q(\sqrt{2\rho\mu_0}) < 0.5 e^{-\rho\mu_0}$
- PDF OF SMI CSNR (Reed, Mallet, Brennan 1974)
- PDF OF EIGENCANCELER CSNR (Haimovich AES 1997)

$$f(\rho) = \frac{\Gamma(K+1)}{\Gamma(N-1)\Gamma(K+2-N)} (1-\rho)^{N-2} \rho^{K+1-N}, \quad 0 \leq \rho \leq 1$$

$$f(\rho) = K\nu^{-1} \rho^{-2} e^{-K(1/\rho-1)/\nu} \quad 0 \leq \rho \leq 1$$

$$\nu = (N\mathcal{P})^2 / (N\mathcal{P} - N_o)^2$$

BER ANALYSIS

- SMI BER BOUND

$$P_e < 0.5 \frac{1}{(1 + \gamma_0)^{N-1}} {}_2F_1 \left(N - 1, N - 1, K + 1, \frac{\gamma_0}{1 + \gamma_0} \right)$$

- SMI BER BOUND APPROXIMATION FOR LARGE K

$$P_e < 0.5 \frac{1}{(1 + \gamma_0)^{N-1}} \left(1 + \frac{(N - 1)^2}{K} \frac{\gamma_0}{1 + \gamma_0} + o(K^{-2}) \right)$$

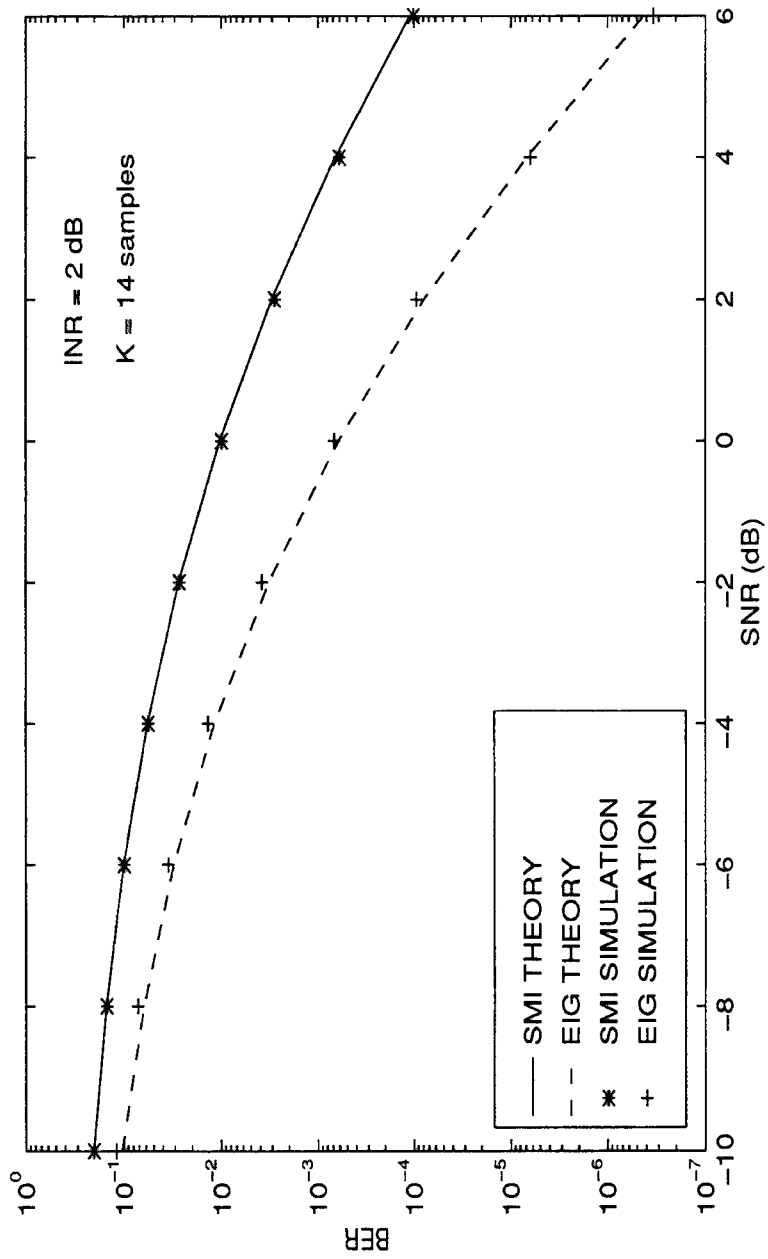
- APPROXIMATION FOR EIGENCANCELER'S CSNR PDF FOR LARGE INR AND LARGE K (Haimovich AES 1997)

$$f(\rho) = K e^{-K(1-\rho)}$$

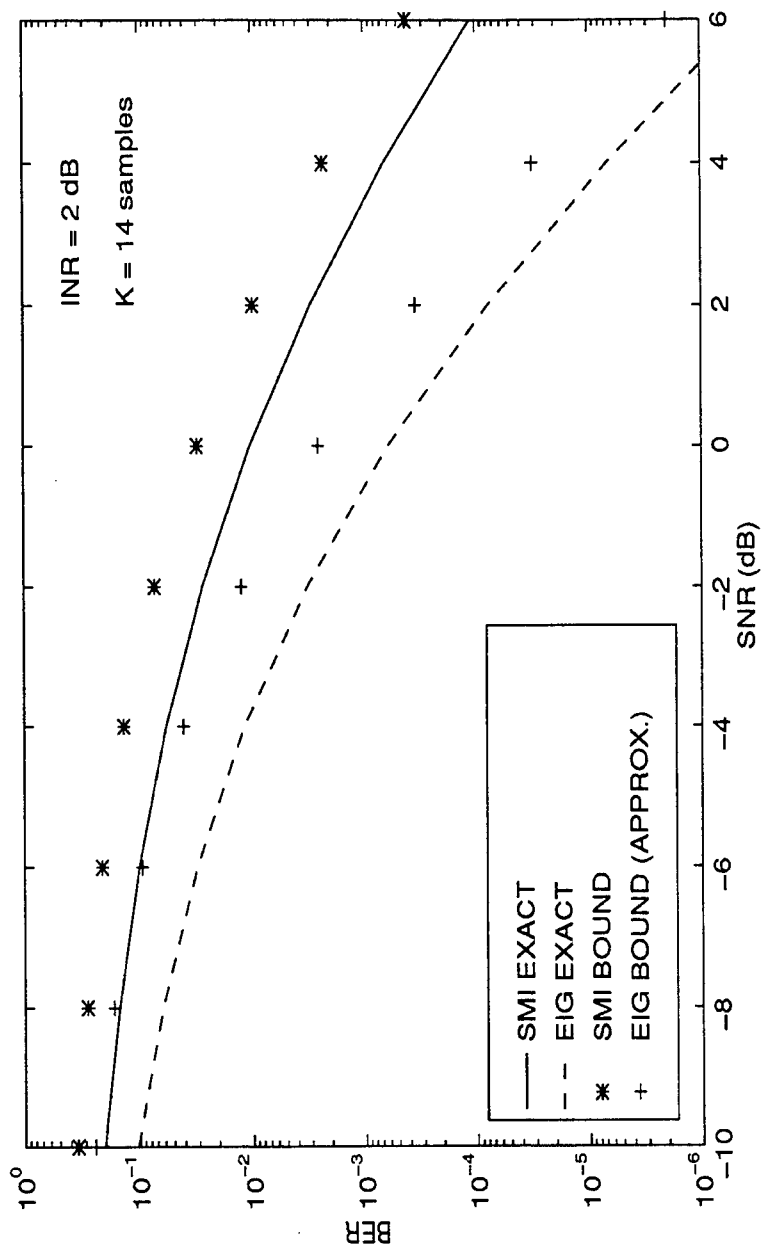
- EIGENCANCELER BER BOUND APPROXIMATION

$$P_e < 0.5 \frac{1}{(1 + \gamma_0)^{N-1}} \left(1 + \frac{N}{K} \frac{\gamma_0}{1 + \gamma_0} + o(K^{-2}) \right)$$

THEORY AND SIMULATIONS



BER APPROXIMATIONS



CONCLUSIONS

- STAP IS APPLICABLE TO MULTIPLE WIRELESS CHANNEL\ SIGNAL MODELS
- STATISTICAL CHARACTERIZATION OF STAP SNR FOR ALL CASES OF RANKS OF THE INTERFERENCE COVARIANCE MATRIX
- SIMPLE CLOSED FORM EXPRESSIONS FOR BER BOUNDS WHICH PROVIDE INSIGHT INTO THE STAP MECHANISM
- COMPARED STAP AND TTAP
- STUDIED APPLICATION OF REDUCED RANK TECHNIQUES - DEVELOPED CLOSED FORM SIMPLE BER BOUNDS
- FUTURE WORK: RICEAN CHANNEL, OTHER MODELS, CHANNEL DOPPLER EFFECTS, SPECIFIC MULTIPLE ACCESS METHODS, CALIBRATION

REPORT DOCUMENTATION PAGE

Form Approved
OMB No. 0704-0188

Public reporting burden for this collection of information is estimated to average 1 hour per response, including the time for reviewing instructions, searching existing data sources, gathering and maintaining the data needed, and completing and reviewing the collection of information. Send comments regarding this burden estimate or any other aspect of this collection of information, including suggestions for reducing this burden, to Washington Headquarters Services, Directorate for Information Operations and Reports, 1215 Jefferson Davis Highway, Suite 1204, Arlington, VA 22202-4302, and to the Office of Management and Budget, Paperwork Reduction Project (0704-0188), Washington, DC 20503.

1. AGENCY USE ONLY (Leave blank)		2. REPORT DATE 25 August 1997	3. REPORT TYPE AND DATES COVERED Project Report ASAP-5, Volume 1	
4. TITLE AND SUBTITLE Proceedings of the Adaptive Sensor Array Processing (ASAP) Workshop, 12-14 March 1997			5. FUNDING NUMBERS C — F19628-95-C-0002 PE — 63326E, 63226E PR — 682	
6. AUTHOR(S) Gina M. O'Donovan, Editor				
7. PERFORMING ORGANIZATION NAME(S) AND ADDRESS(ES) Lincoln Laboratory, MIT 244 Wood Street Lexington, MA 02173-9108			8. PERFORMING ORGANIZATION REPORT NUMBER ASAP-5, Volume 1	
9. SPONSORING/MONITORING AGENCY NAME(S) AND ADDRESS(ES) DARPA 3701 N. Fairfax Drive Arlington, VA 22203-1714			10. SPONSORING/MONITORING AGENCY REPORT NUMBER ESC-TR-97-053	
11. SUPPLEMENTARY NOTES None				
12a. DISTRIBUTION/AVAILABILITY STATEMENT Approved for public release; distribution is unlimited.			12b. DISTRIBUTION CODE	
13. ABSTRACT (Maximum 200 words) The 1997 Adaptive Sensor Array Processing Workshop focuses on the synergism between the sonar and radar ASAP communities in order to encourage future efforts in this direction. Although sonar was included in the first and third ASAP workshops, ASAP has traditionally concentrated on radar — core topics include airborne radar testbed systems, space-time adaptive processing, multipath jamming mitigation, theoretical limits in detection and estimation, and processor architectures. Parallel issues are likewise found in sonar, and both communities have developed adaptive techniques to reduce sensor vulnerability to undesired interference. The similarities between these two fields arise from the common technique of receiving energy on a sensor array, but different missions and propagation environments lead to different signal processing challenges. For airborne early warning (AEW) radar, real-time demands and free-space speed-of-light propagation generally lead to narrowband processing at high data processing throughput. For shallow-water anti-submarine warfare (ASW), the inhomogeneous, dispersive, and attenuation properties of underwater acoustic environments typically require broadband processing at low frequencies, often times with unknown environmental characteristics.				
14. SUBJECT TERMS			15. NUMBER OF PAGES 721	
			16. PRICE CODE	
17. SECURITY CLASSIFICATION OF REPORT Unclassified	18. SECURITY CLASSIFICATION OF THIS PAGE Same as Report	19. SECURITY CLASSIFICATION OF ABSTRACT Same as Report	20. LIMITATION OF ABSTRACT Same as Report	